Lower Passaic River Restoration Project and Newark Bay Study

Final
Hydrodynamic Modeling Report

January 2008

PREPARED BY:
HydroQual, Inc.
1200 MacArthur Blvd.
Mahwah, NJ 07430

UNDER CONTRACT TO:
Malcolm Pirnie, Inc.
104 Corporate Park Drive
White Plains, NY 10602

FOR:
US Environmental Protection Agency
Region 2

US Army Corps of Engineers
Kansas City District
Contract No.
DACW41-02-D-0003

213221

CONTENTS

Section Page

1 INTRODUCTION 1-1
1.1 BACKGROUND 1-1
1.2 STUDY AREA PHYSICAL SETTING 1-3
1.3 CONCEPTUAL SITE MODEL (CSM) 1-5

2 HYDRODYNAMIC MODEL 2-1
2.1 INTRODUCTION 2-1
2.2 RATIONALE FOR A THREE-DIMENSIONAL MODELING FRAMEWORK 2-3
2.3 MODEL DOMAIN 2-4
2.4 HYDRODYNAMIC MODELING FRAMEWORK 2-5
2.5 FLOODING AND DRYING 2-9
2.6 GRID DESIGN 2-9
2.7 BATHYMETRY DATA 2-11

3 BOUNDARY FORCING 3-1
3.1 TIDAL ELEVATION 3-1
3.2 SALINITY AND TEMPERATURE 3-3
3.3 METEOROLOGICAL DATA 3-3
3.4 RIVER DISCHARGE 3-4
3.5 WASTEWATER DISCHARGES 3-6
3.5.1 Wastewater Treatment Plants 3-6
3.5.2 Combined Sewer Overflows and Stormwater Runoff 3-7
3.6 CLOSE EXAMINATION OF FRESHWATER INFLOWS IN THE PASSAIC RIVER BASIN 3-9

4 MODEL CALIBRATION AND VALIDATION 4-1
4.1 AVAILABLE FIELD SURVEY DATA FOR MODEL CALIBRATION AND VALIDATION 4-1
4.2 MODEL CALIBRATION USING THE TSI DATA (1995 AND 1996) FOR THE LPR 4-3
4.2.1 Tidal Elevations 4-3
4.2.2 Current Velocities 4-7
4.2.3 Temperature and Salinity 4-10
4.3 MODEL validation WITH 2004 IMCS DATA SET for the lpr 4-12
4.3.1 Tidal Elevations 4-12
4.3.2 Current Velocities in Lower Passaic River 4-13
4.3.2.1 Current Meter at Station M2 4-13
4.3.2.2 Current Meter at Station M3 4-17
4.3.3 Temperature 4-18
4.3.4 Salinity 4-19
4.4 NEWARK BAY MODEL CLAIBRATION WITH DATA COLLECTED BY IMCS OF RUTGERS UNIVERSITY: MARCH – APRIL, 2002 4-22

CONTENTS (Continued)

Section Page

4.4.1 Tidal Elevations 4-23
4.4.2 Current Velocities 4-25
4.4.3 Temperature 4-33
4.4.4 Salinity 4-34
4.4.5 Net Fluxes in Newark Bay and the Kills 4-40
4.5 NEWARK BAY MODEL VALIDATION USING 2001 SURVEY DATA 4-41
4.5.1 Tidal Elevations 4-41
4.5.2 Current Velocities 4-42
4.5.3 Temperature 4-44
4.5.4 Salinity 4-45
4.5.5 Net Fluxes in Newark Bay And The Kills 4-46

5 SENSITIVITY 5-1
5.1 SENSITIVITY TO MODEL PARAMETERS 5-1
5.1.1 Bottom Roughness Length 5-1
5.1.2 Smagorinsky Coefficient (C_s): HORCON 5-2
5.1.3 Model Sensitivity to Z_0 and C_S 5-2
5.1.4 Summary of Sensitivity to Model Parameters 5-4
5.2 GRID CONVERGENCE TEST 5-20
5.2.1 Model Results 5-20
5.2.2 Elevations 5-21
5.2.3 Current Velocity 5-21
5.2.4 Salinity 5-22
5.2.5 Bottom Shear Stress 5-23
5.2.6 Tracer Simulations: Estimates of flushing time 5-24
5.2.7 Summary of Grid Convergence Test 5-24
5.3 SENSITIVITY TO FRESHWATER INFLOWS IN THE HACKENSACK RIVER5-26

6 SUMMARY OF CALIBRATION/VALIDATION FINDINGS 6-1

7 REFERENCES 7-1

CONTENTS (Continued)

Section		Page
APPENDIX A	Comparison of Computed Water Elevations with Observed TSI Tide Data Over a One-Year Period	
APPENDIX B	Comparison of Computed and Observed Instantaneous Cross-Sectional Velocities at All TSI Transect	
APPENDIX C	Comparison of Computed Hourly Velocities with Near Bottom Data at M1, M2, and M3 Moorings (Round 3)	
APPENDIC D	Comparison of Computed & Observed Cross-Sectional Temperature at All TSI Transects	
APPENDIX E	Comparison of Computed & Observed Cross-Sectional Salinity at All TSI Transect	
APPENDIX F	Testing of Wetting/Drying Scheme	
APPENDIX G	ECOMSED Manual	

FIGURES

Figure

Figure 1 1 Passaic River, Hackensack River, Newark Bay, Kill Van Kull and Arthur Kill Study Area (Map adapted from TSI, 2004)
Figure 1 2 Schematic of the Modeling Framework Processes and their Interaction

Figure 2 1 Bathymetry of study area (in meters). (Pence, 2004)
Figure 2 2 Cross-sectional view of bathymetry in Lower Passaic, Hackensack, and Newark Bay region
Figure 2 3 Monthly average flows of Passaic and Hackensack from 1983 through 2003
Figure 2 4 Surface elevation (top panel), salinity and temperature (middle panels), and surface and bottom currents measured at the head of Newark Bay from Feb-March, 2003 (Pence, 2004)
Figure 2 5 Longitudinal salinity distribution in Passaic River, Water Year 2002
Figure 2 6 Longitudinal salinity distribution in Hackensack River, Water Year 2002
Figure 2 7 SWEM domain and computational grid
Figure 2 8 ECOMSED computational coordinate system
Figure 2 9 Logic diagram for flooding/drying algorithm
Figure 2 10 Full hydrodynamic model domain and computational grid
Figure 2 11 Computational grid for the Lower Passaic River, Hackensack River, and Newark Bay
Figure 2 12 Computational grid for the Harrison Reach of the Lower Passaic River
Figure 2 13 USACE harbor-deepening dredging activities

Figure 3-1 Comparison of 35 hours lowpass water surface elevations at Cape May, Sandy Hook, and Montauk
Figure 3-2a Elevation boundary conditions at four key locations in the New York Bight for July and August, 1995
Figure 3-2b Elevation boundary conditions at four key locations in the New York Bight for April and May, 1996
Figure 3-2c Elevation boundary conditions at four key locations in the New York Bight for March-August, 2001
Figure 3-2d Elevation boundary conditions at four key locations in the New York Bight for March and April, 2002
Figure 3-2e Elevation boundary conditions at four key locations in the New York Bight for August, and September, 2004
Figure 3-3 Temperature and salinity boundary conditions in the New York Bight (used for WY1995 simulation)
Figure 3-4 Temperature and salinity boundary conditions in the New York Bight using WOA98 database (used for WY1996 - 2004)
Figure 3-5a Meteorological data used for heat flux computations (data from JFK station) for July and August, 1995
Figure 3-5b Meteorological data used for heat flux computations (data from JFK station) for April and May, 1996

FIGURES (Continued)

Figure

Figure 3-5c Meteorological data used for heat flux computations (data from JFK station) for March-August, 2001
Figure 3-5d Meteorological data used for heat flux computations (data from JFK station) for March and April, 2002
Figure 3-5e Meteorological data used for heat flux computations (data from JFK station)for August and September, 2004
Figure 3-6 Location map of weather stations for wind stress computations
Figure 3-7 Timeline diagram showing available river discharge data used as model forcing
Figure 3-8a Location map of USGS surface water gauge stations in New York Harbor
Figure 3-8b Location map of USGS surface water gauge stations in Hudson from Tarrytown to Green Island
Figure 3-8c Location map of USGS surface water gauge stations in Connecticut
Figure 3-8d Location map of USGS surface water gauge stations in NJ
Figure 3-9a Temporal variations of river inflows into the model domain from the Hudson, Passaic, Hackensack, and Saddle Rivers for July and August, 1995
Figure 3-9b Temporal variations of river inflows into the model domain from the Hudson, Passaic, Hackensack, and Saddle Rivers for April and May, 1996
Figure 3-9c Temporal variations of river inflows into the model domain from the Hudson, Passaic, Hackensack, and Saddle Rivers for March-August, 2001
Figure 3-9d Temporal variations of river inflows into the model domain from the Hudson, Passaic, Hackensack, and Saddle Rivers for March and April, 2002
Figure 3-9e Temporal variations of river inflows into the model domain from the Hudson, Passaic, Hackensack, and Saddle Rivers for August and September, 2004
Figure 3-10 Temporal variations of river water temperature based on Ashizawa and Cole (1994) (upper panel) and 3 day moving average air temperature from Newark Airport (lower panel)
Figure 3-11 Location map of wastewater treatment plants in the model domain
Figure 3-12a Temporal variations of wastewater inflows compiled by major areas (black lines) during July and August, 1995. Also shown are CSO/SWO water temperature (gray lines) and STP inflow temperature (red lines), water year 1995
Figure 3-12b Temporal variations of wastewater inflows compiled by major areas (black lines) during April and May, 1996. Also shown are CSO/SWO water temperature (gray lines) and STP inflow temperature (red lines), water year 1996
Figure 3-12c Temporal variations of wastewater inflows compiled by major areas (black lines) during March-August, 2001. Also shown are CSO/SWO water temperature (gray dotted lines) and STP inflow temperature (red lines), water year 2001
Figure 3-12d Temporal variations of wastewater inflows compiled by major areas (black lines) during March and April , 2002. Also shown are CSO/SWO water temperature (gray lines) and STP inflow temperature (red lines), water year 2002
Figure 3-12e Temporal variations of wastewater inflows compiled by major areas (black lines) during August and September , 2004. Also shown are CSO/SWO water temperature (gray lines) and STP inflow temperature (red lines), water year 2004
Figure 3-13 Location map of minor tributaries in the Lower Passaic River

FIGURES (Continued)

Figure

Figure 3-14a Temporal variations of Second River, Third River, and McDonald Creek during July and August, 1995. Also shown are inflow water temperatures.
Figure 3-14b Temporal variations of Second River, Third River, and McDonald Creek during April and May, 1996. Also shown are inflow water temperatures.
Figure 3-14c Temporal variations of Second River, Third River, and McDonald Creek during March-August, 2001. Also shown are inflow water temperatures.
Figure 3-14d Temporal variations of Second River, Third River, and McDonald Creek during March and April, 2002. Also shown are inflow water temperatures.
Figure 3-14e Temporal variations of Second River, Third River, and McDonald Creek during August and September, 2004. Also shown are inflow water temperatures.
Figure 3-15 Comparison of USGS gauged Third River flow (black lines) and RRMP computed runoff (red lines) for WY 1995, 1996, and 1997

Figure 4-1 Timeline diagram of TSI field sampling data collected in 1995 and 1996 in the Lower Passaic River
Figure 4-2 Locations of TSI field sampling stations
Figure 4-3 Timeline diagram of IMCS field sampling data collected between 2000 and 2002 (upper panel) and 2004 (lower panel)
Figure 4-4 Locations of IMCS field sampling stations in the Newark Bay, Kill van Kull and Arthur Kill (2000 - 2002)
Figure 4-5 Locations of IMCS field sampling stations in the Lower Passaic River (2004)
Figure 4-6 Comparison of hourly water elevations at TSI stations over a period of one month (May 1995)
Figure 4-7 Comparison of 35 hours low-passed water elevations at TSI stations over a period of two months (May-June 1995)
Figure 4-8 Comparison of instantaneous cross-sectional velocities at Transect 10 (Round 2a)
Figure 4-9 Comparison of hourly computed velocities with near bottom data survey at M1, M2, and M3 moorings (Round 3)
Figure 4-10 Comparison of hourly computed temperature with TSI mooring data over a period of one month (1995) (Group 3, M2, Round 1)
Figure 4-11 Comparison of hourly computed temperature with TSI mooring data over a period of two months (1996) (Group 3 M2 and M3 Round 2a)
Figure 4-12 Comparison of hourly computed temperature with TSI transect data over a period of one month (1995) (Group 2 Round 1)
Figure 4-13 Comparison of hourly computed salinity with TSI transect data over a period of one month (1995) (Group 2 Round 1)
Figure 4-14a Comparison of hourly computed temperature with TSI transect data over a period of two months (1996) (Group 2 Rounds 2a and 3)
Figure 4-14b Comparison of two month averaged model predicted temperature with TSI transect data (1996) (Group 2 Rounds 2a and 3) along the longitudinal axis of the Lower Passaic River
Figure 4-15a Comparison of hourly computed salinity with TSI transect data over a period of two months (1996) (Group 2 Rounds 2a and 3)
Figure 4-15b Comparison of two month averaged model predicted salinity with TSI transect data (1996) (Group 2 Rounds 2a and 3) along the longitudinal axis of the Lower Passaic River

FIGURES (Continued)

Figure

Figure 4-16 Comparison of instantaneous cross-sectional salinities at Transect 10 (Round 2a & 3)

Figure 4-17 Comparison of hourly computed water elevations with IMCS mooring data over a period of two months: August - September 2004

Figure 4-18 Scatter plot of computed water elevation with observed IMCS mooring data: August-September, 2004

Figure 4-19 Comparison of hourly computed current velocities at three depths with IMCS mooring data (M2) over a period of two months: August - September 2004

Figure 4-20 Comparison of hourly computed current velocities at three depths with IMCS mooring data (M2) over a period of 10 days: August 2004

Figure 4-21 Comparison of hourly computed current velocities at three depths with IMCS mooring data (M3) over a period of two weeks: September 2004

Figure 4-22 Scatter plot of computed current velocities with observed IMCS mooring data: August-September, 2004

Figure 4-23 Comparison of hourly computed surface temperature with six IMCS mooring data over a period of two months: August - September 2004

Figure 4-24 Comparison of hourly computed bottom temperature with six IMCS mooring data over a period of two months: August - September 2004

Figure 4-25 Scatter plot of computed temperature with observed IMCS mooring data: August - September 2004

Figure 4-26 Comparison of hourly computed surface salinity with six IMCS mooring data over a period of two months: August - September 2004

Figure 4-27 Comparison of hourly computed bottom salinity with six IMCS mooring data over a period of two months: August - September 2004

Figure 4-28 Longitudinal profiles of salinity at different times: maximum ebb (upper frame), slack (middle frame) and maximum flood (lower frame). Observed values are shown by circles.

Figure 4-29 Scatter plot of computed salinity with observed IMCS mooring data: August - September 2004

Figure 4-30 Comparison of hourly computed water elevations with IMCS mooring data: March-April, 2002

Figure 4-31 Scatter plot of computed water elevation with observed IMCS mooring data: March-April, 2002

Figure 4-32a Comparison of hourly computed current velocities at three depths at NB1 with IMCS mooring data: March - April, 2002

Figure 4-32b Comparison of hourly computed current velocities at three depths at NB3 with IMCS mooring data: March - April, 2002

Figure 4-32c Comparison of hourly computed current velocities at three depths at KVK with IMCS mooring data: March - April, 2002

Figure 4-32d Comparison of hourly computed current velocities at three depths at AK with IMCS mooring data: March - April, 2002

Figure 4-32e Comparison of hourly computed current velocities at three depths at a deeper grid cell (13.4 m) near IMCS NB1 mooring station

Figure 4-32f Comparison of two cell (12.5m and 7.5m) averaged hourly current velocities at three depths near IMCS NB1 mooring station

FIGURES (Continued)

Figure

Figure 4-33a Comparison of 35 hour lowpass computed current velocities at three depths at NB1 with IMCS mooring data: March - April, 2002
Figure 4-33b Comparison of 35 hour lowpass computed current velocities at three depths at NB3 with IMCS mooring data: March - April, 2002
Figure 4-33c Comparison of 35 hour lowpass computed current velocities at three depths at KVK with IMCS mooring data: March - April, 2002
Figure 4-33d Comparison of 35 hour lowpass computed current velocities at three depths at AK with IMCS mooring data: March - April, 2002
Figure 4-34 Scatter plot of computed current velocities with observed IMCS mooring data: March-April, 2002
Figure 4-35 Comparison of hourly computed temperature with IMCS mooring data: March-April, 2002
Figure 4-36 Scatter plot of computed temperature with observed IMCS mooring data: March-April, 2002
Figure 4-37 Comparison of hourly computed salinity with IMCS mooring data: March-April, 2002
Figure 4-38 Scatter plot of computed salinity with observed IMCS mooring data: March-April, 2002
Figure 4-39 Comparison of observed bottom salinity with the results of sensitivity RUN A
Figure 4-40 Comparison of observed bottom salinity with the results of sensitivity RUN B
Figure 4-41 Comparison of observed bottom salinity with the results of sensitivity RUN C
Figure 4-42 Comparison of hourly computed salinity with IMCS mooring data at four stations located 1, 1.5, 2.5 and 3.5 km from the KVK data station
Figure 4-43 Comparison of hourly computed salinity with data at the Hudson River Mooring Station
Figure 4-44a Temporal variations of 35 hour low passed and monthly fluxes through Passaic and Hackensack Rivers, and Newark Bay.
Figure 4-44b Temporal variations of 35 hour low passed and monthly fluxes through Newark Bay, Kill van Kull and Arthur Kill
Figure 4-45 Comparison of hourly computed water elevations with IMCS mooring data: March-August, 2001
Figure 4-46a Comparison of hourly computed current velocities at three depths at NB1 with IMCS mooring data: March - August, 2001
Figure 4-46b Comparison of hourly computed current velocities at three depths at NB3 with IMCS mooring data: March - August, 2001
Figure 4-46c Comparison of hourly computed current velocities at three depths at KVK with IMCS mooring data: March - August, 2001
Figure 4-46d Comparison of hourly computed current velocities at three depths at AK with IMCS mooring data: March - August, 2001
Figure 4-46e Comparison of hourly computed current velocities at three depths at PA with IMCS mooring data: March - August, 2001
Figure 4-47 Comparison of hourly computed temperature with IMCS mooring data: March-August, 2001
Figure 4-48 Comparison of hourly computed salinity with IMCS mooring data: March-August, 2001
Figure 4-49 Temporal variation of the flow through Hudson, Passaic, Hackensack and Raritan rivers: March-August, 2001

FIGURES (Continued)

Figure

Figure 4-50a Temporal variations of 35 hour low passed and monthly fluxes through Passaic and Hackensack Rivers, and Newark Bay.

Figure 4-50b Temporal variations of 35 hour low passed and monthly fluxes through Newark Bay, Kill van Kull and Arthur Kill.

Figure 5-1 Locations of IMCS field sampling stations in the Lower Passaic River (2004)

Figure 5-2 Scatter plot of computed current velocities with observed data for sensitivity to C_s and Z_0

Figure 5-3 Scatter plot of computed surface and bottom temperature and salinity with observed data for sensitivity to C_s.

Figure 5-4 Comparison of surface and bottom salinities under different C_s values at M2

Figure 5-5 Comparison of surface and bottom salinities under different Z_0 values at M2

Figure 5-6 Original grid for the Lower Passaic River

Figure 5-7 High-resolution grid used for the grid convergence test for the Lower Passaic River

Figure 5-8 Comparison of hourly water surface elevation with data for the original and high-resolution grids

Figure 5-9 Comparison of computed cross-sectional velocities with data (Round 2a & 3) at Transect 10 and 15 for the original and high-resolution grids

Figure 5-10 Comparison of computed cross-sectional velocities at three transect locations along the river bends for the original and high-resolution grids

Figure 5-11 Comparison of computed velocities with data at station M2 for the original and high-resolution grids

Figure 5-12 Comparison of hourly computed bottom velocities at three shallow locations for the original and high-resolution grids

Figure 5-13 Comparison of computed cross-sectional salinities for two different times at Transect 10 and 15 for the original and high-resolution grids

Figure 5-14 Comparison of computed surface and bottom salinities with data for the original and high-resolution grids

Figure 5-15 Comparison of longitudinal profile of computed salinities with data along Lower Passaic River for the original and high-resolution grids

Figure 5-16 Comparison of hourly computed bottom shear stress for the original and high-resolution grids

Figure 5-17 Comparison of the flushing time of the Lower Passaic River for the original and high-resolution grids for 1996 (upper frame) and 2004 (lower frame)

Figure 5-18 Comparison of 35 hour low-passed computed salinity with Battelle and MERI data over a period of one year (1994-1995)

Figure 5-19 Sensitivity run results using additional 100 cfs in the Hackensack River

TABLES

Table | Page

Table 2-1. Characteristics of Principal Tidal Constituents in Newark Bay 2-2

Table 3-1. List of Rivers And Discharge Statistics (October 1994-September 2004) 3-5
Table 3-2. List of Wastewater Treatment Plants and Discharges (m^3/s) 3-8

Table 4-1. List of Tide Gauges 4-4
Table 4-2. Statistical Evaluation of Model Performance for Water Elevation 4-5
Table 4-3. Statistical Evaluation of Model Performance for Sub-Tidal Elevation Variations 4-5
Table 4-4. Comparison of Harmonic Constants for Elevation: Using data from April 1 through September 30, 1995 4-6
Table 4-5. List of ADCP Transects and Mooring Station Coordinates (NJ State Plane, NAD83) 4-8
Table 4-6. Maximum Depths of Bins in ADCP Measurements (units: m) 4-9
Table 4-7. Statistical Evaluation of Model Performance for Current Meter Data 4-10
Table 4-8. Statistical Evaluation of Model Performance for Elevation 4-12
Table 4-9. Comparison of Harmonic Constants for Water Elevation 4-14
Table 4-10. Statistical Evaluation of Model Performance for ADCP at M2 (2004) 4-15
Table 4-11. Comparison of Harmonic Constants for ADCP at M2: using data from August 26 through September 23, 20004 4-16
Table 4-12. Statistical Evaluation of Model Performance for ADCP at M3 (September 2004) 4-18
Table 4-13. Comparison of Harmonic Constants for ADCP at M3: using data from September 2004 4-18
Table 4-14. Statistical Evaluation of Model Performance for Temperature 4-20
Table 4-15. Statistical Evaluation of Model Performance for Salinity 4-22
Table 4-16. Statistical Evaluation of Model Performance for Tidal Elevation 4-24
Table 4-17. Comparison of Harmonic Constants for Water Elevation 4-24
Table 4-18. Statistical Evaluation of Model Performance for Current Velocity 4-28
Table 4-19. Comparison of Harmonic Constants for Velocity at NB1: 4-29
Table 4-20. Comparison of Harmonic Constants for Velocity at NB3: 4-30
Table 4-21. Comparison of Harmonic Constants for Velocity at AK: 4-31
Table 4-22. Comparison of Harmonic Constants for Velocity at KVK: 4-32
Table 4-23. Statistical Evaluation of Model Performance for Temperature 4-33
Table 4-24. Statistical Evaluation of Model Performance for Salinity 4-35
Table 4-25. Statistical Evaluation of Model Performance for Salinity for the Model Sensitivity Runs 4-37
Table 4-26. Statistical Evaluation of Model Performance for Bottom Current Velocities for the Model Sensitivity Runs 4-37
Table 4-27. Cross Sectional Fluxes for Each Sensitivity Analysis (units: m^3/sec) 4-38
Table 4-28. Statistical Evaluation of Model Performance for Tidal Elevation 4-42
Table 4-29. ADCP Mooring Depths during 2001 Model Validation Period 4-43
Table 4-30. Statistical Evaluation of Model Performance for Current Velocity 4-44
Table 4-31. Statistical Evaluation of Model Performance for Temperature 4-45
Table 4-32. Statistical Evaluation of Model Performance for Salinity 4-46

TABLES (Continued)

Table | Page

Table 5-1. Simulations Performed With Different Combinations of Z_0 And C_S 5-2
Table 5-2. Statistical Comparison of Measured and Computed Elevations (m) where Model Parameters HORCON(C_S) and Z_0 Were Varied. The Shaded Values are the Selected Parameters 5-6
Table 5-3a. Statistical Comparison of Measured ADCP Velocities (m/s) to Computed Results at M2, where Model Parameters HORCON(C_S) and Z_0 Were Varied. The Shaded Values are the Selected Parameters 5-7
Table 5-3b. Statistical Comparison of Measured ADP Velocities (m/s) to Computed Results at M3, where Model Parameters HORCON(C_S) and Z_0 were Varied. The Shaded Values are the Selected Parameters 5-8
Table 5-4a. Statistical Comparison of Measured and Computed Salinity (psu) at M1, where Model Parameters HORCON (C_S) and Z_0 were Varied. The Shaded Values are the Selected Parameters 5-9
Table 5-4b. Statistical Comparison of Measured and Computed Salinity (psu) at M2, where Model Parameters HORCON (C_S) and Z_0 were Varied. The Shaded Values are the Selected Parameters 5-10
Table 5-4c. Statistical Comparison of Measured and Computed Salinity (psu) at M3, where Model Parameters HORCON (C_S) and Z_0 were Varied. The Shaded Values are the Selected Parameters 5-11
Table 5-4d. Statistical Comparison of Measured and Computed Salinity (psu) at M4, where Model Parameters HORCON (C_S) and Z_0 were Varied. The Shaded Values are the Selected Parameters 5-12
Table 5-4e. Statistical Comparison of Measured and Computed Salinity (psu) at Bridge St. Bridge, where Model Parameters HORCON (C_S) and Z_0 were Varied. The Shaded Values are the Selected Parameters 5-13
Table 5-4f. Statistical Comparison of Measured and Computed Salinity (psu) at M5, where Model Parameters HORCON (C_S) and Z_0 were Varied. The Shaded Values are the Selected Parameters 5-14
Table 5-4g. Statistical Comparison of Measured and Computed Temperature ($^{\circ}$C) at M1, where Model Parameters HORCON (C_S) and Z_0 were Varied. The Shaded Values are the Selected Parameters 5-15
Table 5-4h. Statistical Comparison of Measured and Computed Temperature ($^{\circ}$C) at M2, where Model Parameters HORCON (C_S) and Z_0 were Varied. The Shaded Values are the Selected Parameters 5-16
Table 5-4i. Statistical Comparison of Measured and Computed Temperature ($^{\circ}$C) at M4, where Model Parameters HORCON (C_S) and Z_0 were Varied. The Shaded Values are the Selected Parameters 5-17
Table 5-4j. Statistical Comparison of Measured and Computed Temperature ($^{\circ}$C) at Bridge St. Bridge, where Model Parameters HORCON(C_S) and Z_0 were Varied. The Shaded Values are the Selected Parameters 5-18
Table 5-4k. Statistical Comparison of Measured and Computed Temperature ($^{\circ}$C) at M5, where Model Parameters HORCON (C_S) and Z_0 were Varied. The Shaded Values are the Selected Parameters 5-19

TABLES (Continued)

Table | Page

Table 5-5. Ranks Based on the Water Surface Elevation, Current and Temperature and Salinity Rmses for each Combination of Z_0 and C_S in Tables 5-2, 5-3, and 5-4 5-19
Table 5-6. Statistical Comparisons of Original LPR Grid and High Resolution Grid Model Results with Rutgers DOT1 Survey Data for Elevations 5-25
Table 5-7. Statistical Comparisons of Original LPR Grid and High Resolution Grid Model Results with Rutgers DOT1 Survey Data for ADCP at M2 5-25
Table 5-8. Statistical Comparisons of Original LPR Grid and High Resolution Grid Model Results with Rutgers DOT1 Survey Data for Salinity 5-25

SECTION 1

INTRODUCTION

1.1 BACKGROUND

The Lower Passaic River is the 17-mile tidal stretch of the Passaic River from the Dundee Dam to its confluence with Newark Bay. During the 1800s and through the 20th century, this section of the Passaic River became the center of intense industrial and urban development, and as a result the Lower Passaic River received an array of contaminants that degraded water and sediment quality. This degraded water and sediment quality has further resulted in bans on fish and shellfish consumption, wetlands loss, and degraded habitat for aquatic organisms. In 1984, the U.S. Environmental Protection Agency (USEPA) added the Diamond Alkali site, which is located at about three miles upstream of the mouth of the river, to the National Priority List (NPL) and it became eligible for cleanup under superfund site funding. That site now includes the Lower Passaic River and Newark Bay.

Numerous studies conducted by Federal, State and other agencies have established that the levels of contaminants in the Lower Passaic River sediments are in excess of applicable standards and pose ecological and human health risks. The contaminants that are likely contributors to the risk include dioxin/furans, polychlorinated biphenyls (PCBs), polycyclic aromatic hydrocarbons (PAHs), pesticide and herbicide residues, and metals. Although the list of contaminants of potential concern (COPCs) is not yet finalized, it is likely to include a sub-set or all of the above listed chemicals.

To restore the Lower Passaic River, the USEPA and the US Army Corps of Engineers (USACE) in partnership with State of New Jersey Departments of Transportation (NJDOT) and Environmental Protection (NJDEP) are putting together a comprehensive plan that will improve water and sediment quality in the river as well as restore degraded habitats along the river. This effort will meet the requirements of the Comprehensive Environmental Response Compensation and Liability Act (CERCLA), commonly known as Superfund, and the Water Resources Development Act (WRDA) to implement long-term remedial response actions that permanently and significantly reduce the risks associated with releases or threats of releases of contaminants in the Passaic River. The Lower Passaic River Restoration Project (LPRRP) represents the umbrella under which the integrated effort of the partner agencies is taking place.

As part of the LPRRP draft Work Plan, Quality Assurance Project Plan, Field Sampling Plan, and Modeling Work Plan documents have been prepared. During the preparation of the Data Quality Objectives (DQOs) for the LPRRP study, a number of "fundamental questions" have been formulated (QAPP, MPI, 2005). Answers to those

questions are meant to satisfy the CERCLA and WRDA requirements as well as the needs of a Natural Resource Damage Assessment (NRDA) under CERCLA. The purpose of the NRDA is to provide restoration for natural resources injured by contaminants and to compensate for the public's lost use of those resources. The "fundamental questions" listed below are discussed in "Draft Work Plan" (WP, MPI, 2005).

1. If we take no action on the River, when will the contaminants of potential concern (COPCs) and chemicals of potential ecological concern (COPECs) recover to acceptable concentrations?

2. What actions can we take on the River to significantly shorten the time required to achieve acceptable or interim risk-based concentrations for human receptors and ecological receptors?

3. Are there contaminated sediments now buried that are likely to become "reactivated" following a major flood, possibly resulting in an increase in contaminants within the fish/crab populations?

4. What actions can we take on the river or adjacent areas to significantly improve the functionality of ecosystems within the Lower Passaic River watershed?

5. If the risk assessment for Newark Bay demonstrates unacceptable risks due to export of contaminants from the Passaic River, will the plan proposed to achieve acceptable risks for Passaic River receptors significantly shorten the time required to achieve acceptable or interim risk-based concentrations for human and ecological receptors in Newark Bay, or will additional actions be required on the Passaic River?

6. What actions can we take on the river to significantly reduce the cost of dredged material management for the navigational dredging program?

In order to help answer these questions, an extensive field data collection and analysis program is being conducted. In addition, a state-of-the-science mathematical model is also being developed. The model is comprised of a number of sub-models, including: hydrodynamic, sediment transport, chemical fate and transport, and bioaccumulation. The resulting model will be used, together with results and analyses of the field program, to facilitate evaluation of sediment and water column contaminant fate and transport in the Lower Passaic River. The model will also be used to predict future concentrations of various contaminants of COPCs in the study area under different management scenarios

(e.g., dredging, monitored natural attenuation, capping, etc.). Specifically, the model will be used to:

- Establish the magnitudes and relative importance of specific contaminant sources to the 17-mile tidal reach of the Passaic River, including:
  - Upstream loads over the Dundee Dam,
  - Loads from tributaries and other point and non-point sources (including combined sewer overflows (CSOs) and stormwater overflows (SWOs) along the 17-mile tidal reach,
  - Re-mobilization of contaminants within the 17-mile tidal reach,
  - Inputs from water bodies hydraulically connected to the down-estuary end of the 17-mile tidal reach via Newark Bay (including, for example, re-introduction of contaminants originating from within the 17-mile tidal reach, or seasonal inputs from the Upper New York Harbor)

- Provide management guidance for the adverse ecological and human health effects of the transport and ultimate fate of the chemical of concern within the system.

- Assess the impacts of sediment and chemical contaminant re-mobilization due to various remedial action alternatives that may be conducted within the 17-mile tidal reach of the Passaic River during the period of remediation, as well as during the recovery period.

- Assess sediment quality and contaminant levels if loadings are reduced or eliminated and assess the time frame for improvement under various remedial action alternatives.

1.2 STUDY AREA PHYSICAL SETTING

The primary study area of the Passaic River Restoration Project is located in the northern part of the State of New Jersey and in the southern part of the State of New York. The Passaic River Basin drains approximately 935 mi^2, 85% of which are located in New Jersey and the rest in New York. Due to the tidal interaction between the Lower Passaic River and Newark Bay, the primary study area for the development of the mathematical model consists of the tidal waterways upstream of the junctions of the Kill Van Kull (KVK) with the Upper New York Bay and the Arthur Kill with Raritan Bay as shown in Figure 1-1. This includes the Lower Passaic River, the Lower Hackensack River, Newark Bay, the Kill Van Kull and the Arthur Kill. Most of the freshwater originates from upstream of the Dundee Dam with an annual average discharge rate of about 1,200 cfs (TSI, 2003). There

are, however, three major tributaries to the Lower Passaic River that bring additional fresh water river downstream of the Dundee Dam. These are:

- Saddle River (99 cfs),
- Third River (about 21 cfs), and
- Second River (18 cfs).

Four other tributaries, McDonald Brook, Frank Creek, Lawyer's Creek, and Plum Creek have also been identified historically as contributing freshwater inflow to the Lower Passaic River. However, these tributaries are now urbanized tributaries, having been bulk-headed and now receive freshwater inflows via CSO and SWO inputs. As such, estimates of freshwater inflow from the latter four tributaries are accounted for via the use of an urban runoff model to be described in the following section of this report. The combined flow of the three major tributaries (Saddle River, Third River, and Second River) is estimated to represent less than 10% of the total flow at the mouth of the estuarine section of the combined Lower Passaic River/Hackensack River system.

CSOs, as well as SWOs, also contribute to the inflow of freshwater in the Passaic River. There are 109 inventoried CSOs, and an even larger number SWOs in the Passaic River, Newark Bay, the Kills and the lower section of the Hackensack River, as well as six (6) wastewater treatment plant (WWTP) outfalls distributed in Newark Bay, the Kills and the Hackensack River (TSI, 2004). It is noteworthy that no WWTP outfalls are located in the Passaic River, itself. As will be discussed in the model input section of the report, these CSO, SWO and WWTP sources have been identified and quantified as to their relative contribution to the freshwater volume entering the system.

The waters of the study area are also influenced by semidiurnal tides reaching a mean tidal range of about 5 ft. Density stratification is prevalent in the Lower Passaic River causing a distinct reversal of residual currents between top and bottom layers of the water column.

It is also important to note that the lower section of the Hackensack River consists of vast area of tidal wetlands, the Meadowlands area. The USEPA's National Wetland Inventory identifies about 1,500 acres of wetland area that are submerged with average tidal conditions and that can be flooded during extreme flood conditions. Water storage that occurs in the marshland during tidal cycling and after storm events is expected to have an effect on the hydrodynamic transport through much of the Hackensack River and ultimately to the Passaic River study area. These processes of wetting and drying have been explicitly considered in hydrodynamic model calculations.

1.3 CONCEPTUAL SITE MODEL (CSM)

The CSM framework for the LPRRP includes model components for hydrodynamics, sediment transport and organic carbon cycling, toxic fate and transport, and bioaccumulation as shown in Figure 1-2, which also shows the modeling sequence, input and output. The model will be run with a fine grid resolution (described in Section 2) to capture spatial detail of the transport, fate and bioaccumulation processes within the project domain. For computational efficiency, the overall modeling calculations are being decoupled and performed in four successive model calculations as described below.

Hydrodynamic model calculations will first be performed to determine intra-tidal transport and bottom shear stresses throughout the model domain. This information will be passed forward to a sediment transport/organic carbon cycling model to determine the movement of inorganic particles and particulate organic carbon between the overlying water and the bed. Information from the hydrodynamic and sediment transport/organic carbon cycling models will be passed forward to a chemical fate and transport model and will be used, along with descriptions of contaminant partitioning to organic carbon and other contaminant processes (e.g., volatilization, degradation, etc.), to determine contaminant concentrations in the overlying water and sediment. Finally, contaminant concentrations in the water column and sediment will be used in bioaccumulation and toxicity calculations.

This report presents the development, calibration, and validation of the first component of the integrated mathematical model of the Lower Passaic River and Newark Bay – the hydrodynamic model.

.

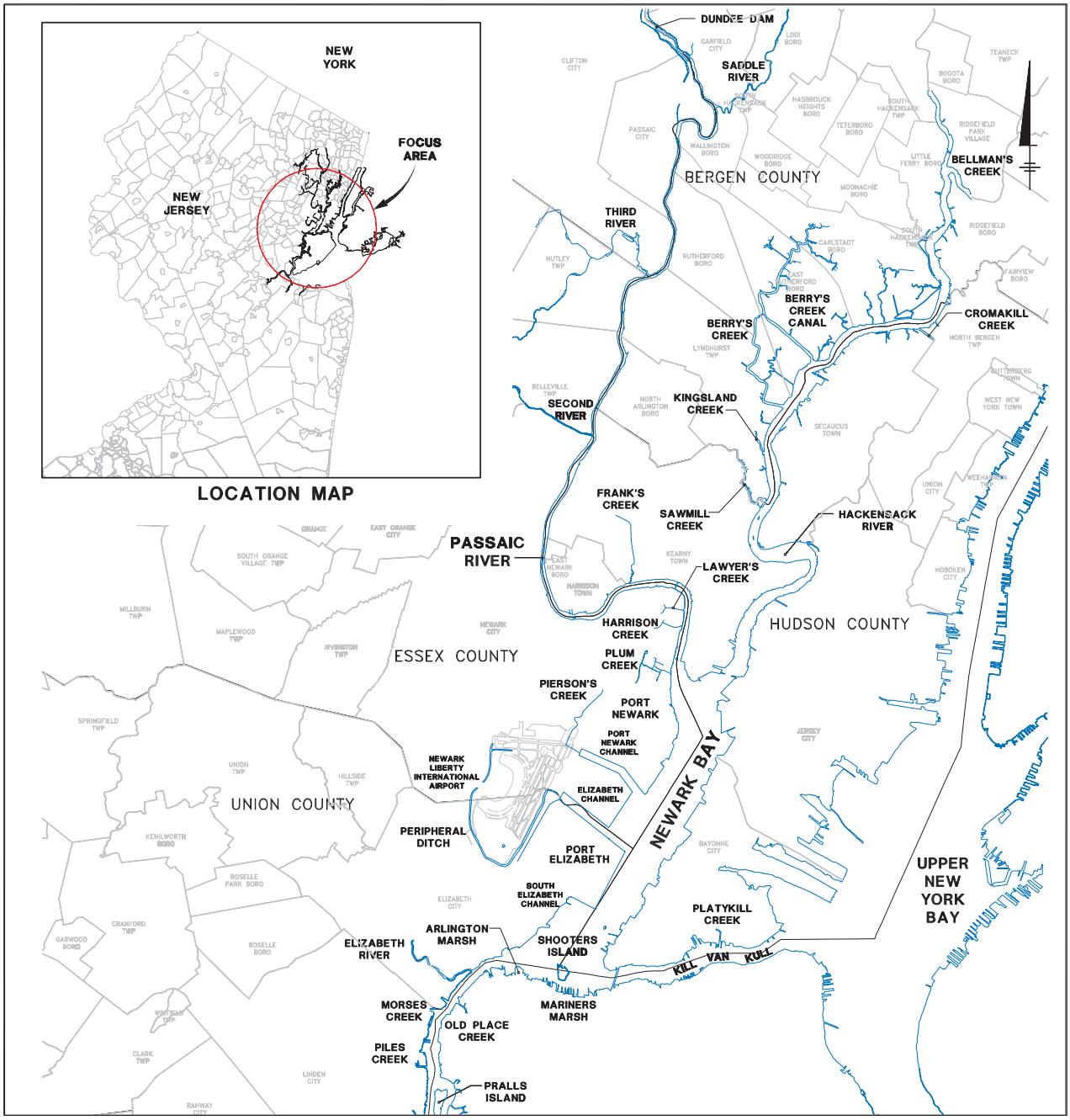

Figure 1-1. Passaic River, Hackensack River, Newark Bay, Kill Van Kull and Arthur Kill Study Area (Map adapted from TSI, 2004)

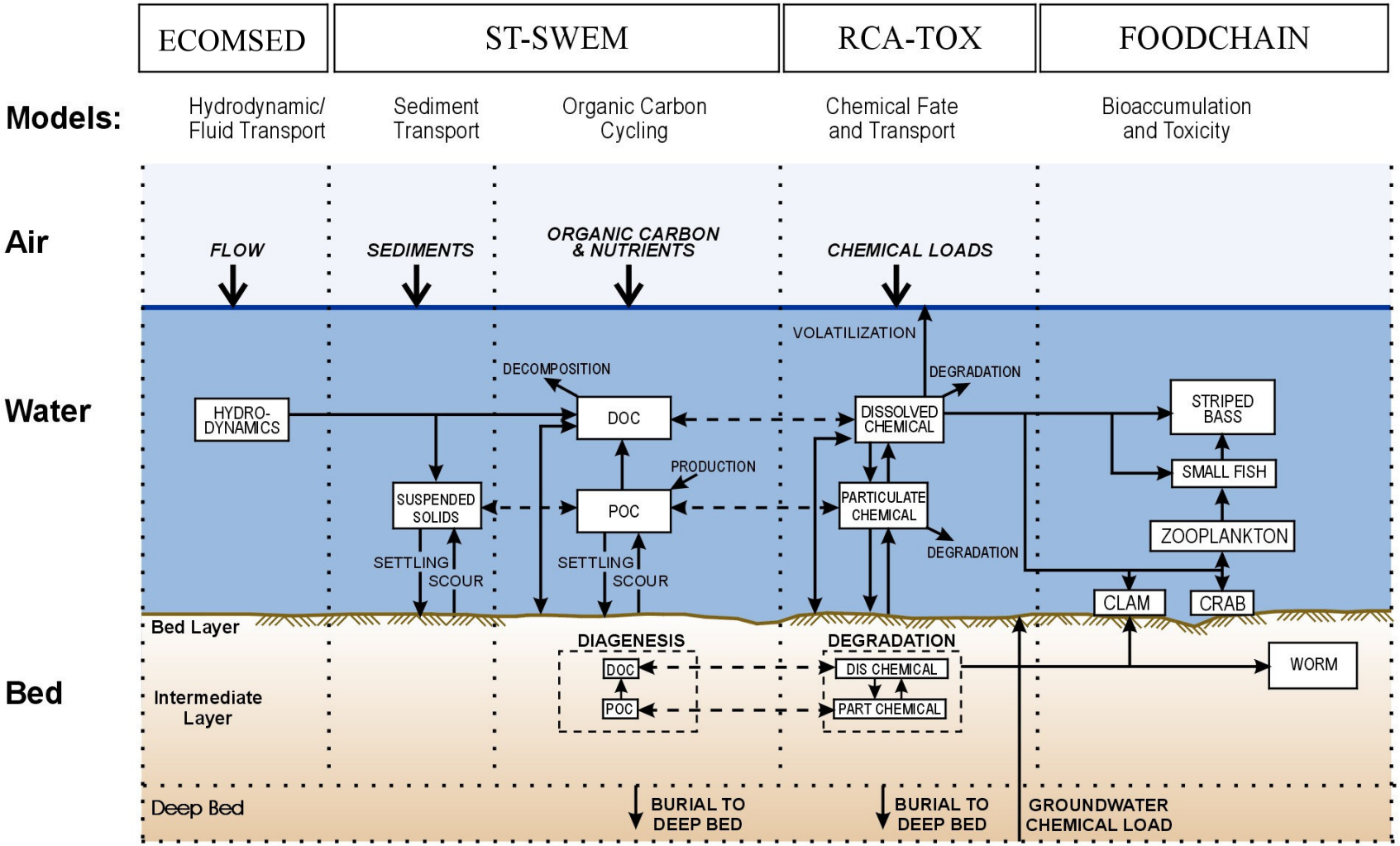

Figure 1-2 Schematic of the Modeling Framework Processes and their Interaction

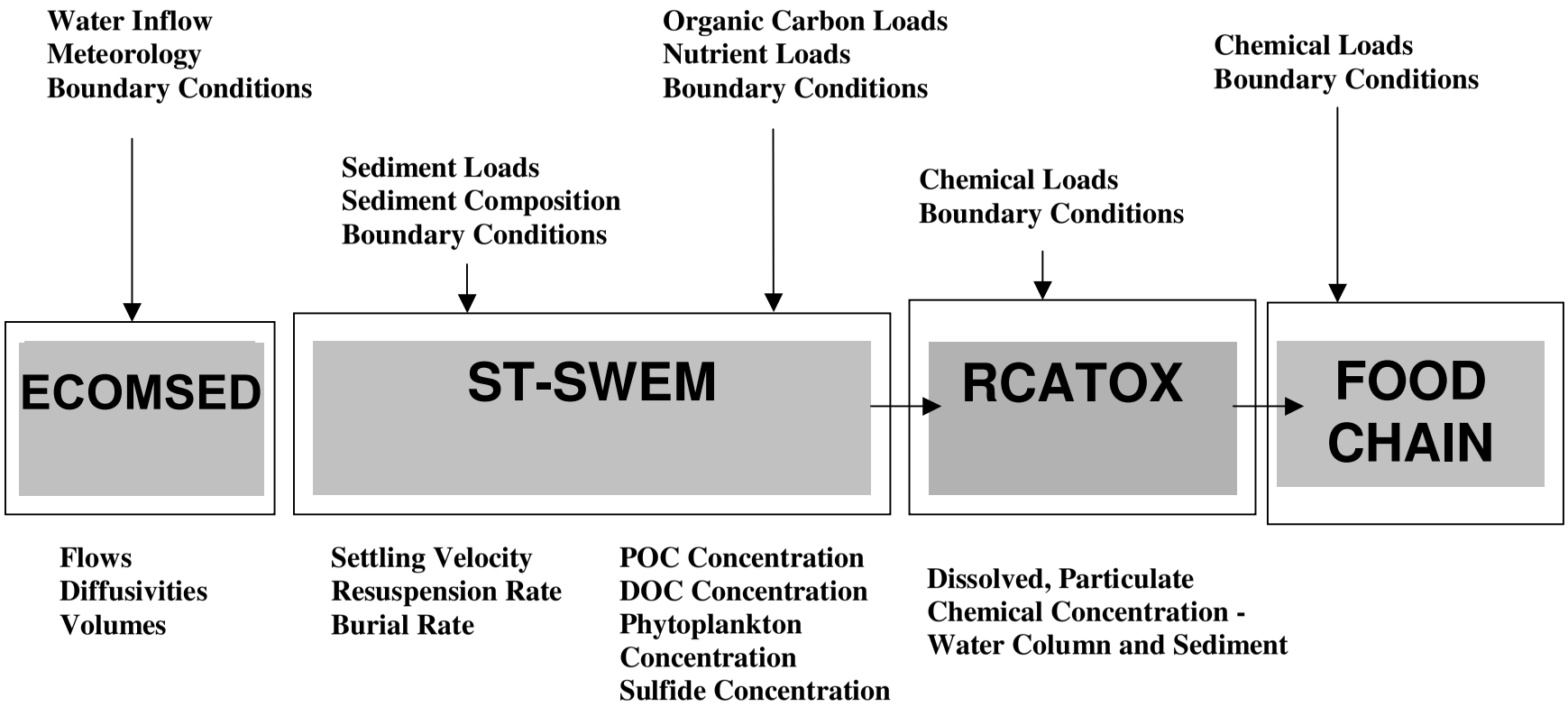

Figure 1-2 Schematic of the Modeling Framework Processes and their Interaction (continued)

SECTION 2

HYDRODYNAMIC MODEL

2.1 INTRODUCTION

The Passaic River along with the Hackensack River and Newark Bay is one of the most complex estuarine systems in the United States. The system is connected to two tidal straits, named the Kill van Kull and the Arthur Kill. These straits connect Newark Bay and the Passaic and Hackensack Rivers with the Upper New York Bay and Raritan Bay, through which tides, originating in the Atlantic Ocean, enter the system. The bathymetry of the Passaic-Hackensack-Newark Bay system is characterized by deep shipping channels along the center of both the Arthur Kill and the Kill van Kull, as well as the west side of Newark Bay through the center of both the Lower Passaic and Hackensack Rivers, with shallower side banks (Figure 2-1). The USACE maintains the navigability of the channels in order to support New York-New Jersey Port operations. The shipping channels, maintained by the USACE to facilitate the movement of container ships in and out of Newark Bay, added additional complexity to the dynamics of the system. The shipping channels in Newark Bay and the Kills are relatively deep (11 -15 m) with respect to the near-shore depths, significant variability in depths across the channels. Figure 2-2 shows the cross sections of different parts of the system. The figure illustrates the relatively deep shipping channels in the rivers and Newark Bay. The average depth of the shipping channel in the Arthur Kill is about 11 meters MSL, while the average shipping channel depth in the Kill van Kull and Newark Bay are 15 m MSL. These channels play an important role in transporting saline water from the ocean into the system.

The hydrodynamics of the Passaic-Hackensack-Newark Bay system is predominantly controlled by three forcing mechanisms, freshwater flows (buoyancy sources), tides, and winds. Two major sources of freshwater inflows, the Passaic and Hackensack Rivers, contribute to the salinity gradients in the system. By far, the largest freshwater contribution is from the Passaic River. Figure 2-3 illustrates 21 years of flows measured at Little Falls on the Passaic River and at the Oradell Dam on the Hackensack River. The long-term daily average flow measured at Little Falls is about 29 m^3/sec (1,000 cfs) and the maximum flow during this 21-year period was approximately 500 m^3/sec (18,000cfs) in April 1984. In contrast the average flow in the Hackensack River is only 1.6 m^3/s (56 cfs) and a maximum flow of approximately 158 m^3/s (5,500 cfs) was measured in September 1999 during Hurricane Floyd. The salinity dynamics in the system are mostly controlled by the freshwater flows from the Passaic and Hackensack Rivers and the saltier ocean waters that enter the system through the Kill van Kull and the Arthur Kill. During most low to moderate flow periods, the salinity front stays within upper Newark Bay and the Lower

Passaic and Hackensack Rivers. However, during extreme high flow periods the front is pushed further downstream to the Arthur Kill and the Kill van Kull. Salinity is, in general, higher during the time of low freshwater flow and is also more uniform both vertically and horizontally throughout the system than during the time of high freshwater flow. Freshwater flows emanating from the Passaic River stay along the western edge of Newark Bay, creating cross channel salinity gradients (Pence, 2004). The deep shipping channels in the system act as conveyances of denser and saltier ocean water to upper Newark Bay and to the Lower Passaic and Hackensack Rivers.

Tidal influence has significant importance within the Passaic-Hackensack-Newark Bay estuarine system. A harmonic analysis (see Figure 2-1 for its location) of tidal elevation data measured at Bergen Point, which is at the entrance to Newark Bay, suggests that the semi-diurnal constituents (M_2 and S_2) dominate the system. A spectral analysis of the tidal elevations also indicated that maximum variance occurred at an interval of approximately 12.4 hours, suggesting a dominant semi-diurnal tidal signal. The resultant tidal harmonic constituents are provided in Table 2-1. The table indicates that the study area has predominant semi-diurnal tides (Figure 2-4).

Table 2-1. Characteristics of Principal Tidal Constituents in Newark Bay

Constituents	Period (Hrs)	Amplitude (m)	Phase (deg)
O_1	25.82	0.05	107.1
K_1	23.93	0.10	108.6
M_2	12.42	0.73	233.7
S_2	12.00	0.14	263.8
N_2	12.66	0.16	220.4

Tidal currents in Newark Bay and in the Passaic and Hackensack Rivers are found to be moderate, with maximum amplitudes of 0.5 m/sec. Most of the time, the surface and bottom tidal currents are of equal magnitude and are in phase in Newark Bay. However, during high-flow periods the surface currents, directed towards the ocean (ebb currents), become much stronger than the bottom currents, indicating the presence of strong vertical shear (Pence, 2004). Figure 2-4 illustrates surface and bottom currents during a high flow season. During high freshwater flow, classical two-layer estuarine circulation is observed during flood tides, with surface currents flowing seaward and bottom currents flowing

upstream. The net flow along the side banks is downstream, with an increased magnitude under higher freshwater flow conditions.

Strong and persistent wind events in Newark Bay can have a strong effect on the circulation in the estuary, and in some extreme cases can disrupt the normal pattern of estuarine circulation. Modeling analysis (Pence, 2004, Pecchioli et al., 2006) suggests that strong winds from the west will flush water and water borne constituents from Newark Bay out through the Kill van Kull, with weaker flow in through the Arthur Kill. Model computations indicate that this flow pattern changes direction when strong winds blow from the east, i.e., flow enters the Kill van Kull from the upper portion of New York/New Jersey Harbor and then enters Newark Bay (Pecchioli et al., 2006).

2.2 RATIONALE FOR A THREE-DIMENSIONAL MODELING FRAMEWORK

The purpose of hydrodynamic modeling is to develop a time-dependent, three-dimensional description of transport through the Passaic River study area, which includes Newark Bay and the Hackensack River. Modeling the hydrodynamics of the Passaic-Hackensack-Newark Bay system is essential to predict the movement and concentrations of various chemicals of concern within the study area under different management scenarios (e.g., dredging, monitored natural attenuation, capping, etc.).

Previous hydrodynamic modeling studies of the Passaic River were performed as part of larger regional studies for eutrophication and toxic contamination for New York-New Jersey Harbor and adjoining waters. Previous modeling efforts, however, are not adequate in describing transport in the Passaic River study area. The grid resolution in the System-Wide Eutrophication Model (SWEM) and Contamination Assessment and Reduction Project (CARP) studies is not sufficient to describe bathymetric features in the Passaic and Hackensack Rivers and Newark Bay sections of the model. Some improvements were made to better represent the Passaic, Hackensack and Raritan Rivers in a subsequent modeling effort (known as the New Jersey Tributaries Modeling Studies) by HydroQual (2002). In the 2002 study, cross-sectional areas and bathymetric representation of the New Jersey tributaries were refined and additional readjustment and reconfiguration of hydrodynamic calibration parameters were made. The hydrodynamic calibration parameters were adjusted to better parameterize small-scale physics not resolved by the initial SWEM grid especially in lateral direction. However, the SWEM grid still utilizes a single lateral grid cell across the width to represent Newark Bay, the LPR and Hackensack River.

It is important to note that to resolve the cross-sectional features of the Passaic and Hackensack Rivers and Newark Bay together with dredged ship channels, as shown in Figure 2-1 and Figure 2-2, requires additional lateral resolution in the computational grid, so

as to resolve the main-channel and river bank geometries. Resolution of bathymetric structure in the lateral direction is important because it plays a key role in determining more realistic bottom shear stresses, which are important in the ultimate transport of sediment and sediment-bound contaminants.

Historical salinity data indicates that salt can travel upstream about 10 miles from the mouth of Passaic River (Figure 2-5) during conditions of low river inflows. The salt front can be pushed out of the LPR under moderately high river flows, i.e., 100 m^3/s or 3,500 cfs (Chant, personal communication). Field studies conducted by TSI in 1995-6 and Rutgers University in 2004 indicate that intra-tidal variations in surface and bottom salinities near the mouth of the LPR can reach as high as 10 psu. Density driven circulation, caused by vertical stratification in the lower section of the LPR and Newark Bay, necessitates the use of a fully three-dimensional modeling framework.

In the Hackensack River, salt can penetrate about 15 miles from the river mouth (Figure 2-6) due to relatively low freshwater inflows over the Oradell Dam. The lower section of the Hackensack River consists of vast area of tidal wetlands, known as the Meadowlands. USEPA's National Wetland Inventory identifies about 1,500 acres of the wetland area that are submerged under average tidal condition. Hydrodynamics in the Passaic River system are complicated by the presence of these large intertidal marshes on the Hackensack River. This is due to the fact that these marshes can provide significant water storage over a tidal cycle and during and after storm events, thereby altering the movement of water up the Hackensack River and to a lesser degree, the Passaic River. The wetting and drying of marshland in the Meadowlands was not included in the SWEM, CARP or New Jersey Tributaries Modeling evaluations.

2.3 MODEL DOMAIN

Complex estuarine systems with irregular coastlines and bathymetric features, such as the Passaic-Hackensack-Newark Bay system, often pose a significant challenge to modelers seeking solutions when resolution of micro-scale physics (order of meters to kilometers) becomes dynamically important. For a credible scientific analysis, however, one must have a high-resolution representation of the model domain in order to resolve the coastline and bathymetry of the system, as well as other important physical, chemical and biological processes and their evolution within the system. The major challenge, however, comes from a computational perspective, even with the fastest and largest computers available to-date balancing desired spatial resolution with reasonable computational burden or "run-times" necessary to complete a model simulation. Thus, in order to provide an effective management tool, a balance must be struck between properly representing the system and its constituents while providing tractable solution times necessary to perform model calibration/validation, sensitivity analyses, and production runs.

Due to the complexities of the Passaic-Hackensack-Newark Bay system, as described earlier in this section, a hydrodynamic model of the system should encompass the Passaic River, the Hackensack River, Newark Bay, their tributaries, the Arthur Kill and the Kill van Kull. The model domain should also include portions of New York Harbor and Raritan Bay as necessary to avoid boundary effects that would contaminate the model results in the region of interest. However, since a hydrodynamic model (SWEM) of the New York/New Jersey Harbor complex that has been calibrated/validated and peer-reviewed (Blumberg et al., 1999) already exists, it was decided to use that model as the basis for the development of the Passaic-Hackensack-Newark Bay hydrodynamic model. The SWEM model (Figure 2-7) was also used as the basis for the development of the CARP hydrodynamic model. Use of the SWEM model, with additional spatial resolution in the Passaic and Hackensack Rivers and Newark Bay, guarantees that the boundary effects are well removed from the area of interest and also provides some benefits in terms of cost efficiencies, since most of the inputs required for setting up a hydrodynamic model of the Passaic-Hackensack-Newark Bay system have already been developed and compiled for use in the SWEM and CARP hydrodynamic models.

The upstream extent in the Passaic River will be the Dundee Dam, which also happens to be the limit of tidal influences within the river. The upstream extent of the Hackensack River will be the Oradell Dam. The model domain also encompasses the Hackensack River wetlands (the Meadowlands), which are represented by model cells in the flood plain, which wet and dry, depending on the tidal elevation and the volume of flow within the Hackensack River free-flowing channel.

2.4 HYDRODYNAMIC MODELING FRAMEWORK

The hydrodynamic model will be based on HydroQual's in-house Estuarine, Coastal and Ocean Model (ECOMSED). The model simulates the spatial and temporal variation of water levels and currents, which advect and disperse contaminants throughout the system, as well as the salinity and temperature fields as they vary with tide, wind, heating from solar and atmospheric radiation and freshwater inflows. ECOMSED also provides the capability of simulating events where water from the main channels can overtop the riverbank and flow into the floodplain, which is an important consideration, especially in wetlands areas of the Meadowlands adjacent to the Hackensack River. The model has been applied in a wide variety of domains from rivers and lakes to estuaries, marine harbors, tidal embayments and across wide coastal regions. ECOMSED is also a fundamental part of the System-Wide Eutrophication Model (SWEM) of the greater New York/New Jersey Harbor, Long Island Sound, and New York Bight system. A description of ECOMSED is provided in Appendix D.

The heat energy content in Passaic River is primarily governed by surface heat exchanges. Measurements of heat fluxes are very difficult and costly to make and are often parameterized to obtain the fluxes, using commonly available meteorological and atmospheric data. The processes that control the heat exchange between the water and atmosphere are well documented (Ahsan and Blumberg, 1999; Adams et al., 1981; Edinger et al., 1974). All of these works relied mostly on bulk formulas to evaluate the components of the heat budget. Estimation of net heat fluxes requires a great deal of judgment in choosing the bulk formulas, which are dependent on many uncertainties in atmospheric parameters such as cloud cover, humidity, and temperature. Four major heat flux components, including short wave solar radiation, longwave atmospheric radiation, sensible heat, and latent heat fluxes have been incorporated in to the ECOMSED modeling framework. The formulations are largely based on the works of Ahsan and Blumberg (1999), Adams et al. (1981) and Cole and Buchak (1995). Appendix D provides a detailed description of the heat flux components incorporated in the ECOMSED framework.

The hydrodynamic model is a three-dimensional, time-dependent, estuarine and coastal circulation model developed by Blumberg and Mellor (1987). ECOMSED has a long history of successful applications to oceanic, coastal and estuarine waters. Among these applications are: Delaware River, Delaware Bay, and adjacent continental shelf (Galperin and Mellor, 1990a,b), the South Atlantic Bight (Blumberg and Mellor, 1983), the Hudson Raritan estuary (Oey et al., 1985a,b,c), the Gulf of Mexico (Blumberg and Mellor, 1985), Chesapeake Bay (Blumberg and Goodrich, 1990), Massachusetts Bay (Blumberg et al., 1993), and most recently in St. Andrew Bay (Blumberg and Kim, 1998), New York Harbor and Bight (Blumberg et al., 1999) and Onondaga Lake (Ahsan and Blumberg, 1999). The model has also been applied in several other lake environments such as Lake Michigan and Green Bay (HydroQual, 2001). In all these studies, model performance was assessed by means of extensive comparisons between predicted and observed data. The predominant physics were realistically reproduced by the model for this wide range of applications.

The model incorporates the Mellor and Yamada (1982) level 2-½ turbulent closure scheme to provide a realistic parameterization of vertical mixing. A system of curvilinear coordinates is used in the horizontal direction, which allows for a smooth and accurate representation of variable shoreline geometry. In the vertical scale, the model uses a transformed coordinate system known as the σ-coordinate transformation to allow for a better representation of bottom topography. Water surface elevation, water velocity in three dimensions, temperature and salinity, and water turbulence are predicted in response to weather conditions (winds and incident solar radiation), tributary inflows, tides, temperature and salinity at open boundaries connected to the coastal waters.

The model solves a coupled system of differential, prognostic equations describing the conservation of mass, momentum, temperature, salinity, turbulence energy, and turbulence macroscale. The governing equations for velocity $U_i = (u, v, w)$, temperature (T), salinity (S), and $x_i = (x,y,z)$ are as follows:

$$\frac{\partial U_i}{\partial x_i} = 0 \tag{2-1}$$

$$\frac{\partial}{\partial t}(U,V) + \frac{\partial}{\partial x_i}\left[U_i(u,v) + f(-v,u)\right]$$
$$= -\frac{1}{\rho_o}\left[\frac{\partial P}{\partial x},\frac{\partial P}{\partial y}\right] + \frac{\partial}{\partial z}\left[K_M \frac{\partial}{\partial z}(u,v)\right] + \left(F_U, F_V\right) \tag{2-2}$$

$$\frac{\partial T}{\partial t} + \frac{\partial}{\partial x_i}\left(U_i T\right) = \frac{\partial}{\partial z}\left[K_H \frac{\partial T}{\partial z}\right] + F_T \tag{2-3}$$

$$\frac{\partial S}{\partial t} + \frac{\partial}{\partial x_i}\left(U_i S\right) = \frac{\partial}{\partial z}\left[K_H \frac{\partial S}{\partial z}\right] + F_S \tag{2-4}$$

The horizontal diffusion terms, (F_U, F_V), F_T and F_S, in Equations (2-2) through (2-4) are calculated using a Smagorinsky (1963) horizontal diffusion formulation (Mellor and Blumberg, 1985). Under the shallow water assumption, the vertical momentum equation is reduced to a hydrostatic pressure equation. Vertical accelerations due to buoyancy effects and sudden variations in bottom topography are not taken into account. The hydrostatic approximation yields:

$$\frac{P}{\rho_o} = g(\eta - z) + \int_z^{\eta} g\,\frac{\rho' - \rho_o}{\rho_o}\,dz' \tag{2-5}$$

where P is pressure, z is water depth, $\eta(x,y,t)$ is the free surface elevation, ρ_o is a reference density, and $\rho = \rho(T,S)$ is the density.

The vertical mixing coefficients, K_M and K_H, in Equations (2-2) through (2-4) are obtained by appealing to a level 2 ½ turbulence closure scheme and are given by:

$$K_M = \hat{K}_M + \upsilon_M, K_H = \hat{K}_H + \upsilon_H \tag{2-6}$$

$$\hat{K}_M = q\ell S_M, \hat{K}_H = q\ell S_H \tag{2-7}$$

where $q^2/2$ is the turbulent kinetic energy, l is a turbulence length scale, S_M and S_H are stability functions defined by solutions to algebraic equations given by Mellor and Yamada (1982) as modified by Galperin et al. (1988), and υ_M and υ_H are constants. The variables q^2 and l are determined from the following equations:

$$\frac{\partial q^2}{\partial t} + \frac{\partial (uq^2)}{\partial x} + \frac{\partial (vq^2)}{\partial y} + \frac{\partial (wq^2)}{\partial z} = \frac{\partial}{\partial z}\left[K_q \frac{\partial q^2}{\partial z}\right] + 2K_M\left[\left(\frac{\partial u}{\partial z}\right)^2 + \left(\frac{\partial v}{\partial z}\right)^2\right] + \frac{2g}{\rho_o} K_H \frac{\partial \rho}{\partial z} - 2\frac{q^3}{B_1 \ell} + F_q \tag{2-8}$$

$$\frac{\partial (q^2\ell)}{\partial t} + \frac{\partial (uq^2\ell)}{\partial x} + \frac{\partial (vq^2\ell)}{\partial y} + \frac{\partial (wq^2\ell)}{\partial z} = \frac{\partial}{\partial z}\left[K_q \frac{\partial (q^2\ell)}{\partial z}\right] + E_1\ell\left\{K_M\left[\left(\frac{\partial u}{\partial z}\right)^2 + \left(\frac{\partial v}{\partial z}\right)^2\right] + \frac{g}{\rho_o} K_H \frac{\partial \rho}{\partial z}\right\} - \frac{q^3}{B_1 \tilde{\omega}} + F_\ell \tag{2-9}$$

where $K_q = 0.2q\ell$, the eddy diffusion coefficient for turbulent kinetic energy; F_q and F_ℓ represent horizontal diffusion of the turbulent kinetic energy and turbulence length scale and are parameterized in a manner analogous to either Equation (2-6) or (2-7); $\tilde{\omega}$ is a wall proximity function defined as $\tilde{\omega} = 1 + E_2 (\ell/\kappa L)^2$, $(L)^{-1} = (\eta - z)^{-1} + (H + z)^{-1}$, κ is the von Karman constant, H is the mean water depth, η is the free surface elevation, and E_1, E_2 and B_1 are empirical constants set in the closure model.

The basic Equations, (2-1) through (2-9), are transformed into a terrain following σ-coordinate system in the vertical scale and an orthogonal curvilinear coordinate system in the horizontal scale. The resulting equations are vertically integrated to extract barotropic variables, and a mode splitting technique is introduced such that the fast-moving, external barotropic modes and relatively much-slower internal baroclinic modes are calculated by

prognostic equations with different time steps. Detailed solution techniques are described in Blumberg and Mellor (1987) and Appendix G.

2.5 FLOODING AND DRYING

The lower section of the Hackensack River consists of vast area of tidal wetlands, the Meadowlands area. The USEPA's National Wetland Inventory identifies about 1,500 acres of the wetland area that are submerged under average tidal condition with a much larger area that can be flooded under extreme flood conditions. Water storage occurs in the wetlands during tidal cycling and after storm events is expected to have an effect on hydrodynamic transport through much of the Hackensack River and may also influence to some degree the Passaic River study area. These processes of wetting and drying need to be explicitly considered in hydrodynamic model calculations. The wetting and drying of marshland in the Meadowlands was not included in the SWEM, CARP or New Jersey Tributaries Modeling evaluations.

During the development of the Lower Passaic River hydrodynamic model, an algorithm, based upon Flather and Heaps (1975) and Kim (1999), that permits the model to simulate the flooding and drying of tidal flats was incorporated into ECOMSED. The treatment is based on both total water depth ($D = H + \eta$) and elevation gradient with adjacent grid cells. For implementation of the flooding and drying scheme, a minimum threshold depth (D_{min}) and a critical elevation gradient (ε) are pre-assigned (via model input). Figure 2-8 illustrates ECOMSED grid conventions. At each external computational timestep, $D_{i,j}$, $D_{i+1,j}$ and $D_{i,j+1}$ are checked (Figure 2-8). The procedure to determine whether a grid cell is either "wet" or "dry" is illustrated in Figure 2-9 (Kim, 1999) and depends upon whether D and elevation gradient ($\Delta\eta$) are greater or less than D_{min} and ε, respectively. When a cell is considered dry, exchange with adjacent cell is prevented. However, hydrodynamic computations such as surface heat exchange, vertical advection and mixing will continue within that cell.

Testing of the wetting/drying scheme has been conducted under various scenarios and confidence has been established in application of this algorithm within the computational framework to be used for application to the Lower Passaic River hydrodynamic model. A brief summary of the testing of the wetting/drying scheme is presented in Appendix F.

2.6 GRID DESIGN

A practical, numerically efficient and accurate approach was taken in order to discretize the Passaic River and connecting waters. While the modeling focus is limited to the Lower Passaic River and its approaches including Newark Bay and the Hackensack

River, it is important to locate the proper open boundary locations in order to avoid unwanted direct impact from the boundary forcing and maintain the robustness of the model performance. From the experience gained in previous modeling efforts in the region (HydroQual, 1999 and 2001), the modeling team identified the regional model grid used for SWEM in the late 1990's and, subsequently for CARP in early 2000's, as the basis of the design of the grid for this study. The CARP model grid covers much of New York Harbor and its tributaries including the Passaic and Hackensack Rivers as well as Raritan Bay, Long Island Sound and New York Bight from Cape May in the south to Nantucket Island in the northeast. While the CARP model was calibrated and validated with extensive field survey data and its grid resolution is adequate for the requirements of CARP, much of the areas of interest for the current study lack spatial detail necessary for the Lower Passaic River Restoration Project. In the CARP model the Kills, Newark Bay and both the Passaic and Hackensack Rivers are resolved with single grid cells in the lateral direction. In order to resolve bathymetric features of the LPR, Newark Bay and the Kills for this study it was necessary to add lateral grid resolution, as well as improve resolution along the major axes (or length) of these water bodies.

The orthogonal, curvilinear grid system designed for the present study is shown in Figure 2-10 and zoomed in views of the grid in the Lower Passaic River, Hackensack River and Newark Bay area and in the Harrison Reach section of the Lower Passaic River, are shown in Figures 2-11 and 2-12, respectively. The entire model grid consists of 74x268 segments in the horizontal plane and 10 equally spaced σ-layers in the vertical plane. The transformed σ-coordinate system in the vertical plane allows the model to have an equal number of vertical segments in all of the computational grid cells. It should be noted that the curvilinear grid allows for finest grid resolution in the areas of interest, such as the Passaic River, Hackensack River and Newark Bay proper. In the lower sections of the Passaic River, from mouth of the river to the mile point 4 near the upstream end of the Harrison Reach, four grid cells in the lateral direction having about 30x120 m grid sizes are configured. The lateral resolution of the grid in the rest of the upstream sections of the Lower Passaic River decreases to two cells as the width of the river narrows. A coarser grid system is adopted in the rest of the region and is maintained at virtually the same resolution of the CARP model. The grid cells become several kilometers in the offshore area (see Figure 2-10). This technique allows for computationally efficient model runs. During the calibration of the model, a number of revisions to the channel configuration were evaluated in order to achieve a better model-data fit. In addition, the geometry (i.e., model surface areas) in the Meadowlands were re-evaluated based on the Meadowlands Environmental Site Investigation Compilation report prepared by the USACE (2004). A series of grid convergence tests were performed to ensure that the grid resolution employed in the Lower

Passaic River was suitable to address the detailed hydrodynamics in the study area. Details of these tests are presented in Section 5.

2.7 BATHYMETRY DATA

Bathymetry data for configuration of model grid were compiled from several historical bathymetric surveys conducted by the USACE in multiple years and a field survey conducted by TSI in 1995. Following is a brief summary of data used for this study:

- Lower Passaic River: TSI bathymetric survey data compiled in 1995 for the first eight-miles of the LPR and high resolution USACE survey data compiled in 2004 for the entire length of the LPR.

- Hackensack River and Meadowlands wetland: USACE survey data compiled in mid-1990,

- Approaches to Newark Bay including the Kill van Kull, upper section of the Arthur Kill, and Newark Bay, including the Port Elizabeth Channel: Survey data from Harbor Deepening Projects between 1999 and 2004.

While the use of the Lower Passaic and Hackensack River data for the configuration of the model depth was straightforward, the use of shipping channel survey data collected during the Harbor Deepening Projects required careful interpretation of the data. The New York District of the USACE started the Harbor Deepening Projects in 1999 in the Kill van Kull, the Arthur Kill and Newark Bay and completed the projects in 2004. Figure 2-13 shows the contract areas for the 50 ft dredging project and dredging schedule. Each contract area had different dredging schedules so that various sections of the waterway leading Newark Bay changed its depths between 1999 and 2004.

Because the available data for the model calibration were from 1995 through early 2005 and because of the Harbor Deepening Project, more than one set of model depth configuration was needed. Numerous bathymetric surveys data sets provided by the NY District of the USACE for the study were carefully reviewed and selected for each bathymetric configuration of the model. After identifying the specific model calibration periods of interest, three different model depths were prepared:

- Model depths representing pre-dredging conditions (before 1999)
- Model depths representing spring of 2002 conditions
- Model depth representing post-dredging conditions (2004)

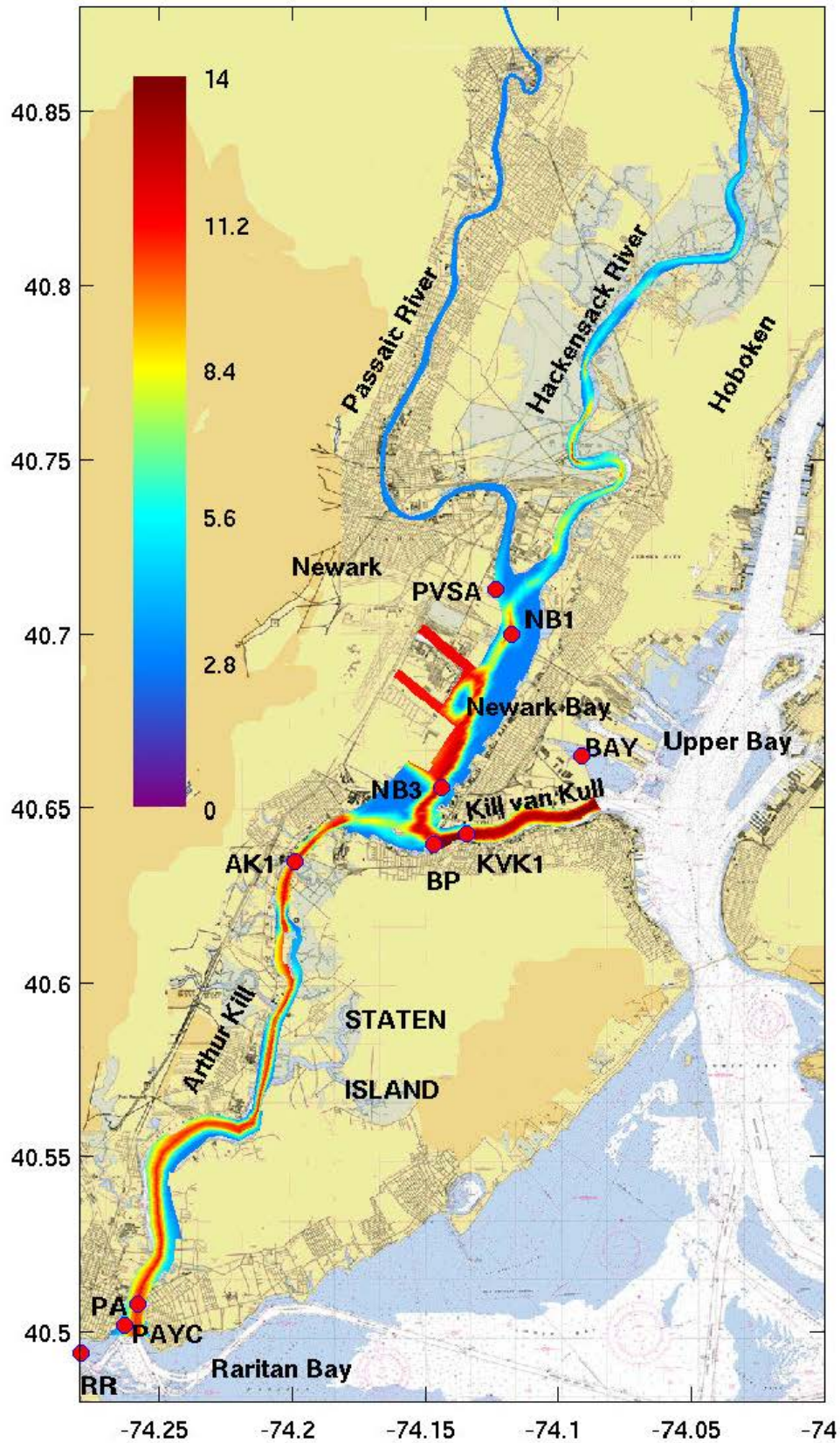

Figure 1.1: Bathymetry of Newark Bay (Pence, 2004)

Figure 2.1: Bathymetry of study area (in meters). (Pence, 2004)

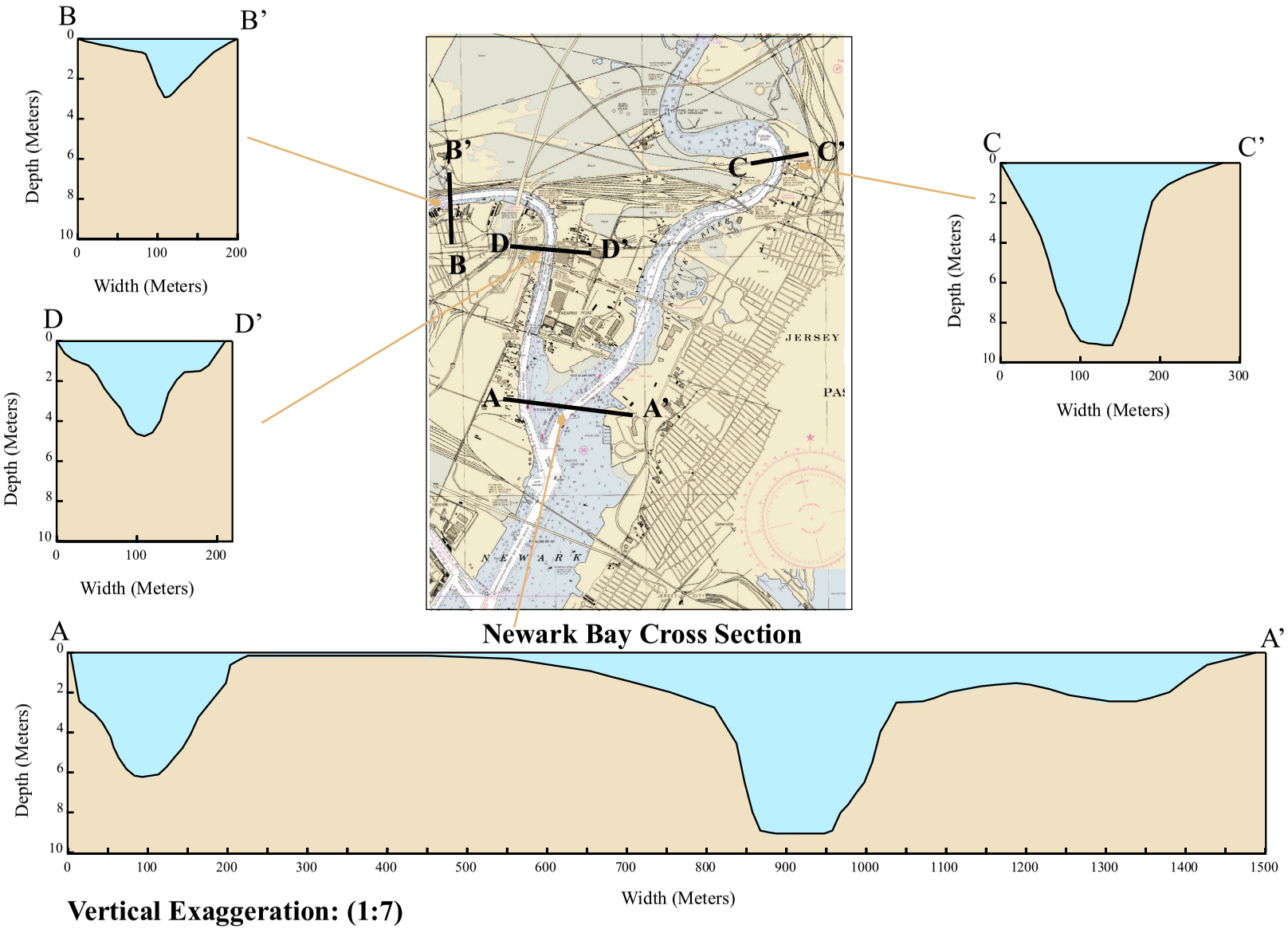

Figure 2-2 Cross-sectional view of bathymetry in Lower Passaic, Hackensack, and Newark Bay region.

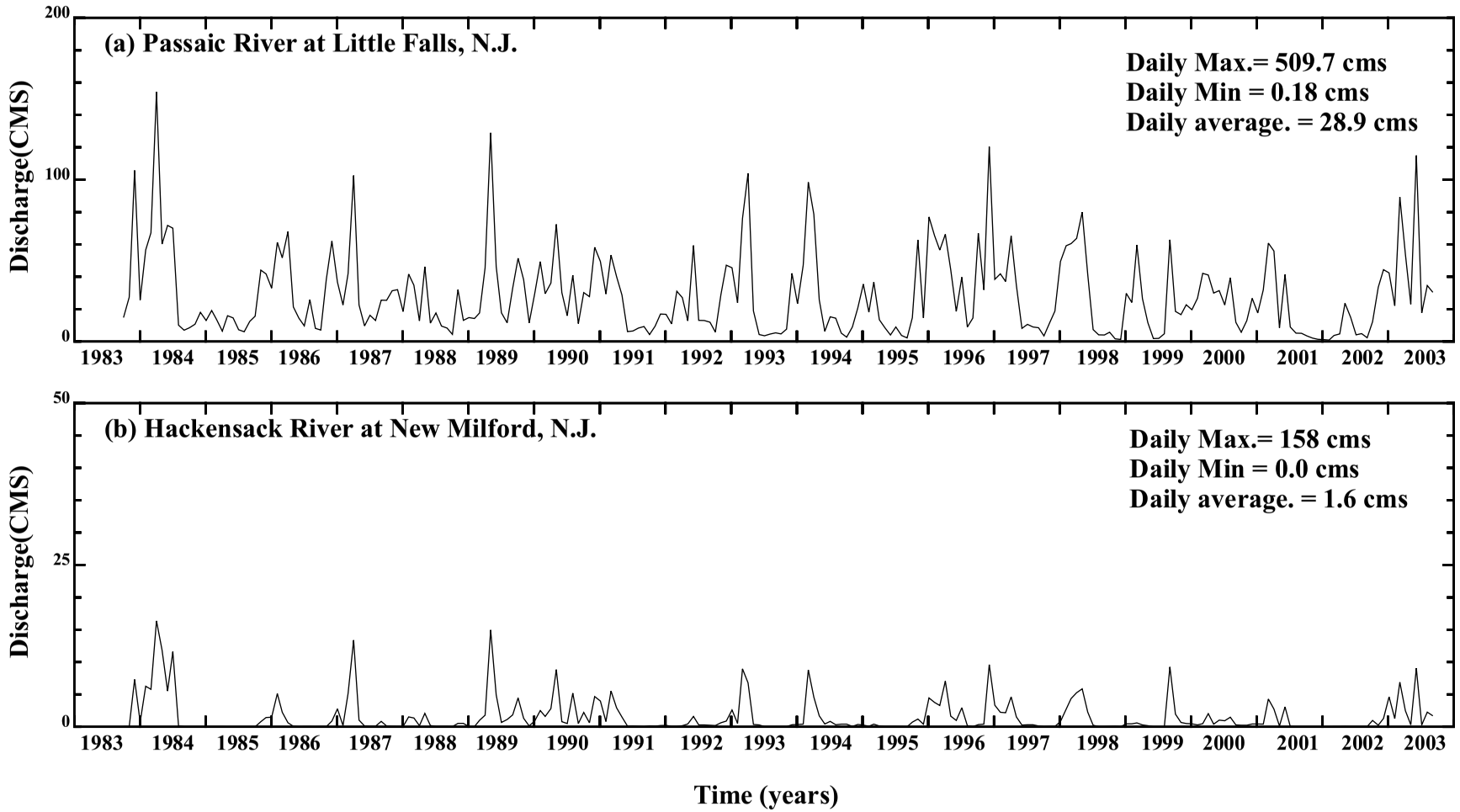

Figure 2-3. Monthly average flows of Passaic and Hackensack from 1983 through 2003.

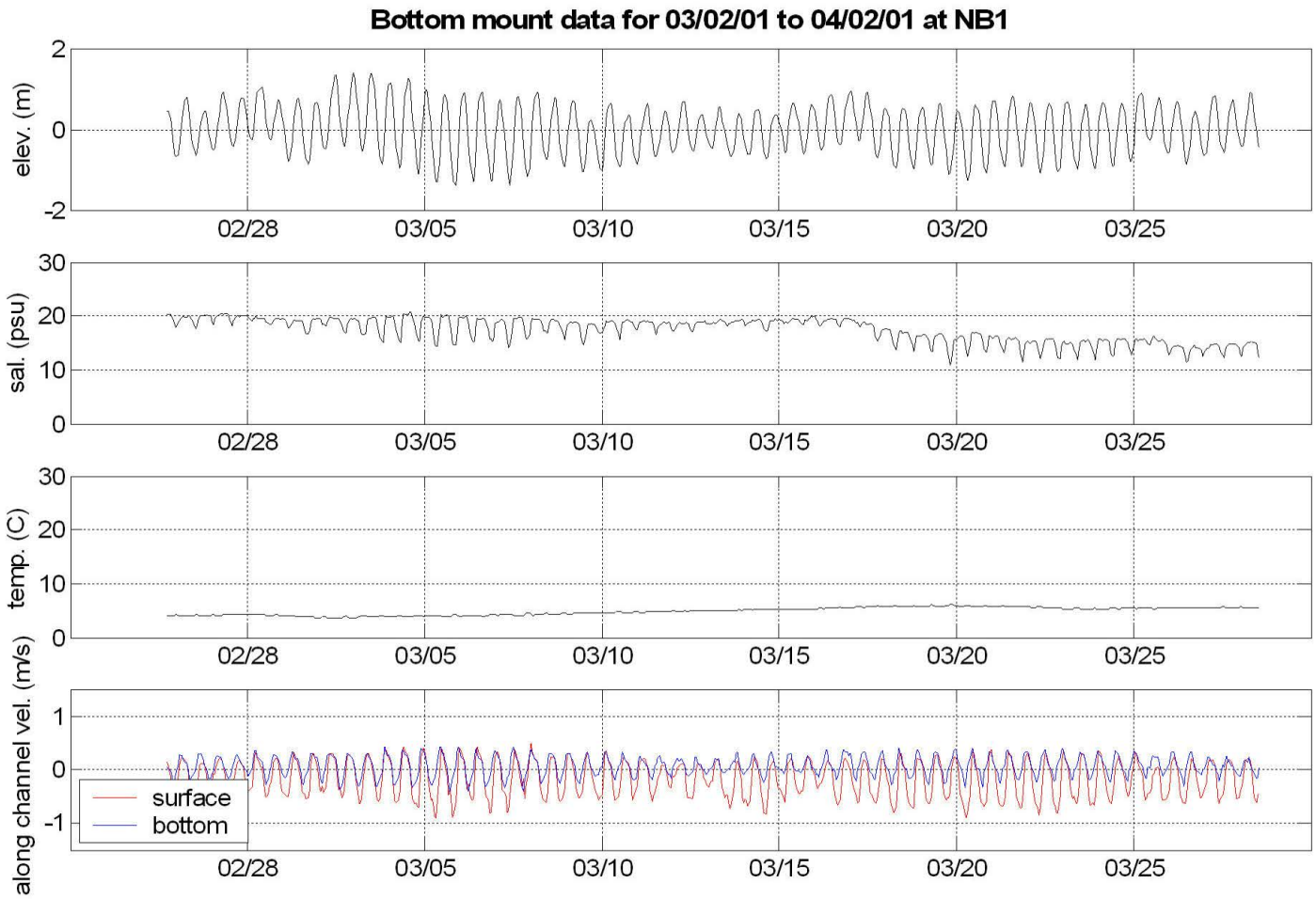

Figure 2 4. Surface elevation (top panel), salinity and temperature (middle panels), and surface and bottom currents measured at the head of Newark Bay from Feb- March, 2003 (Pence, 2004)

Note: Bottom velocity is measured 1.9 m from bottom and surface velocity is measured 8.4 m from bottom

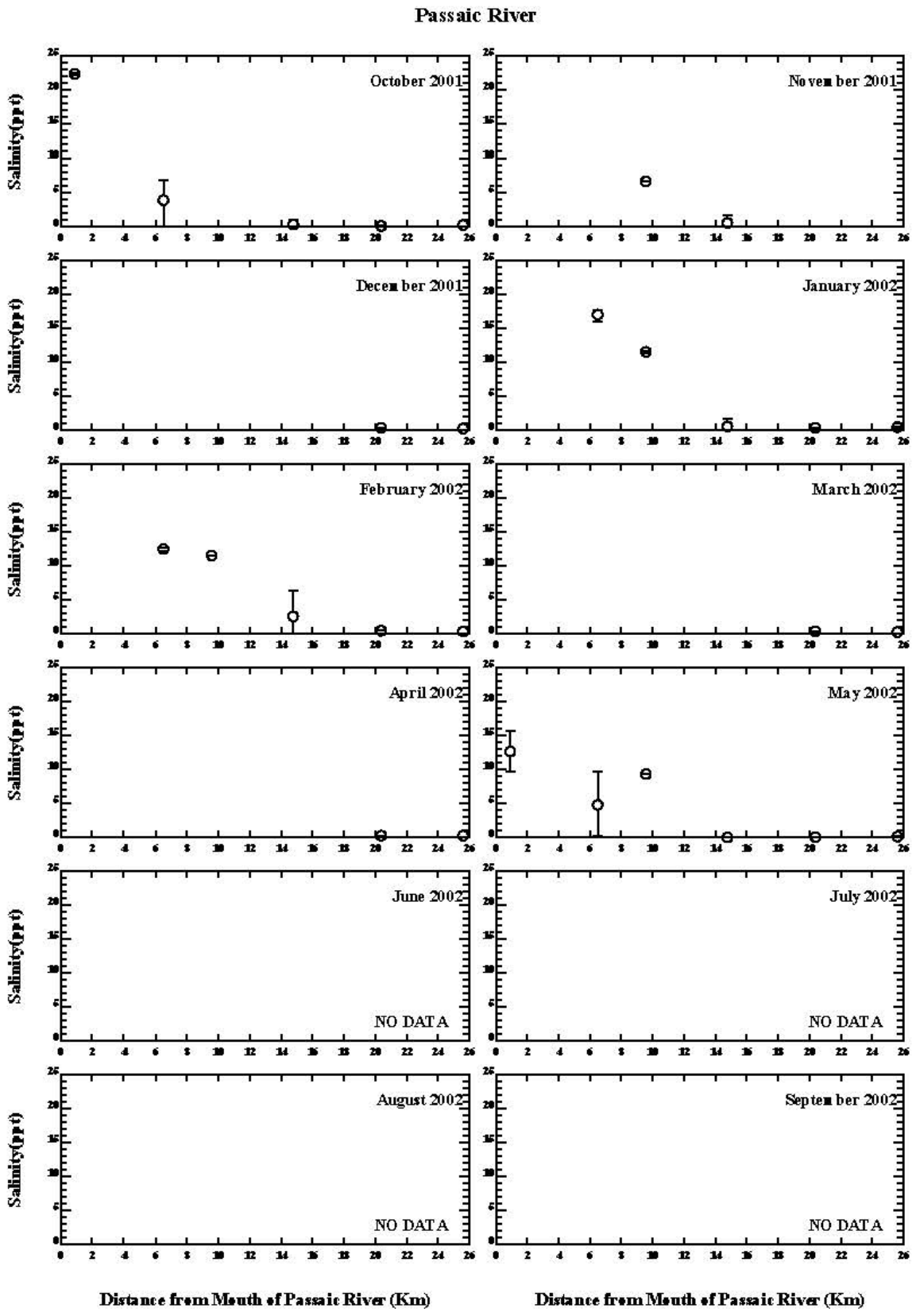

Figure 2-5 Longitudinal salinity distribution in Passaic River, Water Year 2002.

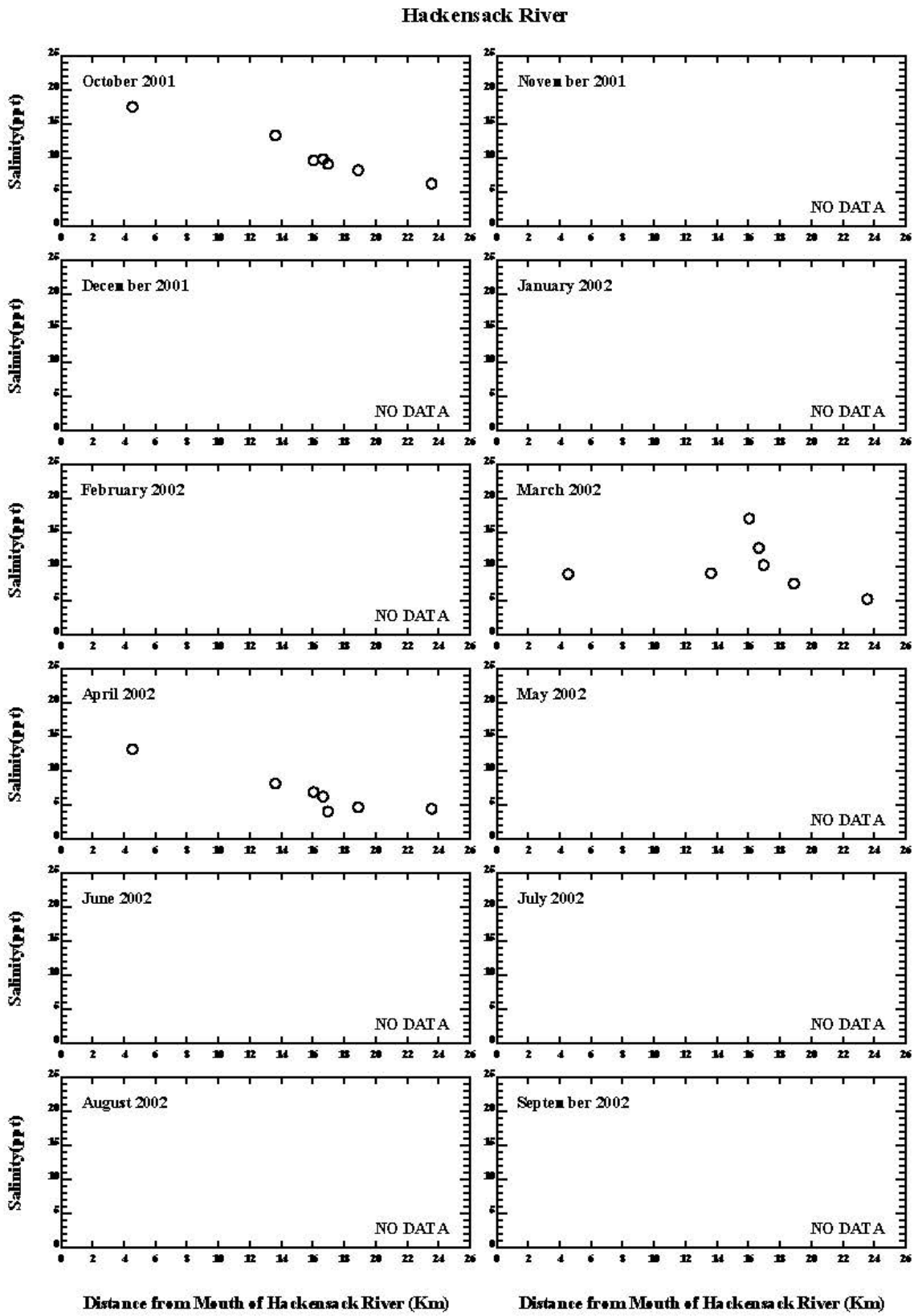

Figure 2-6 Longitudinal salinity distribution in Hackensack River, Water Year 2002.

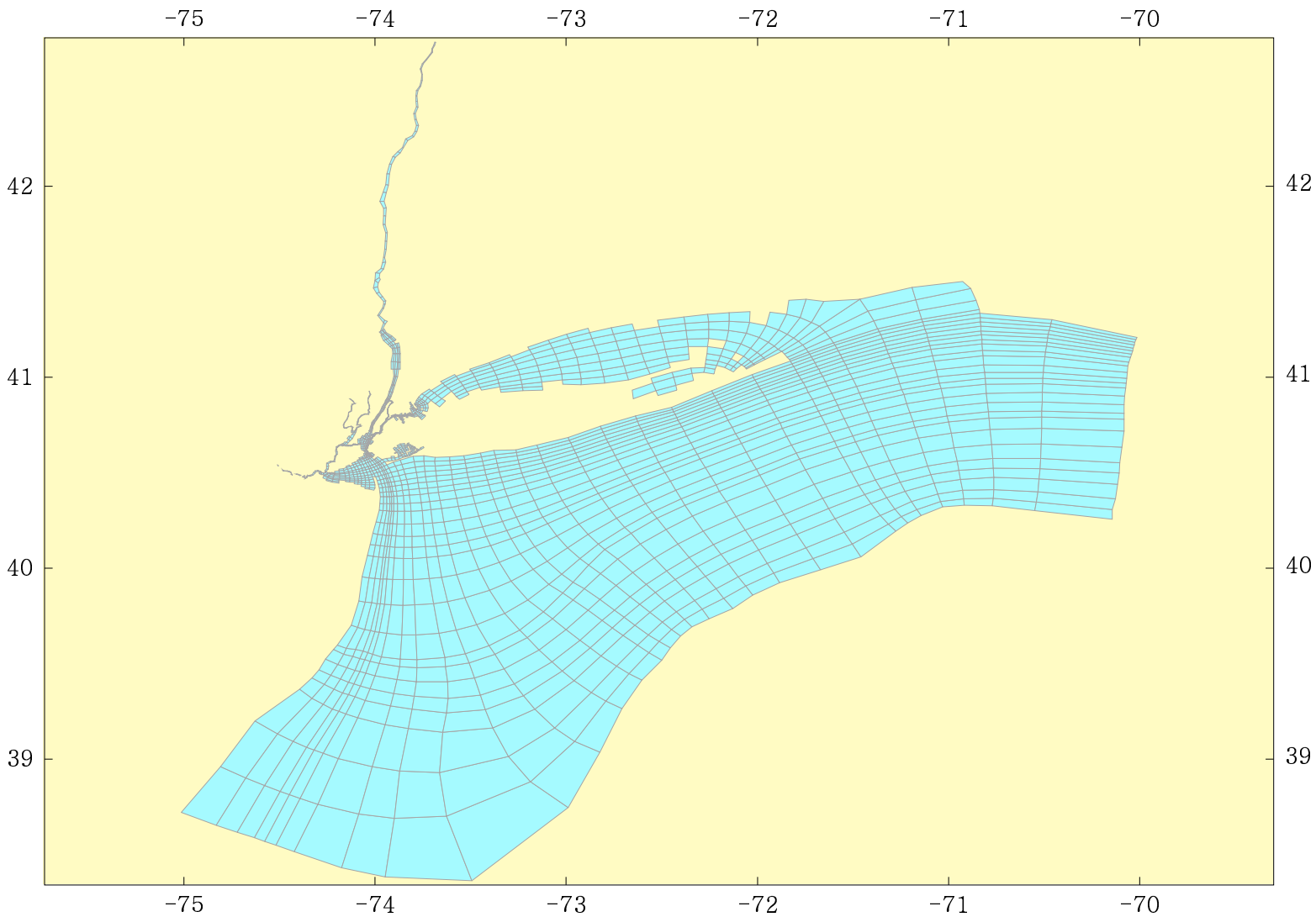

Figure 2-7. SWEM domain and computational grid.

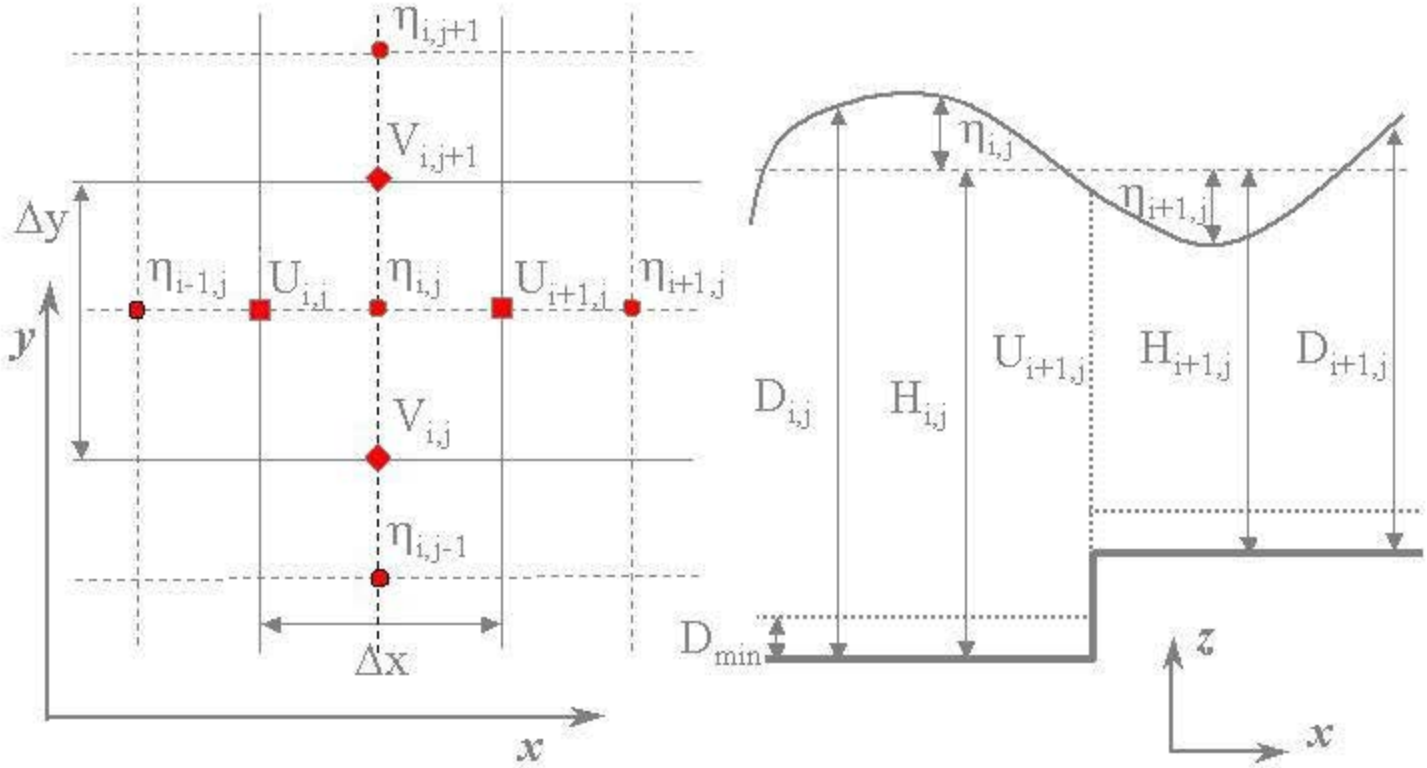

Figure 2 8. ECOMSED computational coordinate system

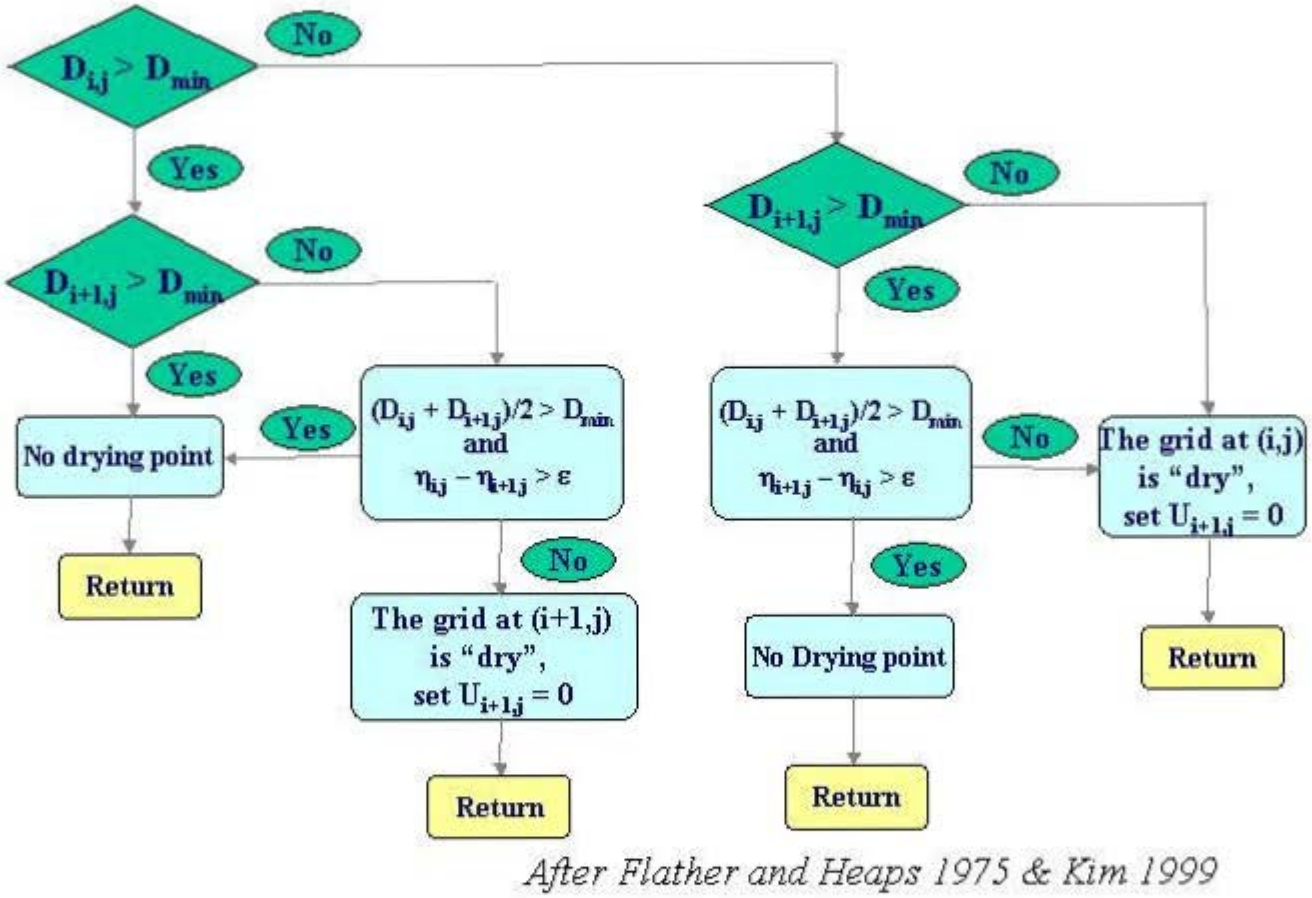

Figure 2 9. Logic diagram for flooding/drying algorithm

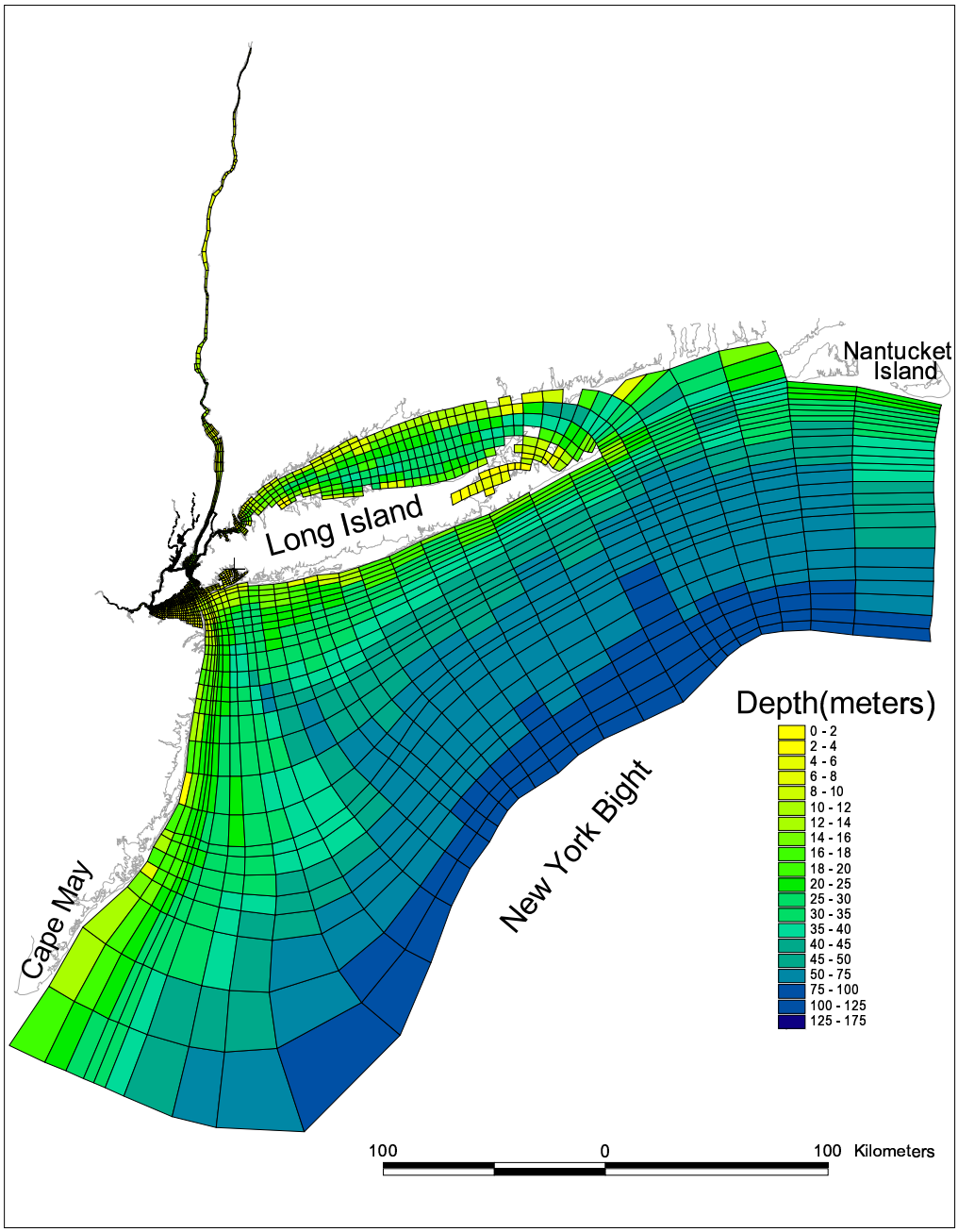

Figure 2-10. Full hydrodynamic model domain and computional grid.

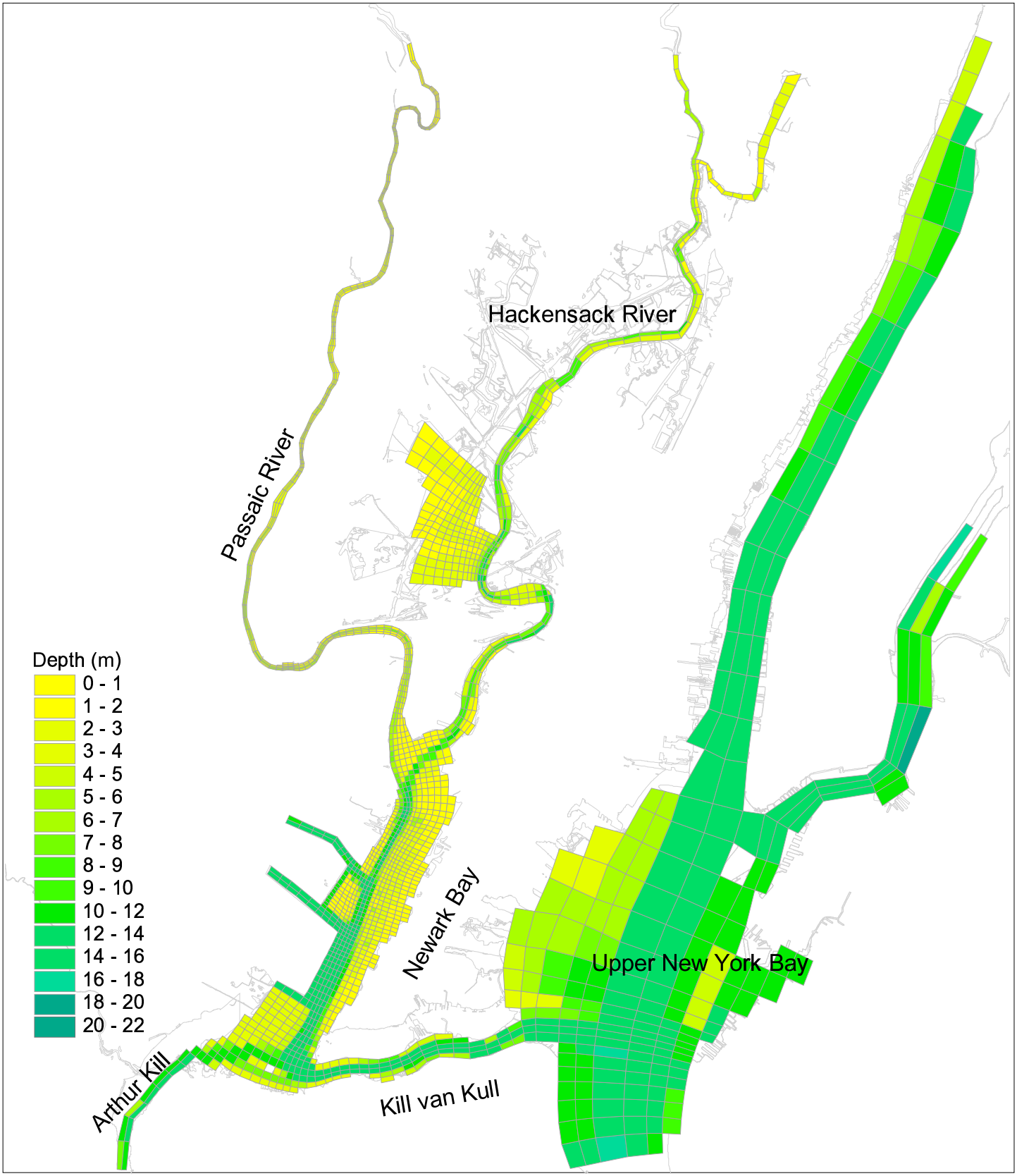

Figure 2-11. Computional grid for the Lower Passaic River, Hackensack River, and Newark Bay.

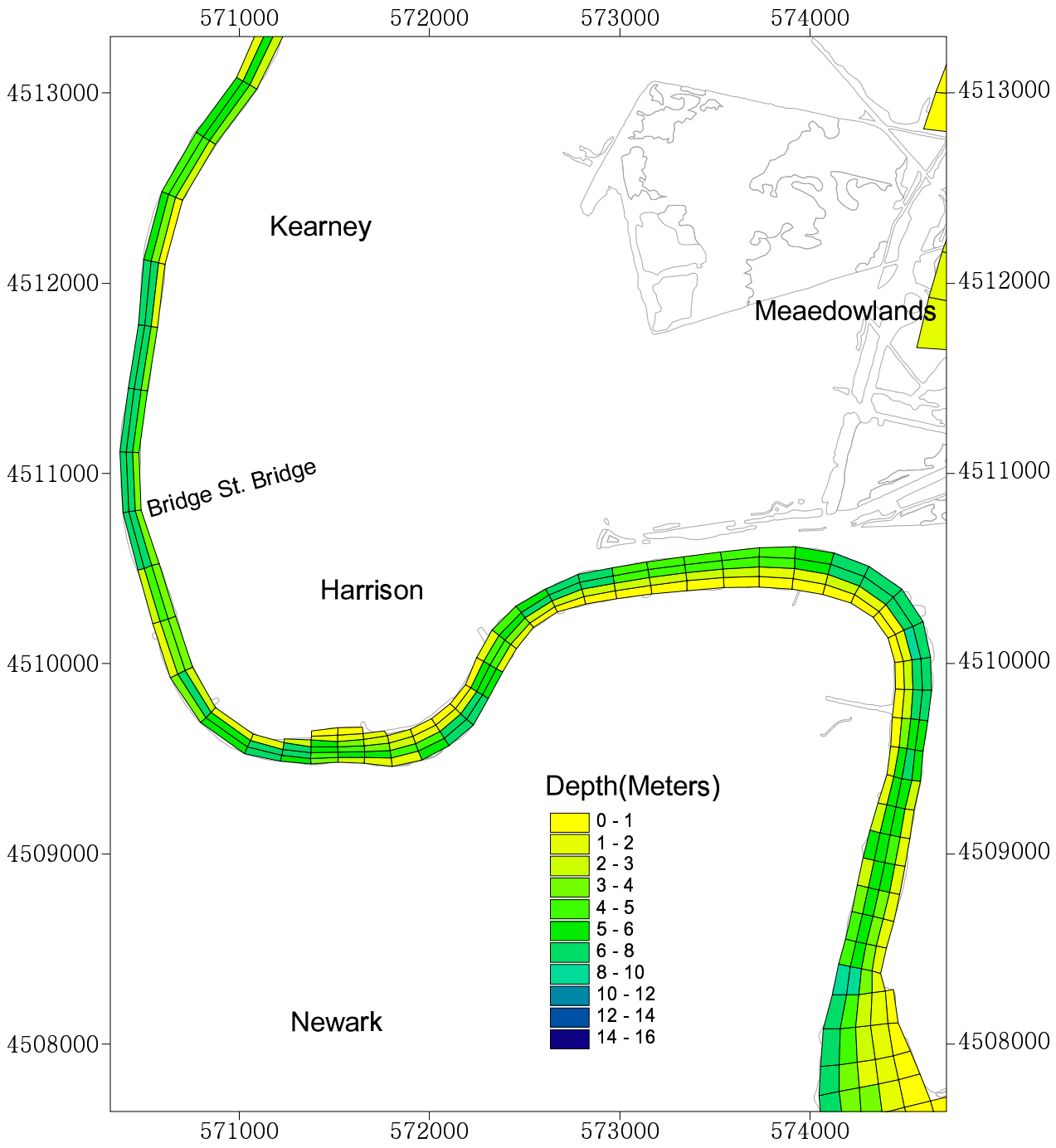

Figure 2-12. Computional grid for the Harrison Reach of the Lower Passaic River.

SHIPPING CHANNEL DATA PROVIDED BY COE NY DISTRIC (AUG 2005)

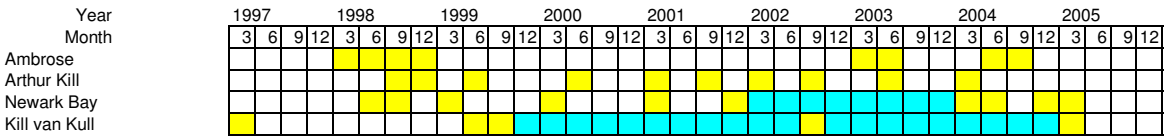

Bathymetric data received for each quarter (3: Jan-March, 6: April-June, 9: July-Sept 12:Oct-Dec)

Significant depths changes occurred during this period

SHIPPING CHANNEL DEPTHS IN KILL VAN KULL, ARTHUR KILL, AND NEWARK BAY

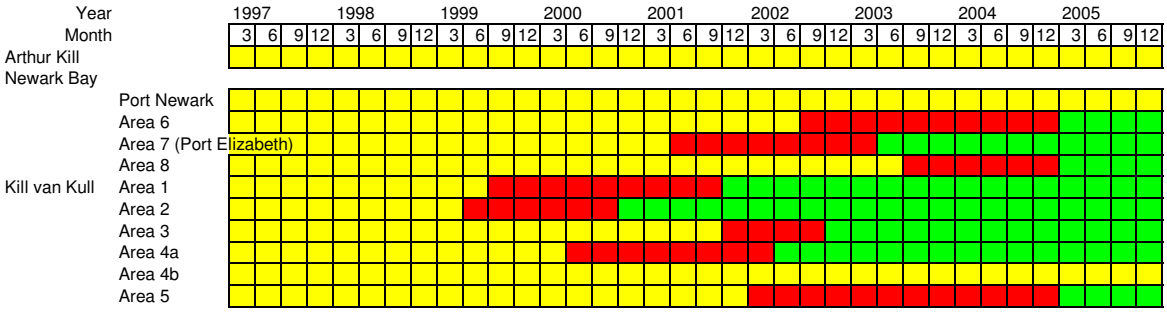

40-45'
Dredging Occurred This Period
50-55'

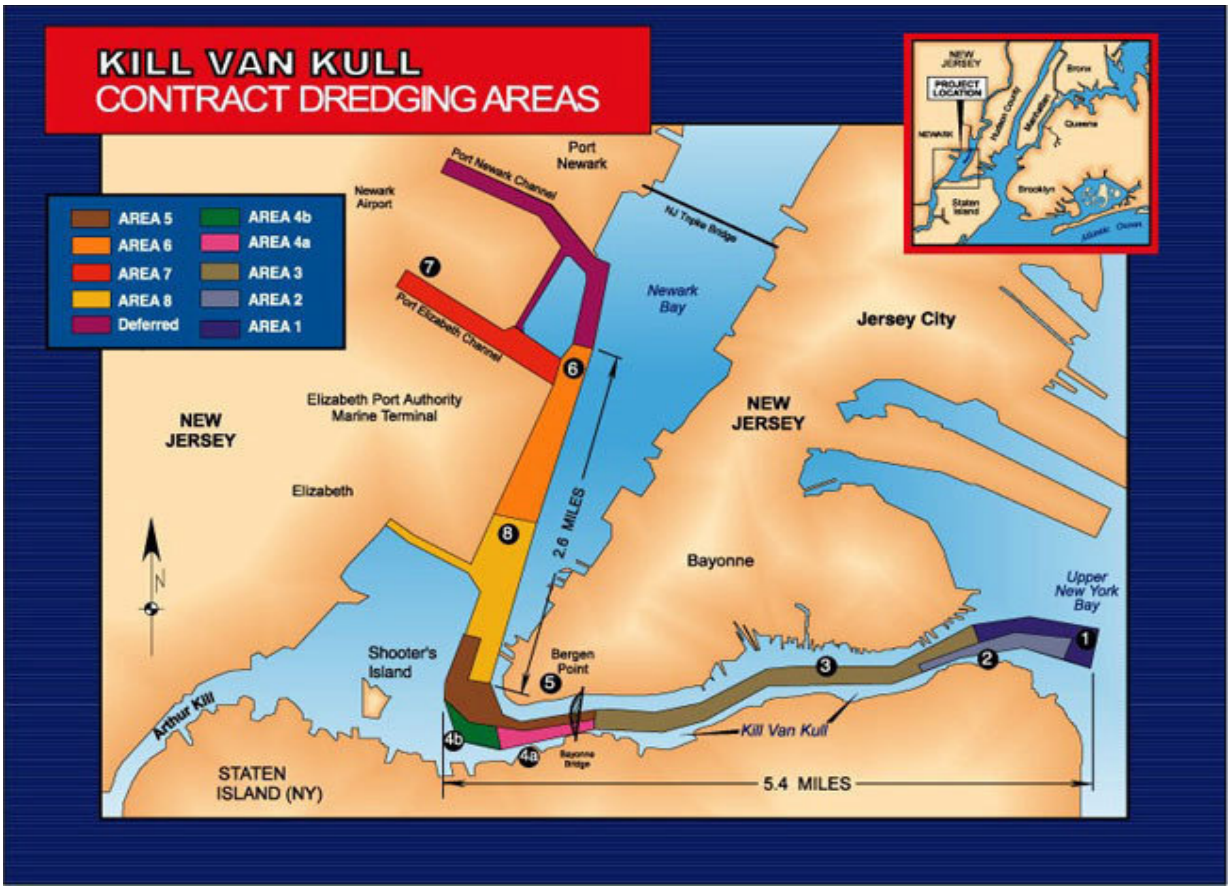

Figure 2-13. USACE harbor-deepening dredging activities.

SECTION 3

BOUNDARY FORCING

The boundary forcing functions of the hydrodynamic model consist of:

- water surface elevation along open ocean boundaries incorporating astronomical tide, cross-shelf elevation gradient and shelf-break elevation;

- three-dimensional fields of temperature and salinity along the open boundaries;

- meteorological information consisting of wind speed and direction, shortwave solar radiation, cloud cover, air temperature, atmospheric vapor pressure and relative humidity to compute surface wind stress and heat flux; and

- freshwater inflows from rivers, wastewater treatment plants, combined sewer overflow and surface runoff.

The details of these boundary conditions are described in this section.

3.1 TIDAL ELEVATION

To produce a simulation of the tidal scale circulation, including the effects of baroclinicity, it is necessary to prepare a data base containing the astronomical dynamics and climatological thermodynamic properties prevailing in New York Bight. The low frequency dynamics in the shelf break are important to the circulation in New York Bight. This phenomenon has already been addressed, among others, by Hopkins and Dieterle (1983, 1987) and Blumberg and Galperin (1990). Low frequency dynamics of continental shelves are associated, among others, with a geostrophic balance. Hence, the cross-shelf slope of the sea surface elevation at the boundaries is highly significant. Because low frequency cross-shelf sea surface elevation records at the boundaries are not available, a practical approach is developed in order to adequately define forcing conditions at these locations.

For the model simulation period, the sea surface elevation $\eta(x,t)$ at the boundary is assumed to be composed of three parts. The first part drives the long-term circulation (geostrophic currents) due to the cross-shelf slope ($\eta_g(x,t)$); the second part deals with the tidal fluctuations ($\eta_I(x,t)$); and the third part represents sub-tidal (meteorological) forcing ($\eta_M(t)$). The resulting water surface elevation is given by:

$$\eta(x,t) = \eta_g(x,t) + \eta_T(x,t) + \eta_M(x,t) \tag{3-1}$$

The effect of the along-shelf elevation gradient imposed at the shelf break on the barotropic circulation in New York Bight has been studied by Hopkins and Dieterle (1983). They found that the parabathic elevation gradient at the shelf-break affects the total transport through the cross-shelf boundaries. For August 1978, a typical summertime period, a diabathic gradient of 13 cm across a Narragansett Bay shelf-break section and a 11 cm gradient across a Cape May shelf-break section could produce the observed summer along-shelf flux of water. Following the findings of Hopkins and Dieterle, Blumberg and Galperin (1990) adopted the same approach to specifying the boundary elevation in a summer average circulation study in the New York Bight.

In the present study, a 13 cm gradient along the northeastern Nantucket Shoals boundary, a 11 cm gradient across the Cape May shelf-break southern boundary and a zero gradient along the shelf boundary are imposed.

Astronomical tide, $\eta_T(x,t)$ due to eight primary harmonic constituents (M_2, S_2, N_2, K_2, K_1, O_1, P_1 and Q_1), is obtained from a global model of ocean tide, TPXO.2, developed by Oregon State University (Egbert et al., 1994). The input to the tidal synthesis program is gridded data of the harmonic constants. The output is η_T as function of time and space (longitude and latitude). The tidal synthesis program uses interpolation of the tidal admittances in the diurnal and semi-diurnal bands to include 9 additional mirror constituents ($2N_2$, MU_2, NU_2, L_2, T_2, J_1, NO_1, OO_1, RHO_1). The synthesis program also adds the long period constituents MF, MM, SSA using the standard equilibrium forms.

Figure 3-1 compares temporal variations in sub-tidal (35 hours) water surface elevations at Cape May, Sandy Hook and Montauk. The figure indicates that the response of water surface to meteorological forcing are essentially in phase throughout the New York Bight and the adjacent estuarine waters. The differences in amplitude at different locations, due to local bathymetry and coastline, are also small. Therefore, in this study $\eta_M(t)$ is expressed as:

$$\eta_M(t) = \alpha\eta_{35h}(t) \tag{3-2}$$

where α is a calibration parameter and $\eta_{35h}(t)$ is the 35 hour low-passed water surface elevation at Sandy Hook. As a tidal wave propagates over the continental shelf, its amplitude is increased by shoaling and shallow water effects. As a result α is expected to have a value less than one. Its value (α = 0.5) has been determined previously by performing a series of simulation runs and comparing model results with data (HydroQual,

2001). The resulting elevation boundary conditions at four key locations in the New York Bight are shown in Figure 3-2.

Also a modified form of the Sommerfield radiation boundary conditions (Blumberg and Kantha (1985) is applied across the Cape May shelf-break section with a function, which tends to force the elevation to a specified (elevation) boundary condition within a given time scale. Thus, long waves are allowed to propagate and they are free to advect through the boundary.

3.2 SALINITY AND TEMPERATURE

Temperature and salinity boundary conditions are obtained from climatological data from World Ocean Atlas 1998 (WOA98), published by NOAA. The published data set contains gridded monthly temperature and salinity at one-degree latitude-longitude. The monthly data are tabulated at 19 levels from 0 to 1000 m. At the model boundary, temperature and salinity are linearly interpolated from the surrounding gridded data.

As climatological data do not represent true monthly variations of temperature and salinity for the periods of the model calibration, it was necessary to adjust the boundary conditions defined from WOA98 so that computed temperature and salinity matched the monthly mean temperature and salinity in the Long Island Sound, the New York Bay and the Hudson River. The temporal variations of the adjusted salinity and temperature at the continental shelf break are shown in Figures 3-3 and 3-4, respectively. They are defined as follows:

$$S(x,t) = S_L(x,t) - 2.0 \tag{3-3}$$

$$T(x,t) = T_L(x,t) - 2.0 \tag{3-4}$$

where S_L and T_L are climatological salinity and temperature in psu and ^oC from WOA98.

3.3 METEOROLOGICAL DATA

Two major boundary forcings applied to the water surface are wind stress and heat flux. Wind stress is computed from wind speed and wind direction. Heat flux computations require the specification of air temperature, relative humidity, barometric pressure, shortwave solar radiation and cloud cover. Data from J.F.K. airport are used for the heat flux computation (Figure 3-5). Hourly meteorological data were obtained from NOAA for 5 airports including, Newark Airport, N.J., Atlantic City Airport, N.J., J.F.K. Airport, N.Y., Albany Airport, N.Y., Bridgeport Airport, C.T. and several buoys in New York Bight and Long Island Sound. Figure 3-6 shows the locations of the meteorological data stations. Spatially varying wind stress was computed from these monitoring locations.

3.4 RIVER DISCHARGE

Fresh water inflows from 25 rivers and tributaries are considered in the model. Discharge data were compiled from 34 verified USGS surface water gauges for New York, New Jersey and Connecticut from October 1994 through September 2004. Table 3-1 lists these rivers and the availability of data is shown in Figure 3-7. Table 3-1 also indicates the maximum, minimum and the mean river inflows for the calibration/validation period. In many cases, multiple sources that are physically located close to each other are placed in the same computational cell of the hydrodynamic model. Locations of the USGS gauging stations are shown in Figure 3-8, and the temporal variation of river discharges used for the model calibration are shown in Figure 3-9.

If there is no gauge on a river, then a nearby gauge is used to calculate the river flow using the ratio of the ungauged drainage area to the gauged drainage area. For example, the ungauged Catskill Creek includes drainage basins in Green and Columbia Counties. The inflow was calculated based on specific discharge (flow/area) from the adjacent Wallkill and Esopus Creeks. A similar procedure was used to determine discharge from ungauged Westecunk Creek based on specific discharge from the Oswego, Batso and Bass Rivers basin.

The annual mean flow from the rivers listed in Table 3-1 is 1377 m^3/sec. The highest discharge is from the Connecticut River, followed by the Hudson River. The mean flow of the Hudson is about 84 percent of the Connecticut River. These two rivers account for 65.8 percent of the total flow into the SWEM model domain. The tributaries of the Hudson in the New York areas contribute an additional 11.0 percent of the freshwater. The contributions of the rivers from New Jersey and Connecticut, excluding the Connecticut river, are approximately 15.8 and 7.4 percent, respectively.

Long term averaged (107 years) flow of Passaic River measured at the most downstream gauging station at Little Falls is about 1,140 cfs. During the past 100 years, the maximum peak flow measured at the Little Falls is 31,700 cfs which was observed on October 10, 1903. During the last few decades, the maximum peak flow of 18,400 cfs was measured on April 7, 1984. On a yearly averaged basis, Water Year 1902 yielded the largest flow of 2,400 cfs while the driest year (1965) yielded 270 cfs. During the study, USGS flow records from the Little Falls gauging station were analyzed for ten years. Out of the ten years, only WY 1996, 2003, and 2004 exceeded the long term average flow of the Passaic River: i.e. 1,800, 1,900, and 1,500 cfs, respectively. WY 1995 and 2002 were relatively dry years, which yielded 660 and 450 cfs, respectively.

Table 3-1. List of Rivers And Discharge Statistics
(October 1994-September 2004)

River	Gauging Station #	Discharge (m^3/sec)		
		Maximum	Minimum	Mean
1. Hudson River(Green Island + Wappingers)	01358000/01372500(1)	1062.06	58.21	413.28
2. Hackensack River	01378500	158.01	0.00	1.51
3. Passaic River	01389500	319.98	0.18	28.78
4. Saddle River	01391500	51.54	0.14	2.85
5. Raritan River	01403060	1727.33	2.60	32.31
6. South R.(Manalapan) +Lawrence Brook(Raritan)	01404054/01403060	133.36	0.22	5.65
7. Normans Kill (Wappinger)	01372500	50.75	0.88	3.16
8. Moordener Kill (Wappinger)	01372500	9.85	0.17	0.61
9. Esopus Creek	01364500	297.33	0.16	13.78
10. Roundout Creek+Wallkill River	01367500/01371500	681.59	1.42	48.42
11. Wappinger Creek+Fishkill	01372500	278.82	0.20	16.39
12. Croton River	01375000	132.12	0.05	15.37
13. Saw Mill River	01376500(2)	8.36	0.17	1.12
14. Bronx River	01302000(3)	16.29	0.00	1.80
15. Navesink +Shrewsbury	01407500	85.29	0.00	2.61
16. Catskill River(Esopus + Wallkill)	01364500/01371500	663.03	0.60	50.37
17. Norwalk River	01209700	25.49	0.03	1.56
18. Housatonic River + Naugatuck River	01205500/01208500	845.82	3.68	94.03
19. Quinnipiac River	01196500	73.91	0.93	6.43
20. Connecticut River	01184000	2803.36	44.17	492.47
21. Thames River(Shetucket + Quinebaug)	01122500/01127000	534.06	1.78	56.89
22. Manasquan + Shark Rivers	01408000/01407705	58.26	0.63	3.77
23. Metedeconk + Toms Rivers	01408120/01408500	161.38	1.79	19.50
24. Mulica River + Westconk River (Oswego, Batso, Bass)	01409400/01410000/ 01409500/01410150	282.48	7.43	37.16
25. Great Egg Harbor + Tuckahoe River	01411000/01411300	199.72	3.18	27.22

(1) If no Gauge for 01358000 then add Mohawk and Hudson R. above Lock #1 (01357500+01335754)
(2) Use Croton River (0137500) if there is no gauge data
(3) No data after 9/30/89, use Croton R. (01375000)

During initial model calibration, daily surface water temperature data measured at the NOAA Battery tide gauge station were used for the specification of temperature associated with the Passaic River inflows due to lack of continuous observation of river water temperature at upstream USGS gauges. It was found, not surprisingly, that computed water temperatures in the upper portion of LPR were extremely sensitive to the water temperature specified for the river inflows. This is because the volume of the narrow and shallow section of the upper LPR is relatively small compared to the inflow volumes. On the other hand as one nears the mouth of the LPR the cross-sectional areas and water depths increase and water volumes are more strongly influenced by tidal exchange with Newark Bay. Using water temperature data from the Battery did not produce reasonable receiving water temperatures in the LPR during relatively high inflow events. Lacking continuous water temperature observations at upstream USGS gauges, different prescriptions of river water temperature were attempted: interpolation of infrequent monthly or bi-monthly observed water temperature at upstream USGS stations, air temperature measured at nearby airports, and so on. Among these approaches, a 3-day moving average of air temperature recorded at Newark International Airport produced the most favorable water temperature in the upper portion of LPR. Therefore, the river inflow temperatures for the Passaic River, Hackensack River and Saddle River were prescribed with the 3-day moving average air temperature measured at Newark International Airport. The remaining river temperatures were based on daily surface water temperature measured at the Battery with missing data filled in from the NOAA's Bergen Point West Reach Station. Temporal variation of river water temperature used in the model is shown in Figure 3-10.

3.5 WASTEWATER DISCHARGES

Wastewater flows of 99 wastewater treatment plants, and discharges due to combined sewer overflows and stormwater runoff at 1297 grid locations for a total of 1396 inputs. In many cases, multiple sources that are physically located close to each other are placed in the same computational cell of the hydrodynamic model

3.5.1 Wastewater Treatment Plants

The wastewater treatment plants used in this study are shown in Figure 3-11. Their respective discharges, listed in Table 3-2, have been compiled from HydroQual (1991a, 1991b), Interstate Sanitation Commission Report (ISC, 1989), and in consultation with NYCDEP.

The total effluent from the treatment plants is 114.05 m^3/sec. The highest effluent flow rate of 12.7 m^3/sec is from Newtown Creek, closely followed by Wards Island (8.2 m^3/sec). The Passaic Valley plant discharges about 11.9 m^3/sec of effluent, which discharges its effluent in the Upper New York Bay of New York Harbor. The effluents

from these three treatment plants account for approximately 32 percent of the flows from this category of input. There is no wastewater treatment plant effluent discharge within the LPR. There are three wastewater treatment plant discharges within the Hackensack River basin but their discharge volumes are relatively small (less than 5 m^3/sec combined).

Monthly mean temperatures of the effluents were obtained from NYCDEP. Figure 3-12 shows the temporal variation of temperature of wastewater from wastewater treatment plants. The maximum, minimum and mean temperatures are 23.0, 14.0 and 18.6°C respectively.

3.5.2 Combined Sewer Overflows and Stormwater Runoff

The runoff volumes due to combined sewer overflows and stormwater runoff were obtained from two landside models developed during other water quality modeling efforts. They include RAINMAN, for the New York and Northern New Jersey area and Rainfall Runoff Modeling Program (RRMP), for Connecticut and southern New Jersey, which includes counties south of Monmouth County. These landside models are driven by rainfall records to generate CSO and stormwater volumes. Hourly rainfall data from regional airports or from local rain gauges installed in the drainage area were used as input. The resulting outflows were distributed throughout the domain at 1297 locations. Figure 3-12 also shows the total flow from surface runoffs (CSO and stormwater) and compares it to the wastewater treatment flow compiled by major areas. As indicated, CSO results in high total flows over the simulation period. In the lower end, surface runoffs from some of the CSO are very small – close to zero. The temperature of runoff is taken as the temperature of the river water as shown in Figure 3-12.

Table 3-2. List of Wastewater Treatment Plants and Discharges (m^3/s)

#	Plant Name	Discharge
New York		
1	26th Ward	3.067
2	Bowery Bay	6.326
3	Coney Island	4.904
	Hunts Point	6.146
5	Jamaica	4.153
6	Newtown Creek	12.714
7	North River	8.293
8	Oakwood Beach	1.671
9	Owls Head	5.449
10	Port Richmond	1.767
11	Red Hook	1.990
12	Rockaway	1.183
13	Tallman Island	3.006
14	Wards Island	8.249
15	Lawrence	0.051
16	Long Beach	0.252
17	Huntington, New York	0.079
18	Port Jefferson SCSD#1	0.032
19	Oyster Bay	0.049
20	Great Neck Village	0.036
21	Town of Cornwall	0.048
22	Cedarhurst	0.034
23	Highland Falls	0.033
24	Kings Park SCSD#6	0.029
25	USMA - West Point	0.078
26	Orange town SD#2	0.486
27	City of Poughkeepsie	0.324
28	Arlington	0.149
29	City of Newburgh	0.311
30	Inwood	0.552
31	Bay Park	2.313
32	Glen Cove STP	0.190
33	Yonkers	3.416
34	New Rochelle	0.652
35	Mamaroneck	0.722
36	Blind Brook	0.140
37	Port Washington	0.114
38	Port Chester	0.171
39	Bel Grave STP	0.056
40	Cedar Creek	2.474
41	Great Neck SD	0.105
42	Haverstraw	0.226
43	Stony Point	0.041
44	Rockland County SD#1	0.818
45	Peekskill	0.263
46	Suffolk County Sewer District 3	0.905
47	Ossining	0.289
48	Stonybrook SCSD#21	0.085
New Jersey		
49	Ciba-Geigy	0.000
50	Bergen County	3.169
51	Middlesex County	5.028
52	Cape May-Cape May	0.041
53	Edgewater	0.158
54	Passaic Valley	11.868
55	Ocean Township SA	0.226
56	S.Monmouth Regional SA	0.189
57	Rahway	1.108
58	Monmouth County Bayshore	0.678
59	Bayshore Region SA	0.353
60	Joint Meeting Essex	2.898
61	Long Branch SA	0.164
62	Neptune Township SA	0.192
63	Linden-Roselle	0.514
64	Secaucus	0.135
65	Asbury Park	0.124
66	West New York	0.443
67	Atlantic County UA/Middletown SA	0.335
68	Ocean County UA Southern	0.219
69	Hoboken/North Hudson SA	0.498
70	NE Monmouth SA/ Two Rivers WRA	0.442
71	Ocean County UA	0.842
72	North Bergen Woodcliff	0.118
73	Ocean County UA Central	0.876
74	North Bergen Central/North Bergen MUA	0.309
75	Cape May-Ocean City	0.117
76	Cape May - Wildwood	0.239
Connecticut		
77	Ansonia WPCF	0.107
78	Branford	0.180
79	Bridgeport Westside	1.024
80	Derby WPCF	0.090
81	Greenwich Central STP	0.398
82	Gronton Town	0.011
83	East Shore/New Haven East Shore WPAF	1.511
84	New London	0.342
85	North Haven	0.158
86	Norwich	0.276
87	Seymour WPCF	0.053
88	Westport WPCF	0.078
89	Shelton WPCF	0.111
90	Milford-Beaver Brook	0.092
91	Montville	0.059
92	Bridgeport Eastside	0.306
93	Stratford WPF	0.479
94	Fairfield Town Hall	0.379
95	West Haven	0.372
96	Stamford, Connecticut	0.674
97	Groton City WPCF	0.161
98	Norwalk WPCF	0.735
99	New Canaan STP	0.057

3.6 CLOSE EXAMINATION OF FRESHWATER INFLOWS IN THE PASSAIC RIVER BASIN

In the Lower Passaic River basin, there are several ungauged streams. These include McDonald Brook, Third River, and Second River between Dundee Dam and Harrison Reach, and Franks Cr., Harrison Cr., Plum Cr., and Lawyer's Cr., which are downstream of the Harrison Reach. Figure 3-13 shows the locations of these minor tributaries. The three tributaries upstream of the Harrison Reach have clearly defined drainage boundaries in the RAINMAN input. The drainage boundaries of other "tributaries" between Harrison Reach and the mouth of Passaic River are not so well defined. In fact, these three downstream "tributaries" are found in highly urbanized environments and have been largely bulkheaded and receive their freshwater inputs via CSO and stormwater inputs. Therefore, estimates of the runoff volumes are handled as CSOs and SWOs in RAINMAN. Freshwater inflows of three upstream tributaries generated by RAINMAN runoff model are shown in Figure 3-14.

Further examination of RAINMAN generated freshwater inflows was conducted for the Third River basin, which drains into the Lower Passaic River near Passaic, New Jersey. USGS maintained the monitoring station in the river up to WY 1997 and drainage area upstream of the station is 11.8 square miles (7,500 acres) and the gauging station covers more than 90% of total drainage basin. Flows from RAINMAN and gauged flows are compared from WY 1995 to 1997 (Figure 3-15). As shown in the figure, RAINMAN generated flows (red lines) as direct function of rainfall events. The flow peaks and decreases sharply without retention of flows over time as shown in USGS gauge data (blue lines). The average inflow over WY 1995 estimated by RAINMAN is 8.4 cfs while the USGS reported a gauged flow of average 12.7 cfs. The comparison indicates that RAINMAN generated about 66% of the measured flow. The USGS gauge data suggest that while the inflows are highly correlated to rainfall events, there is six to eight cfs base flow in the Third River in WY 1995 through WY 1997.

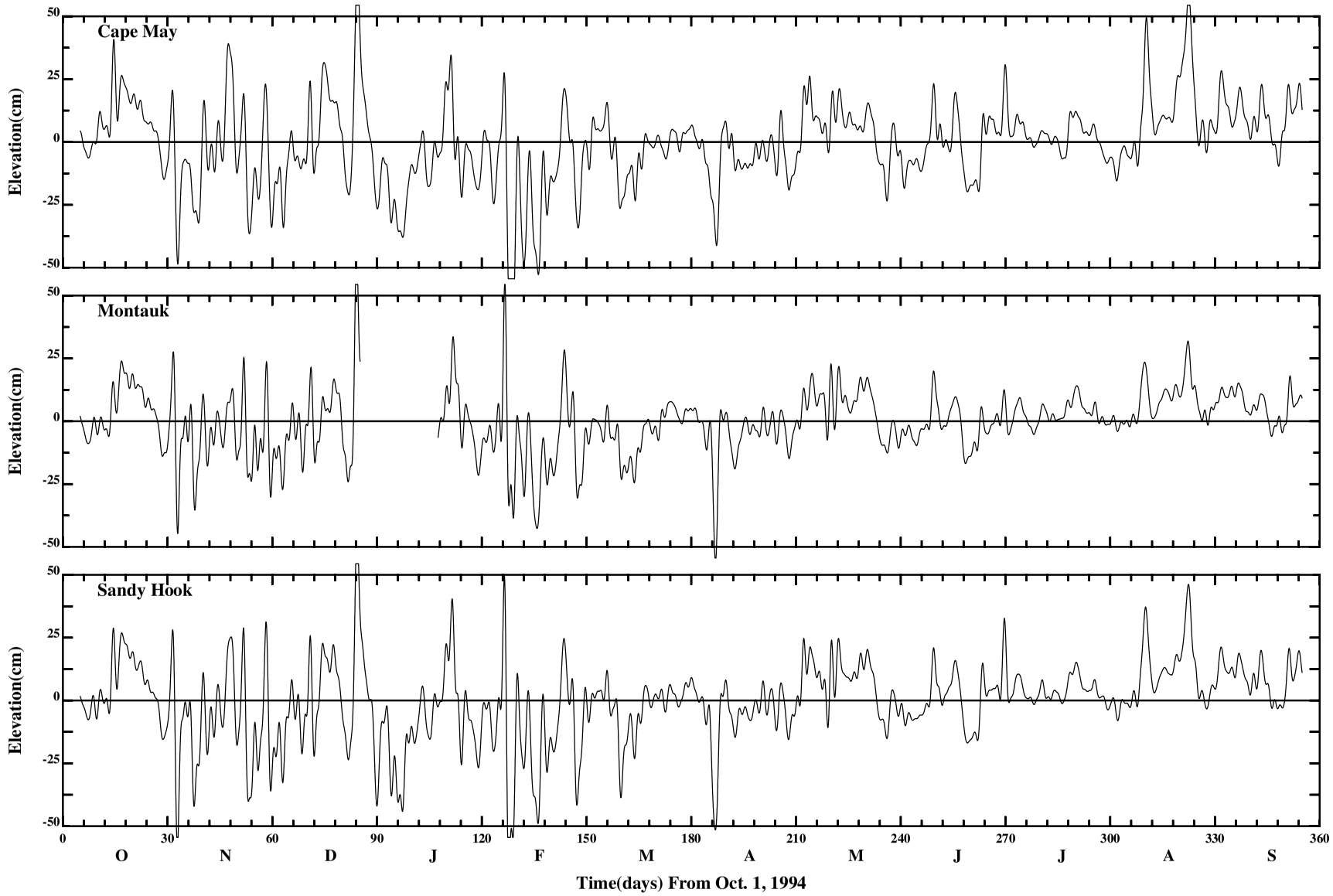

Figure 3-1 Comparison of 35 hours lowpass water surface elevations at Cape May, Sandy Hook, and Montauk

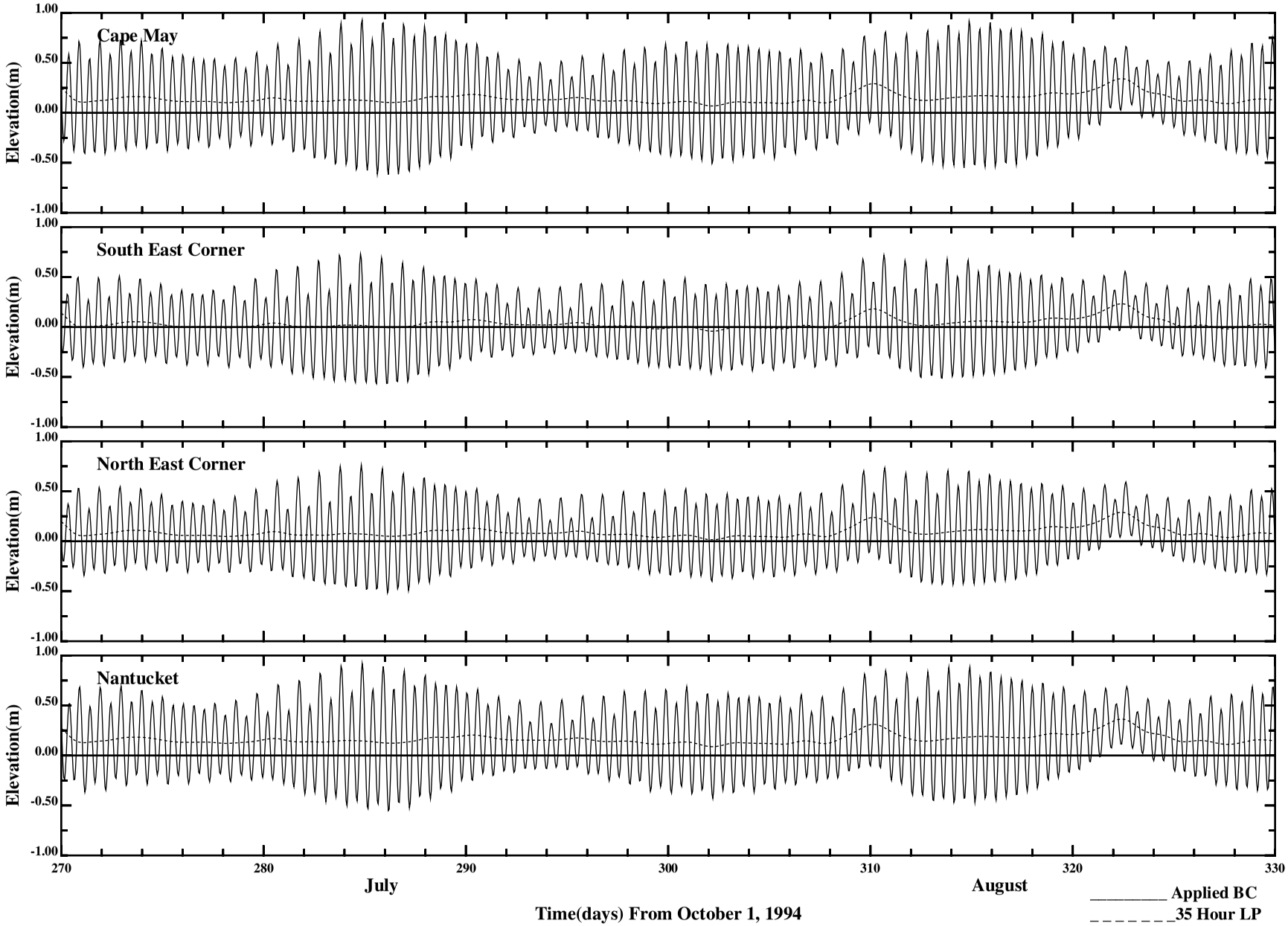

Figure 3-2a Elevation boundary conditions at four key locations in the New York Bight for July and August,1995

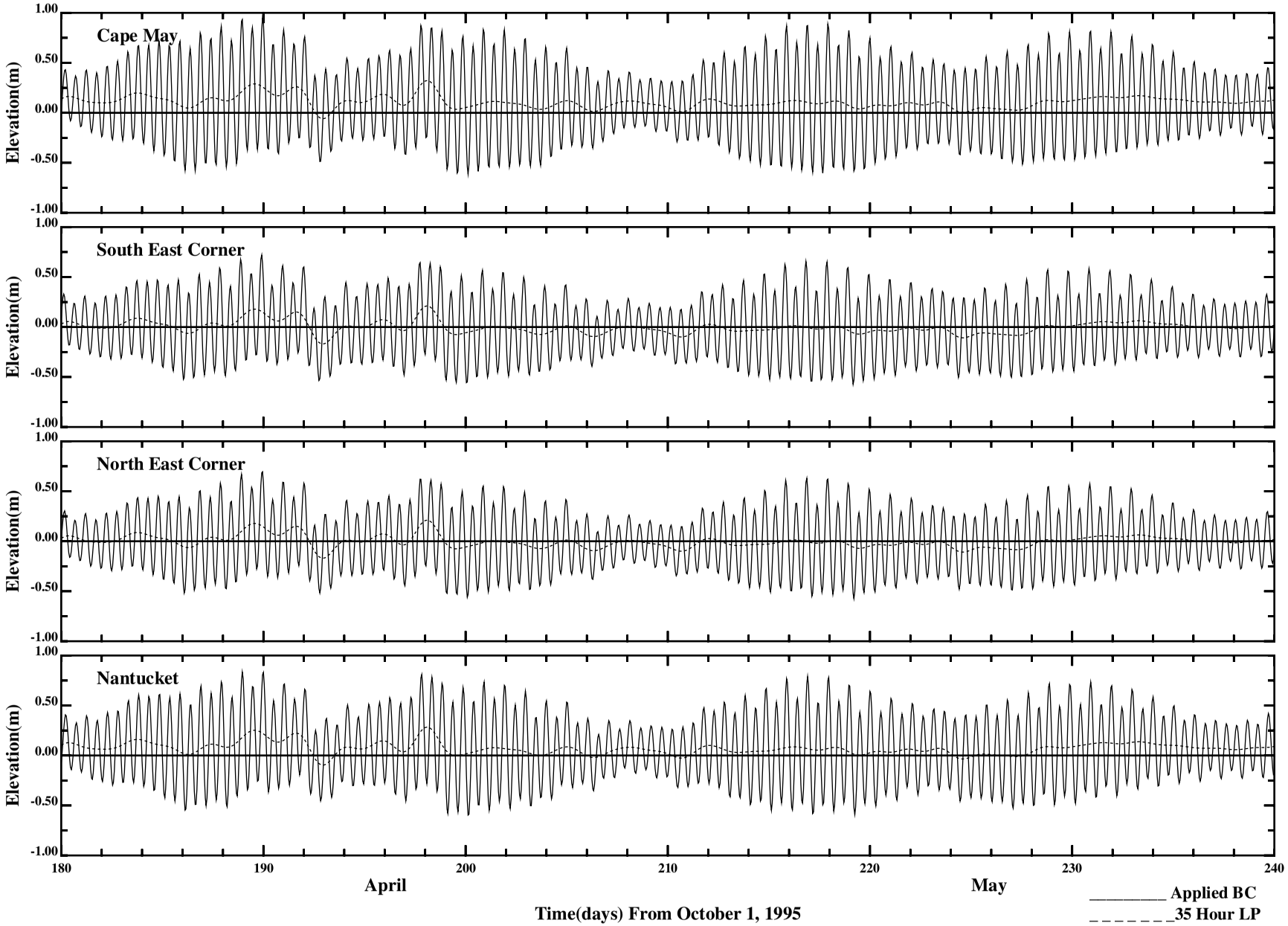

Figure 3-2b Elevation boundary conditions at four key locations in the New York Bight for April and May, 1996

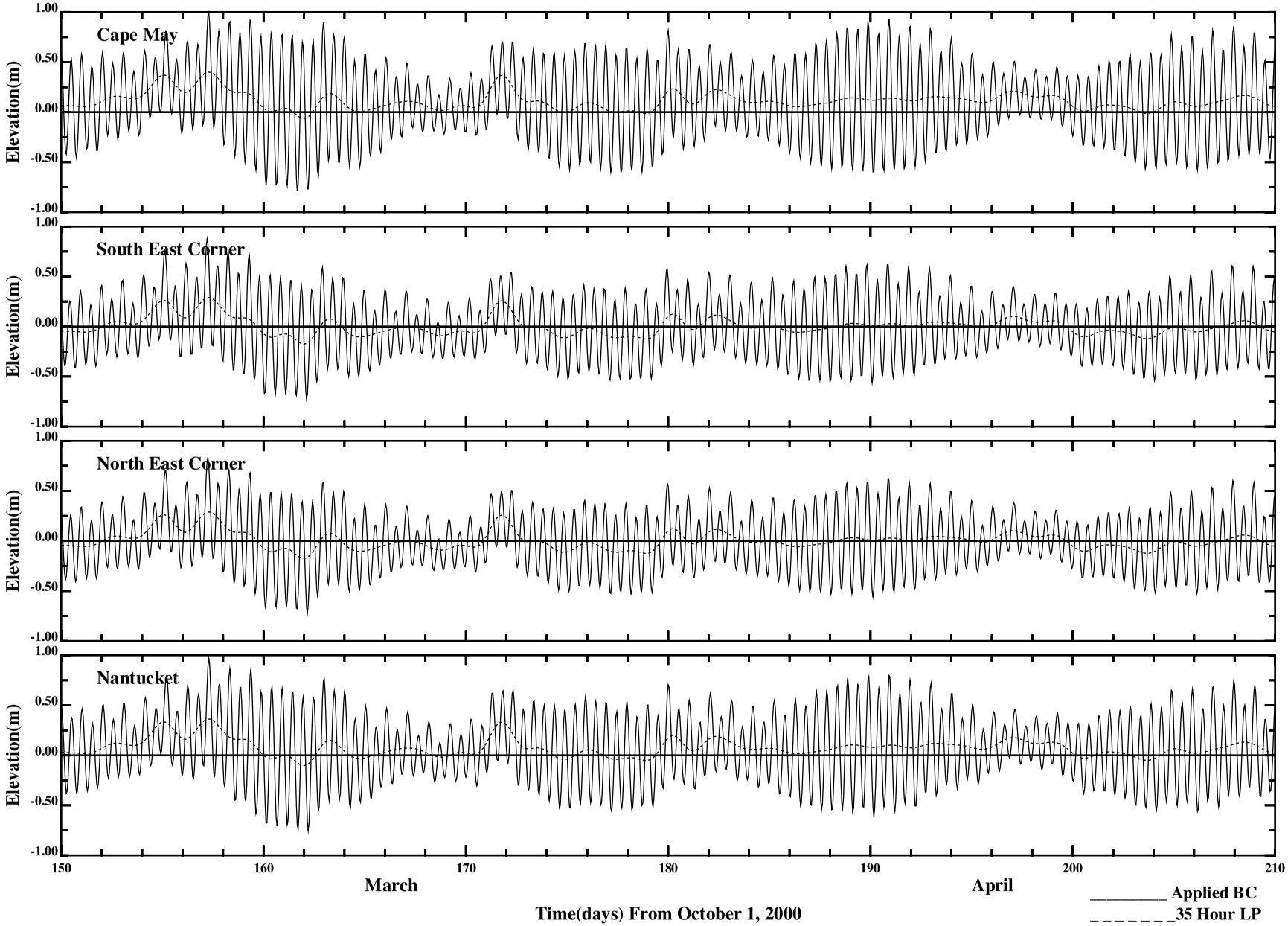

Figure 3-2c Elevation boundary conditions at four key locations in the New York Bight for March-August, 2001

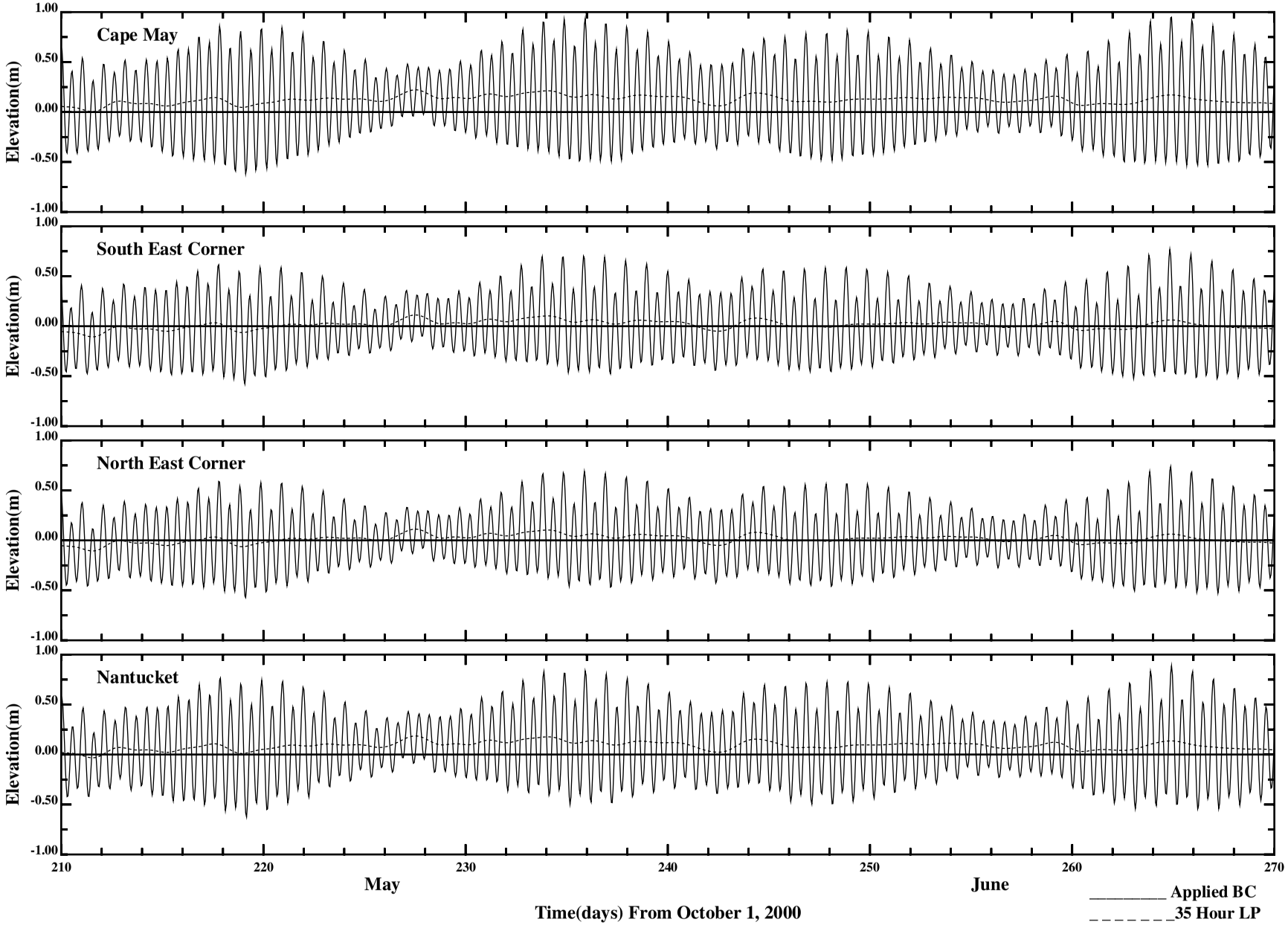

Figure 3-2c Elevation boundary conditions at four key locations in the New York Bight for March-August, 2001 (continued)

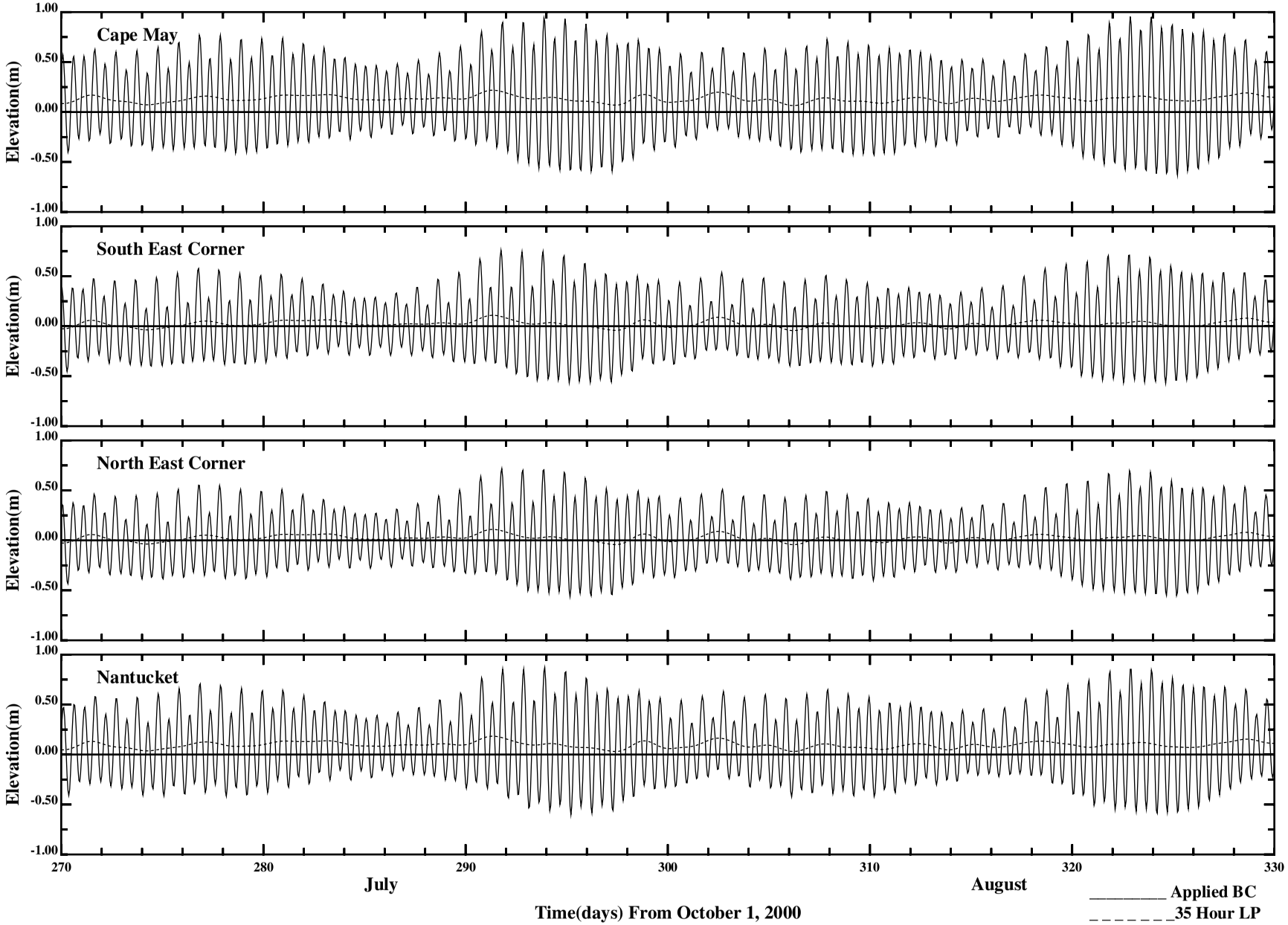

Figure 3-2c Elevation boundary conditions at four key locations in the New York Bight for March-August, 2001 (continued)

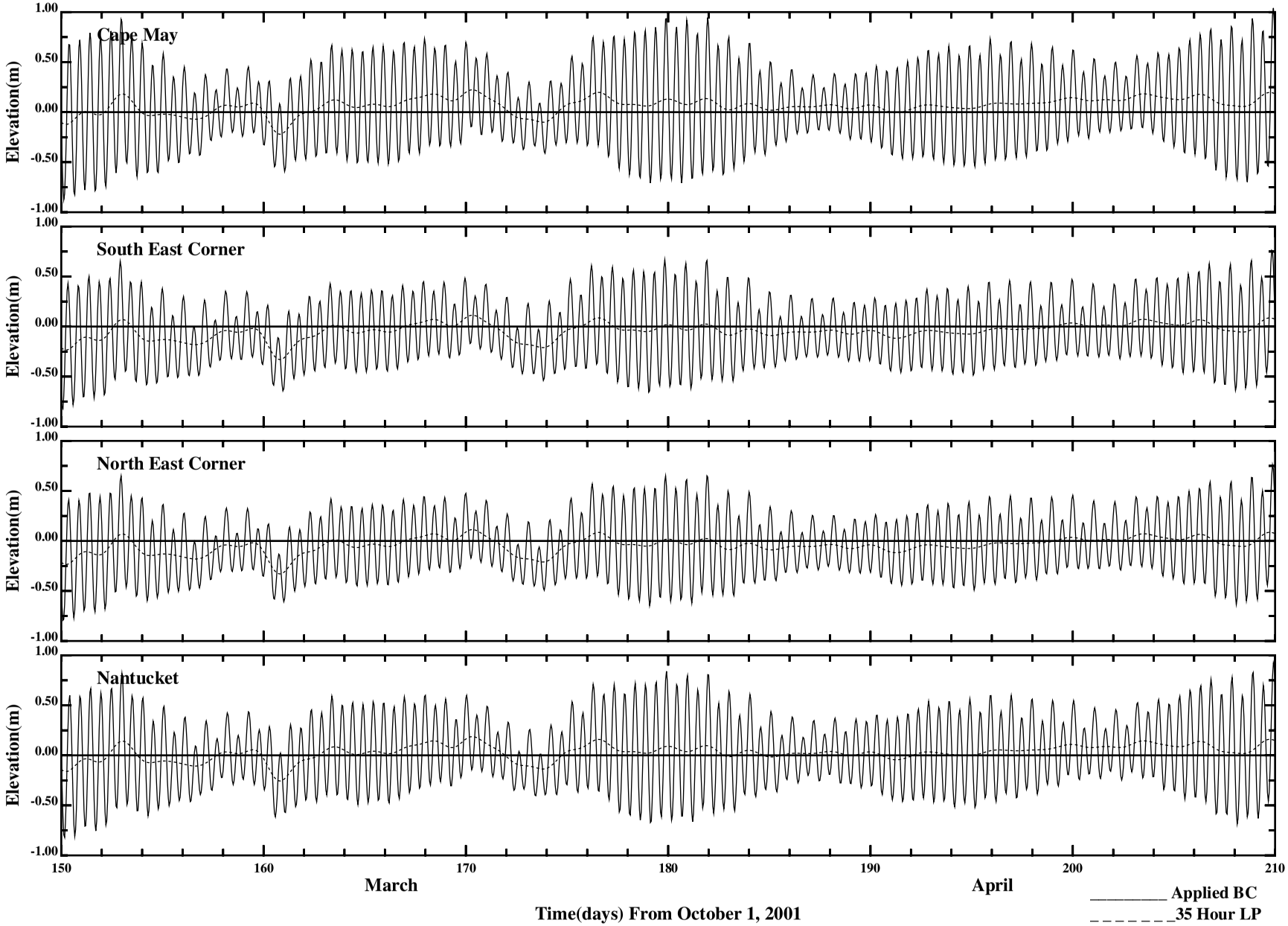

Figure 3-2d Elevation boundary conditions at four key locations in the New York Bight for March and April, 2002

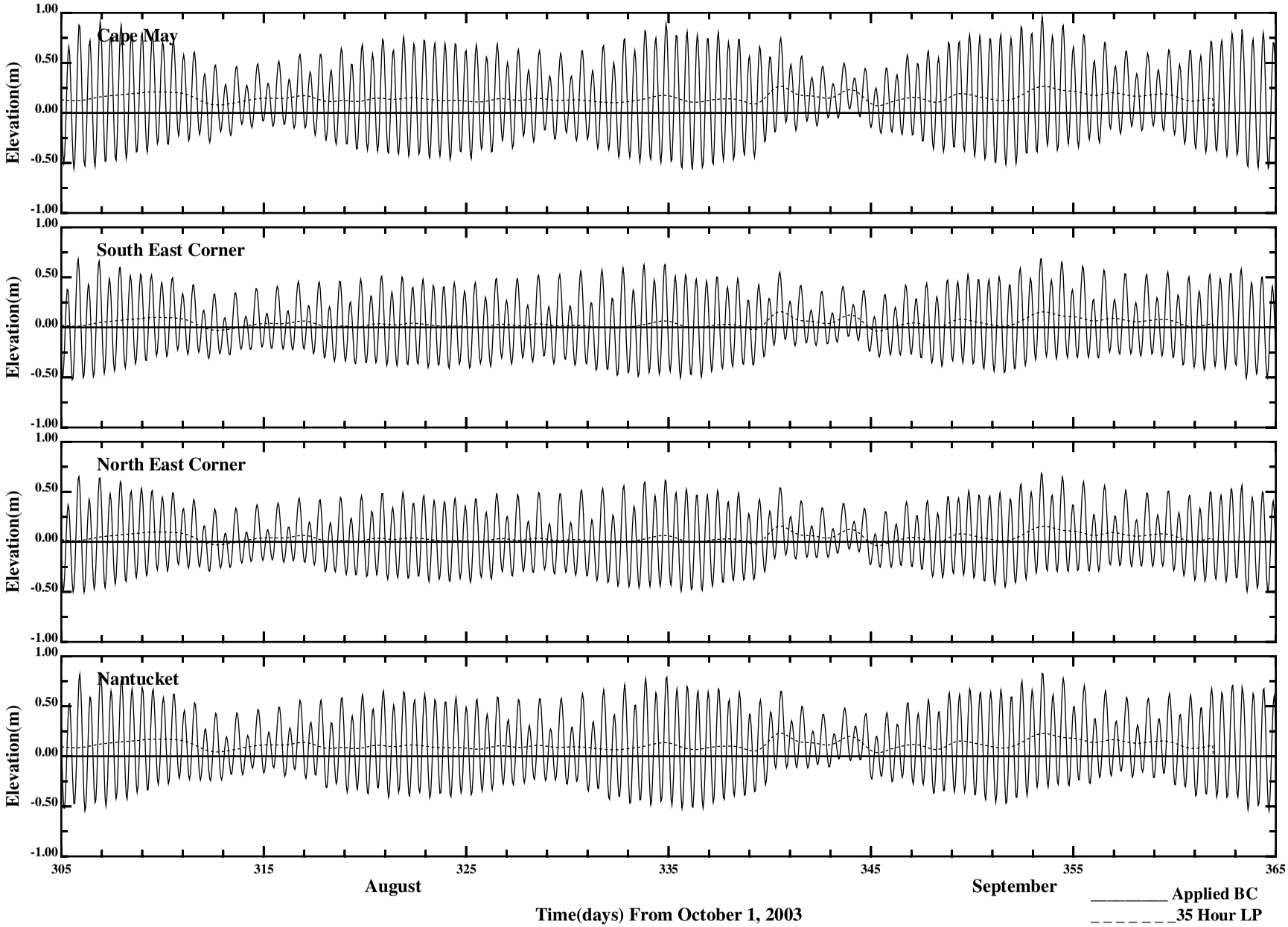

Figure 3-2e Elevation boundary conditions at four key locations in the New York Bight for August and September, 2004

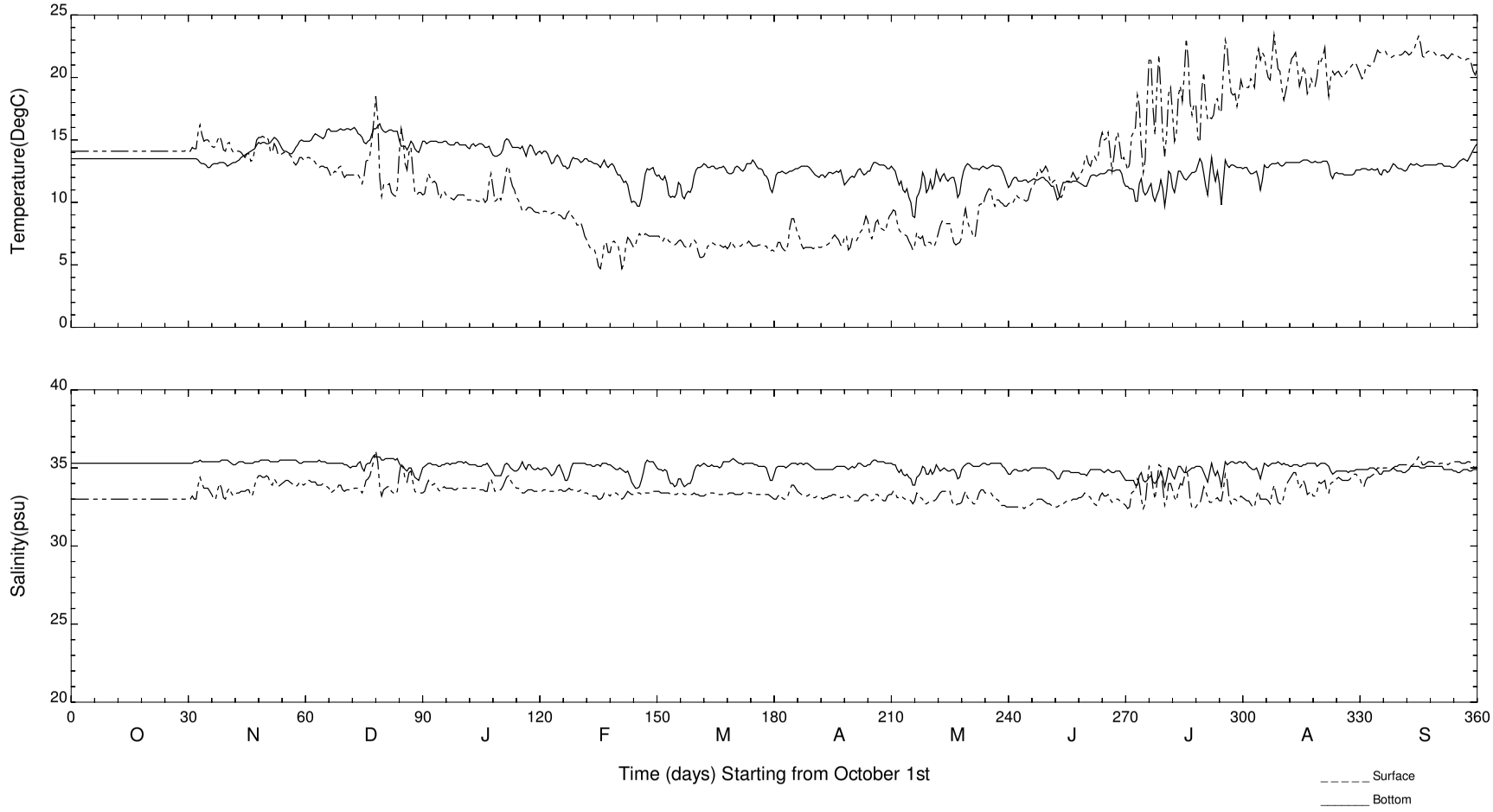

Figure 3-3 Temperature and salinity boundary conditions in the New York Bight (used for WY1995 simulation)

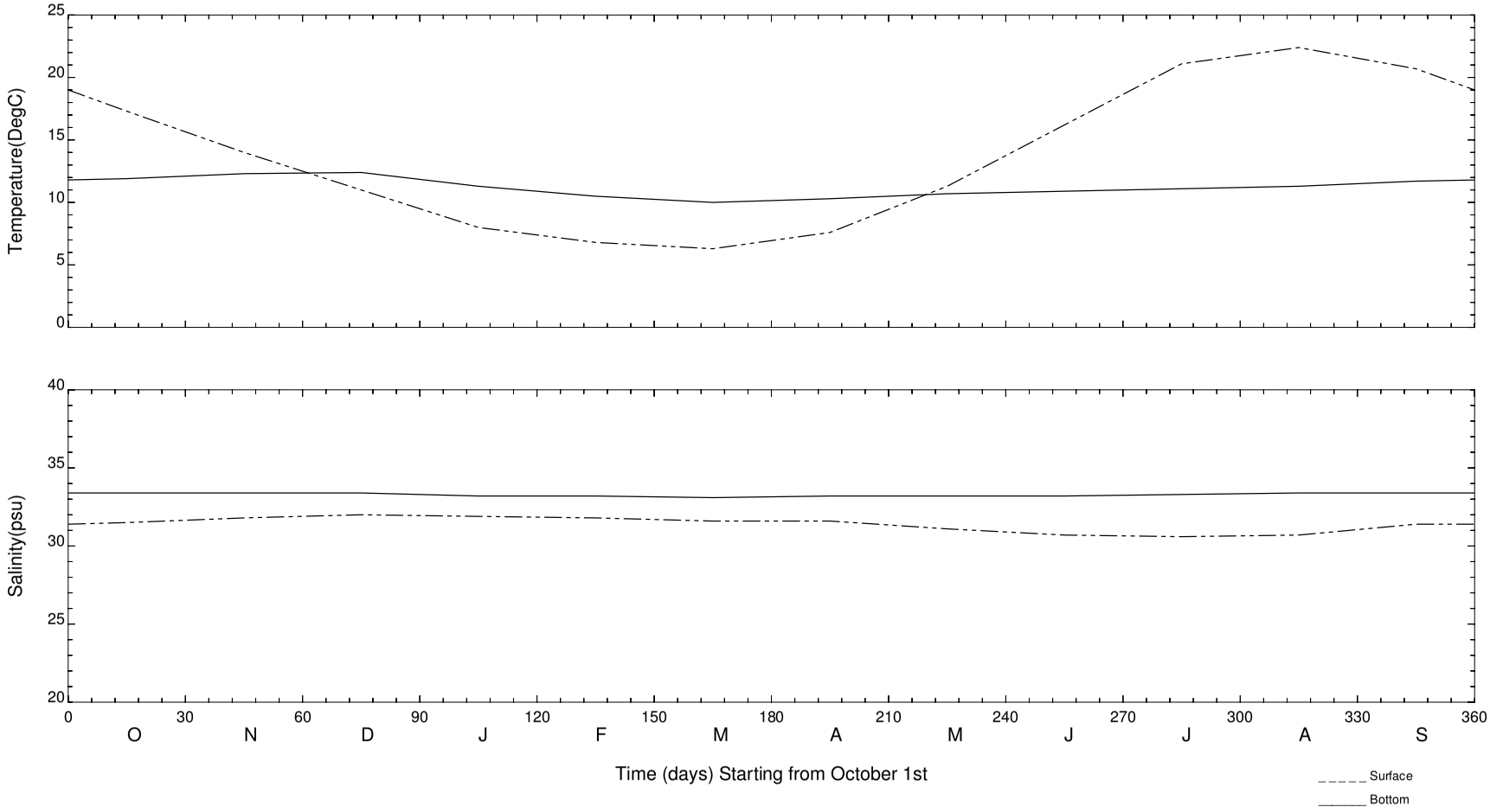

Figure 3-4 Temperature and salinity boundary conditions in the New York Bight using WOA98 database (used for WY1996 - 2004)

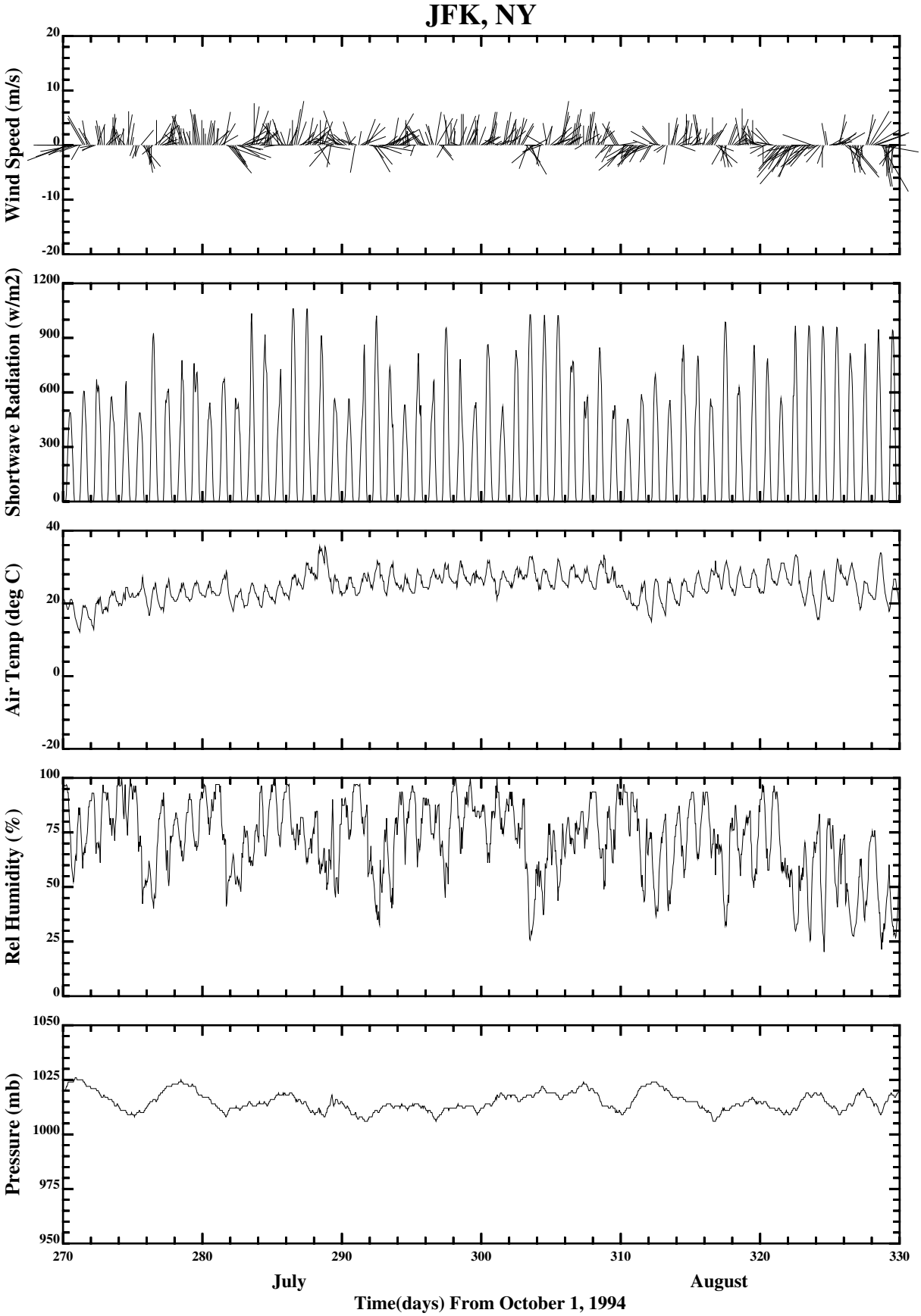

Figure 3-5a Meteorological data used for heat flux computations (data from JFK station) for July and August, 1995

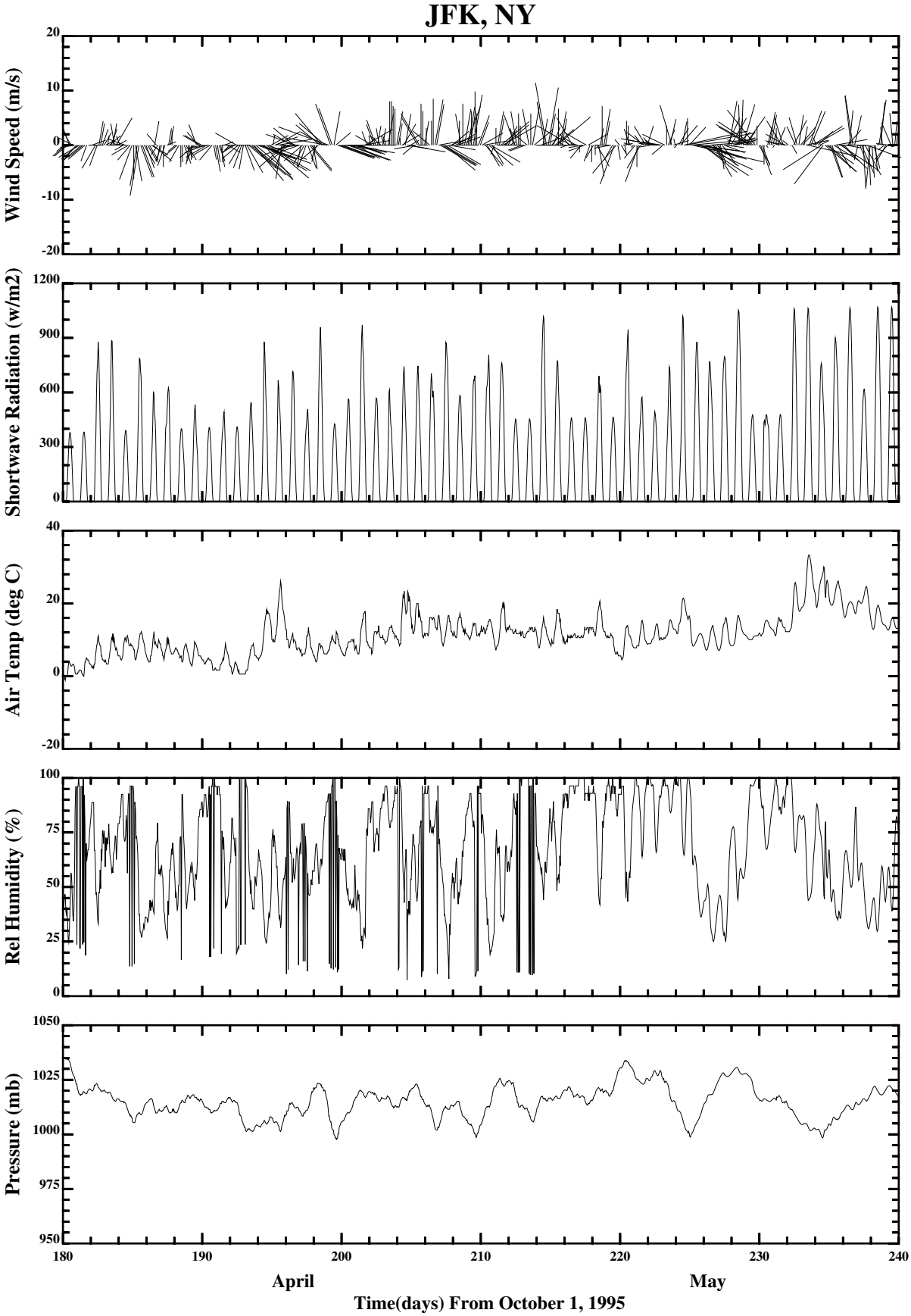

Figure 3-5b Meteorological data used for heat flux computations (data from JFK station) for April and May, 1996

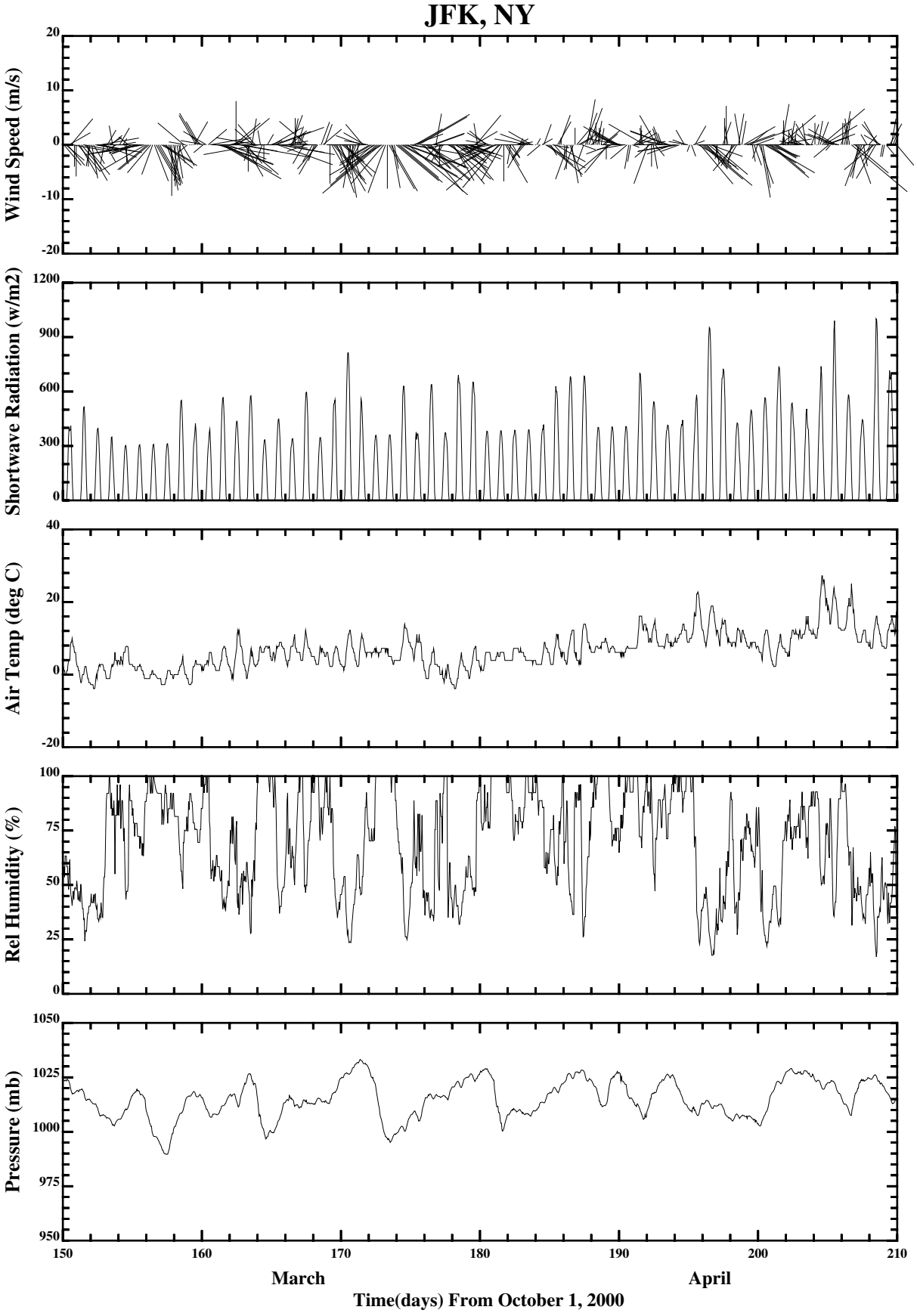

Figure 3-5c Meteorological data used for heat flux computations (data from JFK station) for March-August, 2001

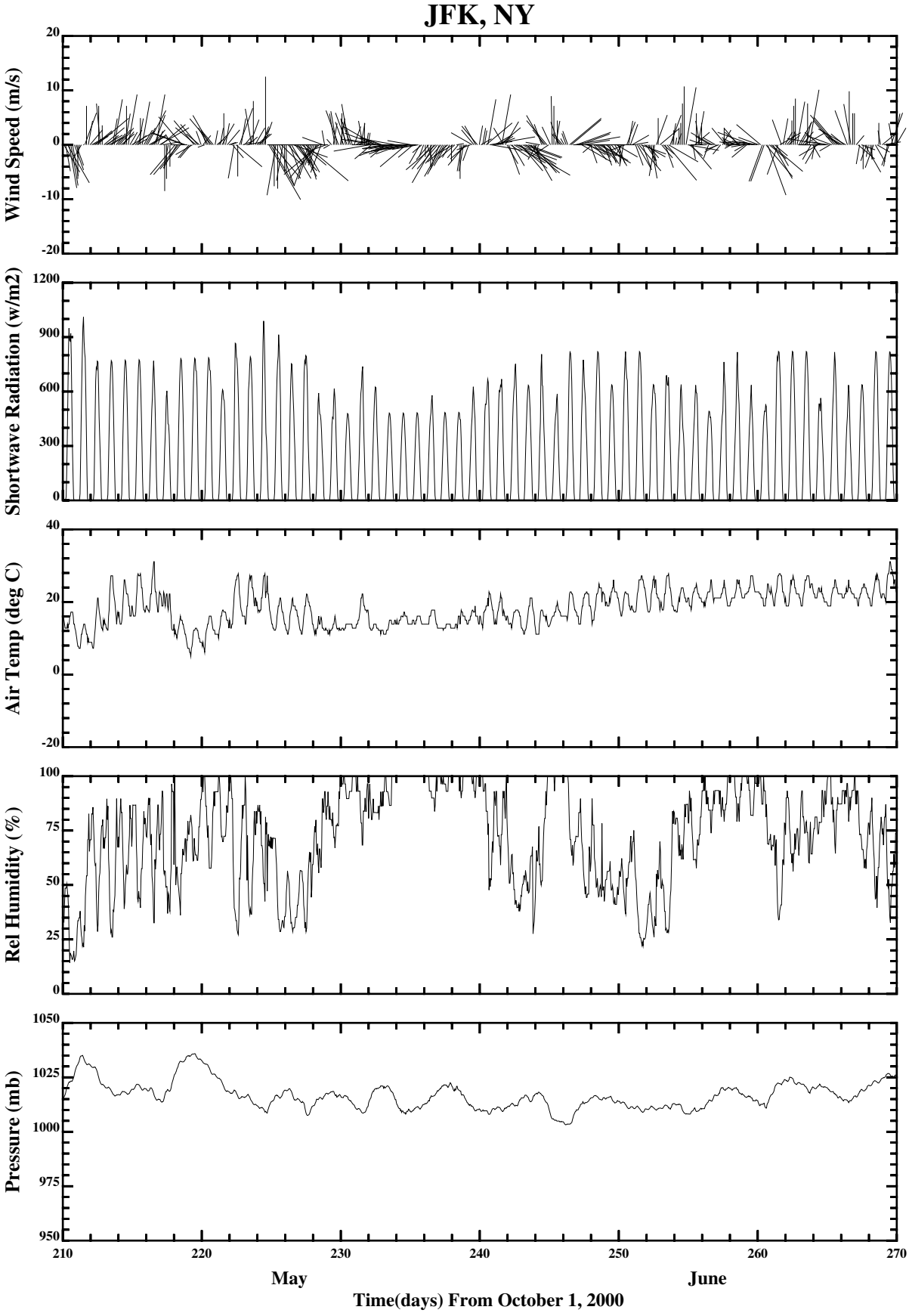

Figure 3-5c Meteorological data used for heat flux computations (data from JFK station) for March-August, 2001

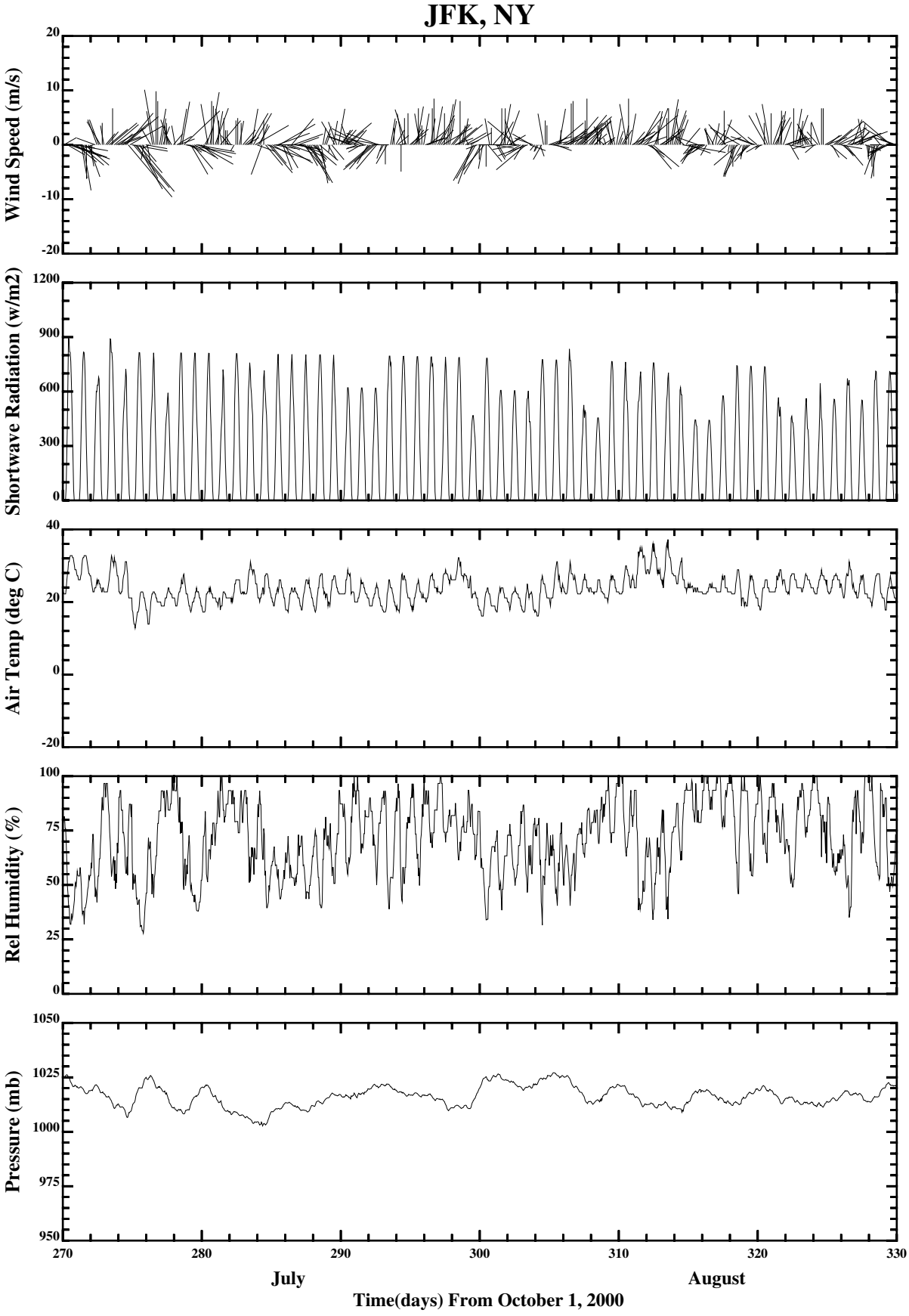

Figure 3-5c Meteorological data used for heat flux computations (data from JFK station) for March-August, 2001

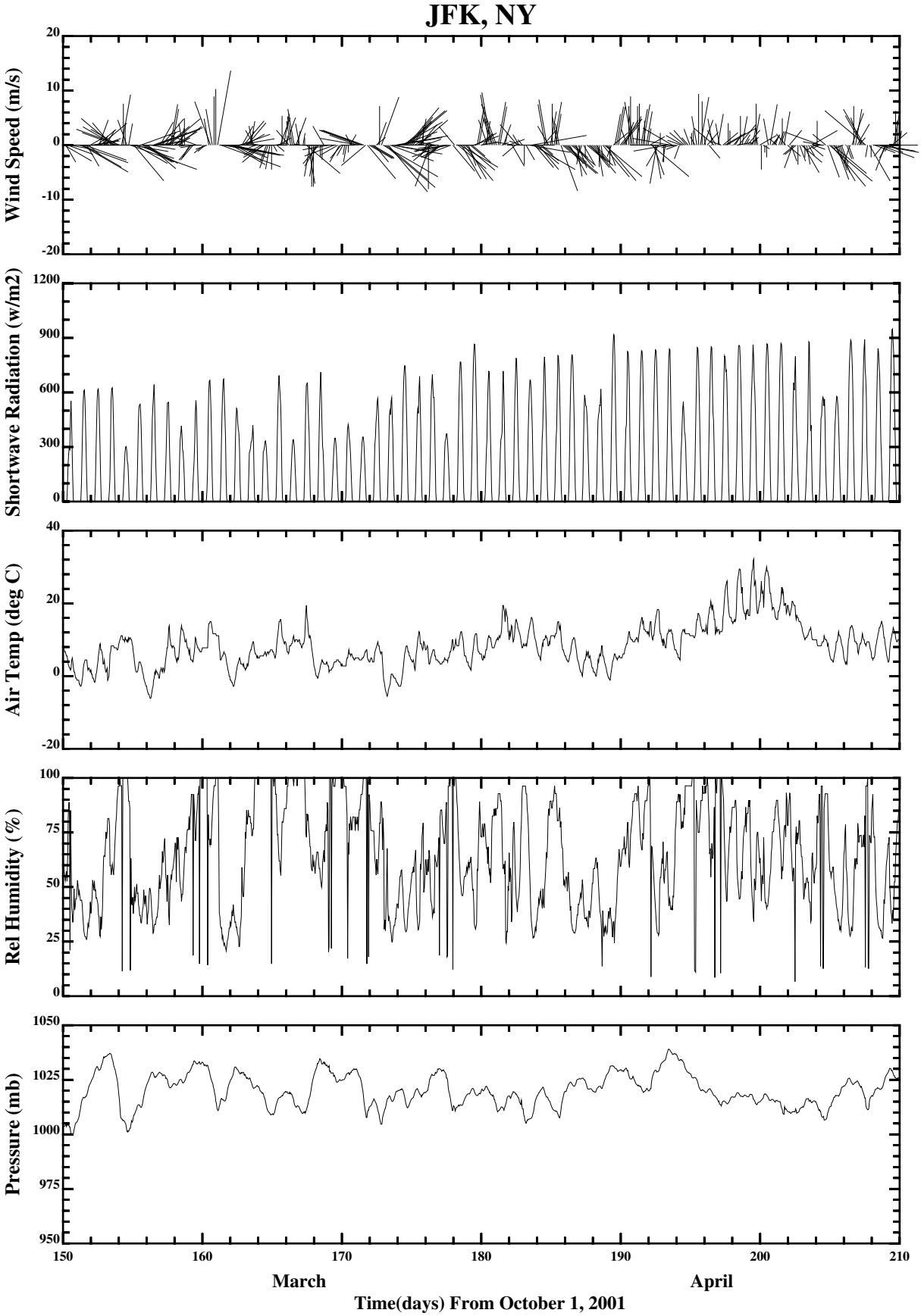

Figure 3-5d Meteorological data used for heat flux computations (data from JFK station) for March and April, 2002

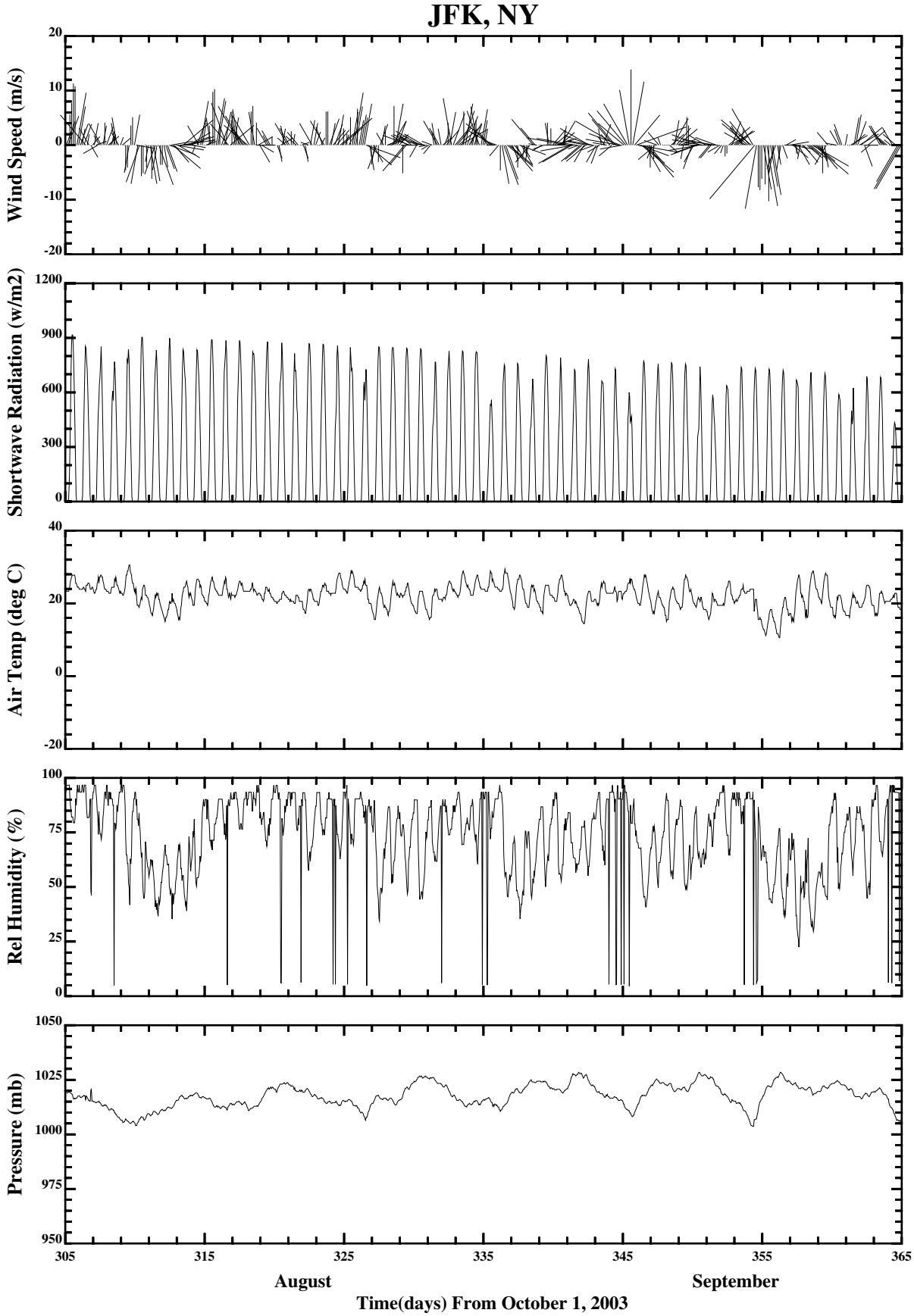

Figure 3-5e Meteorological data used for heat flux computations (data from JFK station)for August and September, 2004

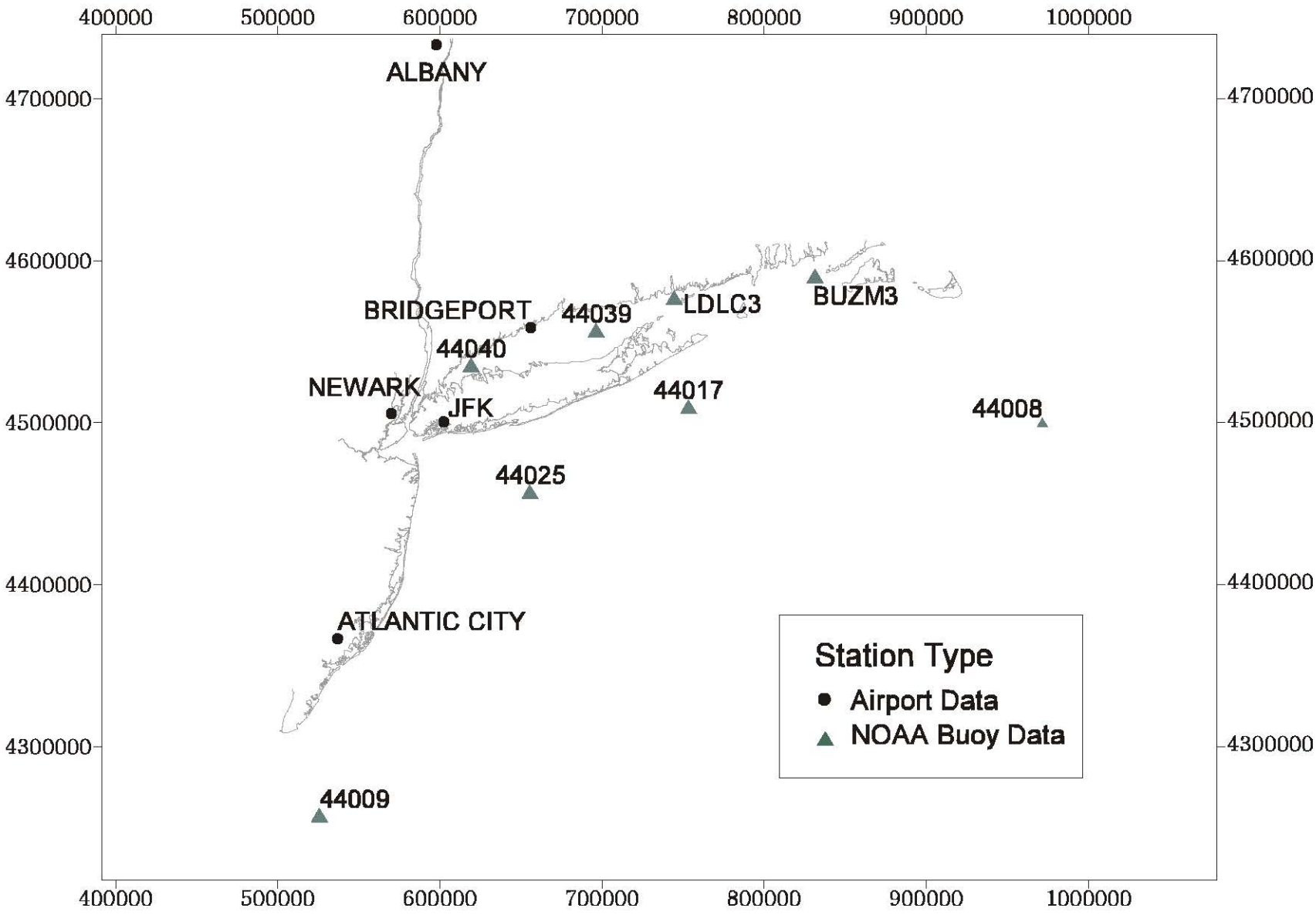

Figure 3-6 Location map of weather stations for wind stress computations

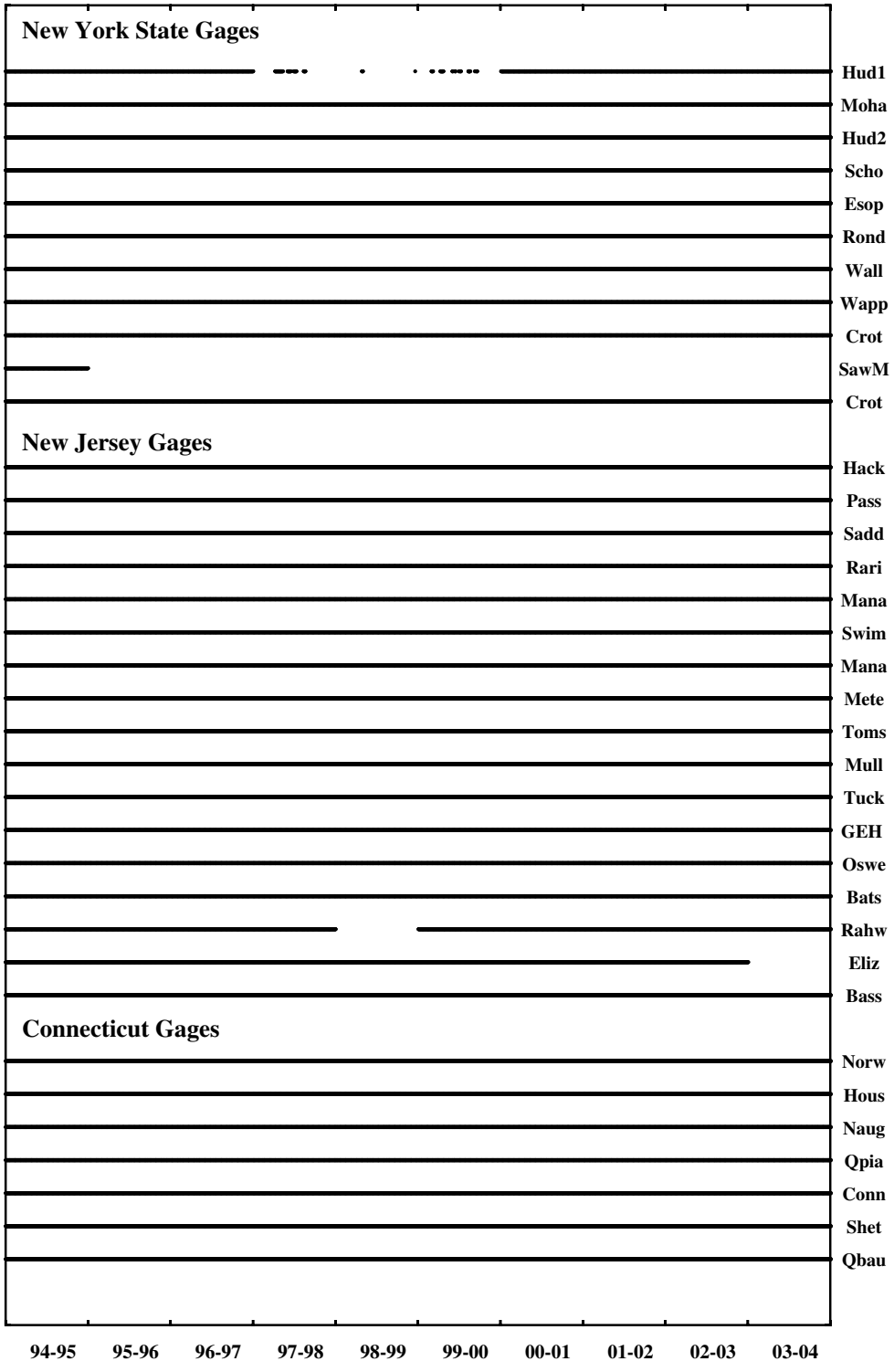

Figure 3-7 Timeline diagram showing available river discharge data used as model forcing

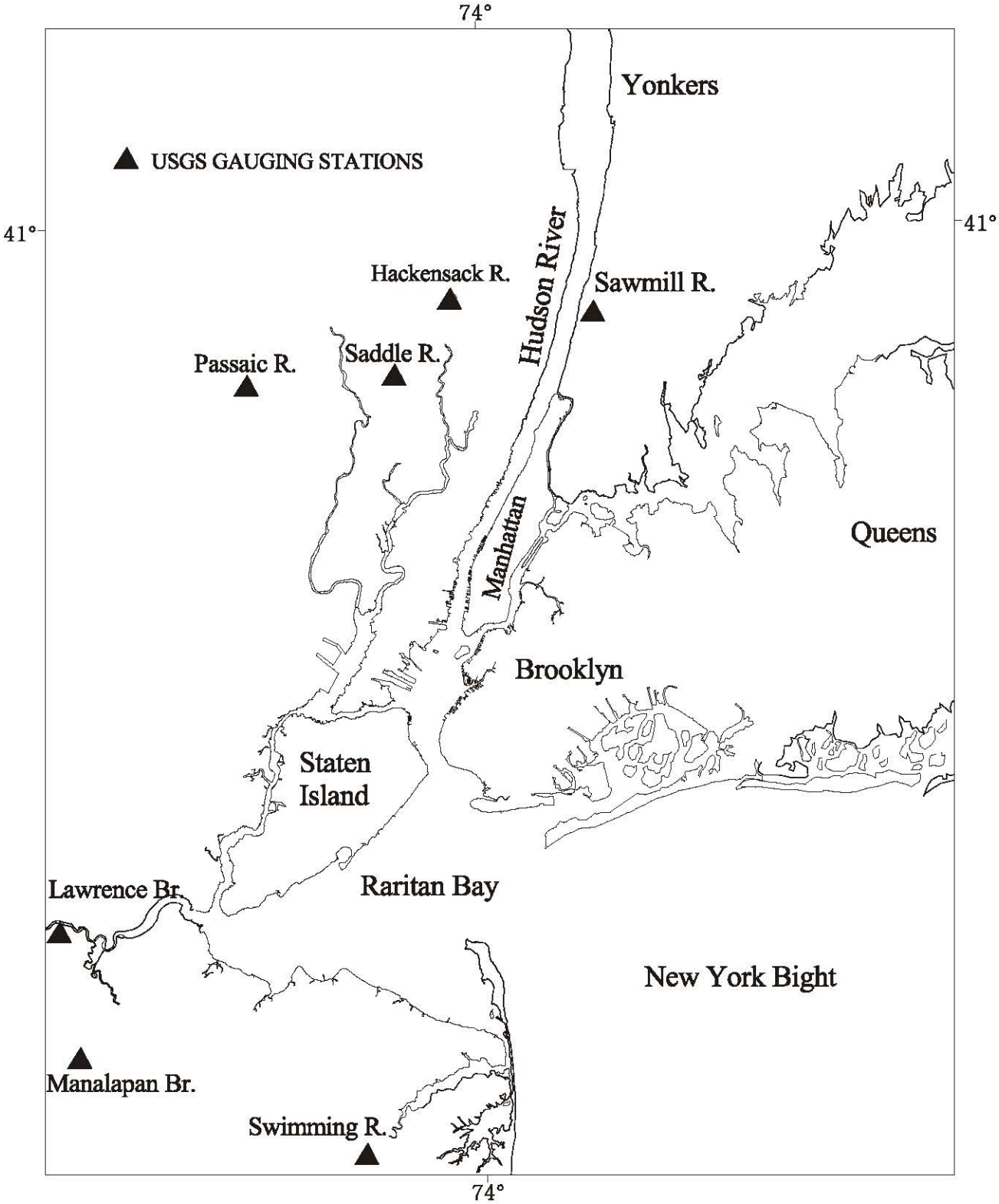

Figure 3-8a Location map of USGS surface water gauge stations in New York Harbor

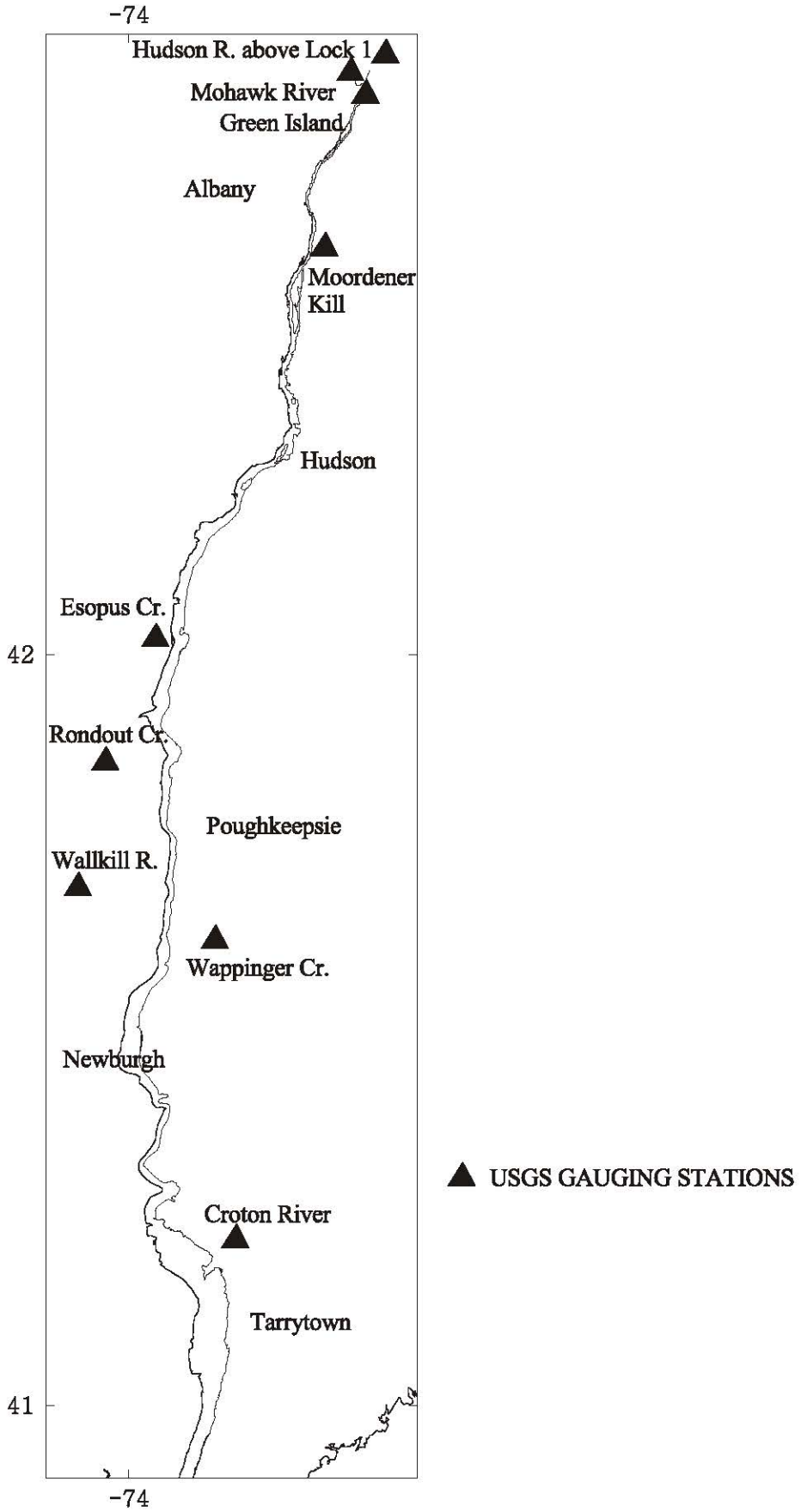

Figure 3-8b Location map of USGS surface water gauge stations in Hudson from Tarrytown to Green Island

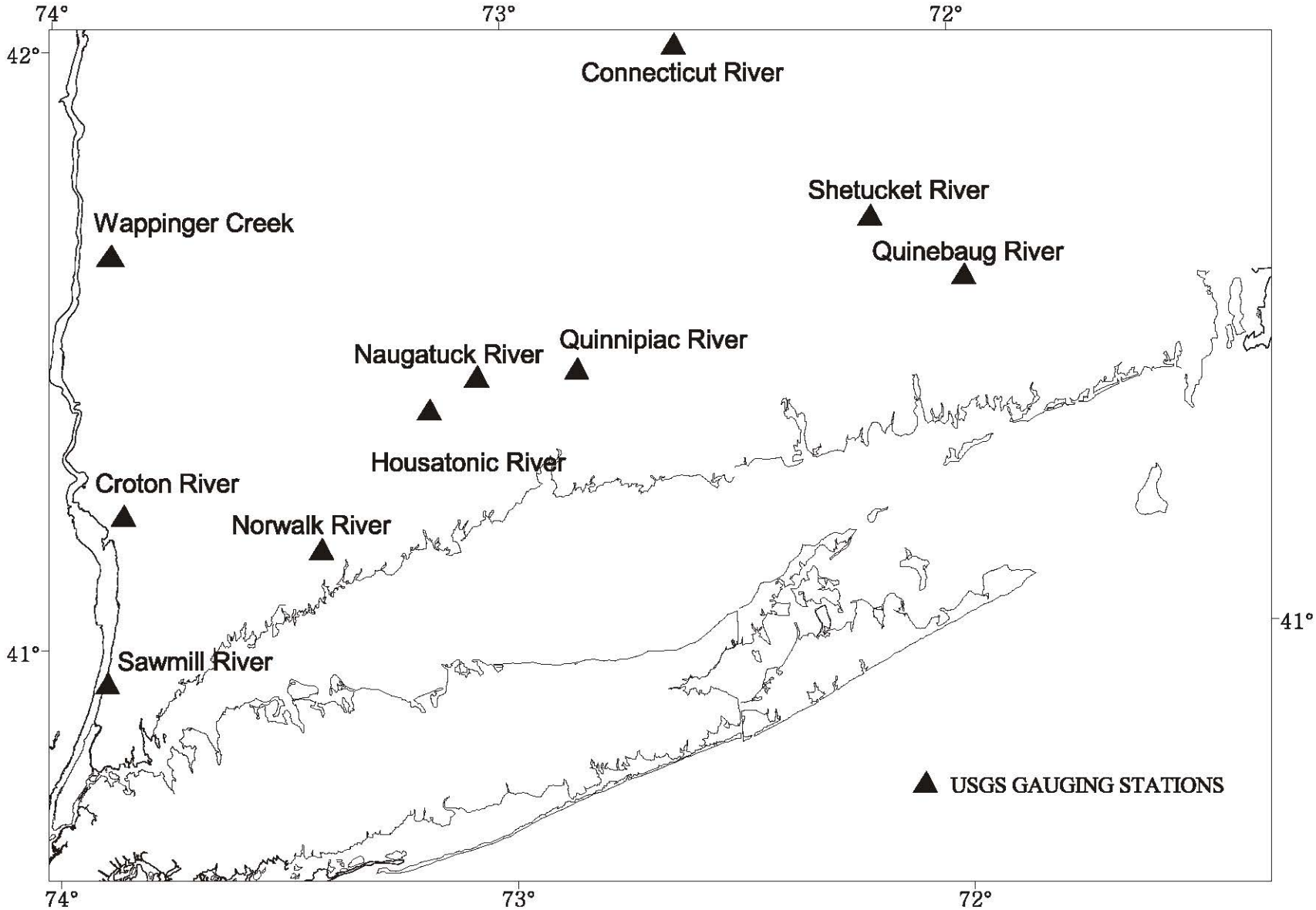

Figure 3-8c Location map of USGS surface water gauge stations in Connecticut

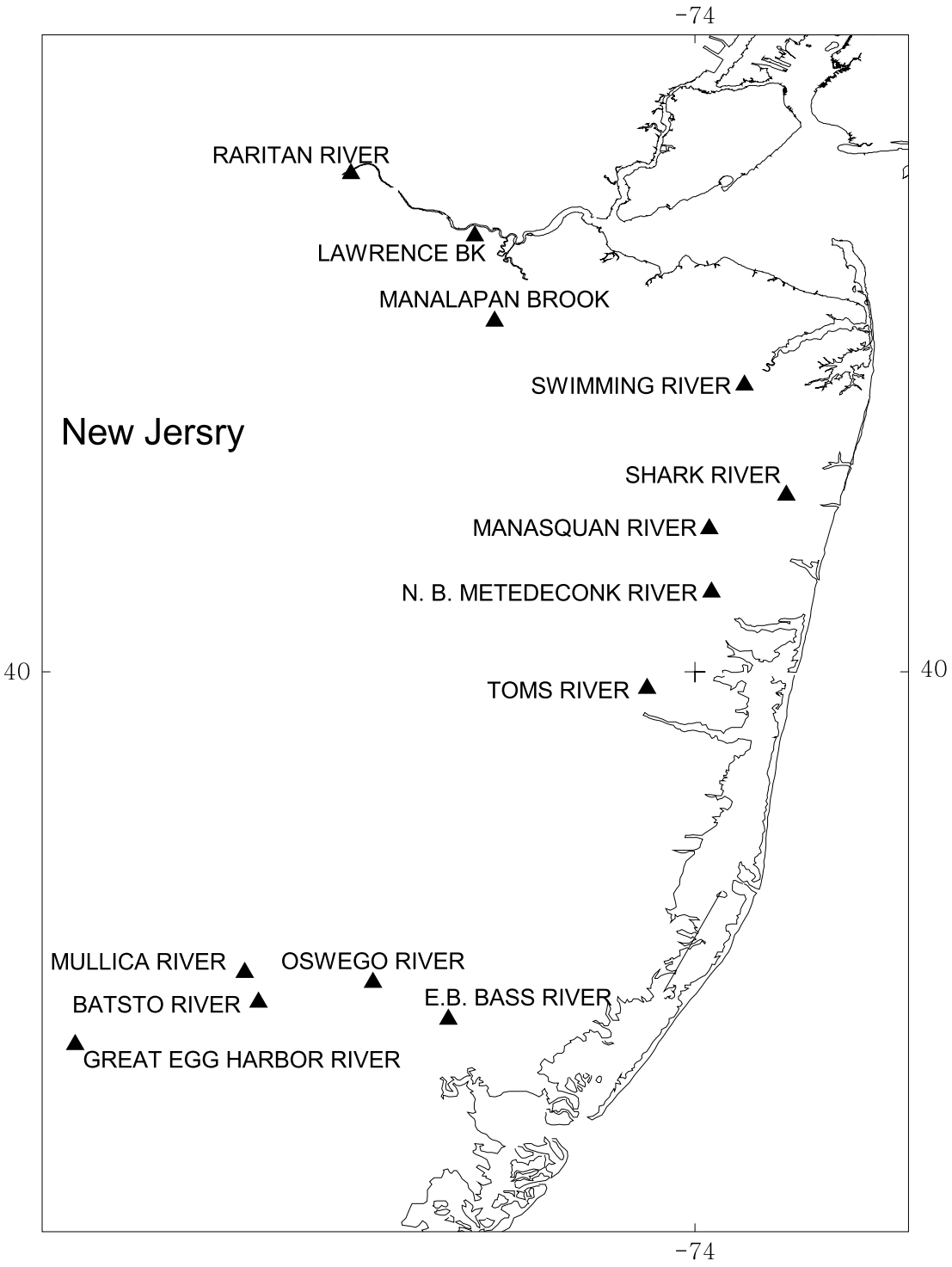

Figure 3-8d Location map of USGS surface water gauge stations in NJ

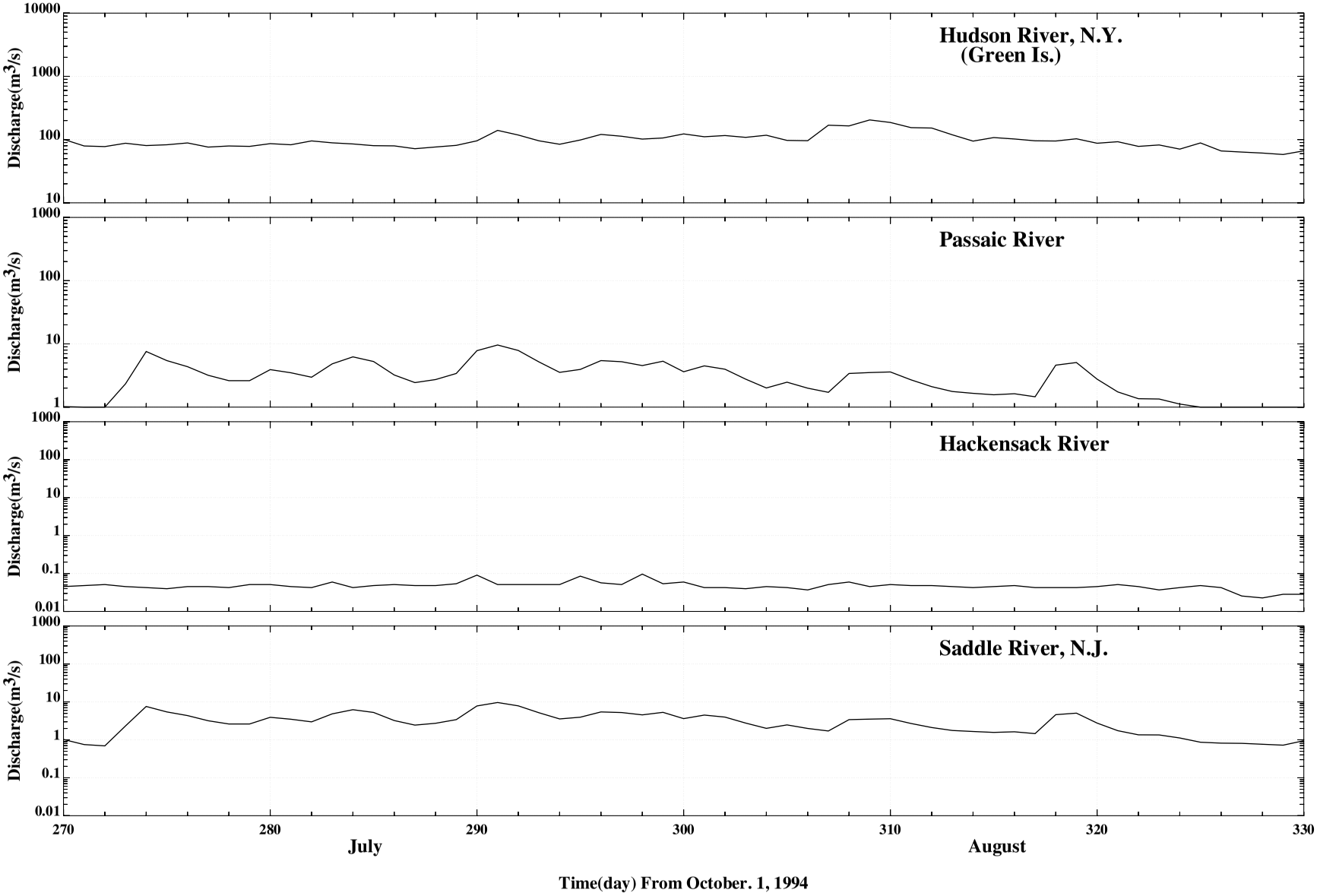

Figure 3-9a Temporal variations of river inflows into the model domain from the Hudson, Passaic, Hackensack, and Saddle Rivers for July and August, 1995

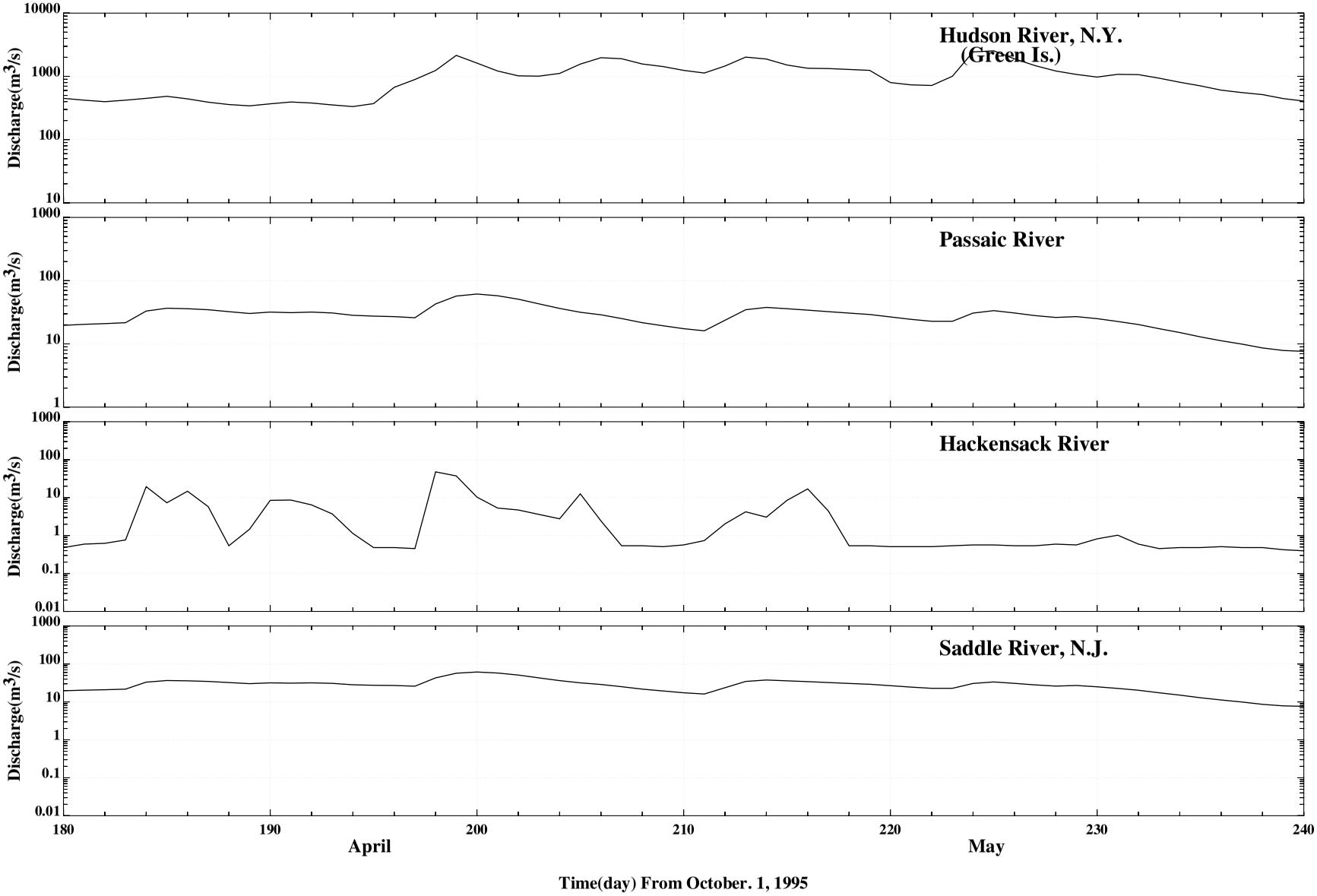

Figure 3-9b Temporal variations of river inflows into the model domain from the Hudson, Passaic, Hackensack, and Saddle Rivers for April and May, 1996

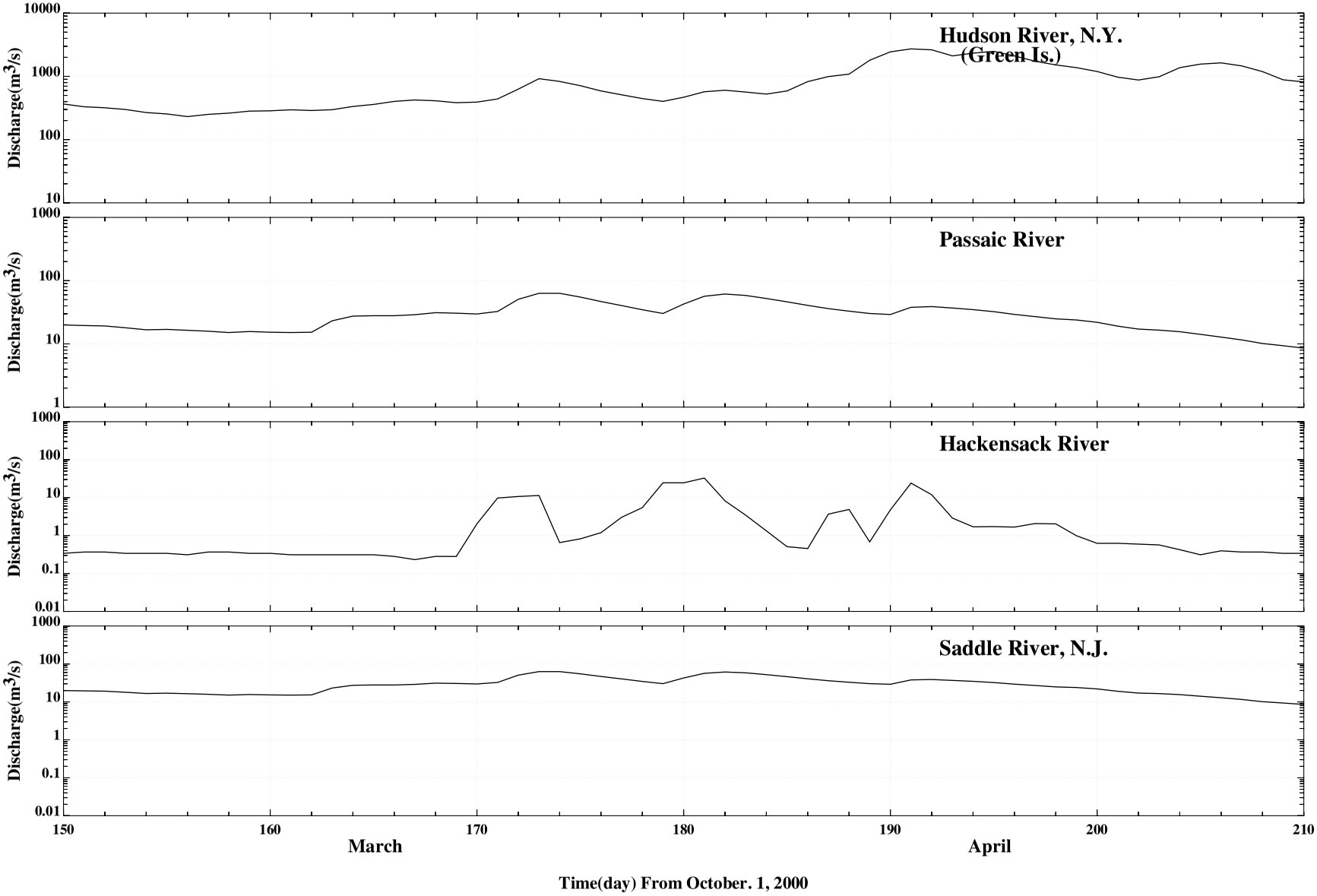

Figure 3-9c Temporal variations of river inflows into the model domain from the Hudson, Passaic, Hackensack, and Saddle Rivers for March-August, 2001

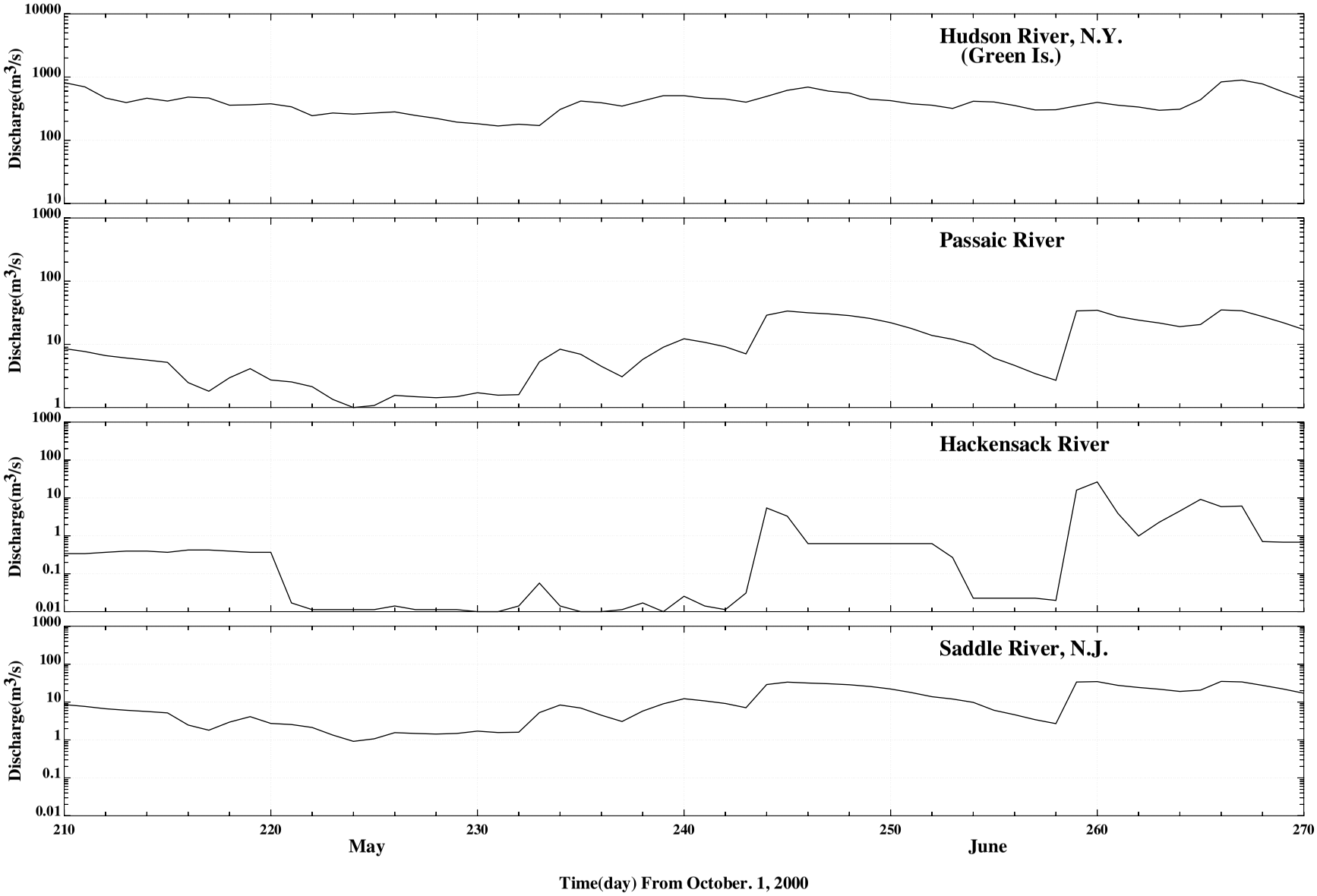

Figure 3-9c Temporal variations of river inflows into the model domain from the Hudson, Passaic, Hackensack, and Saddle Rivers for March- August, 2001 (continued)

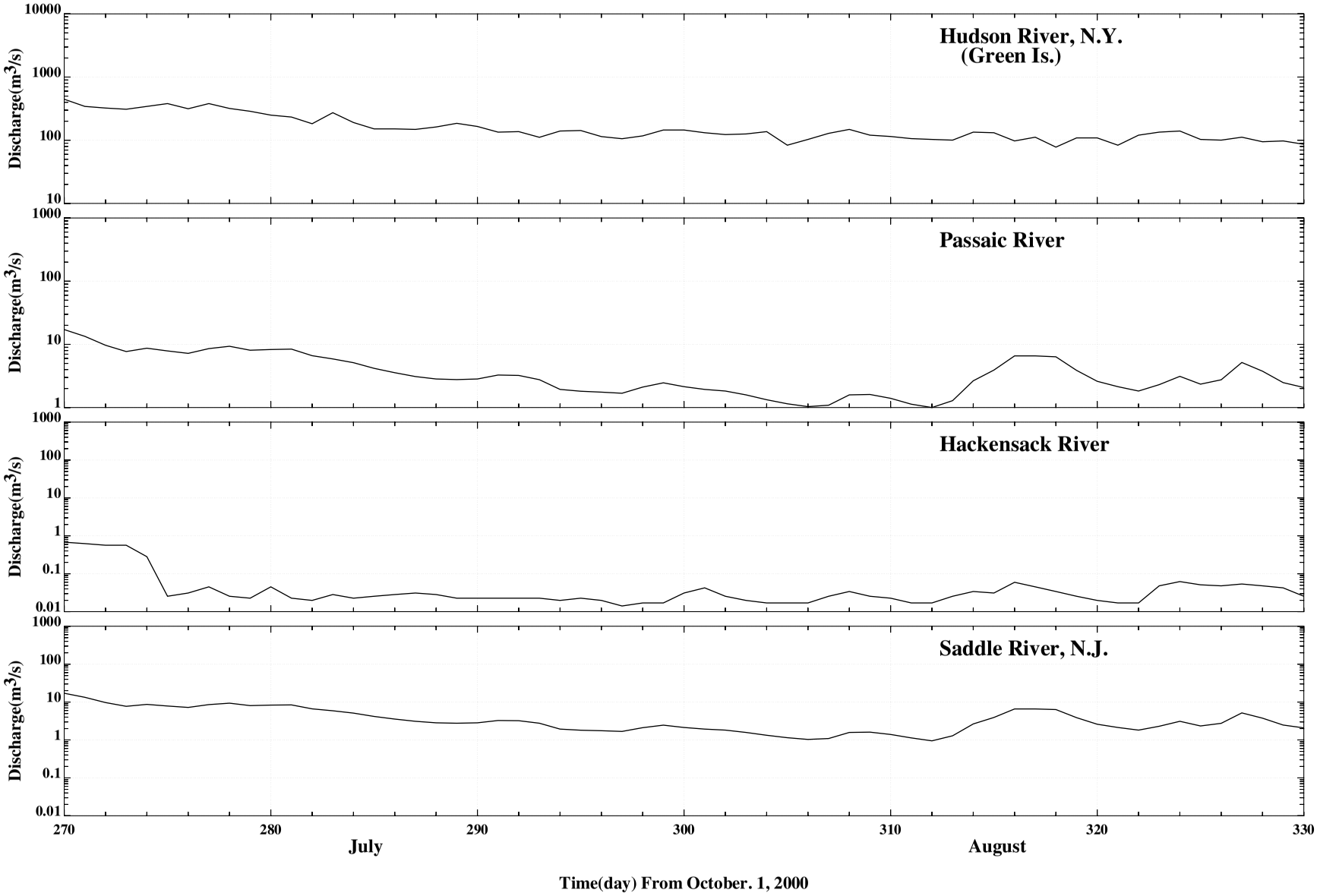

Figure 3-9c Temporal variations of river inflows into the model domain from the Hudson, Passaic, Hackensack, and Saddle Rivers for March- August, 2001 (continued)

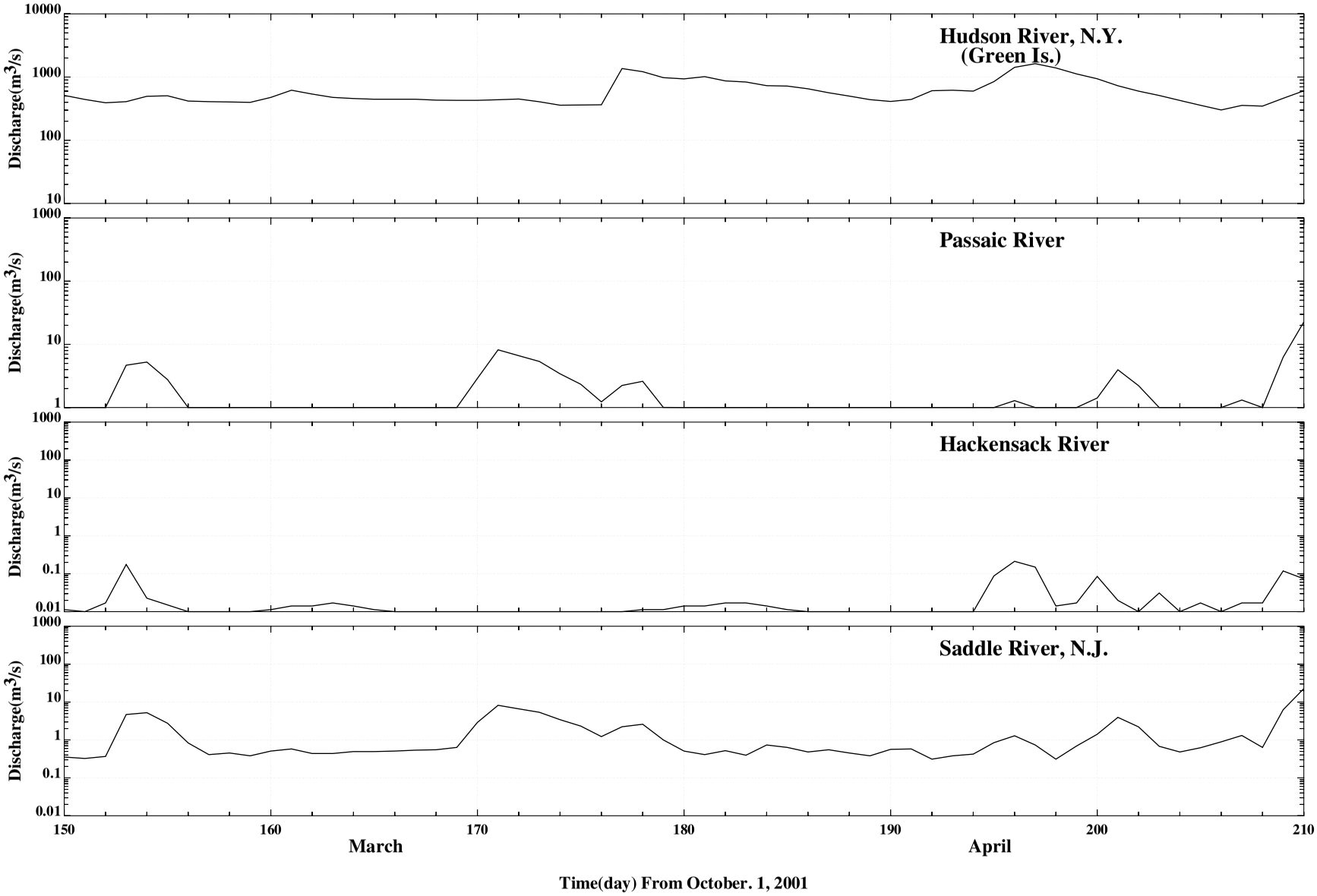

Figure 3-9d Temporal variations of river inflows into the model domain from the Hudson, Passaic, Hackensack, and Saddle Rivers for March and April, 2002

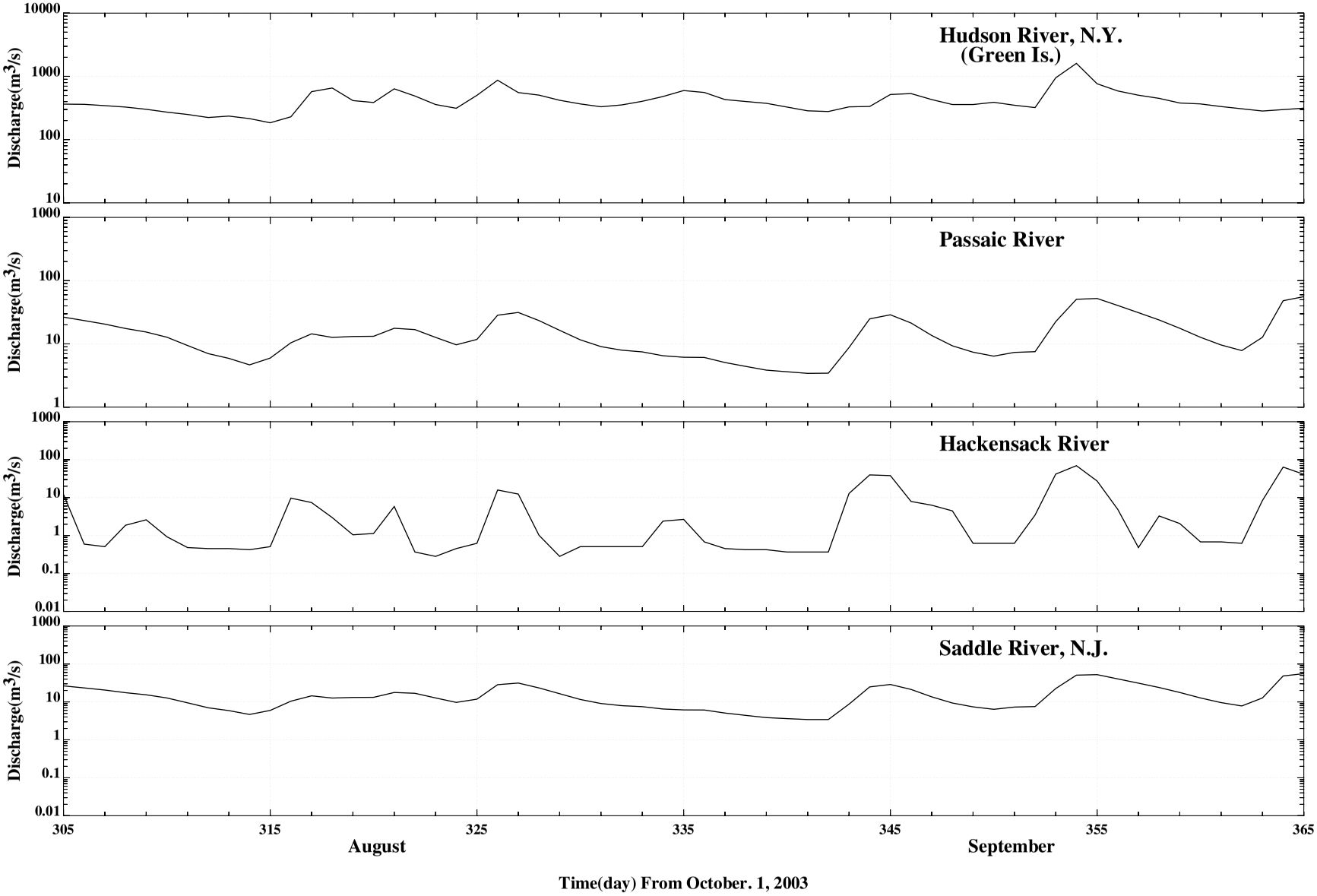

Figure 3-9e Temporal variations of river inflows into the model domain from the Hudson, Passaic, Hackensack, and Saddle Rivers for August and September, 2004

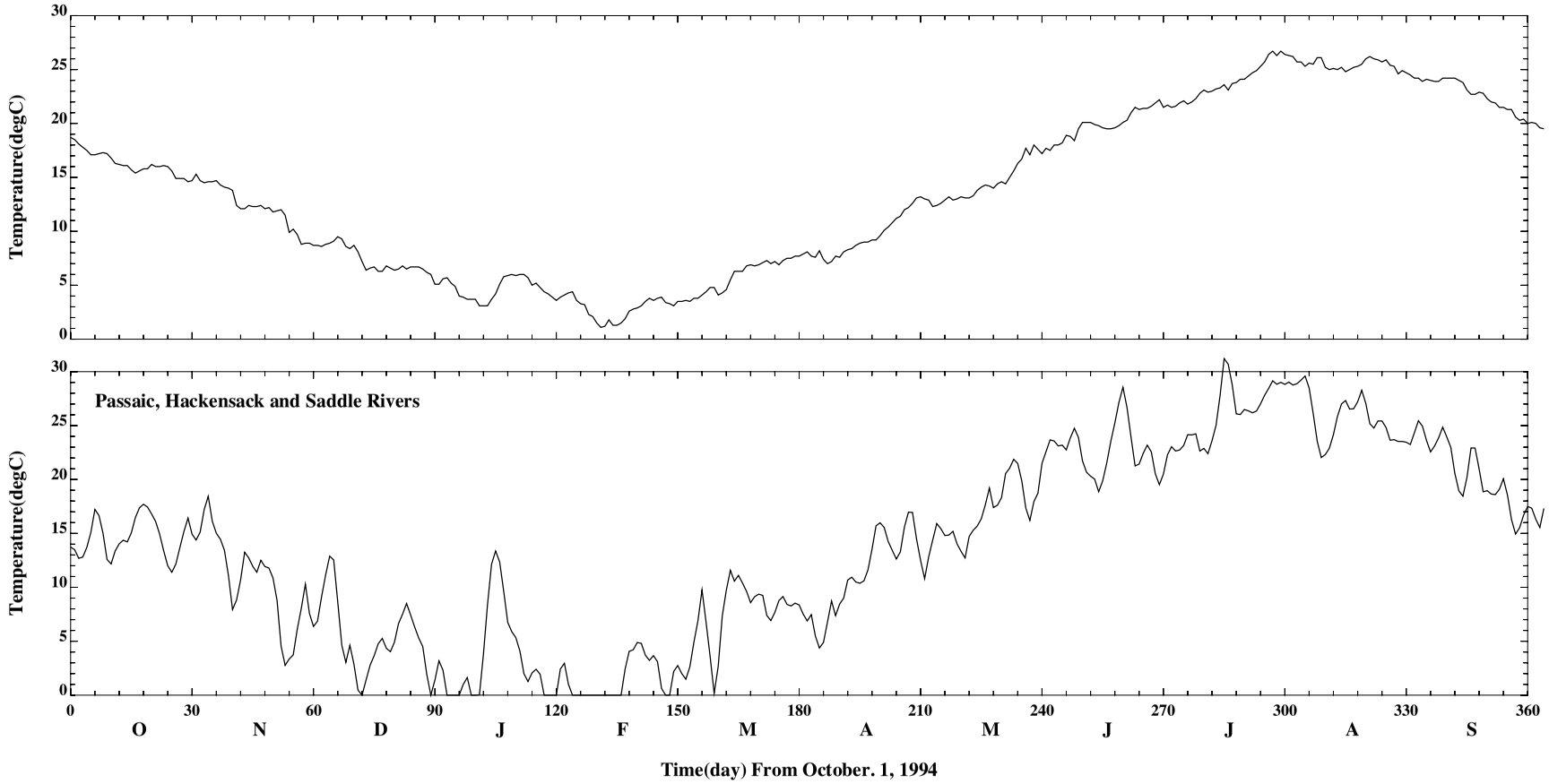

Figure 3-10 Temporal variation of river water temperature based on Ashizawa and Cole (1994) (upper panel) and 3 day moving average air temperature from Newark Airport (lower panel)

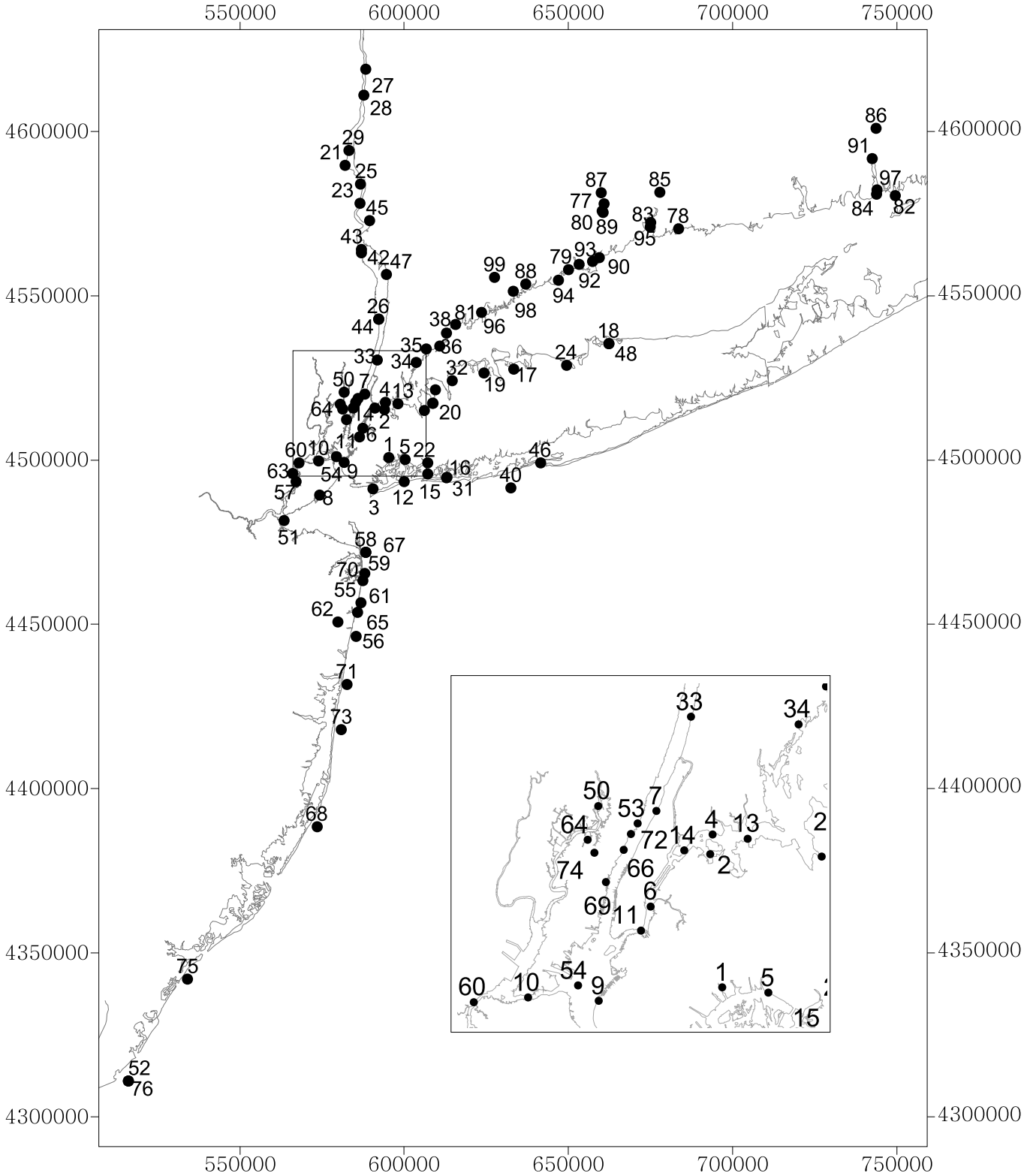

Figure 3-11 Location map of wastewater treatment plants in the model domain

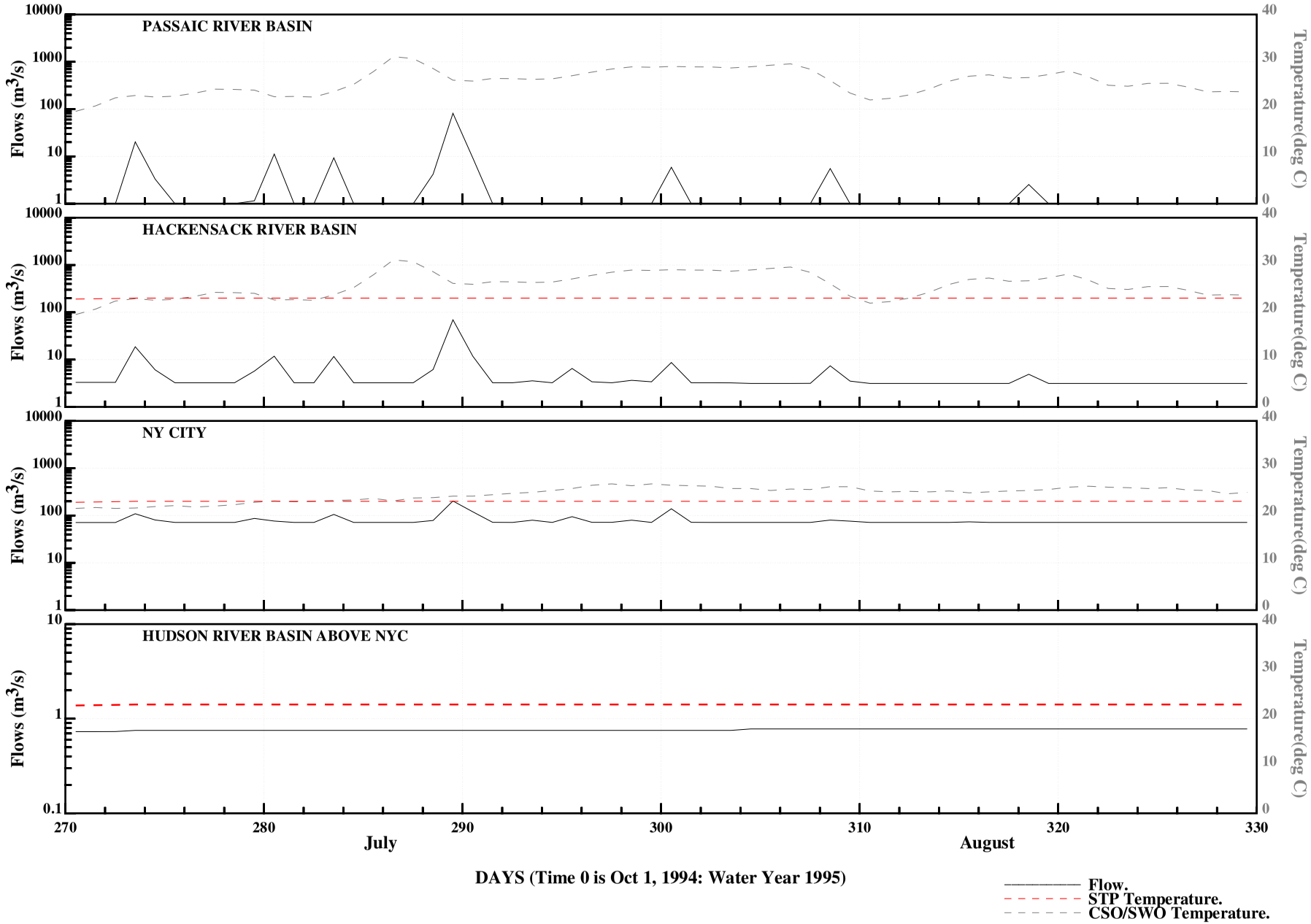

Figure 3-12a Temporal variations of wastewater inflows compiled by major areas (black lines) during July and August, 1995. Also shown are CSO/SWO water temperature (gray dotted lines) and STP inflow temperature (red lines), water year 1995

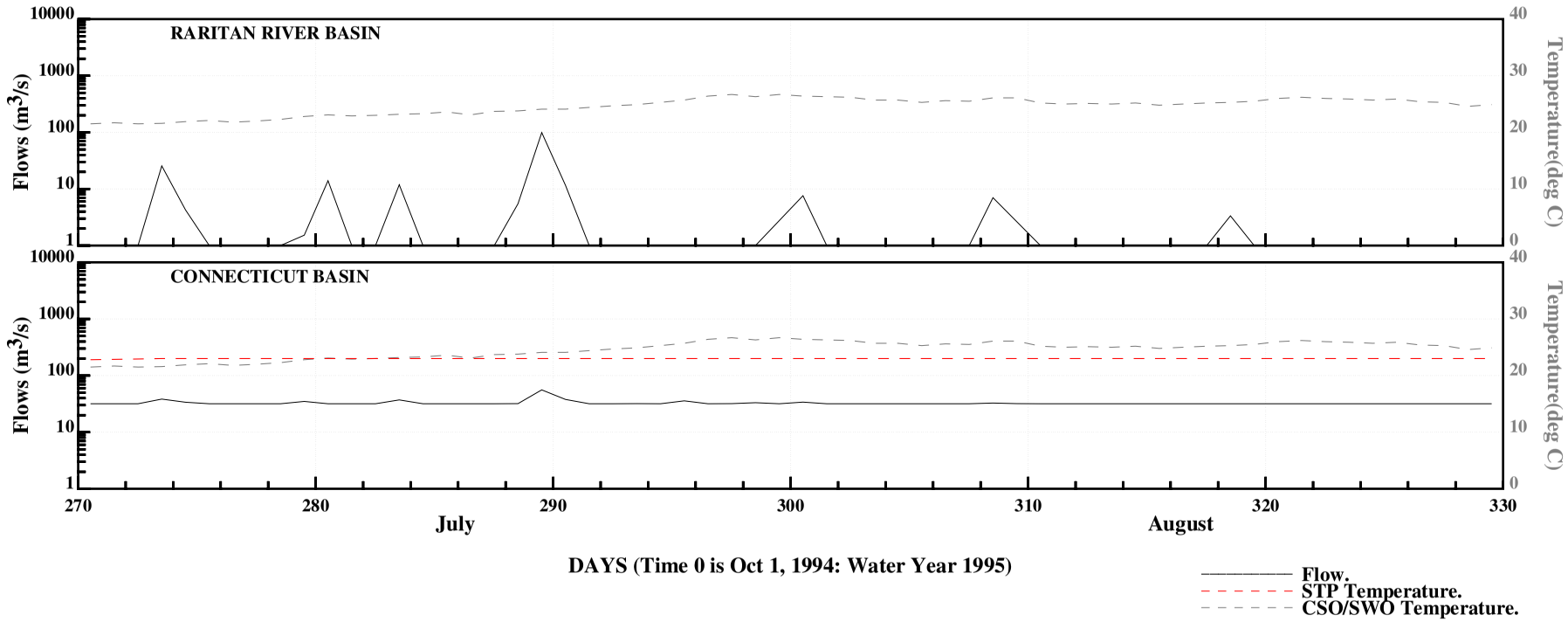

Figure 3-12a Temporal variations of wastewater inflows compiled by major areas (black lines) during July and August, 1995. Also shown are CSO/SWO water temperature (gray dotted lines) and STP inflow temperature (red lines), water year 1995 (Continued)

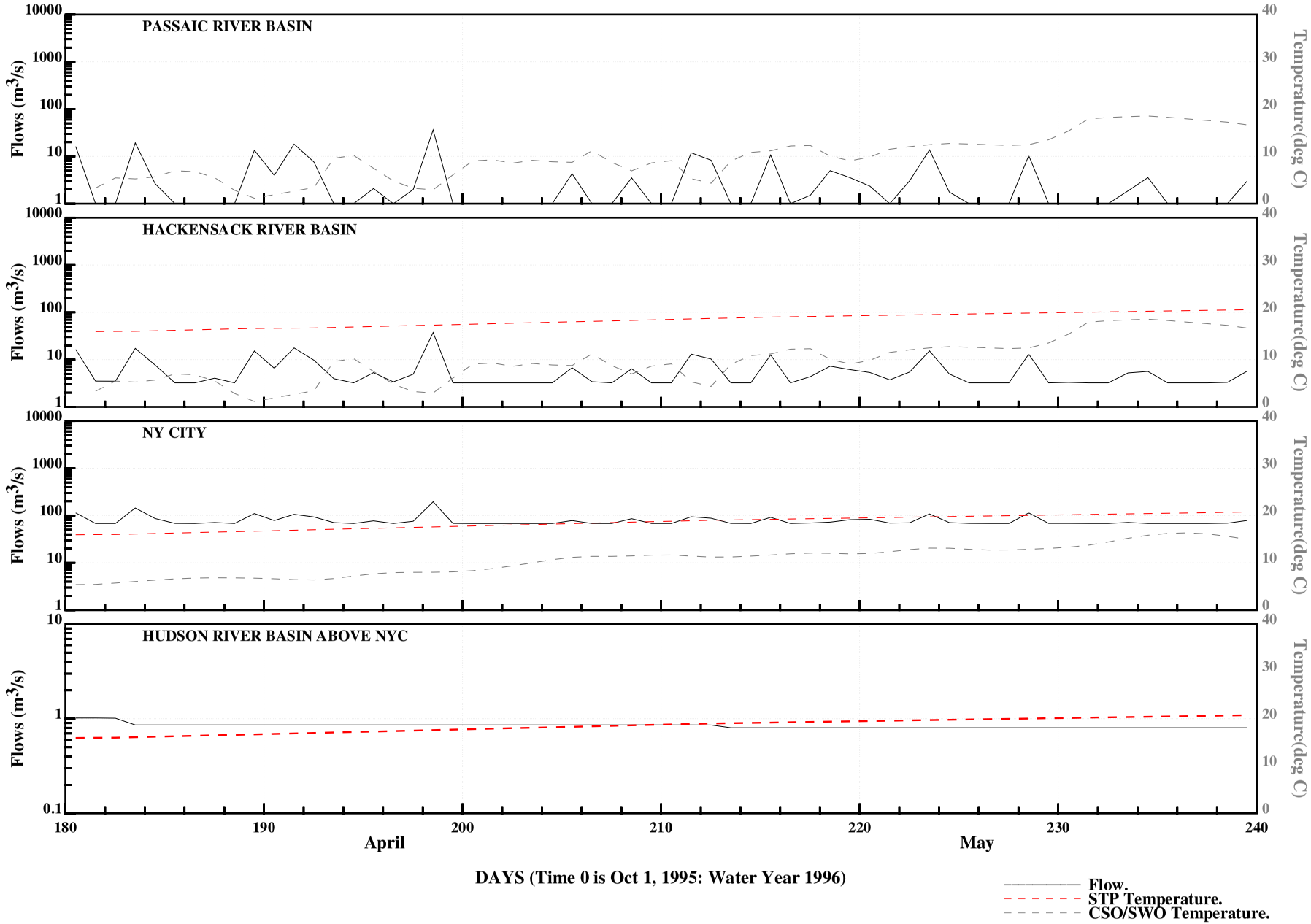

Figure 3-12b Temporal variations of wastewater inflows compiled by major areas (black lines) during April and May, 1996. Also shown are CSO/SWO water temperature (gray dotted lines) and STP inflow temperature (red lines), water year 1996

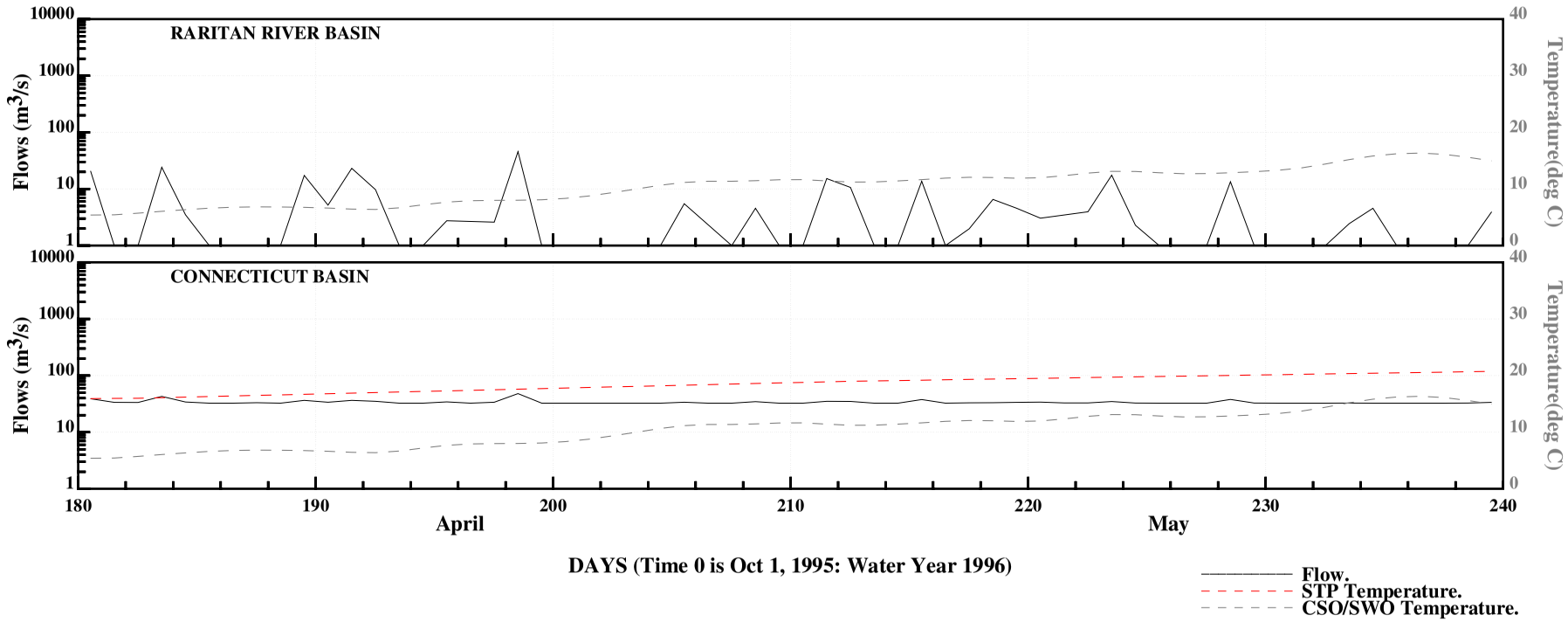

Figure 3-12b Temporal variations of wastewater inflows compiled by major areas (black lines) during April and May, 1996. Also shown are CSO/SWO water temperature (gray dotted lines) and STP inflow temperature (red lines), water year 1996 (Continued)

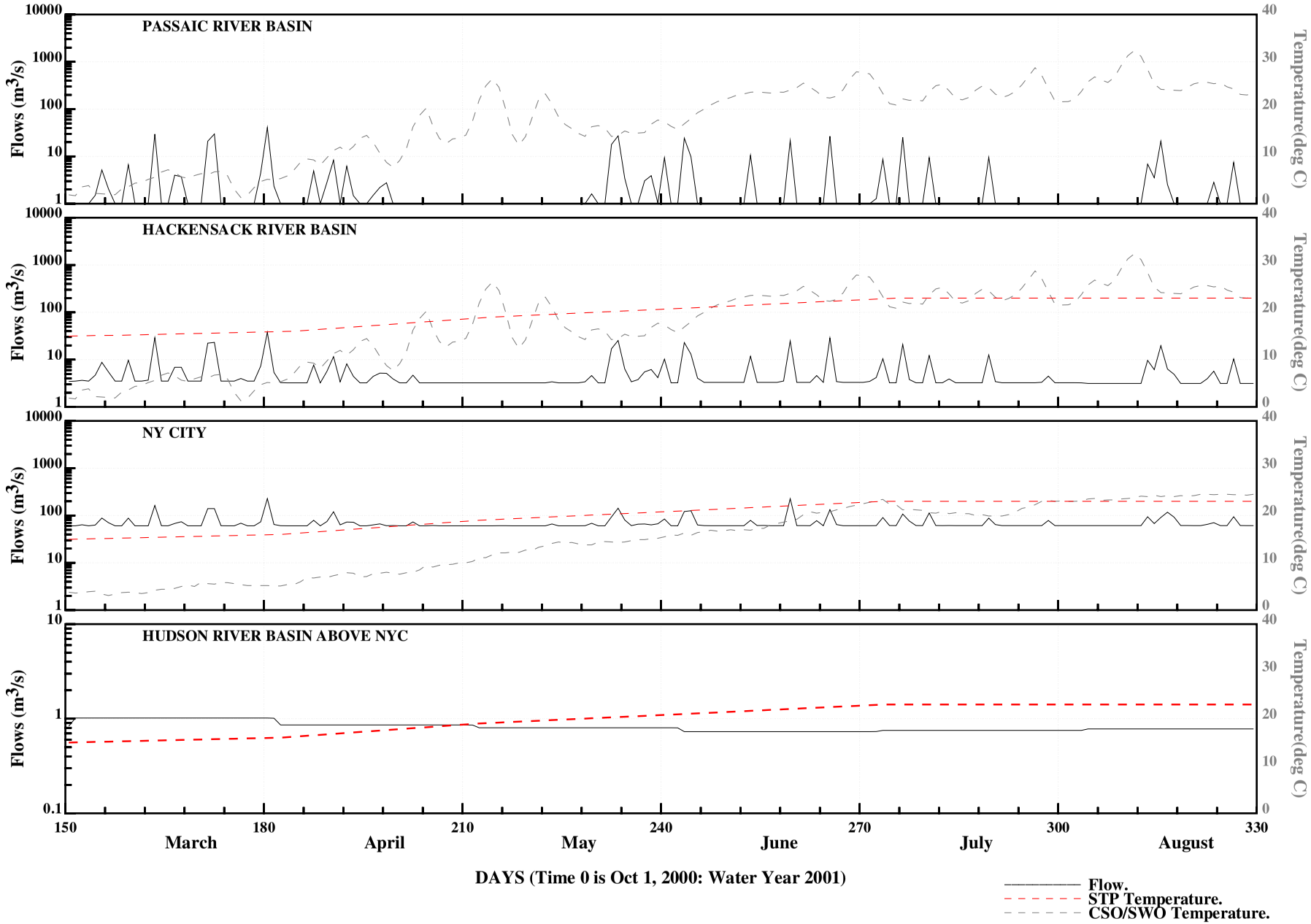

Figure 3-12c Temporal variations of wastewater inflows compiled by major areas (black lines) during March-August, 2001. Also shown are CSO/SWO water temperature (gray dotted lines) and STP inflow temperature (red lines), water year 2001

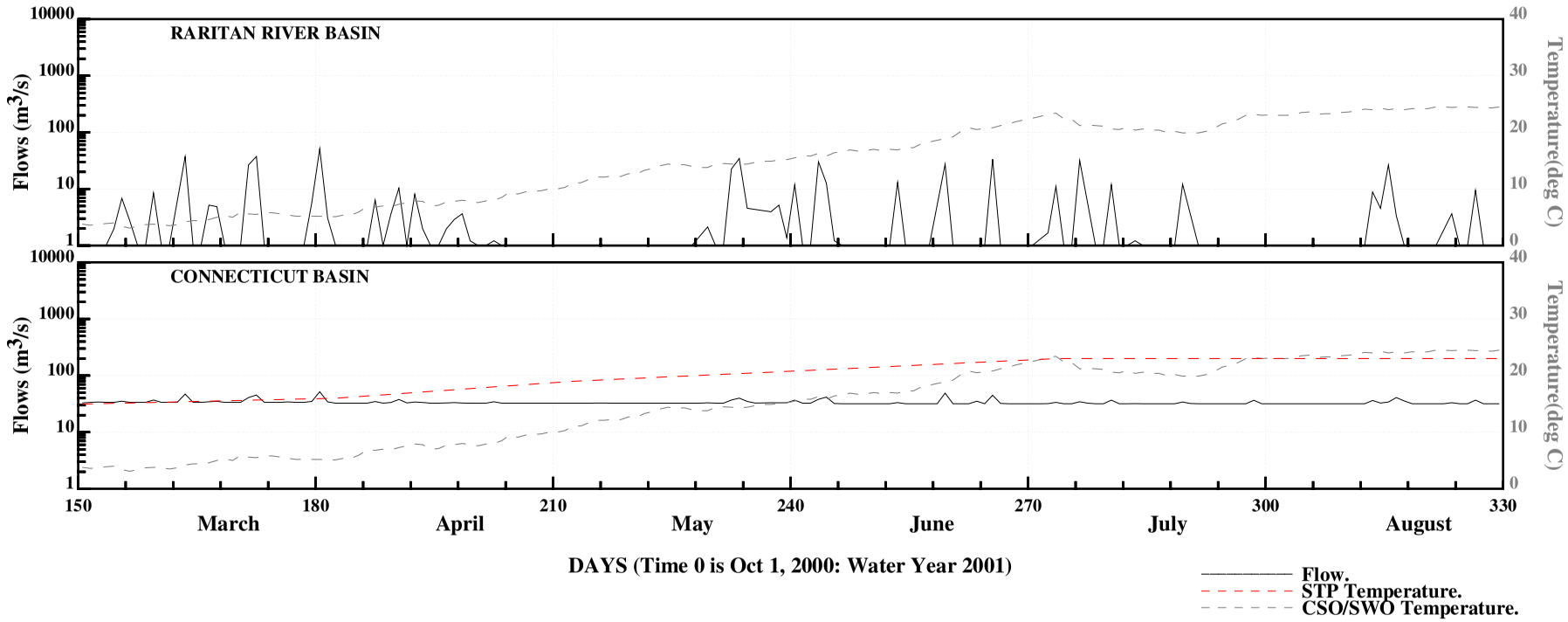

Figure 3-12c Temporal variations of wastewater inflows compiled by major areas (black lines) during March-August, 2001. Also shown are CSO/SWO water temperature (gray dotted lines) and STP inflow temperature (red lines), water year 2001 (Continued)

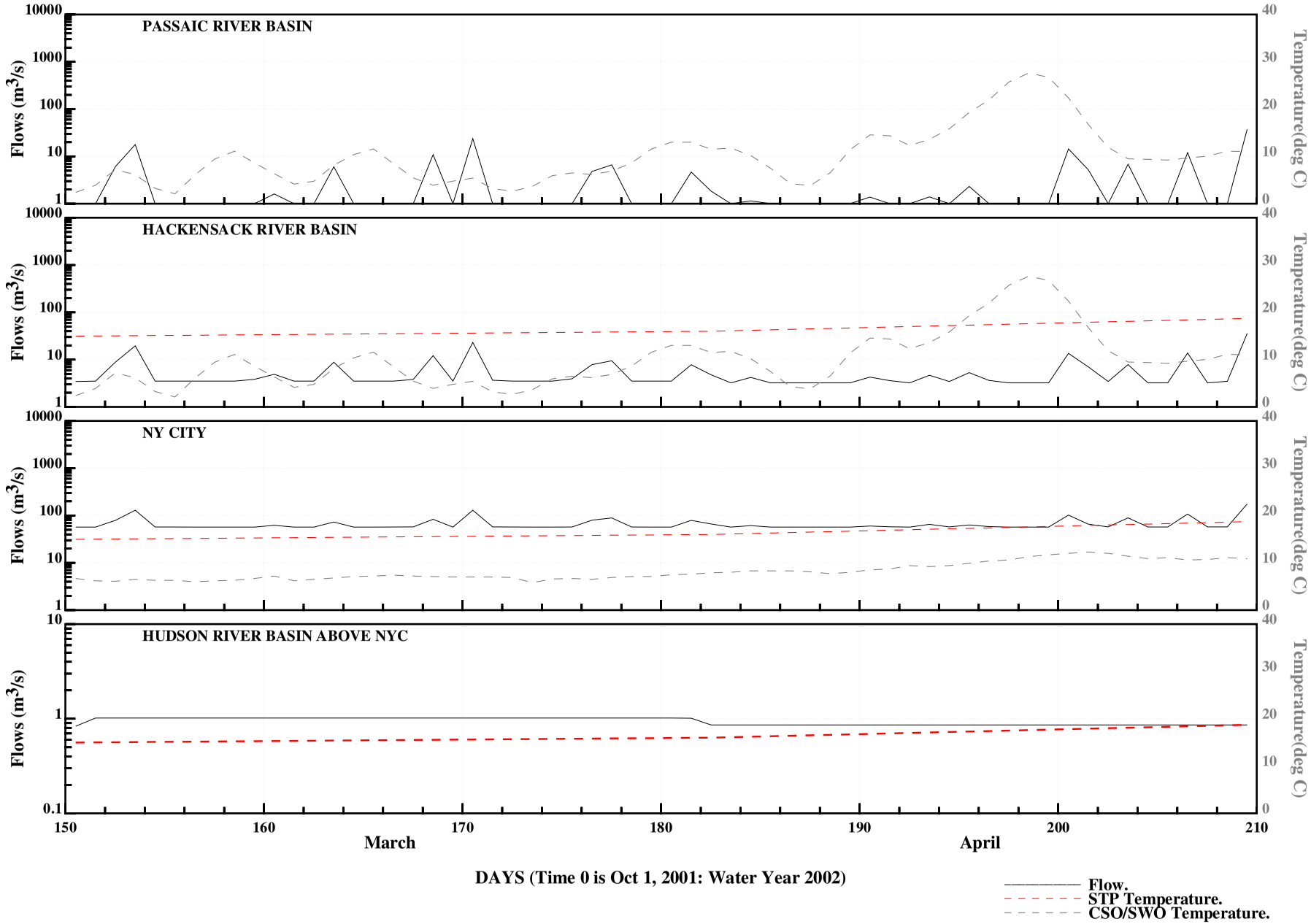

Figure 3-12d Temporal variations of wastewater inflows compiled by major areas (black lines) during March and April , 2002. Also shown are CSO/SWO water temperature (gray dotted lines) and STP inflow temperature (red lines), water year 2002

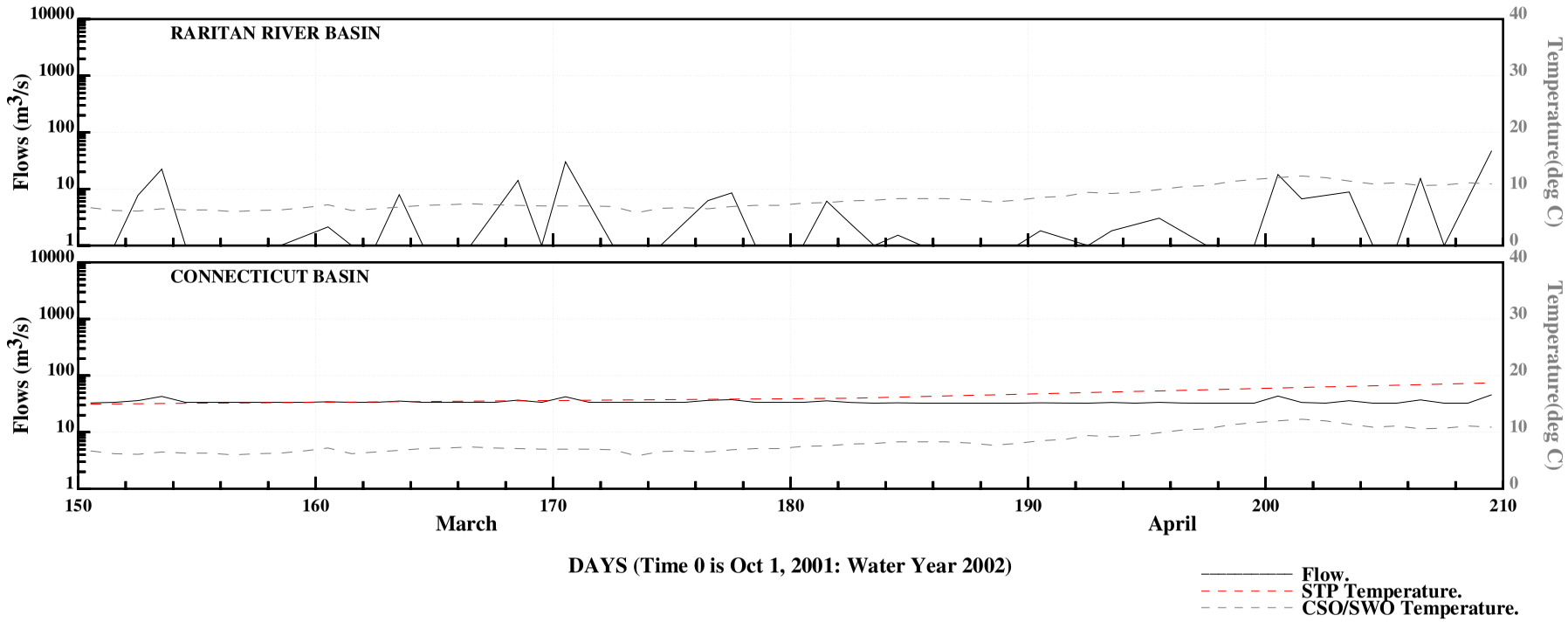

Figure 3-12d Temporal variations of wastewater inflows compiled by major areas (black lines) during March and April , 2002. Also shown are CSO/SWO water temperature (gray dotted lines) and STP inflow temperature (red lines), water year 2002 (Continued)

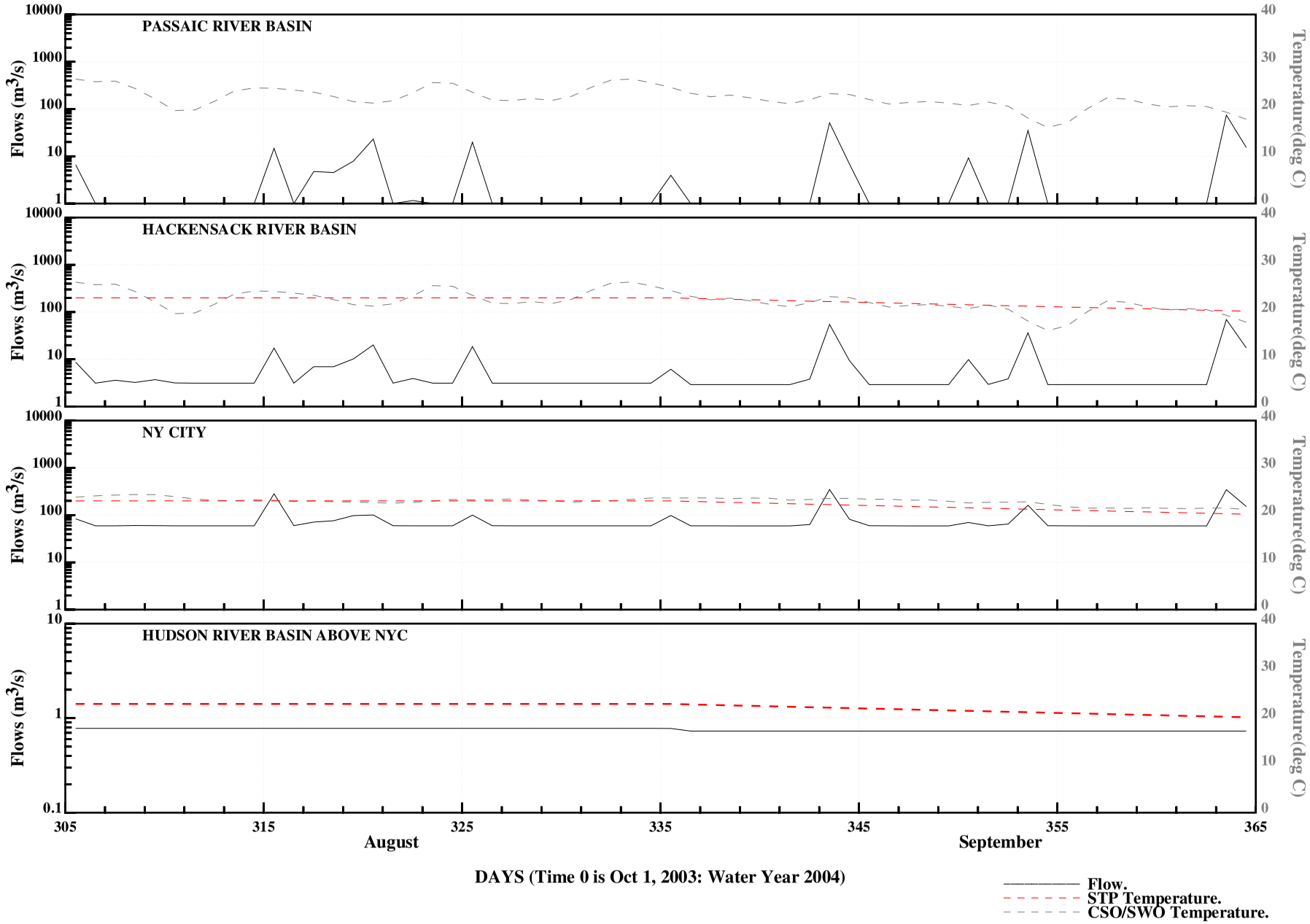

Figure 3-12e Temporal variations of wastewater inflows compiled by major areas (black lines) during August and September , 2004. Also shown are CSO/SWO water temperature (gray dotted lines) and STP inflow temperature (red lines), water year 2004

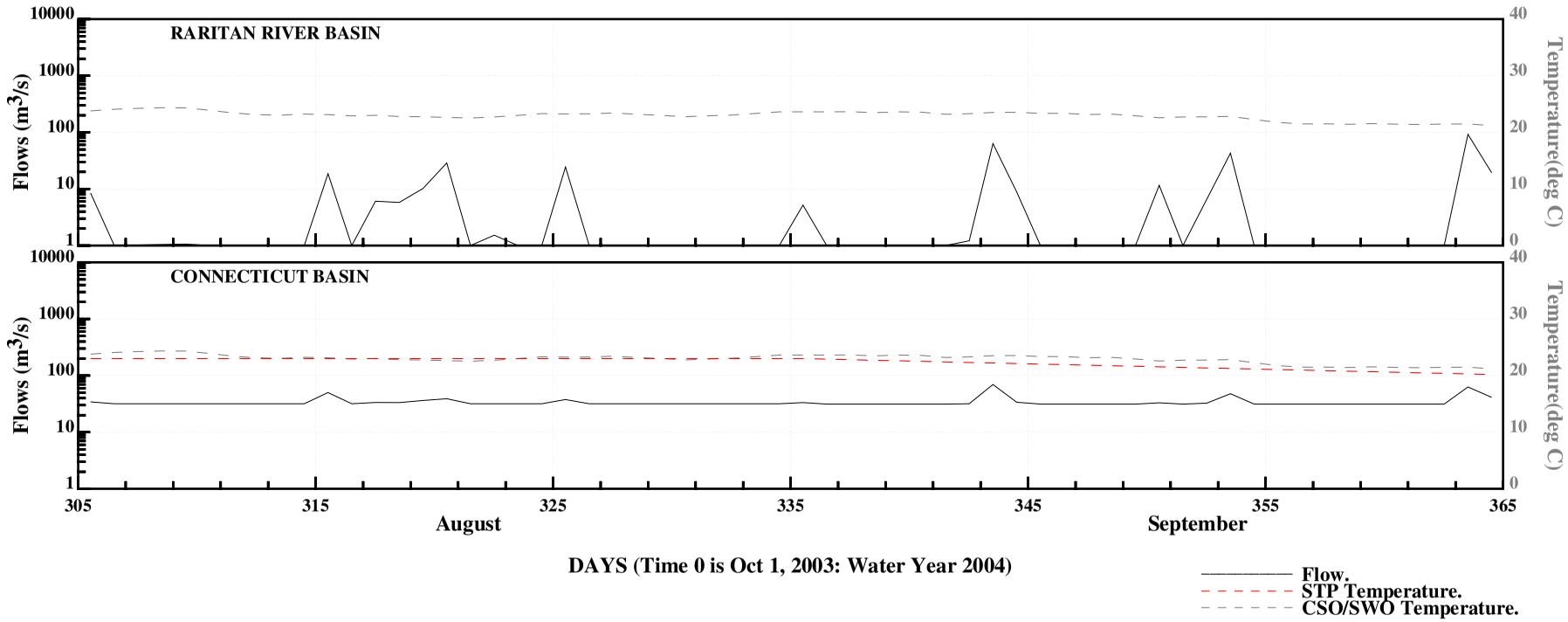

Figure 3-12e Temporal variations of wastewater inflows compiled by major areas (black lines) during August and September , 2004. Also shown are CSO/SWO water temperature (gray dotted lines) and STP inflow temperature (red lines), water year 2004 (Continued)

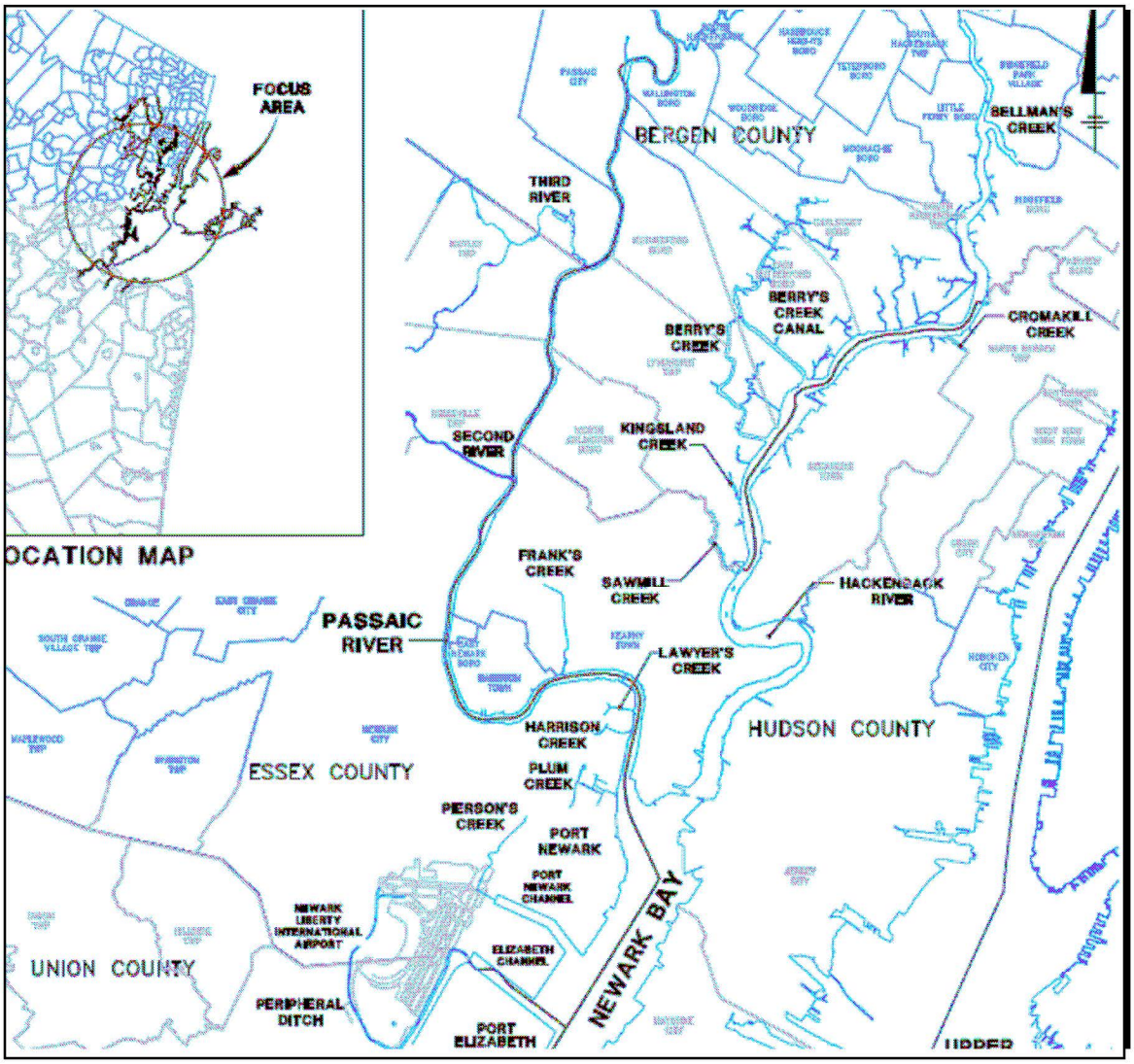

Figure 3-13 Location map of minor tributaries in the Lower Passaic River

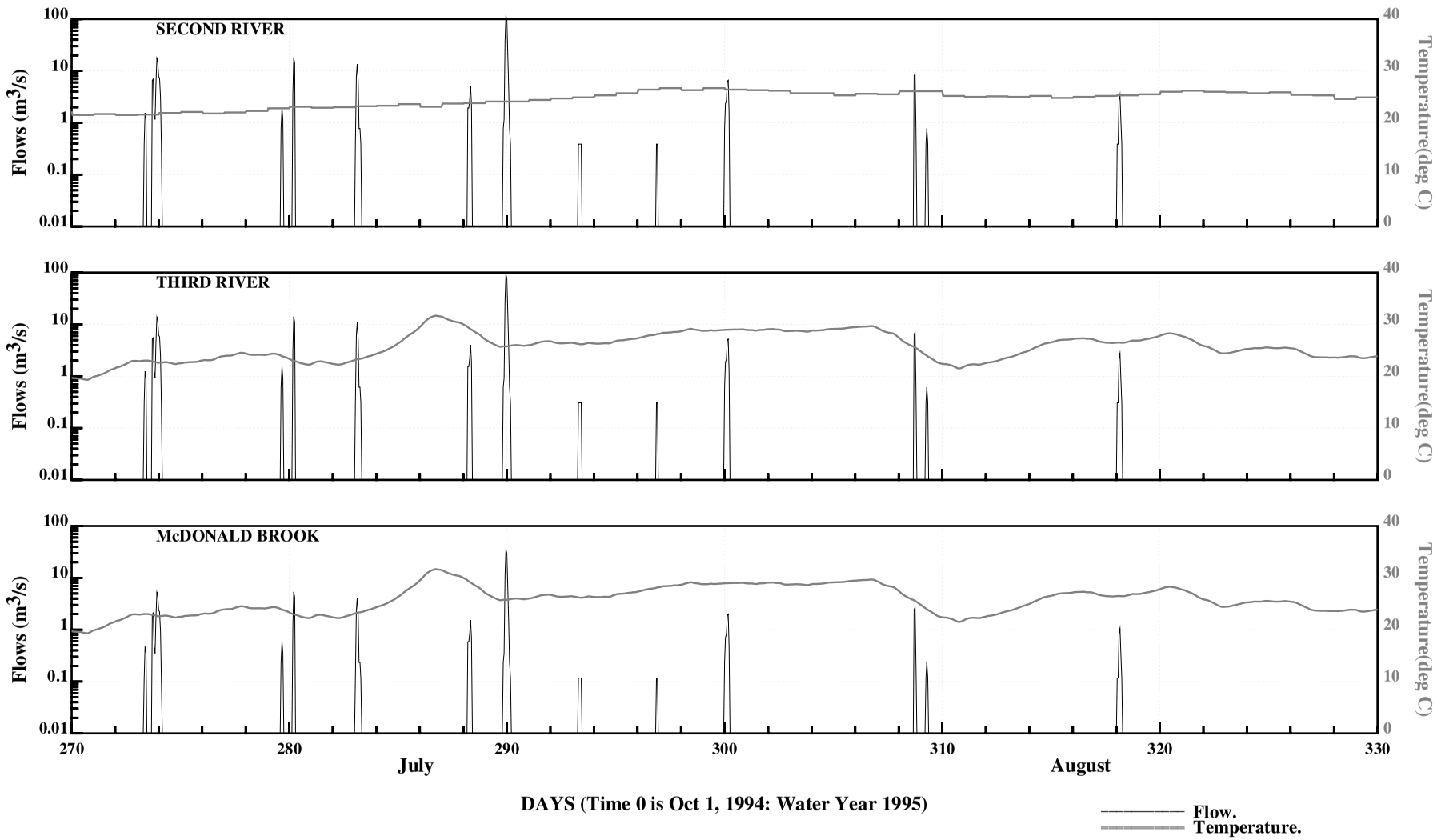

Figure 3-14a Temporal variations of Second River, Third River, and McDonald Creek during July and August, 1995. Also shown are inflow water temperatures.

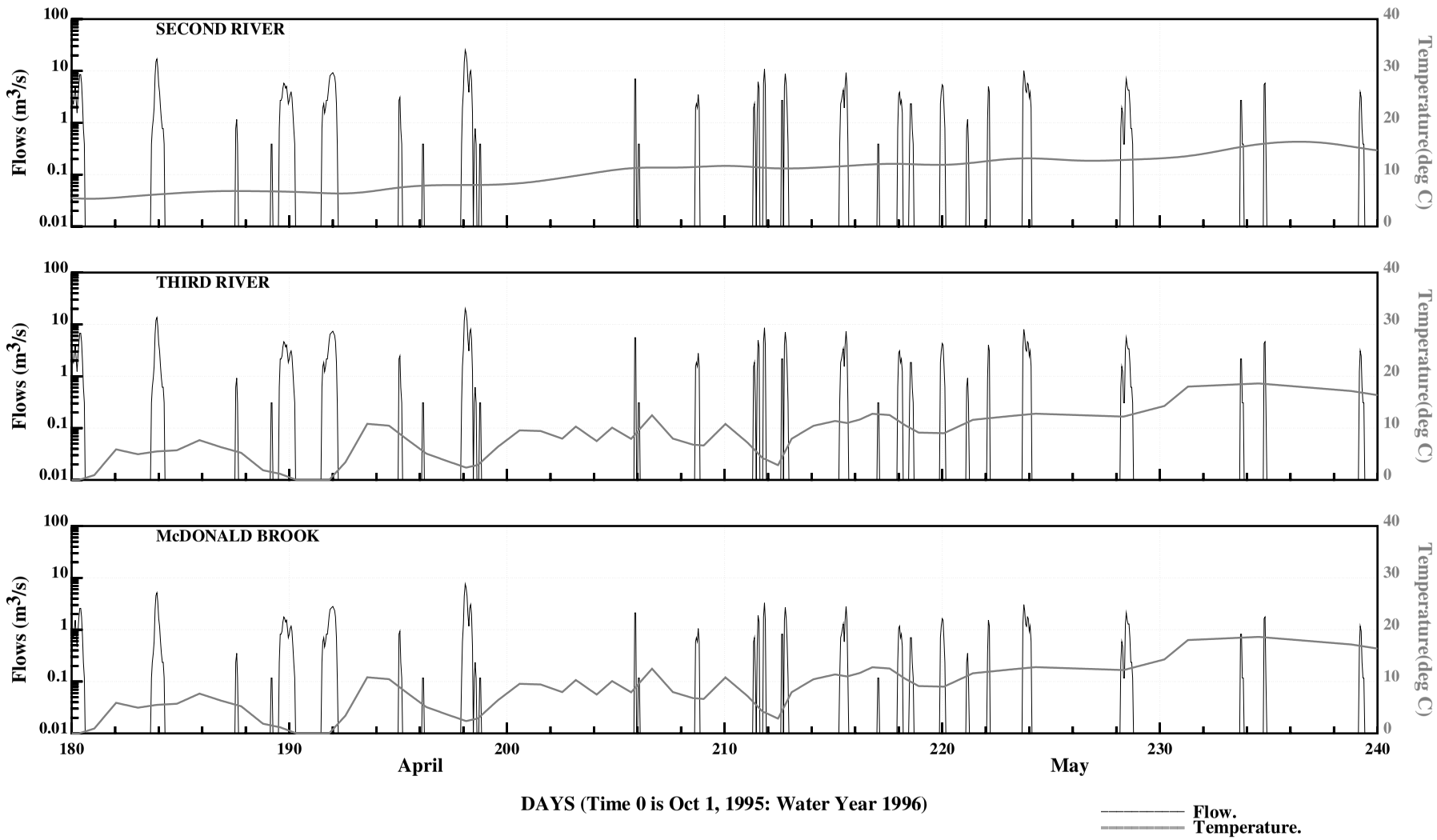

Figure 3-14b Temporal variations of Second River, Third River, and McDonald Creek during April and May, 1996. Also shown are inflow water temperatures.

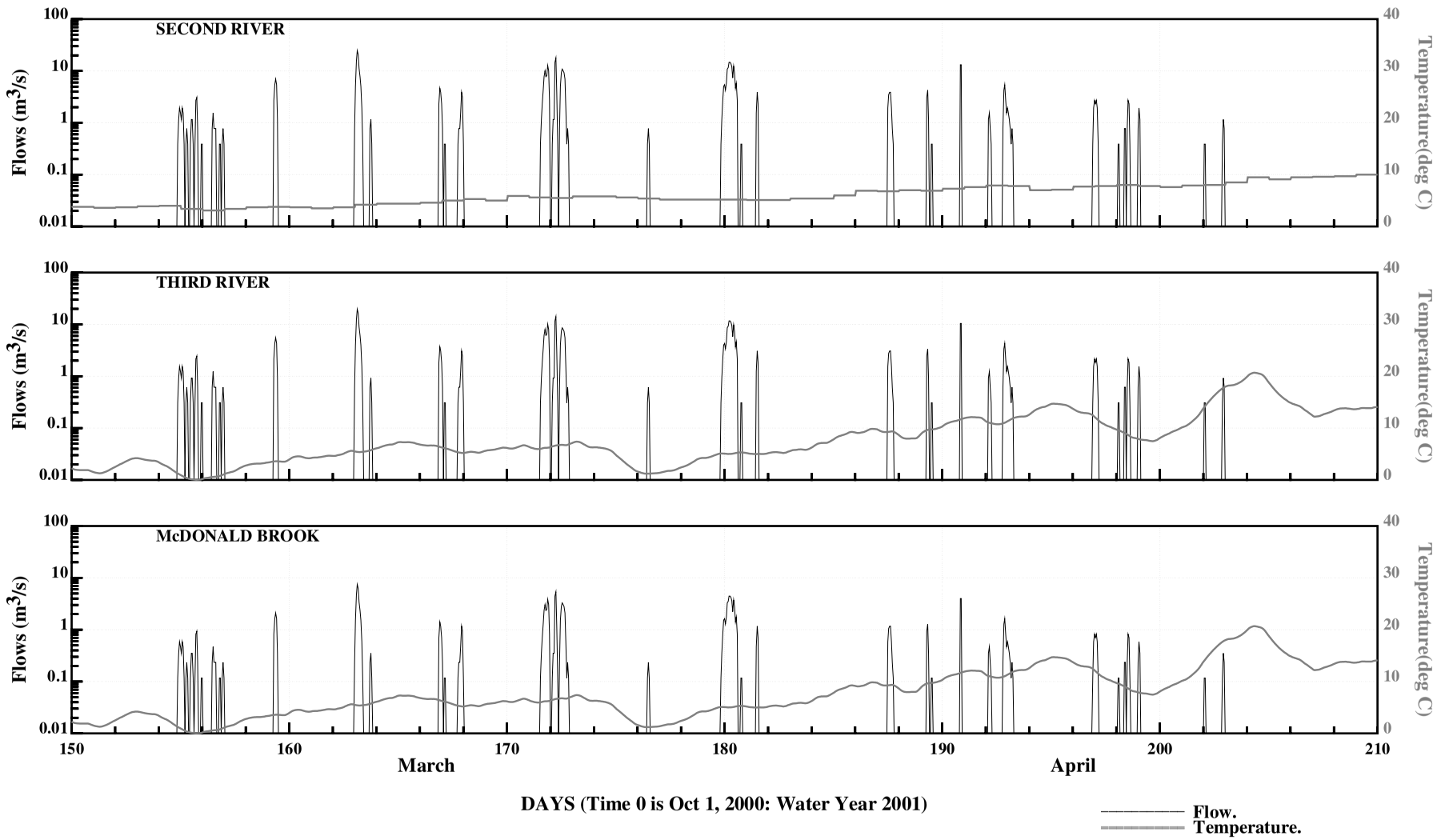

Figure 3-14c Temporal variations of Second River, Third River, and McDonald Creek during March-August, 2001. Also shown are inflow water temperatures.

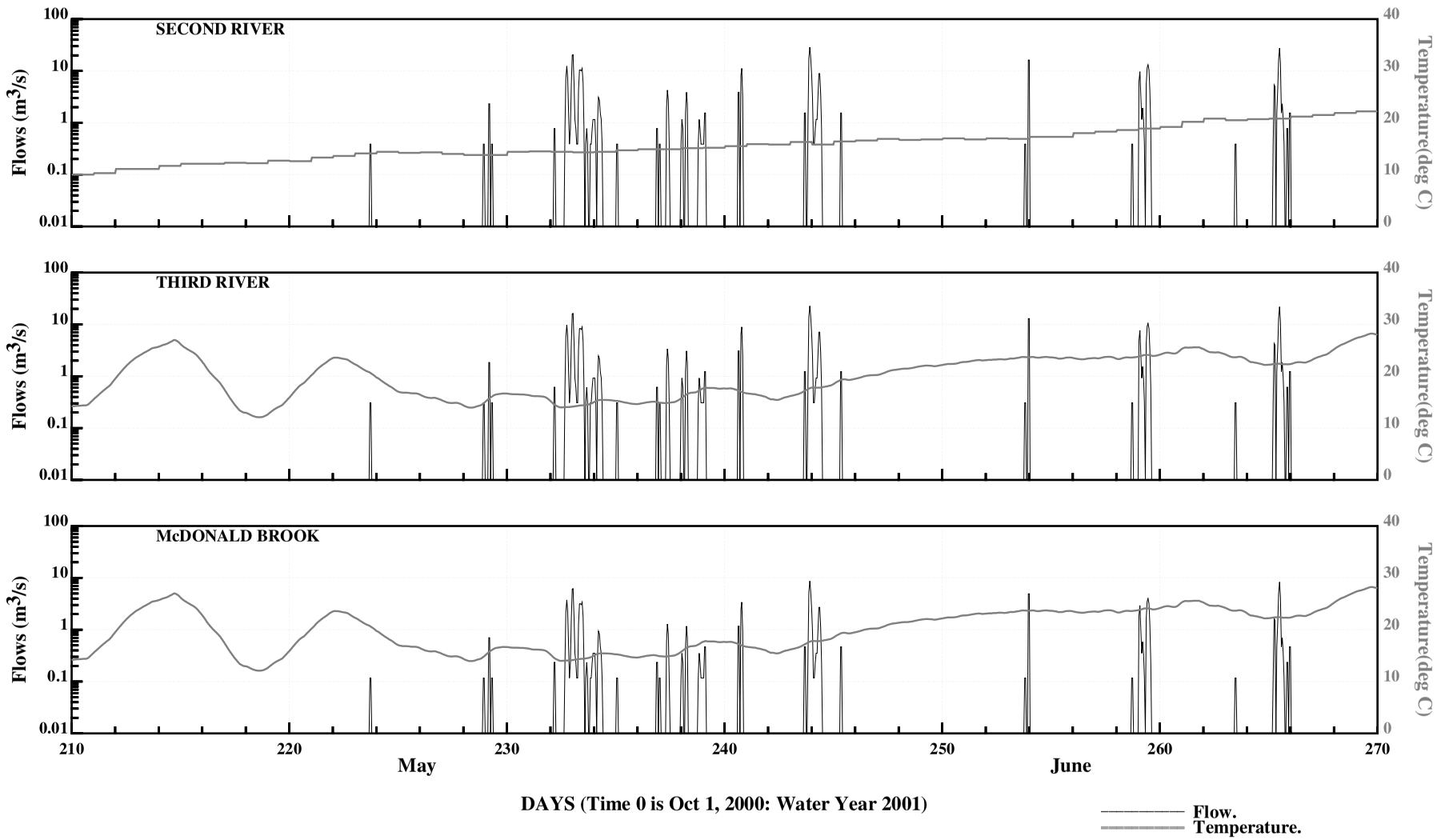

Figure 3-14c Temporal variations of Second River, Third River, and McDonald Creek during March-August, 2001. Also shown are inflow water temperatures (Continued)

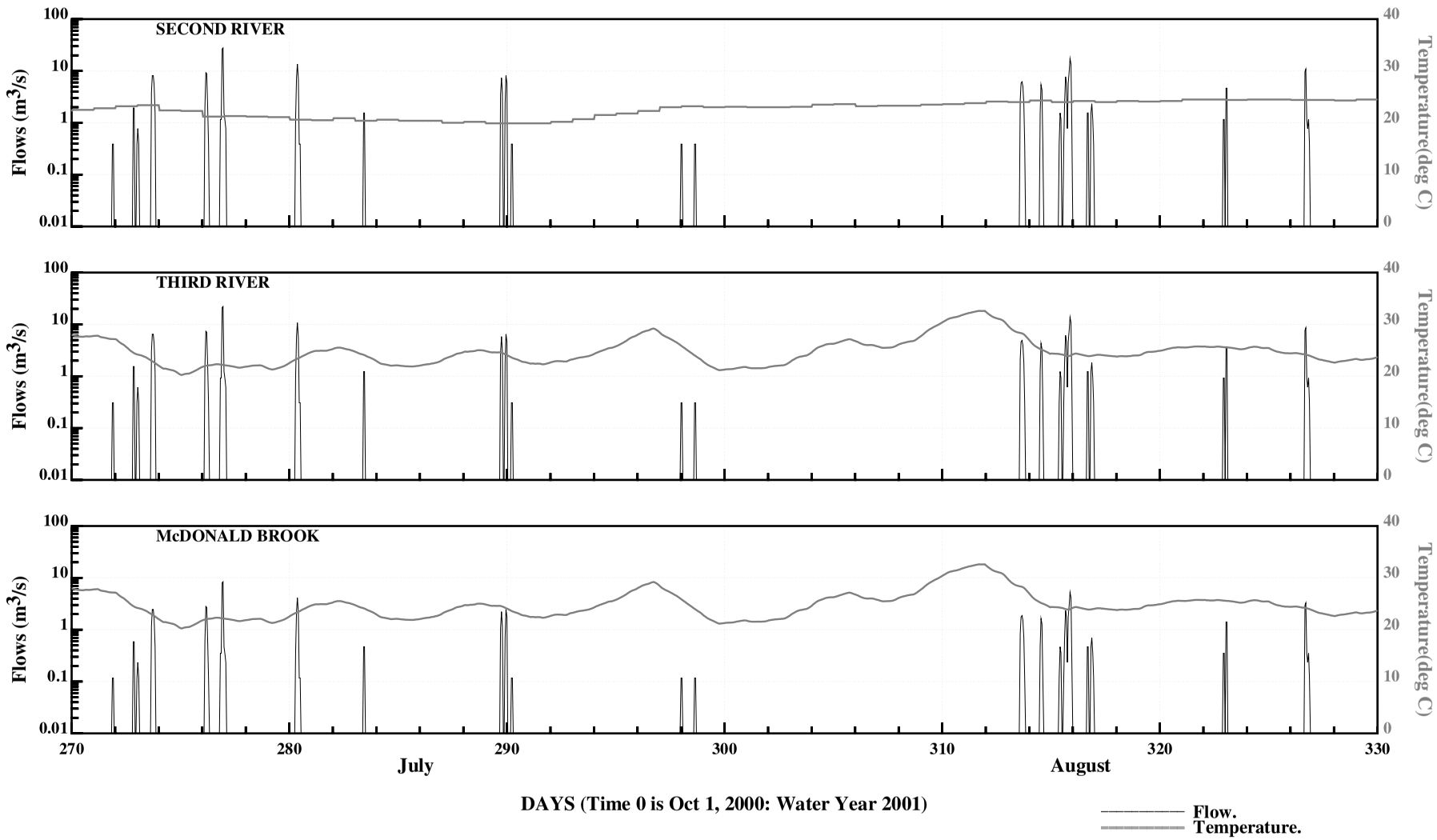

Figure 3-14c Temporal variations of Second River, Third River, and McDonald Creek during March-August, 2001. Also shown are inflow water temperatures (Ccontinued)

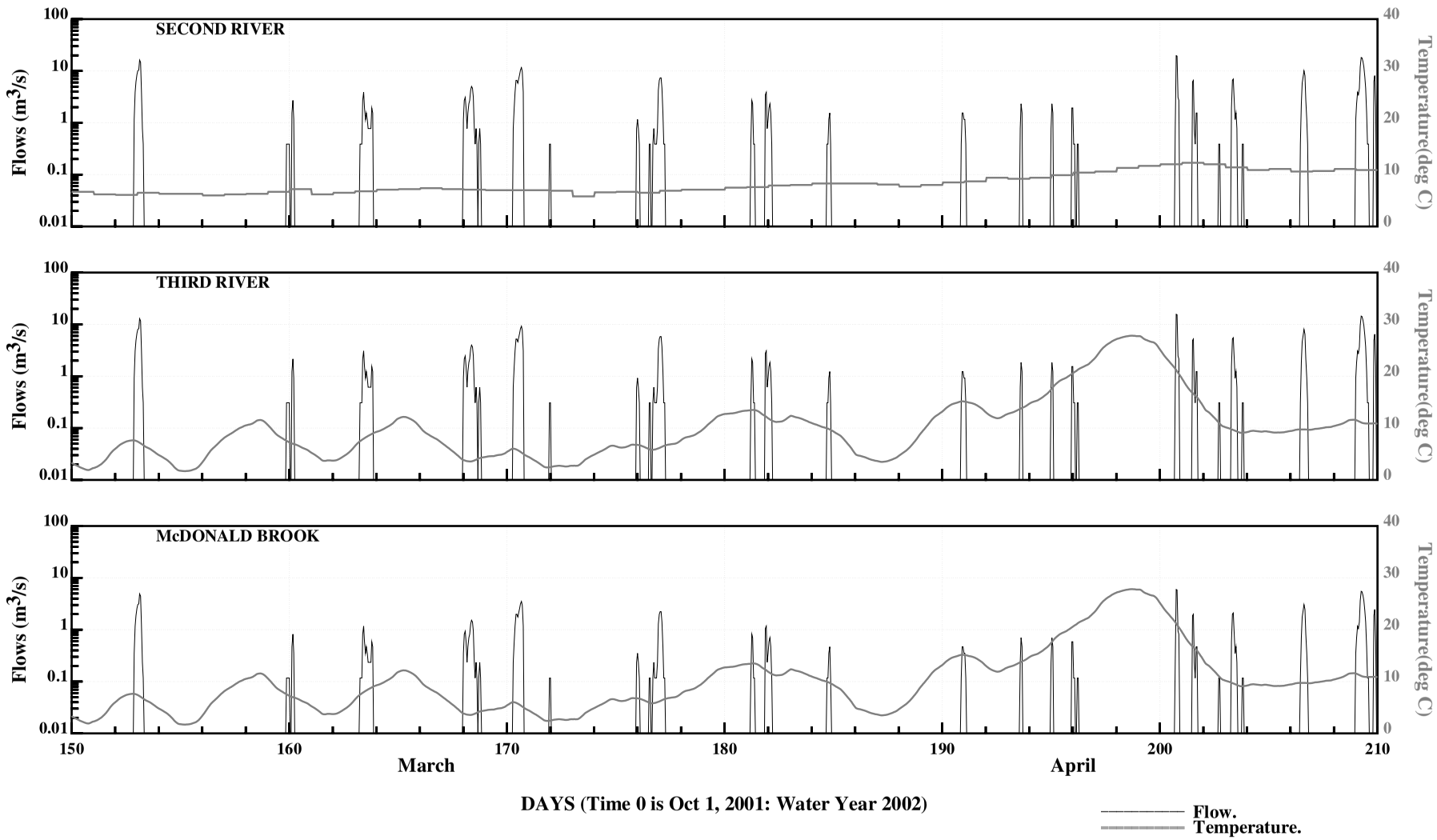

Figure 3-14d Temporal variations of Second River, Third River, and McDonald Creek during March and April, 2002. Also shown are inflow water temperatures.

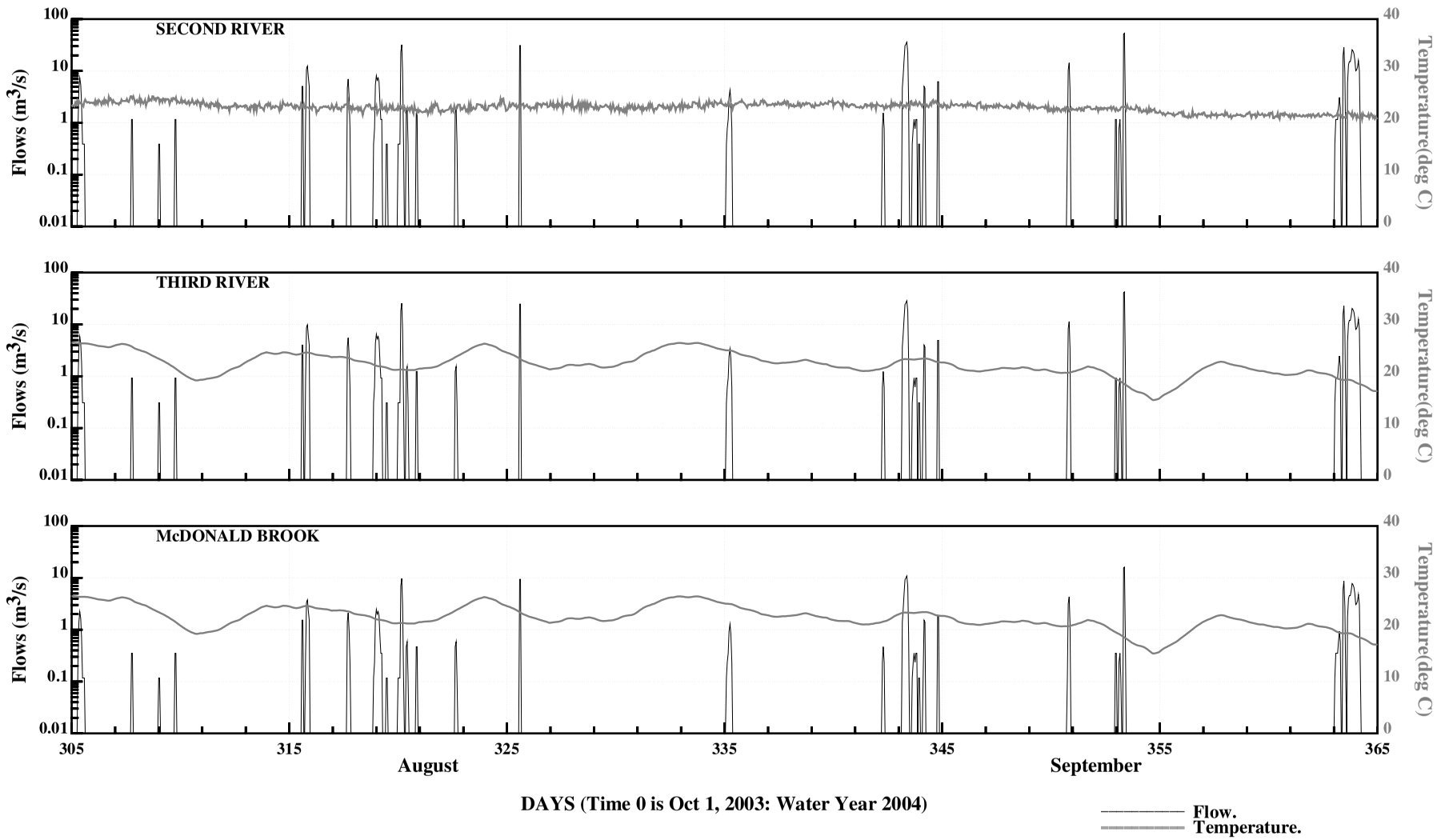

Figure 3-14e Temporal variations of Second River, Third River, and McDonald Creek during August and September, 2004. Also shown are inflow water temperatures.

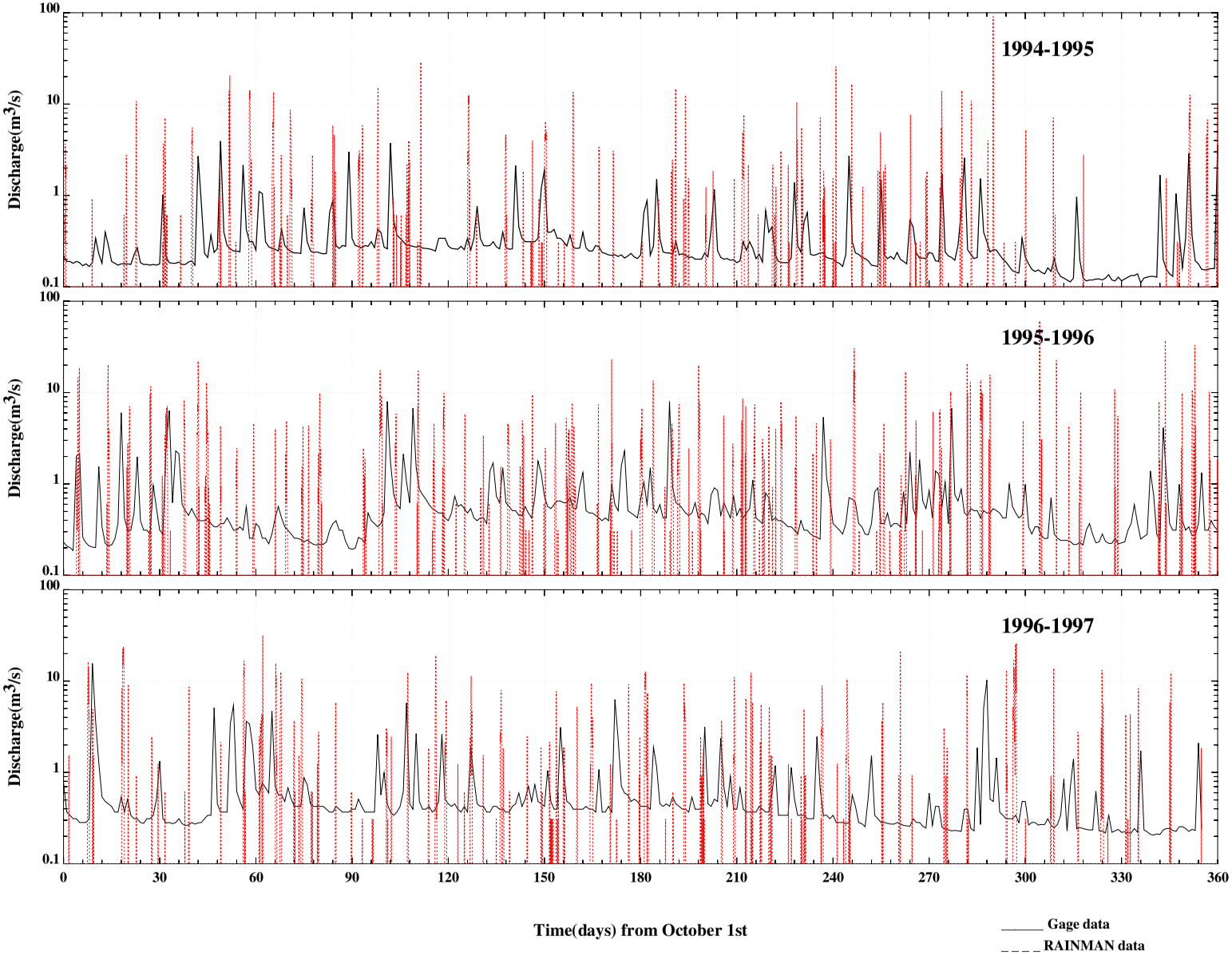

Figure 3-15 Comparison of USGS gauged Third River flow (black lines) and RRMP computed runoff (red lines) for WY 1995, 1996, and 1997

SECTION 4

MODEL CALIBRATION AND VALIDATION

Calibrating a model is an iterative procedure whereby model parameters are evaluated and refined by comparing model results to observed data. Model validation is an extension to the calibration process to insure that a calibrated model will represent variables and conditions that the model must reproduce over longer time periods. Though related, the two procedures can be separated into two processes where a portion of the available data is used to calibrate and remaining data are used to validate. The calibration data might be in a period where there is a particularly high quality and/or high density of data, whereas validation data, which must be statistically independent to the data used for calibration, may be less dense and extend over a different period. This section focuses on the model calibration procedures and the calibration results of the Lower Passaic River and Newark Bay hydrodynamic model as well as model validation results. Calibration/validation data, rationale for selection of the calibration/validation periods, model parameters and statistical methods to assess model performance are also presented.

4.1 AVAILABLE FIELD SURVEY DATA FOR MODEL CALIBRATION AND VALIDATION

Model calibration/validation for a model as large as the Lower Passaic River requires extensive field data, including surface water elevation, current velocity, temperature, salinity, and freshwater discharge. Since there is no unique data source with enough spatial and temporal coverage to be used as the sole basis of model calibration and validation, a number of datasets were collected, reduced and analyzed. For the present study, emphasis is placed only on the years for which extensive data are available. For example, although the System Wide Eutrophication Modeling (SWEM) 1988-89 database is sufficient for validation purposes in the New York Harbor-Raritan Bay system, it does not provide for a robust model skill assessment in the Passaic and Hackensack Rivers and Newark Bay. The available datasets begin with the 1994-95 Battelle and Meadowland Environmental Research Institute (MERI) programs and end with the 2004 Rutgers University, Institute of Marine & Coastal Sciences (IMCS) hydrographic measurements, as described in the following:

- Monthly field survey data collected as a part of SWEM study in 1994-1995: Temperature/Salinity (T/S).

- Quarterly T/S data collected by MERI in the Hackensack River from 1993 to present.

- Field data collected by Tierra Solutions Inc. (TSI) in 1995-1996 in the Lower Passaic River: bottom mounted moorings (T/S, and current meters) and transect surveys.

- Field data collected by IMCS of Rutgers University in 2000-2002: Acoustic Doppler Current Profilers (ADCP) and bottom mounted temperature, conductivity, and pressure sensors at various locations in Newark Bay and the Kills.

- Field data collected by IMCS in 2004: bottom mounted ADCP and pressure sensors, and surface and bottom mounted T/S sensors in the Lower Passaic River.

The detailed timelines and sampling locations for available tidal elevations, current meter, temperature and salinity data are presented in Figures 4-1 and 4-2 for the March 1995-June 1996 period for the TSI data set, in Figures 4-3, 4-4, and 4-5 for the IMCS data collected between 2000 and 2004 at various locations in the Kills, Newark Bay, and the Lower Passaic River.

The monthly T/S monitoring data collected for the SWEM program were available in the Passaic and Hackensack Rivers as well as the Kills from November 1994 and September 1995. These data are a subset of the field sampling that covered the entire SWEM study area including most of New York Harbor, Long Island Sound, and New York Bight from Cape May to Nantucket Island. Due to the paucity in the temporal resolution of this data set, no calibration or validation of model using this data set was attempted.

The TSI data collected between 1995 and 1996 provided valuable hydrodynamic information in the Lower Passaic River consisting of three bottom moorings that measured tidal currents, water elevations, temperature, and conductivity as well as a series of transect measurements of current velocities using ship-mounted ADCPs and vertical T/S casts to obtain snapshots of hydrographic conditions.

The IMCS data sets consist of a multi-year deployment - from December 2000 through April 2002 - of bottom mounted ADCP, pressure, temperature, and conductivity sensors at five locations: Perth Amboy, the Arthur Kill, the Kill van Kull, and two in Newark Bay. However, the instruments were rotated between the locations at different periods so that there are many gaps in the data as shown in Figure 4-3 (upper panel). A calibration period was selected for two months in the spring of 2002 when there were concurrent observations of current velocities and T/S in Newark Bay. Data collected in 2001 were used for the validation of model for the Newark Bay area.

During the review of available data for use in calibrating and validating the Newark Bay portion of the LPR/NB hydrodynamic model, a sulfur hexafluoride (SF_6) tracer study performed by Caplow et al. (2003) in Newark Bay and the Kills was considered. The field

program consisted of the release of SF_6 at the head of Newark Bay during July 2002 and following its tract at various points in Newark Bay and the Kills for a period of 11 days. However, due to the uncertainties in the exact time and locations of the field sampling, it would not have been possible to perform an exact matchup of observed data and model computations. This would have compromised the ability to perform a conclusive model skill assessment. Therefore, the tracer study was not utilized for model calibration or validation.

Another high quality data set collected by IMCS between mid-August 2004 and the end of September in 2004, focusing on the lower Passaic River itself, was also available for the validation of the model in the LPR. This data set consists of three bottom-mounted pressure, six surface and bottom temperature and conductivity sensors and two bottom-mounted ADCPs (Figure 4-3 (lower panel) and Figure 4-5).

Data from all of the above studies, except the 1994-1995 Battelle survey data, were processed and prepared for numerical model calibration/validation and for the evaluation of the physical mechanisms driving the flow through the Lower Passaic River. This analysis also helped select the two periods for the calibration/validation of the Lower Passaic River and the two periods for the calibration/validation of Newark Bay area, i.e., the first period between 1995 and 1996, and the second period in 2004 for the LPR and two periods in 2001 and 2002 for the Newark Bay area. This section will present the model calibration/validation procedures and results for these four periods.

The hydrodynamic model calibration was performed by adjusting bottom friction (C_D) and horizontal eddy diffusion coefficients to reproduce measured tidal elevations, current velocities, salinities and temperatures at different locations inside the model domain. In addition, fluxes through the Kills and Newark Bay were compared with estimates of fluxes from previous SWEM studies. The calibrated value of Smagorinsky (1963) horizontal diffusion formulation is equal to 0.01 throughout the model domain. The minimum bottom friction coefficient (C_D) was set equal to 0.003, except for the East River and Harlem River where C_D is equal to 0.06. Selection of these parameters is further described in Section 5 titled "Sensitivity Analyses".

4.2 MODEL CALIBRATION USING THE TSI DATA (1995 AND 1996) FOR THE LPR

4.2.1 Tidal Elevations

The 1995-1996 TSI data provided tidal stage measurements at three locations on the Lower Passaic River (Figure 4-2 and Table 4-1). The data collection periods extend from

mid-April 1995 to mid-June 1996 (Figure 4-1). Water surface elevations were measured at five- and six-minute intervals and the data were used for model calibration for these periods.

The model was run for a period of two years (WY1995 and WY1996), and the model computations compared against the observations taken at the tidal gauge locations. Figure 4-6 shows the comparison of the computed surface elevations with field data over a one-month period, May 1995. (The comparison over the entire survey period is presented in Appendix A). In this figure, observations are shown as solid lines, while the model results are shown as dashed lines. The May 1995 calibration indicates that the model slightly underestimates the amplitudes at the three tidal gauges, and the model-data discrepancies become more significant during the neap tide period (Figure 4-6). Otherwise, the model results agree very well with the observed data. The ranges between spring and neap tidal cycles, and times of high and low waters are very well reproduced.

Table 4-1. List of Tide Gauges

Station	River/Bay	Northing (ft)*	Easting (ft)*
1. Upper Reach Tidal Gauge	Lower Passaic River	708170	2142958
2. Middle Reach Tidal Gauge	Lower Passaic River	695738	2146946
3. Lower Reach Tidal Gauge	Lower Passaic River	688835	2151062

* NJ State Plane NAD83 in ft

Statistical analyses were conducted to evaluate the model performance, in which the model-computed results were compared against the measured data. Statistical parameters include the root mean square errors (RMSE) and the relative RMSE. The RMSE is a measure of the error between the model and observed data (variability unaccounted for by the model) as expressed by the following equation:

$$\text{RMSE} = \sqrt{\frac{\sum (C_{OBS_i} - C_{MODEL_i})^2}{n}},$$

where C_{OBS} is observed variable, C_{MODEL} is model calculated variable, and n is number of paired variables. The relative RMSE (%) is defined as RMSE/(data range). The data range is the difference between the minimum and maximum values observed during the survey.

Table 4-2 presents statistical evaluation of model performance in terms of RMSE, relative RMSE and correlation coefficient between model and data. The number of data points used in the calculations and the tidal range, based on data, are also shown in the table.

The RMSE decreases from upstream to downstream in the Lower Passaic River (0.18 to 0.16 m). For the three tide gauge stations, involving more than several hundred thousand data points, the mean RMSE and the mean correlation coefficient are 0.17 m and 0.96, respectively. In general, the relative RMSEs at those tidal gauges are about 5.0 percent.

Table 4-2. Statistical Evaluation of Model Performance for Water Elevation

	No. Data	Data Range (m)	RMSE (m)	Rel. RMSE (%)	Correlation Coefficient (R^2)
Upper Reach Tidal Gauge	103846	358	0.18	5.1	0.96
Middle Reach Tidal Gauge	101033	348	0.17	4.8	0.96
Lower Reach Tidal Gauge	89689	350	0.16	4.6	0.96

At the same tidal gauges, 35 hr low-pass filtered data are compared in Figure 4-7 over a period of two months (May - June 1995). Since off-shore boundary conditions are used to force the model, the discrepancies between model results and data are mainly due to the approximate nature of the derived elevation boundary conditions as discussed in Section 3 (off-shore boundary forcings). Considering these approximations, the model manages to reproduce the subtidal variations in water surface elevations as illustrated in Table 4-3.

Table 4-3. Statistical Evaluation of Model Performance for Sub-Tidal Elevation

	35 Hour Low Passed		
	RMSE (m)	Rel. RMSE (%)	Corr. Coefficient (R^2)
Upper Reach Tidal Gauge	0.10	5.0	0.84
Middle Reach Tidal Gauge	0.10	5.3	0.82
Lower Reach Tidal Gauge	0.10	5.7	0.83

.

Table 4-3 presents RMSEs, relative RMSEs, and correlation coefficients between model and data for low-frequency of 35 hours. For this sub-tidal frequency, the coefficients of correlation vary from 0.82 to 0.84. The model and data comparisons also indicate that the mean RMSEs are 0.10 m and the mean relative RMSEs are 5.3% for the 35 hour low-passed water surface elevation.

The statistical assessment compares favorably against the results of the earlier SWEM study (Blumberg et al., 1999). The mean correlation coefficients and RMSE of hourly water elevation reported by Blumberg et al. for SWEM were 0.97 and 0.15 m, respectively, at Bergen Point, which is located at the entrance to Newark Bay. For the same location, Blumberg et al. reported RMSEs and correlation coefficients of 35- hour low-passed water levels of 0.07 m and 0.93, respectively.

Table 4-4 compares results of harmonic analyses of computed and observed water surface elevations at the tide gauge stations. The amplitudes and phases of five tidal constituents, M_2, N_2, S_2, K_1 and O_1 are presented in the table. The dominant tidal constituent is M_2, with observed amplitude varying from 0.79 m at the Upper Reach Tidal Gauge to 0.74 m at the Lower Reach Tidal Gauge. For the M_2 tide, the maximum error in amplitude is about 0.04 m, and the maximum phase error is about 10º (20 minutes). Among all five tidal constituents, amplitude errors never exceed 0.04 m, while phase errors are less than 20°. At the three tidal gauges, the amplitudes of the semi-diurnal constituents M_2 and N_2, and the diurnal constituent K_1 are underestimated and the computed phases lead the observations by about 3-18° (6-36 minutes) and 7-18° (28-72 minutes) for the semi-diurnal and the diurnal constituents, respectively.

Table 4-4. Comparison of Harmonic Constants for Elevation: Using data from April 1 through September 30, 1995

M_2 Component

	Observed		Calculated	
	Amp. (m)	**Phase (°)**	**Amp. (m)**	**Phase (°)**
Upper Reach Tidal Gauge	0.79	248	0.77	238
Middle Reach Tidal Gauge	0.77	241	0.73	235
Lower Reach Tidal Gauge	0.74	239	0.72	233

N_2 Component

	Observed		Calculated	
	Amp. (m)	**Phase (°)**	**Amp. (m)**	**Phase (°)**
Upper Reach Tidal Gauge	0.20	243	0.18	225
Middle Reach Tidal Gauge	0.18	228	0.17	220
Lower Reach Tidal Gauge	0.19	228	0.17	218

S_2 Component

	Observed		Calculated	
	Amp. (m)	**Phase (°)**	**Amp. (m)**	**Phase (°)**
Upper Reach Tidal Gauge	0.12	285	0.15	275
Middle Reach Tidal Gauge	0.13	273	0.14	270
Lower Reach Tidal Gauge	0.12	274	0.14	267

K_1 Component

	Observed		Calculated	
	Amp. (m)	**Phase (°)**	**Amp. (m)**	**Phase (°)**
Upper Reach Tidal Gauge	0.10	108	0.08	90
Middle Reach Tidal Gauge	0.11	106	0.08	88
Lower Reach Tidal Gauge	0.11	102	0.8	87

O_1 Component

	Observed		Calculated	
	Amp. (m)	**Phase (°)**	**Amp. (m)**	**Phase (°)**
Upper Reach Tidal Gauge	0.05	120	0.05	104
Middle Reach Tidal Gauge	0.05	112	0.05	105
Lower Reach Tidal Gauge	0.05	113	0.05	105

4.2.2 Current Velocities

As part of TSI's hydrodynamic field program, currents were measured by boat-mounted ADCPs along eight transects and at three near-bottom moorings in the Lower Passaic River. Table 4-5 shows the coordinates of the starting and the ending locations in each transect and the current mooring stations during Round 1 survey (Figure 4-1). Figure 4-2 shows the locations of the transects and the current meters. As it can be seen, the first three ADCP transects, Tr -1, Tr 00 and Tr 01, are located near the mouth of the Lower Passaic River and in upper Newark Bay while, Tr 27 is in the upper portion of the Lower Passaic River. The three moorings, Meter 3, Meter 2, and Meter 1, are near the three tidal

gauges, Upper, Middle, and Lower Reach Tidal Gauges, respectively. The data available for model calibration are shown in Figure 4-1.

Table 4-5. List of ADCP Transects and Mooring Station Coordinates (NJ State Plane, NAD83)

	Northing (ft)	Easting (ft)
1. Tr –1	686504 - 686592	2150566 - 2151467
2. Tr 00	687732 - 687449	2150683 - 2151575
3. Tr 01	689283 - 689096	2151062 - 2151644
4. Tr 10	695259 - 695725	2147043 - 2147065
5. Tr 15	692451 - 692905	2142270 - 2142274
6. Tr 19	695329 - 695375	2138956 - 2139304
7. Tr 26	703417 - 703182	2139970 - 2140228
8. Tr 27	708543 - 708434	2142952 - 2143253
9. Meter 1	691253	2151915
10. Meter 2	695291	2146194
11. Meter 3	703792	2140380

Instantaneous ADCP measurements along the eight transects have a bin interval of 0.25 m, starting from approximately 1.1 m below the river surface. The maximum depths of ADCP bins on each transect in each round of surveys, with respect to river surface, are listed in Table 4-6.

The other set of current velocities measured at the fixed mooring stations have time intervals of 5, 15 and 20 minutes. No information was provided to indicate the depth from bottom for the near-bottom moorings. Among the three rounds of data collections, current directions could not be determined at Meters 1 and 3 from the round 1 survey, because of questionable data quality. This problem was noted in the field logs and may have resulted from biofouling of the instruments.

Table 4-6. Maximum Depths of Bins in ADCP Measurements (units: m)

Transect	Round 1	Round 2	Round 3
Tr –1	9.58	9.58	9.58
Tr 00	7.83	7.58	7.33
Tr 01	7.83	7.58	7.83
Tr 10	6.08	6.33	6.58
Tr 15	6.08	6.33	6.58
Tr 19	5.58	5.83	6.08
Tr 26	5.83	5.83	6.33
Tr 27	5.08	5.08	5.33

Contours of computed cross-sectional velocities are plotted against ADCP data in the eight transects. Figure 4-8 shows the model and data comparison on Tr 10 for a period of six hours (Round 2a). Open colored circles represent data locations and observed velocities. A color match between the open circle and the colored model domain indicates a perfect agreement (within the contour intervals chosen) between observed and calculated velocities. The model domain in these figures represents the sloping side and the stair-stepped bottom of the river cross section. Comparison over the complete observation period is presented in Appendix B. In the figure, negative velocity means that the current is going downstream in the Lower Passaic River towards Newark Bay, and positive velocity indicates that the water is traveling upstream in the river away from Newark Bay. Figure 4-8 shows that the magnitudes and the lateral/vertical structure of velocities are very well reproduced by the model during the ebb, ebb-to-flood transition, and flood tidal periods. Both model and data show that stronger currents usually occur near the surface layers of the deep channel. However, there are some discrepancies of current magnitudes between model and data along the transect (for example at 17:24 April 15, 1996) during the flood period, as shown in Figures 4-8.

Since survey depths at the mooring stations are not available, model output is extracted at three standard levels. They are 1 m (near bottom), 3 m (mid-depth) and 4.5 m (near surface) from the bottom. Figure 4-9 compares near bottom velocities for the round 3 measurements at Meters 1, 2 and 3. The comparison presented is based on the length of survey periods, which are 27, 20, and 38 days for round 1 through round 3, respectively. Comparisons between the model output and the complete surveys are presented in Appendix C. The resulting RMSEs, relative RMSEs and correlation coefficients are shown in

Table 4-7. The table clearly shows that the model-data correlation for round 1 survey is low compared to those of round 2a and 3. If one neglects the round 1 survey, RMSEs vary from 0.09 m/s to 0.19 m/s, with a mean of 0.14 m/s and relative RMSEs from 8.9% to 17.1%, with a mean of 12.8%. The correlation coefficient ranges from 0.29 at Meter 1, round 2a to 0.91 at Meters 2 and 3, round 3. The table indicates that the upstream moorings have relatively smaller RMSEs and relative RMSEs, and higher correlation coefficients.

Table 4-7. Statistical Evaluation of Model Performance for Current Meter Data

	Round 1			Round 2a			Round 3		
Station	**RMSE (m/s)**	**Rel. RMSE (%)**	**Corr. Coef. (R^2)**	**RMSE (m/s)**	**Rel. RMSE (%)**	**Corr. Coef (R^2).**	**RMSE (m/s)**	**Rel. RMSE (%)**	**Corr. Coef (R^2).**
Meter 1	0.19	25.1	0.38	0.19	17.1	0.29	0.17	16.0	0.83
Meter 2	0.24	20.7	0.39	0.19	14.6	0.80	0.11	8.9	0.91
Meter 3	0.21	36.1	0.05	0.1	11.3	0.88	0.09	9.1	0.91

4.2.3 Temperature and Salinity

The model was calibrated against 30-day continuous bottom temperature and conductivity measurements made at two locations (M1 and M2) in the Lower Passaic River in 1995 and 1996. In addition, the TSI field survey program conducted in the spring 1996 consisted of a series of six CTD casts at eight transects (Group 2 Round 2 and 3 data set) along the axis of the Lower Passaic River. Figure 4-1 and Figure 4-2 show the sampling timelines and the transect locations. These CTD casts were obtained in the middle of each transect coincident with the ship-mounted current velocity profiles (discussed in the previous section).

Figure 4-10 and Figure 4-11 show the time series of temperature at the 1995 and 1996 mooring locations, respectively. Because the conductivity data were unable to be converted to salinity values (due to the absence of sensor information), only the bottom temperature data (red lines) are examined against model results (black lines) for the 1995 data. The results show good agreement between observed and computed bottom temperature. Both the range of tidal fluctuation and general trend of temperature over the deployment periods are well reproduced. However, in 1996, there are significant differences between the computed and observed bottom water temperature. It was found that during high inflow events the computed temperatures were significantly lower than the observed

temperature (see Figure 3-9b for river inflow data used for the simulation). This is attributed to uncertainty in the water inflow temperature assigned to the river and CSO/SWO inflows.

Figures 4-12 and 4-13 show the time series of temperature and salinity, respectively, for 30 days at eight transect locations in late July through early August 1994. All CTD cast data at each transect were plotted regardless of sample depth and their position within each transect. The vertical lines plotted in the figure indicate the range of data. The mean values of each transect survey are indicated as open circles. The paucity of the observed data makes it difficult to draw definitive statements regarding the agreement between model and field data. Yet, using the available data, Figures 4-12 and 4-13 show that both the model computed salinity and temperature match quite well with the data at all transects. The model reproduced the observed ranges in salinity varying with the tidal cycle as well as the degree of upstream salinity intrusion.

Figures 4-14a and 4-15a show the time series of temperature and salinity for 60 days at each transect in the spring of 1996. Both the model computed salinity and temperature match the data well at all transect locations. There were, however, some times when the computed temperatures were lower than the observed data. This also is attributed to when uncertainty in the river inflow water temperature to be used in the model. It should also be noted that, during the spring 1996 survey, the salinity in the Lower Passaic River is much lower than was observed during the summer low flow condition (see Figure 4-13). The tidal variation of salinity is also higher in this period reflecting a greater higher horizontal salinity gradient that results from the high volume of upstream freshwater inflow. Figures 4-14b and 4-15b show the range of temperature and salinity, respectively, over two months in the spring of 1996 both at surface and depth along the longitudinal section of the LPR. The ranges in the observed TSI transect data are also shown in the figures. As the figures indicate the ranges of computed values of salinity are in good agreement with the data both in terms of maximum and minimum values along the transect as well as the position of the salt intrusion in the LPR during this period. However, the model computed temperature values over this period show much larger ranges as compared to the observed data.

Figure 4-16 shows the vertical profiles of computed and observed salinity at Transect 10. As shown in the figure, the vertical variation of salinity at different times at this transect were very well reproduced by the model. Additional figures of computed salinity and temperature profiles compared against vertical CTD cast data are shown in Appendices D and E, respectively.

4.3 MODEL VALIDATION WITH 2004 IMCS DATA SET FOR THE LPR

4.3.1 Tidal Elevations

Three tidal gauges deployed in the Lower Passaic River (M1, M3, M5 in Figure 4-4) were used to compare against the model. Computed versus observed hourly sea surface elevations at these three locations are shown in Figure 4-17. The results indicate that the model was able to reproduce the water elevations very well. The mean range of spring tide in the LPR and the Newark Bay areas varies between 1.2 and 1.5 m. The figure shows that the maximum water surface variation (i.e. maximum-minimum water elevations) at those gauges is about 3.3 m during the validation period. The model-data comparisons shown in Figure 4-17 also indicate that the amplitudes of tide, the ranges between spring and neap tidal cycles, and times of high and low waters are very well reproduced at those three locations in the river except around day 365 when observed data at the upstream station M5 show an increase in water elevations not reproduced by the model. Both the model results and the observations show that there is no significant change in the tidal amplitude from downstream at M1 to upstream locations at M5.

Table 4-8 presents the statistical analysis of model performance in terms of RMSE, relative RMSE and correlation coefficient between model and data. The RMSE in tidal elevations vary from 0.14 m to 0.19 m and with relative RMSE of about 6%. The correlation coefficients are greater than 0.92 at all locations. A previous model study performed in the Chesapeake Bay (Johnson et.al., 1993) reports the model-data error for tidal elevations in the range of 0.03 to 0.2 m at various locations in the bay. Another study done in New York Harbor (Blumberg et al., 1999) reports the RMSE in the stations within the harbor ranges between 0.1 to 0.19m. Figure 4-18 shows the correlation plots of computed and observed water elevations at M1, M3, and M5. The figure indicates that there is strong correlation between computed and observed water elevations.

Table 4-8. Statistical Evaluation of Model Performance for Elevation

	No. Data	Data Range (m)	RMSE (m)	Rel. RMSE (%)	Correlation Coefficient (R^2)
M5	6264	3.11	0.19	6.2	0.92
M3	1417	2.38	0.14	5.8	0.98
M1	5824	2.58	0.15	5.8	0.97

The results of harmonic analyses between the observed and computed tidal elevations are presented in Table 4-9. The results confirm that the model reproduced the tidal signal in the study area quite well. Dominant tidal constituents in the Lower Passaic River are semidiurnal. The amplitude and phase of semidiurnal components (M_2, N_2 and S_2) are in good agreement between the computed and observed tides. The diurnal components, K_1 and O_1 show about 30-60 minutes phase lag in model results, which is consistent with previous analyses conducted using TSI mooring data.

4.3.2 Current Velocities in Lower Passaic River

This section presents the model validation results using the current velocities measured by two bottom moored acoustic current meters (M2 and M3) deployed in the Lower Passaic River between August and September 2004 (See Figure 4-4 for locations).

4.3.2.1 Current Meter at Station M2

The time series of hourly current velocities at M2 at three depths (0.4 m, 2.1 m, and 3.6 m from bottom) are shown in Figure 4-19. Positive values depict downstream currents while negative values indicate upstream currents. The figure indicates that there are strong tidal currents in the LPR during the validation period. The maximum flood and ebb tidal velocities at the surface are about 1.0 m/s. Current velocities decrease at depth. At the bottom layer, the maximum ebb tidal velocities are about 0.4 m/s and the maximum flood tidal velocities about 0.6 m/s. Stronger flood current at depth indicates the influence of density-driven gravitational circulation, with higher salinity in the lower layer, at this location. A zoomed-in view of 10 days of current velocities is shown in Figure 4-20 for visual clarity. The figure indicates that the model reproduced the current velocities very well at all depths at M2. The variations in magnitudes of current speed and phase, as well as the variations between spring and neap tidal cycles at surface and bottom, are also well reproduced by model. Two non-tidal events recorded at Day 343 and around 354 are also well captured by the model.

Table 4-9. Comparison of Harmonic Constants for Water Elevation

M_2 Component

	Observed		Calculated	
	Amp. (m)	Phase (°)	Amp. (m)	Phase (°)
M5 (SBE16)	0.83	245	0.72	245
M3 (CTD)	0.84	244	0.70	244
M1 (SBE16)	0.82	240	0.68	240

S_2 Component

	Observed		Calculated	
	Amp. (m)	Phase (°)	Amp. (m)	Phase (°)
M5 (SBE16)	0.20	288	0.18	290
M3 (CTD)	0.21	286	0.17	287
M1 (SBE16)	0.20	280	0.16	282

K_1 Component

	Observed		Calculated	
	Amp. (m)	Phase (°)	Amp. (m)	Phase (°)
M5 (SBE16)	0.10	116	0.06	104
M3 (CTD)	0.10	118	0.06	103
M1 (SBE16)	0.10	116	0.06	102

O_1 Component

	Observed		Calculated	
	Amp. (m)	Phase (°)	Amp. (m)	Phase (°)
M5 (SBE16)	0.05	112	0.05	108
M3 (CTD)	0.06	114	0.05	108
M1 (SBE16)	0.06	112	0.05	107

The statistical analysis of model performance against observed data at M2 current meter is presented in Table 4-10. As can be seen in the table, the RMSEs vary from 0.11 to 0.19 m/s, with a mean of 0.16 m/s and relative RMSEs from 8.0 to 9.1%, with a mean of 8.9%. The correlation coefficient ranges from 0.80 to 0.89. The RMSE values demonstrate that on average, the model does perform better in simulating the current velocities at the bottom as compared to mid depth and surface; however, the model and data values seem to be better correlated at the surface than at the bottom and mid-depth. The statistical analysis of currents obtained in this study compare well with the results of the earlier SWEM study (Blumberg et al., 1999), where the RMSE on the ADCP deployed in the East River varied between 0.15 m/s in the Upper East River (College Point) to 0.43 m/s in the Lower East River (Red Hook). The correlation coefficients of current velocities in SWEM were above 0.95.

Table 4-10. Statistical Evaluation of Model Performance for ADCP at M2 (2004)

	No. Data	Data Range (m/s)	RMSE (m/s)	Rel. RMSE (%)	Correlation Coefficient (R^2)
Surface (3.6m)	2004	2.10	0.19	9.1	0.89
Mid-depth (2.1m)	3106	1.99	0.14	7.3	0.87
Bottom (0.4m)	3074	1.40	0.11	8.0	0.80

Table 4-11 lists the results of harmonic analyses of computed and observed current velocities at M2. The amplitudes and phases of four tidal constituents, M_2, S_2, K_1 and O_1 at M2 are presented in the table. The dominant tidal constituent is M_2, with observed amplitude varying from 0.29 m at the bottom to 0.55 m at the surface at station M2. The results of the harmonic analyses of tidal currents at M2 indicate that model-data comparison of tidal constituents is in good agreement, with less than 10 % differences in amplitudes and less than 15 degrees in phase (about 30 minutes). At the bottom, the differences of the observed and computed amplitude of M_2 components are 0.01 cm/sec. Minor components such as N_2, S_2, K_1, and O_1 also show very good agreements between observed and computed currents at M2.

Table 4-11. Comparison of Harmonic Constants for ADCP at M2: using data from August 26 through September 23, 2004

M_2 Component

	Observed		Calculated	
	Amp. (m/sec)	Phase (°)	Amp. (m/sec)	Phase (°)
Surface(3.6 m)	0.55	333	0.61	335
Mid-Depth(2.1 m)	0.50	348	0.45	335
Bottom (0.4 m)	0.29	342	0.28	328

N_2 Component

	Observed		Calculated	
	Amp. (m)	Phase (°)	Amp. (m)	Phase (°)
Surface (3.6 m)	0.09	301	0.13	302
Mid-Depth (2.1 m)	0.08	324	0.08	313
Bottom (0.4 m)	0.05	330	0.05	320

S_2 Component

	Observed		Calculated	
	Amp. (m)	Phase (°)	Amp. (m)	Phase (°)
Surface (3.6 m)	0.11	348	0.13	0
Mid-Depth (2.1 m)	0.10	13	0.10	13
Bottom (0.4 m)	0.08	20	0.08	20

K_1 Component

	Observed		Calculated	
	Amp. (m)	Phase (°)	Amp. (m)	Phase (°)
Surface (3.6 m)	0.02	182	0.02	182
Mid-Depth (2.1 m)	0.02	207	0.02	198
Bottom (0.4 m)	0.02	213	0.02	196

4.3.2.2 Current Meter at Station M3

The time series of hourly current velocities at M3 at three depths (0.5 m, 2.5 m, and 5.5 m from bottom) are shown in Figure 4-21. Positive values depict downstream currents while negative values indicate upstream currents. At this location, the observed and computed currents are compared for about 14 days in September 2004. The figure indicates that the model reproduced the current velocities well at M3 at all depths. The variations of magnitudes of current speed from surface and bottom are also well reproduced by the model. At this upstream location, surface tidal currents are not as strong as those at the downstream current meter, M2. The maximum ebb tidal velocities at the surface are about 0.8 m/s and the maximum flood tidal velocities are about 0.7 m/s. As depth increases, current velocities decrease. At the bottom layer, the maximum ebb and flood tidal velocities are about 0.4 m/sc and 0.6 m/sec, respectively, which also indicate the stronger upstream component at the bottom due to gravitational circulation. The non-tidal event recorded around day 364 is captured reasonably well by the model.

The statistical analysis of model performance against observed data at Station M3 is presented in Table 4-12. RMSE vary from 0.15 to 0.17 m/sec and relative RMSE vary from 9 to 10%. The correlation coefficients for model-data comparison are between 0.72 at the bottom and 0.86 at surface. The table indicates that, in general, the downstream station (M2) has relatively smaller RMSEs and relative RMSEs, and higher correlation coefficients compared to the upstream station M3.

The results of harmonic analysis of tidal current velocities at Station M3 are presented in Table 4-13. Due to the short period of record available for this station (~14 days), the harmonic analysis could only be conducted for the M_2 and K_1 components. The results are consistent with those analyzed at Station M2. The amplitude of semi-diurnal component, M_2, at the surface is about 0.12 m/sec or 20% smaller than that observed at the downstream station M2. However, the bottom currents are slightly stronger than those observed at M2, which was reproduced by the model.

Figure 4-22 shows the cross correlation plots of computed and observed current velocities at depths from M2 and M3. The figure indicates that overall correlation between the computed and observed currents are in good agreements and shows better correlation at the surface than at the bottom at both locations.

Table 4-12. Statistical Evaluation of Model Performance for ADCP at M3 (September 2004)

	No. Data	Data Range (m/sec)	RMSE (m/sec)	Rel. RMSE (%)	Correlation Coefficient (R^2)
Surface (5.5 m)	648	1.68	0.15	9.0	0.86
Mid-Depth (2.5 m)	648	1.69	0.17	10.0	0.80
Bottom (0.5 m)	648	1.64	0.16	10.0	0.72

Table 4-13. Comparison of Harmonic Constants for ADCP at M3: using data from September 2004

M_2 Component

	Observed		Calculated	
	Amp. (m/sec)	Phase (°)	Amp. (m/sec)	Phase (°)
Surface (5.5 m)	0.43	345	0.49	340
Mid-Depth (2.5 m)	0.40	355	0.46	342
Bottom (0.5 m)	0.35	6	0.33	344

K_1 Component

	Observed		Calculated	
	Amp. (m/sec)	Phase (°)	Amp. (m/sec)	Phase (°)
Surface (5.5 m)	0.03	225	0.03	171
Mid-Depth (2.5 m)	0.04	245	0.03	179
Bottom (0.5 m)	0.03	237	0.02	205

4.3.3 Temperature

Continuous observations of surface and bottom water temperatures were made at six locations in the Lower Passaic River in the summer of 2004 (See Figure 4-5 for locations). The model-data comparisons of surface and bottom temperature at these locations are

shown in Figures 4-23 and 4-24, respectively. The blue lines represent the computed values and the red lines the observations at surface and bottom layers. The shaded areas on the figure denote the time periods when the temperature sensors were in place in the water. During the simulation period, temperatures remained above 20ºC in the LPR except for brief period around day 354 due to a high flow event. Figures 4-23 and 4-24 indicate that the model computed surface and bottom temperatures follow the observed temperatures very closely for most of the simulation period, but the model does not quite capture the temperature decrease following the high flow event. The discrepancy in the computed and the measured temperatures around the day 354 flow event may be attributed to the water temperature assigned to freshwater inflows, which was discussed earlier in Section 4.1.3. The model-data differences are relatively small at the downstream locations (M1, M2 and M3) but become more apparent at upstream locations (M4, Bridge St. Bridge and M5). In general, both the surface and bottom temperatures and temperature variations were reproduced reasonably well at all locations.

Table 4-14 shows the statistical evaluation of model performance in terms of RMSE, relative RMSE and correlation coefficient between computed and observed water temperature at surface and bottom. The RMSE in water temperature predictions varies from 0.9 to 1.8ºC and with relative RMSE varying from 12.3% to 42.8%. In general, the model does a better job simulating the surface temperatures than those at the bottom and the model predictions at the downstream stations than at the upstream stations. The RMSE increases in the upstream direction. This may be due to a lack of knowledge concerning the water temperatures for river inflows and stormwater run-off during the high flow event.

Figure 4-25 shows the statistical correlation between the model and data values. Station M5 has been excluded from the figure because of a lack of data. The figure confirms the results of the statistical analysis, which shows relatively good model-data agreement in downstream stations.

4.3.4 Salinity

Hourly surface and bottom salinity observations are plotted against computed values in Figures 4-26 and 4-27, respectively. The shaded areas in the figures denote the periods of time when the sensors were placed in the water. The figures indicate that both the surface and bottom salinities at most stations are in good agreement with the observed salinity. The ranges of tidal variation of salinity, as well as in response to high inflow water conditions, are very well reproduced both at surface and at the bottom by the model. In particular, the model reproduced the high freshwater inflow events that occurred on day 343 and on day 353. In response to freshwater inflows, both the timing and magnitude of the salinity fluctuations were accurately represented by the model.

Table 4-14. Statistical Evaluation of Model Performance for Temperature

	No. Data	Data Range (°C)	RMSE (°C)	Rel. RMSE (%)	Correlation Coefficient (R^2)
M5					
Surface		NO DATA			
Bottom	35	3.0	1.3	42.8	0.78
Bridge Street Bridge					
Surface	335	5.1	1.6	31.1	0.45
Bottom	400	8.2	1.8	22.1	0.52
M4					
Surface	935	8.2	1.3	15.5	0.66
Bottom		NO DATA			
M3					
Surface	671	4.1	0.7	16.9	0.68
Bottom	671	4.1	0.8	19.0	0.54
M2					
Surface	1007	8.0	1.1	13.9	0.73
Bottom	1007	8.0	1.2	14.5	0.73
M1					
Surface	1007	8.1	1.0	12.3	0.78
Bottom	709	5.7	0.9	15.3	0.85

At M1, the surface salinity can decrease to near 0 psu while the corresponding bottom salinity has a value of about 13.5 psu around day 355. The observed tidal variation in the surface salinity at M1 can be as much as 12 psu. This represents the tidal excursion of high salinity water entering the river from Newark Bay during flood tides and low salinity water from the upstream Lower Passaic River on ebb tides. The model was able to reproduce the magnitude of tidal variation in the surface and bottom salinity very well. Moving upstream, salt intrusion and vertical stratification become weaker and the influence

of fresh water flow becomes dominant. At M5 and Bridge St. Bridge, the surface-to-bottom salinity differences are only about 1-2 psu during the low flow periods and salinities at surface and bottom approach 0 psu during the high flow period. During high flow events, the surface salinity can decrease from 17 psu to close to 0 psu at the downstream stations and from 7 to 0 psu at the upstream stations.

The computed temporal variations of surface salinity, as well as vertical stratification due to tidal movement of water, are in good agreement with the observations. At stations M5 and Bridge St. Bridge, the most upstream locations of the survey, the computed salinities at the surface and bottom agree very well with the observed data. The drifting lines of bottom salinity observations at M2 and M3 near day 343 in Figure 4-27 is attributed to malfunctioning of sensors due to contamination with bottom sediments (Chant, personal communication). During this period, the upstream mooring M3 recorded higher salinities than those recorded at the downstream station M2. The field crew reported that the bottom sensors were often retrieved with debris such as plastic bags and mud during scheduled maintenance. The extent of the salt intrusion into the LPR was well represented by the model. This suggests that the physical configuration (geometry) of the LPR is adequately addressed and hydrodynamic transport and mixing characteristics are well resolved by the model.

Figure 4-28 shows the vertical profile of salinity along the longitudinal section of the LPR from RM 0 through RM 7 during the calibration period. Three different hours within a tidal cycle are shown in the figures: maximum ebb, slack before flood, and maximum flood. In each panel, observed salinity values are also posted. The colors of each circle correspond to the observed value of salinity. The figures show that model performed well, reproducing observed salinity in the lower seven miles of the LPR. The positions of salt front at difference phases of tide, as well as the vertical distribution of salinity, are also well reproduced.

Table 4-15 lists the statistical evaluation of model performance in terms of RMSE, relative RMSE and correlation coefficient between computed and observed salinity at surface and bottom. The RMSE in salinity predictions varies from 1.0 psu to 3.9 psu, while the relative RMSE varies from 8.6 to 30.3%. It can be observed that the model does a better job simulating the surface salinities as compared to bottom salinities. This may be the results of the aforementioned fouling of the bottom sensors. Figure 4-29 shows the statistical correlation between the model and data values. The station M5 has not been included in the Figure 4-29 because of the paucity of data. The correlation figures also confirm that the model-data comparisons at the surface are generally better than those at the bottom. Earlier studies in Chesapeake Bay (Blumberg and Goodrich, 1990 and Johnson el. al., 1993) reports

the RMSE for salinity of 1.1 to 1.4 psu and 0.7 to 2.2 psu, respectively, and the relative RMSE of 5 to 10% and 11 to 21%, respectively.

Table 4-15. Statistical Evaluation of Model Performance for Salinity

	No Data.	Data Range (psu)	RMSE (psu)	Rel. RMSE (%)	Correlation Coefficient (R^2)
M5					
Surface		NO DATA			
Bottom	35	4.5	1.4	30.3	0.12
Bridge Street Bridge					
Surface	318	6.4	1.0	16.3	0.50
Bottom	98	11.0	1.9	17.7	0.70
M4					
Surface	900	12.1	1.0	8.6	0.90
Bottom		NO DATA			
M3					
Surface	637	12.5	1.5	11.7	0.85
Bottom	369	16.0	3.8	23.9	0.59
M2					
Surface	972	16.5	1.8	10.9	0.86
Bottom	1007	17.3	3.9	22.5	0.51
M1					
Surface	972	17.1	1.7	9.7	0.88
Bottom	709	19.0	1.7	8.9	0.72

4.4 NEWARK BAY MODEL CLAIBRATION WITH DATA COLLECTED BY IMCS OF RUTGERS UNIVERSITY: MARCH – APRIL, 2002

Extensive arrays of ADCPs and bottom mounted T/S and pressure sensors deployed by IMCS between December 2000 and May 2002, provided a high quality data set for calibration of Newark Bay, the Kill van Kull, and the Arthur Kill portion of the hydrodynamic model. The timelines of the data collection period and the station locations are shown in Figure 4-3 (upper panel) and Figure 4-4, respectively. After a careful review of

the available data, a two month period was selected when the most contiguous data are available for the Newark Bay area. This section focuses on the model calibration of tidal elevations, current velocities, temperature, and salinity using IMCS data collected during March–April, 2002 at two stations in Newark Bay (NB1 & NB3), the Kill van Kull (KVK), and upper Arthur Kill (AK). During this period, observations made at Perth Amboy (PA) were not available.

4.4.1 Tidal Elevations

Bottom mounted pressure sensor data collected at four locations in the study area between March and April 2002 were compared against model computations. Figure 4-30 shows the model-data comparisons of hourly elevations during the survey period. The plots indicate that the model reproduced the tidal elevations in Newark Bay and the Kills very well. Both the amplitude and phases of tides at all locations are in good agreement with the observed data.

During this period, the data shows considerable low-frequency sea level fluctuations between day 160 and 170 that are usually associated with 3-5 day band meteorological events such as passage of low pressure systems or perturbations from the offshore coastal ocean. The model was able to reproduce these low frequency variations well.

Table 4-16 presents the statistical evaluation of model performance in terms of RMSE, relative RMSE and correlation coefficient between model and data. The number of data points used in the statistical analysis, based on the available data, along with the statistical parameters are presented in the table. For all four stations, the RMSE in tidal elevations is about 0.12m and with relative RMSE of less than 5%. These values compare favorably with those reported (average RMSE of 11.2% and a range from 7.6 to 29.8%) by Blumberg et al. (1999) for New York Harbor. The correlation coefficients (R^2) are 0.96 for all four locations.

The results of the statistical correlation analysis in the form of scatter plots are shown in the Figure 4-31. As can be noticed, the model and data values are closely correlated and show no apparent biases with respect to water elevation.

Table 4-17 presents the results of harmonic analyses performed on both the observed and computed tidal elevations. The amplitudes and phases of four tidal constituents, M_2, S_2, K_1 and O_1 are presented in the table. The dominant tidal constituent is M_2, with observed amplitudes varying from 0.65 m at the NB3 tidal gauge to 0.74 m at the NB1. For the M_2 tide, the maximum error in amplitude is about 0.06 m which is less than 10%, and the phase error is always less than 3° (6 minutes). The comparison between the observed and the calculated amplitudes and phases looks very good for the two main

dominant components M_2 and S_2, with the maximum phase error never exceeding 7° (about 15 minutes). The results from this analysis indicate that the model developed in this study is quite capable in capturing both the amplitude and phase of the dominant tidal components accurately. The comparisons between model computations and observations consistently show that the model does an equally good job in predicting the amplitude and phase of the tidal components at all the stations, an observation consistent with the results from the RMSE analysis.

The results confirm that the model reproduced the tidal signal in the study area quite well. The amplitude and phase of M_2 component are in good agreement between the computed and observed tides.

Table. 4-16. Statistical Evaluation of Model Performance for Tidal Elevation

	No. of Data	Data Range (m)	RMSE (m)	Rel. RMSE (%)	Correlation Coefficient (R^2)
Newark Bay (NB1)	2310	2.66	0.12	4.5	0.96
Newark Bay (NB3)	1544	2.46	0.12	4.9	0.96
Arthur Kill (AK)	2098	2.63	0.12	4.6	0.96
Kill van Kull (KVK)	1985	2.5	0.12	4.8	0.96

Table. 4-17. Comparison of Harmonic Constants for Water Elevation

M_2 Component

	Observed		Calculated	
	Amp (m)	Phase (deg)	Amp (m)	Phase (deg)
Newark Bay (NB1)	0.74	229	0.69	227
Newark Bay (NB3)	0.65	230	0.59	228
Arthur Kill (AK)	0.72	224	0.68	222
Kill van Kull (KVK)	0.70	225	0.65	224

S_2 Component

	Observed		Calculated	
	Amp (m)	Phase (deg)	Amp (m)	Phase (deg)
Newark Bay (NB1)	0.24	256	0.20	260
Newark Bay (NB3)	0.25	255	0.22	262
Arthur Kill (AK)	0.23	251	0.20	254
Kill van Kull (KVK)	0.22	250	0.19	256

K_1 Component

	Observed		Calculated	
	Amp (m)	Phase (deg)	Amp (m)	Phase (deg)
Newark Bay (NB1)	0.08	84	0.06	62
Newark Bay (NB3)	0.07	80	0.05	51
Arthur Kill (AK)	0.08	82	0.06	60
Kill van Kull (KVK)	0.08	82	0.06	62

O_1 Component

	Observed		Calculated	
	Amp (m)	Phase (deg)	Amp (m)	Phase (deg)
Newark Bay (NB1)	0.04	97	0.04	95
Newark Bay (NB3)	0.04	97	0.05	102
Arthur Kill (AK)	0.04	95	0.04	94
Kill van Kull (KVK)	0.04	96	0.04	95

4.4.2 Current Velocities

Bottom mounted ADCP data, collected at four locations in the study area between March and April 2002, were compared with model results. Figure 4-32 (a through f) shows the model-data comparisons of hourly current velocities during the survey period. Current velocities at three depths (surface, mid-depth, and bottom) for a sixty-day period are shown. All current velocities data collected in Newark Bay and the Kills exhibit predominantly uni-directional currents, following the orientation of coastlines or shipping channels so that all model-data comparisons were conducted for the currents along the major axis. The plots indicate that the model reproduced the tidal current velocities in the Kills and Newark Bay

reasonably well. Both the amplitude and phases of tidal currents at all locations are generally in good agreement with the observed data.

Comparison of observed and computed current velocities in estuaries is often a difficult task. The observed current velocities usually reflect current patterns highly influenced by local features such as sharp bathymetric gradients and small scale underwater structures, which may not be adequately addressed in model grids. This is quite apparent by comparing the observed data recorded over different time periods. For example, IMCS moved the ADCP mooring position in the Kill van Kull a number of times during the deployment period (See Figure 4-4 for the mooring locations) and at one point in time the ADCP was even deployed on the other side of the shipping channel. In particular, Figure 4-32c shows the observations made at two different locations which are separated by about 300m. Even within this relatively close proximity, the observed currents on the western side of the area from day 157 to day 174 are slightly larger than those computed by the model while the model-data comparison was generally more favorable for the period of time (from days 175 through 210) when the meter was located on the eastern side of the channel. Hourly surface tidal currents at NB1 station (Figure 4-8a) are generally lower than those computed by the model. The model computed current velocities increase as they move from bottom to surface. In contrast, the measured current velocities at surface (8.4m from the bottom) are slightly reduced compared to those at mid-depth (4.9 m from the bottom).

Chant (2006) reports that the NB1 mooring was placed on the eastern flank of the shipping channel, where depths change from about 13 m in the center of the channel to less than 4 m within a distance of less than a few hundred meters. During the March-April 2002 deployment, the mooring was placed at about 9.2 m below MSL. The grid cell that coincides with the mooring location was configured with an average depth of 12.5 m based on the average of the USACE survey data for this location. Current velocities at nearby grid cells were also compared with the results at the "mooring" grid cell which is shown in Figure 4-32a. The model computed current velocities in the deeper section (13.4 m) (one cell to the left looking upstream, i.e. about 75 m away) are shown in Figure 4-32e and the two-cell (12.4 m and 7.5 m) averaged current velocities are shown in Figure 4-32f. Figure 4-32f is the result of averaging the "mooring" cell (12.4 m) (shown in Figure 4-32a) and the shallow grid cell (7.5 m) on the right. Figure 4-32e shows that, at the deeper section, the current velocities are significantly larger than those shown in Figure 4-32a. The two-cell averaged current velocities (Figure 4-32f) show very good agreement with the data. The results illustrate the highly variable lateral current structure computed by the model in the vicinity of the NB1 mooring location. Given the highly-variable bathymetric features of the Newark Bay system, the model appears to have produced reasonable current profiles at NB1.

Figure 4-33 (a through d) shows 35 hour low-passed current velocities for the same four stations. Both the model and data are low-passed for comparison. At most of the stations, both the model and data show reasonable agreement in both the low frequency fluctuations and the direction of the currents. At Station NB1, the observed currents at surface show near-zero or positive low-passed currents, which indicate neutral or upstream direction of the currents (Figure 4-33a). The model results show a predominantly downstream direction, which is expected in an estuarine environment wherein low salinity water is directed downstream in the surface layer. At the Arthur Kill station (Figure 4-33d), where the strongest residual currents are observed, both the model and data show very good agreement in the timing and magnitudes of the fluctuations in the low frequency currents at all depths.

Statistical evaluation of model performance in terms of RMSE, relative RMSE and correlation coefficient between computed and observed current velocities is presented in Table 4-18. The RMSE in tidal currents vary from 0.09 m/s to 0.23 m/s and with a relative RMSE of about 10%, which is higher than those computed for the tidal elevations. However, the 10% RMSE still compares favorably to those reported by Blumberg et al. (1999) for New York Harbor. Blumberg et al. reported a mean RMSE of 11.3% for eight stations within New York Harbor and a range from 7.1% to 16.4%. The correlation coefficients are also lower with range varying from 0.77 to 0.91. The model performed relatively well in Upper Arthur Kill and Newark Bay and less favorably in the Kill van Kull. The poor model performance in the Kill van Kull might be related to the lack of accurate depth information during the survey and calibration period, which coincided with the Harbor Deepening Project that was carried out by the New York District of the USACE. The RMSE values demonstrate that on average, the model does perform better in simulating the current velocities at the bottom as compared to mid-depth and surface; however, the model and data values seem to be better correlated at the surface than at the bottom and mid-depth. In general, the relative RMSE seems to be higher at the bottom as compared to mid-depth. Based on this table, the model performance in reproducing the current velocities looks favorable. In the SWEM study, the RMSE evaluated for ADCPs deployed in the East River varied between 0.15 m/s in the Upper East River (College Point) to 0.43 m/s in the Lower East River (Red Hook). The correlation coefficients of current velocities in SWEM were above 0.95.

The results of the statistical correlation analysis in the form of scatter plots are presented in Figure 4-34 at all three depth levels for all four stations. As can be observed, the model and data values seem to be closely correlated. Most of the points are well distributed around the one-to-one correlation line in the plot and, as suggested by the correlation coefficient themselves (Table 4-18), indicate good agreement between model and data.

However, although the correlation coefficients are all high at the KVK station, the model-data scatter plots show larger deviations than those observed at the other locations. As mentioned earlier in this section, the model under/over-predicted tidal currents at this station.

Table 4-18. Statistical Evaluation of Model Performance for Current Velocity

Station	No. of Data	Data Range (m/s)	RMSE (m/s)	Rel. RMSE (%)	Correlation Coefficient (R^2)
Newark Bay (NB1)					
Surface	2310	1.23	0.11	8.90	0.87
Mid-depth		1.18	0.12	10.17	0.83
Bottom		1.00	0.10	10.00	0.78
Newark Bay (NB3)					
Surface	1542	1.14	0.10	8.77	0.85
Mid-depth		1.01	0.09	8.91	0.85
Bottom		0.86	0.09	10.47	0.77
Arthur Kill (AK)					
Surface	1930	1.43	0.13	9.09	0.91
Mid-depth		1.37	0.12	8.76	0.90
Bottom		1.13	0.10	8.85	0.88
Kill van Kull (KVK)					
Surface	1889	2.61	0.23	8.81	0.86
Mid-depth		2.55	0.22	8.63	0.84
Bottom		1.92	0.18	9.37	0.79

Tables 4-19 through 4-22 compare the results of harmonic analyses of computed and observed current velocities at the four stations, NB1, NB3, AK, and KVK, respectively. The amplitudes and phases of the four tidal constituents, M_2, S_2, K_1 and O_1, at all four stations are presented in the tables. The dominant tidal constituent is M_2, with observed amplitude varying in the range of 0.3 m to 0.73 m at the surface, 0.29 m to 0.66 m at the mid depth and 0.23 m to 0.43 m at the bottom. The amplitude of the dominant component M_2 is the largest at the KVK station and smallest at the NB3 station. Generally, the errors in amplitude and phase predictions are lower at the bottom and higher at the surface, an observation consistent with the RMSE analysis. It can also be seen from the tables that with the exception of NB1 where the model overestimates the magnitude of the tidal components at

all three levels, the model and data are usually in good agreement for all components of tidal amplitude.

Table 4-19. Comparison of Harmonic Constants for Velocity at NB1:

M_2 Component

	Observed		Calculated	
	Amp (m)	**Phase (deg)**	**Amp (m)**	**Phase (deg)**
Surface(8.4 m)	0.30	160	0.36	152
Mid-Depth(4.9 m)	0.32	157	0.34	144
Bottom (1.9 m)	0.27	152	0.27	152

S_2 Component

	Observed		Calculated	
	Amp (m)	**Phase (deg)**	**Amp (m)**	**Phase (deg)**
Surface(8.4 m)	0.09	185	0.11	182
Mid-Depth(4.9 m)	0.09	180	0.10	176
Bottom (1.9 m)	0.09	181	0.08	181

K_1 Component

	Observed		Calculated	
	Amp (m)	**Phase (deg)**	**Amp (m)**	**Phase (deg)**
Surface(8.4 m)	0.01	34	0.01	280
Mid-Depth(4.9 m)	0.01	0	0.01	284
Bottom (1.9 m)	0.02	349	0.02	349

O_1 Component

	Observed		Calculated	
	Amp (m)	**Phase (deg)**	**Amp (m)**	**Phase (deg)**
Surface(8.4 m)	0.01	8	0.01	342
Mid-Depth(4.9 m)	0.01	3	0.01	13
Bottom (1.9 m)	0.01	359	0.01	359

Table 4-20. Comparison of Harmonic Constants for Velocity at NB3:

M_2 Component

	Observed		Calculated	
	Amp (m)	**Phase (deg)**	**Amp (m)**	**Phase (deg)**
Surface(11.0 m)	0.32	153	0.29	152
Mid-Depth(6.0 m)	0.29	149	0.30	142
Bottom (2.5 m)	0.23	147	0.23	135

S_2 Component

	Observed		Calculated	
	Amp (m)	**Phase (deg)**	**Amp (m)**	**Phase (deg)**
Surface(11.0 m)	0.10	179	0.11	185
Mid-Depth(6.0 m)	0.09	171	0.10	166
Bottom (2.5 m)	0.07	159	0.07	154

K_1 Component

	Observed		Calculated	
	Amp (m)	**Phase (deg)**	**Amp (m)**	**Phase (deg)**
Surface(11.0 m)	0.01	18	0.02	321
Mid-Depth(6.0 m)	0.01	325	0.01	234
Bottom (2.5 m)	0.01	346	0.01	227

O_1 Component

	Observed		Calculated	
	Amp (m)	**Phase (deg)**	**Amp (m)**	**Phase (deg)**
Surface(11.0 m)	0.01	2	0.01	26
Mid-Depth(6.0 m)	0.02	11	0.01	43
Bottom (2.5 m)	0.01	26	0.02	49

Table 4-21. Comparison of Harmonic Constants for Velocity at AK:

M_2 Component

	Observed		Calculated	
	Amp (m)	**Phase (deg)**	**Amp (m)**	**Phase (deg)**
Surface(10.9 m)	0.51	202	0.56	196
Mid-Depth(5.9 m)	0.48	201	0.47	191
Bottom (1.9 m)	0.35	198	0.37	187

S_2 Component

	Observed		Calculated	
	Amp (m)	**Phase (deg)**	**Amp (m)**	**Phase (deg)**
Surface(10.9 m)	0.15	231	0.15	234
Mid-Depth(5.9 m)	0.12	229	0.12	226
Bottom (1.9 m)	0.10	233	0.09	223

K_1 Component

	Observed		Calculated	
	Amp (m)	**Phase (deg)**	**Amp (m)**	**Phase (deg)**
Surface(10.9 m)	0.02	359	0.03	350
Mid-Depth(5.9 m)	0.02	357	0.02	348
Bottom (1.9 m)	0.01	8	0.01	341

O_1 Component

	Observed		Calculated	
	Amp (m)	**Phase (deg)**	**Amp (m)**	**Phase (deg)**
Surface(10.9 m)	0.01	62	0.01	358
Mid-Depth(5.9 m)	0.01	72	0.01	66
Bottom (1.9 m)	0.01	69	0.01	74

Table 4-22. Comparison of Harmonic Constants for Velocity at KVK:

M_2 Component

	Observed		Calculated	
	Amp (m)	**Phase (deg)**	**Amp (m)**	**Phase (deg)**
Surface(9.4 m)	0.73	308	0.73	299
Mid-Depth(6.4 m)	0.66	308	0.68	296
Bottom (1.9 m)	0.43	306	0.51	292

S_2 Component

	Observed		Calculated	
	Amp (m)	**Phase (deg)**	**Amp (m)**	**Phase (deg)**
Surface(9.4 m)	0.23	336	0.23	335
Mid-Depth(6.4 m)	0.23	335	0.22	332
Bottom (1.9 m)	0.18	339	0.18	331

K_1 Component

	Observed		Calculated	
	Amp (m)	**Phase (deg)**	**Amp (m)**	**Phase (deg)**
Surface(9.4 m)	0.04	182	0.02	137
Mid-Depth(6.4 m)	0.04	175	0.02	149
Bottom (1.9 m)	0.03	168	0.01	140

O_1 Component

	Observed		Calculated	
	Amp (m)	**Phase (deg)**	**Amp (m)**	**Phase (deg)**
Surface(9.4 m)	0.02	189	0.02	191
Mid-Depth(6.4 m)	0.01	197	0.02	185
Bottom (1.9 m)	0.01	179	0.01	197

4.4.3 Temperature

The model was calibrated by comparing model results to temperature measured by bottom mounted sensors collected at four locations in Newark Bay and the Kills between March and April 2002. Figure 4-35 shows the model-data comparison of hourly bottom water temperature during the survey period. The results indicate that the model reproduced the bottom temperature in the Kills and Newark Bay very well, following the warming temporal trends observed in the data during March-April of 2001. However, at the AK station, model computed bottom water temperatures are consistently lower than those observed by about 2°C. It is suspected that model may have not accounted for additional sources of heat in the area such as industrial thermal discharges.

Table 4-23 presents the statistical evaluation of model performance in terms of RMSE, relative RMSE and correlation coefficient between computed and observed bottom water temperature. The RMSE in water temperature predictions varies from 0.51ºC to 0.98ºC, with the relative RMSE varying from 6.5% to 11.3%. The RMSE in temperature predictions are always less than 1ºC, signifying that the model does a good job in simulating the temperature values in the system.

The statistical correlation between the model and data values is shown in Figure 4-36. The correlation coefficient varies in the range of 0.92 to 0.97 with a mean value of 0.95. As can be seen from the values of the correlation coefficient, the model and data values are highly correlated. The scatter plots show that most of the data and model values are more or less uniformly distributed around the one-to-one correlation line at the stations within Newark Bay. However, the plot indicates that model under-predicted bottom water temperature at the Arthur Kill station and slightly over-predicted at the Kill van Kull station.

Table 4-23. Statistical Evaluation of Model Performance for Temperature

Station	No. of Data	Data Range (°C)	RMSE (°C)	Rel. RMSE (%)	Correlation Coefficient (R^2)
NB1	2310	11.1	0.79	7.1	0.97
NB3	1544	7.7	0.51	6.5	0.97
AK	2098	9.6	0.98	10.2	0.94
KVK	1889	7.2	0.81	11.3	0.92

4.4.4 Salinity

Bottom mounted conductivity sensor data collected at four locations in the Kills and Newark Bay between March and April 2002 were compared with model results. Figure 4-37 shows the model-data comparison of hourly bottom salinity during the survey period. The results indicate that the model computed bottom salinity follows the general pattern of observed salinity in the Kills and Newark Bay. However, model computed bottom salinity during the 2002 calibration period failed to reproduce observed bottom salinity around day 187 and 203, particularly at the KVK and NB3 stations. It should also be noted that significant dredging activities took place between October 2001 and October 2002 in the shipping channels located in the Kill van Kull. The model depth configured for the simulations used pre-dredging depths measured in 2001. It may well be that at certain times during the simulations, the depths of the model grid cells may not accurately represent the real, but "unknown" bathymetric conditions during this period. By "unknown", we mean that the channel depths were known prior to the beginning of the dredging project and were known at the end of the dredging project but the times, locations, and depths during the actual dredging were not recorded and, therefore, are not known on a day by day or month by month basis.

Table 4-24 presents the statistical evaluation of model performance in terms of RMSE, relative RMSE and correlation coefficient between computed and observed bottom salinity. The RMSE of salinity vary from 1.4 psu to 3.0 psu with an average of 2.0 psu, and the relative RMSE vary from 26.9 to 34.7%. The correlation coefficients are between 0.04 and 0.74. The low values of correlation coefficients are most likely a result of the interplay of above discussed factors. The model does perform well in reproducing the salinity in the month of March. However, the model doesn't do quite as well in reproducing the rapid rise in salinity in the following month during the neap tide period, resulting in a poor correlation. Figure 4-38 shows the statistical correlation between the model and data values. The statistical correlation plots indicate a bias in the model predictions. Mostly the model underestimates the data values, particularly the high bottom salinities observed around day 187 and 203.

Table 4-24. Statistical Evaluation of Model Performance for Salinity

Station	No. of Data	Data Range (psu)	RMSE (psu)	Rel. RMSE (%)	Correlation Coefficient (R^2)
NB1	2310	5.72	1.74	30.4	0.53
NB3	1544	6.36	2.05	32.2	0.06
AK	2098	5.02	1.35	26.9	0.74
KVK	1889	8.64	3	34.7	0.04

Further analyses of model simulations were conducted in an attempt to identify the causes of this mis-calibration of model. Sensitivity runs were performed wherein changes were made to a few calibration parameters. In addition, adjustments to the model bathymetry in the Kill van Kull and Newark Bay (KVK-NB) were also considered. The latter reflects the uncertainty in actual depths in this region given the activities of the USACE Harbor Deepening Project.

A coefficient (HORCON) in the Smagorinsky(1961) horizontal turbulence closure formula and the bottom roughness length (Z_0) are the two typical ECOMSED calibration parameters to adjust horizontal and vertical density gradients. Lower HORCON values produce less horizontal mixing and thus enhance vertical stratification. For model calibration, a value of 0.01 was used for HORCON. The bottom roughness length Z_0 is being used in ECOMSED in the computation of bottom drag coefficient, C_D, which in turn is being used to compute bottom stress. The bottom drag coefficient is estimated by an equation:

$$C_D = \left[\frac{1}{\kappa} \ln(0.5 * Z_b / Z_0) / Z_0 \right]^{-2}$$

where Z_0 is the bottom roughness length, Z_b is the thickness of the model grid point nearest the bottom and κ is the von Karman constant. Lower values of Z_0 are used to represent smooth bottom and thus produce lower bottom drag coefficient which leads to less vertical turbulent mixing. Thus lower values of Z_0 should result in increased vertical stratification. During the model calibration, a value of 0.001 was used to represent bottom roughness of the model domain.

A series of sensitivity model runs were designed:

- RUN A: decrease the coefficient in the Smagorinsky horizontal turbulence formulation (HORCON) to 0.002

- RUN B: RUN A plus decreasing the bottom roughness length (Z_0) to 0.0005
- RUN C: use the post-dredging model depths in the Kill van Kull and Newark Bay together with using a HORCON value of 0.002

The results of sensitivity runs are shown in Figures 4-39 through 4-41. Figure 4-39 (RUN A) shows that the model reproduced some of the surge in bottom salinity around day 187. However, it failed to reproduce the second surge observed around day 203. The model results indicate that prior to the second salinity surge event the model computed bottom salinities at the KVK station were lower than those observed and remained lower throughout the event.

RUN B, which used a Z_0 value of 0.0005, shows slightly increased bottom salinities compared to those of RUN A, but the improvement is not significant (Figure 4-40). The third sensitivity run, RUN C, used post-dredging depths in the Kill van Kull and Newark Bay while maintaining the same model parameters used for RUN A. The post-dredging depths reflect the depth condition wherein all 50-ft Harbor Deepening Projects were assumed completed in the area. Figure 4-41 shows the results of RUN C. At the KVK station, the model reproduced the surge of bottom salinities around days 187 and 203 better than those of RUN A and B. However, under the deepened water depths in the Kills, the bottom salinities at other interior stations were also increased significantly, particularly prior to the surge events, which is not consistent with the observed data.

In order to understand model's inability to bring in high salinity water from the mouth of Kill van Kill, bottom salinities from few more locations east of the KVK stations were compared with observed data at KVK. Figure 4-42 shows bottom salinities at 1.0, 1.5, 2.5, and 3.5 km from east of the KVK station, respectively. The figure indicates that model computed surges of salinities are at around 2.5 km east of the KVK station but the model failed to bring in further to the west close to the KVK station.

Statistics of model-data comparison for each sensitivity run for salinity and current velocities were compiled in Table 4-25 and 4-26, respectively. RMSE, relative RMSE, and correlation coefficients of sensitivity runs are presented along with original model calibration results. The results indicate that there are no significant changes in model skills among these sensitivity runs, which suggest relatively little effect of these changes in model parameters/bathymetric changes on calibration scores and bottom velocities/shear stress even though the model is computing relatively large changes in the model skill for salinity.

Table 4-25. Statistical Evaluation of Model Performance for Salinity for the Model Sensitivity Runs

	RMSE (psu)				Correlation Coefficient (R^2)			
	Calibration	RUN A	RUN B	RUN C	Calibration	RUN A	RUN B	RUN C
NB1	1.74	1.03	1.01	1.48	0.53	0.55	0.53	0.69
NB3	2.05	1.48	1.39	1.58	0.06	0.07	0.07	0.16
AK	1.35	0.95	0.83	1.14	0.74	0.71	0.69	0.71
KVK	3.00	2.98	2.83	1.89	0.04	0.01	0.01	0.08

Table 4-26. Statistical Evaluation of Model Performance for Bottom Current Velocities for the Model Sensitivity Runs

Surface

	RMSE (m/s)				Correlation Coefficient (R^2)			
	Calibration	RUN A	RUN B	RUN C	Calibration	RUN A	RUN B	RUN C
NB1	0.16	0.17	0.17	0.17	0.74	0.72	0.71	0.74
NB3	0.16	0.17	0.17	0.17	0.74	0.72	0.71	0.74
AK	0.17	0.20	0.21	0.17	0.86	0.86	0.86	0.86
KVK	0.23	0.27	0.27	0.27	0.86	0.81	0.79	0.81

Mid-depth

	RMSE (m/s)				Correlation Coefficient (R^2)			
	Calibration	RUN A	RUN B	RUN C	Calibration	RUN A	RUN B	RUN C
NB1	0.15	0.15	0.15	0.14	0.76	0.74	0.72	0.74
NB3	0.10	0.10	0.10	0.09	0.85	0.85	0.85	0.85
AK	0.11	0.12	0.13	0.10	0.90	0.92	0.92	0.92
KVK	0.22	0.26	0.27	0.27	0.84	0.77	0.77	0.77

Bottom

	RMSE (m/s)				Correlation Coefficient (R^2)			
	Calibration	RUN A	RUN B	RUN C	Calibration	RUN A	RUN B	RUN C
NB1	0.12	0.12	0.13	0.12	0.74	0.72	0.72	0.74
NB3	0.10	0.10	0.10	0.09	0.76	0.72	0.71	0.76
AK	0.10	0.10	0.11	0.09	0.88	0.90	0.90	0.90
KVK	0.17	0.20	0.21	0.20	0.80	0.74	0.71	0.72

Cross-sectional fluxes of these sensitivity runs at three locations within the Kills are tabulated in Table 4-27. These values represent two-month averaged total fluxes at each transect. Negative values indicate either westerly or southerly direction of fluxes. The results indicate that with lowering HORCON and bottom roughness length (Z_0) the net flux in the Kills increases slightly but less than 10%. With increasing water depths in the Kill van Kull and Newark Bay (RUN C), the net flux decreases about 10%. The results suggest that changing calibration parameters and bathymetry within the ranges used for this sensitivity analysis does not significantly affect the overall volume fluxes in the system.

Table 4-27. Cross Sectional Fluxes for Each Sensitivity Analysis (units: m^3/sec)

	Calibration	RUN A	RUN B	RUN C
Kill van Kull	-152	-154	-162	-137
Newark Bay	-10	-10	-10	-10
Arthur Kill	-161	-165	-173	-147

Lowering the HORCON and Z_0 values helped the model to come closer to reproducing the bottom salinity surge events at KVK and NB3 stations but the model was not able to fully reproduce these events. In addition, some of these changes degraded model performance during other parts of the calibration period. Further lowering the parameters caused the model to become unstable. Deepening the depths in the Kills helped greatly to reproduce the model results but resulted in unacceptable increases in salinity intrusion during other periods.

The various sensitivity runs produced no meaningful improvement of the model performance so additional analysis of the model performance was considered by looking at the performance of the model in the open waters of NY-NJ Harbor and how the performance of the model in that region may have affected the calibration in the Kills and Newark Bay. A separate field survey data set was available in the Hudson River in the spring of 2002 (Warner et al., 2005). A 43-day record of surface and bottom temperature and salinity observations (from April 23 to June 5, 2002) was utilized to compare against model computations. Warner et al. (2005) deployed data recording instruments just upstream of the Hudson River-Harlem River confluence which is about 23 km upstream of the Battery, where the water depth is about 15 m.

Figure 4-43 shows model-data comparison at this location. The figure also presents the Hudson River flows in the lower panel. The solid line indicates the flow measured at the USGS Green Island gauging station and the dotted line indicates the total Hudson River inflow including tributaries downstream of Green Island. In general, model computed water temperature and salinity match the data very well. The increasing trend in temperature both at surface and bottom is well reproduced by the model. Spring-neap variations of vertical salinity stratification are also very well reproduced by the model. However, close examination of the bottom salinity during high flow events reveals that model does not quite match the levels observed in the salinity. The model reproduced observed salinities for the 700 m^3/sec event (around days 210-215) very well but failed to reproduce subsequent high flow (~2,000 m^3/sec) event which occurred around day 225-230. Warner et al. (2005), presenting computations of their hydrodynamic model against the same data set, found similar problems. Their results show good agreement with high flow event (days 225-230) but over compute bottom salinity during the smaller high flow event (days 210-215).

We believe that the difference between the model versus data discrepancies in the two models may be attributed to uncertainties in the estimates of the tributary inflows that provide freshwater to the Hudson River, i.e., the ungauged drainage area below the USGS gauge at Green Island. Without having a detailed watershed model of the lower Hudson Valley together with detailed temporal and spatial rainfalls distribution for this region, one is dependent on making simplifying assumptions concerning runoff volumes for the ungauged drainage area. In the HydroQual hydrodynamic model estimates of the ungauged flows were extrapolated from a few USGS gauging stations (Wappinger Creek, Croton Rivers, and Esopus Creek), while Warner et al. (2005) estimated their Hudson River flow by multiplying the values recorded at Green Island by 1.4. This appears a little high but reasonable considering that the drainage area downstream of the Green Island gauge account for ~25% of the total Hudson River drainage area. Taking the long-term average of HydroQual's data analysis, our correction factor for the total Hudson River flow would be 1.2 times the Green Island. Hence, our flow estimates are lower than those developed by Warner et al.. It is possible then that our estimated flows for the low flow event better represent actual flow conditions since we match the first event salinity better than Warner et al., but that their estimated flows for the second event are more accurate since they reproduce the observed second event salinities.

In summary, model computed bottom salinity matches data very well during low flow periods both in the Passaic-Hackensack Rivers and Hudson River. However, model underestimates salinity intrusion in the Kills after high flow events in the Hudson River. The sensitivity runs indicate that model somewhat responded to the adjustments of model parameters (i.e. HORCON, bottom roughness length (Z_0), and shipping channel depths) but

not to the level of satisfaction. Even using the post-dredging depths in the Kills failed to reproduced the salinity intrusion, which indicates inadequate model performance outside of the Kills and Newark Bay region and was evident in the model-data comparison at the Hudson mooring station. It may be concluded that transport through Newark Bay/Kills is reasonable although some uncertainty exists due to problems with salinity computed in NY/NJ Harbor. Results show relatively little effect on calibration scores and bottom velocities/shear stress.

4.4.5 Net Fluxes in Newark Bay and the Kills

Sub-tidal volume fluxes reflect the system's response to meteorological events such as storms, floods, or low-frequency perturbation of offshore coastal oceans. The time series of fluxes in Newark Bay, the Kill van Kull and the Arthur Kill for March-April 2002 are shown in Figures 4-44a and b. The fluxes are low-pass filtered with a cut-off period of 35 hours to remove the tidal component of volume exchanges. The figures show the total flux in black, upper layer flux in red and lower layer flux in blue. The monthly mean fluxes in m^3/sec are also indicated in the upper part of each frame in the figures. While the monthly averaged volume fluxes in the system remain less than 200 m^3/sec, the downstream volume fluxes out of Newark Bay are consistently balanced by the sum of the Passaic and Hackensack Rivers inflows (Figure 4-44a). In the 35-hour sub-tidal band, the total volume flux in the Passaic River is almost always in the downstream direction, reflecting the dominant freshwater inflows from above Dundee Dam. However, in the Hackensack River, the sub-tidal fluxes vary over time reflecting the relatively small inflow of freshwater to the system, since most of the natural inflow to the system is captured for water supply purposes. During this period, the monthly volume fluxes at the mouth of the LPR and Hackensack River indicate that very limited freshwater inflows came into the basin. Within the Newark Bay system, Figure 4-44a indicates that there is a strong two layer estuarine circulation in Newark Bay and at the mouth of both the LPR and Hackensack River, in which the upper layer with low salinity water flows downstream and the denser lower layer flows upstream.

In the Kill van Kull and the Arthur Kill, the flux is predominantly toward Raritan Bay. Maximum rates for these sub-tidal fluxes are about 600 m^3/sec (Figure 4-44b) during this two month period. The flux in the Arthur Kill is quite similar to the one in the Kill van Kull. The results indicate that there is very limited two layer circulation in the Kill van Kull with no evidence of two layer circulation in the Arthur Kill. During this period, the average net volume fluxes in the Kills are about 150 m^3/sec toward Raritan Bay. The magnitude and its direction are consistent with earlier SWEM and CARP studies (HydroQual, 2002), which reported the net volume flux of about 130 m^3/sec toward Raritan Bay during March-April in 1995.

Several studies indicate that there are "flow-through" flushing events in Newark Bay (Pence, 2004, Pecchioli et al., 2006, and Chant, 2006). Under persistent westerly wind conditions in the NY-NJ Harbor area, coastal set-downs result in the "emptying" of the Newark Bay water. During easterly wind conditions, coastal set-ups causes transport of waters from Raritan Bay and the Upper New York Bay mostly through the Kill van Kull into Newark Bay, resulting in the "filling up" of the Bay. During the 2002 calibration period, a few emptying/filling events of Newark Bay were observed. Figure 4-44b shows the low-passed cross-sectional fluxes in the Newark Bay system. On days 153, 160, 171, and 177, the total volume fluxes of Newark Bay are the southerly (downstream) direction. During these periods, the wind data observed at JFK Airport indicate that there were westerly or northerly winds in preceding days (Figure 3-5c). On other days, when the upstream fluxes were computed (i.e. days 162 and 192), the winds were dominantly southerly in preceding days. There were no significant easterly wind events during the simulation period so no filling events exclusively due to easterly winds were identified.

4.5 NEWARK BAY MODEL VALIDATION USING 2001 SURVEY DATA

Using the same model configuration, consistent model parameters and input files used for the 2002 model calibration, a model validation was performed. This is to evaluate whether the model calibrated for 2002 conditions can be used to reproduce hydrodynamic conditions at different period. IMCS field survey data collected between March through August 2001 were selected for the model validation. Unlike in the spring of 2002, only three relatively long deployment data are available during this period: one in the Kill van Kull (KVK), one in upper Newark Bay (NB1), and the other at the southern mouth of the Arthur Kill near Perth Amboy (PA). No data are available at the AK station in 2001. At the NB3 station, only two weeks of observations were available in August 2001.

All forcing data including open boundary elevations, temperature and salinity data, freshwater inputs, and meteorological data were assembled for this period. Model initial conditions were extracted from a model archive from the ten year simulations conducted in the earlier phase of this study. A month of model spin-up was applied to let the model reach its equilibrium with open boundary forcing. An evaluation of model output showed that model reached its equilibrium within a month.

4.5.1 Tidal Elevations

Bottom mounted pressure sensor data collected at three locations in the study area between March and August 2001 were compared against model computed tidal elevations. Figure 4-45 shows the model-data comparisons of hourly elevations during the survey period. Each panel shows 60 days of model and data comparison. The plots indicate that

the model reproduced the tidal elevations measured at all stations very well. Both the amplitude and phases of tides as well as low-frequency sea level fluctuations are in good agreement with the observed data.

Table 4-28 presents the statistical evaluation of model performance in terms of RMSE, relative RMSE and correlation coefficient between model and data. The number of data points used in the statistical analysis, based on the data, along with the statistical parameters are presented in the table. For all four stations, the RMSE in tidal elevations is about 0.12 m and with relative RMSE of between 4.2% and 5.1%. The correlation coefficients (R^2) for tidal elevation vary from 0.96 to 0.98. These values are comparable with the results achieved during the 2002 model calibration.

Table 4-28. Statistical Evaluation of Model Performance for Tidal Elevation

Station	No. of Data	Data Range (m)	RMSE (m)	Rel. RMSE (%)	Correlation Coefficient (R^2)
NB1	4462	2.86	0.13	4.6	0.97
NB3	774	2.37	0.12	5.1	0.98
PA	1960	2.86	0.12	4.2	0.97
KVK	3468	2.76	0.12	4.4	0.96

4.5.2 Current Velocities

Bottom mounted ADCP data, collected at four locations in the study area between March and August 2002, were compared with model results. Figure 4-46 (a through e) shows the model-data comparison of hourly current velocities during the survey period. Current velocities at three depths (surface, mid-depth, and bottom) for a sixty-day period are shown in each frame. The plots indicate that the model reproduced the tidal current velocities in the Kills and Newark Bay reasonably well. Both the amplitude and phases of tidal currents at all locations are generally in good agreement with the observed data. However at certain times, the computed current velocities do not match well with observed values. For example, at KVK, the computed current velocities do not agree well during April 2001 (from day 190 to 215). Observed values are significantly lower than those computed. As discussed in Section 4.4.2, comparison of observed and computed current velocities in estuaries is often a difficult task. The observed current velocities are highly influenced by local features such as small scale underwater structures, which may not be adequately addressed in model grids. In 2001, IMCS deployed the ADCP at different

locations a number of times during the deployment period (See Figure 4-4 for the mooring locations). Table 4-29 lists the station depths for each deployment at each station. As evident in the table, the instrument depths sometimes vary significantly despite the proximity of each deployment. This in turn makes it difficult to assign model results to the proper vertical level to compare with the observed current velocities. Table 4-29 indicates that during this period the current mooring at the KVK station was in about 10.6 m of water whereas at other times the mooring was placed at 13 to 14 m water depths.

Table 4-29. ADCP Mooring Depths during 2001 Model Validation Period

Station	Period of Data Measurement		Depth (m)
	Start Date (mm/dd/yy)	End Date (mm/dd/yy)	
NB1	03/02/01	04/02/01	9.1
	04/09/01	05/09/01	11.6
	05/14/01	05/30/01	10.2
	08/06/01	08/22/01	12.1
NB3	08/06/01	08/22/01	12.3
PA	03/07/01	03/28/01	12.3
	04/05/01	05/06/01	12.7
KVK	03/02/01	04/03/01	14.3
	04/09/01	05/03/01	10.6
	05/14/01	05/30/01	13.4

Statistical evaluation of model performance in terms of RMSE, relative RMSE and correlation coefficient between computed and observed current velocities is presented in Table 4-30. The RMSE in tidal currents vary from 0.11 m/s to 0.26 m/s and relative RMSE varied between 9% and 15%, which are comparable to those computed for the 2002 calibration period. As in the 2001 calibration period, the model performed relatively well in Newark Bay and less favorably in the Kill van Kull. The RMSE values demonstrate that on average, the model does perform better in simulating the current velocities at the bottom as compared to those at mid depth and surface. The validation results for the current velocities are consistent with the calibration results.

Table 4-30. Statistical Evaluation of Model Performance for Current Velocity

Station	No. of Data	Data Range (m/s)	RMSE (m/s)	Rel. RMSE (%)	Correlation Coefficient (R^2)
NB1					
Surface	3998	1.91	0.18	9.4	0.80
Mid-depth		1.24	0.15	12.1	0.80
Bottom		1.08	0.13	12.0	0.77
NB3					
Surface	774	1.02	0.11	10.8	0.83
Mid-depth		1.10	0.12	10.9	0.79
Bottom		0.92	0.12	13.0	0.71
PA					
Surface	1931	1.66	0.19	11.4	0.79
Mid-depth		1.45	0.19	13.1	0.76
Bottom		1.21	0.18	14.9	0.59
KVK					
Surface	3468	1.81	0.26	14.4	0.67
Mid-depth		1.66	0.23	13.9	0.66
Bottom		1.40	0.20	14.3	0.59

4.5.3 Temperature

Figure 4-47 shows the model-data comparison of hourly bottom water temperature during the 2001 validation period. The results indicate that the model reproduced the bottom temperature in the Kill van Kull, Perth Amboy, and Newark Bay very well, following the temporal trends observed in the data during this period. One exception is during August 2001 (between day 310 and 325) when the computed water temperature is about 2ºC lower than those observed water temperature. Figure 4-47 indicates that the model under-computed bottom water temperature at NB1 and NB3 in August 2001 about 2ºC. The figure also shows that bottom water temperatures were depressed during the month of July 2001 and failed to recover in August at the NB1 and NB3 stations. This may be due to inadequate prescription of upstream freshwater inflow temperatures or the meteorological forcing data during this period.

Table 4-31 presents the statistical evaluation of model performance in terms of RMSE, relative RMSE and correlation coefficient between computed and observed bottom water temperature. The RMSE in water temperature predictions varies from 0.4ºC to 1.8ºC, with the relative RMSE varying from 2.9% to 66.8%. The high values of 1.75ºC and 66.8% for RMSE and relative RMSE, respectively, are from the NB3 where only a relatively short period of observations was available in August 2001. At other stations, the RMSE in temperature predictions are always less than 1ºC, signifying that the model does a good job in simulating the temperature values in the system.

Table 4-31. Statistical Evaluation of Model Performance for Temperature

Station	No. of Data	Data Range (°C)	RMSE (°C)	Rel. RMSE (%)	Correlation Coefficient (R^2)
NB1	2310	23.6	0.8	3.6	0.99
NB3	1544	2.6	1.8	66.8	0.42
PA	1960	13.3	0.4	2.9	0.99
KVK	3468	13.3	0.5	3.6	0.99

4.5.4 Salinity

Bottom mounted conductivity sensor data collected in the KVK, Perth Amboy, and Newark Bay between March and August 2002 were compared with model results. Figure 4-48 shows the model-data comparison of hourly bottom salinity during the validation period. The results indicate that the model computed bottom salinity follows the general pattern of observed salinity in the Kills and Newark Bay. There are, however, events that the model was not able to reproduce such as the sudden increase in salinity in April 2001 – between day 190 and day 210 at the KVK station, which is similar to model-data mismatch observed in the calibration period. As in the 2001 calibration period, this event is correlated with high freshwater flows in the Hudson River. Figure 4-49 shows the freshwater flows used for the model simulations. There are high flow events in the Hudson between day 190 and 210.

Table 4-32 presents the statistical evaluation of model performance in terms of RMSE, relative RMSE and correlation coefficient between computed and observed bottom salinity. The RMSE of salinity vary from 0.7 to 2.7 psu with an average of 1.5 psu, and the relative RMSE vary from 8.2 to 22.5%. The correlation coefficients are between 0.19 and 0.89. The low values of correlation coefficients are also from NB3 where limited data were

collected during the model validation period (about 15 days). It is unclear, however, as to the cause of this discrepancy.

Table 4-32. Statistical Evaluation of Model Performance for Salinity

Station	No. of Data	Data Range (psu)	RMSE (psu)	Rel. RMSE (%)	Correlation Coefficient (R^2)
NB1	3278	16.6	1.4	8.2	0.89
NB3	774	3.2	0.7	22.5	0.19
PA	1960	7.9	1.1	14.2	0.50
KVK	2712	16.8	2.7	15.9	0.52

4.5.5 Net Fluxes in Newark Bay And The Kills

Sub-tidal volume fluxes in Newark Bay, the Kill van Kull and the Arthur Kill for March-August 2001 are shown in Figures 4-50 a and b. The fluxes are low-pass filtered with a cut-off period of 5 days to remove the tidal component of volume exchanges. The figures show the total flux in black lines, upper layer flux in red lines, and lower layer flux in blue lines. The monthly mean fluxes in m^3/sec are also indicated in the upper part of each frame in the figures. During the 2001 validation period, the general direction of the net fluxes in the KVK-Newark Bay system is consistent with the fluxes computed during the 2002 calibration period (see Figures 4-44a and b): counter-clock-wise around Staten Island. During this period, the monthly volume fluxes at the mouth of the LPR and Hackensack River indicate that some large freshwater inflows entered into the basin, particularly during the months of March, April, and June (see Figure 4-49 for river flow data). Within the Newark Bay system, Figure 4-50a indicates that there is strong two layer estuarine circulation in Newark Bay and at the mouths of both the LPR and the Hackensack River. The magnitude of two layer circulation intensified during the high flow months (March, April and June).

In the Kills, while the direction of net fluxes remained the same as during the calibration period, it appears that the magnitude of net fluxes increased with the high freshwater flow volumes in the LPR system and the Hudson River (Figure 50b). During April (day 180 – 210) the net volume fluxes almost doubled compared to those during low flow months (day 270 – 330). Also during the low flow period, the model results suggest that very weak two-layer circulation exists in the Kill van Kull. However, in the Arthur Kill cross-section, both the surface and lower layer flows toward Raritan Bay.

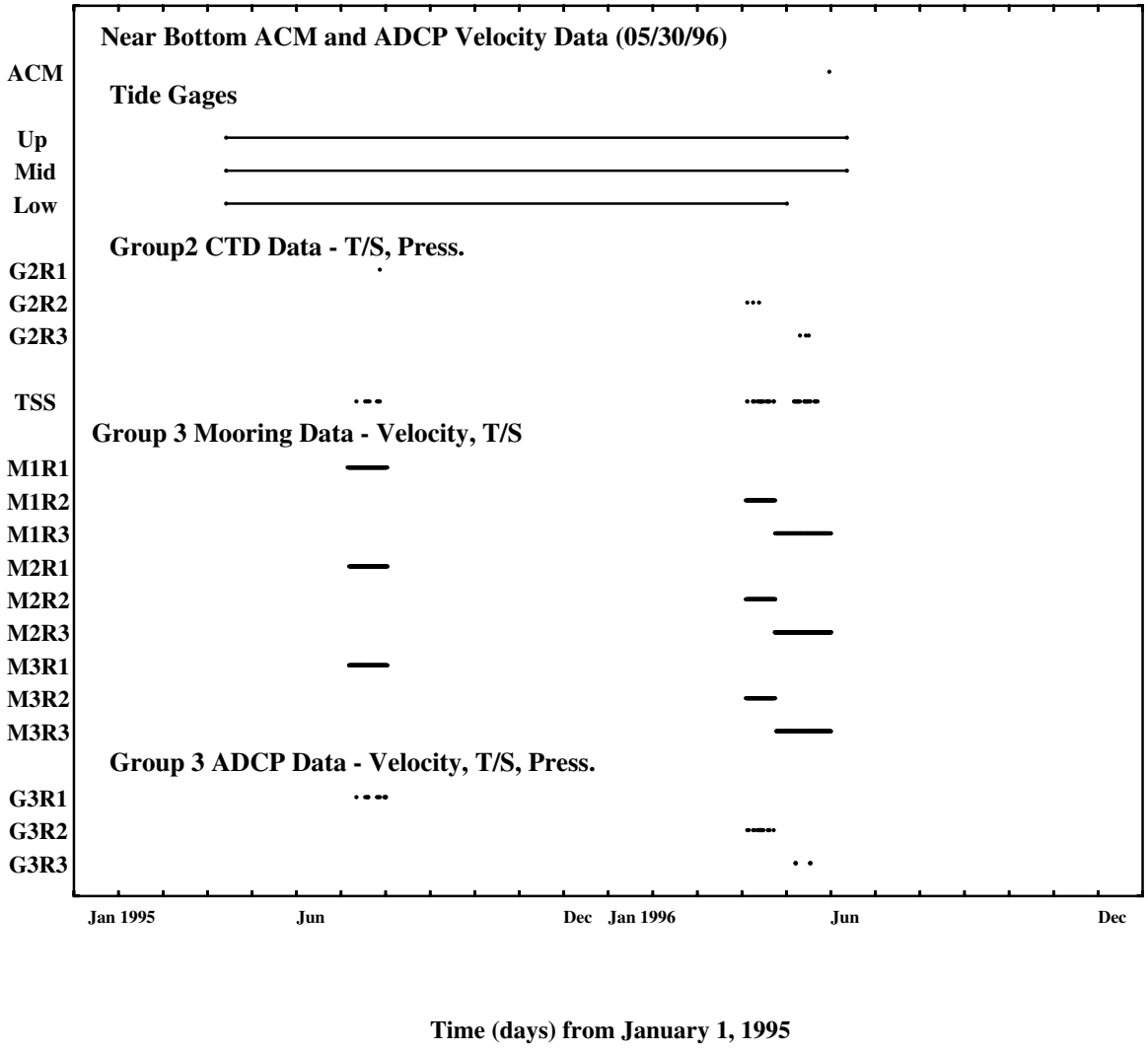

Figure 4-1 Timeline diagram of TSI field sampling data collected in 1995 and 1996 in the Lower Passaic River

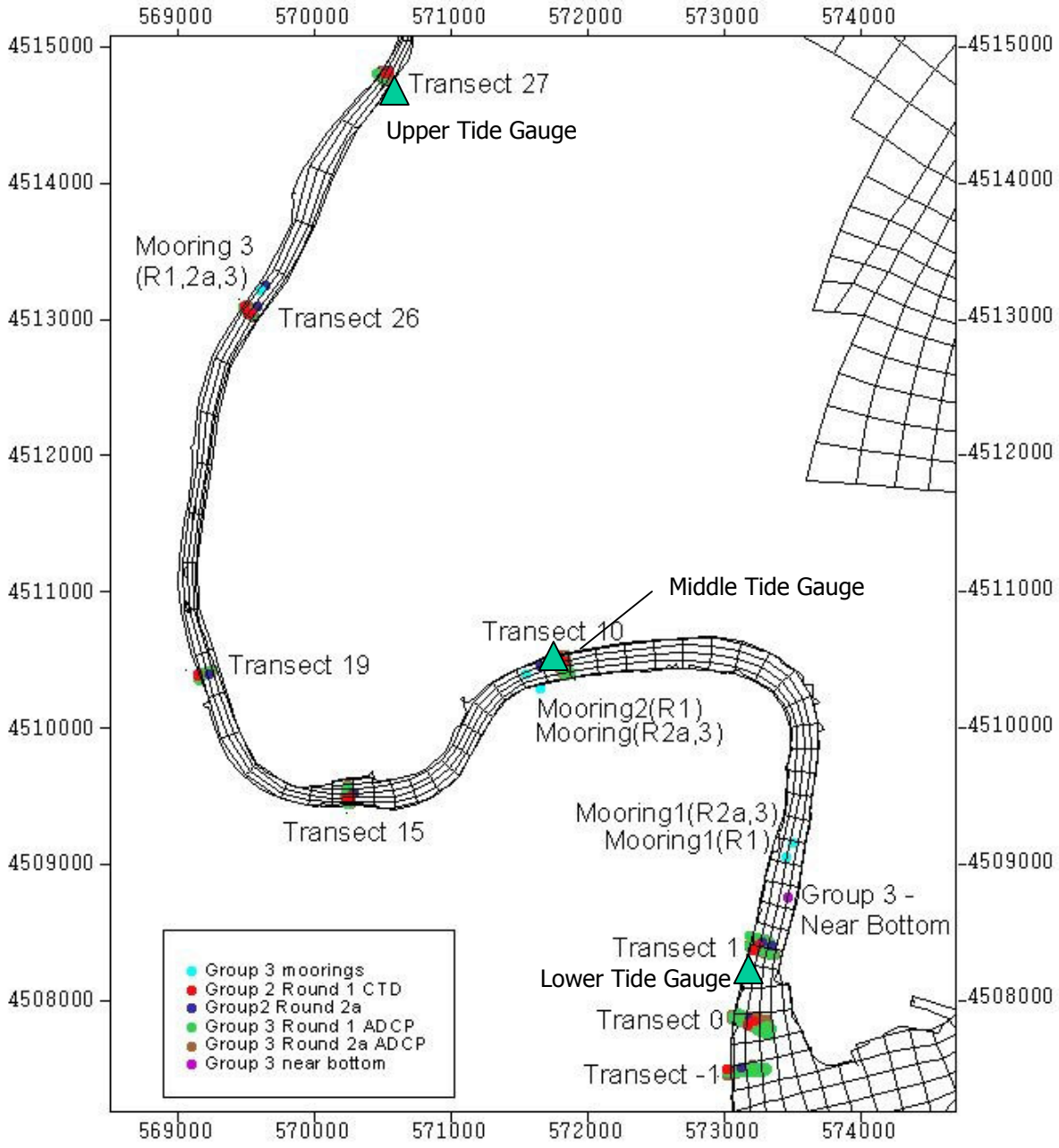

Figure 4-2 Locations of TSI field sampling stations

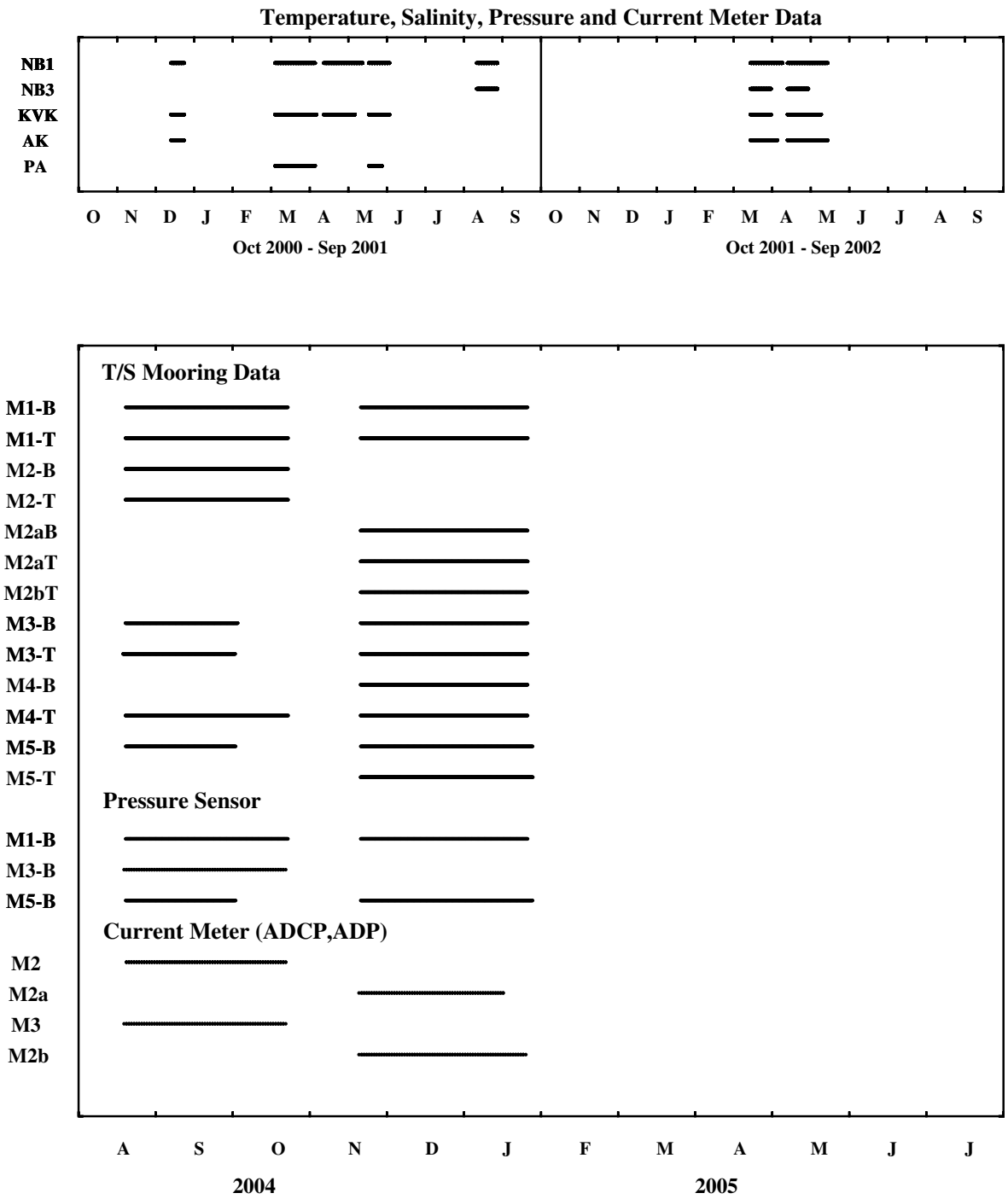

Figure 4-3 Timeline diagram of IMCS field sampling data collected between 2000 and 2002 (upper panel) and 2004 (lower panel) (T: surface B: bottom)

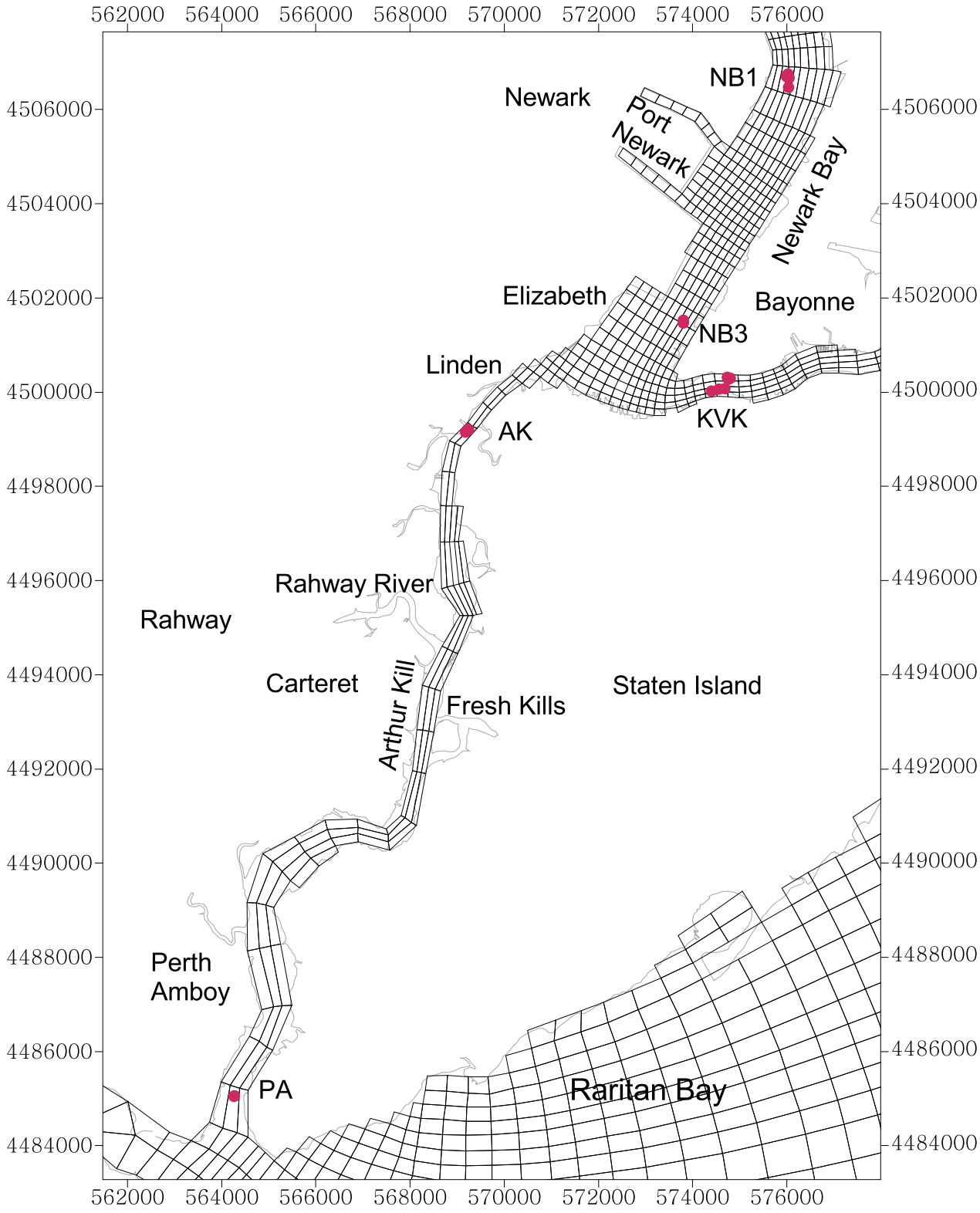

Figure 4-4 Locations of IMCS field sampling stations in Newak Bay, the Kill van Kull and the Arthur Kill (2000 - 2002)

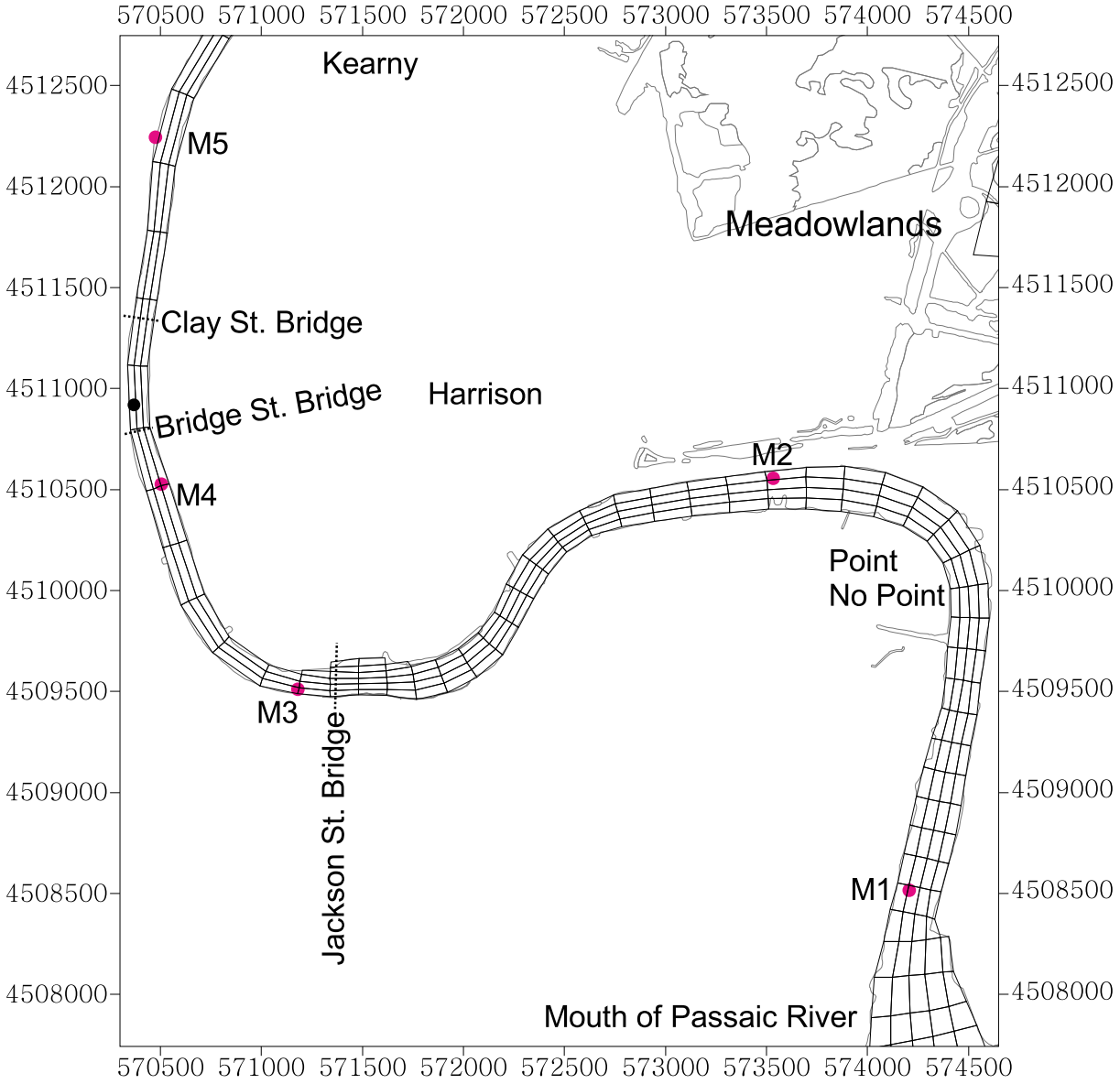

Figure 4-5 Locations of IMCS field sampling stations in the Lower Passaic River (2004)

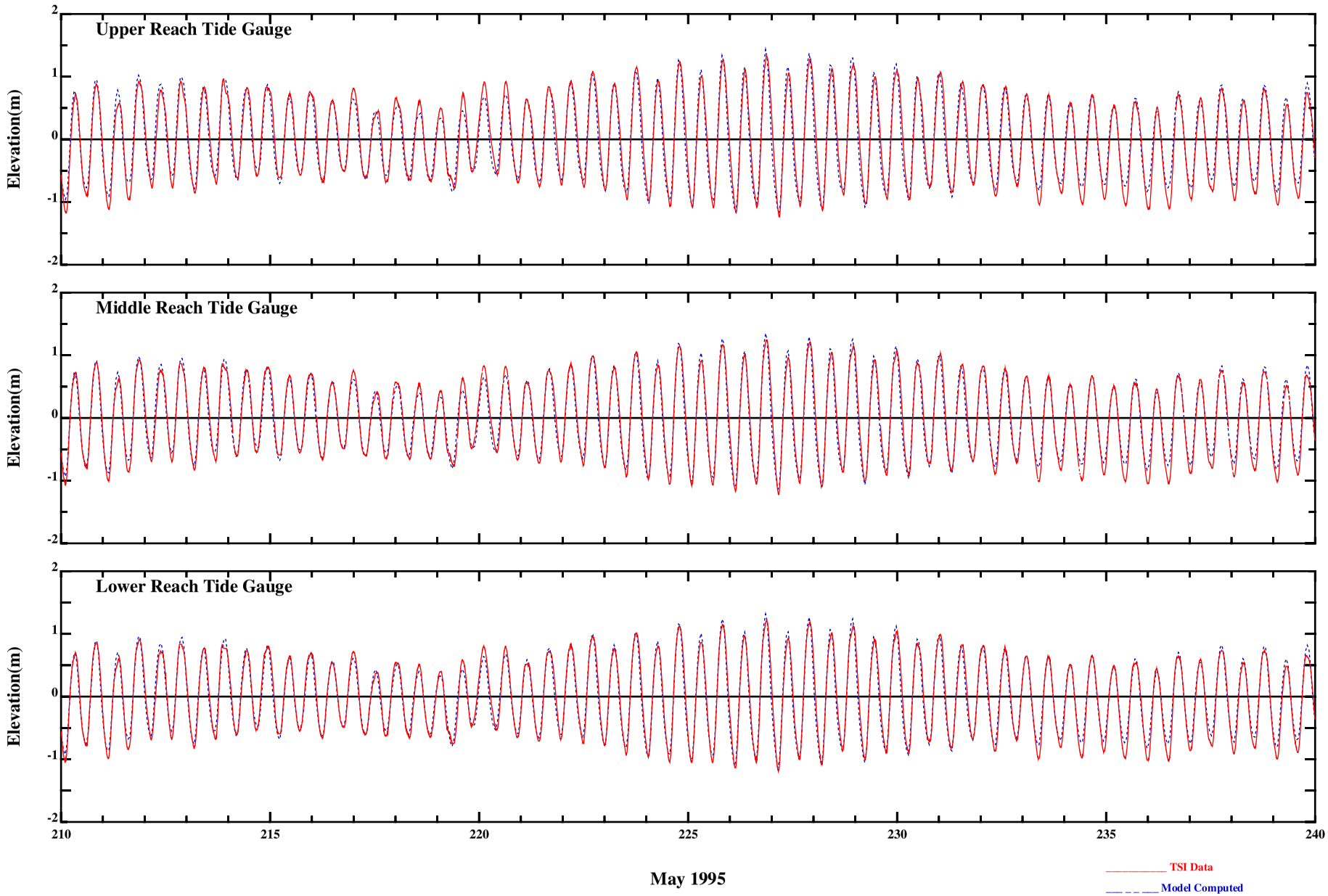

Figure 4-6 Comparison of hourly water elevations at TSI stations over a period of one month (May 1995)

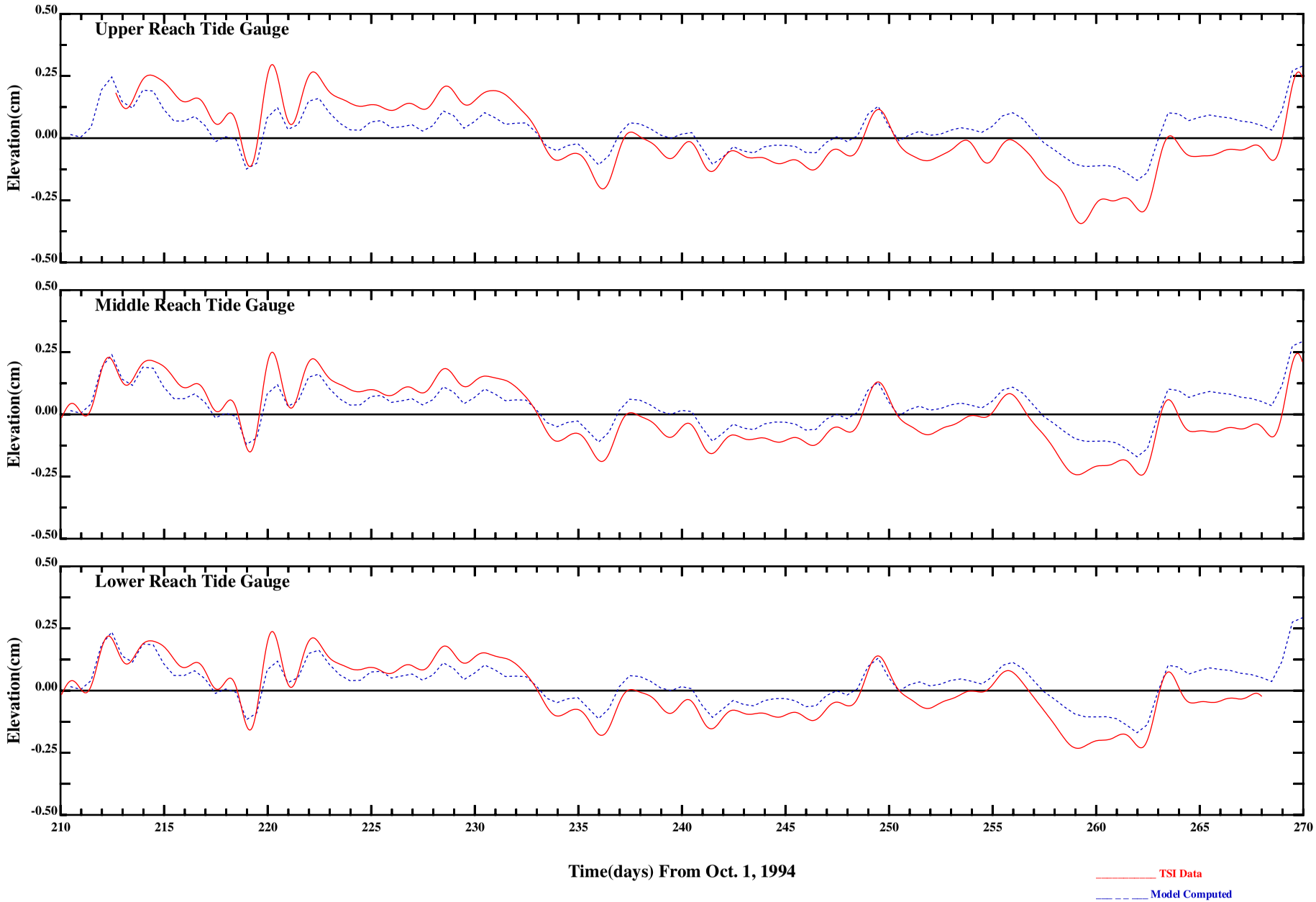

Figure 4-7 Comparison of 35 hours low-passed water elevations at TSI stations over a period of two months (May-June 1995)

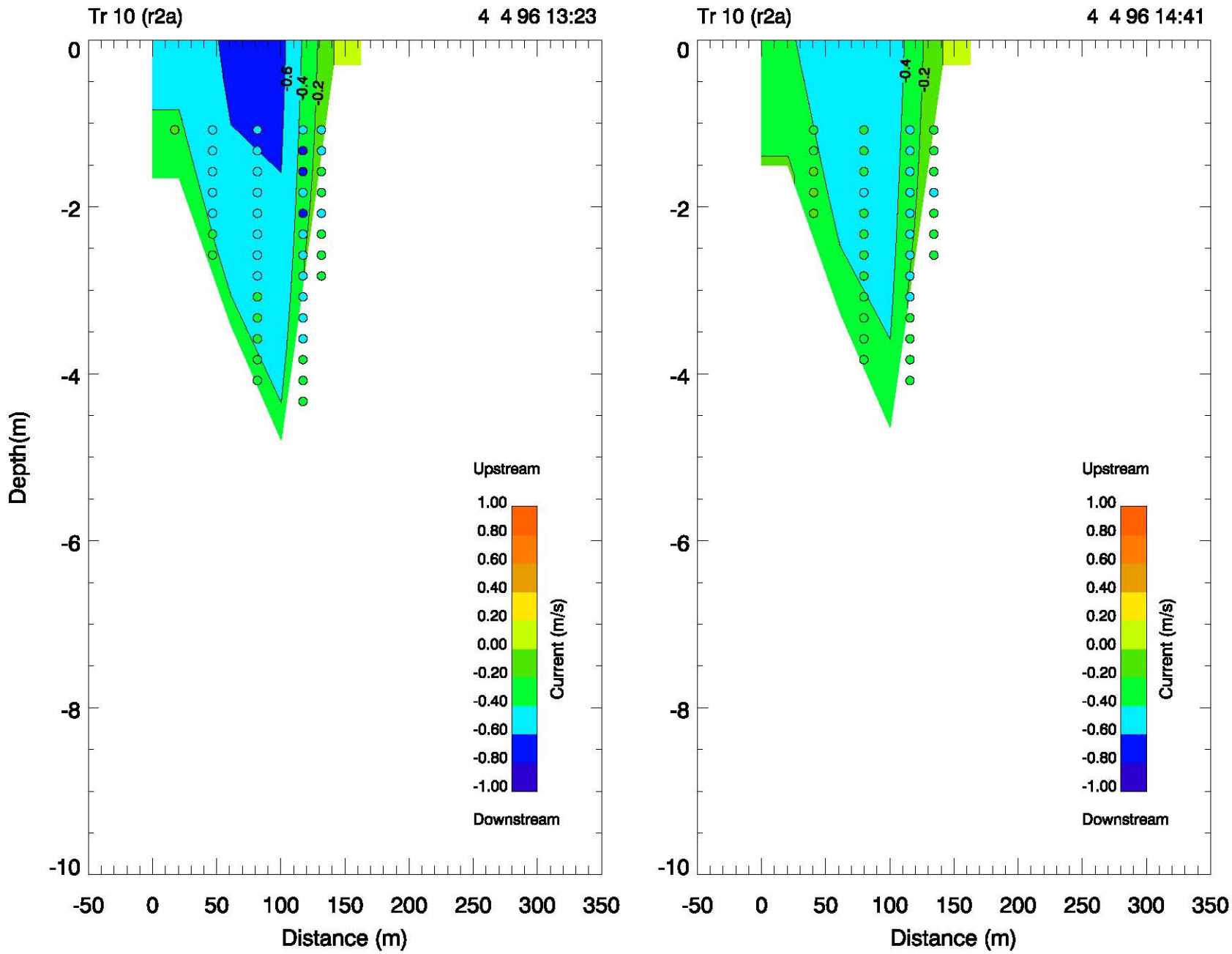

Figure 4-8 Comparison of instantaneous cross-sectional velocities at Transect 10 (Round 2a)

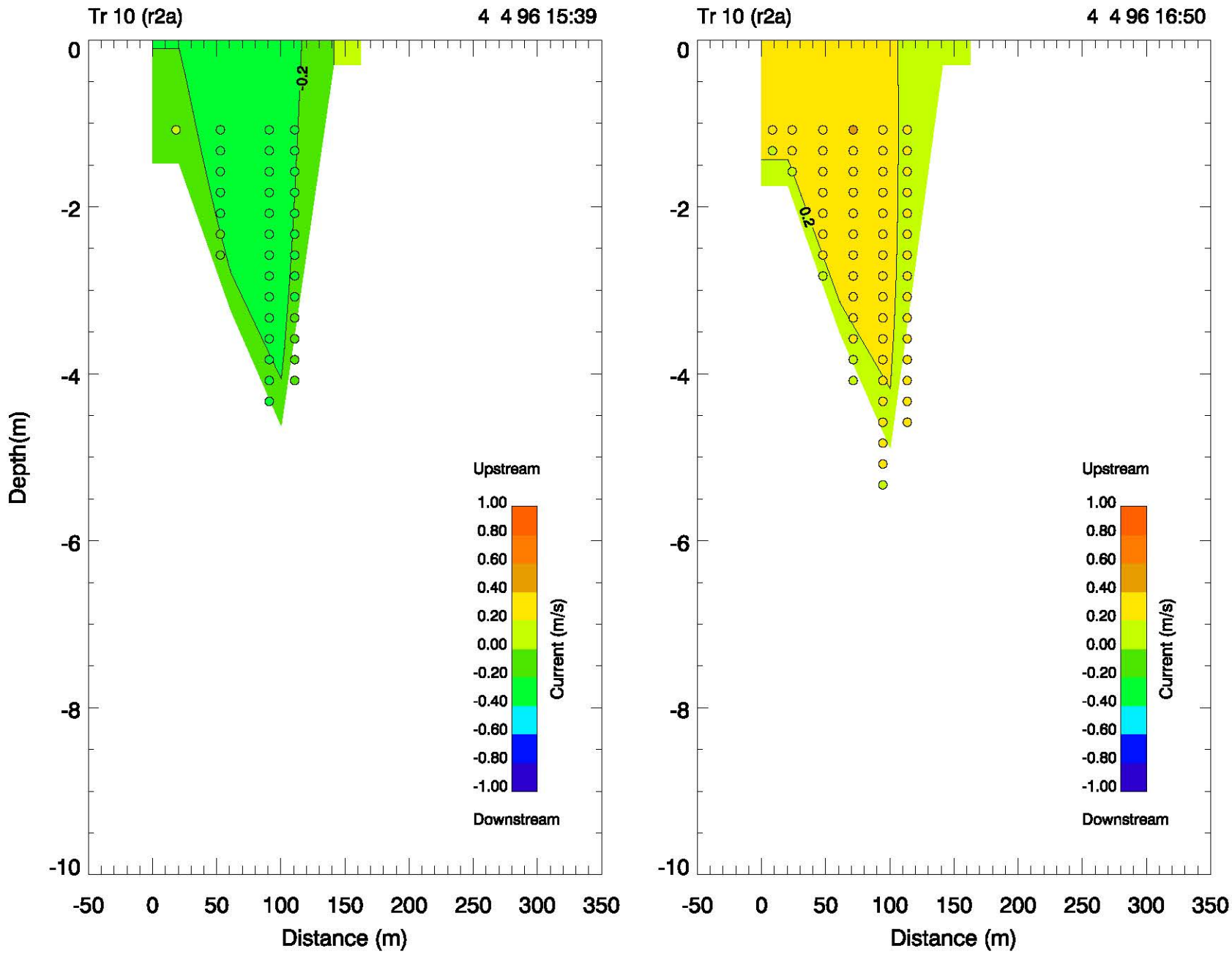

Figure 4-8 Comparison of instantaneous cross-sectional velocities at Transect 10 (Round 2a) (continued)

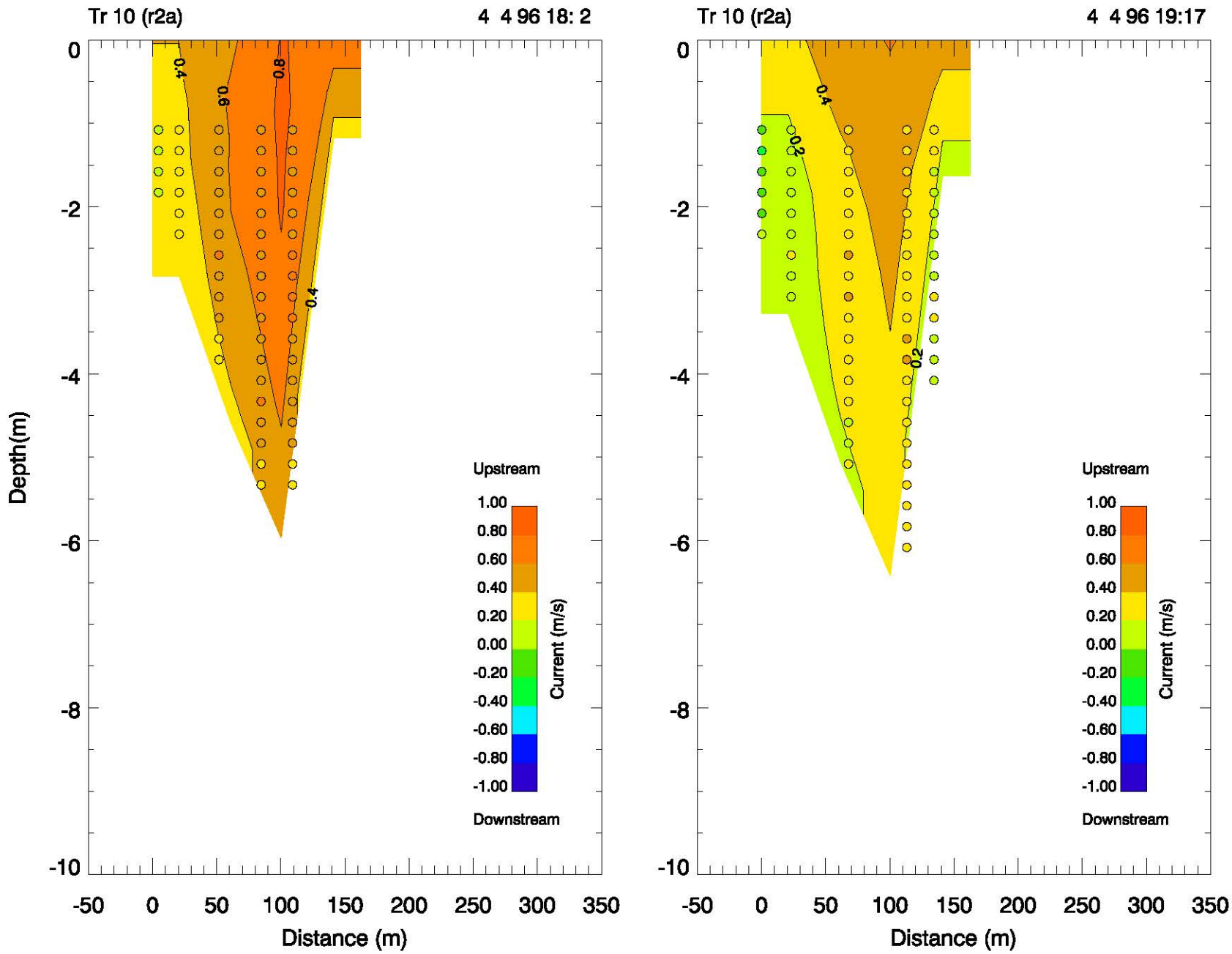

Figure 4-8 Comparison of instantaneous cross-sectional velocities at Transect 10 (Round 2a) (continued)

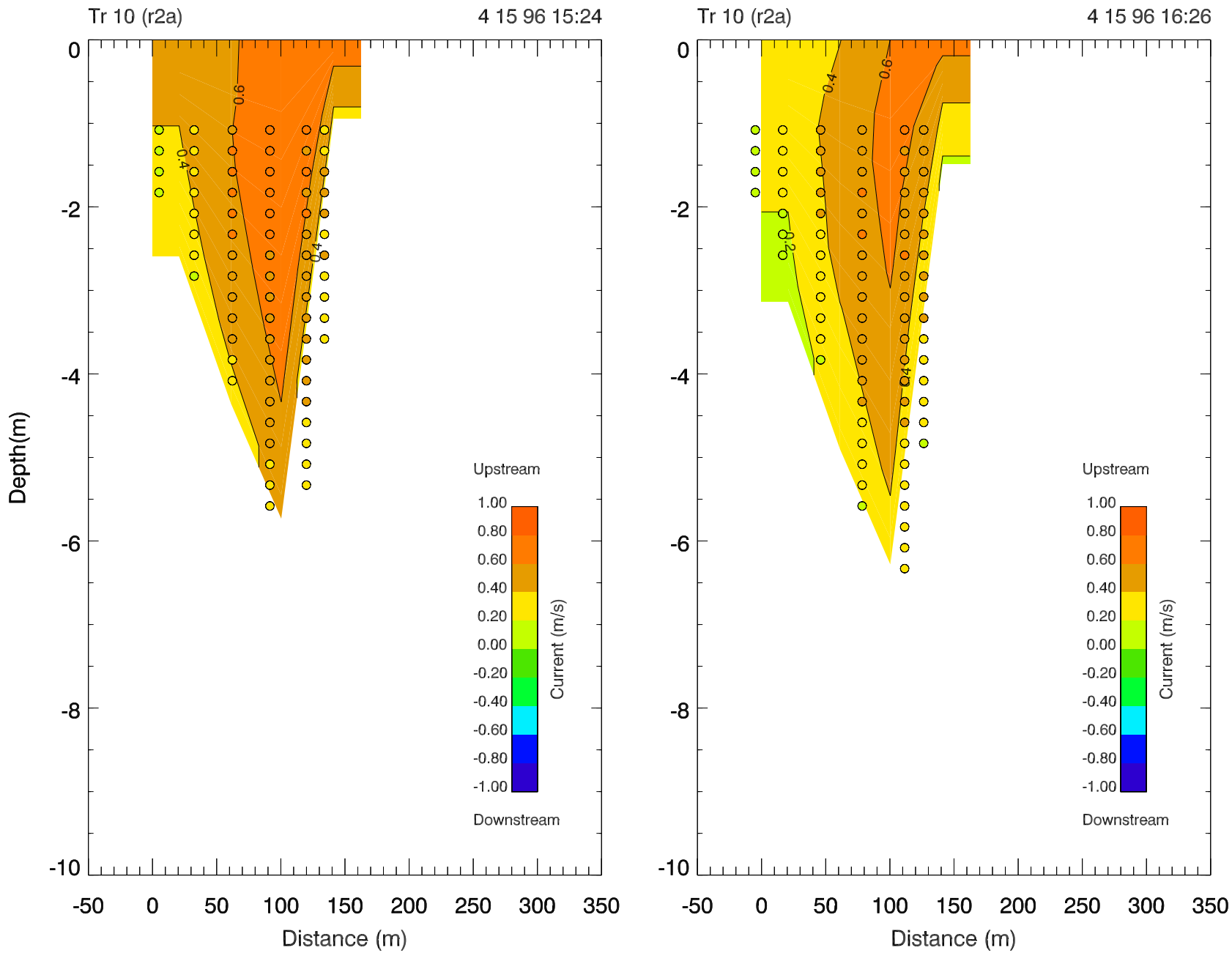

Figure 4-8 Comparison of instantaneous cross-sectional velocities at Transect 10 (Round 2a) (continued)

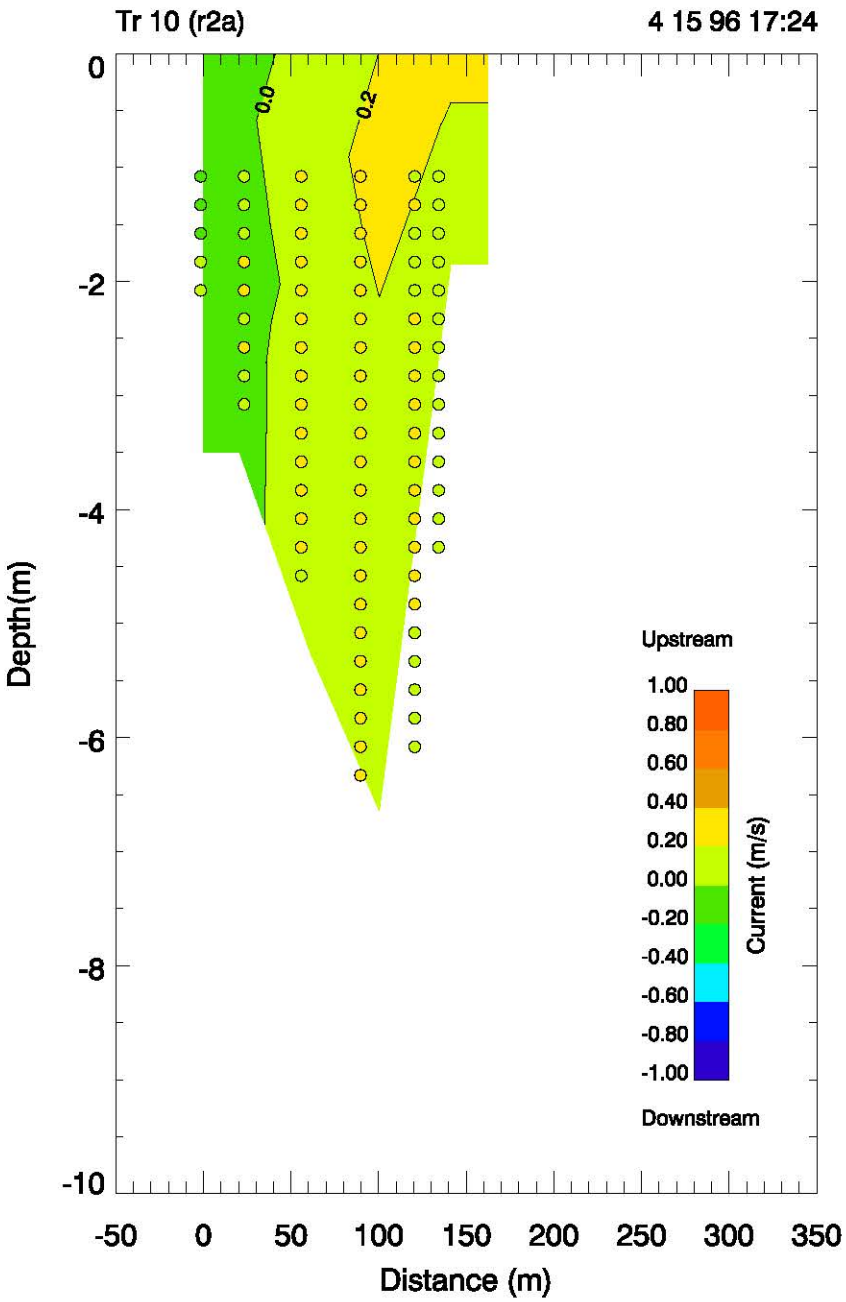

Figure 4-8 Comparison of instantaneous cross-sectional velocities at Transect 10 (Round 2a) (continued)

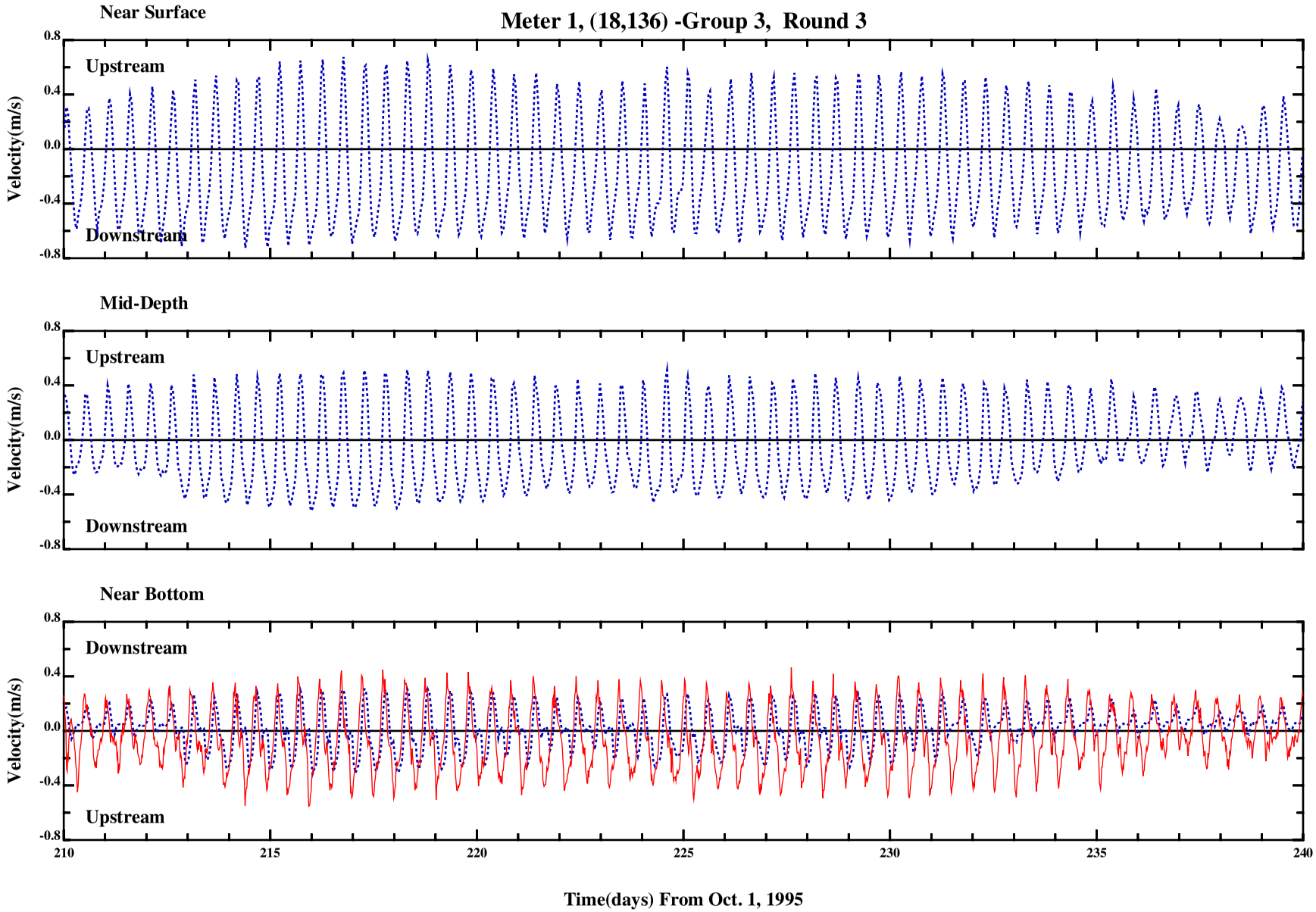

Figure 4-9 Comparison of hourly computed velocities with near bottom data survey at M1, M2, and M3 moorings (Round 3)

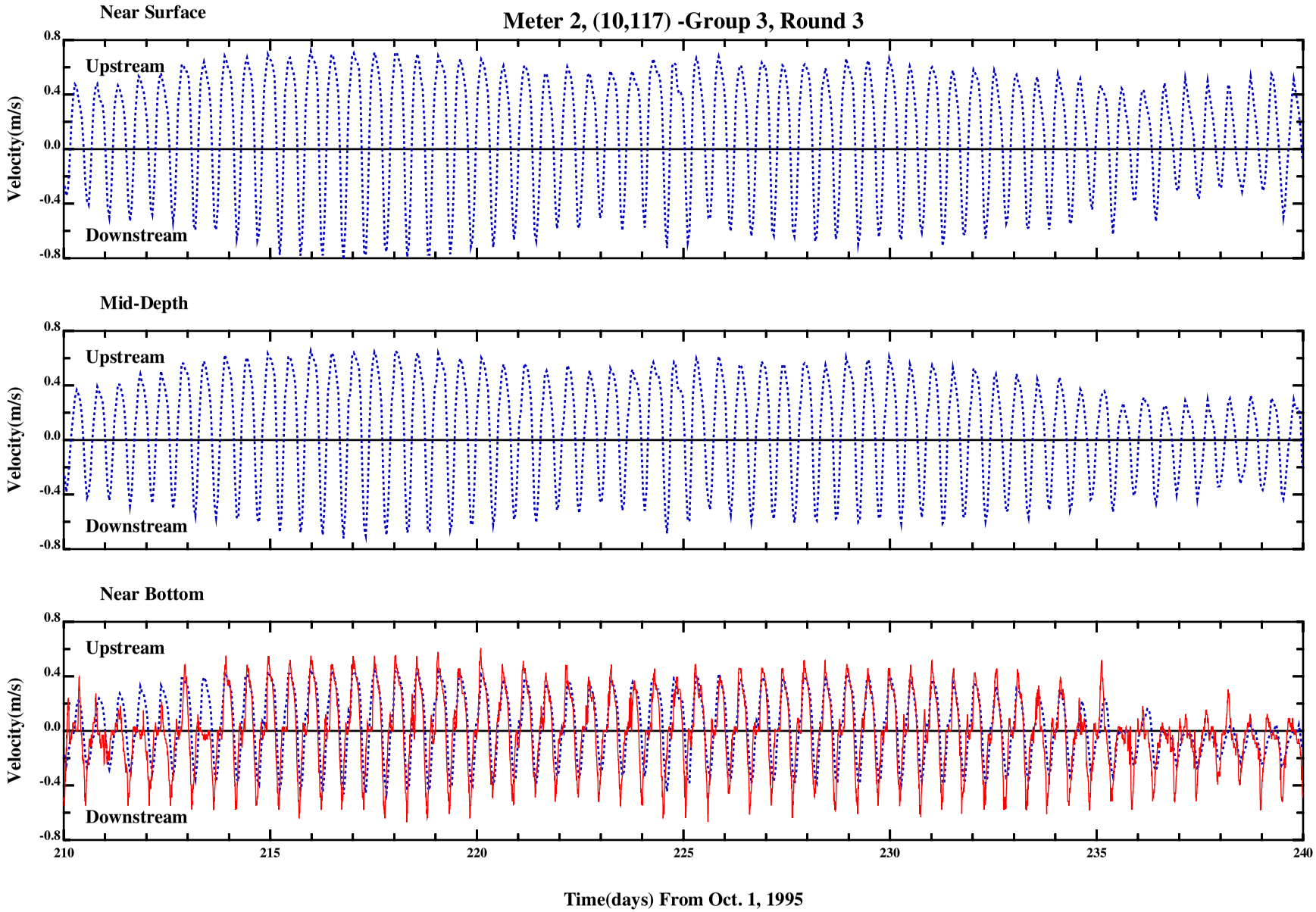

Figure 4-9 Comparison of near bottom current velocites for the Round 3 survey at M1, M2, and M3 moorings (continued)

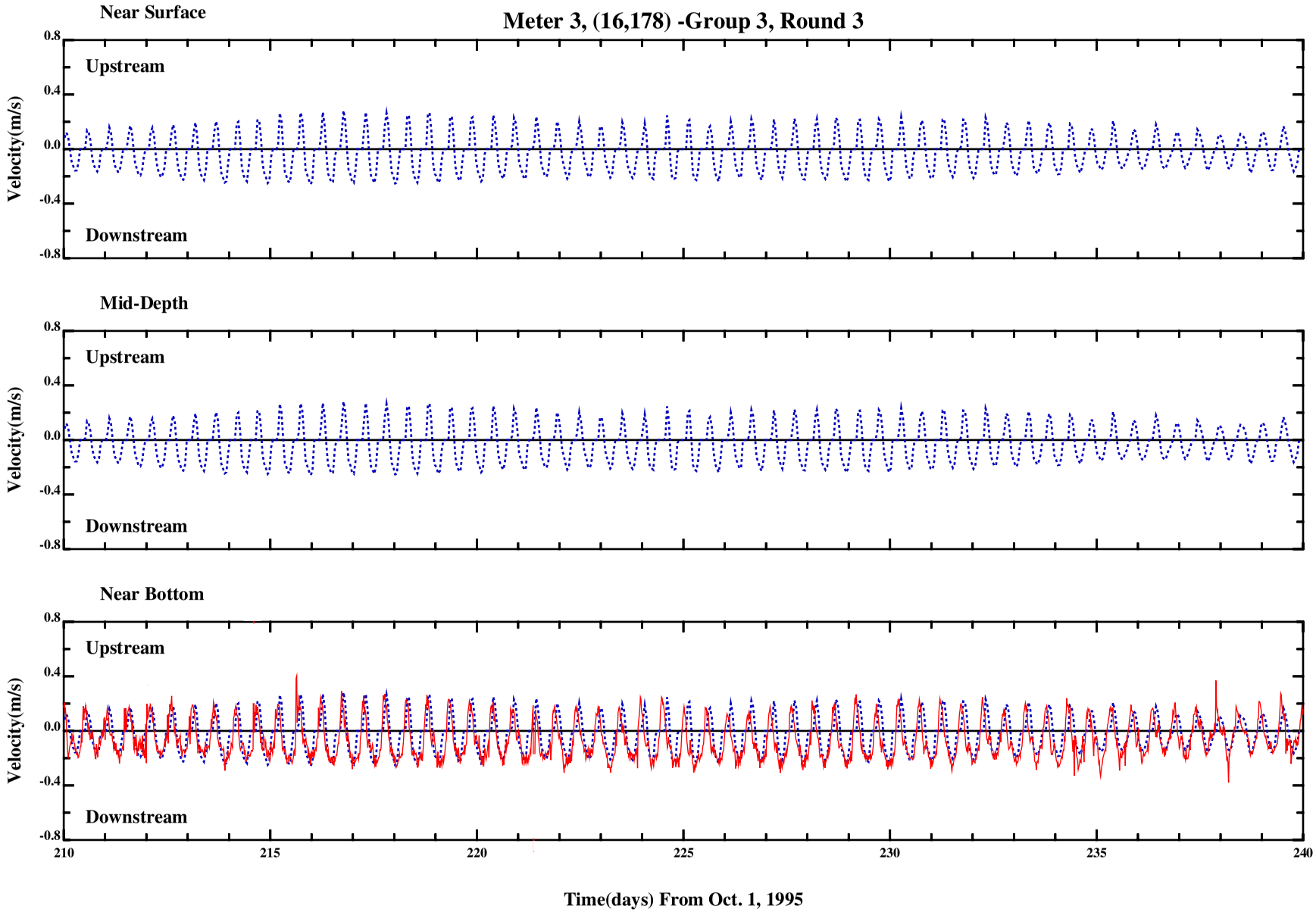

Figure 4-9 Comparison of near bottom current velocites for the Round 3 survey at M1, M2, and M3 moorings (continued)

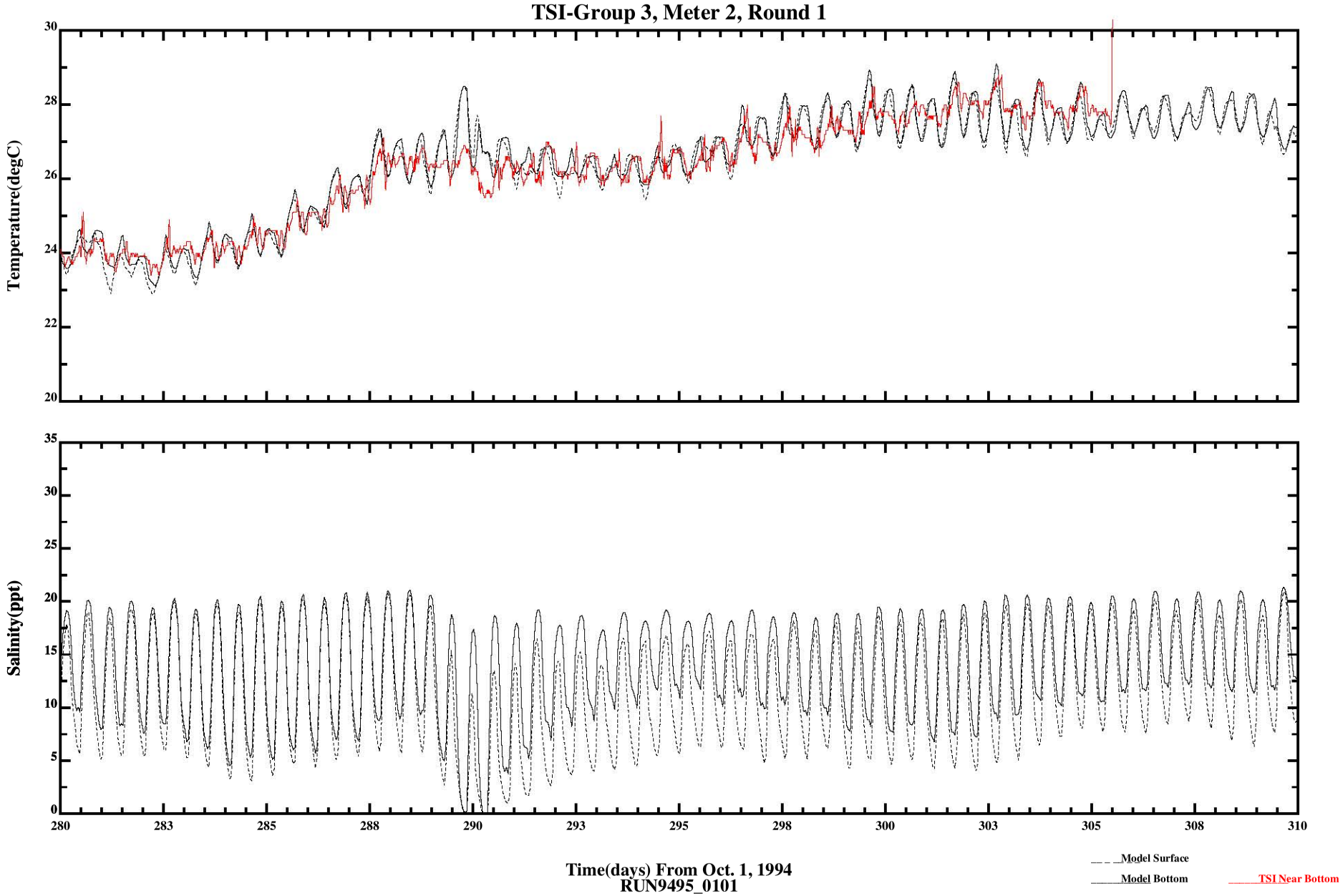

Comparison of Instantaneous Surface and Bottom Salinity

/black4/mpin0021/HYDRO/RUN9495_0101/PLOTS/TSI/TANDS/tands_g3m2r1

Figure 4-10 Comparison of hourly computed temperature with TSI mooring data over a period of one month (1995) (Group 3, M2, Round 1)

DATE: 4/24/2007 TIME: 10:43:21

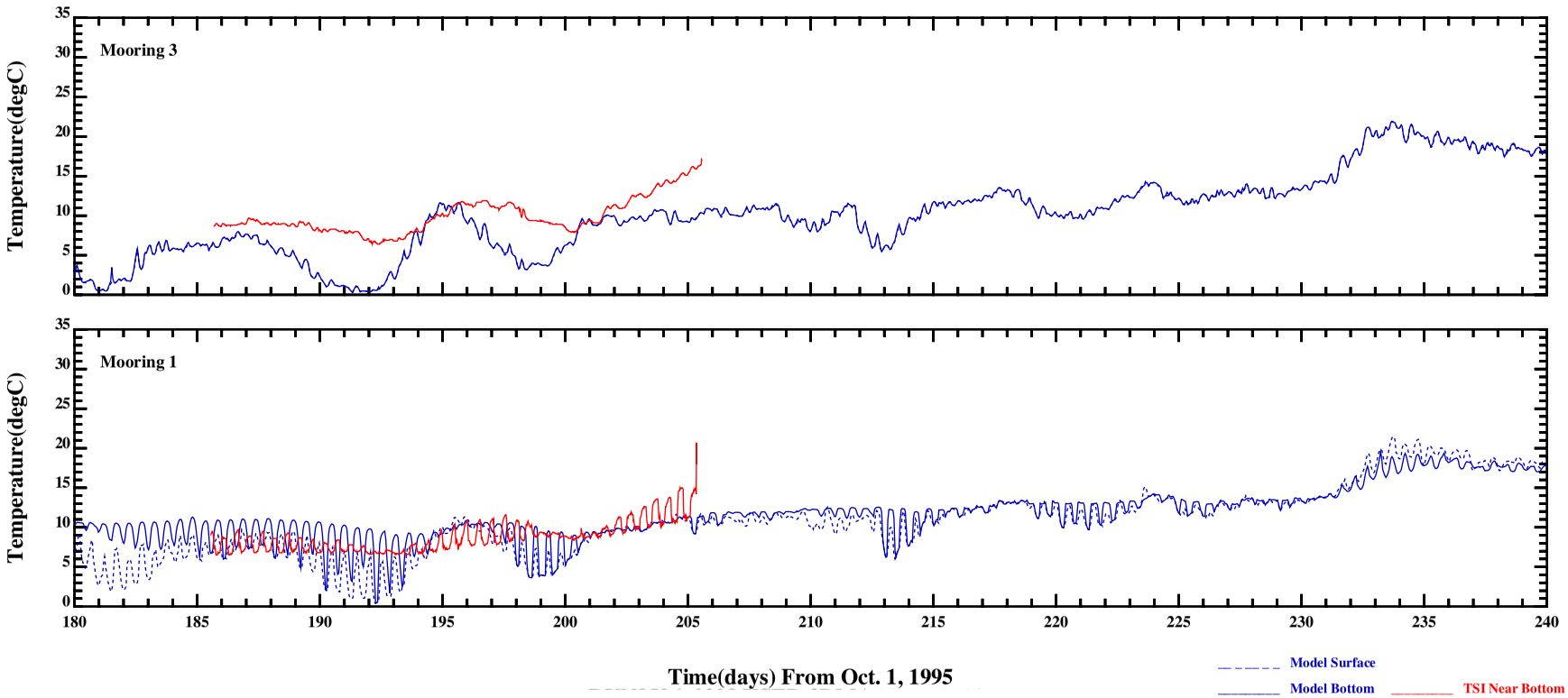

Figure 4-11 Comparison of hourly computed temperature with TSI mooring data over a period of two months (1996) (Group 3 M2 and M3 Round 2a)

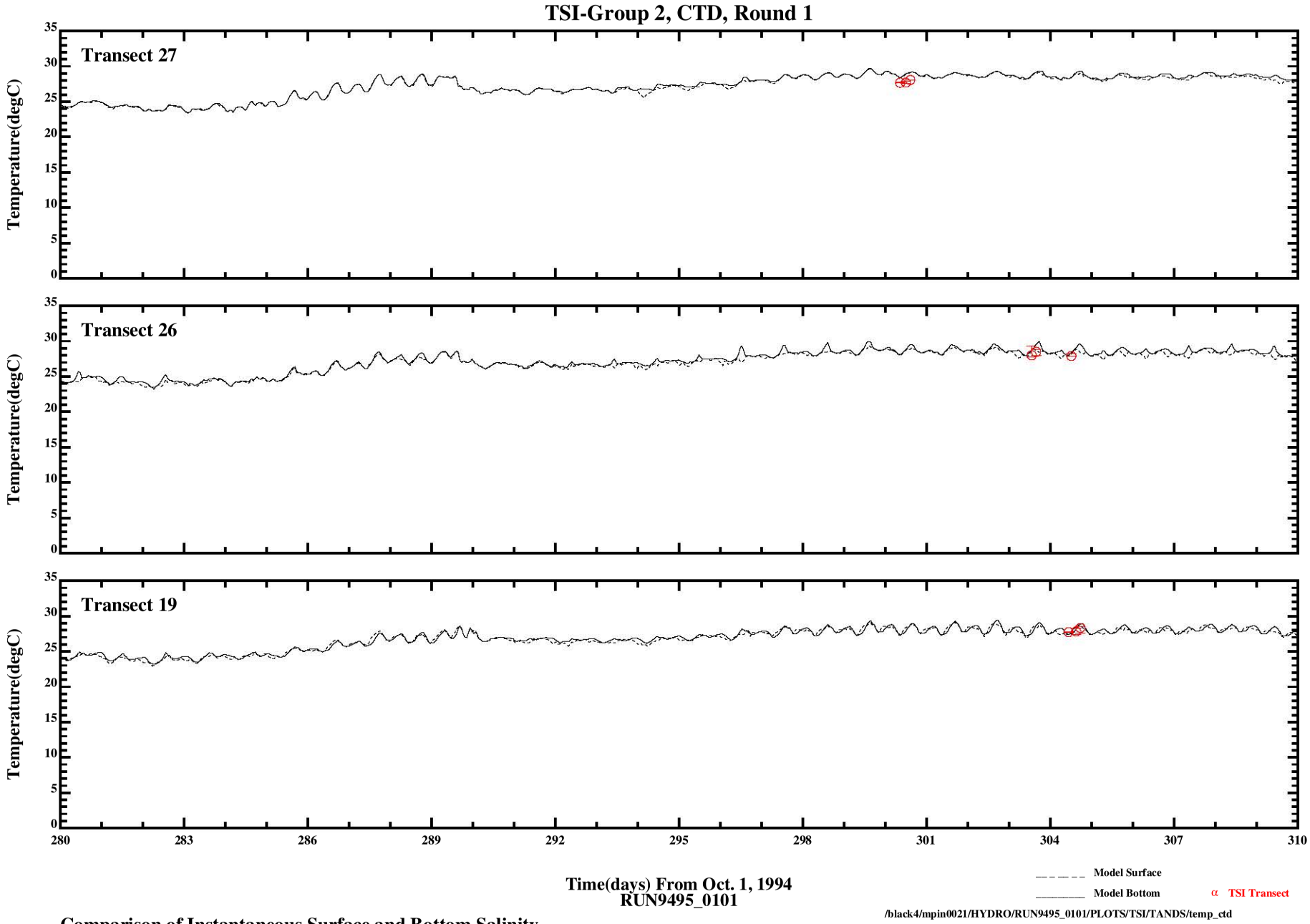

Comparison of Instantaneous Surface and Bottom Salinity

Figure 4-12 Comparison of hourly computed temperature with TSI transect data over a period of one month (1995) (Group 2 Round 1)

DATE: 4/24/2007 TIME: 10:43:40

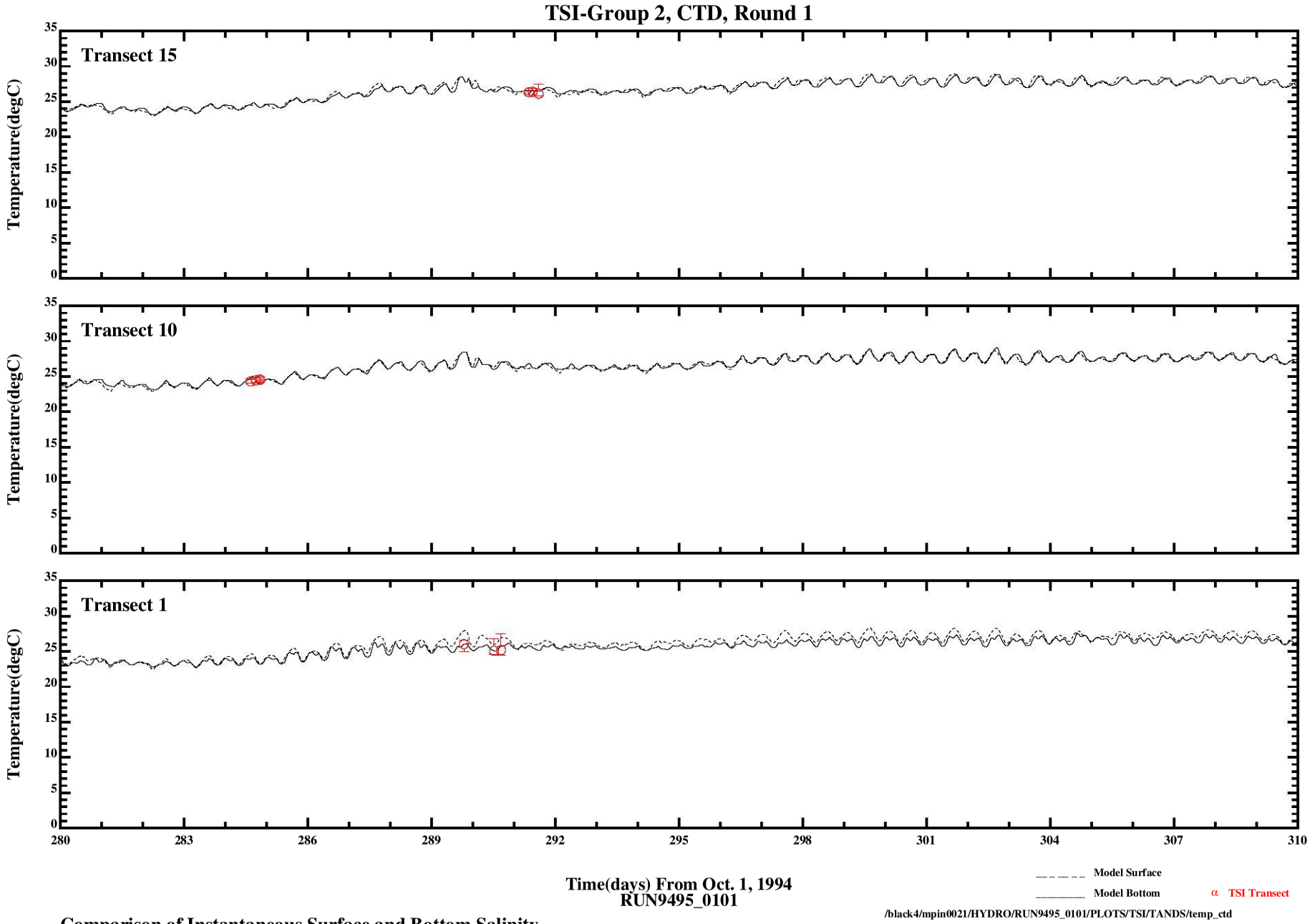

Comparison of Instantaneous Surface and Bottom Salinity

Figure 4-12 Comparison of hourly computed temperature with TSI transect data over a period of one month (1995) (Group 2 Round 1) (continued)

DATE: 4/24/2007 TIME: 10:43:40

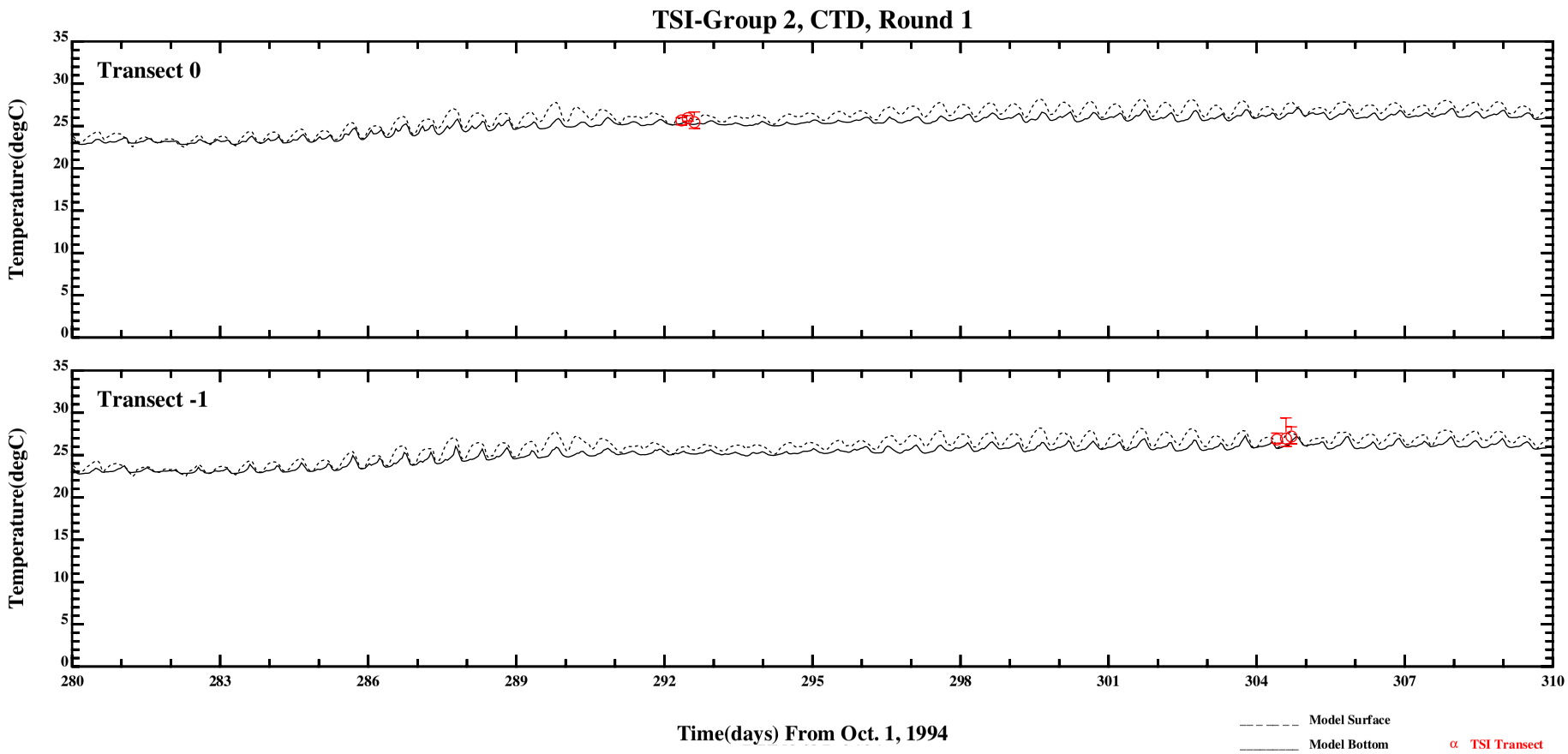

Figure 4-12 Comparison of hourly computed temperature with TSI transect data over a period of one month (1995) (Group 2 Round 1) (continued)

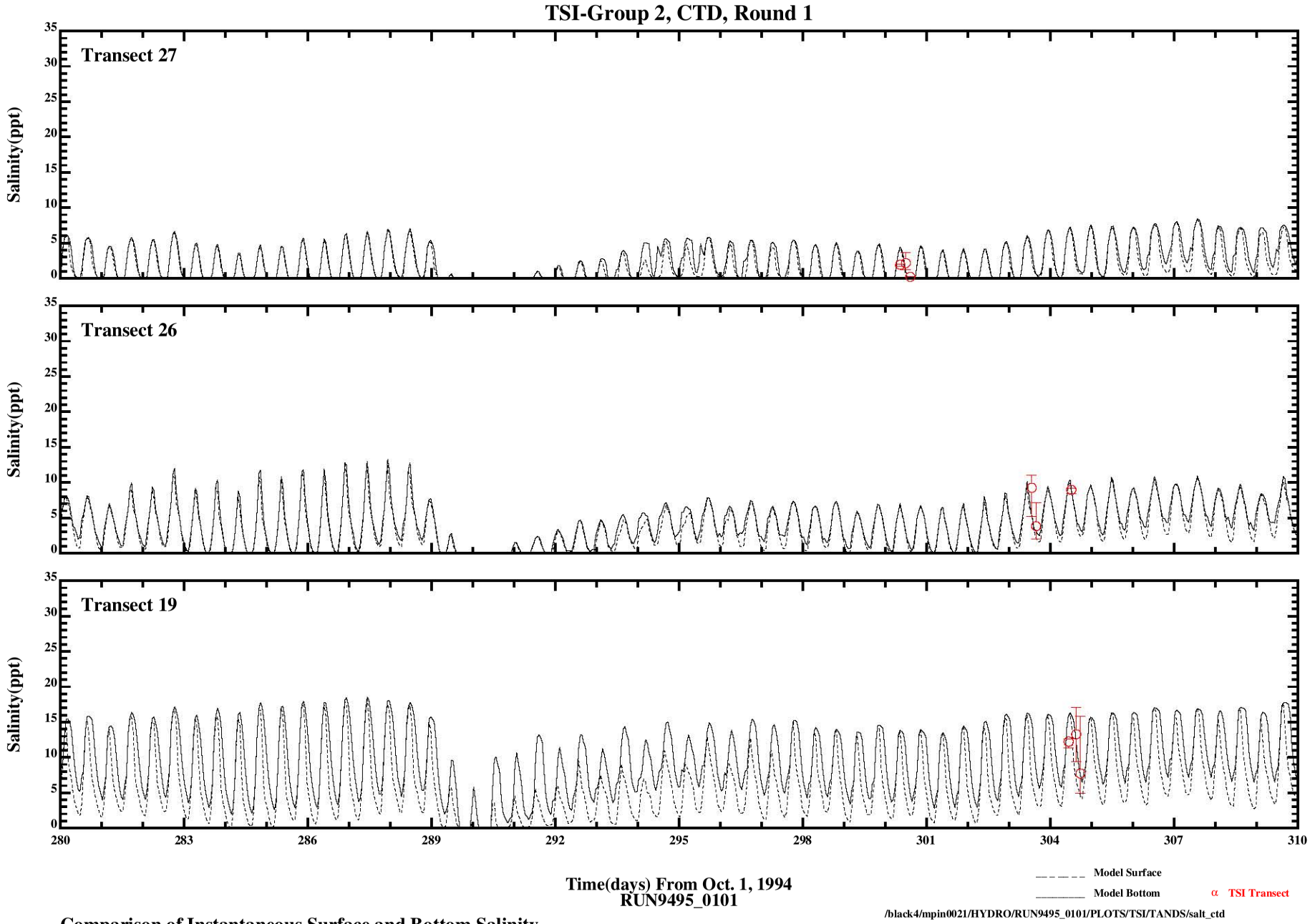

Comparison of Instantaneous Surface and Bottom Salinity

Figure 4-13 Comparison of hourly computed salinity with TSI transect data over a period of one month (1995) (Group 2 Round 1)

DATE: 4/24/2007 TIME: 10:42:40

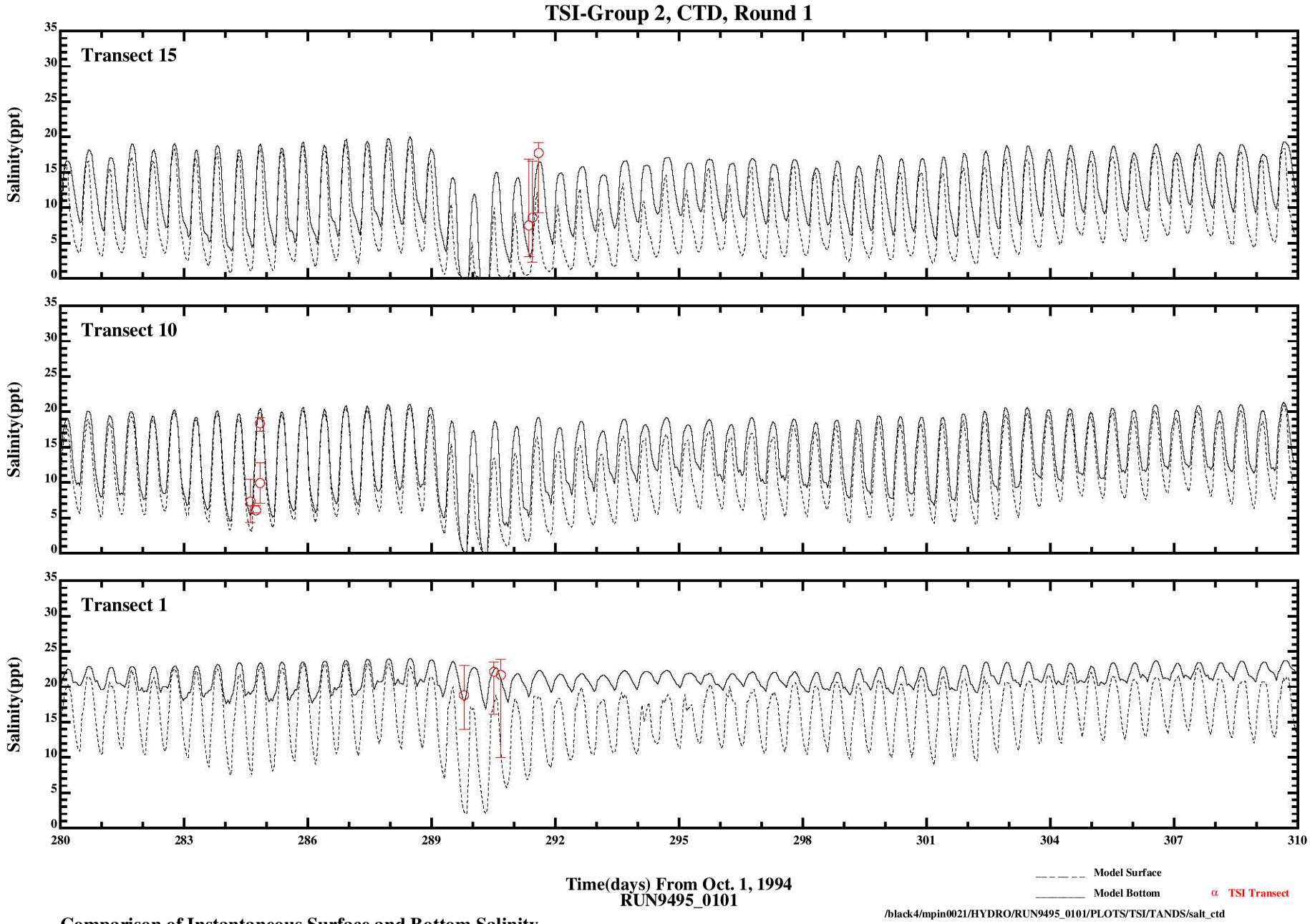

Comparison of Instantaneous Surface and Bottom Salinity

Figure 4-13 Comparison of hourly computed salinity with TSI transect data over a period of one month (1995) (Group 2 Round 1) (continued)

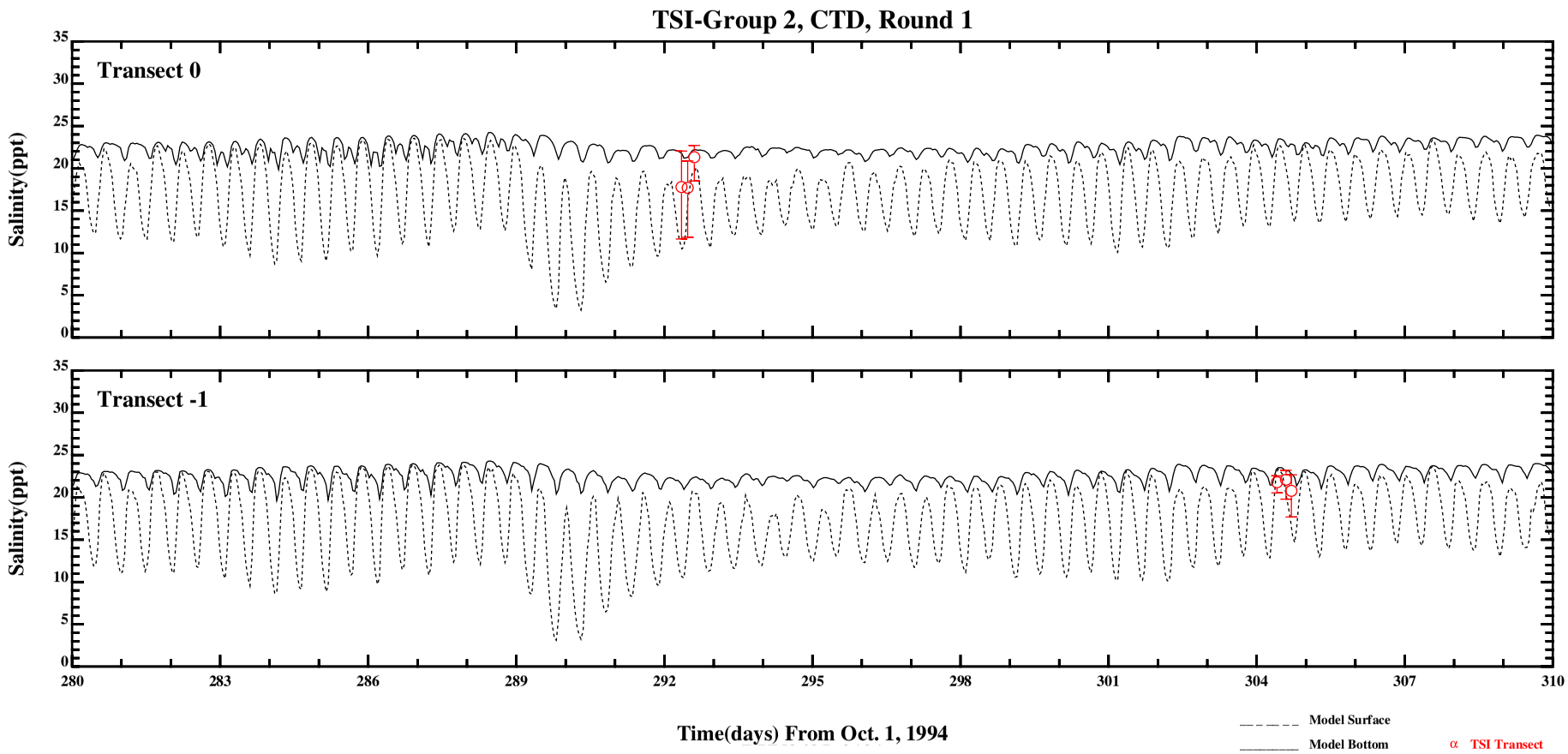

Figure 4-13 Comparison of hourly computed salinity with TSI transect data over a period of one month (1995) (Group 2 Round 1) (continued)

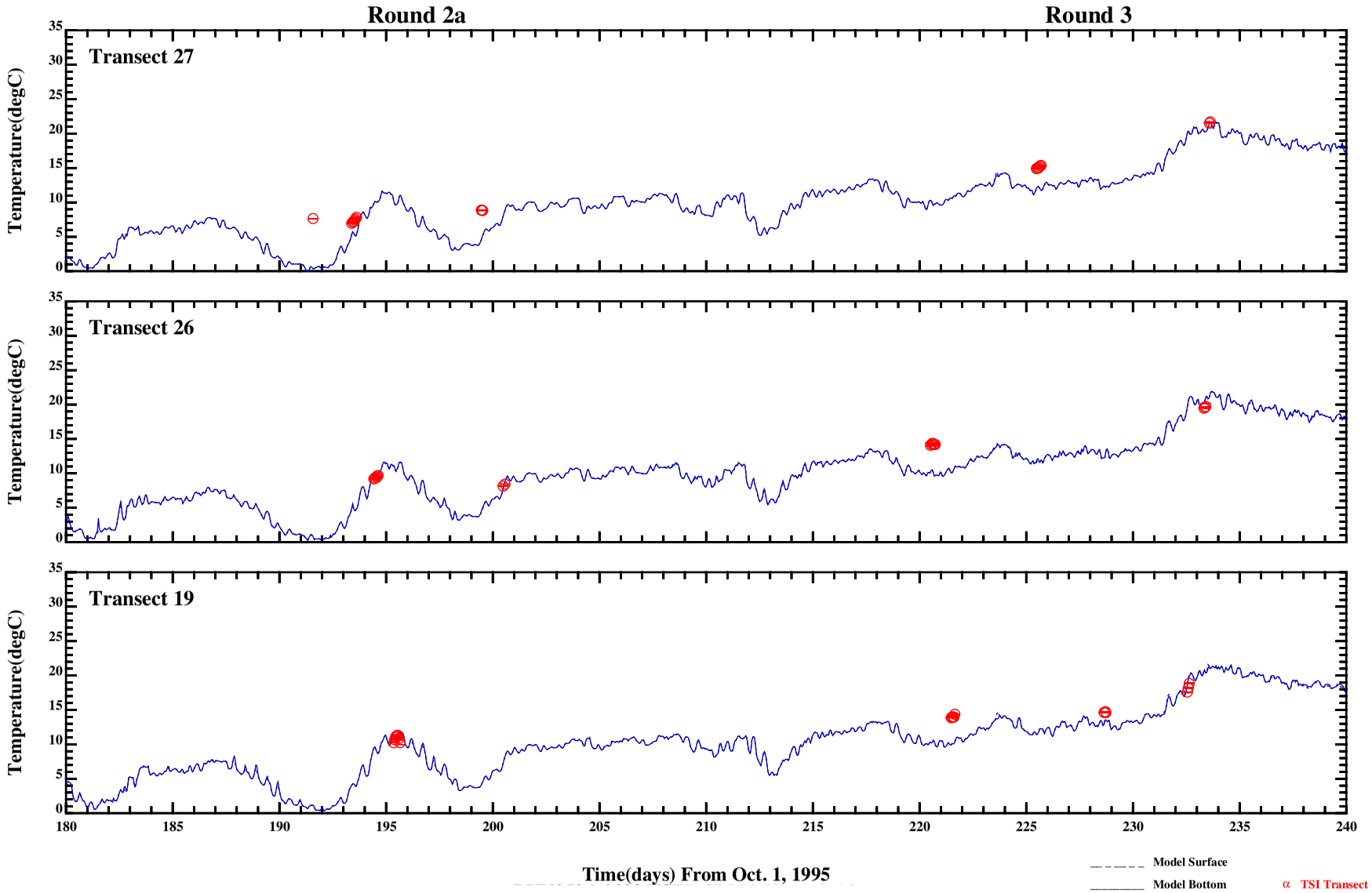

Figure 4-14a Comparison of hourly computed temperature with TSI transect data over a period of two months (1996) (Group 2 Rounds 2a and 3)

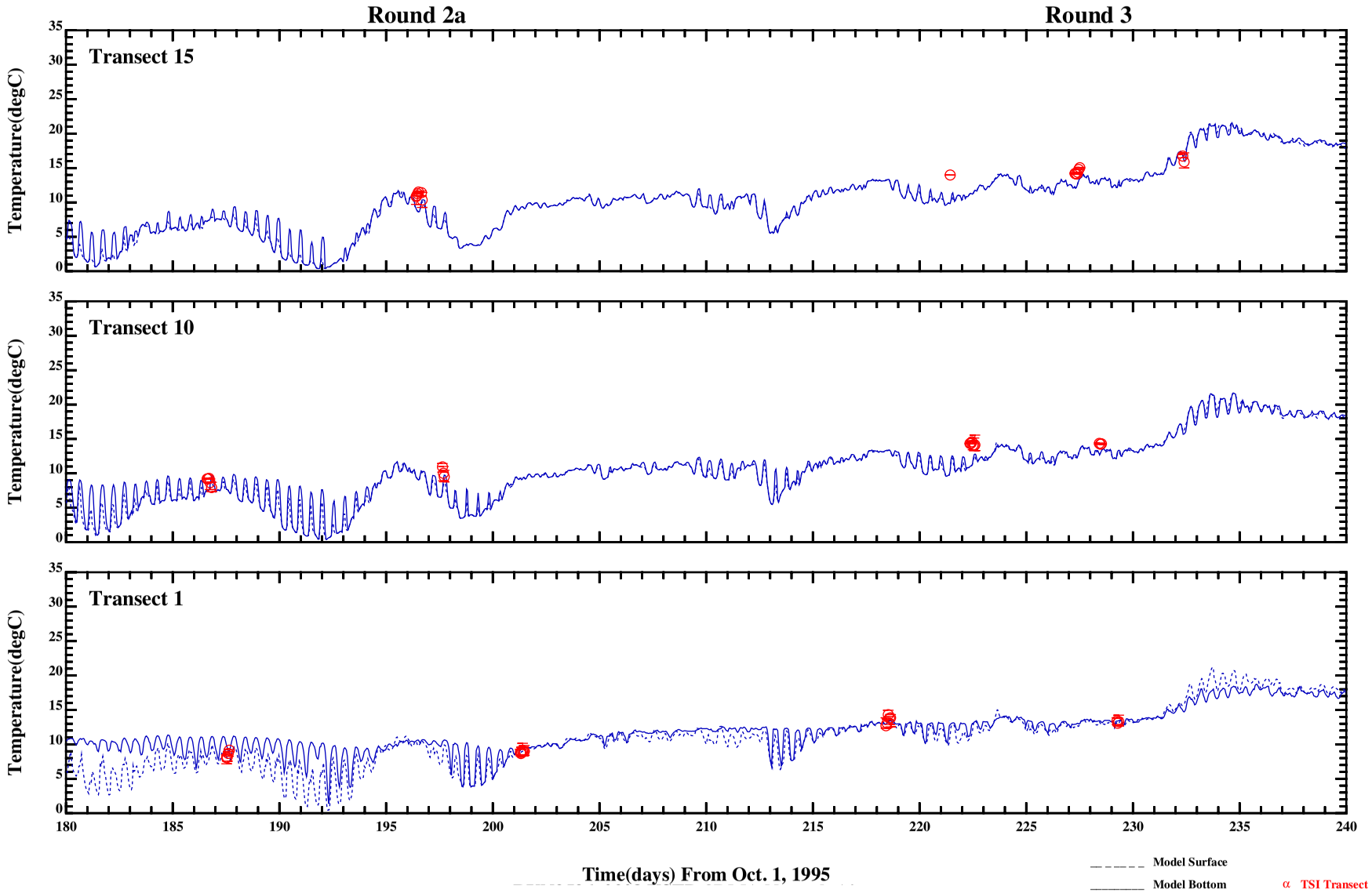

Figure 4-14a Comparison of hourly computed temperature with TSI transect data over a period of two months (1996) (Group 2 Rounds 2a and 3) (continued)

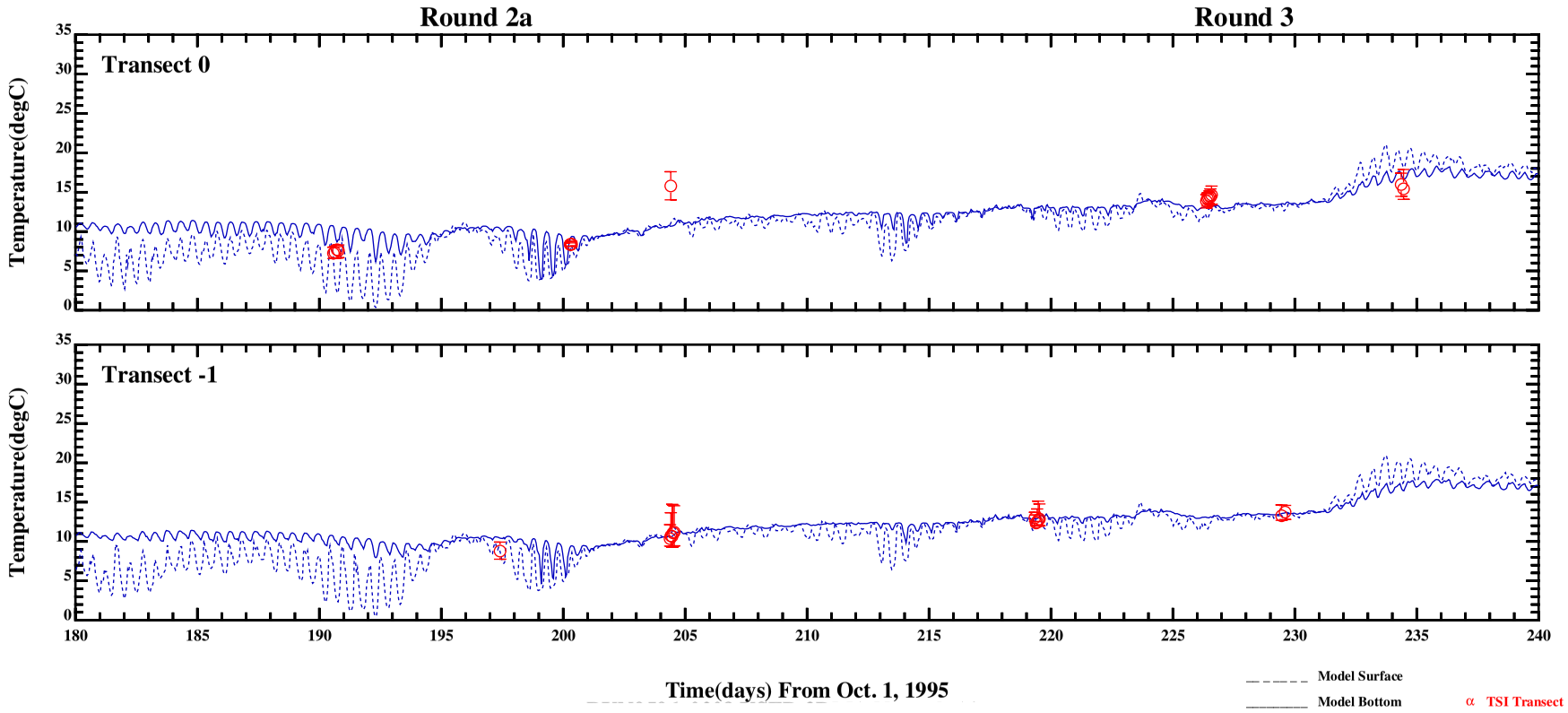

Figure 4-14a Comparison of hourly computed temperature with TSI transect data over a period of two months (1996) (Group 2 Rounds 2a and 3) (continued)

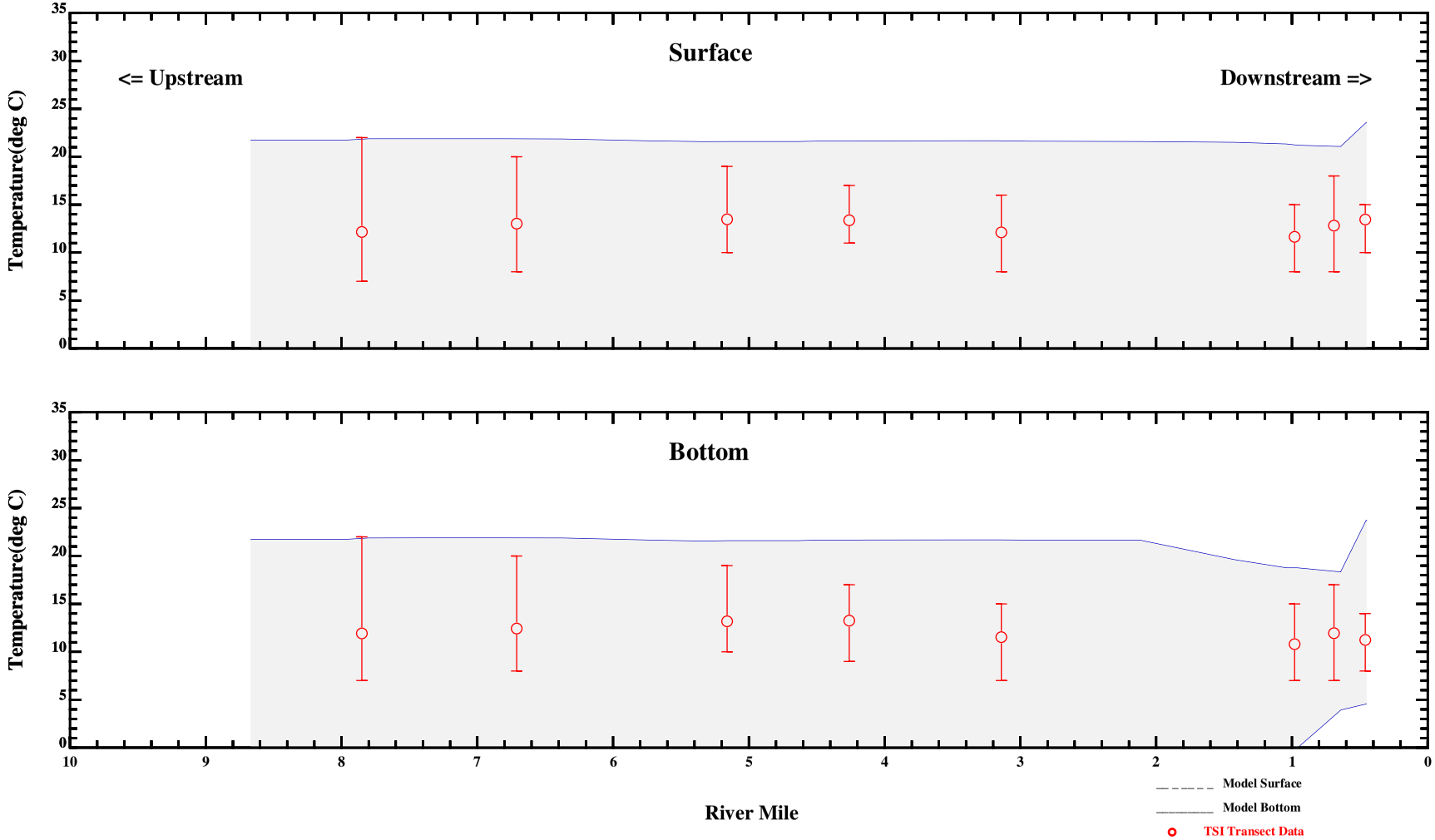

Figure 4-14b Comparison of two month averaged model predicted temperature with TSI transect data (1996) (Group 2 Rounds 2a and 3) along the longitudinal axis of the Lower Passaic River

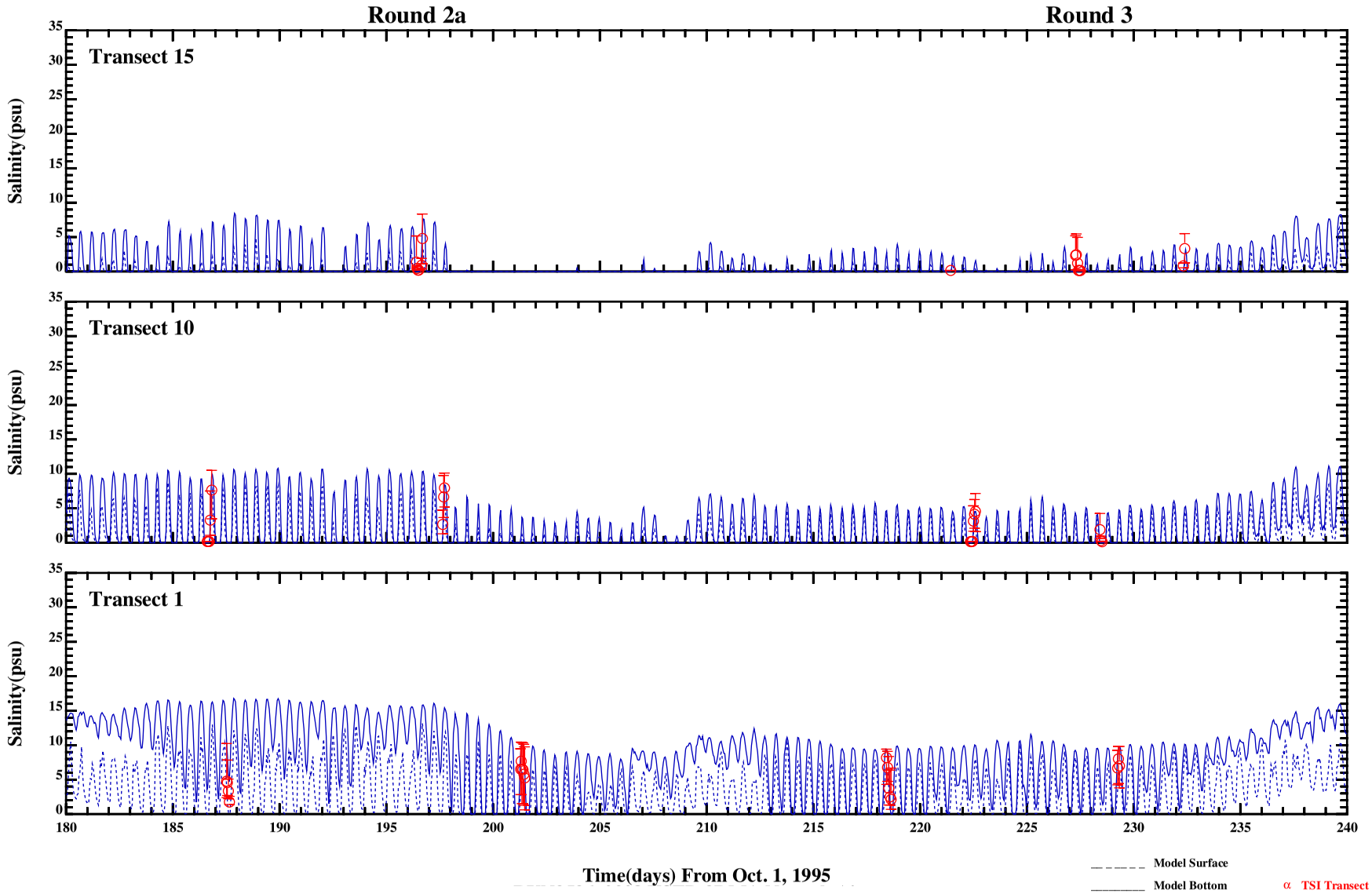

Figure 4-15a Comparison of hourly computed salinity with TSI transect data over a period of two months (1996) (Group 2 Rounds 2a and 3) (continued)

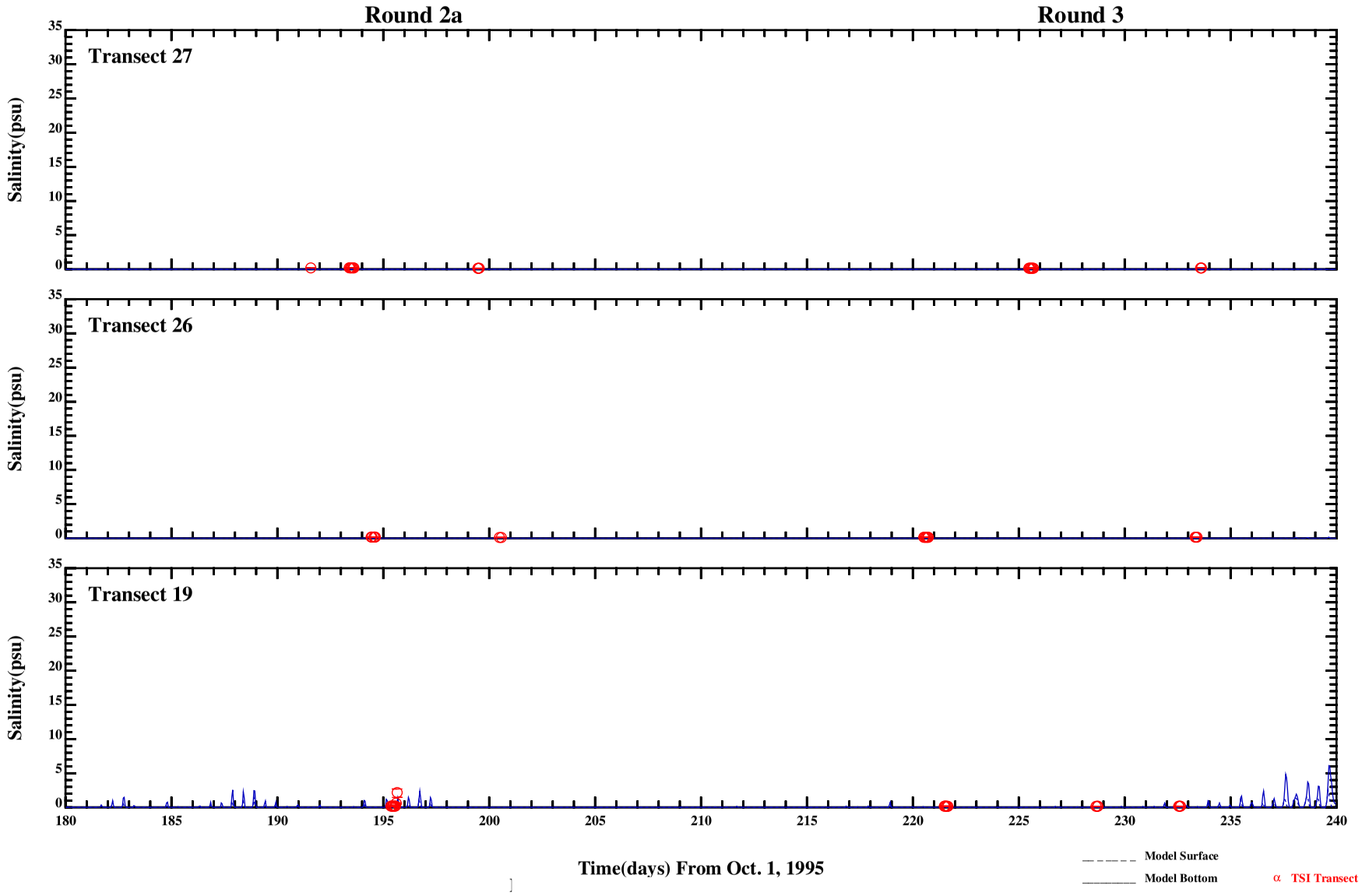

Figure 4-15a Comparison of hourly computed salinity with TSI transect data over a period of two months (1996) (Group 2 Rounds 2a and 3)

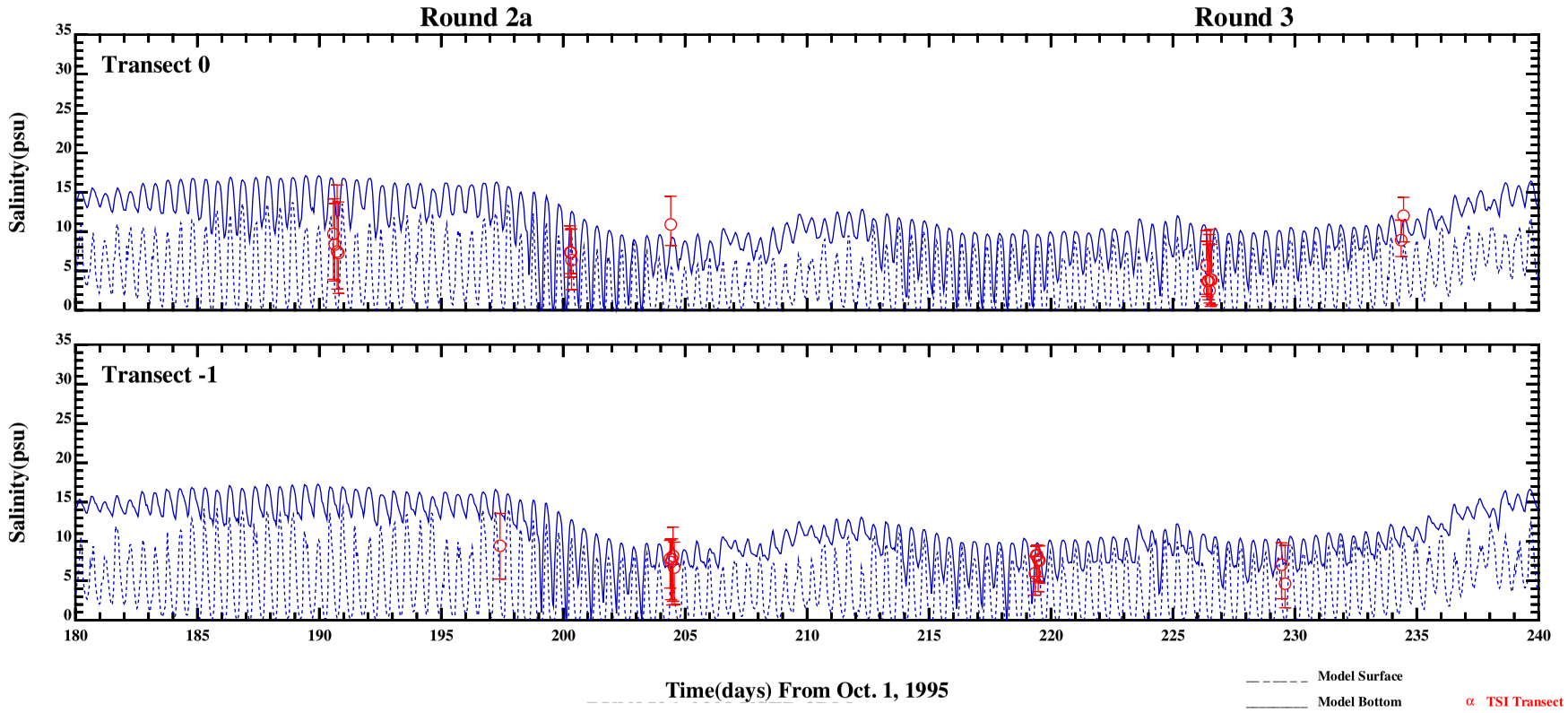

Figure 4-15a Comparison of hourly computed salinity with TSI transect data over a period of two months (1996) (Group 2 Rounds 2a and 3) (continued)

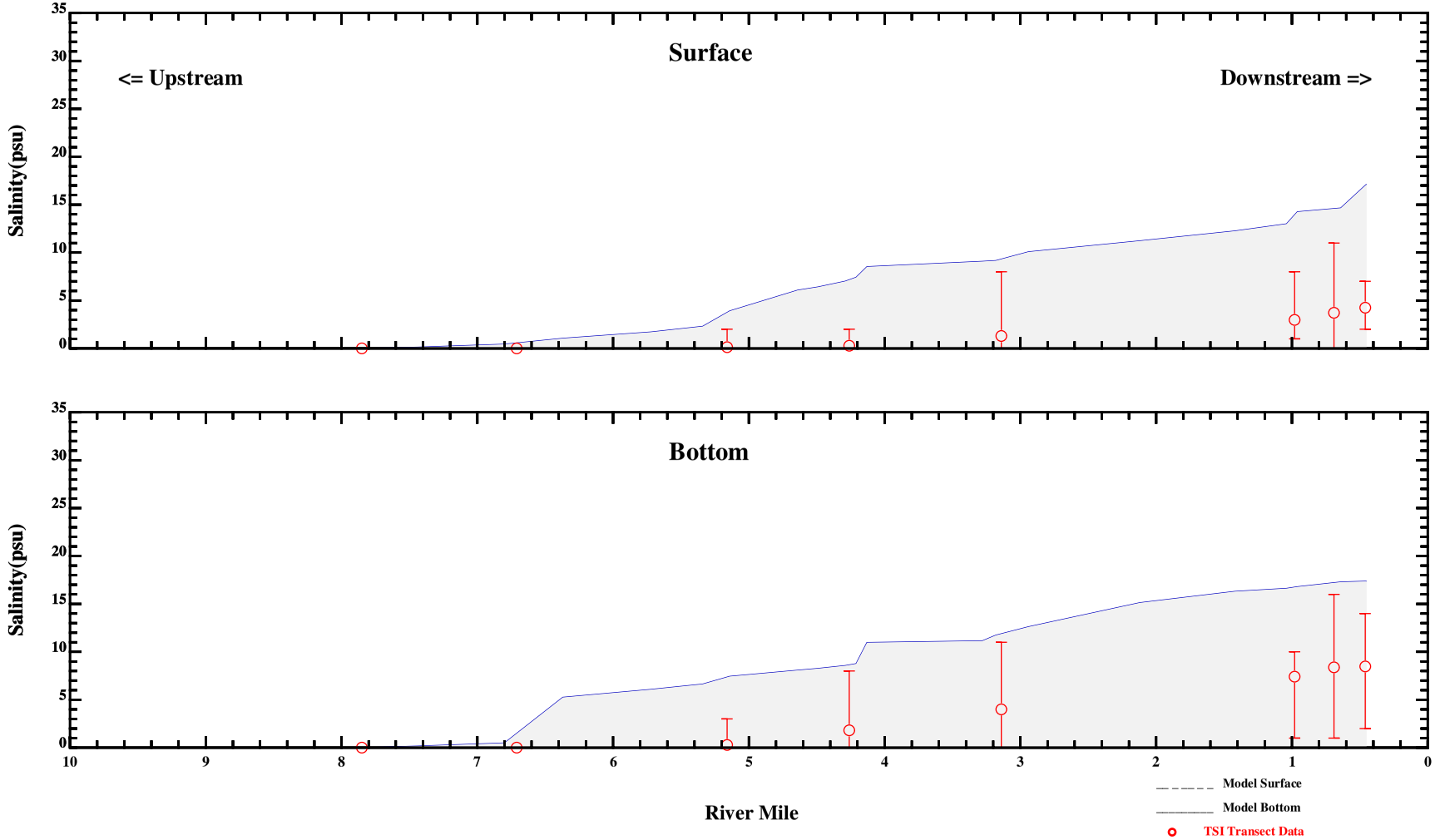

Figure 4-15b Comparison of two month averaged model predicted salinity with TSI transect data (1996) (Group 2 Rounds 2a and 3) along the longitudinal axis of the Lower Passaic River

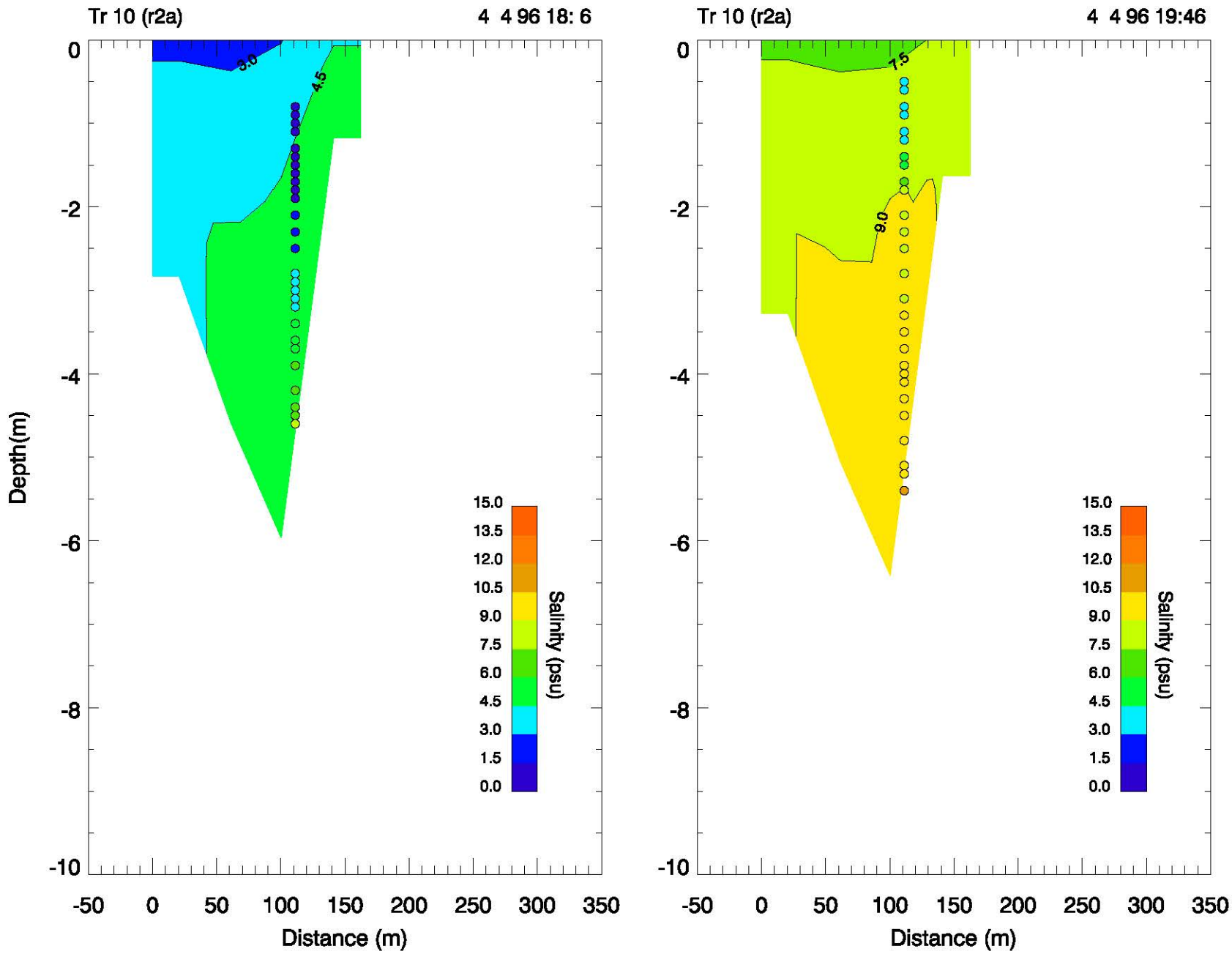

Figure 4-16 Comparison of instantaneous cross-sectional salinities at Transect 10 (Round 2a & 3)

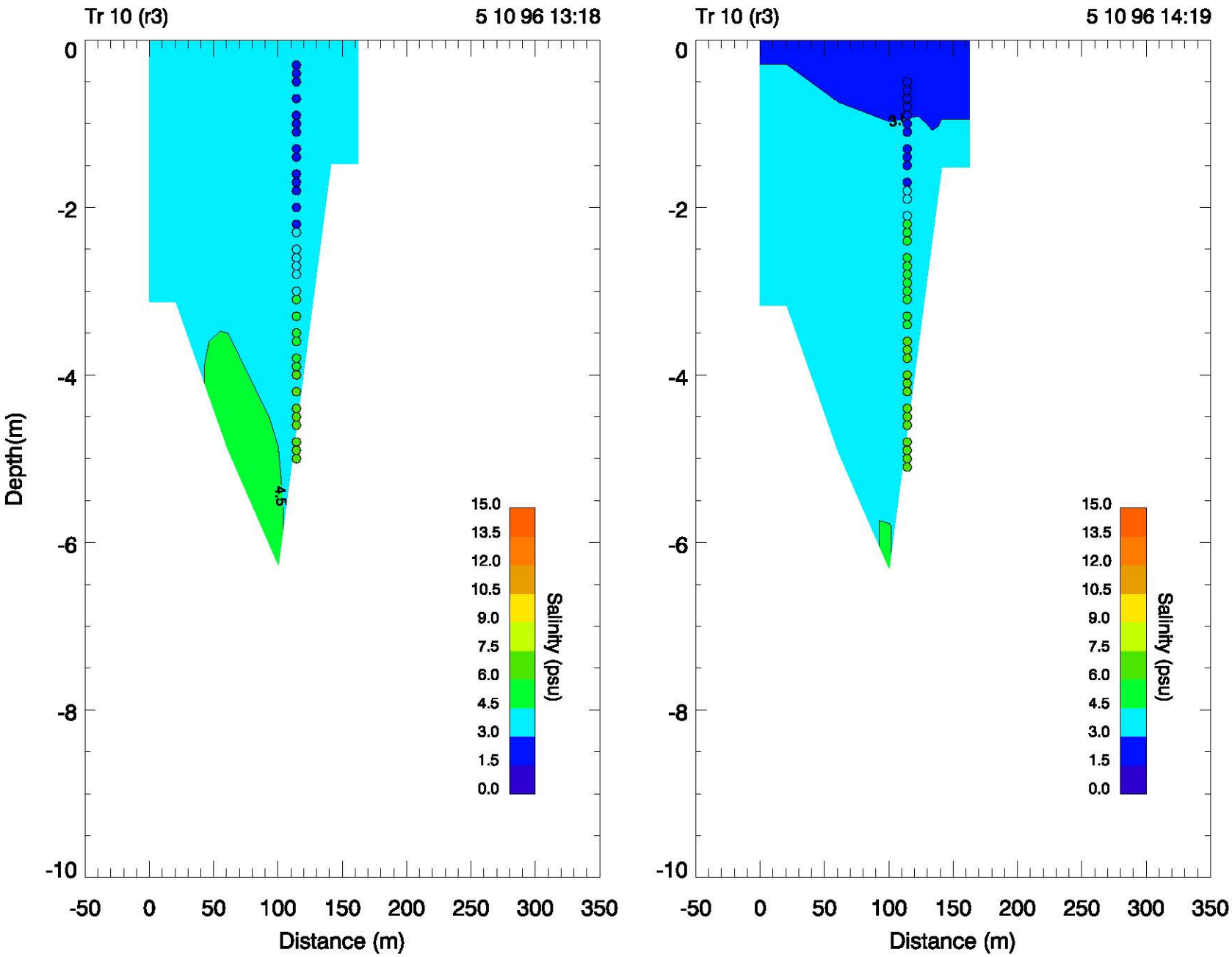

Figure 4-16 Comparison of instantaneous cross-sectional salinities at Transect 10 (Round 2a & 3) (continued)

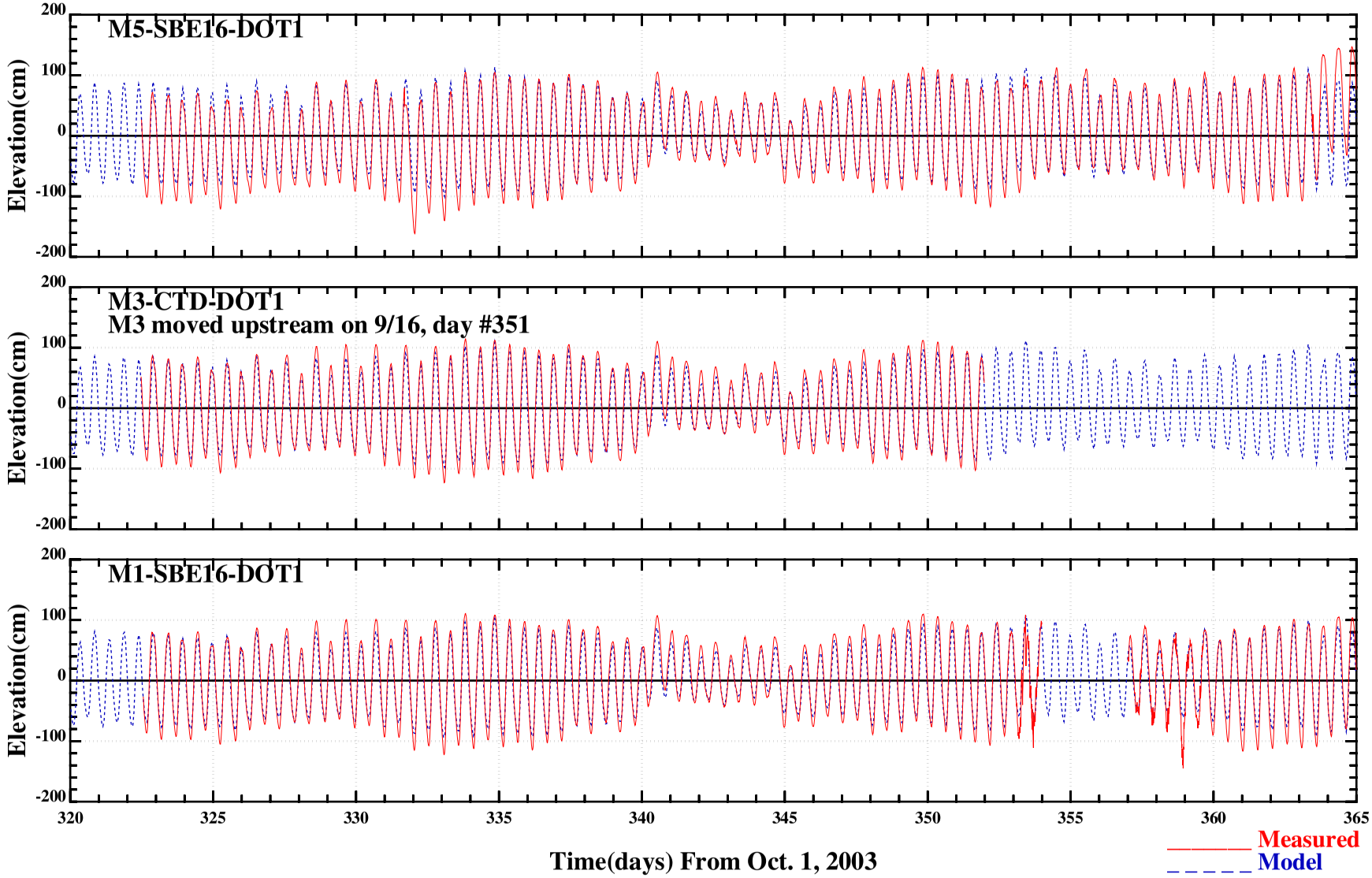

Figure 4-17 Comparison of hourly computed water elevations with IMCS mooring data over a period of two months: August - September 2004

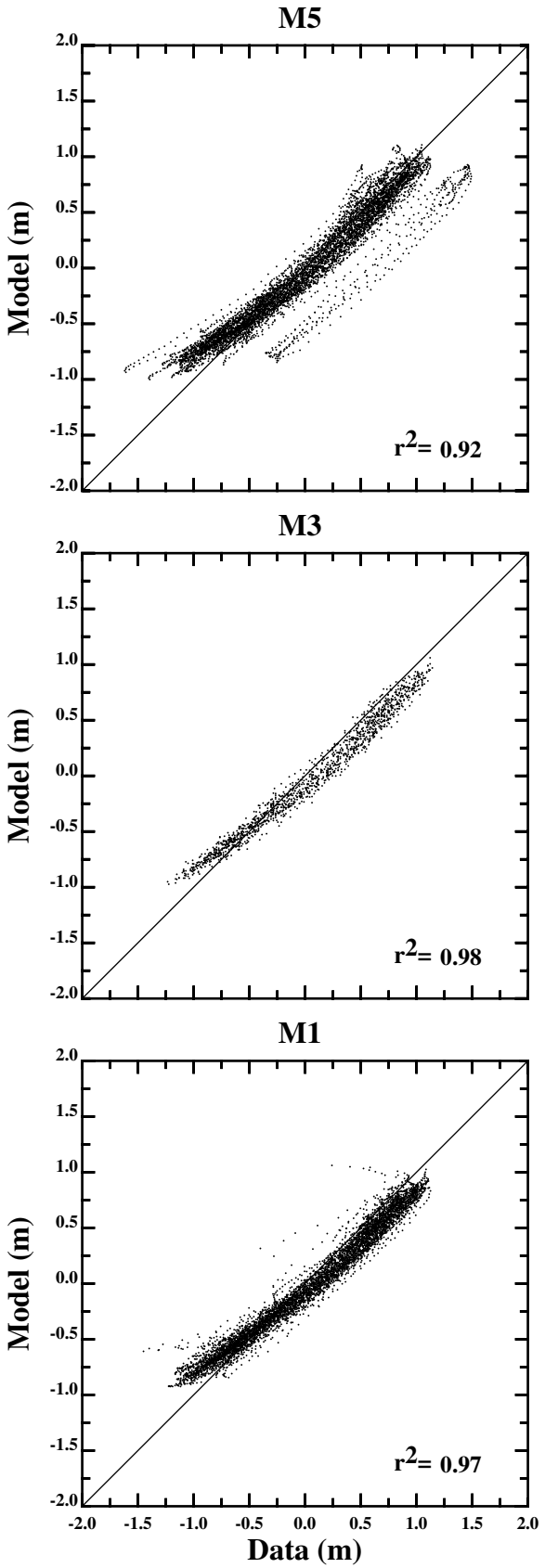

Figure 4-18 Scatter plot of computed water elevation with observed IMCS mooring data: August-September, 2004

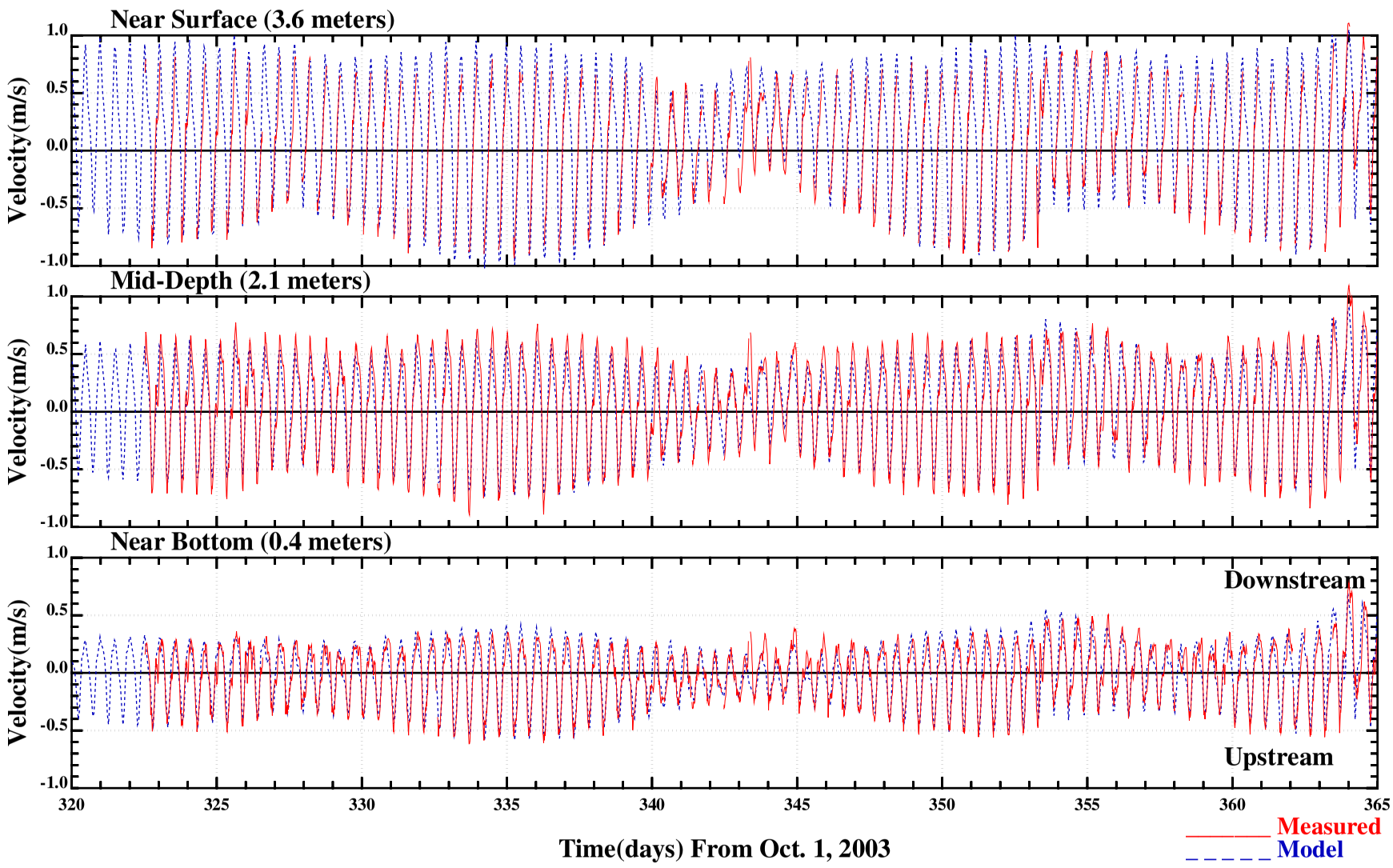

Figure 4-19 Comparison of hourly computed current velocities at three depths with IMCS mooring data (M2) over a period of two months: August - September 2004

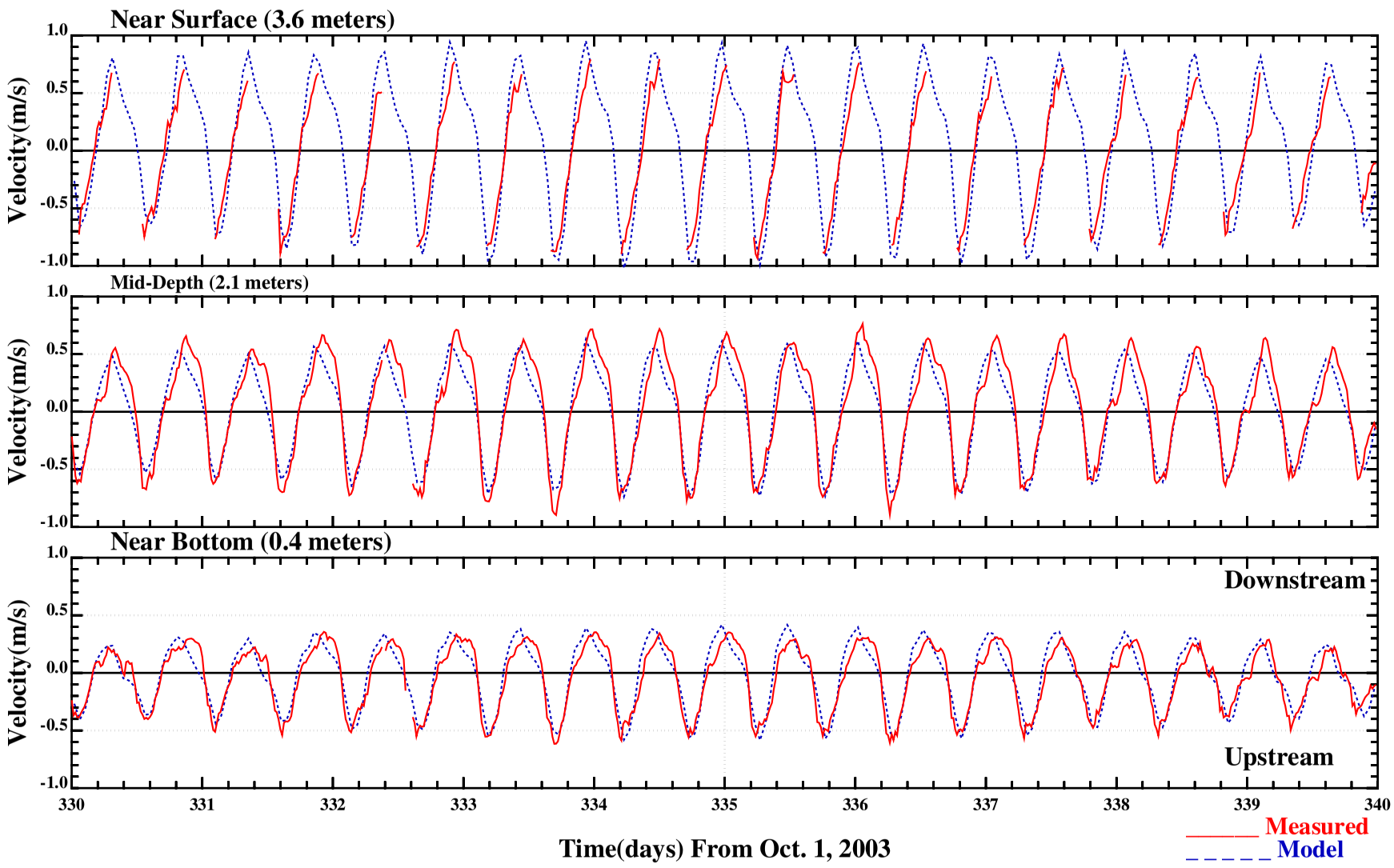

Figure 4-20 Comparison of hourly computed current velociteis at three depths with IMCS mooring data (M2) over a period of 10 days: August 2004

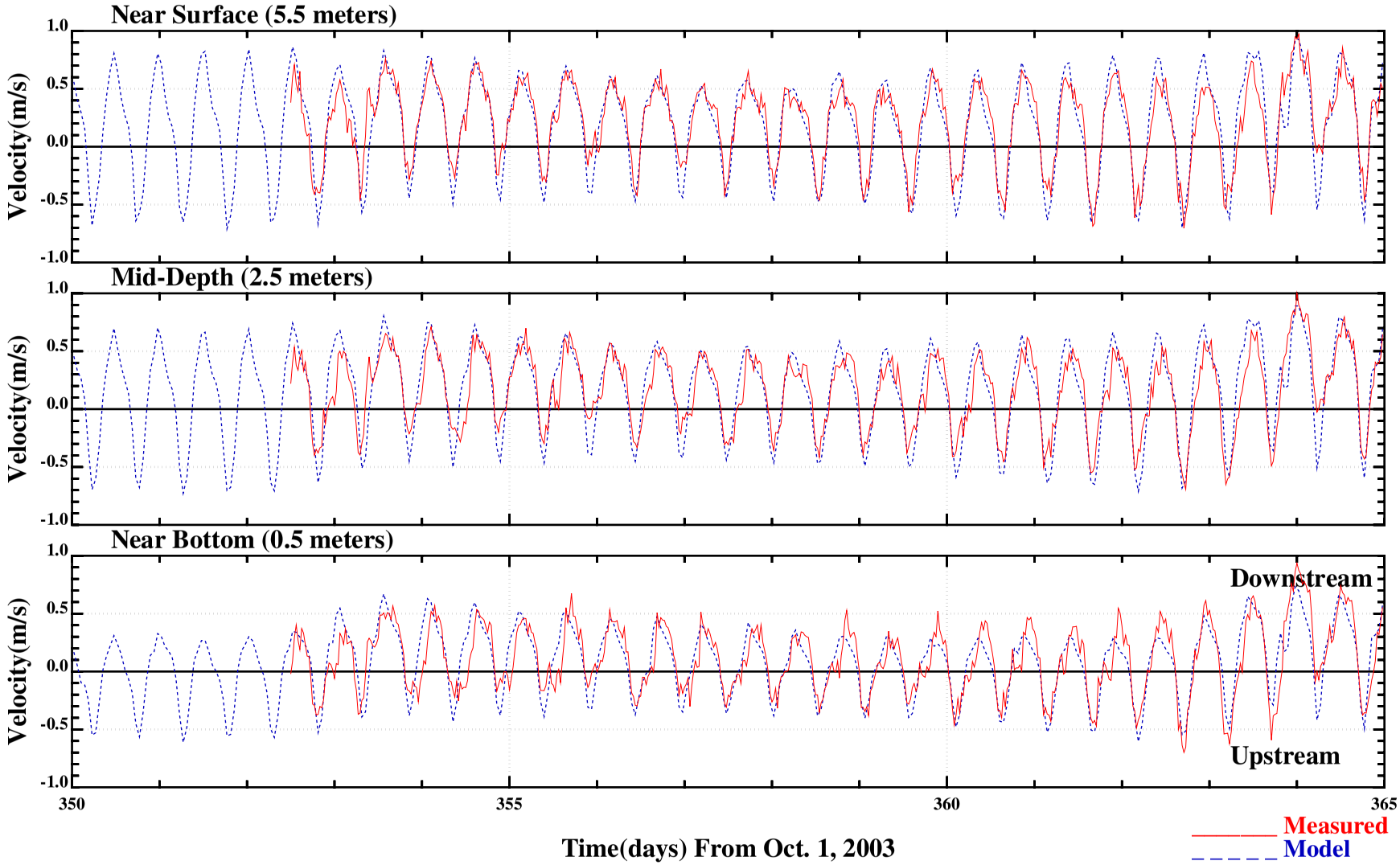

Figure 4-21 Comparison of hourly computed current velocities at three depths with IMCS mooring data (M3) over a period of two weeks: September 2004

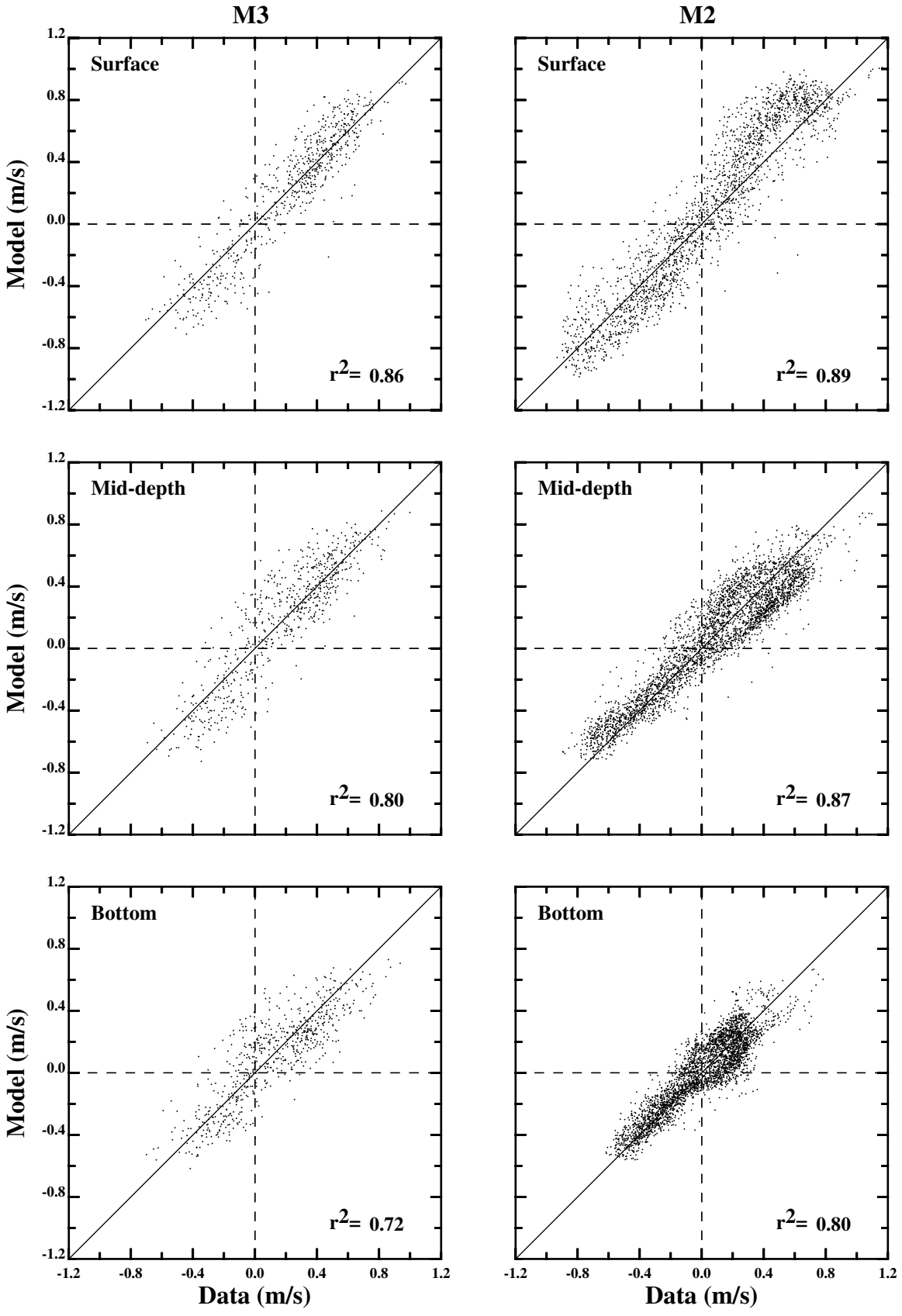

Figure 4-22 Scatter plot of computed current velocities with observed IMCS mooring data: August-September, 2004

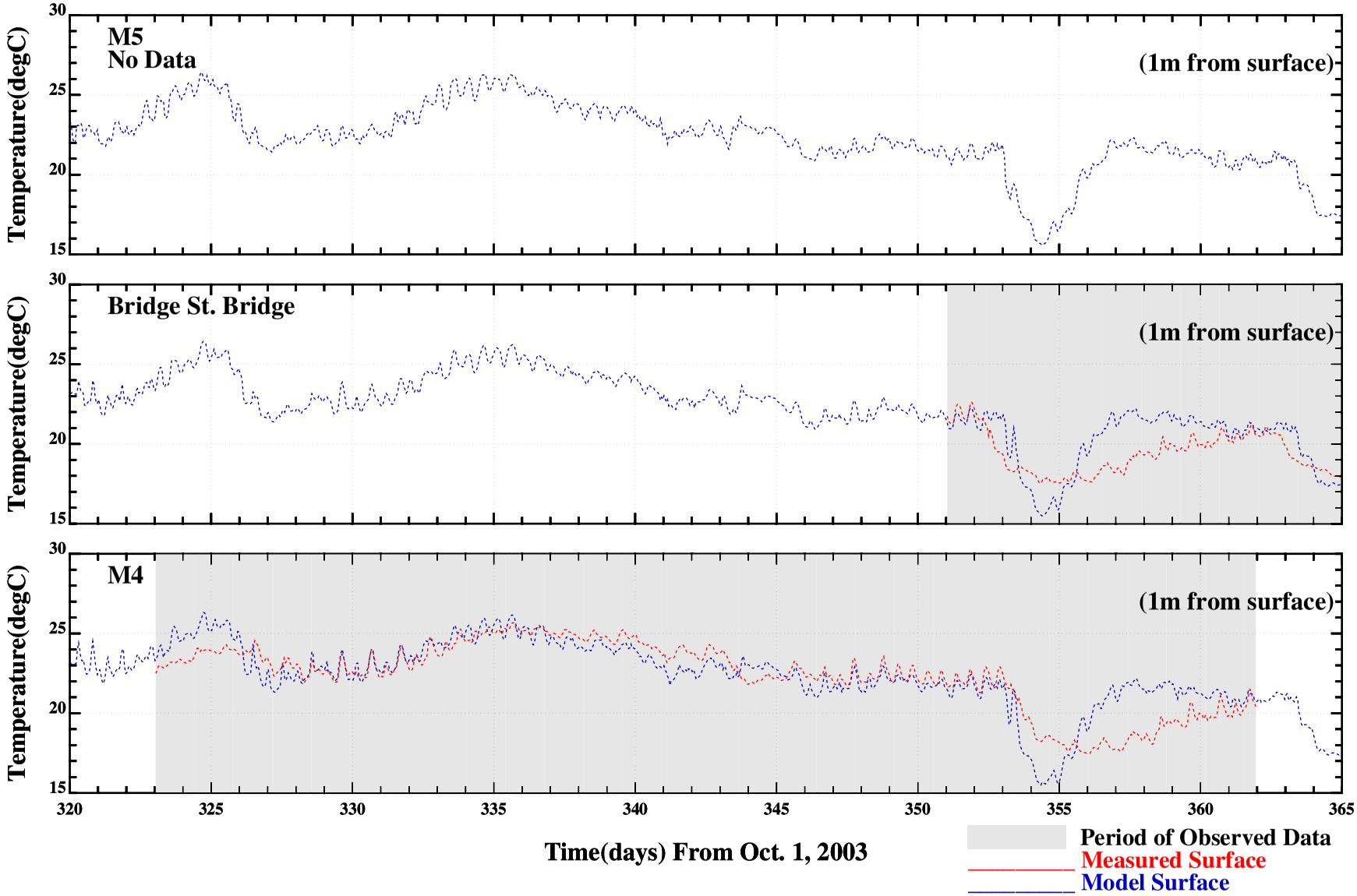

Figure 4-23 Comparison of hourly computed surface temperature with six IMCS mooring data over a period of two months: August - September 2004

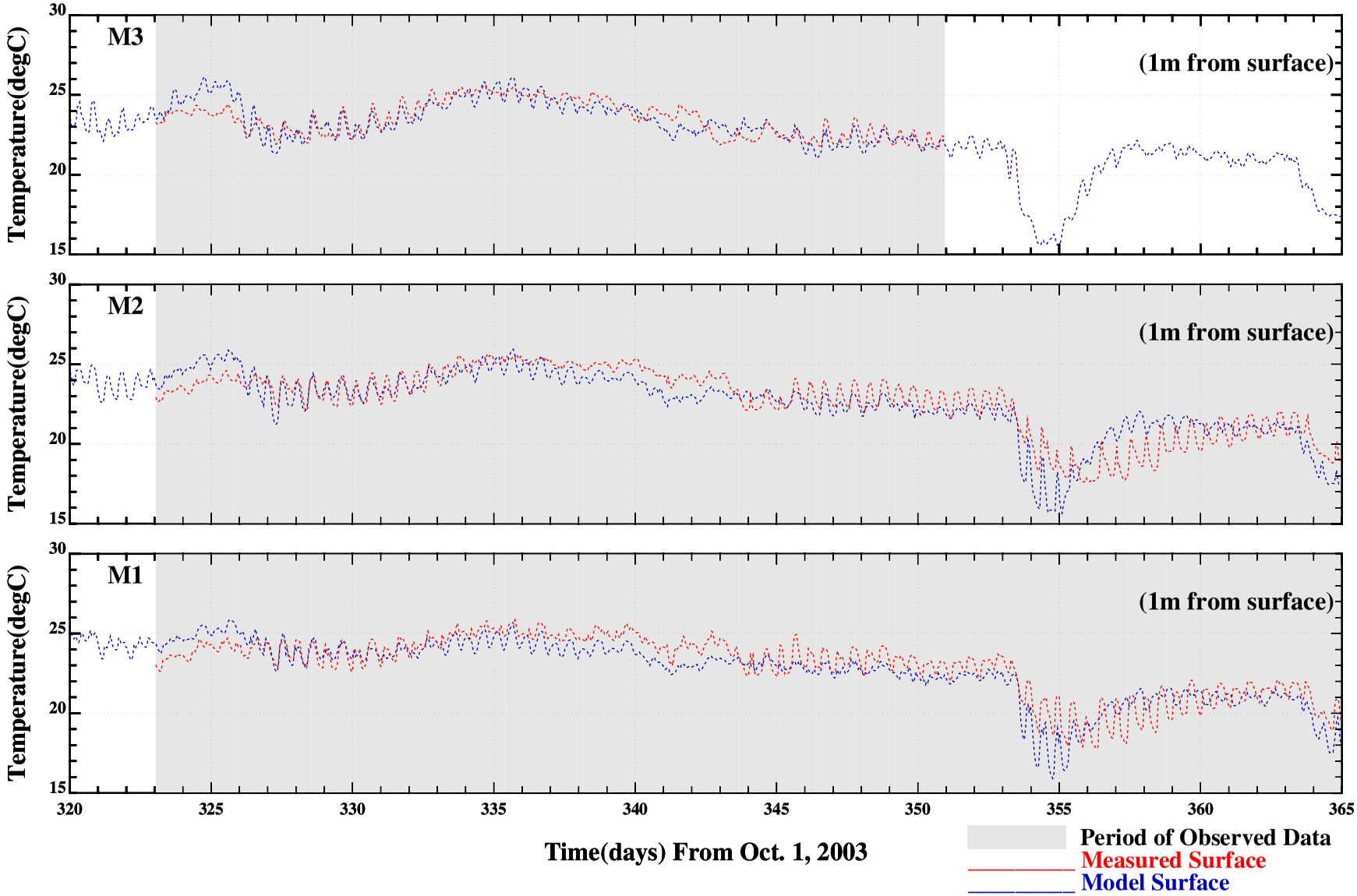

Figure 4-23 Comparison of hourly computed surface temperature with six IMCS mooring data over a period of two months: August - September 2004 (continued)

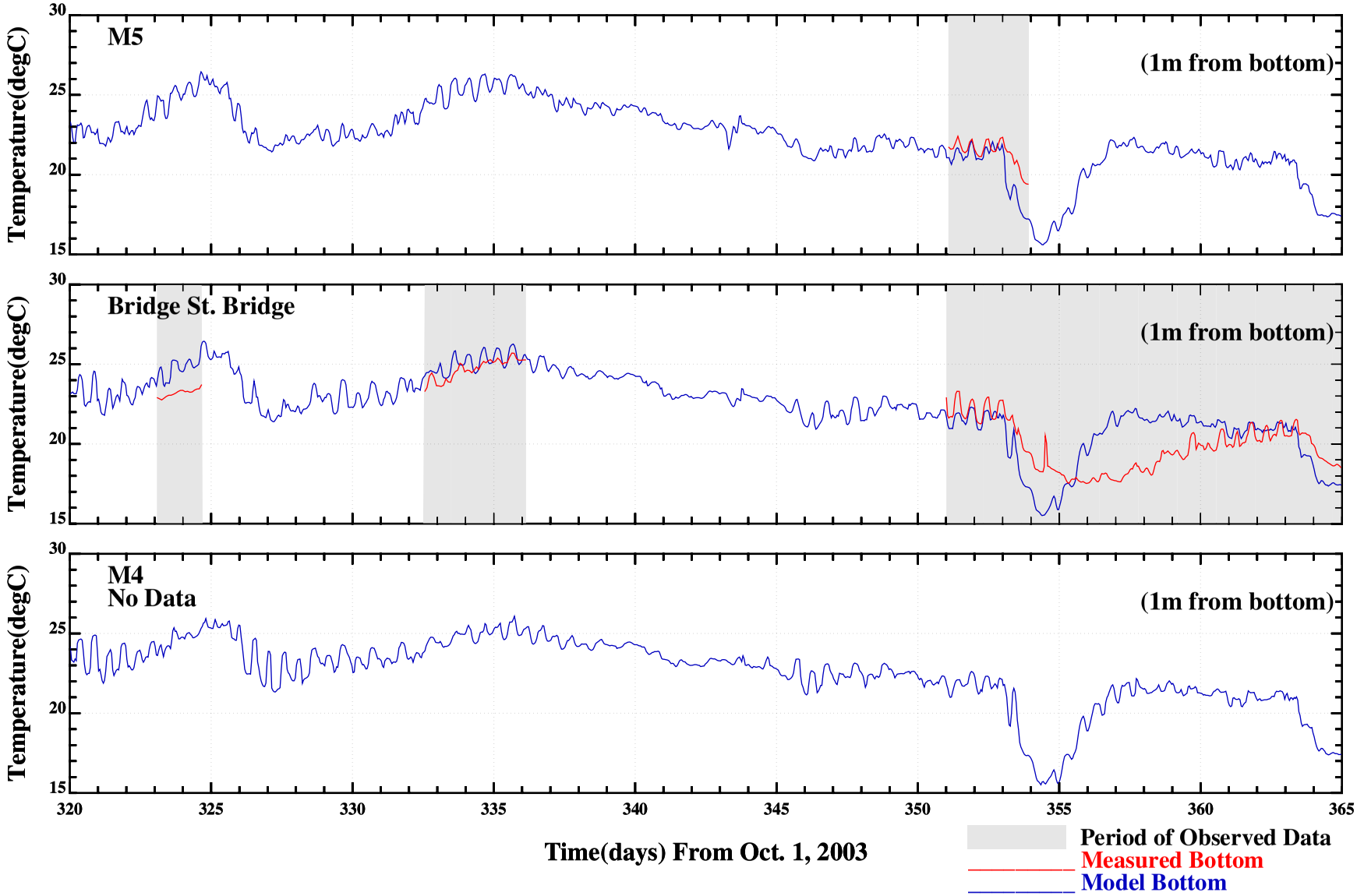

Figure 4-24 Comparison of hourly computed bottom temperature with six IMCS mooring data over a period of two months: August - September 2004

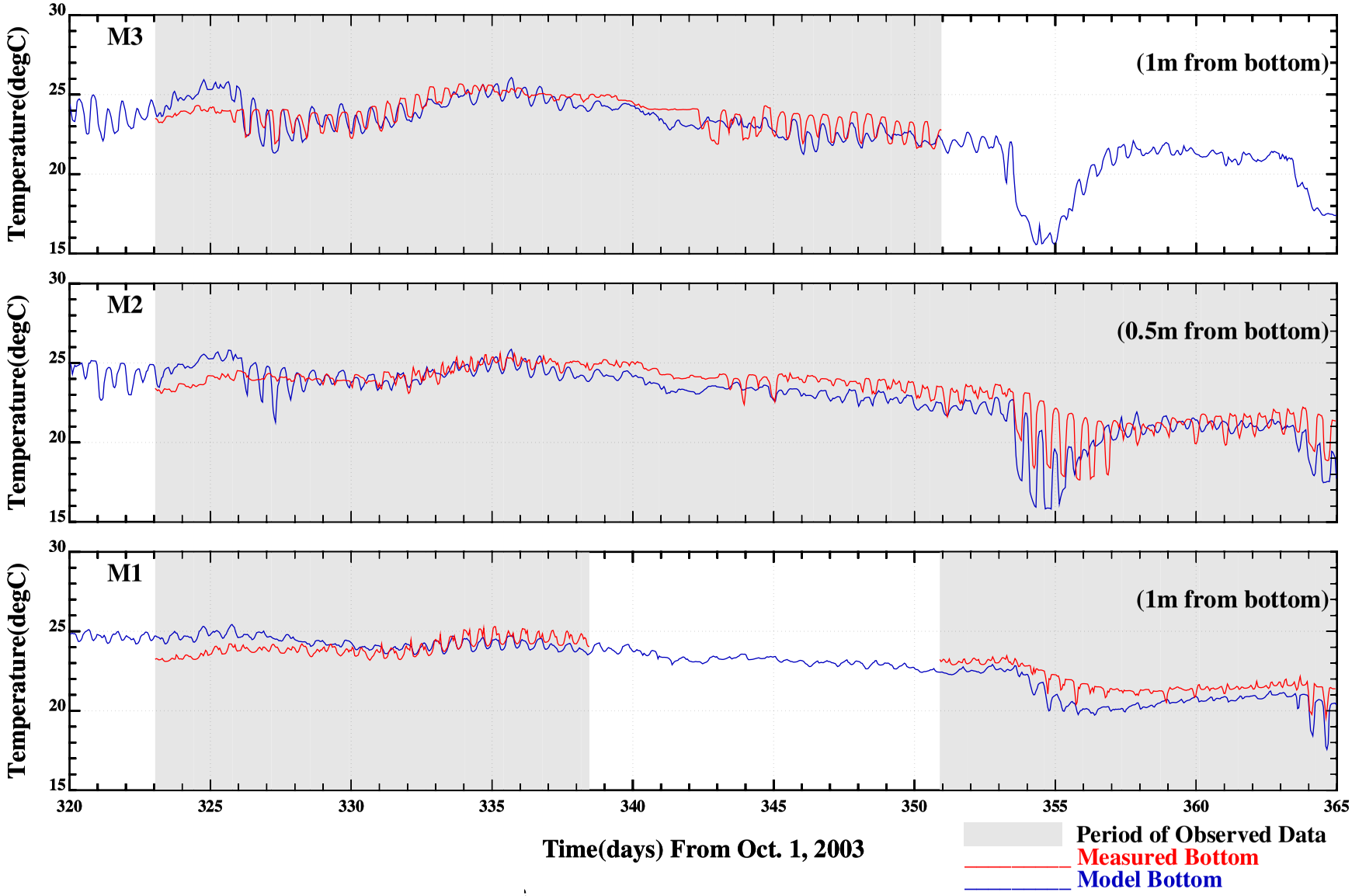

Figure 4-24 Comparison of hourly computed bottom temperature with six IMCS mooring data over a period of two months: August - September 2004 (continued)

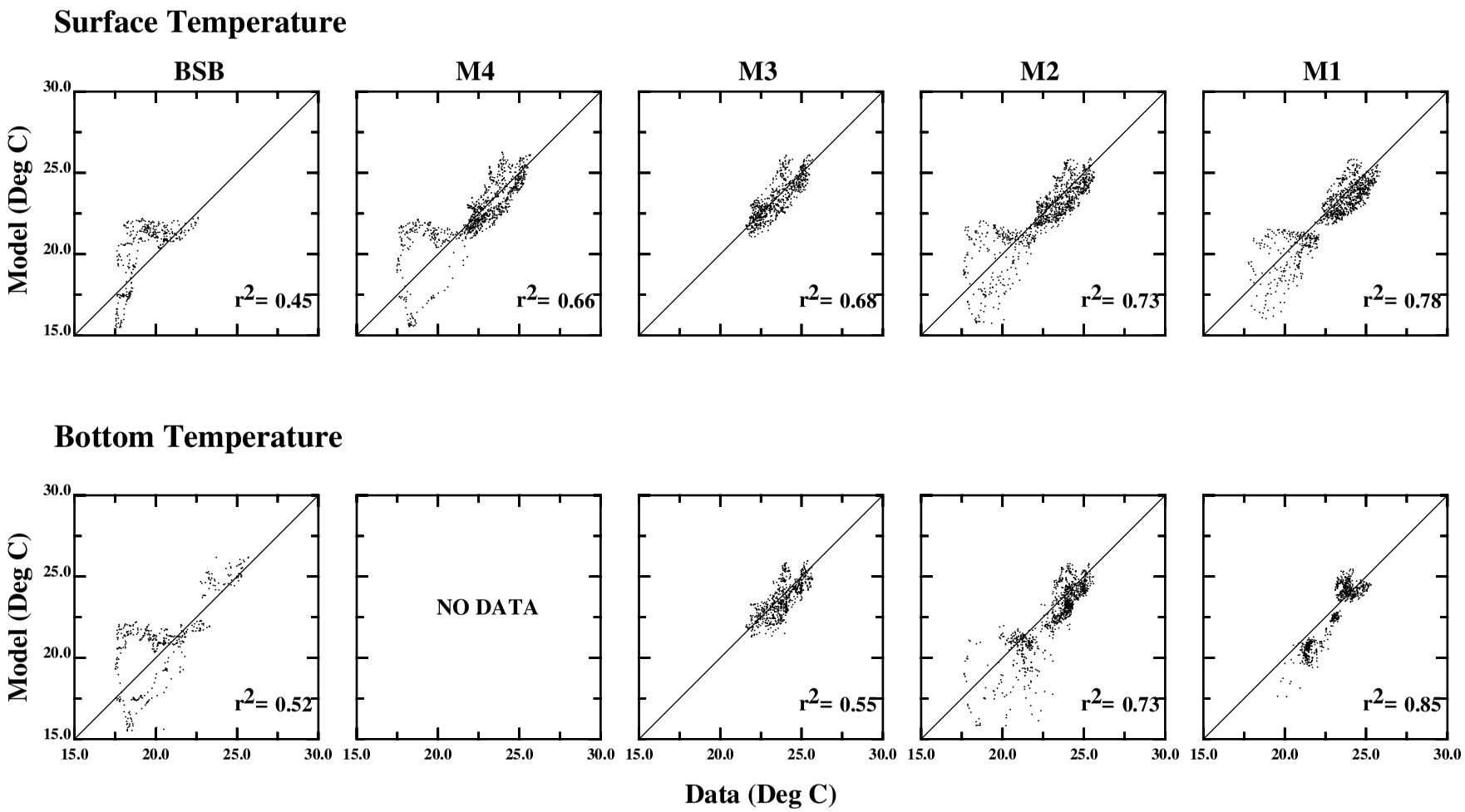

Figure 4-25 Scatter plot of computed temperature with observed IMCS mooring data: August - September 2004

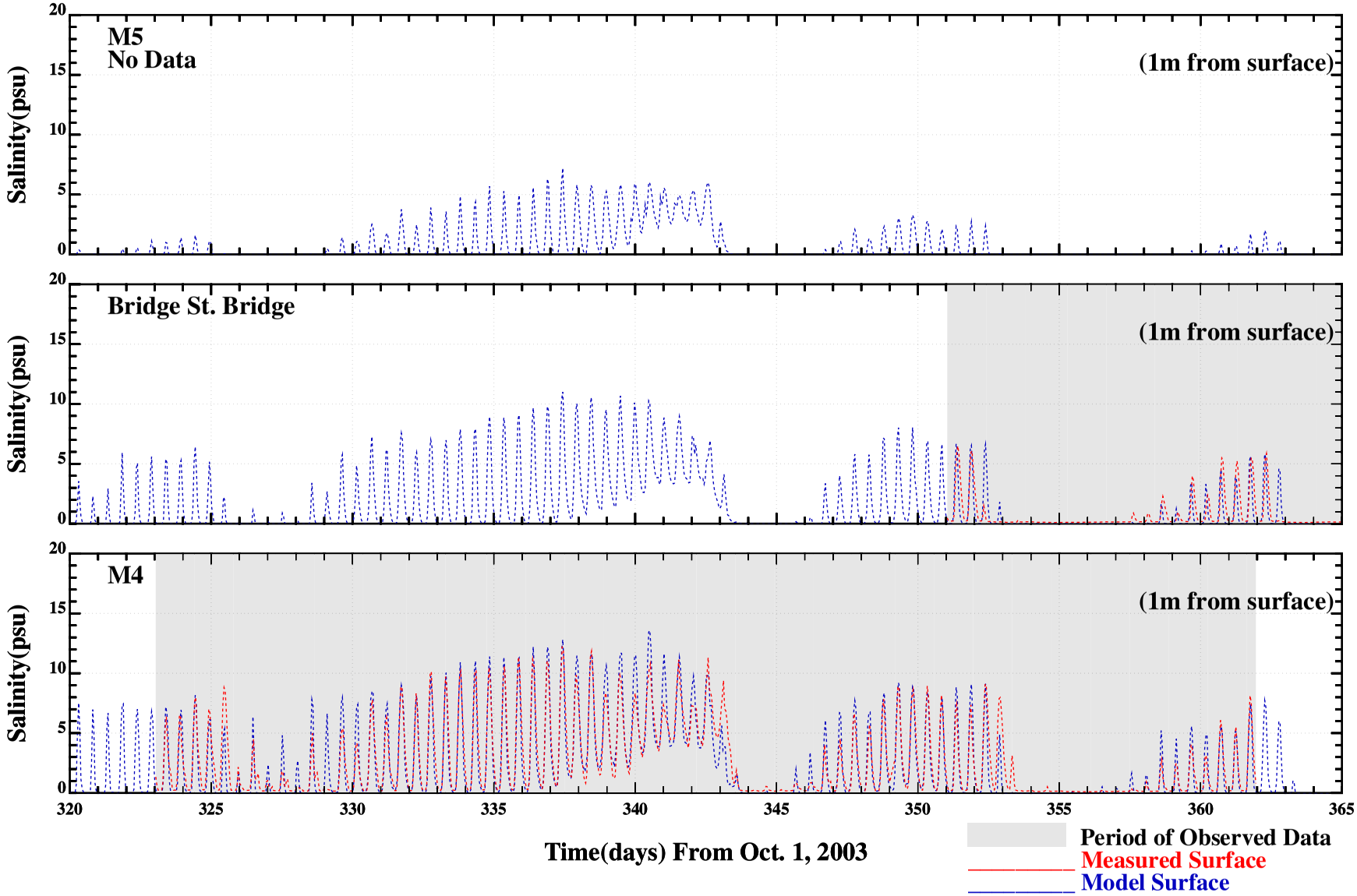

Figure 4-26 Comparison of hourly computed surface salinity with six IMCS mooring data over a period of two months: August - September 2004

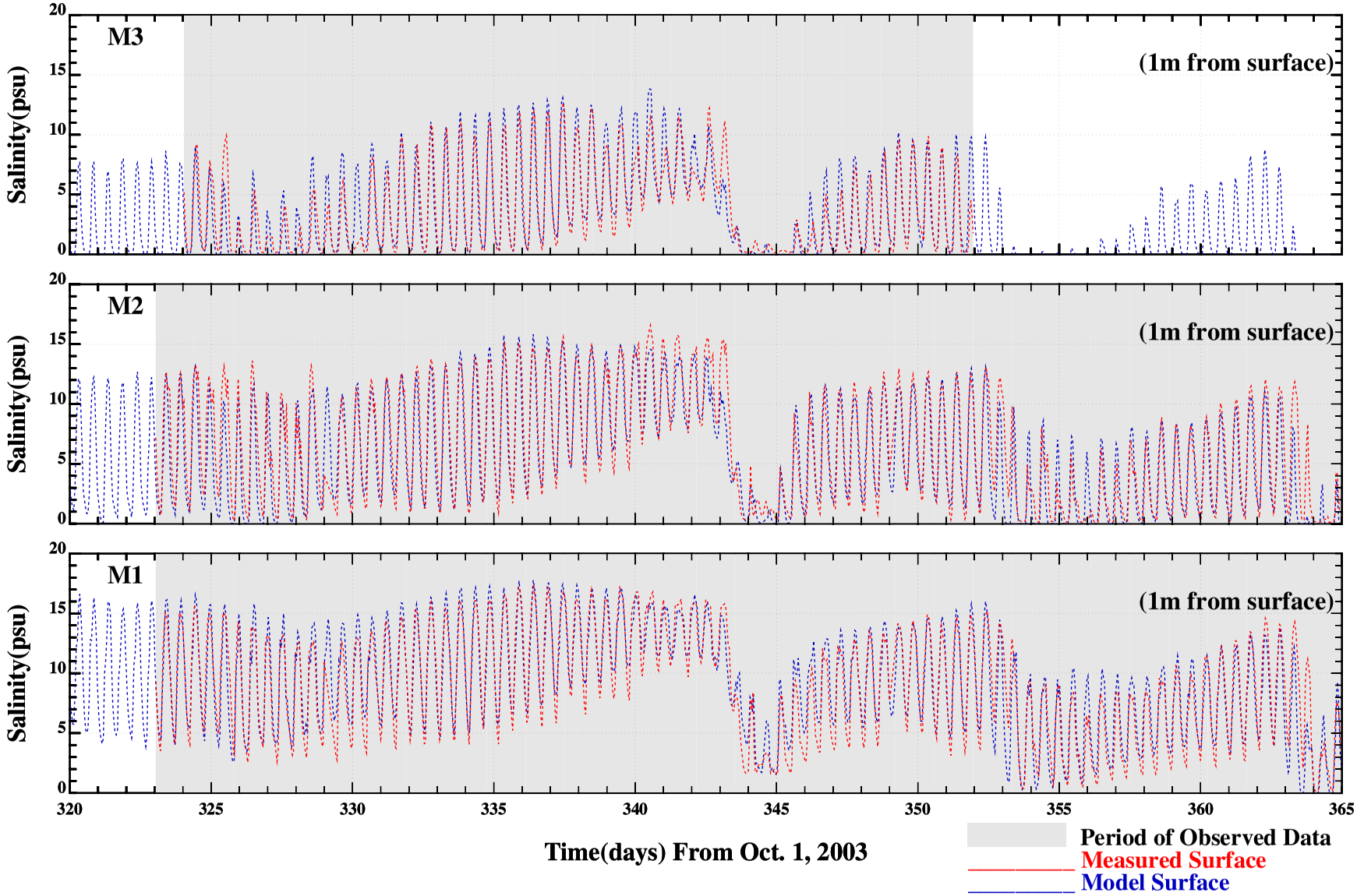

Figure 4-26 Comparison of hourly computed surface salinity with six IMCS mooring data over a period of two months: August - September 2004 (continued)

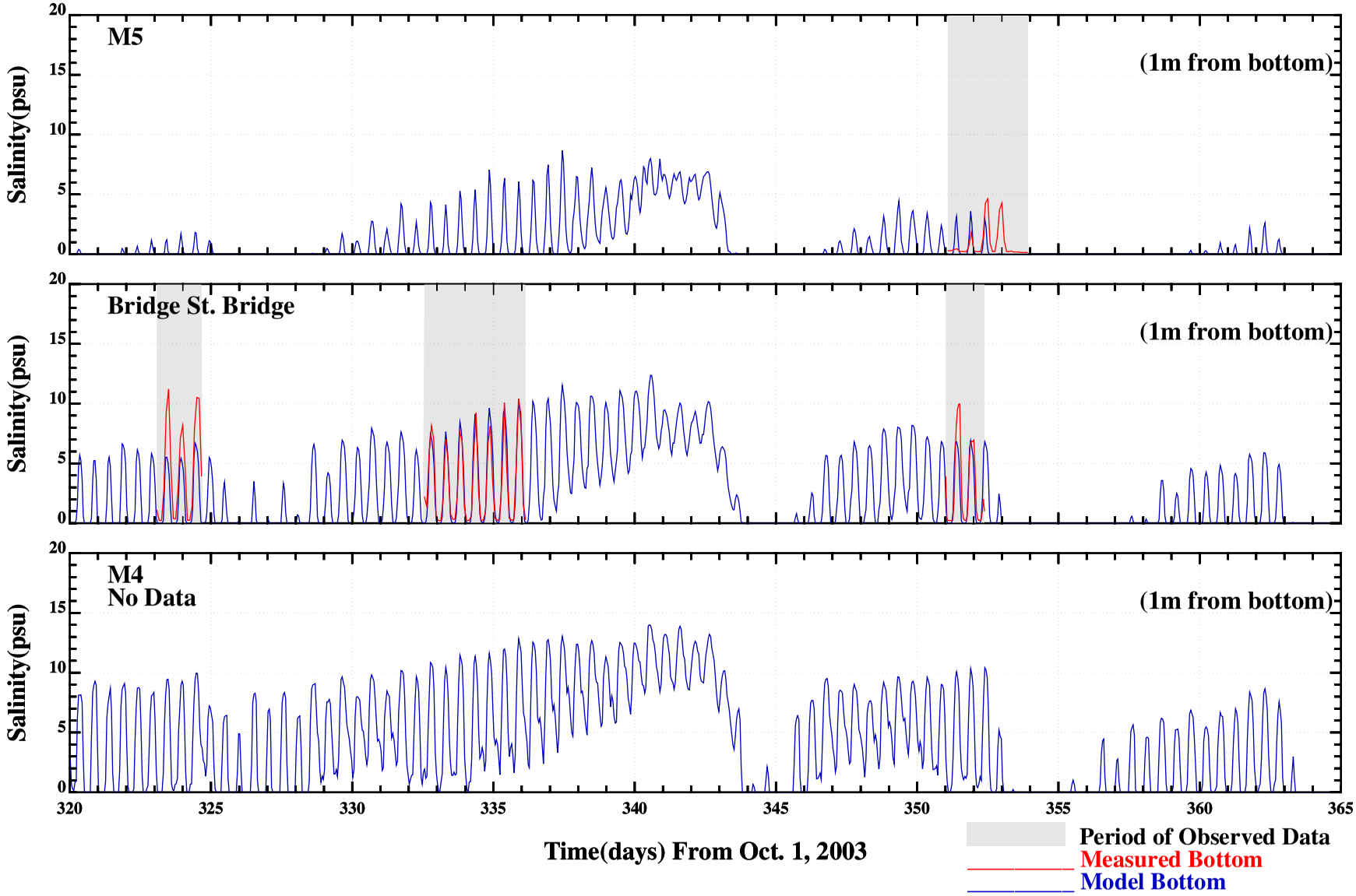

Figure 4-27 Comparison of hourly computed bottom salinity with six IMCS mooring data over a period of two months: August - September 2004

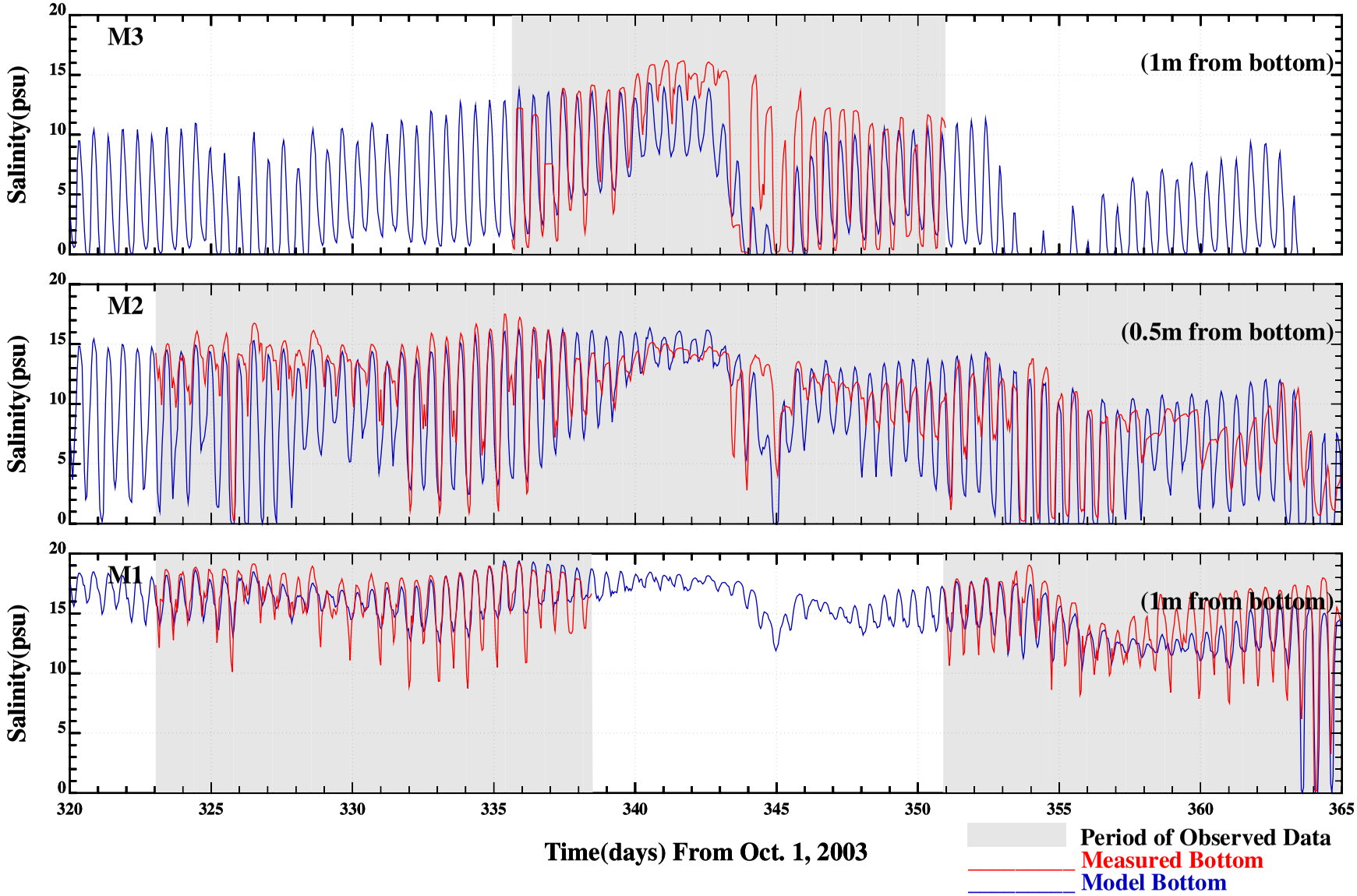

Figure 4-27 Comparison of hourly computed bottom salinity with six IMCS mooring data over a period of two months: August - September 2004 (continued)

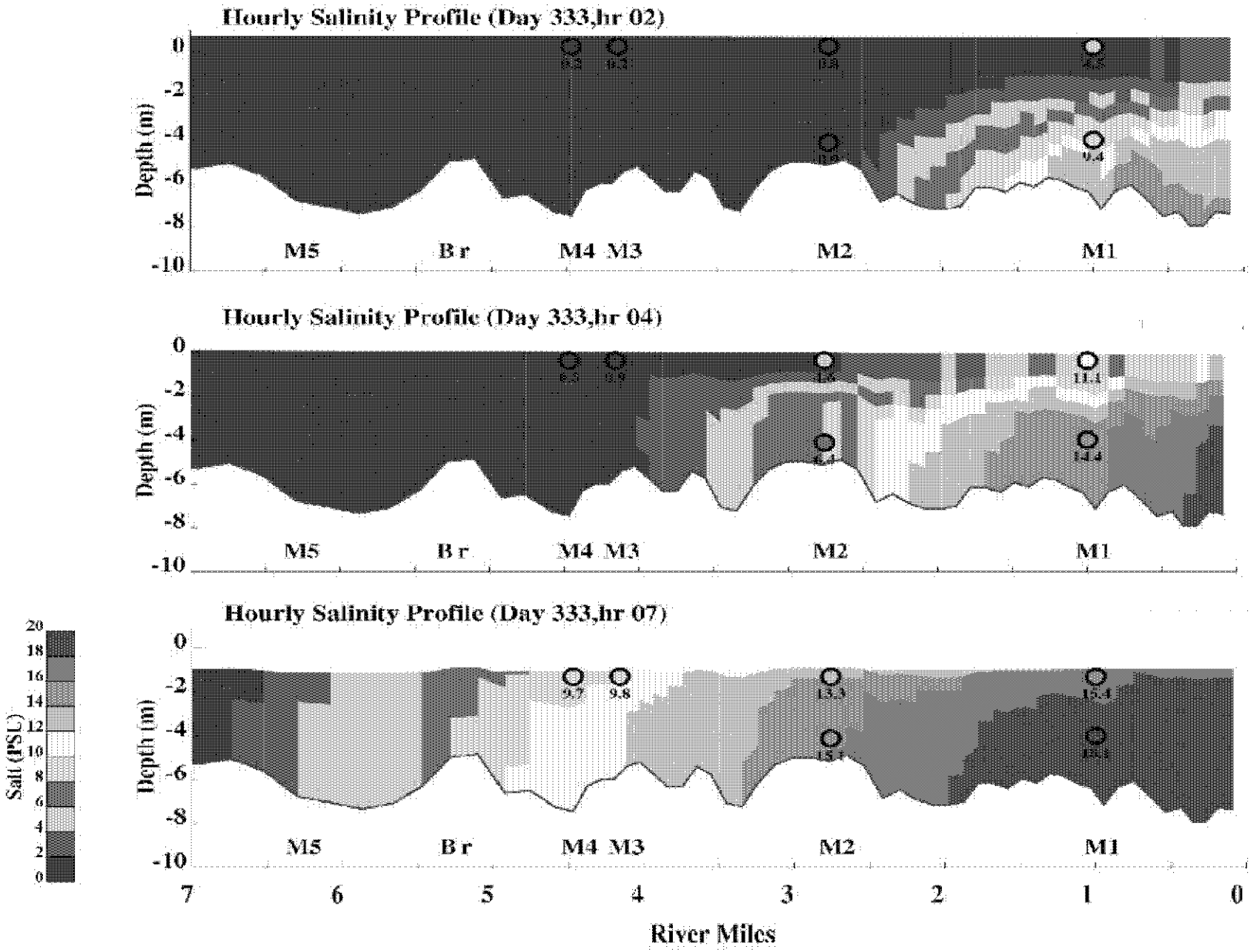

Figure 4-28 Longitudinal profiles of salinity at different times: maximum ebb (upper frame), slack (middle frame) and maximum flood (lower frame). Observed values are shown by circles.

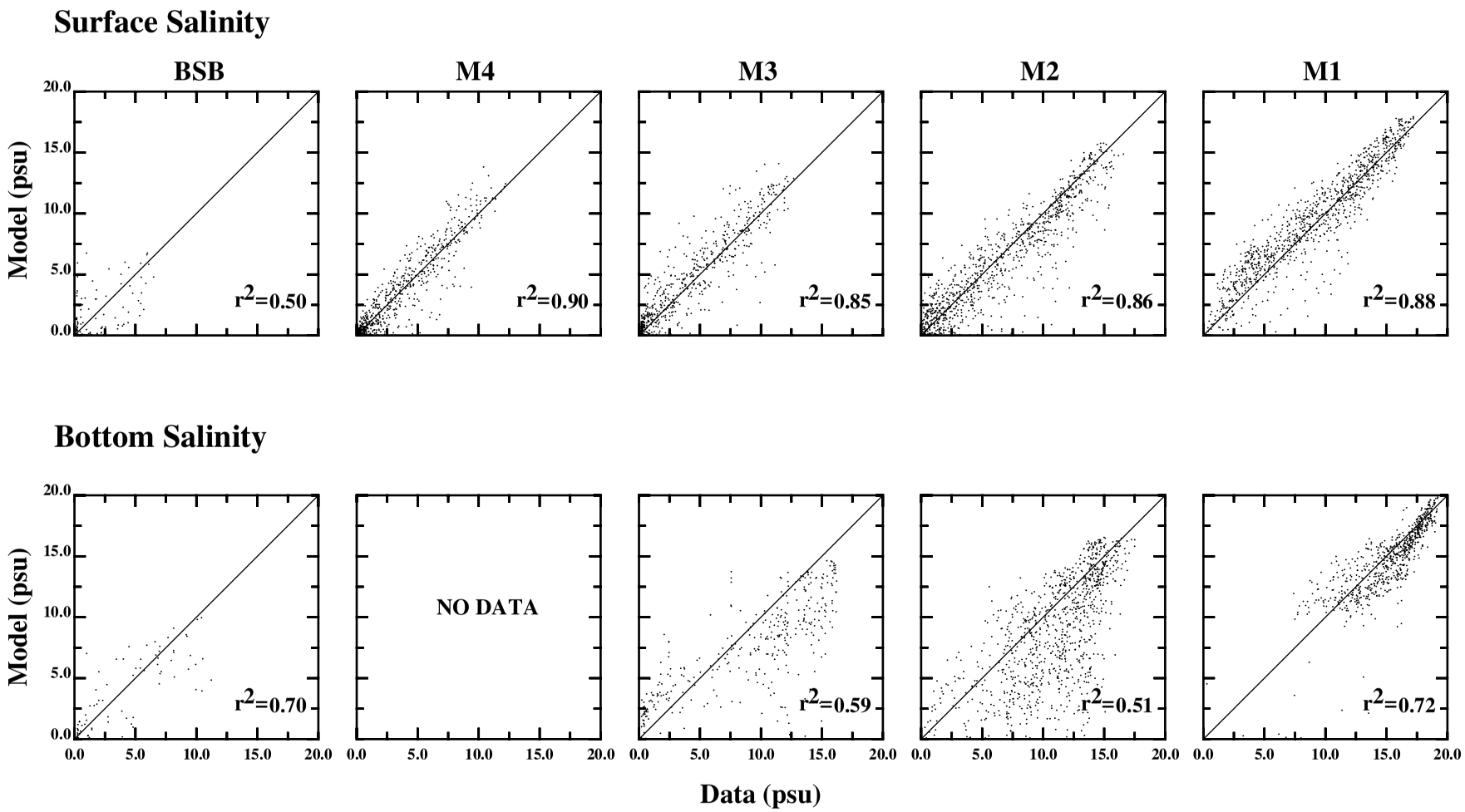

Figure 4-29 Scatter plot of computed salinity with observed IMCS mooring data: August - September 2004

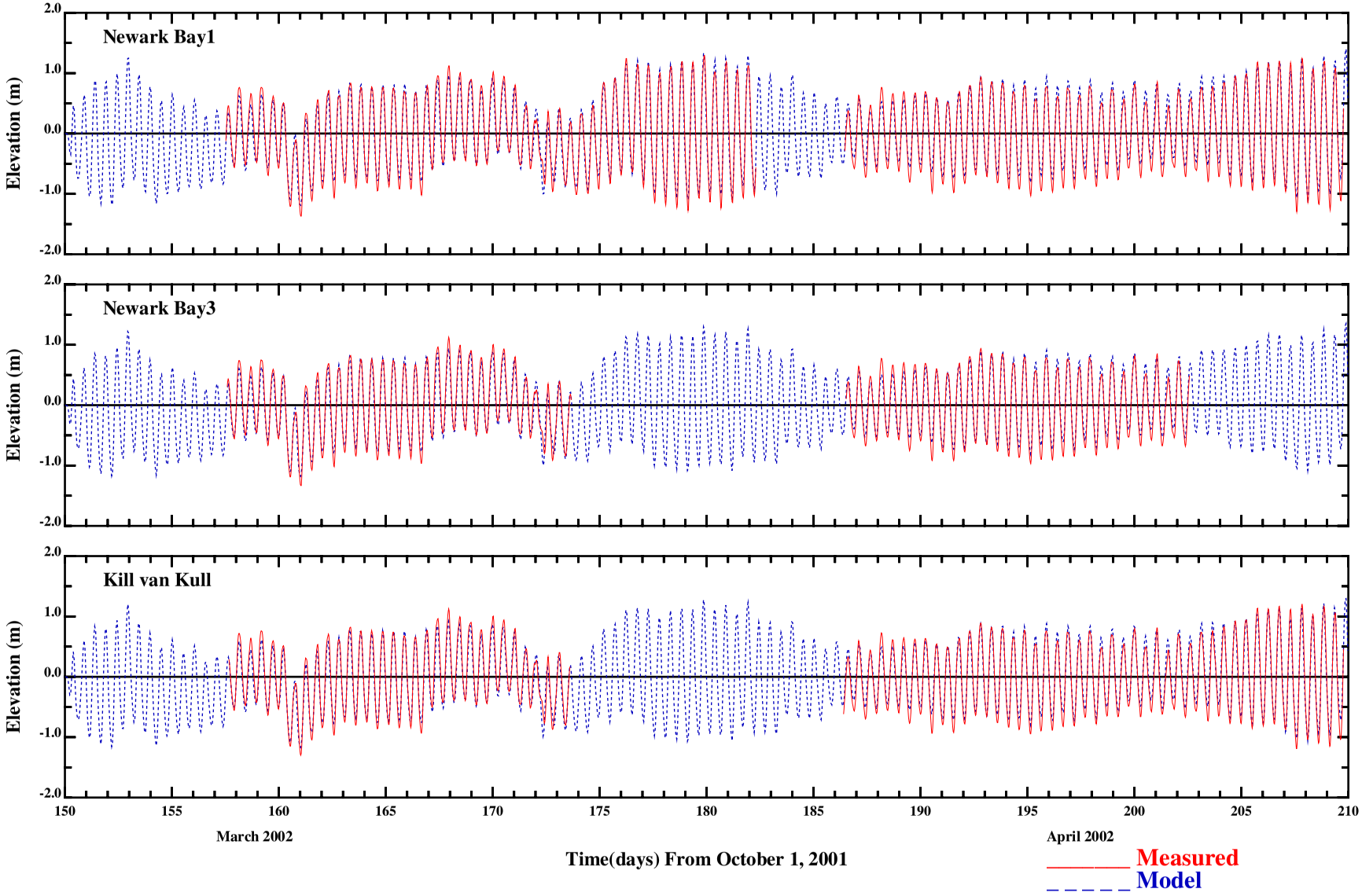

Figure 4-30 Comparison of hourly computed water elevations with IMCS mooring data: March-April, 2002

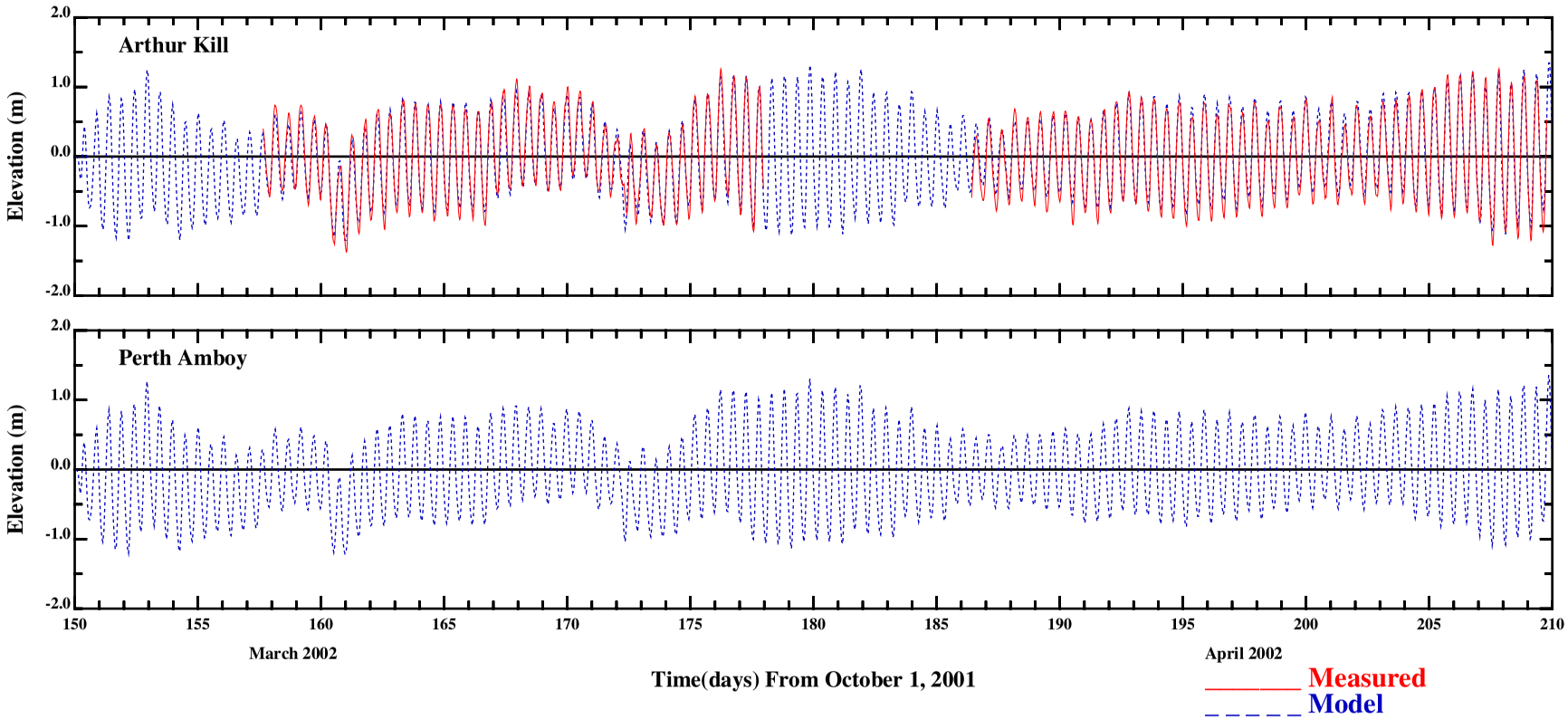

Figure 4-30 Comparison of hourly computed water elevations with IMCS mooring data: March-April, 2002 (continued)

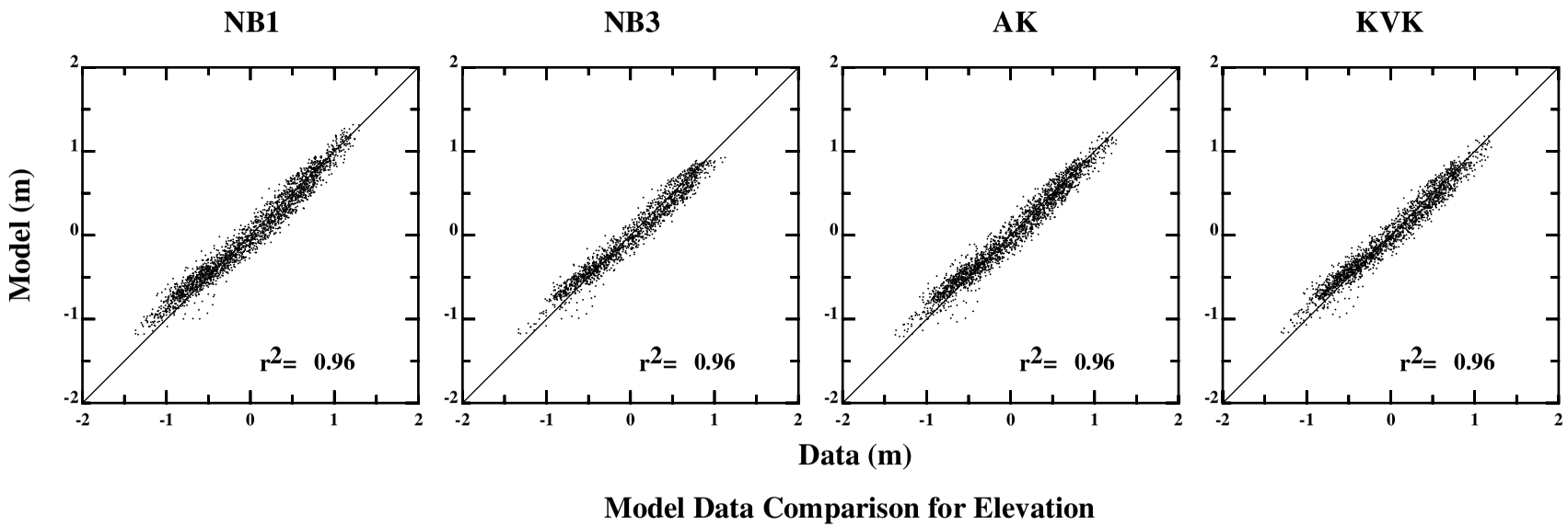

Figure 4-31 Scatter plot of computed water elevation with observed IMCS mooring data: March-April, 2002

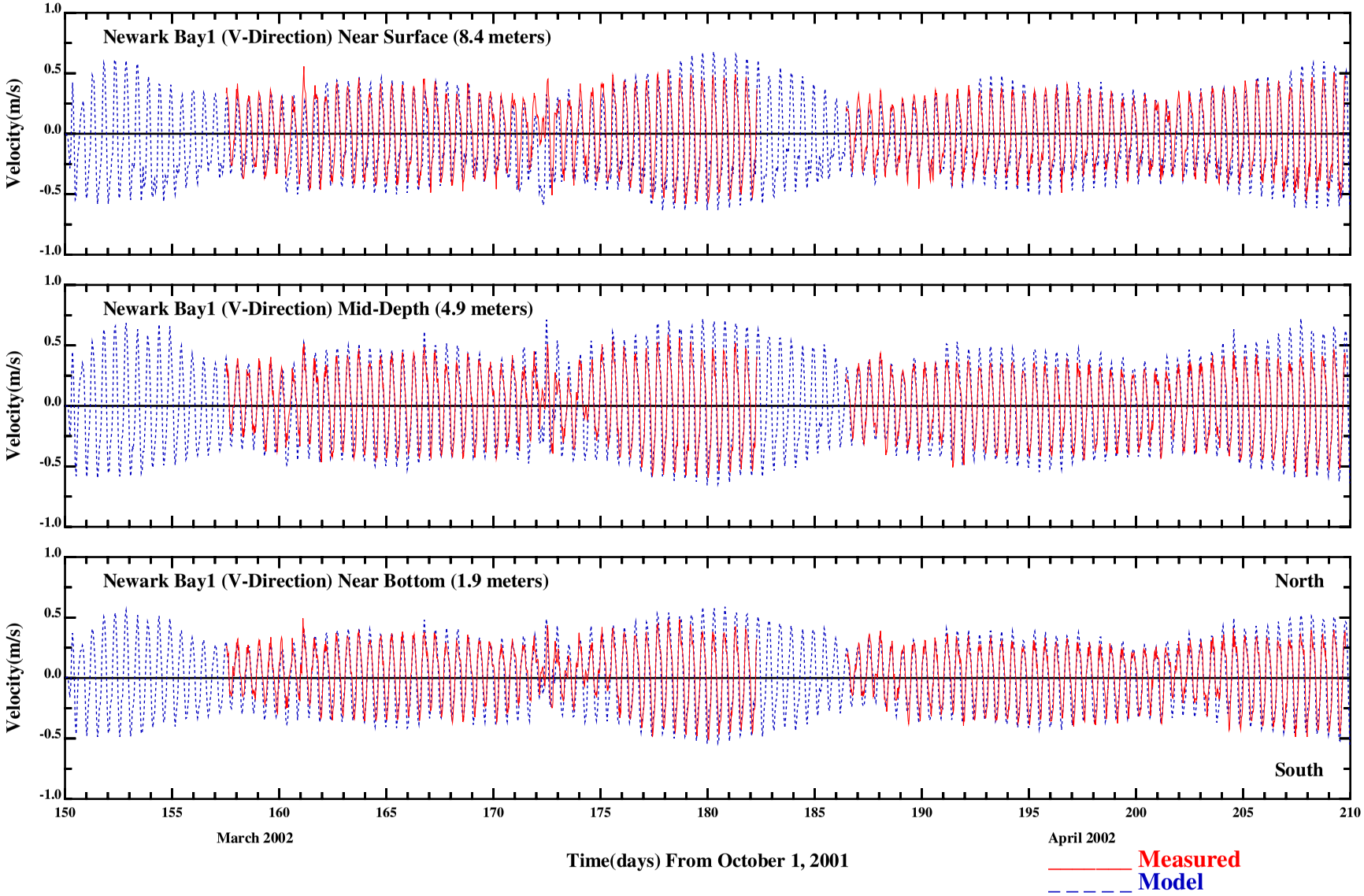

Figure 4-32a Comparison of hourly computed current velocities at three depths at NB1with IMCS mooring data: March - April, 2002

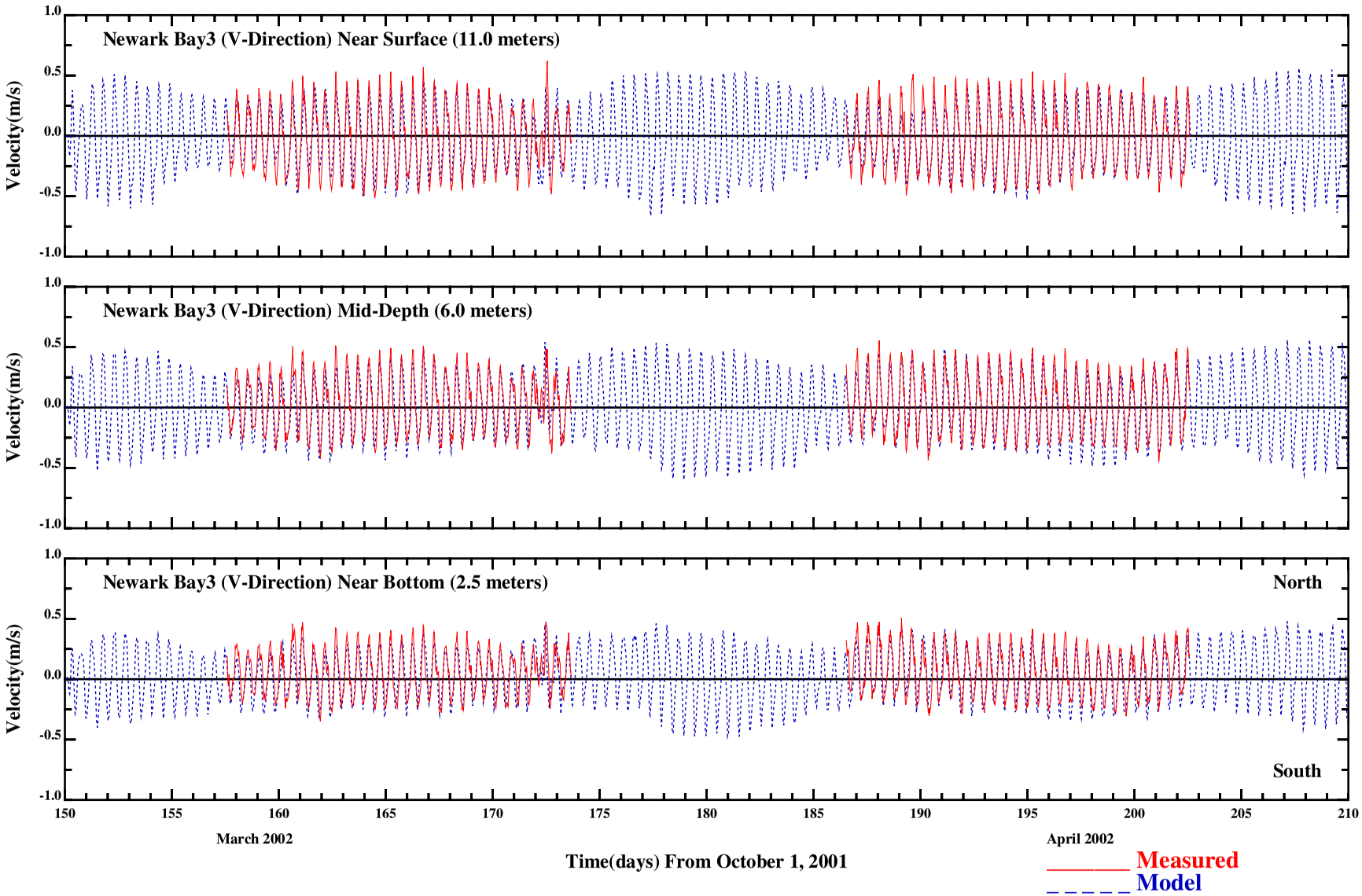

Figure 4-32b Comparison of hourly computed current velocities at three depths at NB3 with IMCS mooring data: March - April, 2002

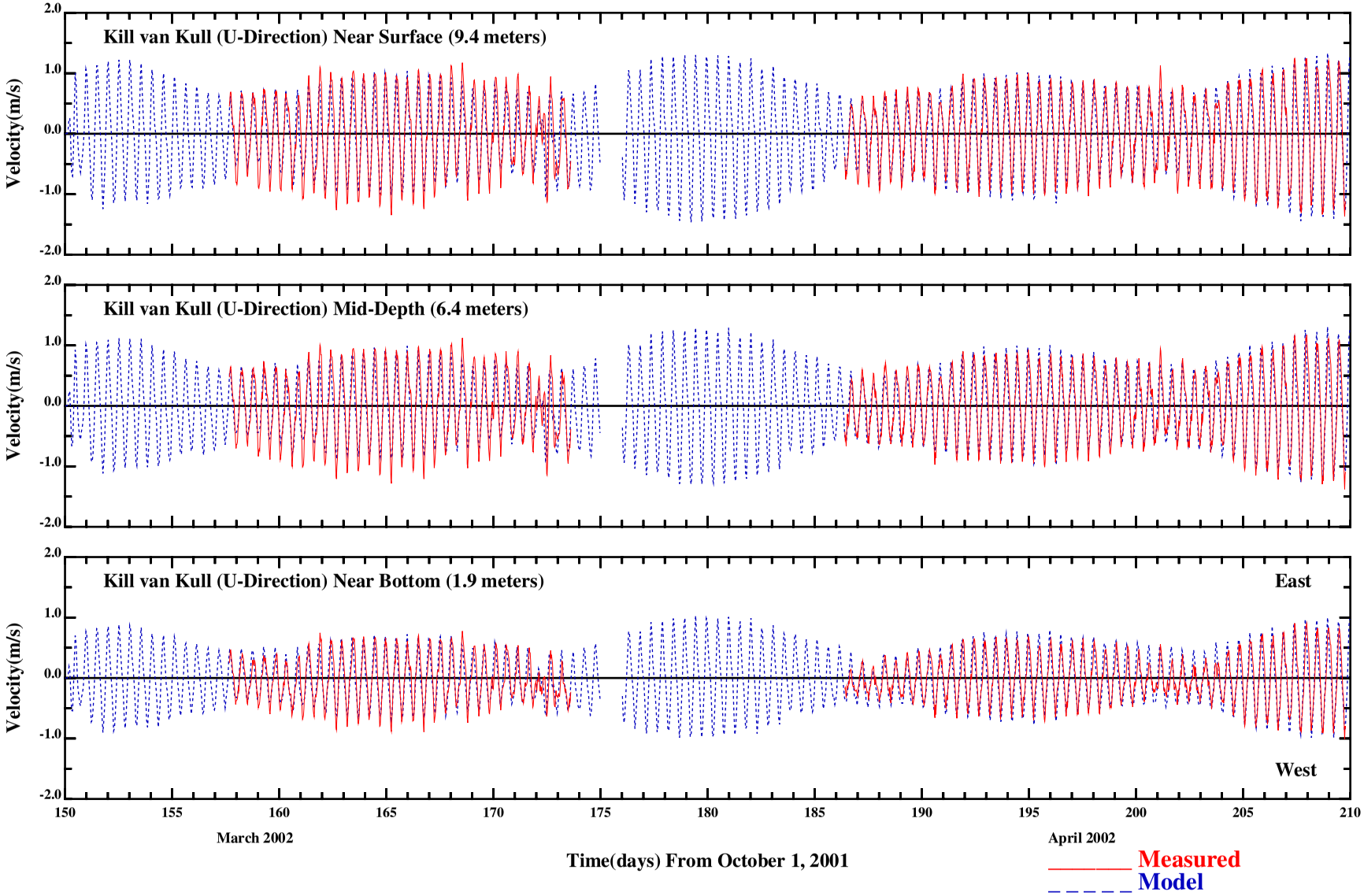

Figure 4-32c Comparison of hourly computed current velocities at three depths at KVK with IMCS mooring data: March - April, 2002

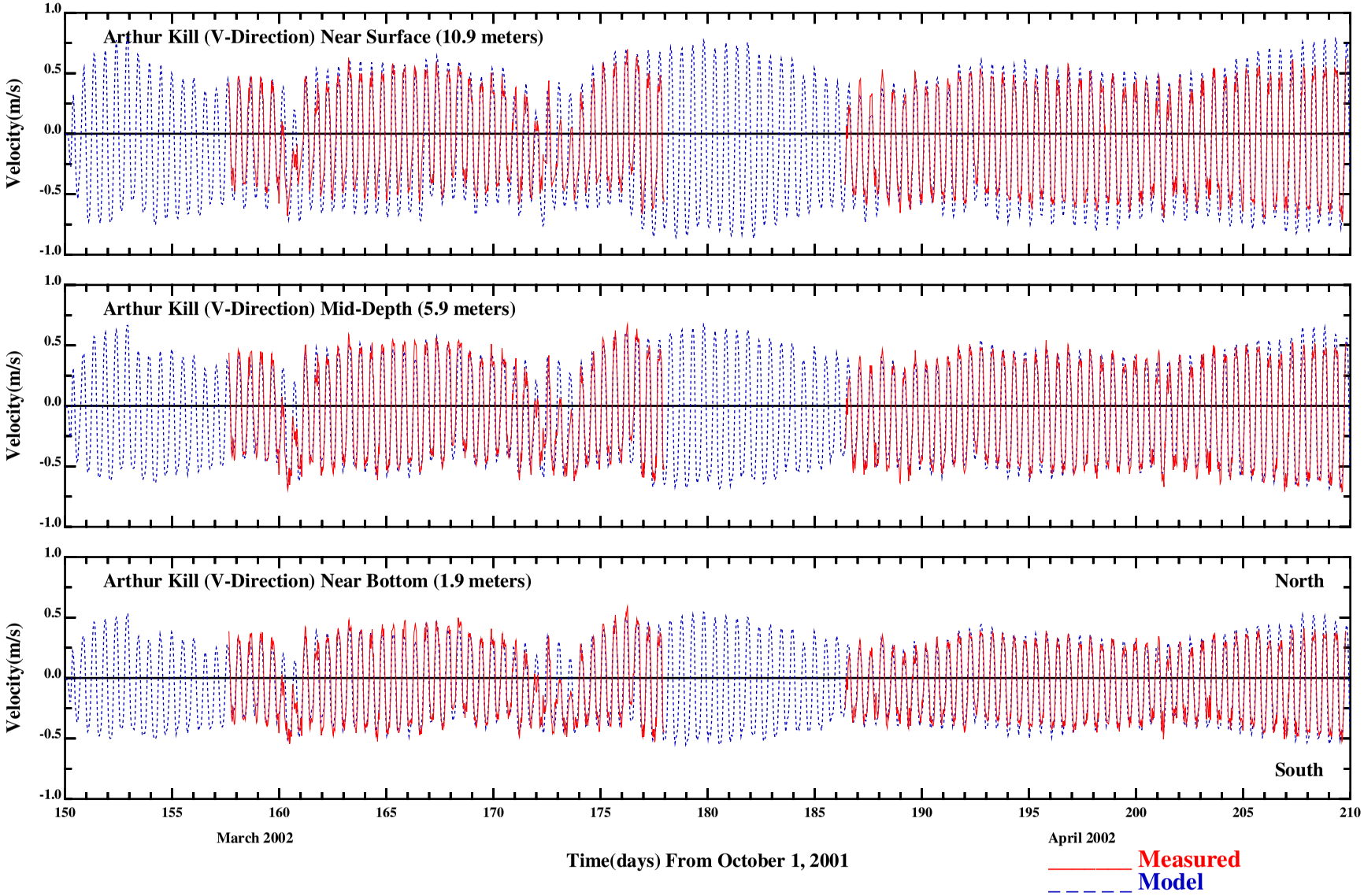

Figure 4-32d Comparison of hourly computed current velocities at three depths at AK with IMCS mooring data: March - April, 2002

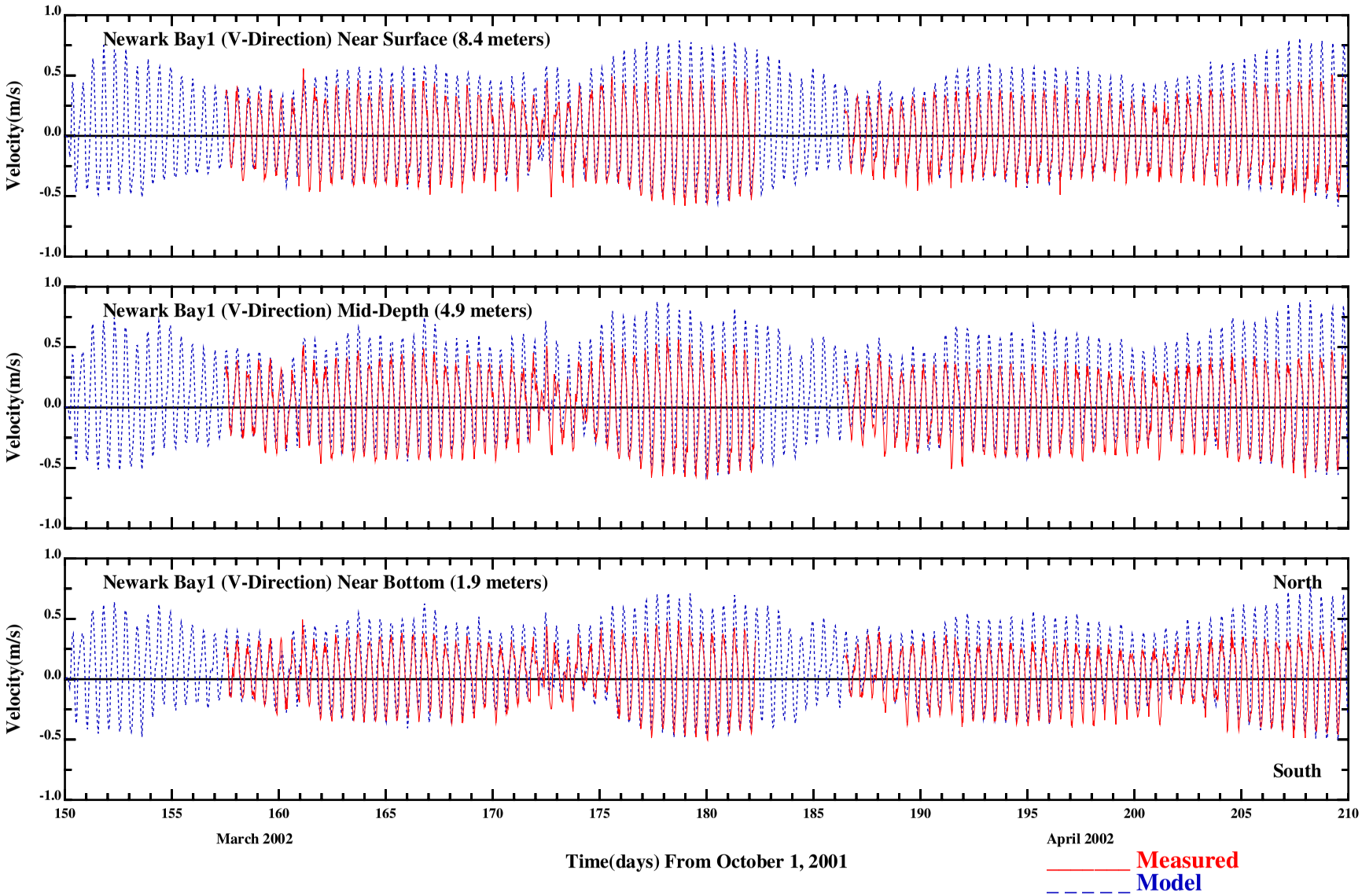

Figure 4-32e Comparison of hourly computed current velocities at three depths at a deeper grid cell (13.4 m) near IMCS NB1 mooring station

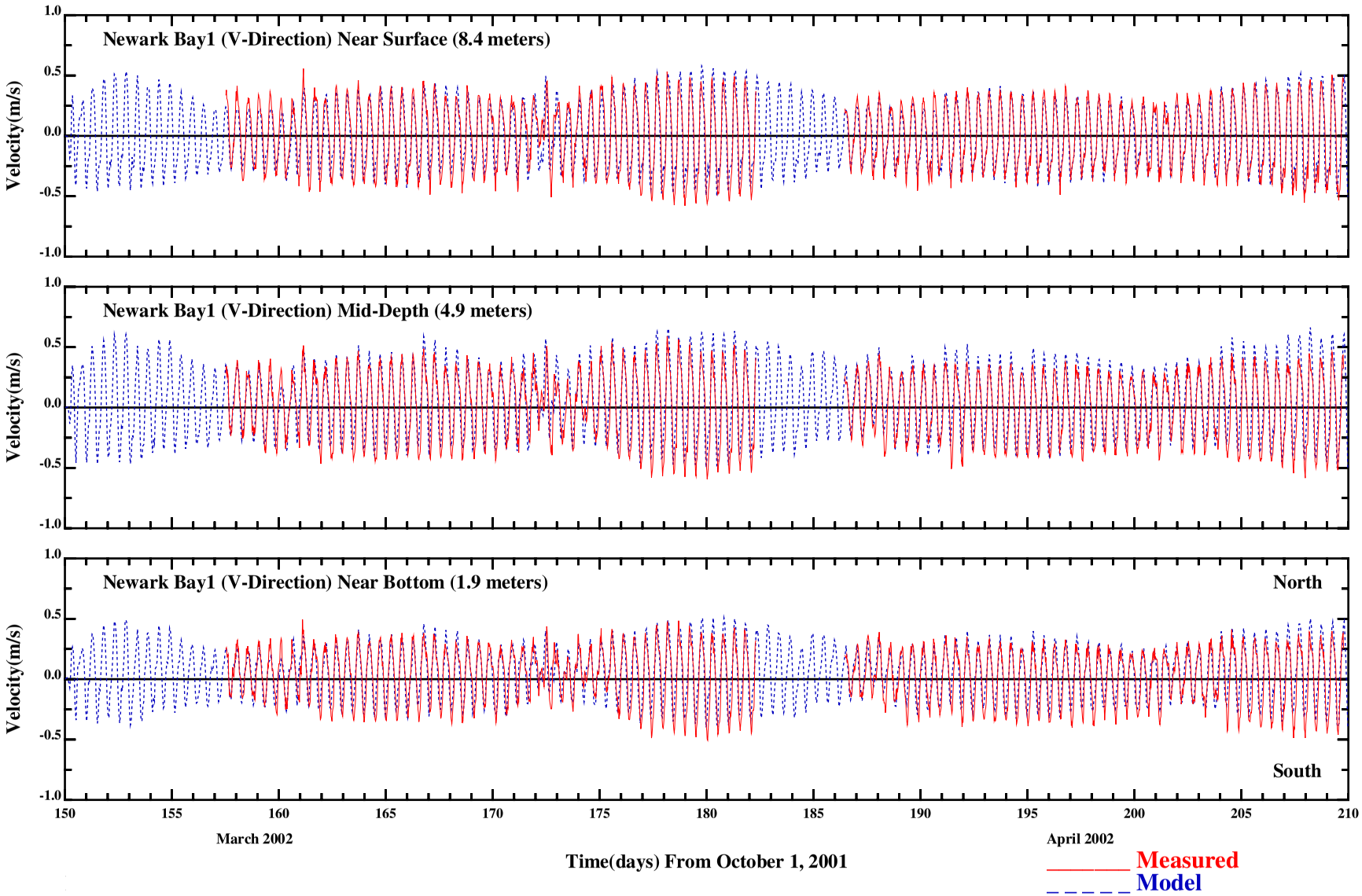

Figure 4-32f Comparison of two cell (12.5m and 7.5m) averaged hourly current velocities at three depths near IMCS NB1 mooring station

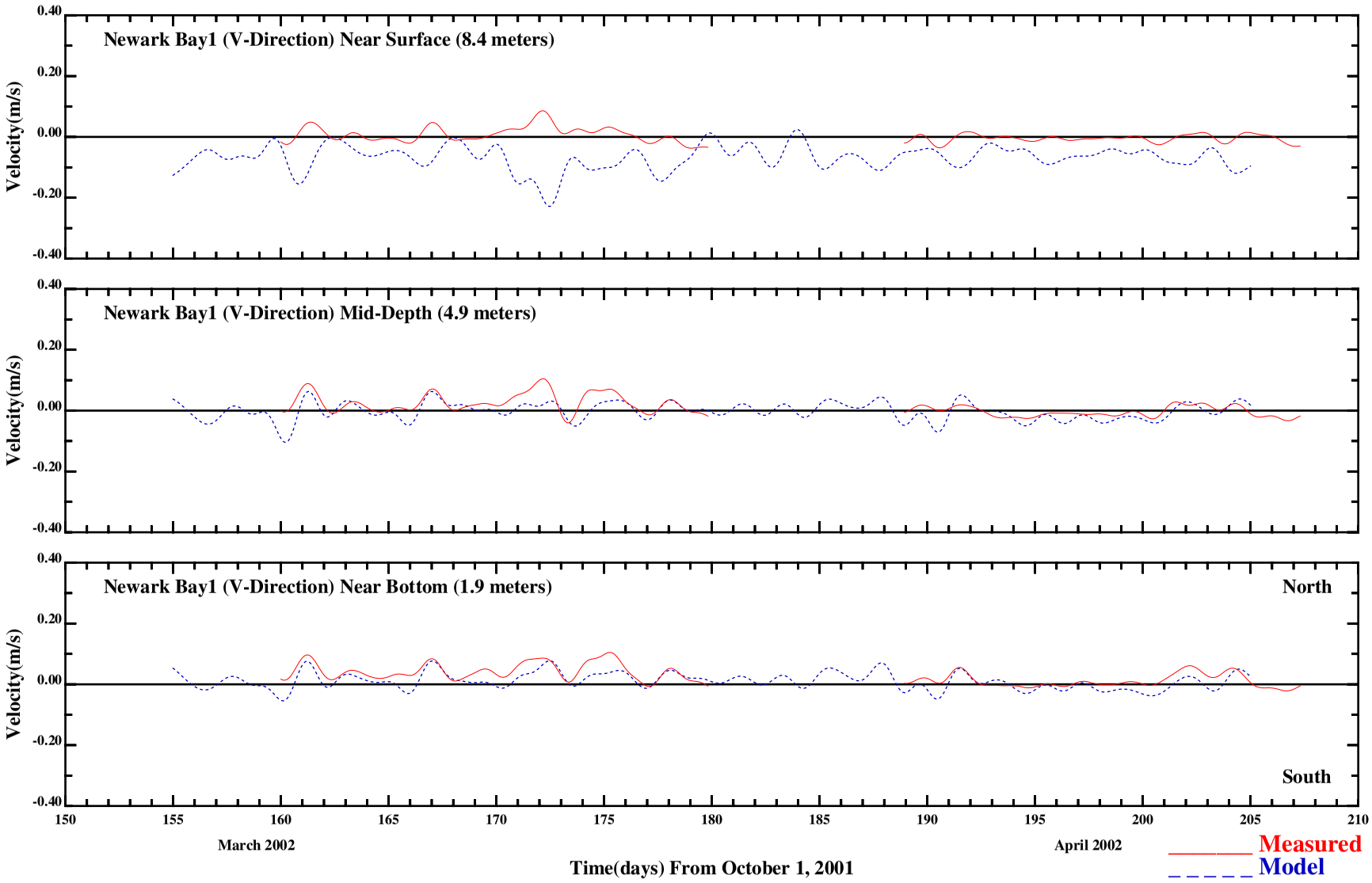

Figure 4-33a Comparison of 35 hour low-passed computed current velocities at three depths at NB1 with IMCS mooring data: March - April, 2002

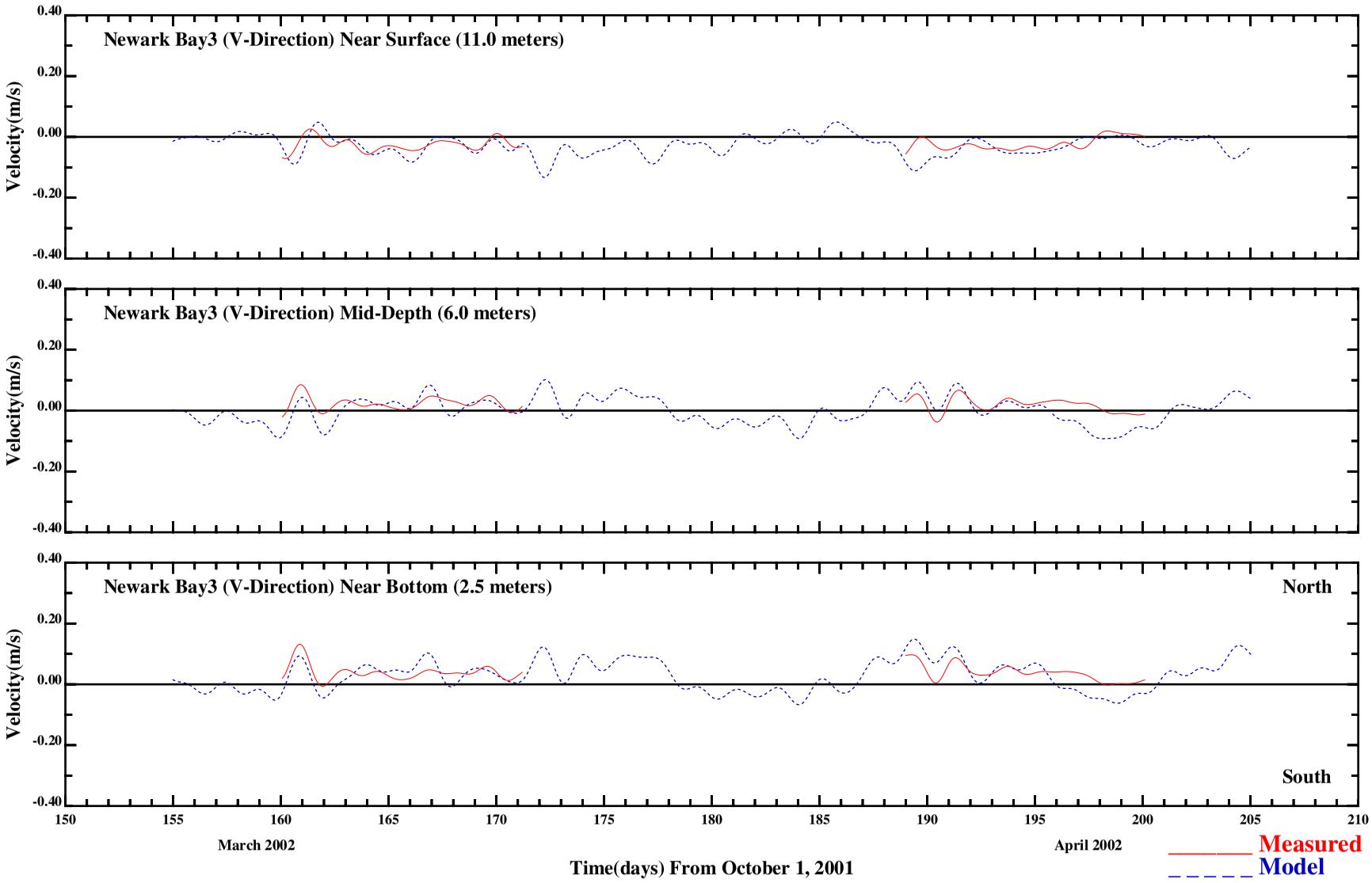

Figure 4-33b Comparison of 35 hour low-passed computed current velocities at three depths at NB3 with IMCS mooring data: March -April, 2002

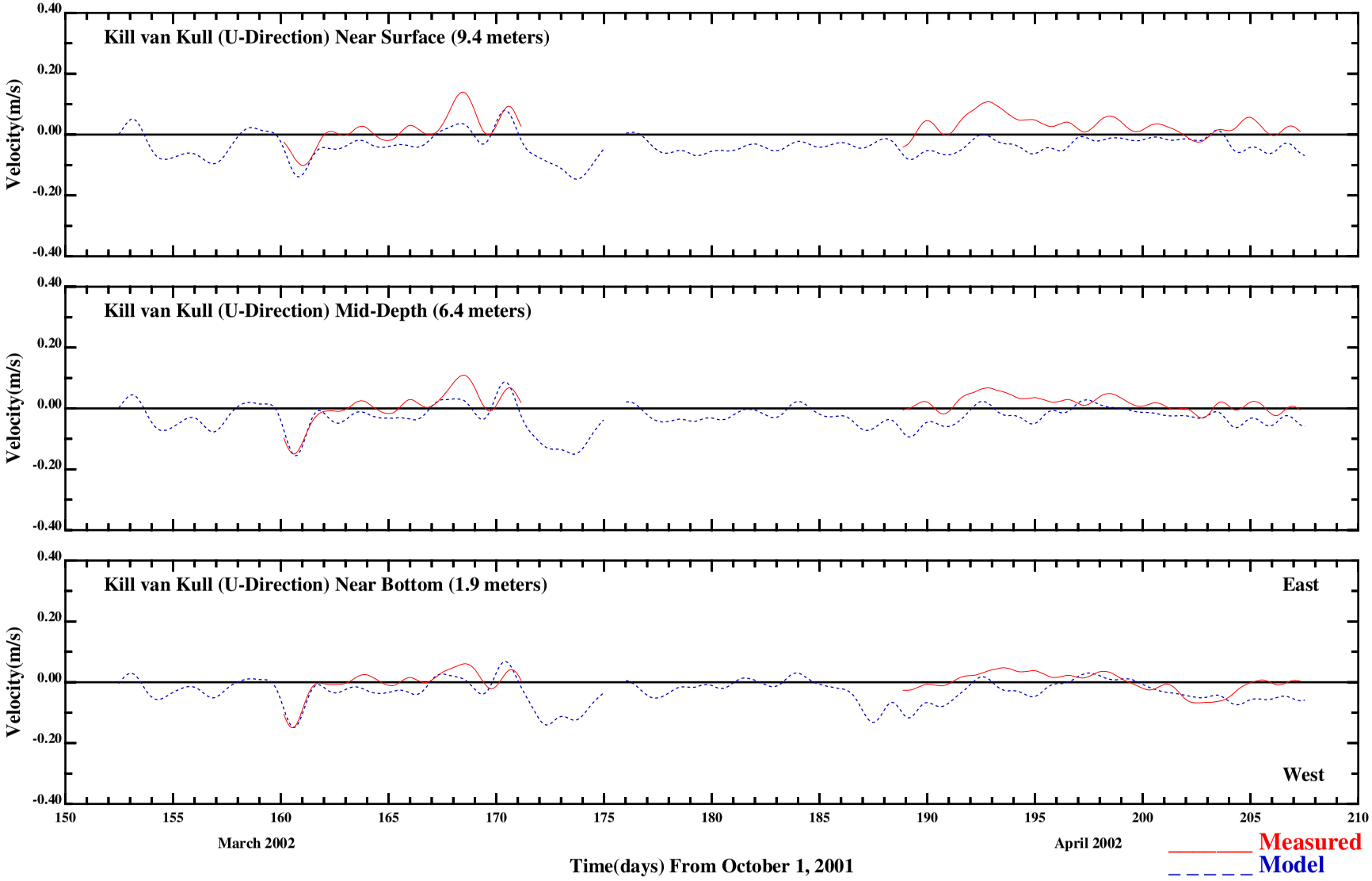

Figure 4-33c Comparison of 35 hour low-passed computed current velocities at three depths at KVK with IMCS mooring data: March -April, 2002

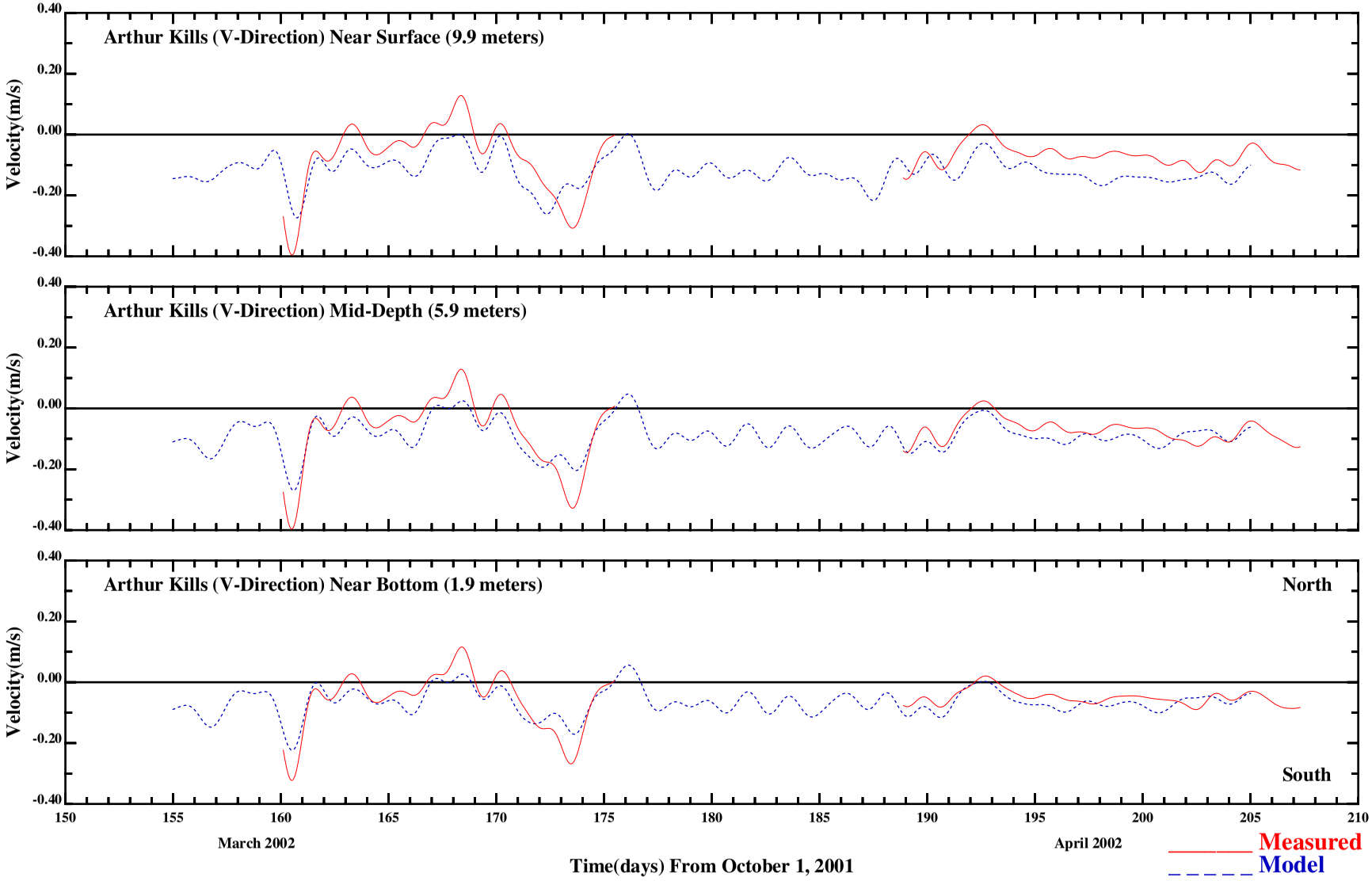

Figure 4-33d Comparison of 35 hour low-passed computed current velocities at three depths at AK with IMCS mooring data: March -April, 2002

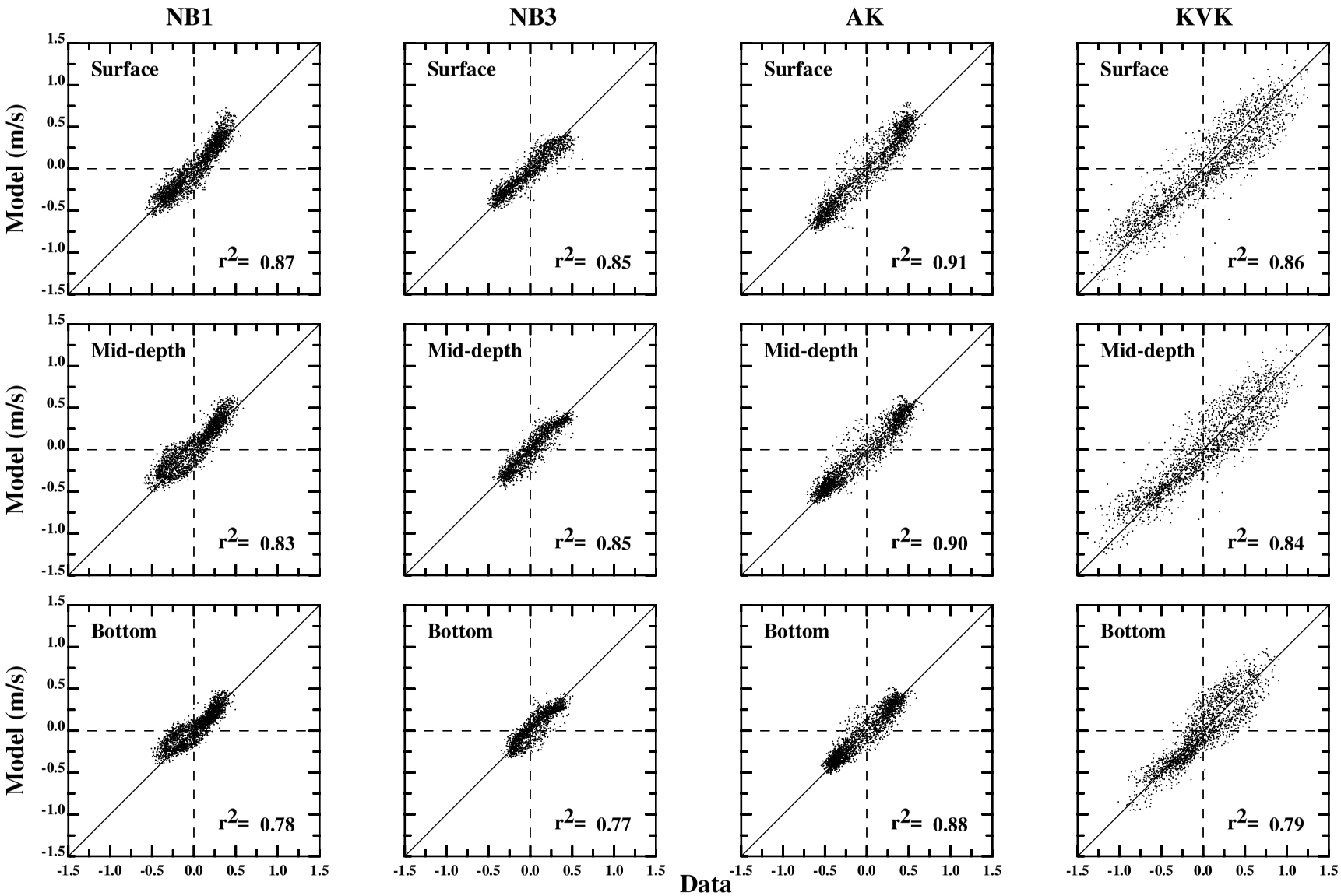

Figure 4-34 Scatter plot of computed current velocities with observed IMCS mooring data: March-April, 2002

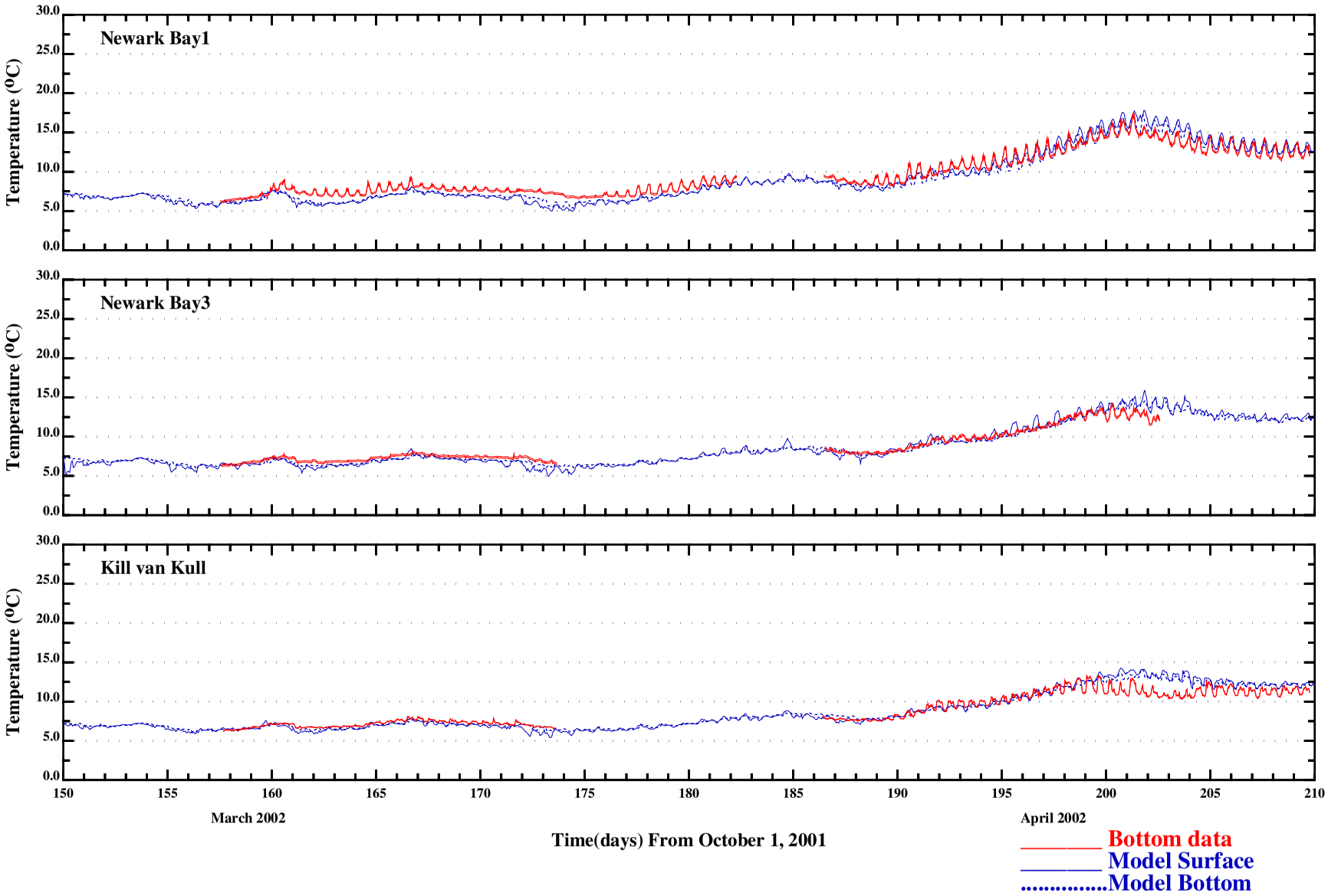

Figure 4-35 Comparison of hourly computed temperature with IMCS mooring data: March-April, 2002

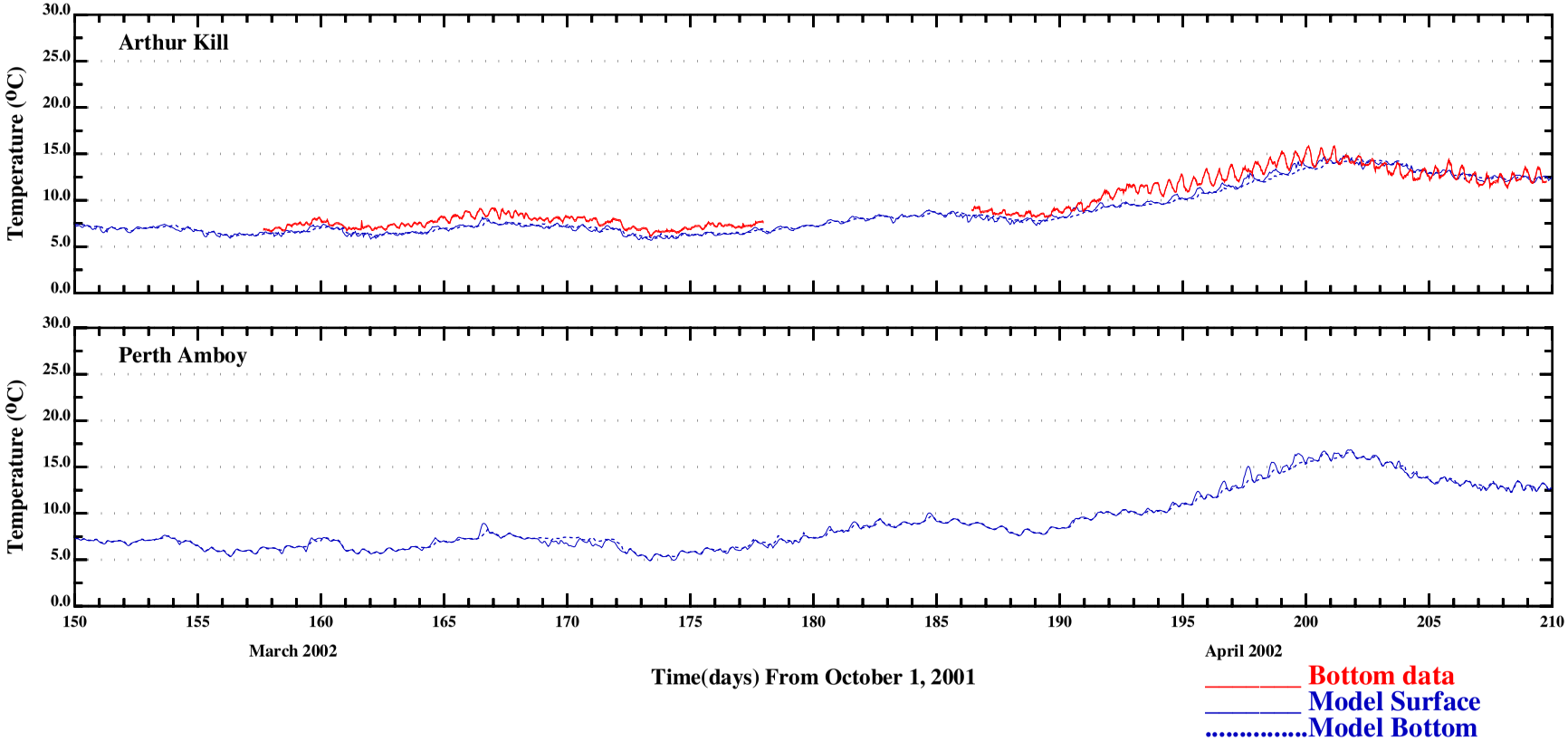

Figure 4-35 Comparison of hourly computed temperature with IMCS mooring data: March-April, 2002 (continued)

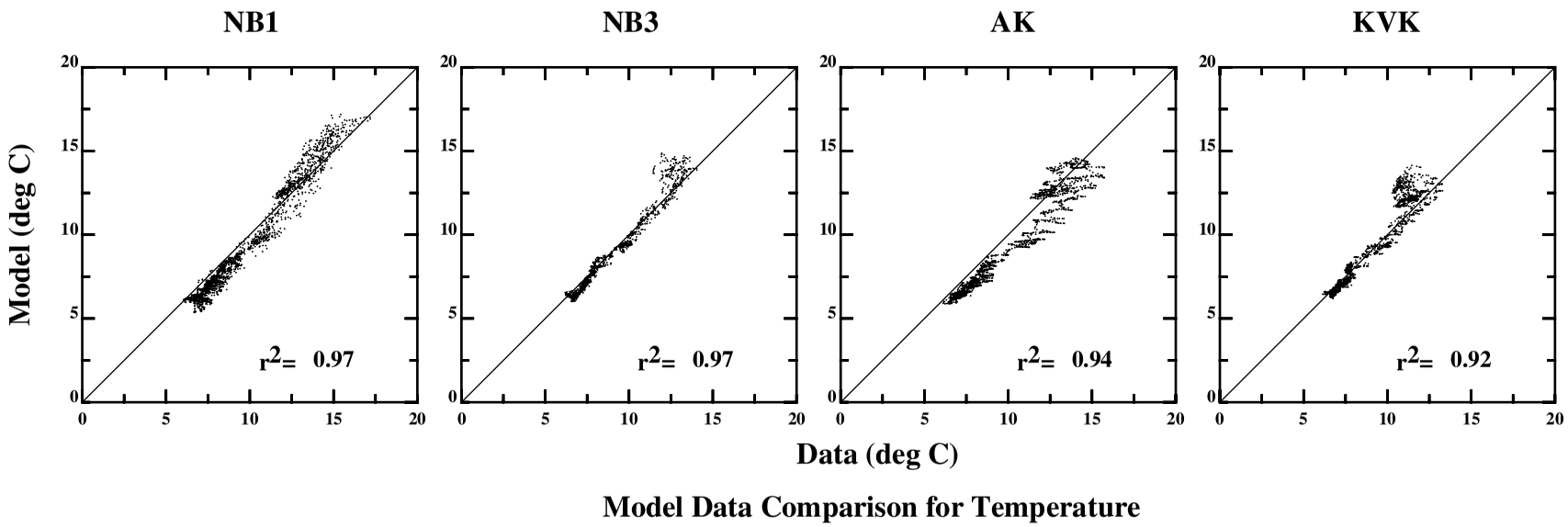

Figure 4-36 Scatter plot of computed temperature with observed IMCS mooring data: March-April, 2002

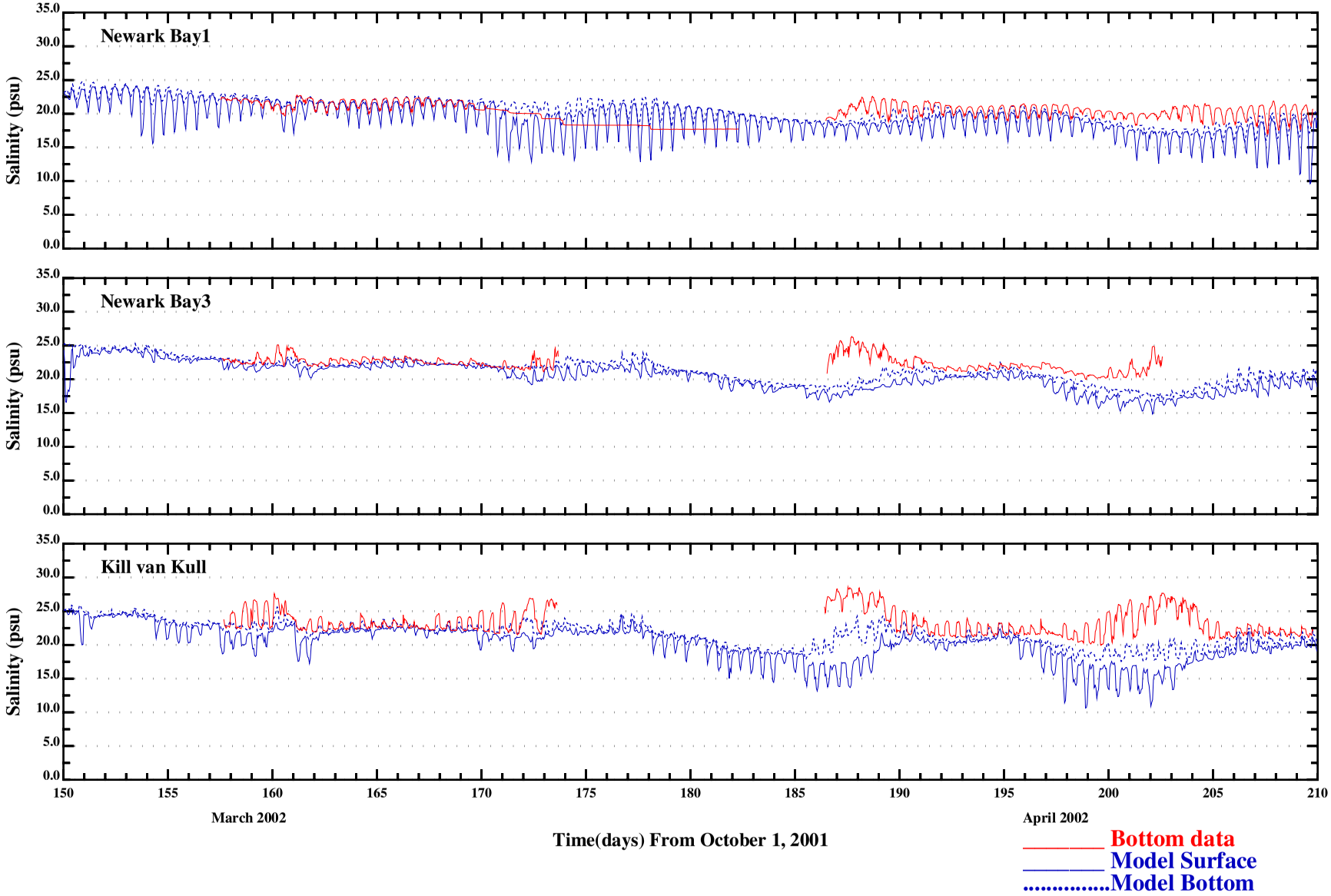

Figure 4-37 Comparison of hourly computed salinity with IMCS mooring data: March-April, 2002

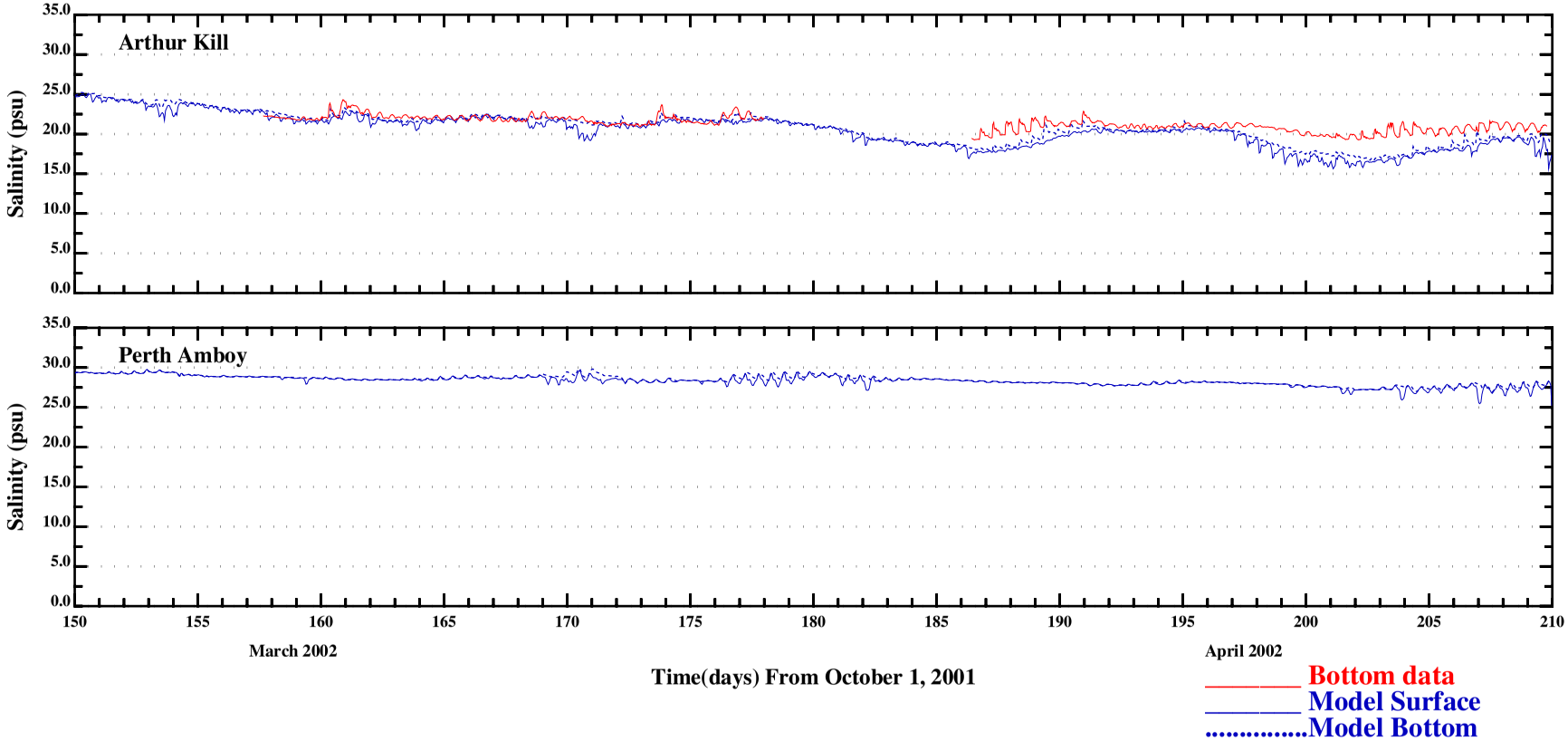

Figure 4-37 Comparison of hourly computed salinity with IMCS mooring data: March-April, 2002 (continued)

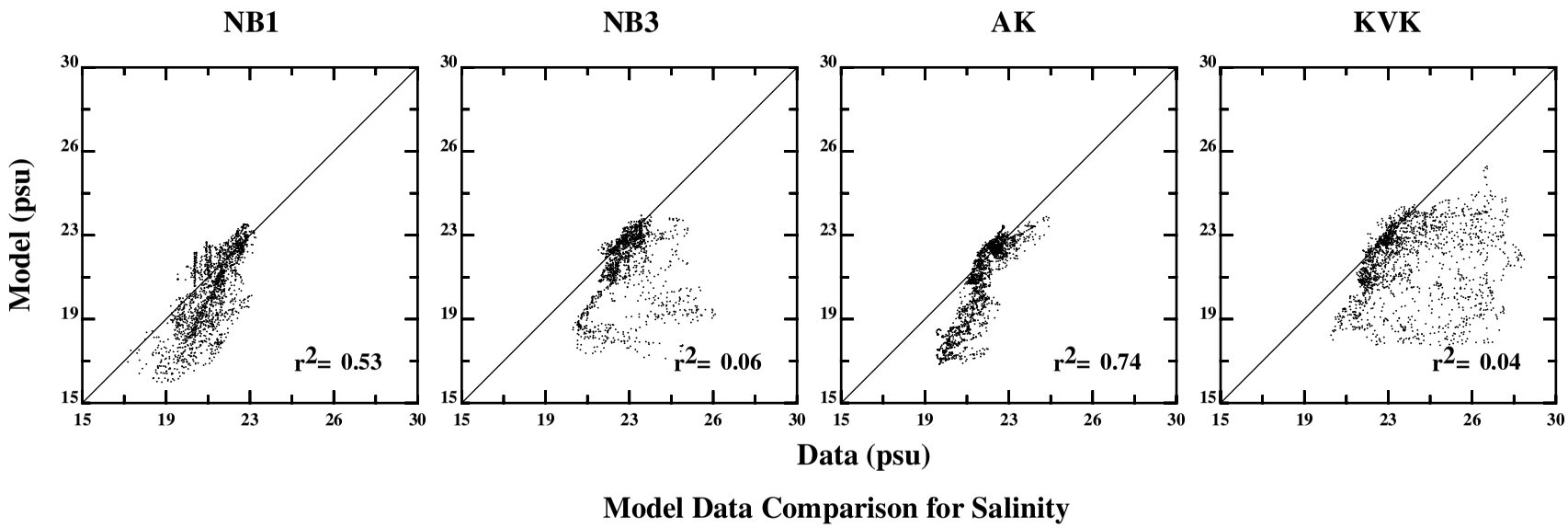

Figure 4-38 Scatter plot of computed salinity with observed IMCS mooring data: March-April, 2002

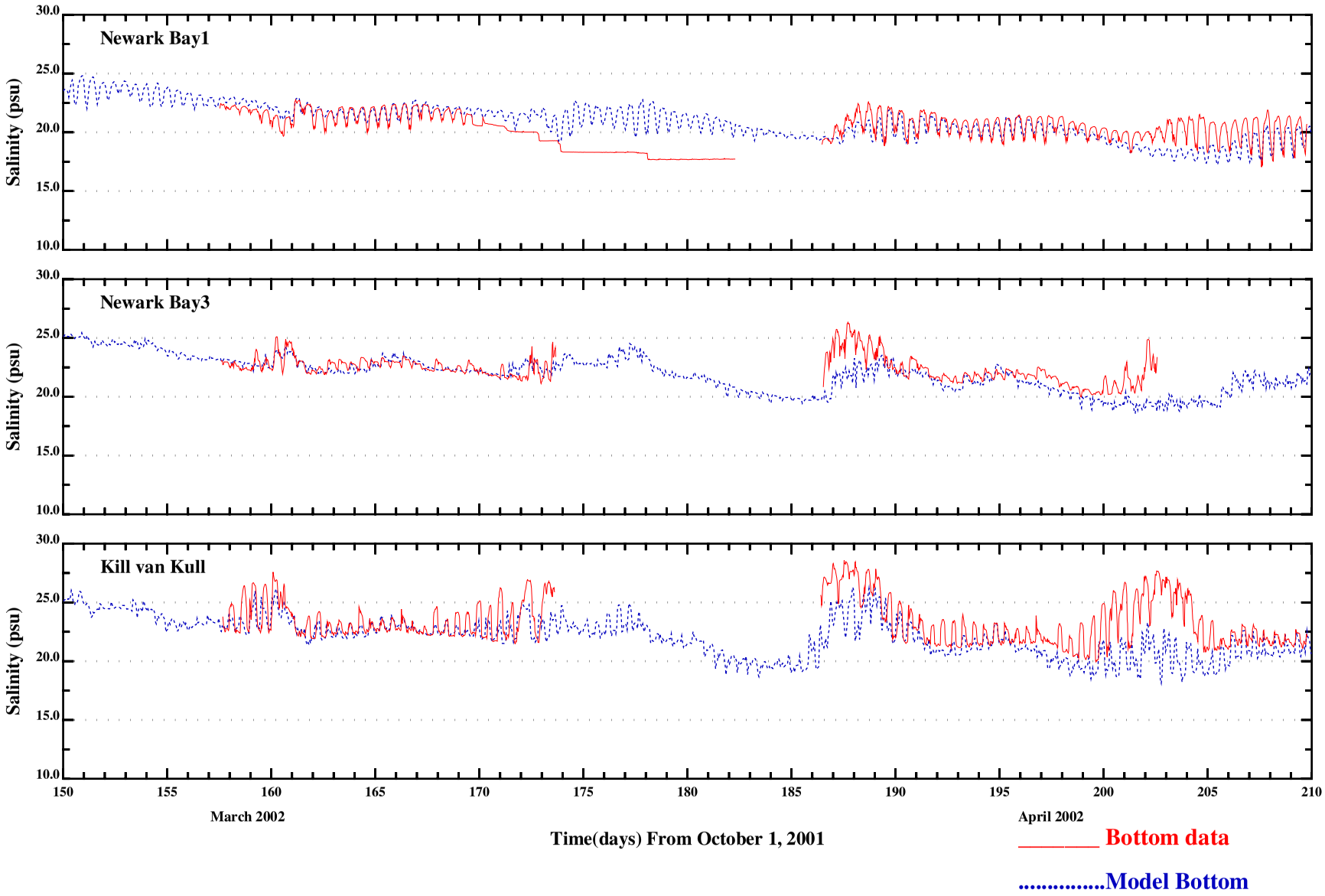

Figure 4-39 Comparison of observed bottom salinity with the results of sensitivity RUN A

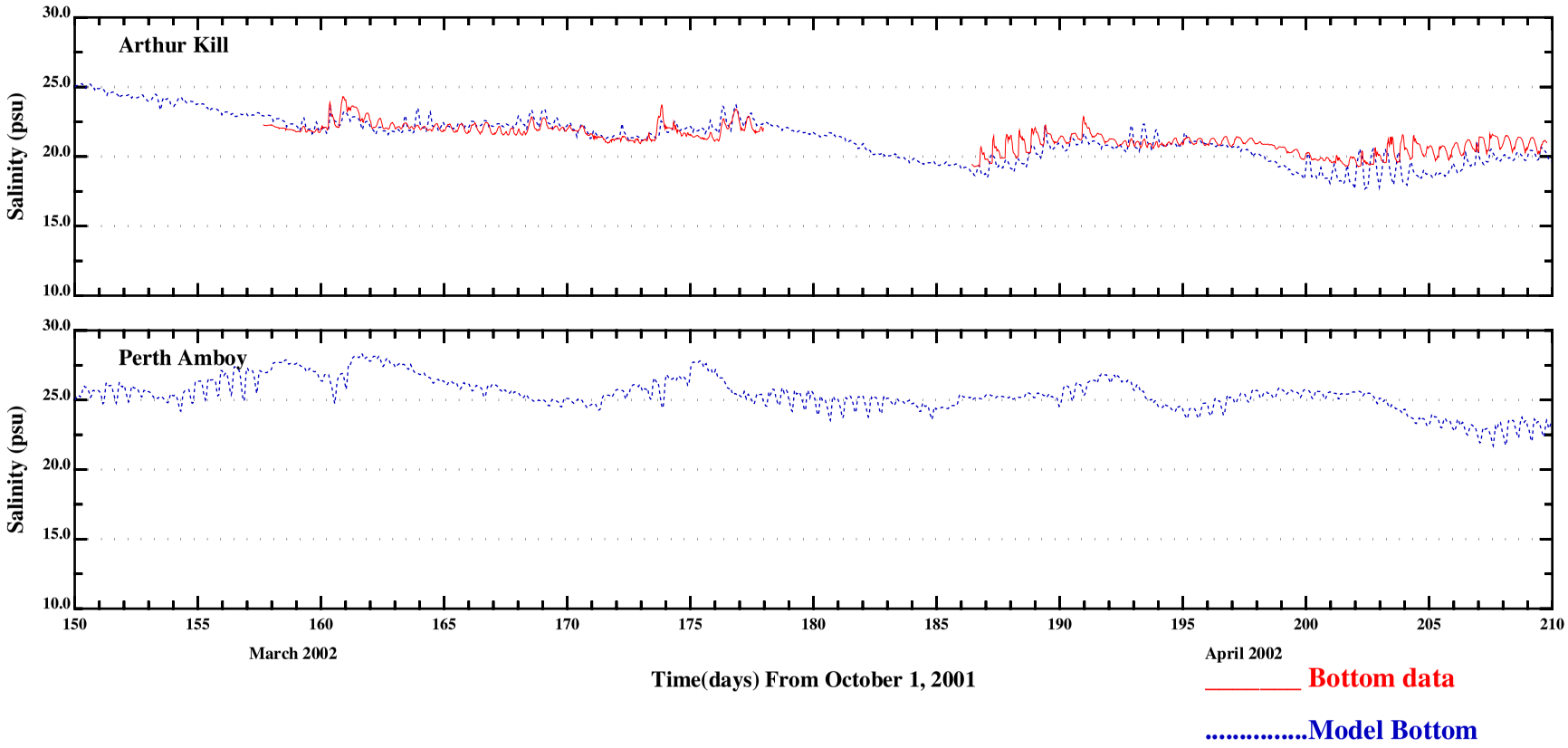

Figure 4-39 Comparison of observed bottom salinity with the results of sensitivity RUN A (continued)

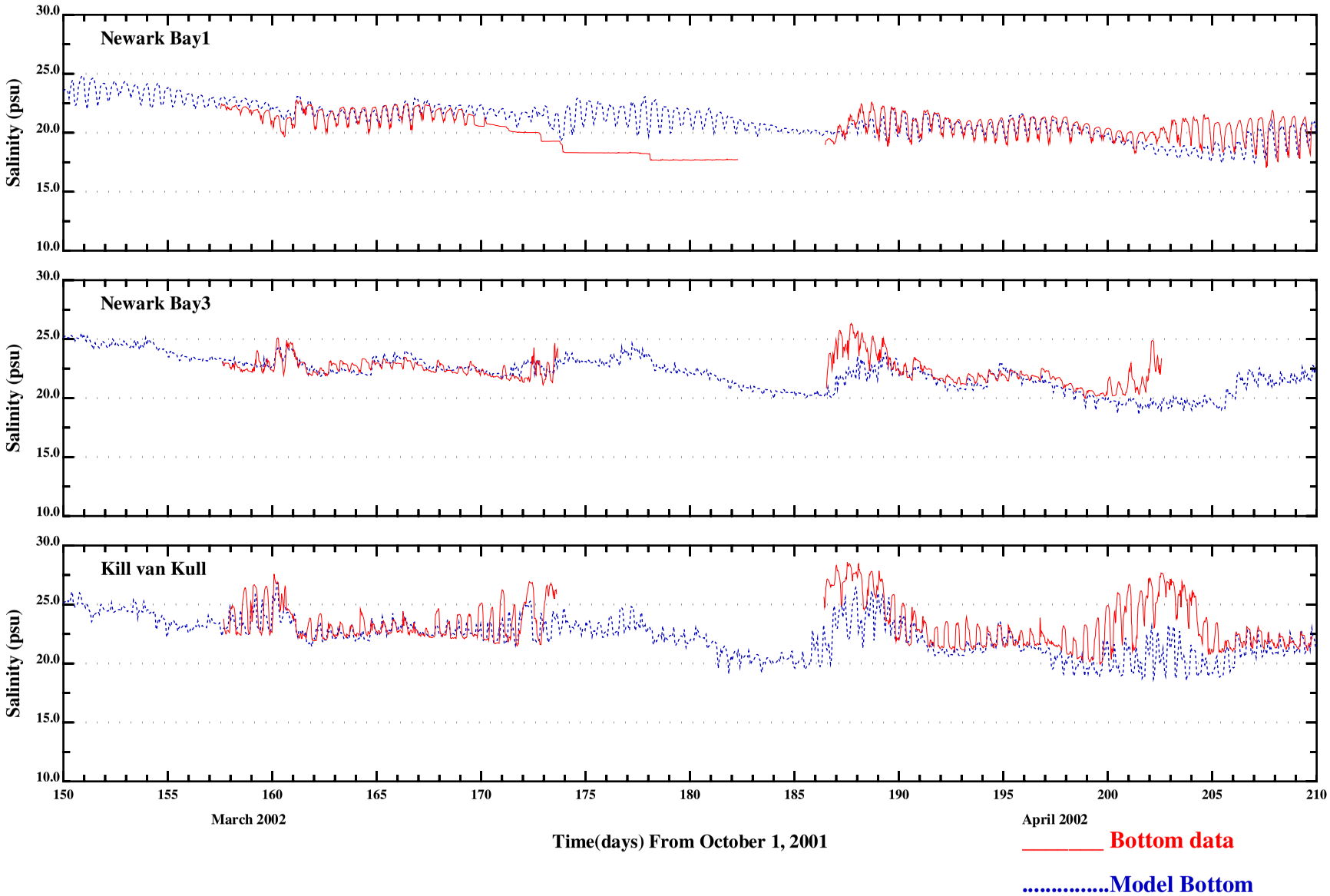

Figure 4-40 Comparison of observed bottom salinity with the results of sensitivity RUN B

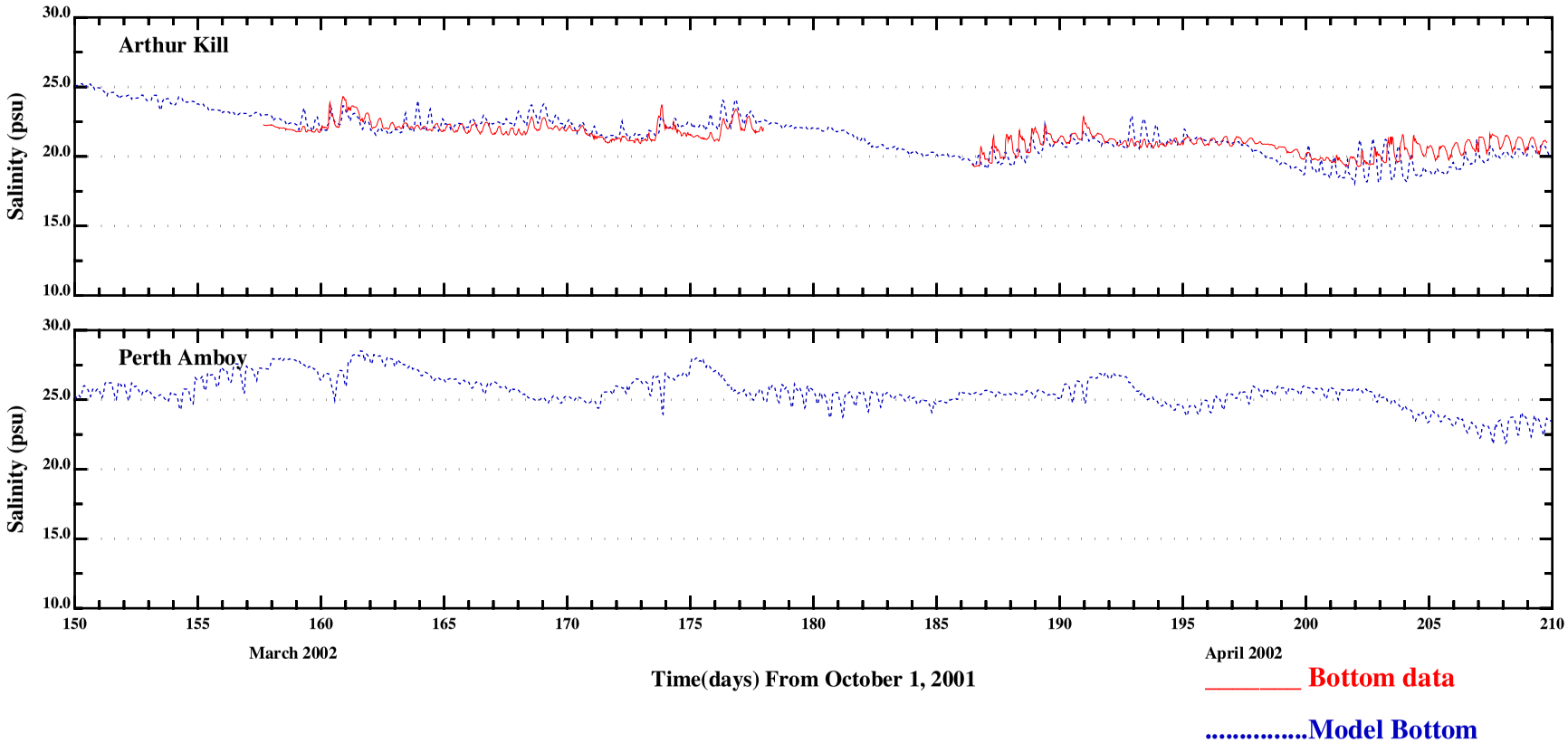

Figure 4-40 Comparison of observed bottom salinity with the results of sensitivity RUN B (continued)

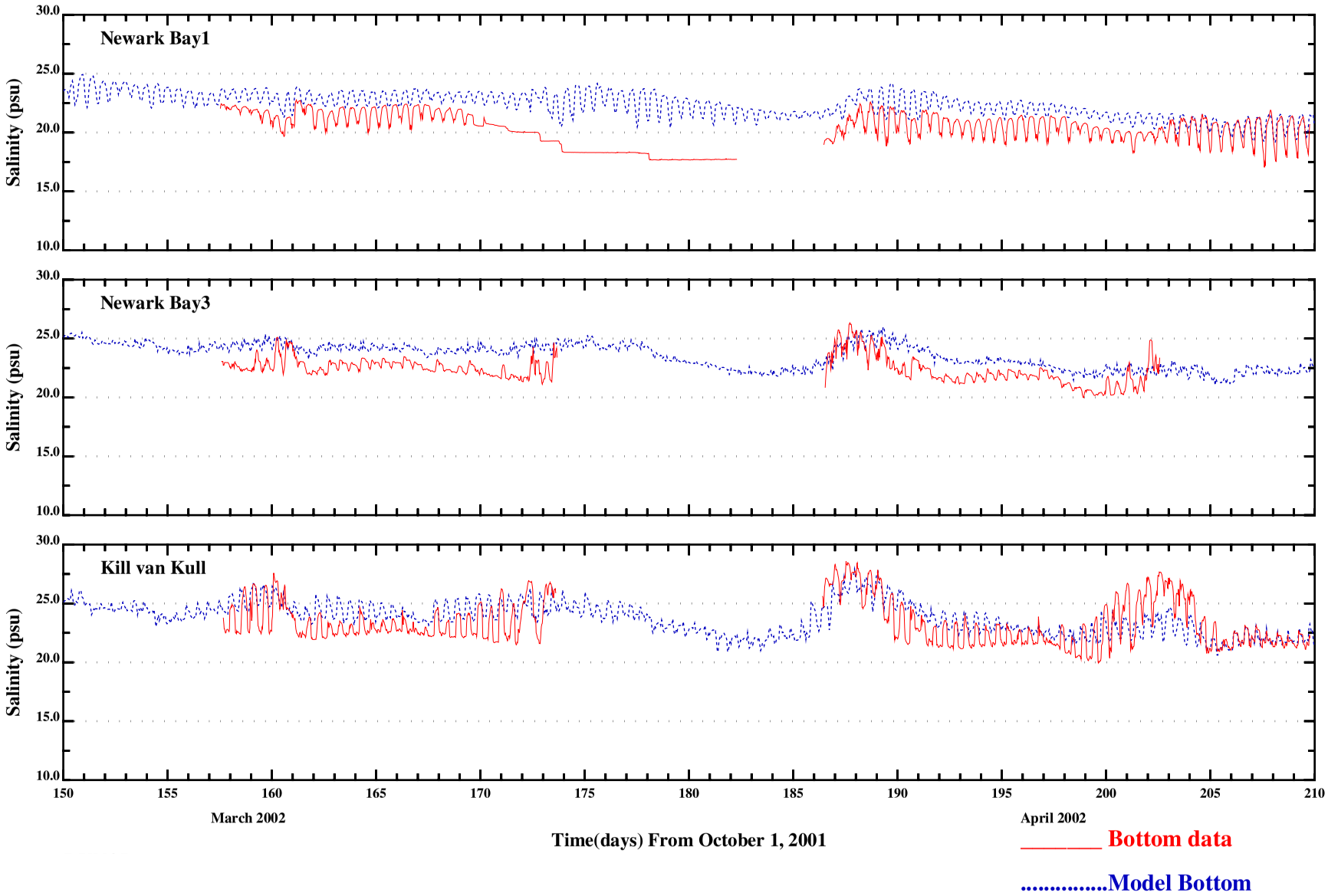

Figure 4-41 Comparison of observed bottom salinity with the results of sensitivity RUN C

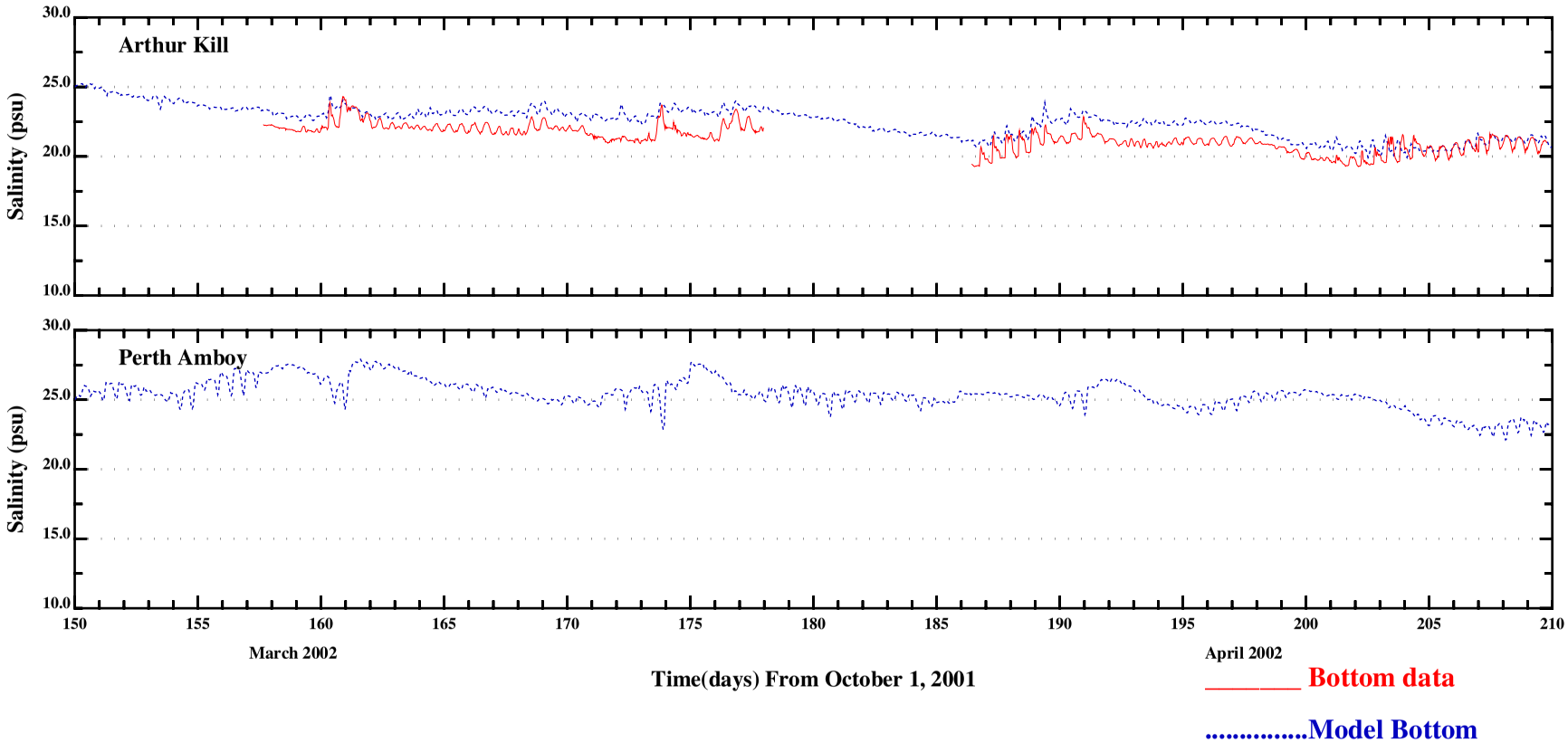

Figure 4-41 Comparison of observed bottom salinity with the results of sensitivity RUN C (continued)

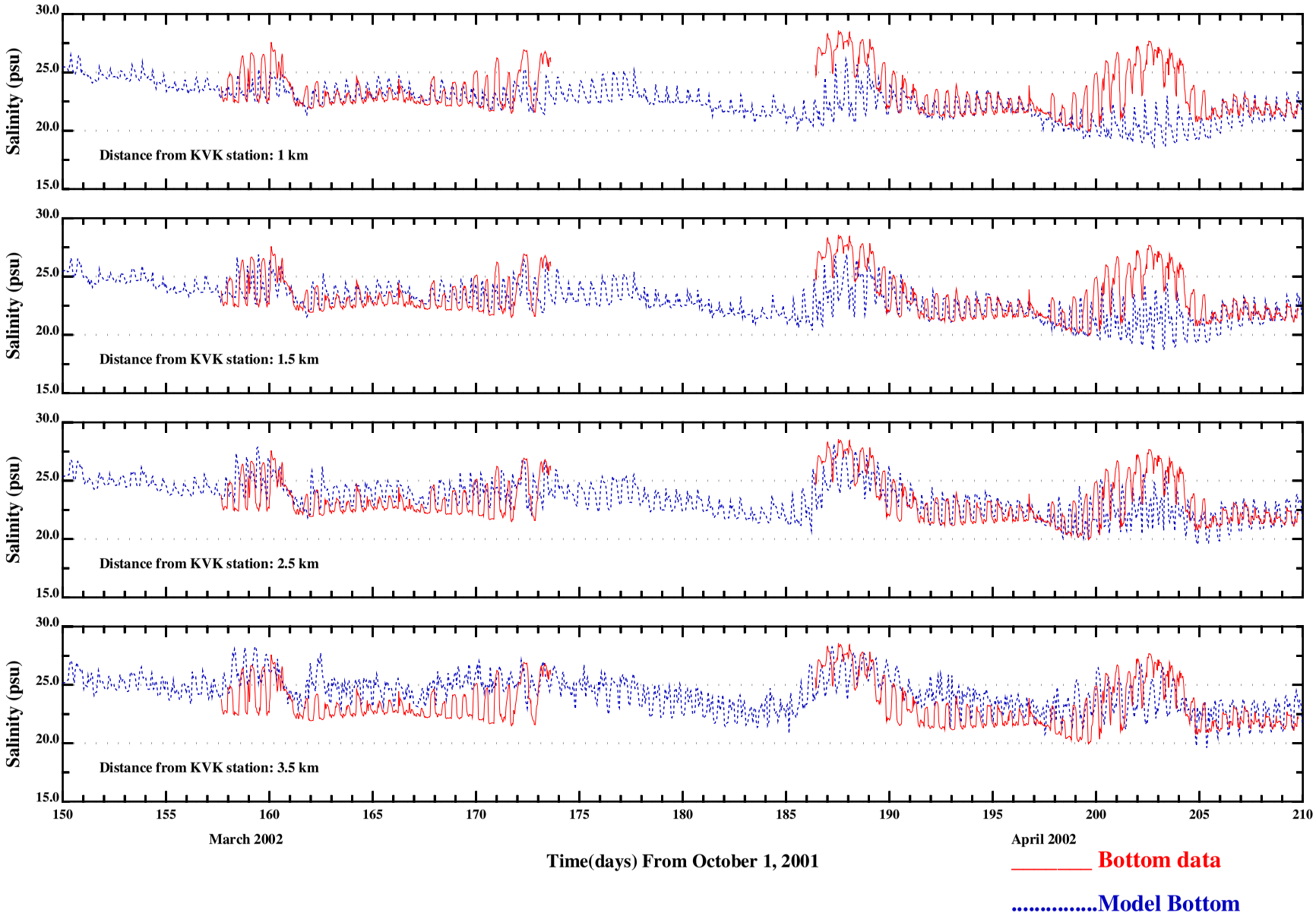

Figure 4-42 Comparison of hourly computed salinity with IMCS mooring data at four stations located 1, 1.5, 2.5 and 3.5 km from the KVK data station

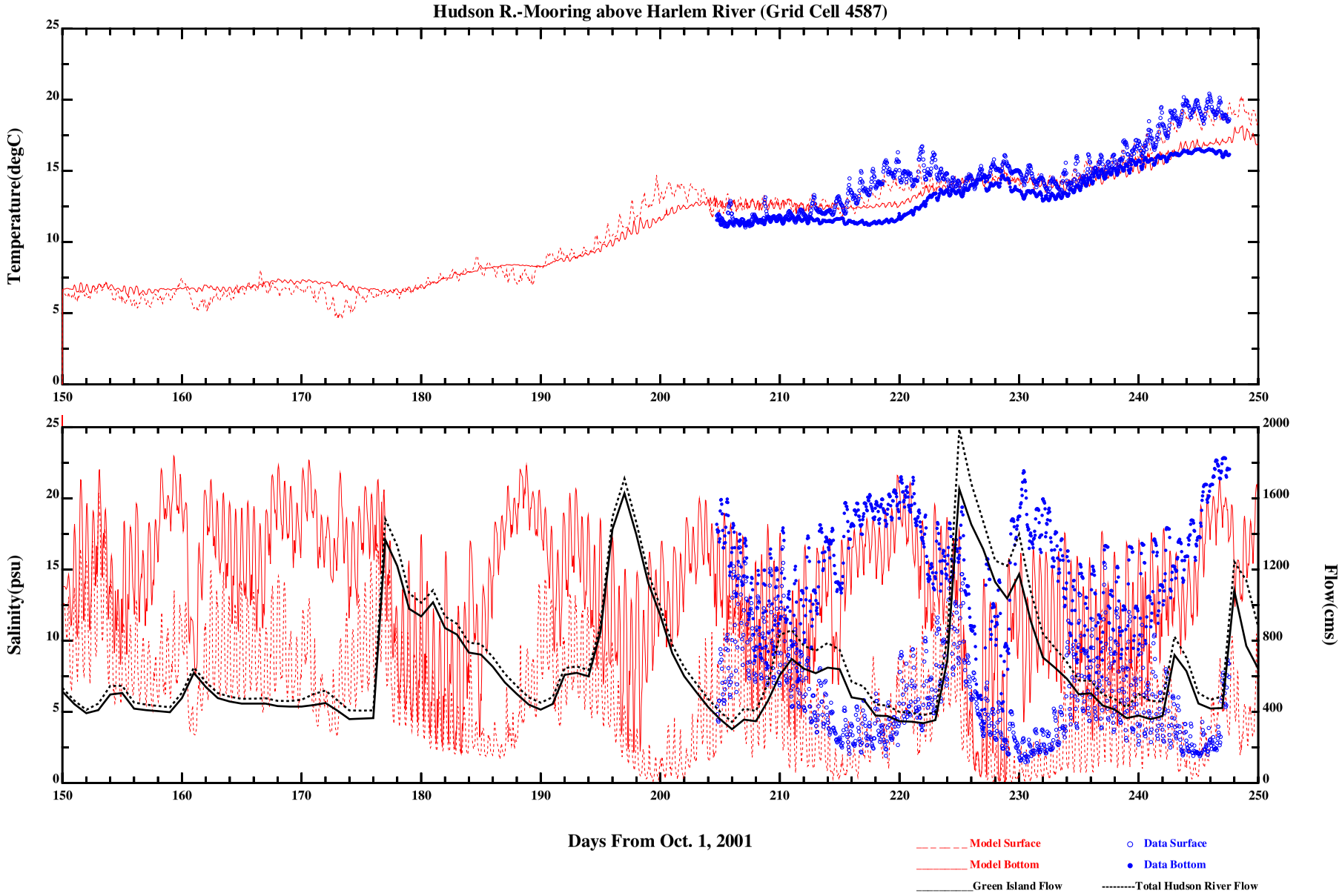

Figure 4-43 Comparison of hourly computed salinity with data at the Hudson River Mooring Station

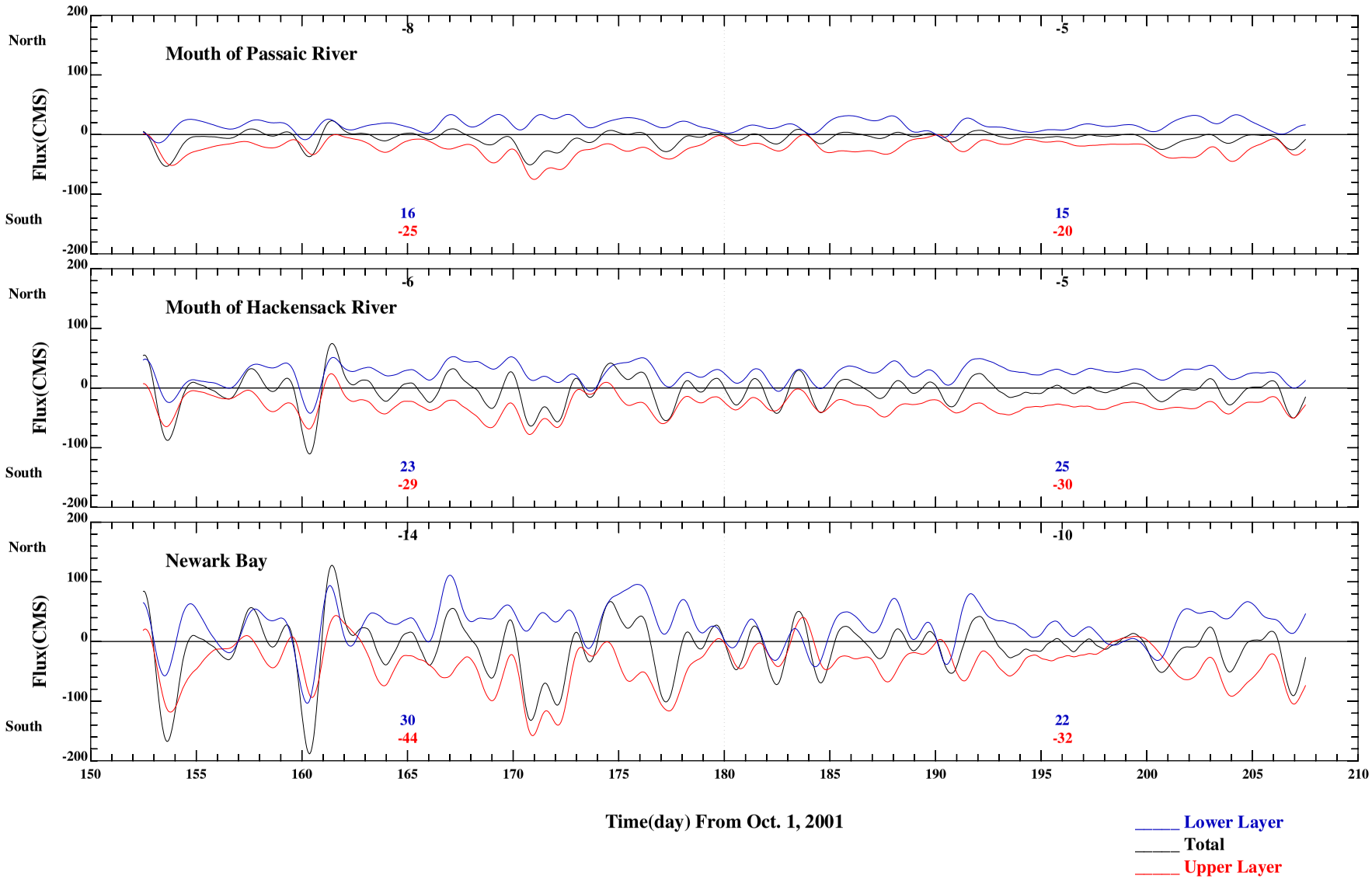

Figure 4-44a Temporal variations of 35 hour low-passed and monthly fluxes through Passaic and Hackensack Rivers, and Newark Bay.

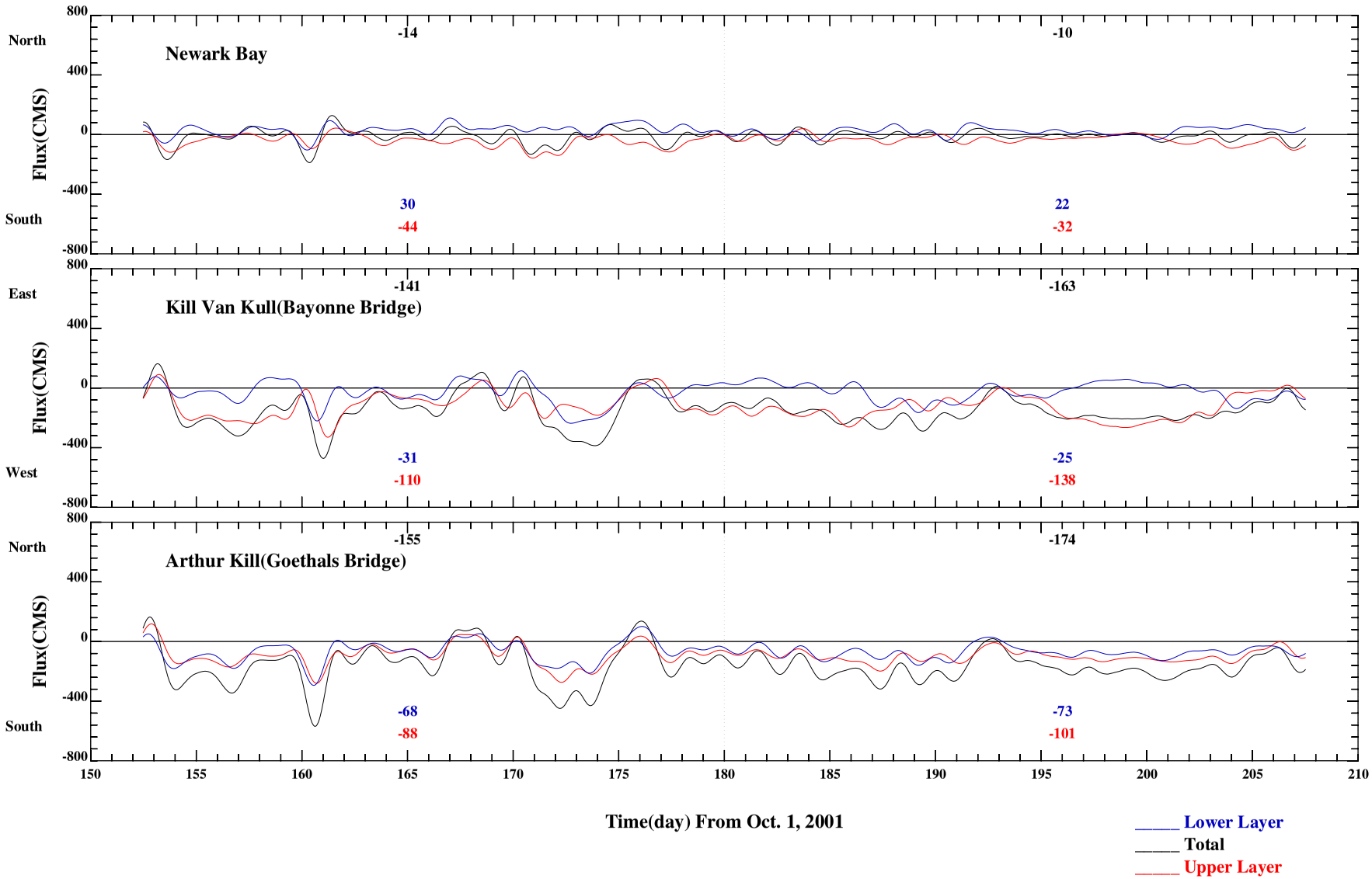

Figure 4-44b Temporal variations of 35 hour low-passed and monthly fluxes through Newark Bay, the Kill van Kull and the Arthur Kill

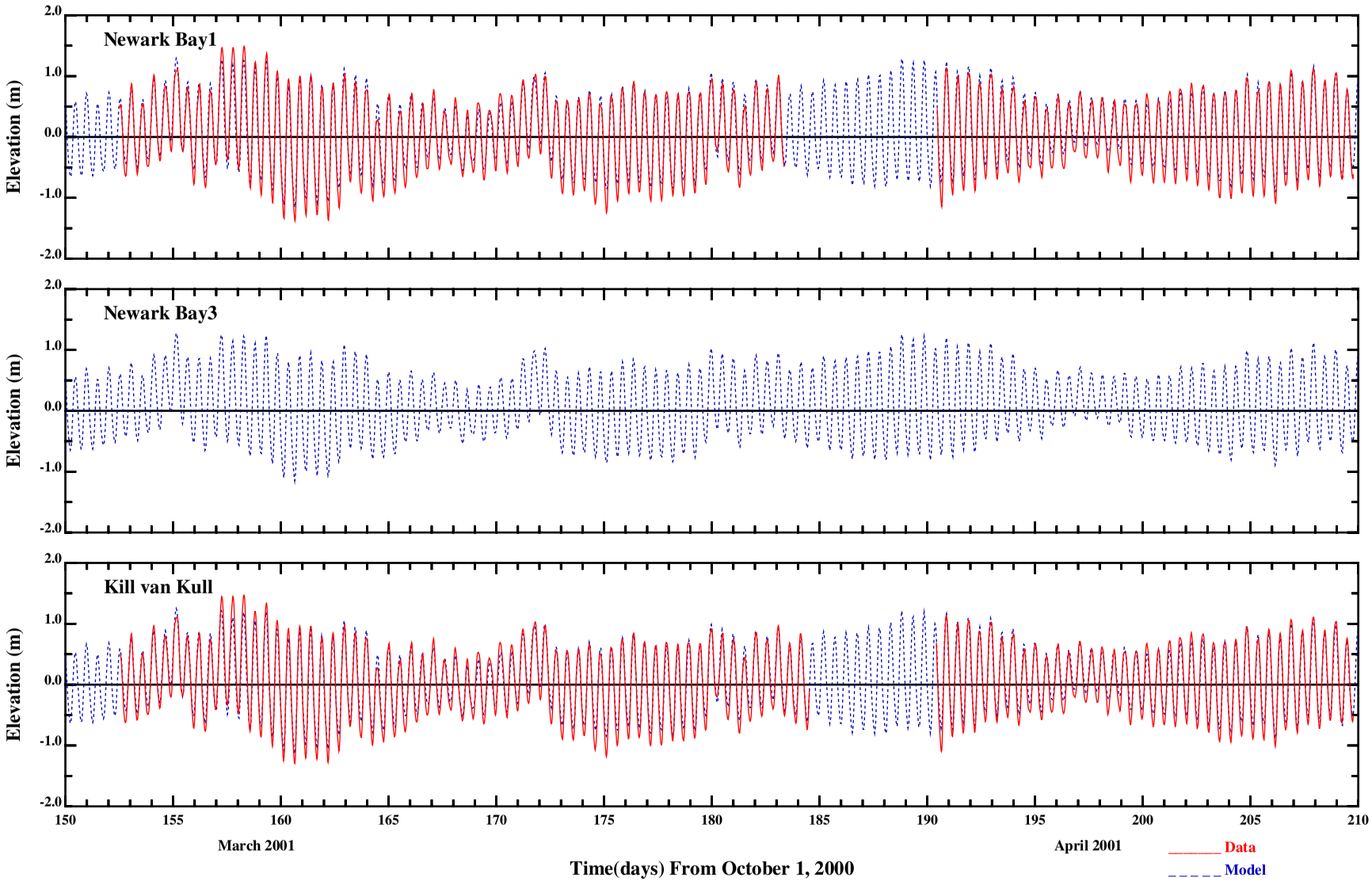

Figure 4-45 Comparison of hourly computed water elevations with IMCS mooring data: March-August, 2001

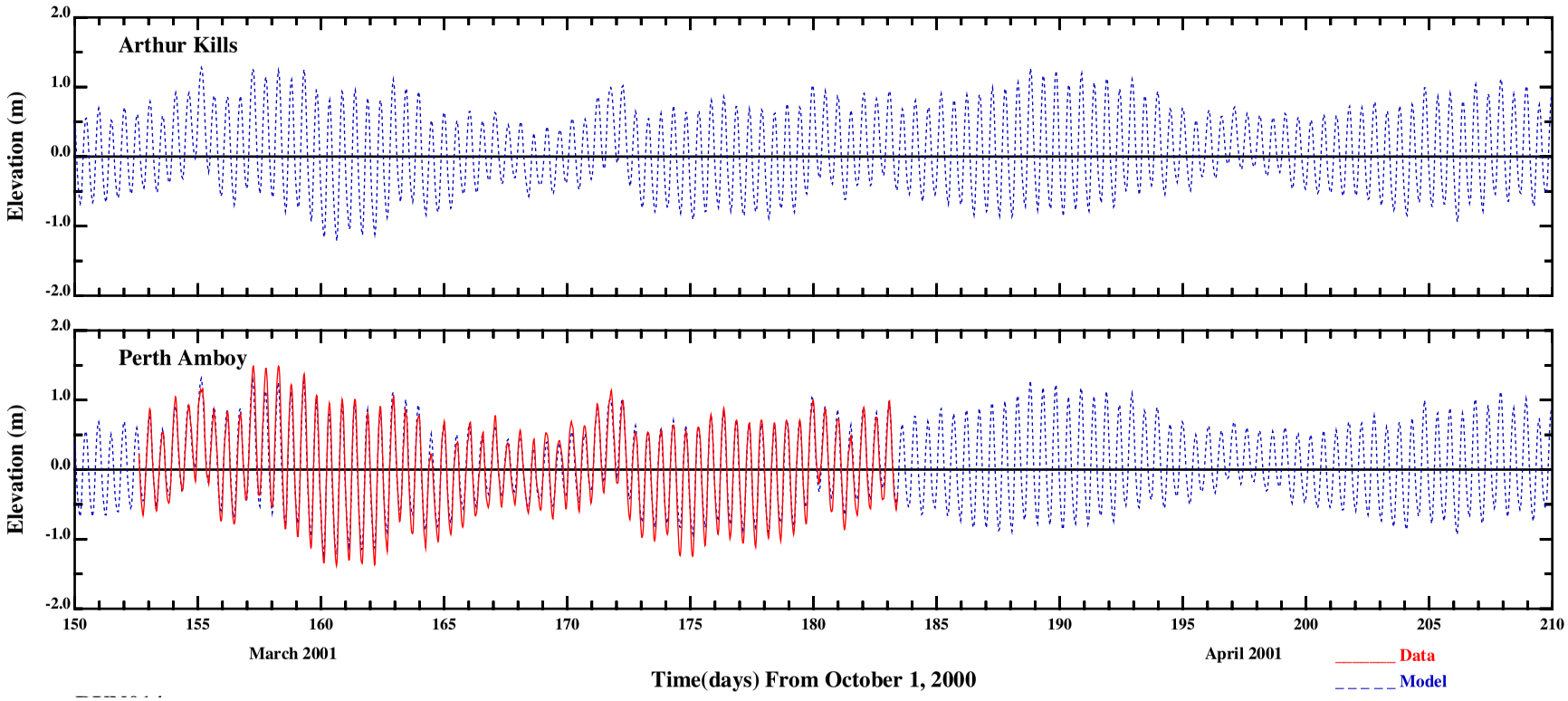

Figure 4-45 Comparison of hourly computed water elevations with IMCS mooring data: March-August, 2001 (continued)

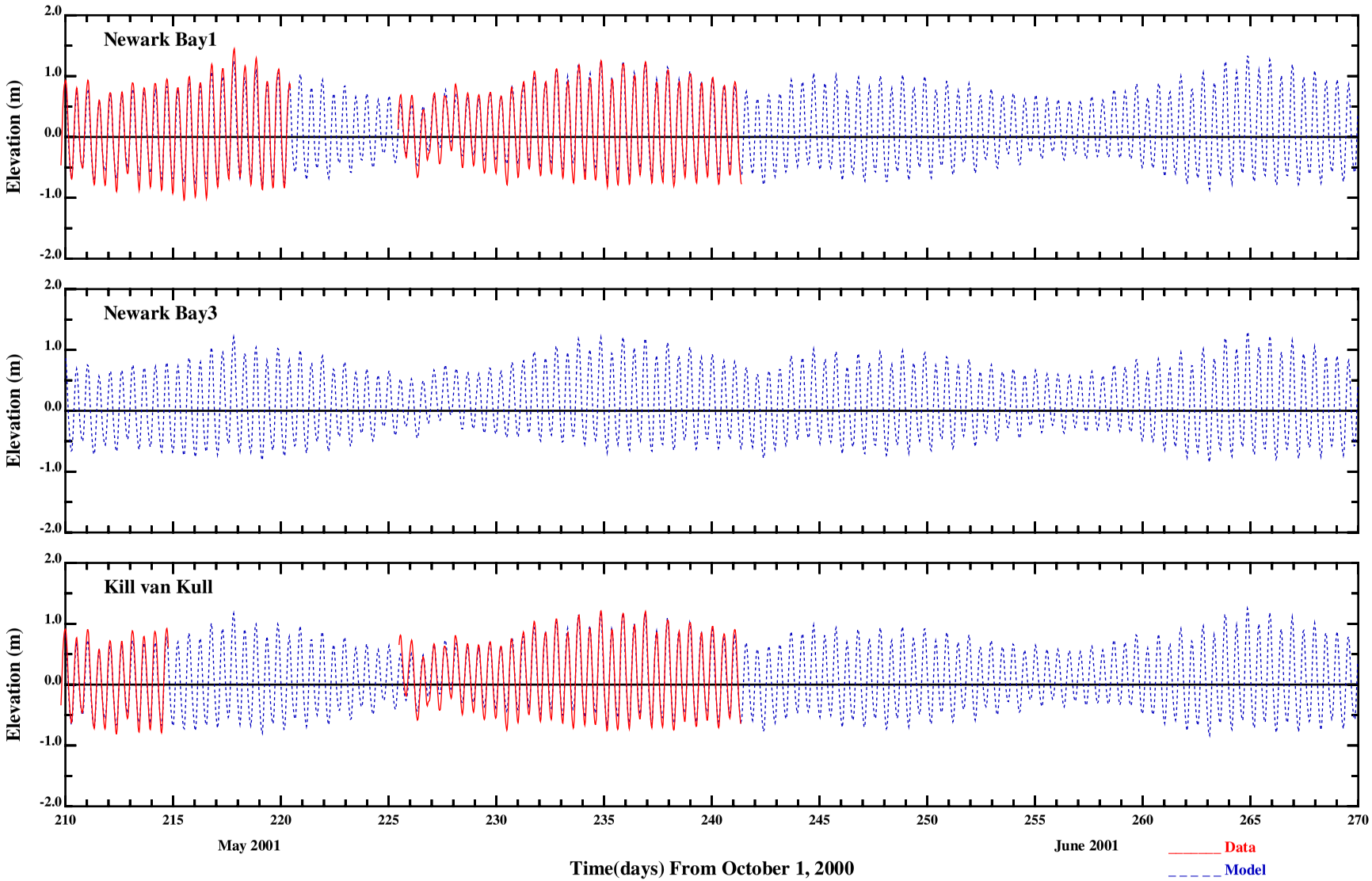

Figure 4-45 Comparison of hourly computed water elevations with IMCS mooring data: March-August, 2001 (continued)

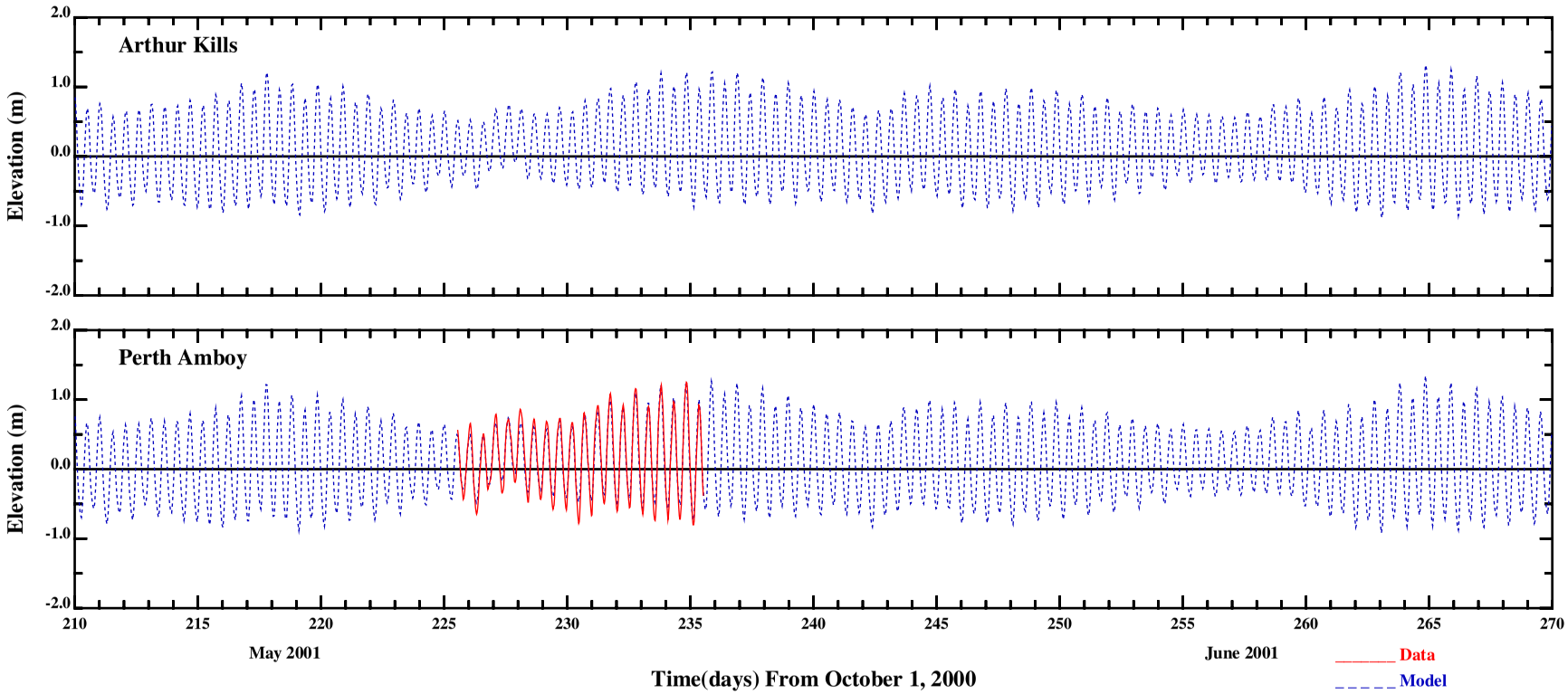

Figure 4-45 Comparison of hourly computed water elevations with IMCS mooring data: March-August, 2001 (continued)

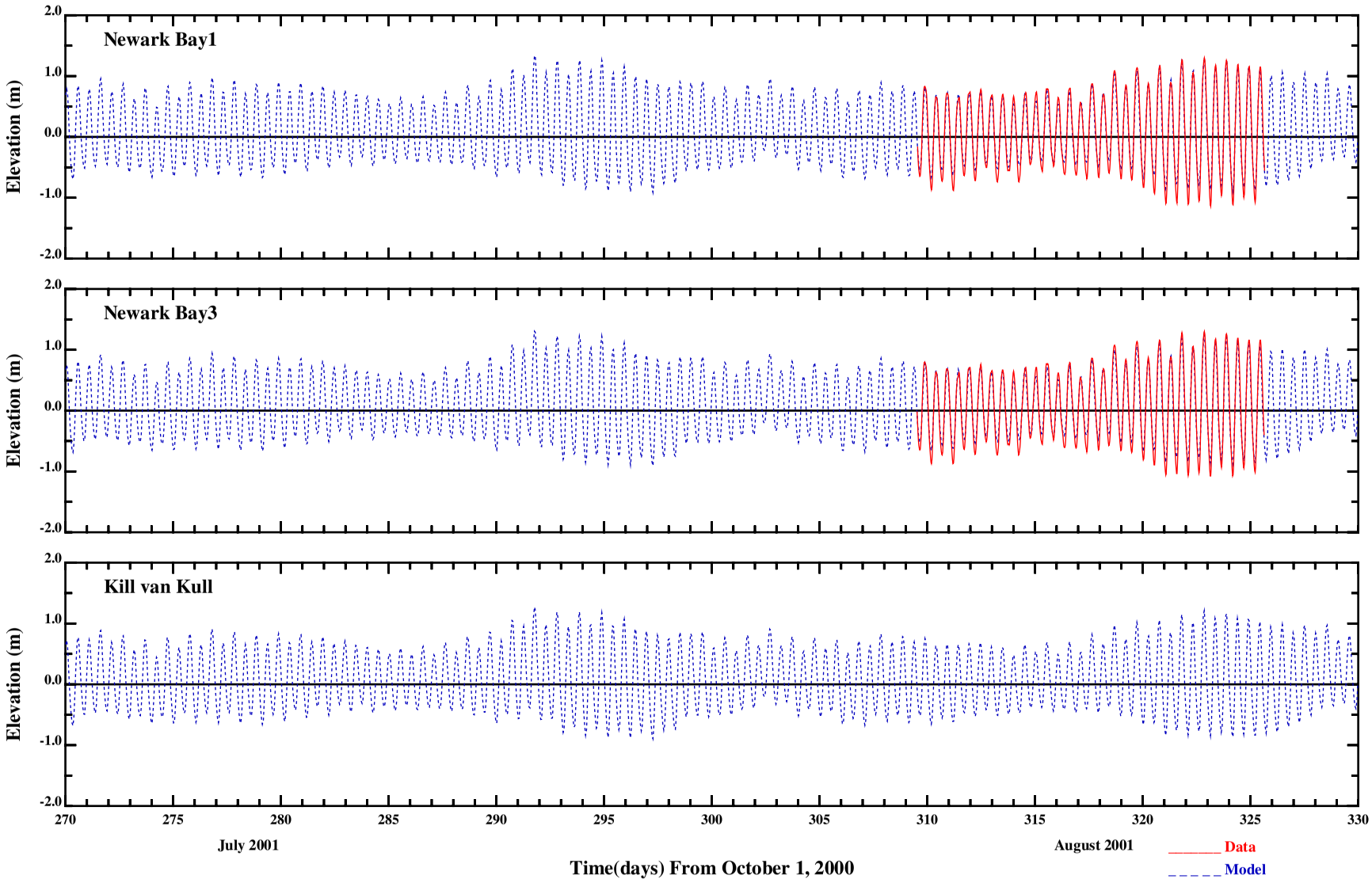

Figure 4-45 Comparison of hourly computed water elevations with IMCS mooring data: March-August, 2001 (continued)

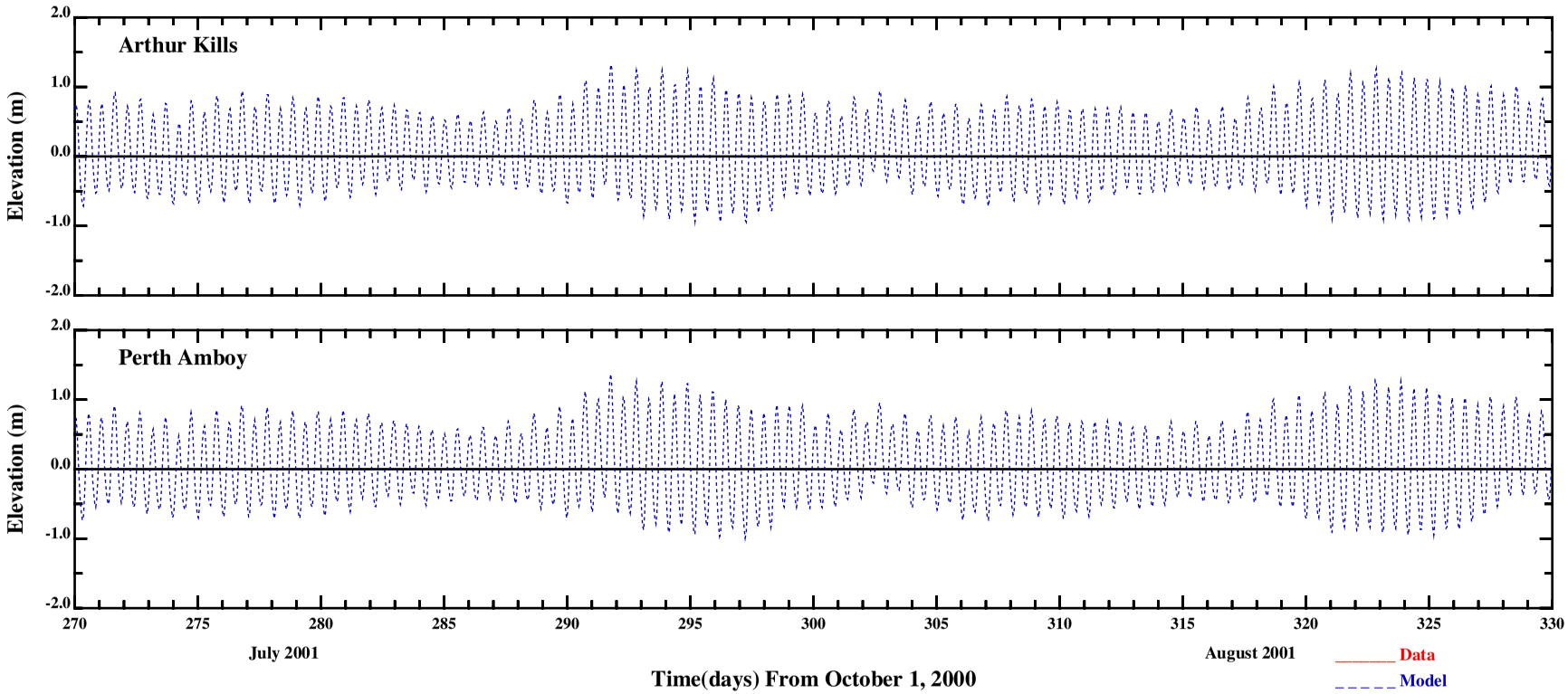

Figure 4-45 Comparison of hourly computed water elevations with IMCS mooring data: March-August, 2001 (continued)

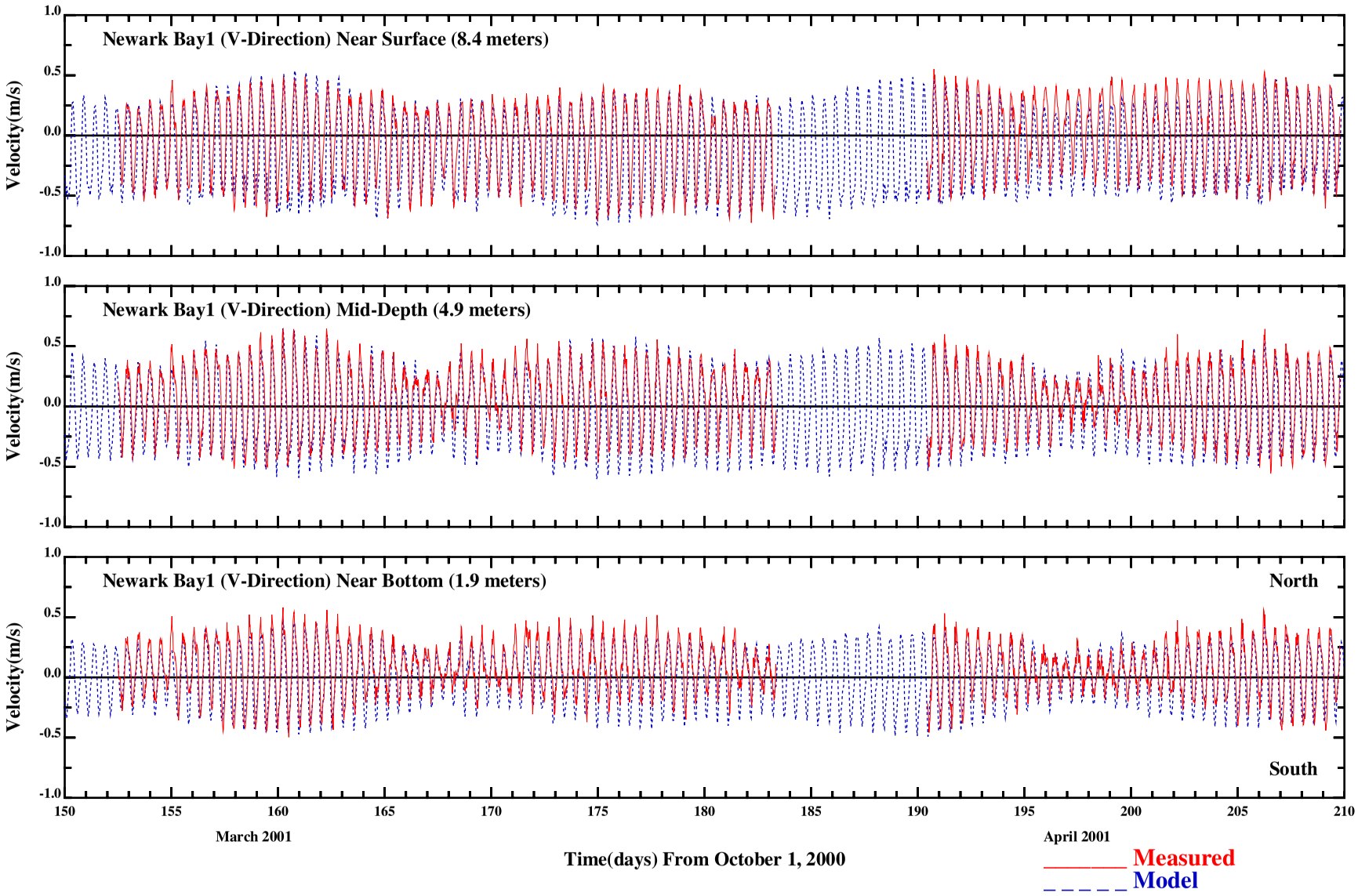

Figure 4-46a Comparison of hourly computed current velocities at three depths at NB1 with IMCS mooring data: March - August, 2001

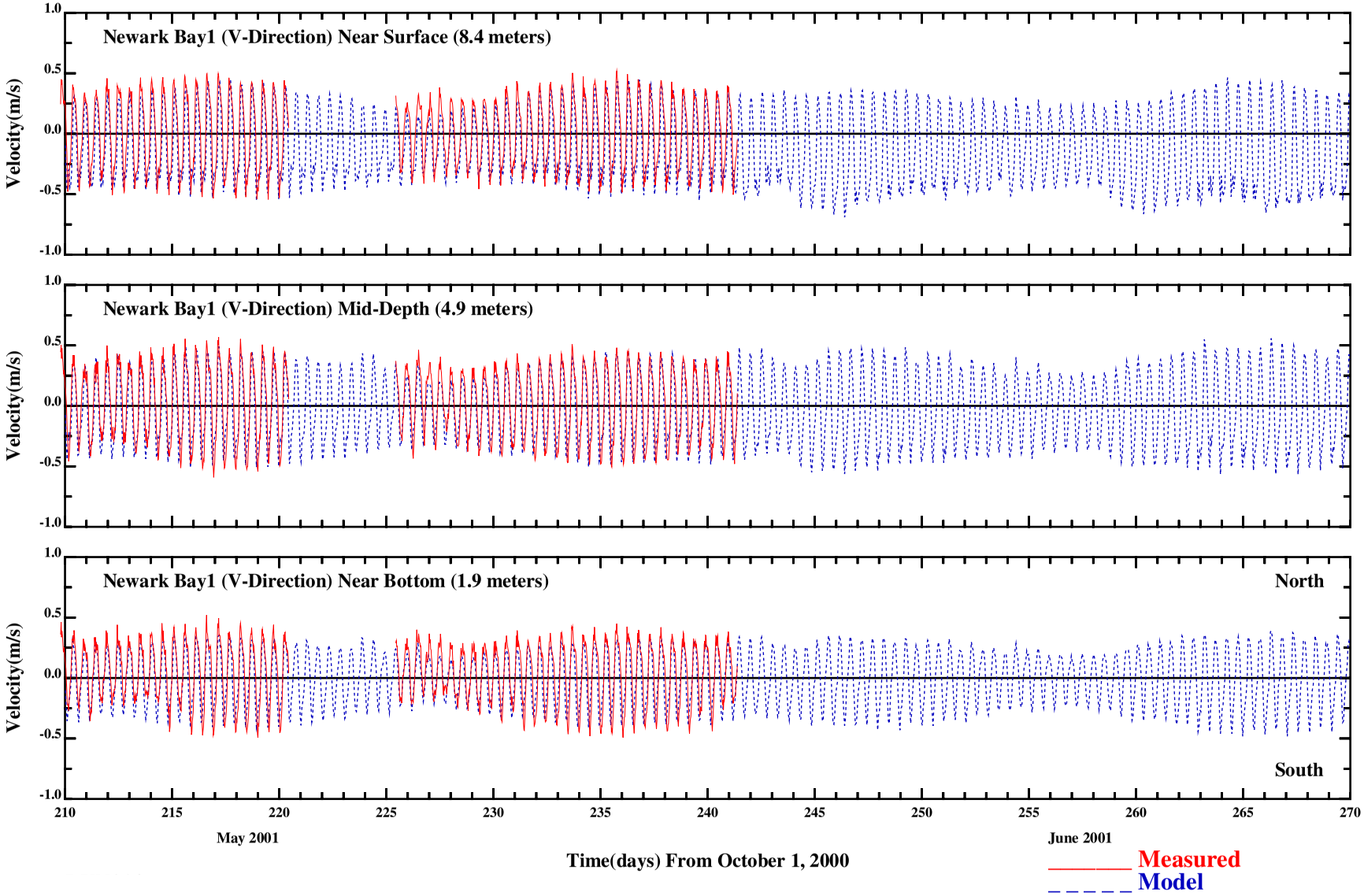

Figure 4-46a Comparison of hourly computed current velocities at three depths at NB1 with IMCS mooring data: March - August, 2001 (continued)

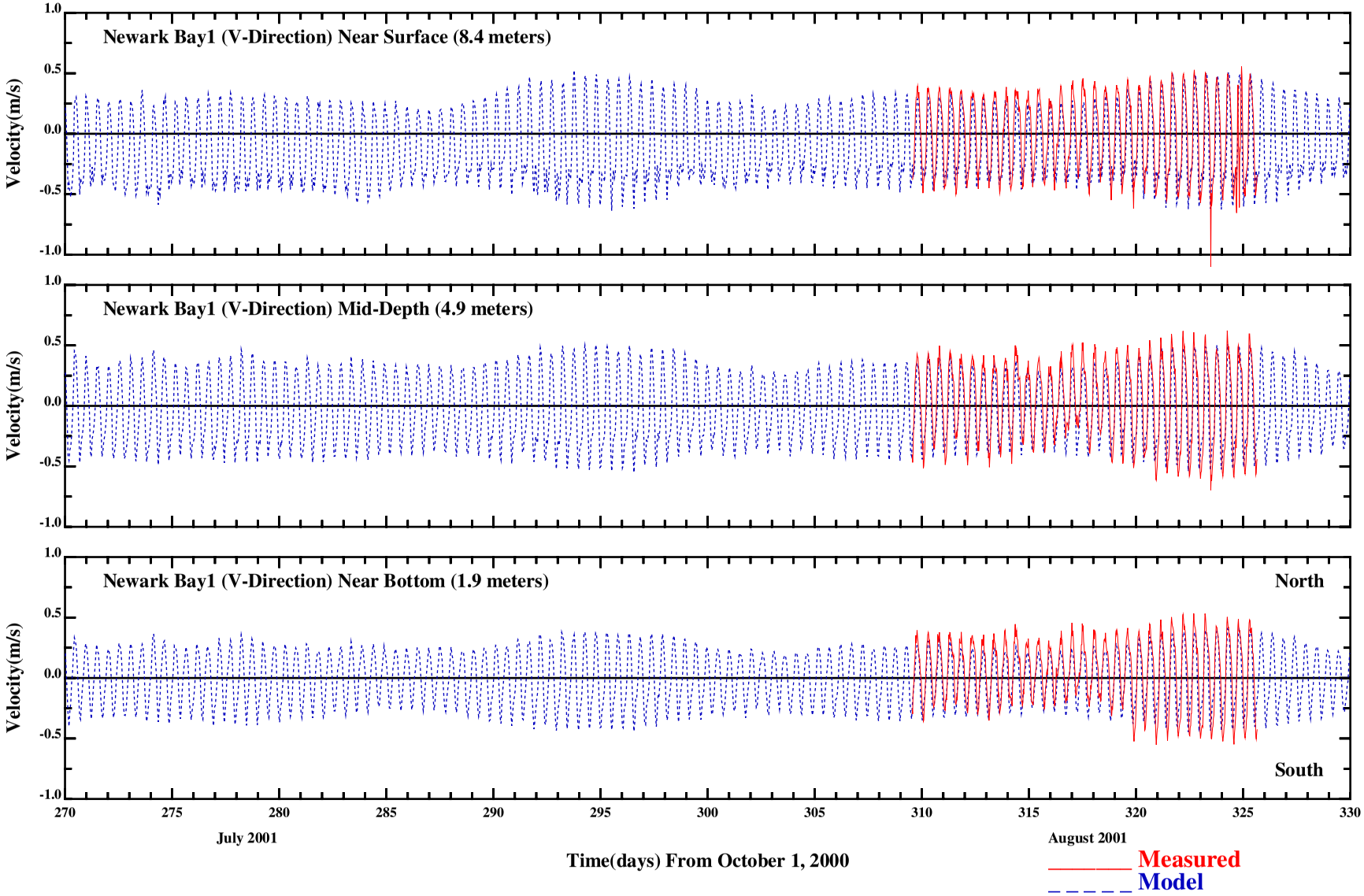

Figure 4-46a Comparison of hourly computed current velocities at three depths at NB1 with IMCS mooring data: March - August, 2001 (continued)

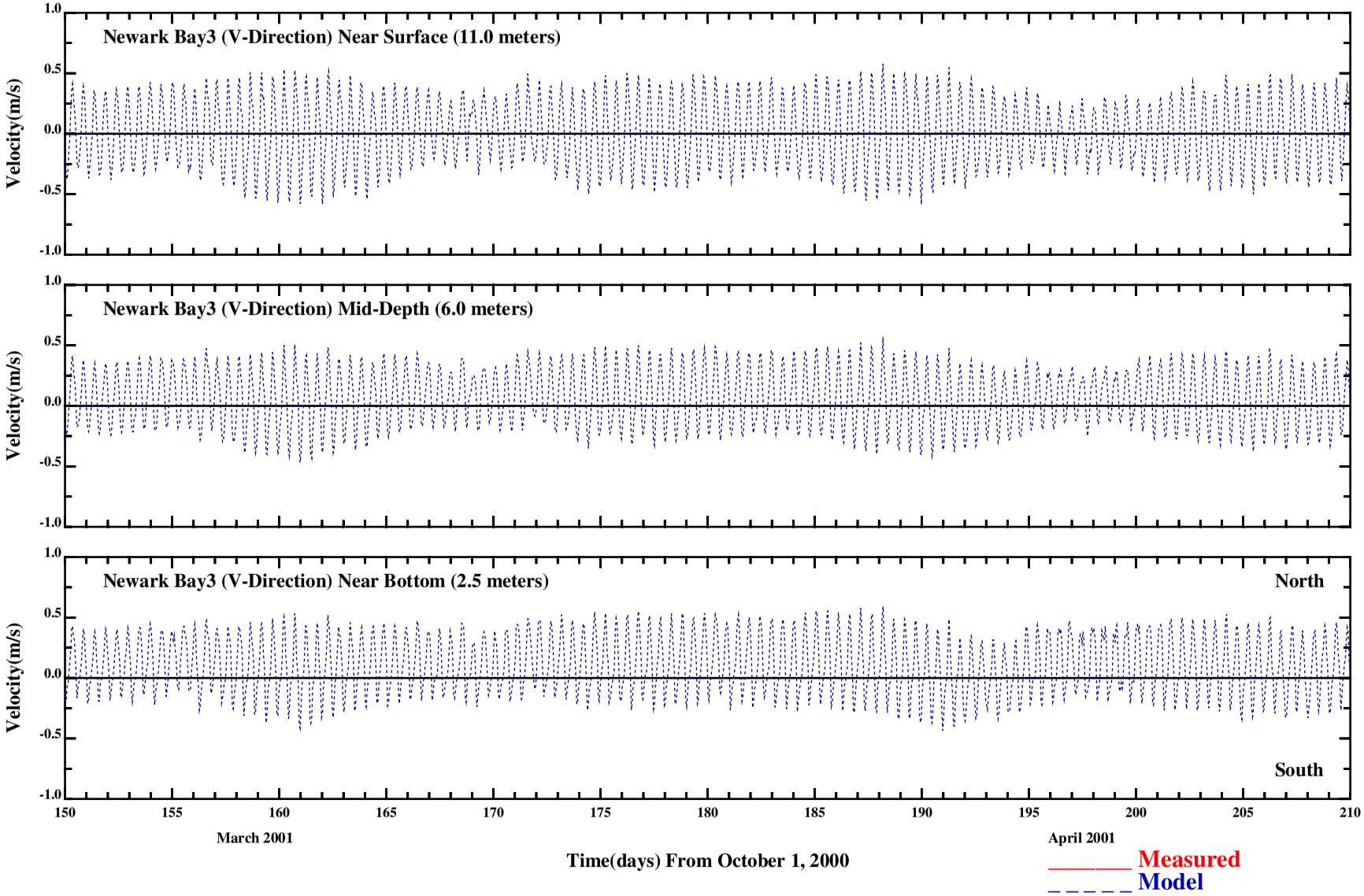

Figure 4-46b Comparison of hourly computed current velocities at three depths at NB3 with IMCS mooring data: March - August, 2001

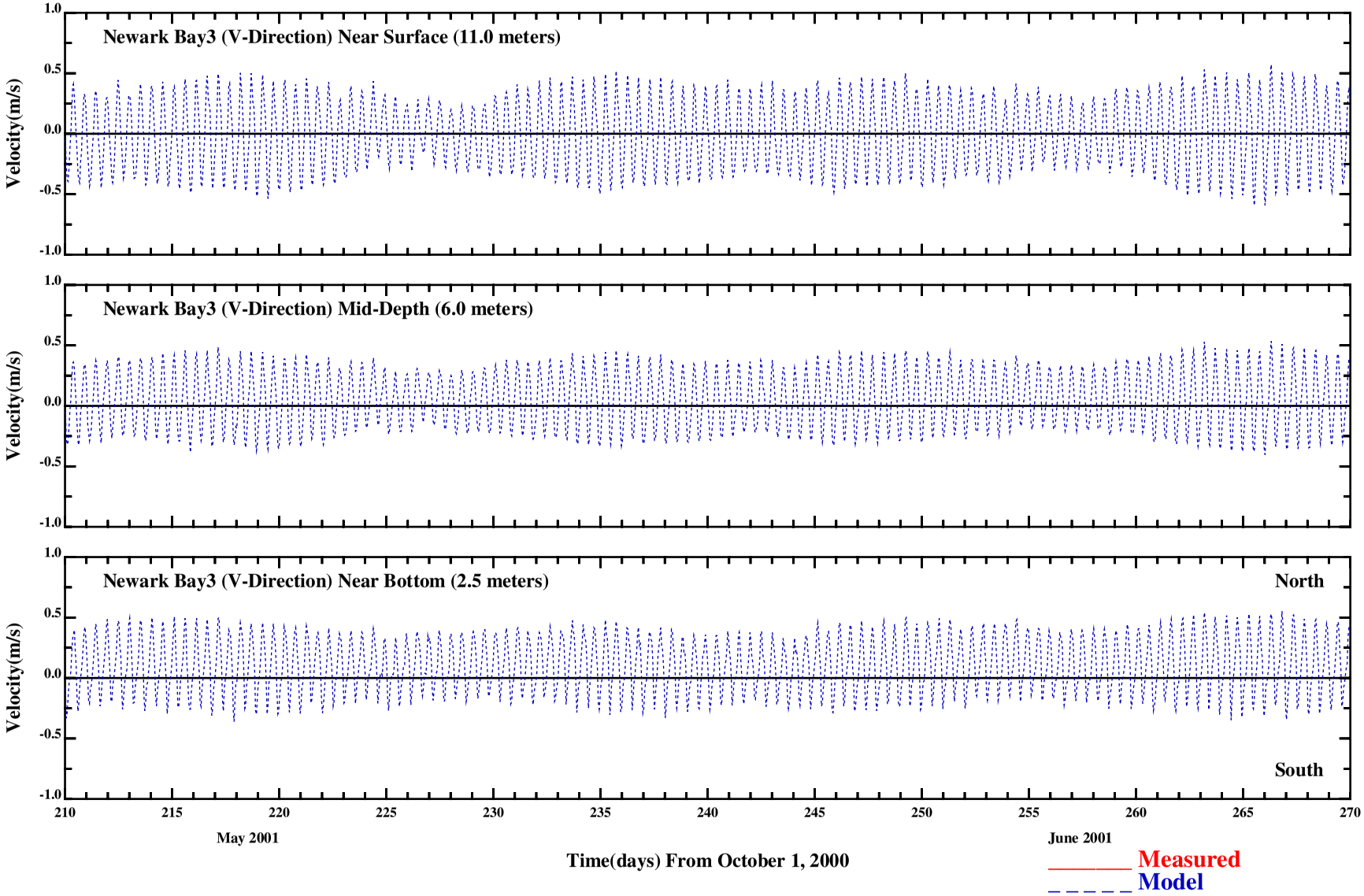

Figure 4-46b Comparison of hourly computed current velocities at three depths at NB3 with IMCS mooring data: March - August, 2001 (continued)

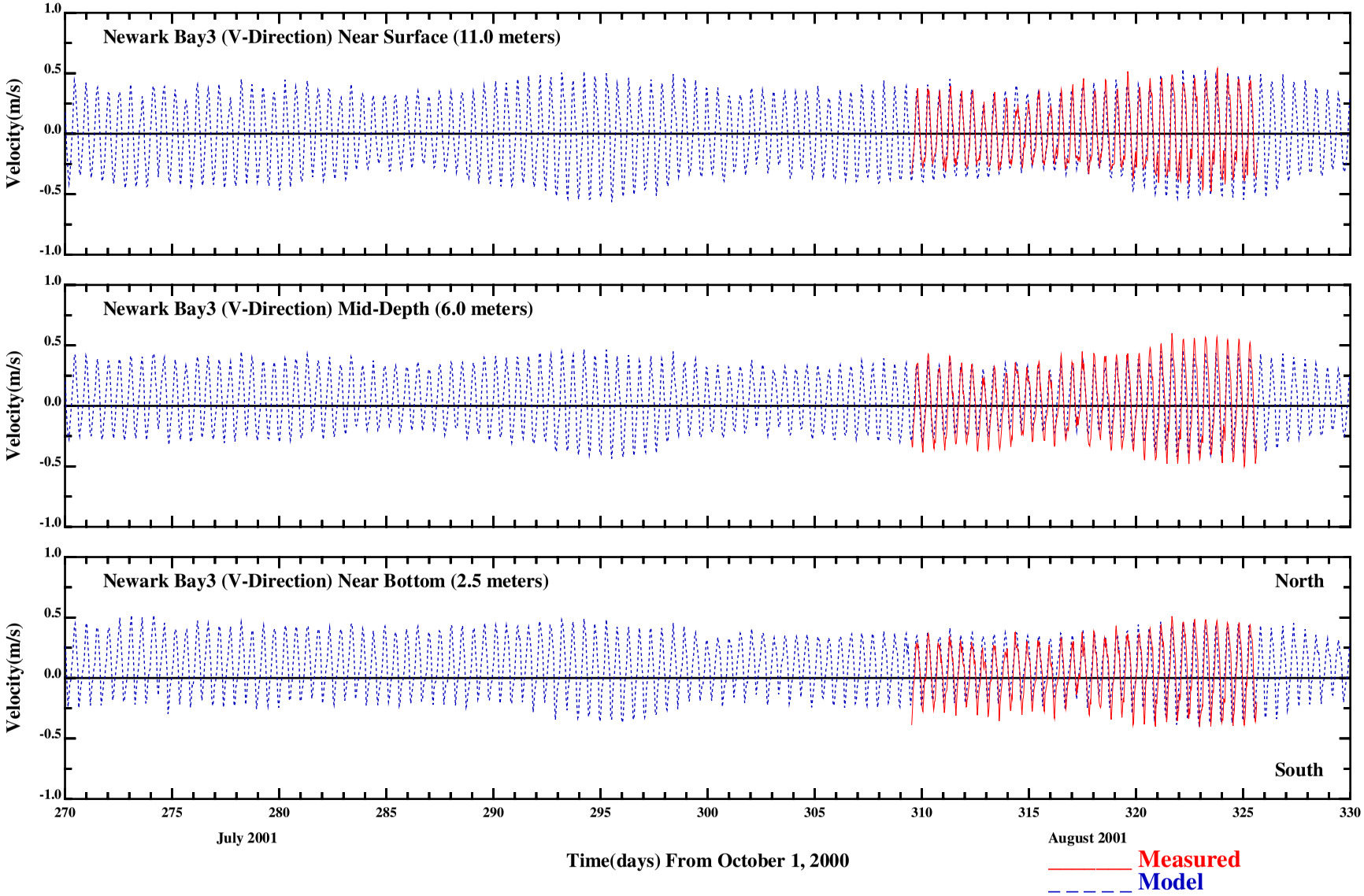

Figure 4-46b Comparison of hourly computed current velocities at three depths at NB3 with IMCS mooring data: March - August, 2001 (continued)

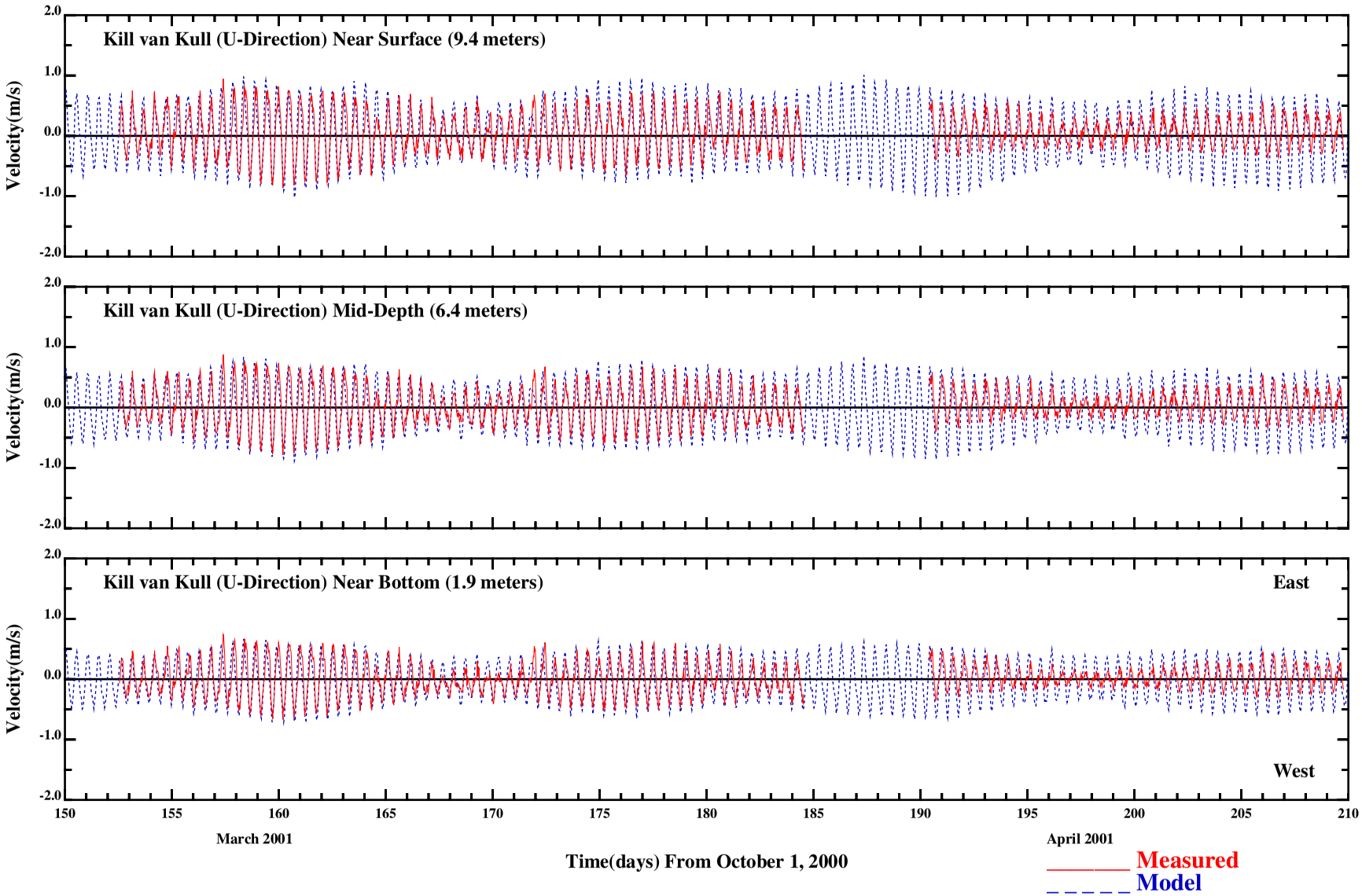

Figure 4-46c Comparison of hourly computed current velocities at three depths at KVK with IMCS mooring data: March - August, 2001

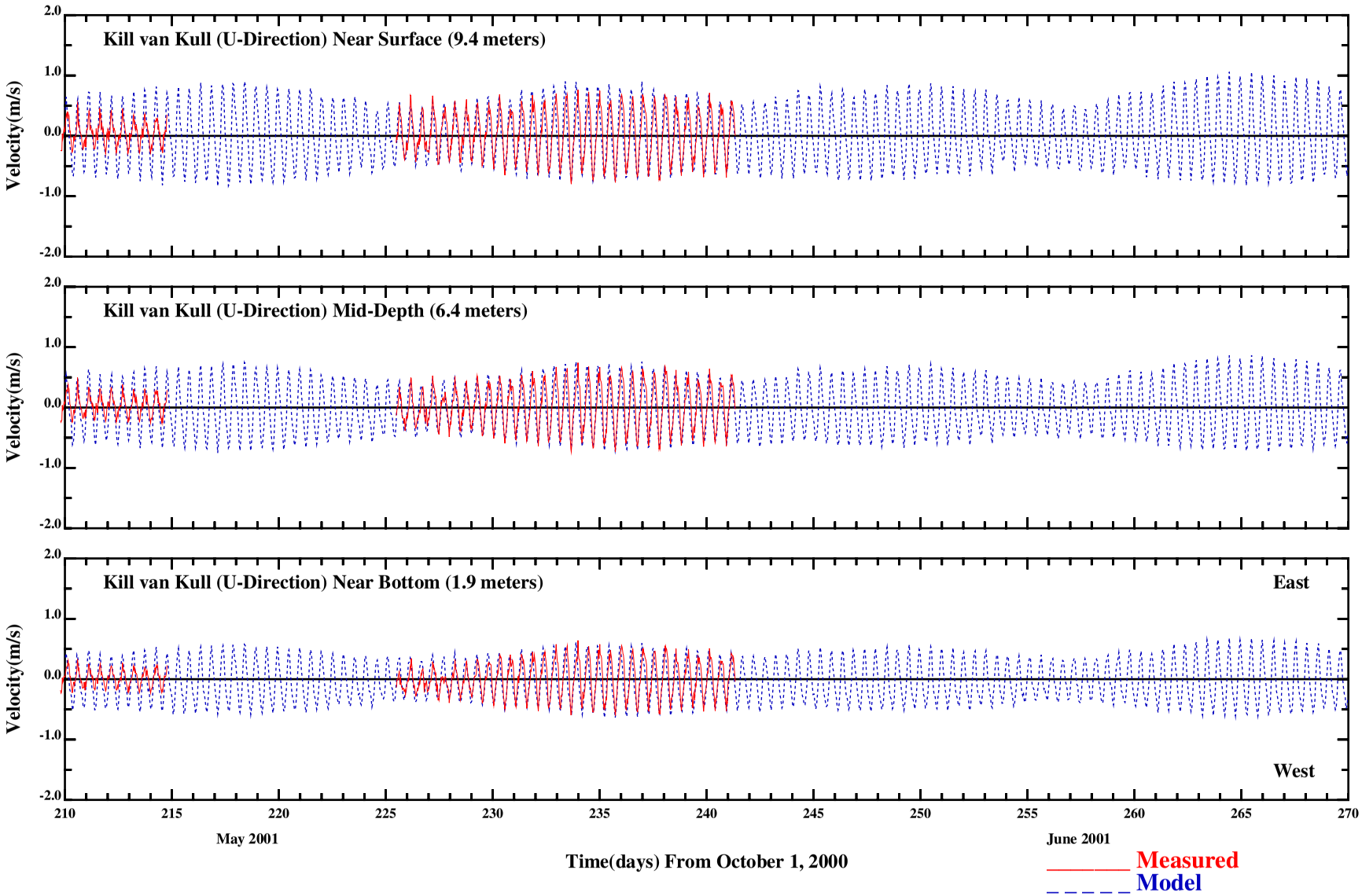

Figure 4-46c Comparison of hourly computed current velocities at three depths at KVK with IMCS mooring data: March - August, 2001 (continued)

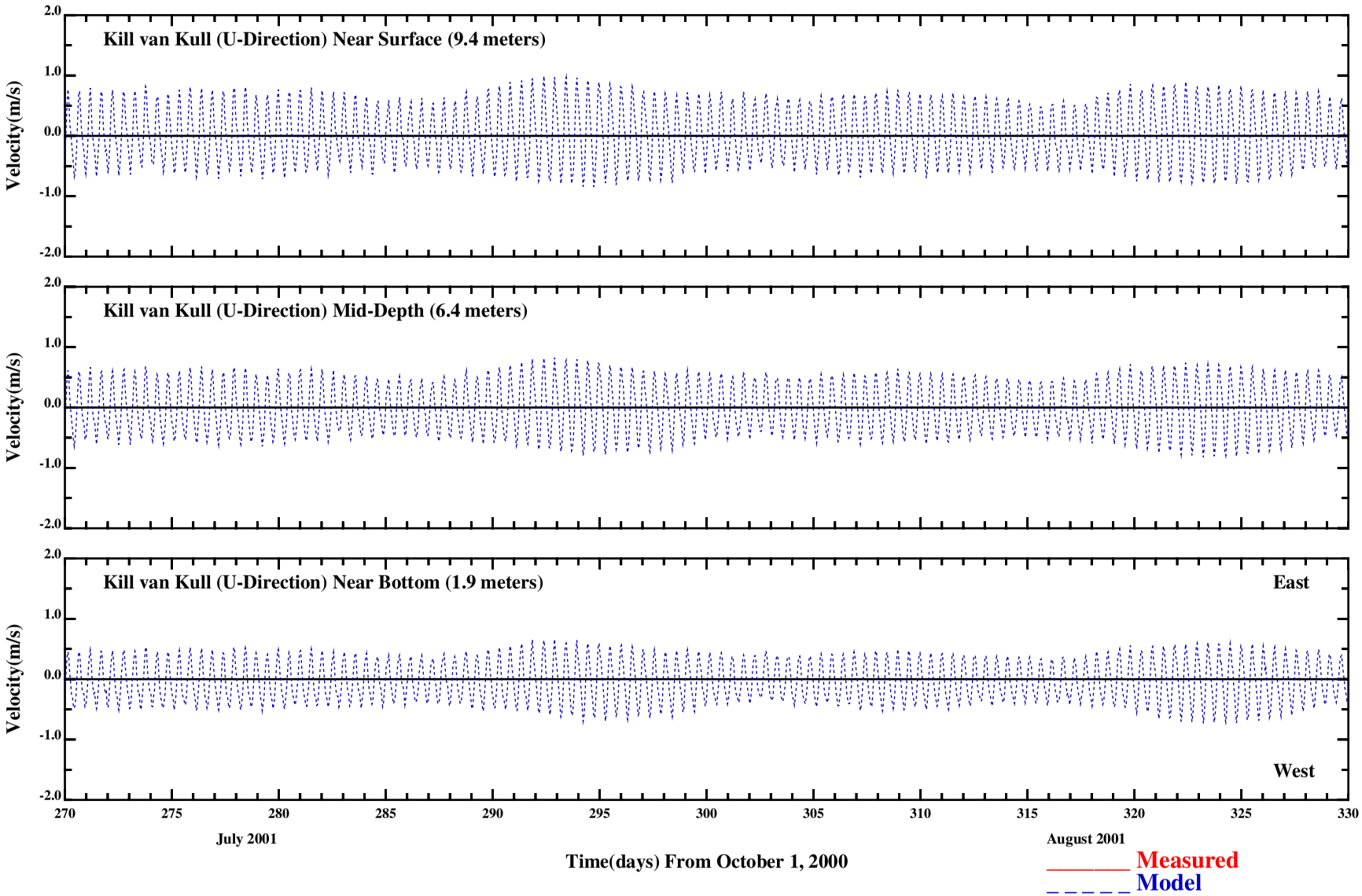

Figure 4-46c Comparison of hourly computed current velocities at three depths at KVK with IMCS mooring data: March - August, 2001 (continued)

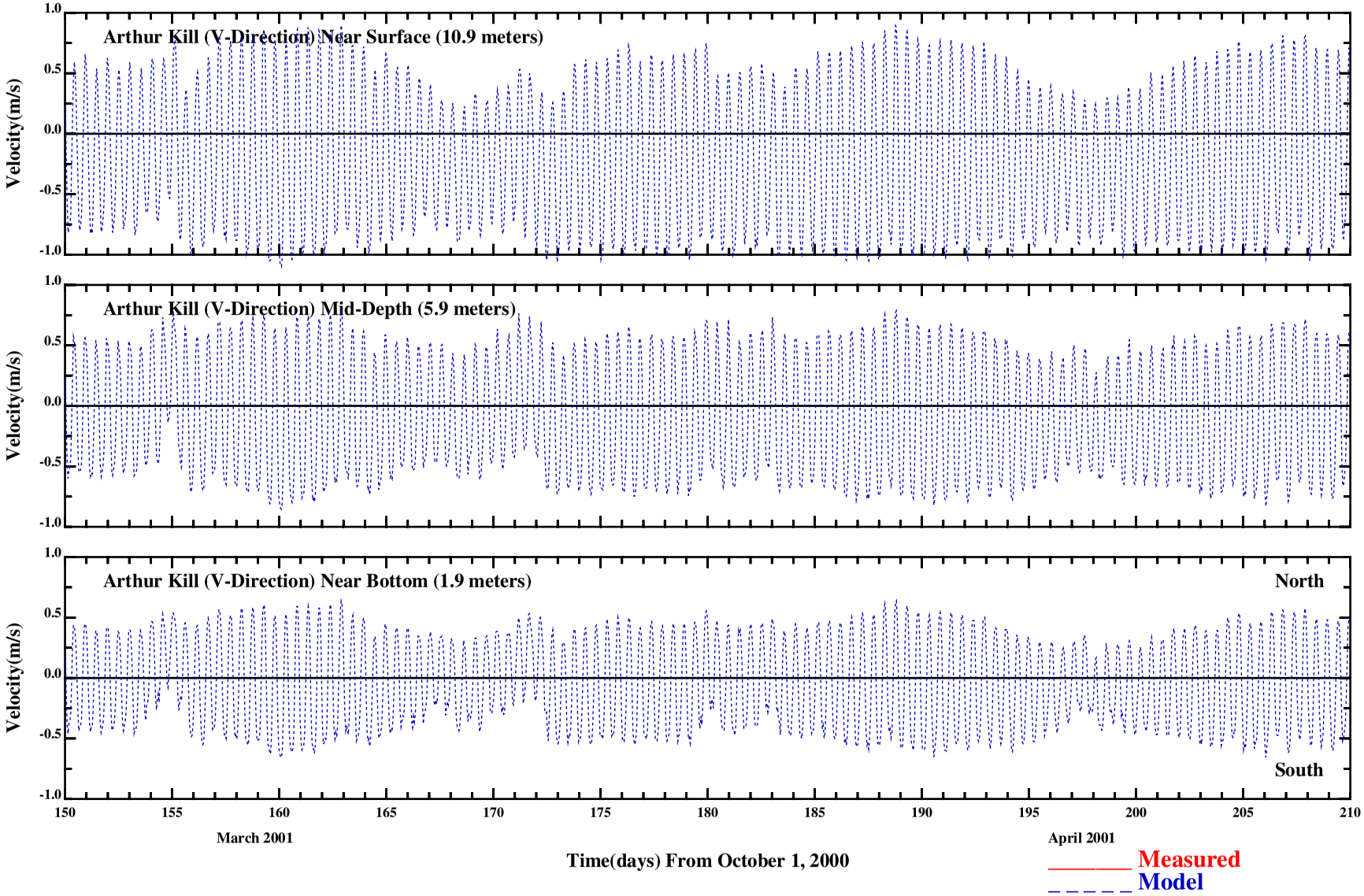

Figure 4-46d Comparison of hourly computed current velocities at three depths at AK with IMCS mooring data: March - August, 2001

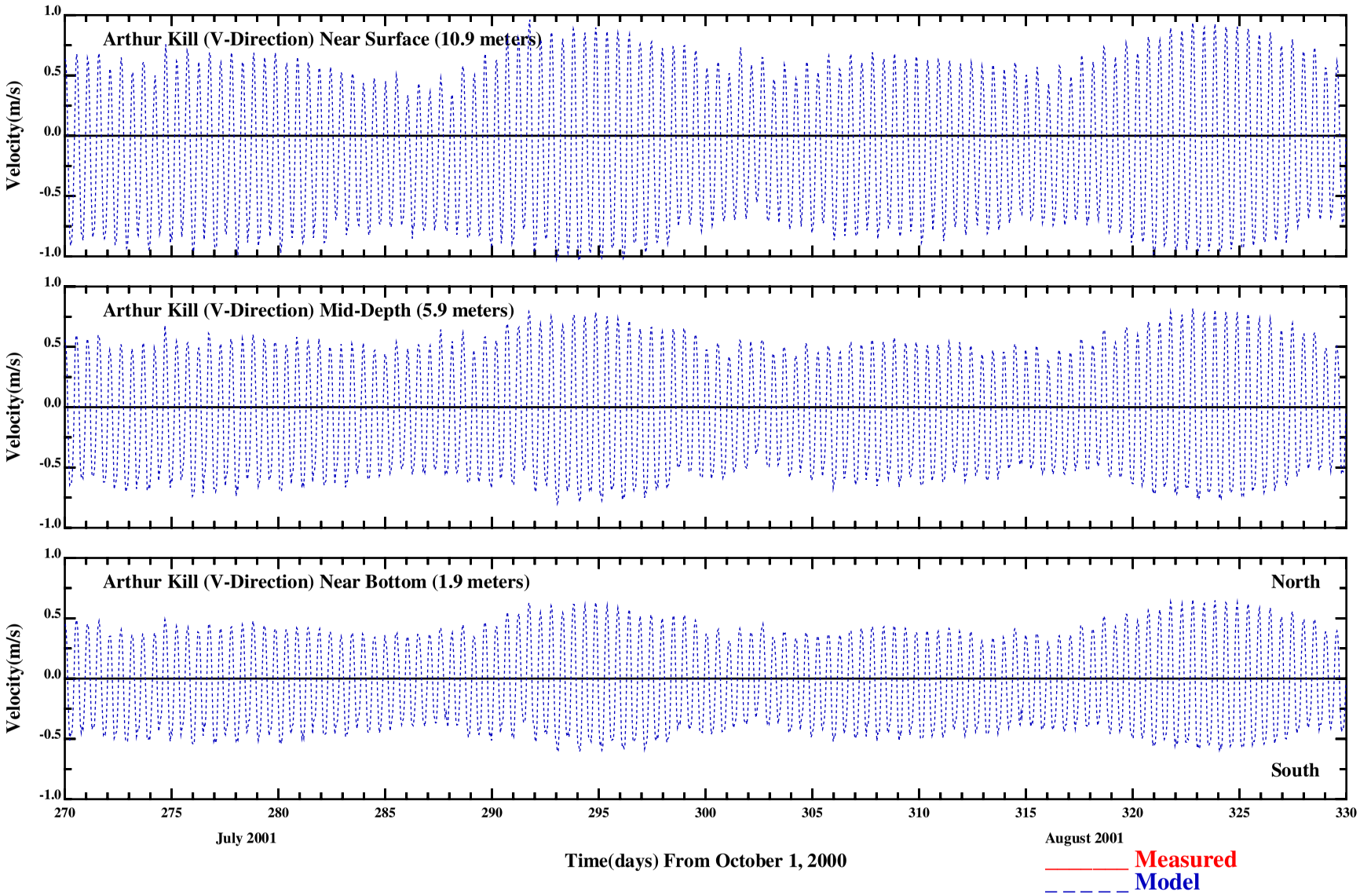

Figure 4-46d Comparison of hourly computed current velocities at three depths at AK with IMCS mooring data: March - August, 2001 (continued)

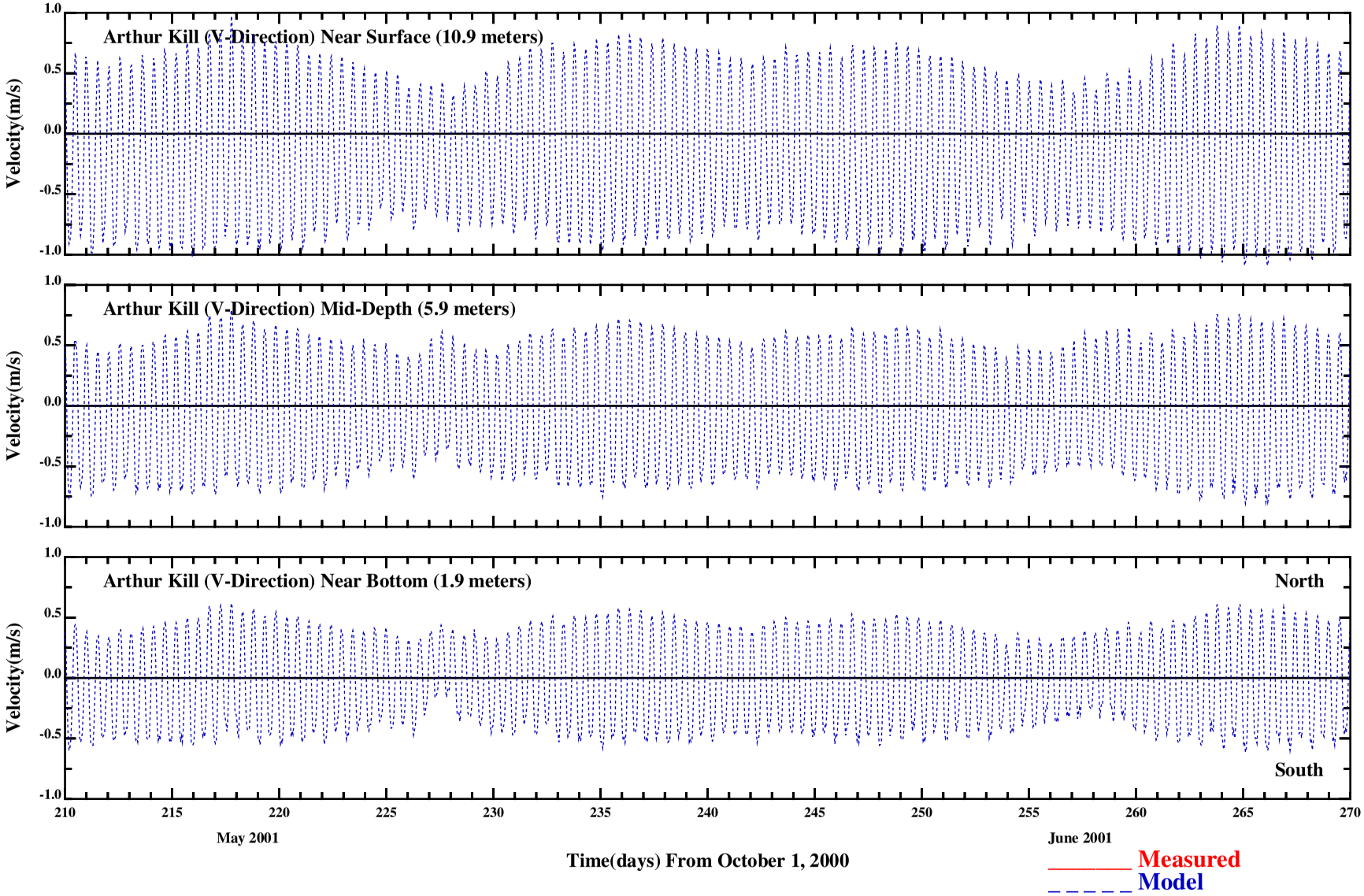

Figure 4-46d Comparison of hourly computed current velocities at three depths at AK with IMCS mooring data: March - August, 2001 (continued)

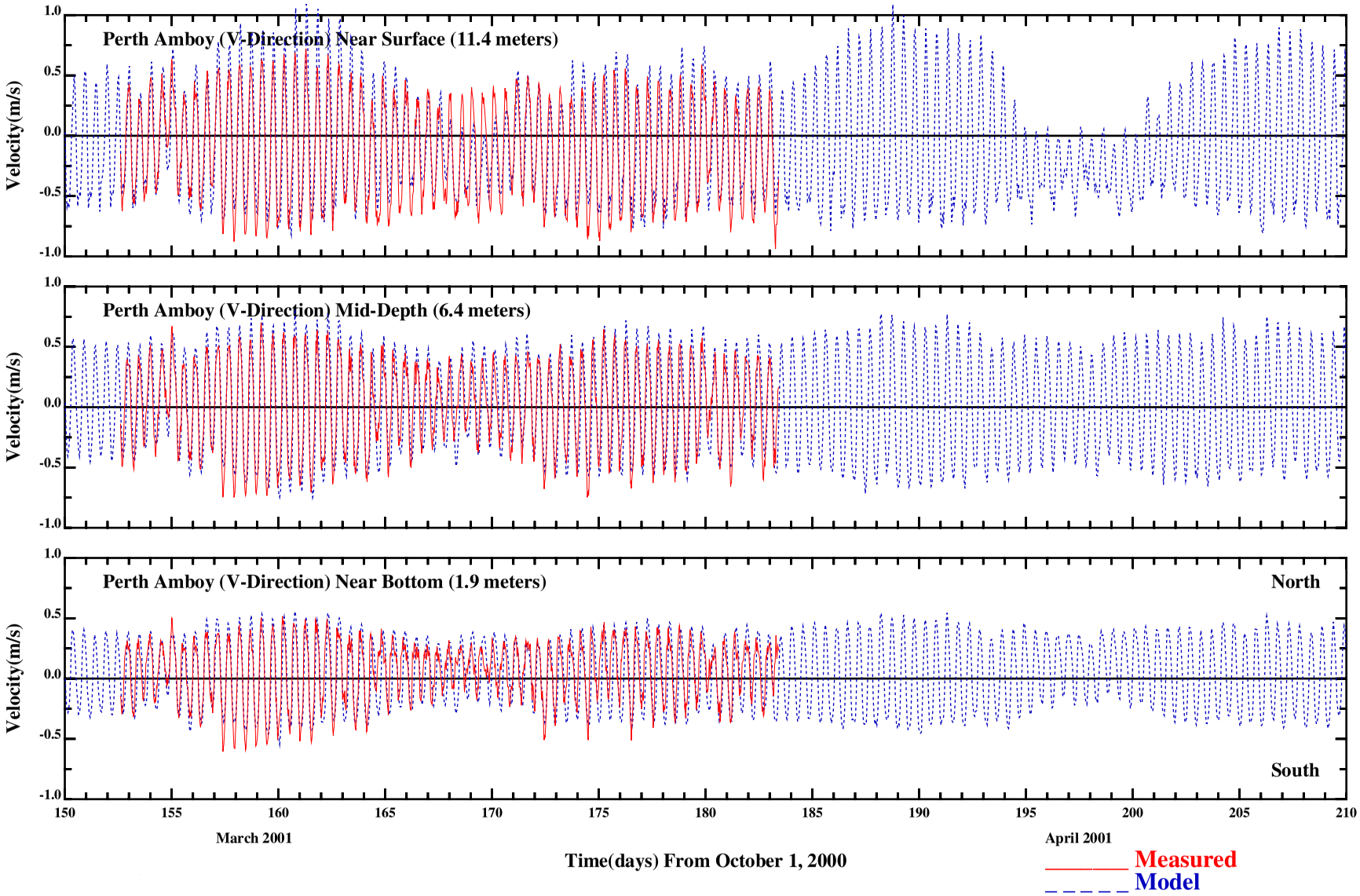

Figure 4-46e Comparison of hourly computed current velocities at three depths at PA with IMCS mooring data: March - August, 2001

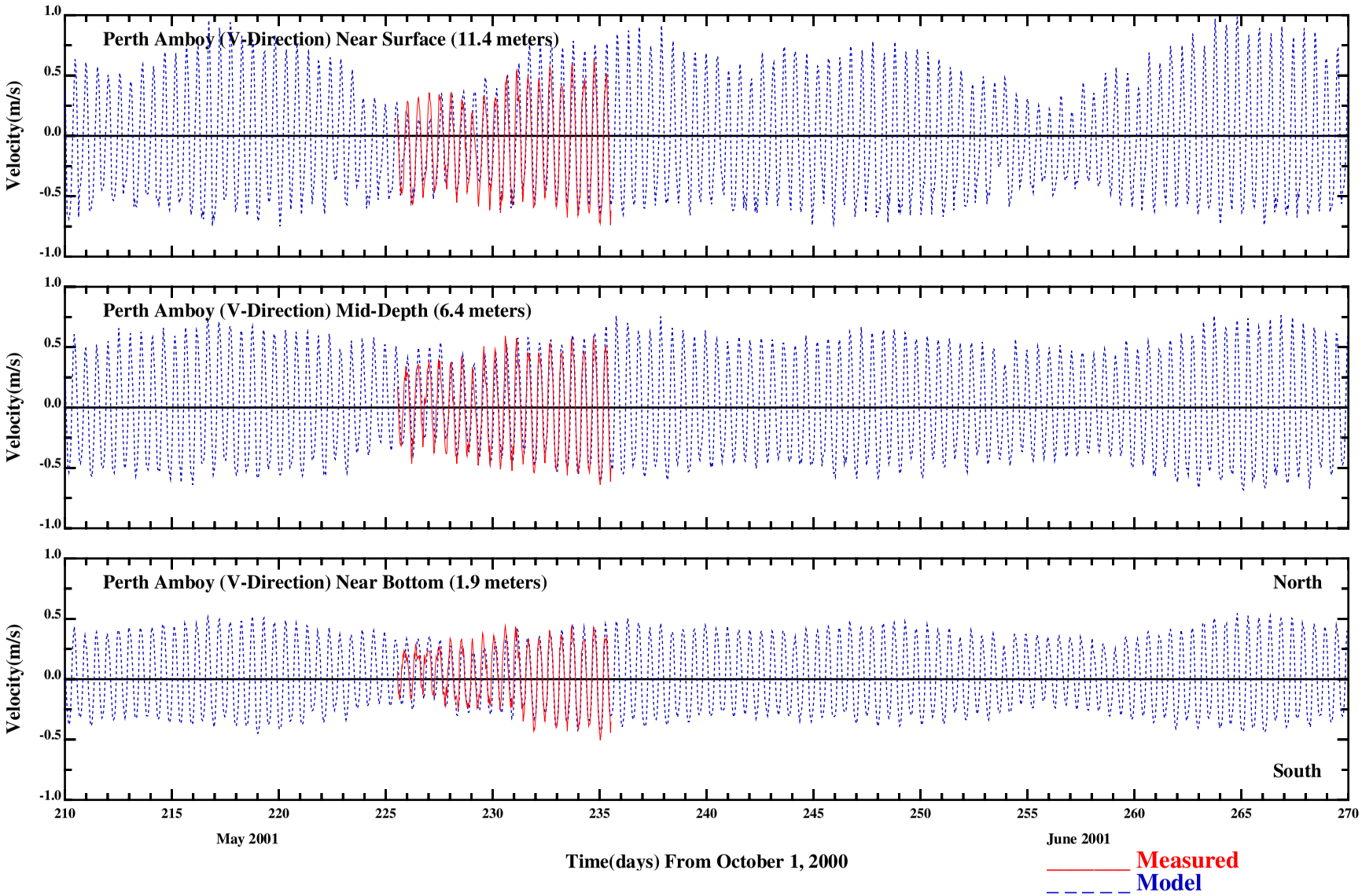

Figure 4-46e Comparison of hourly computed current velocities at three depths at PA with IMCS mooring data: March - August, 2001 (continued)

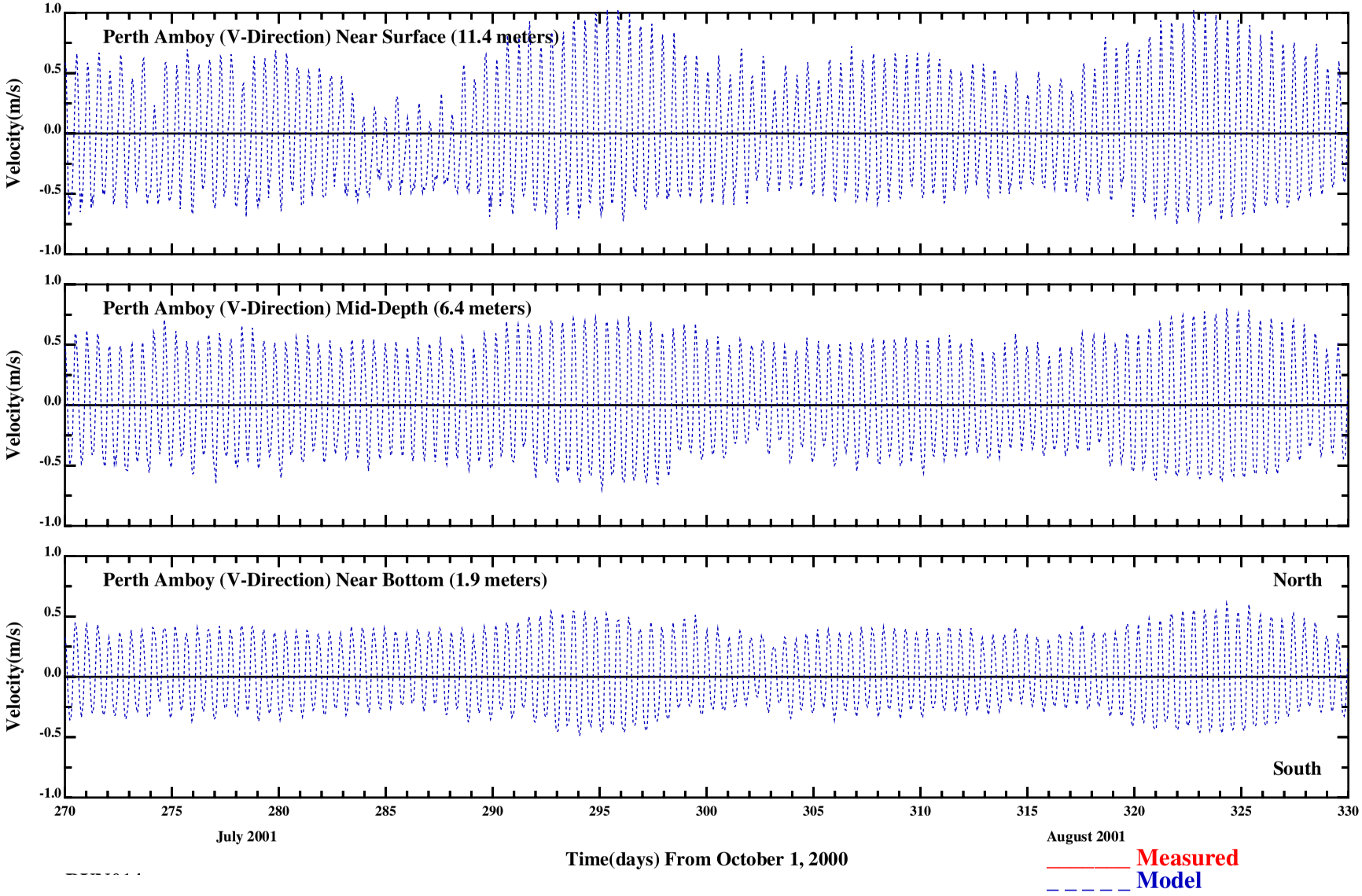

Figure 4-46e Comparison of hourly computed current velocities at three depths at PA with IMCS mooring data: March - August, 2001 (continued)

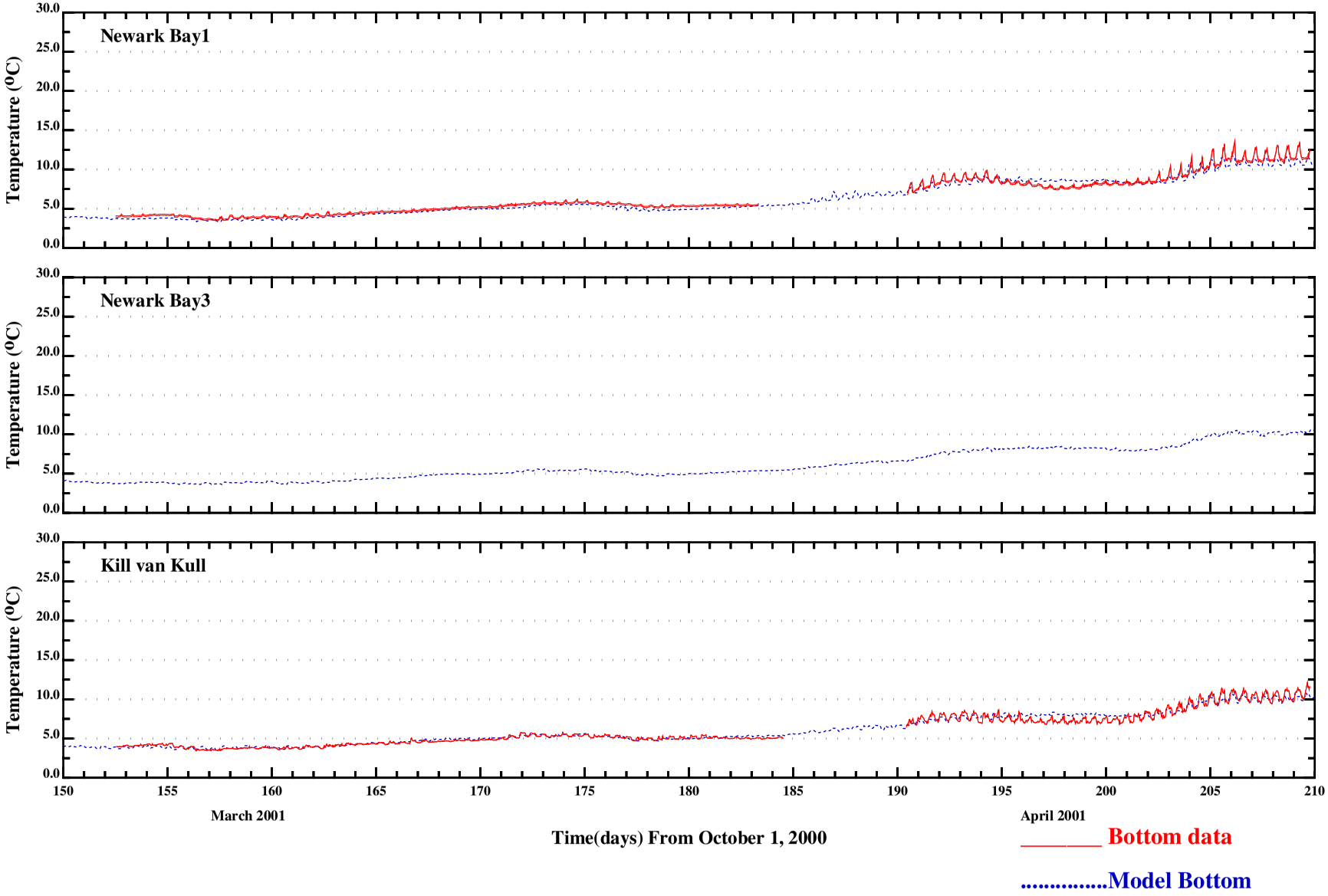

Figure 4-47 Comparison of hourly computed temperature with IMCS mooring data: March-August, 2001

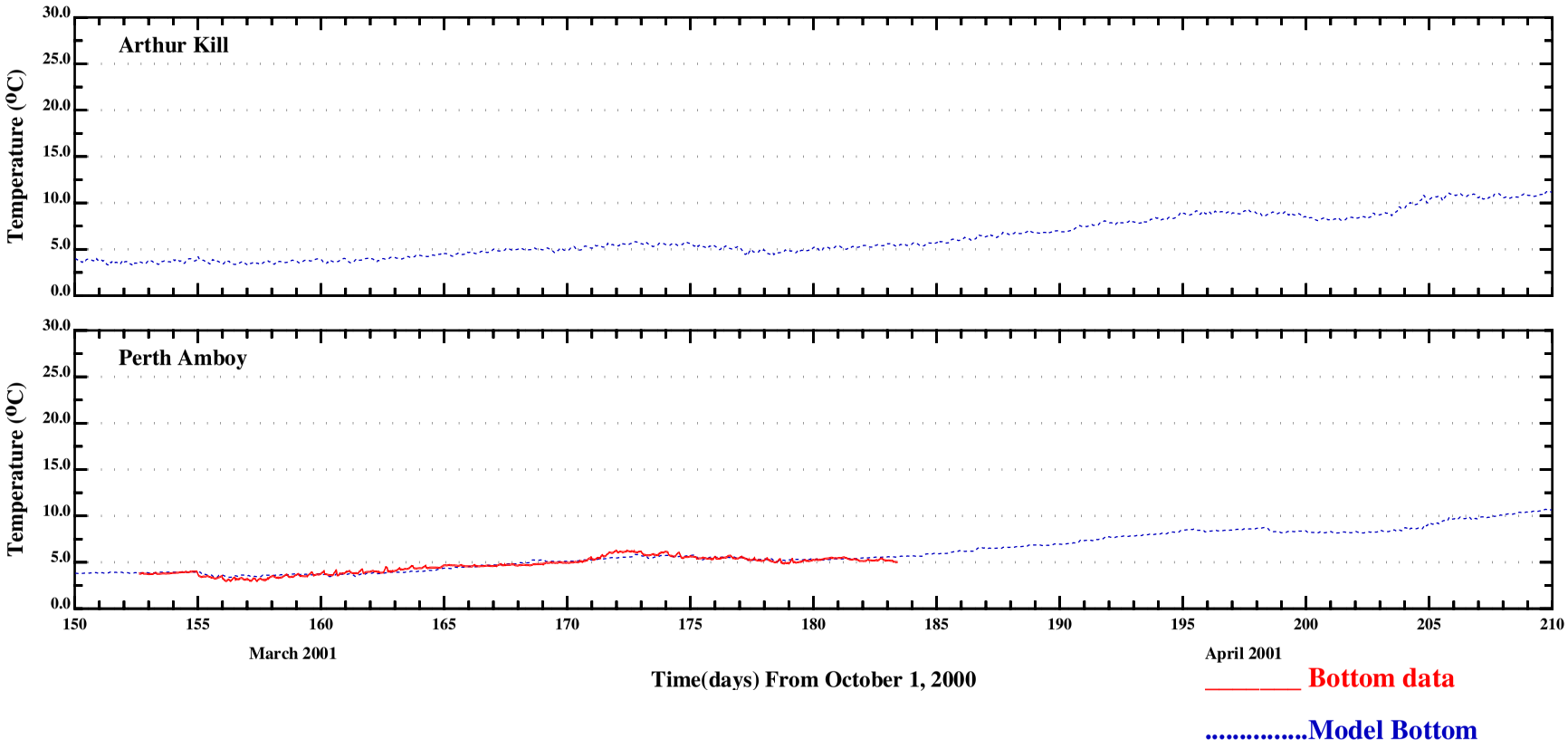

Figure 4-47 Comparison of hourly computed temperature with IMCS mooring data: March-August, 2001 (continued)

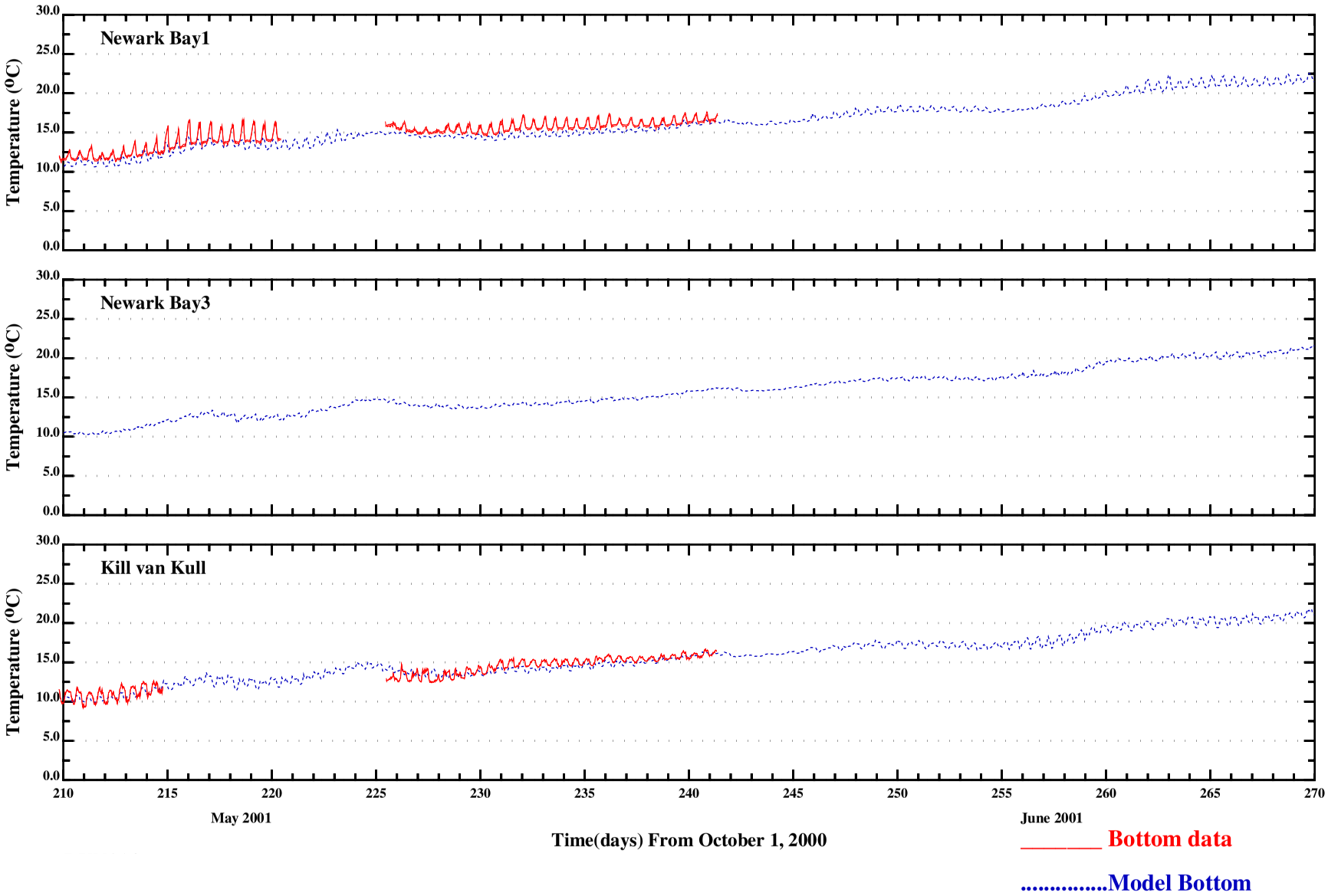

Figure 4-47 Comparison of hourly computed temperature with IMCS mooring data: March-August, 2001 (continued)

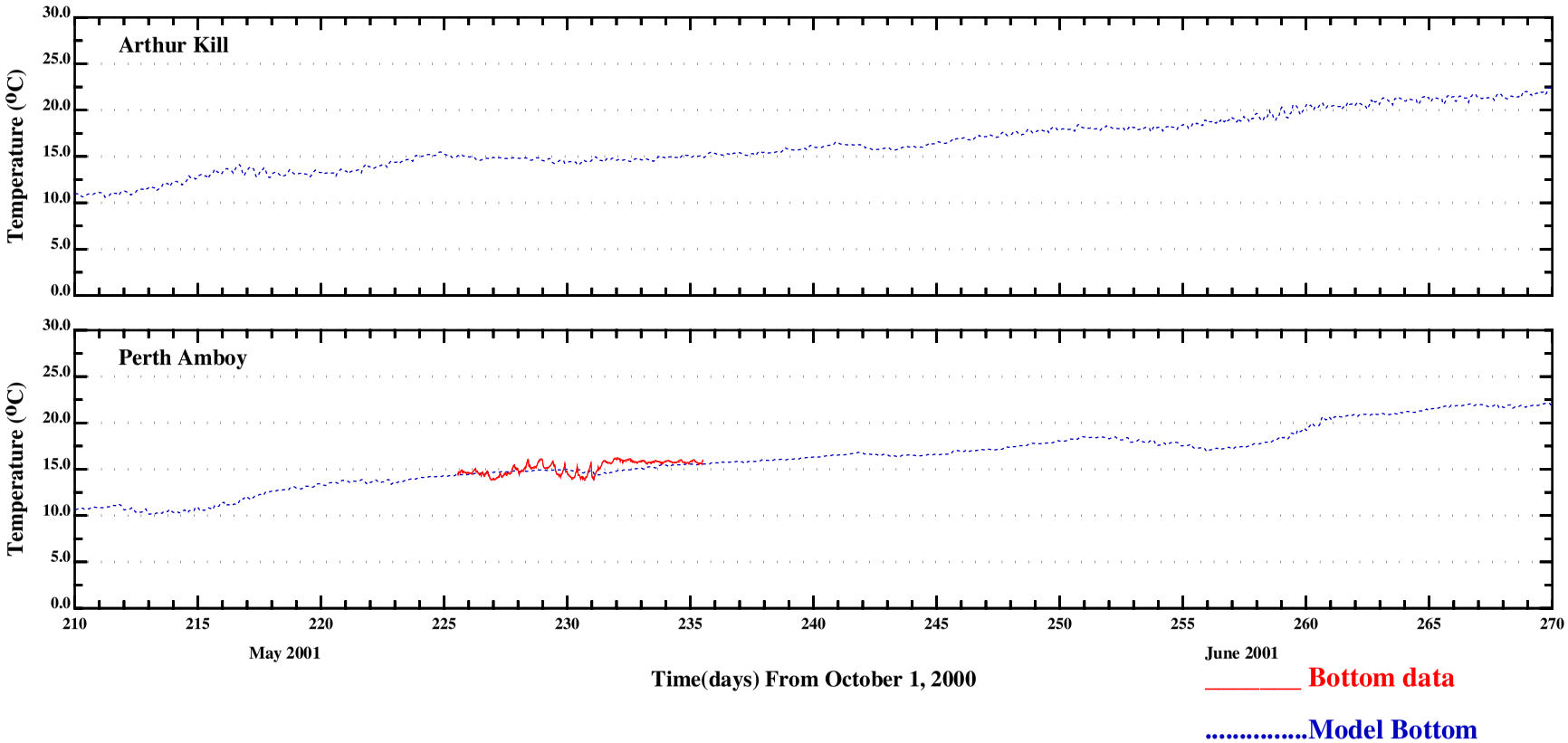

Figure 4-47 Comparison of hourly computed temperature with IMCS mooring data: March-August, 2001 (continued)

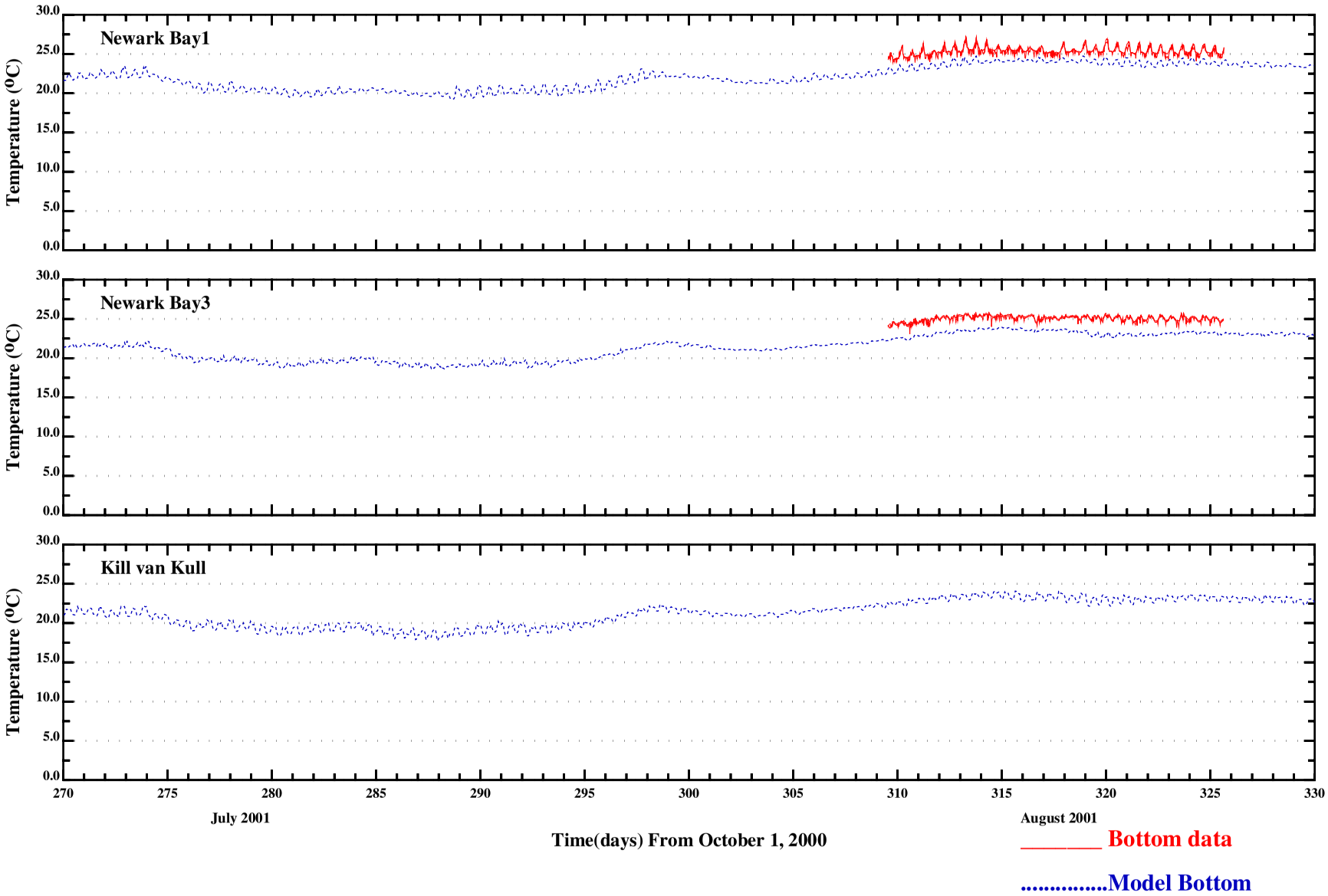

Figure 4-47 Comparison of hourly computed temperature with IMCS mooring data: March-August, 2001 (continued)

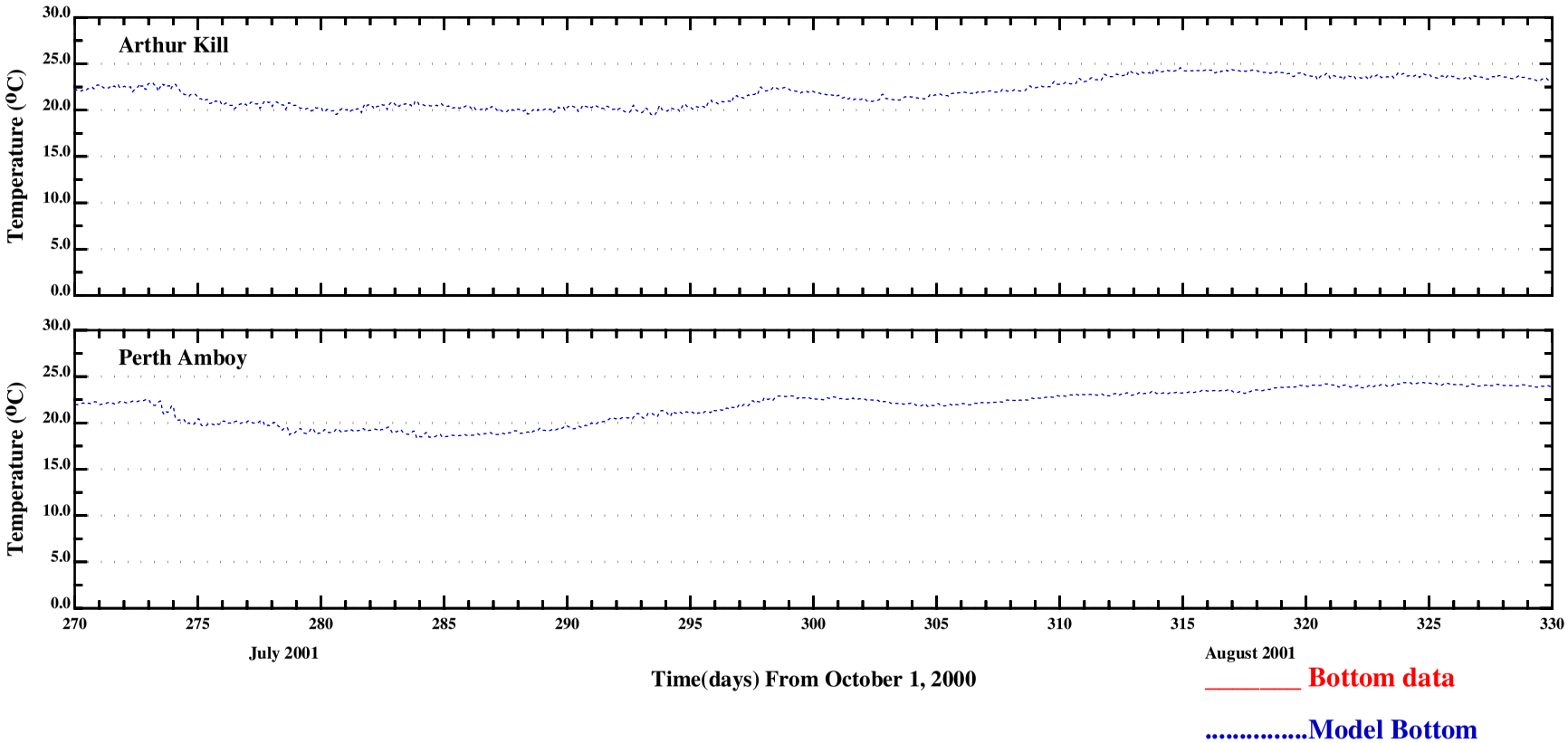

Figure 4-47 Comparison of hourly computed temperature with IMCS mooring data: March-August, 2001 (continued)

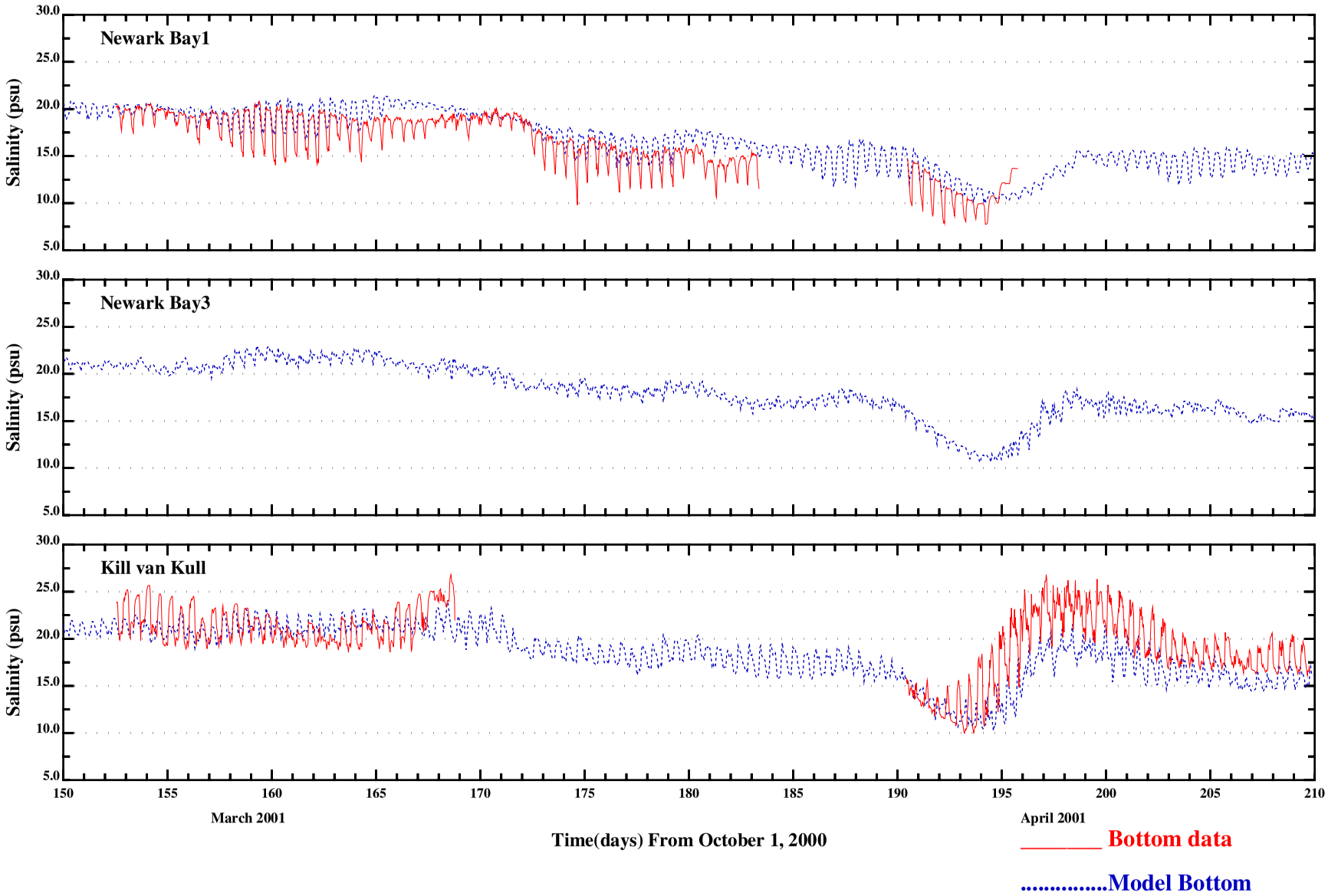

Figure 4-48 Comparison of hourly computed salinity with IMCS mooring data: March-August, 2001

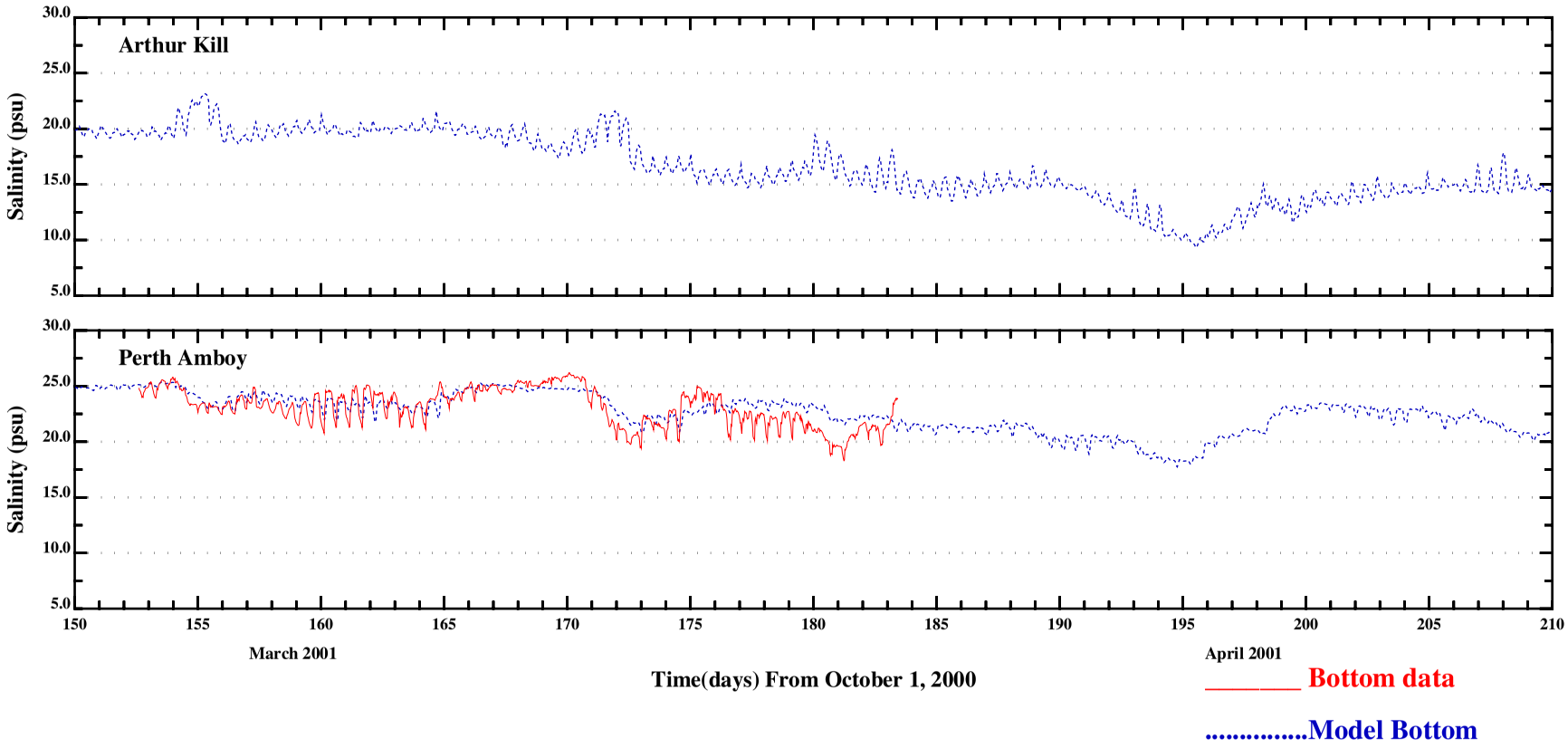

Figure 4-48 Comparison of hourly computed salinity with IMCS mooring data: March-August, 2001 (continued)

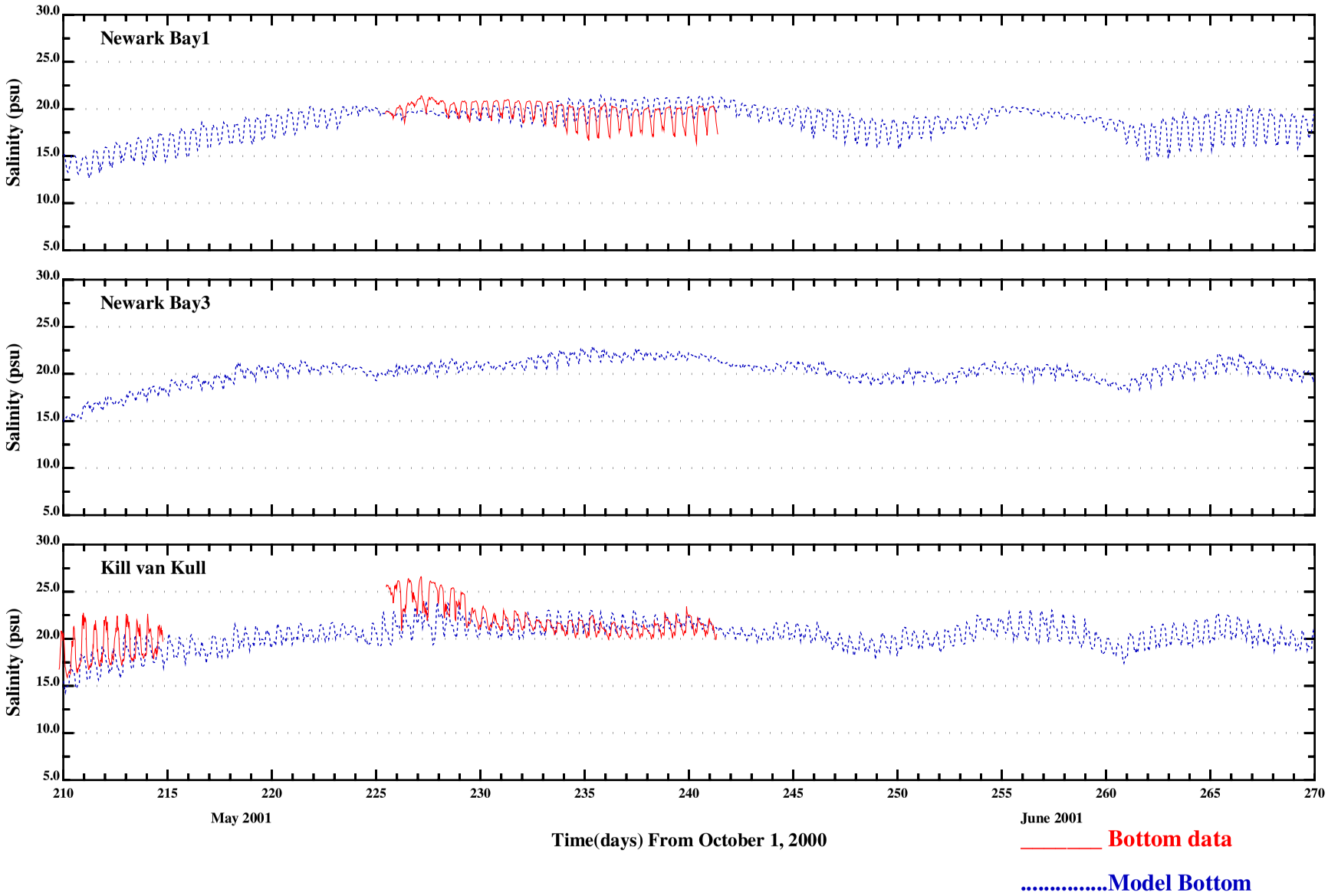

Figure 4-48 Comparison of hourly computed salinity with IMCS mooring data: March-August, 2001 (continued)

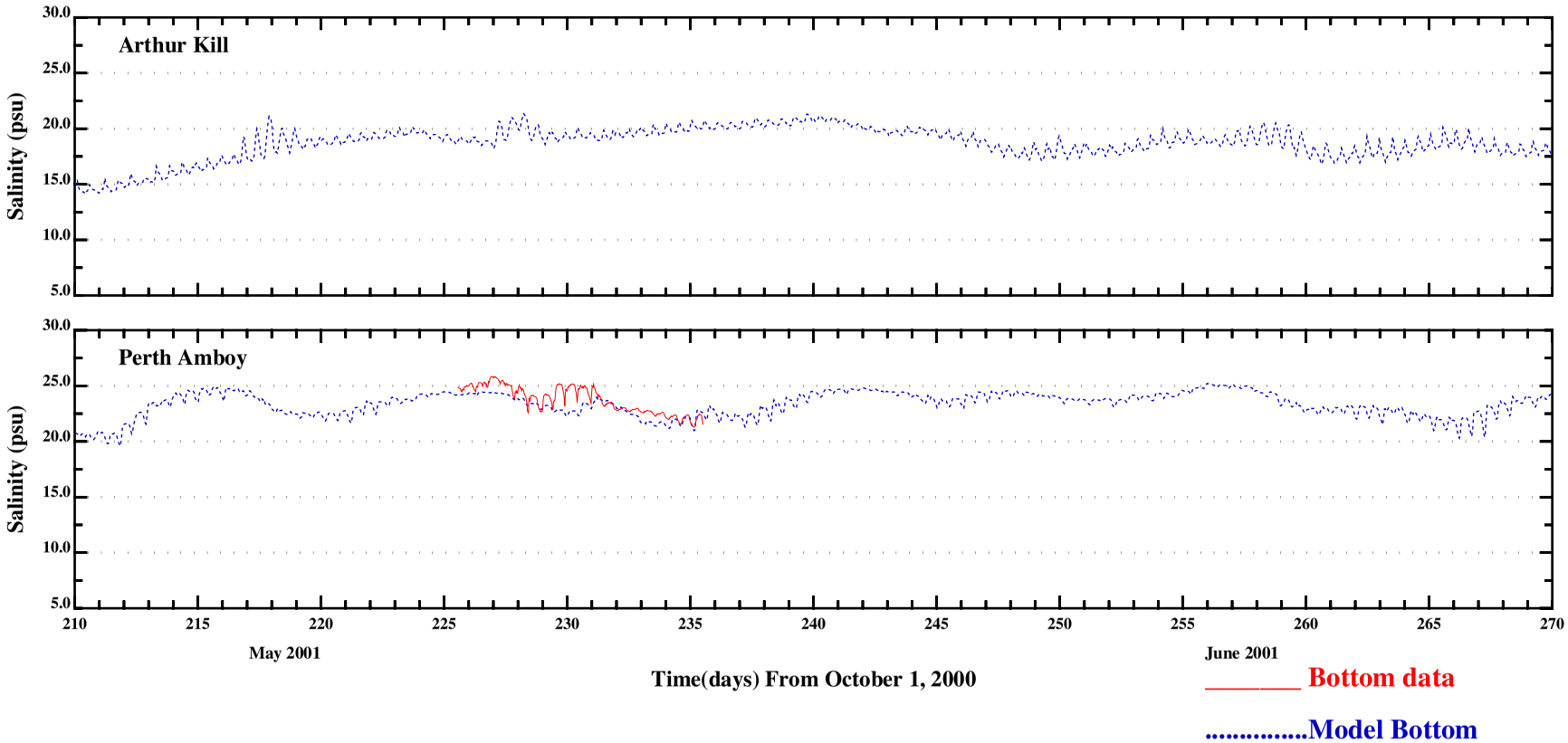

Figure 4-48 Comparison of hourly computed salinity with IMCS mooring data: March-August, 2001 (continued)

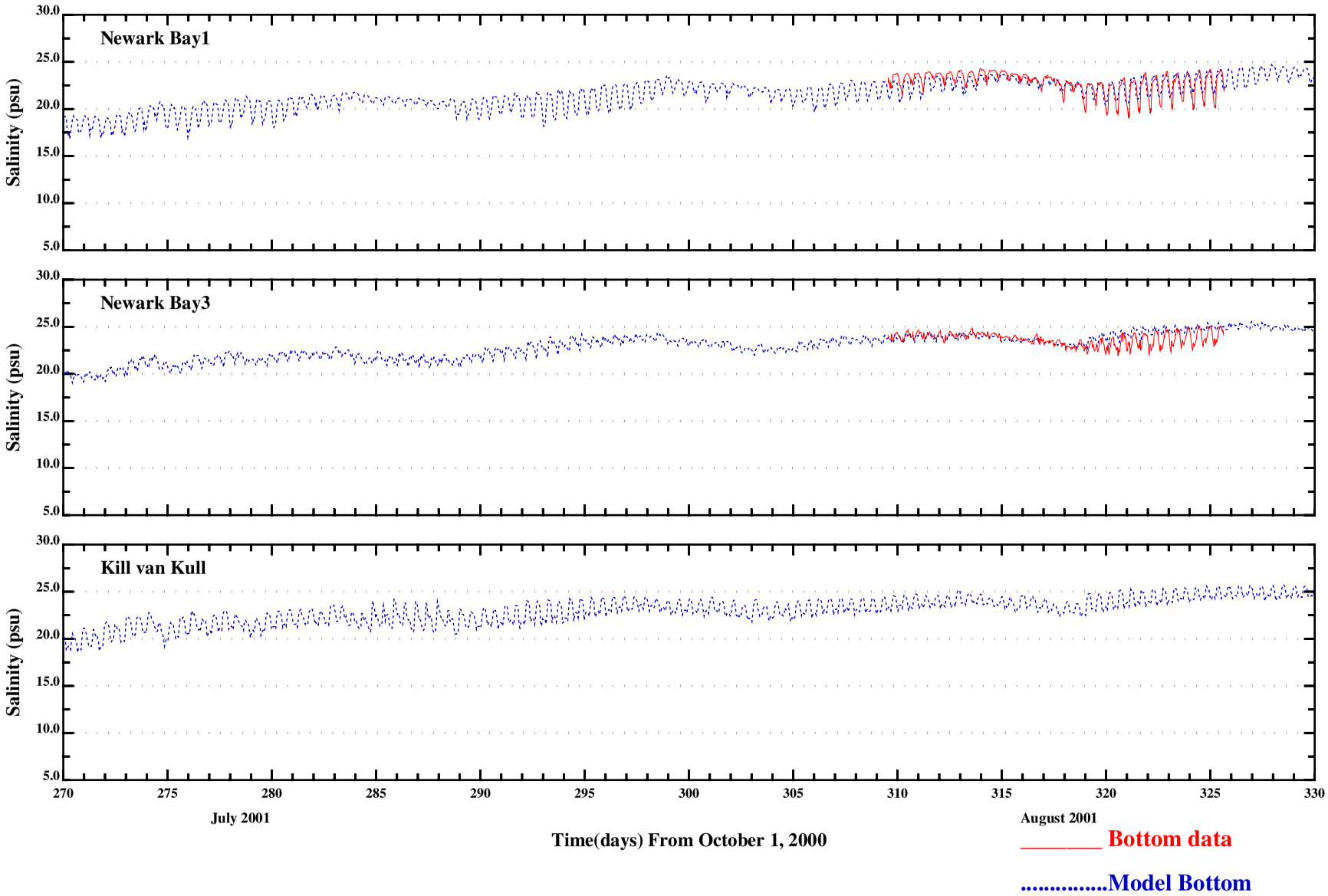

Figure 4-48 Comparison of hourly computed salinity with IMCS mooring data: March-August, 2001 (continued)

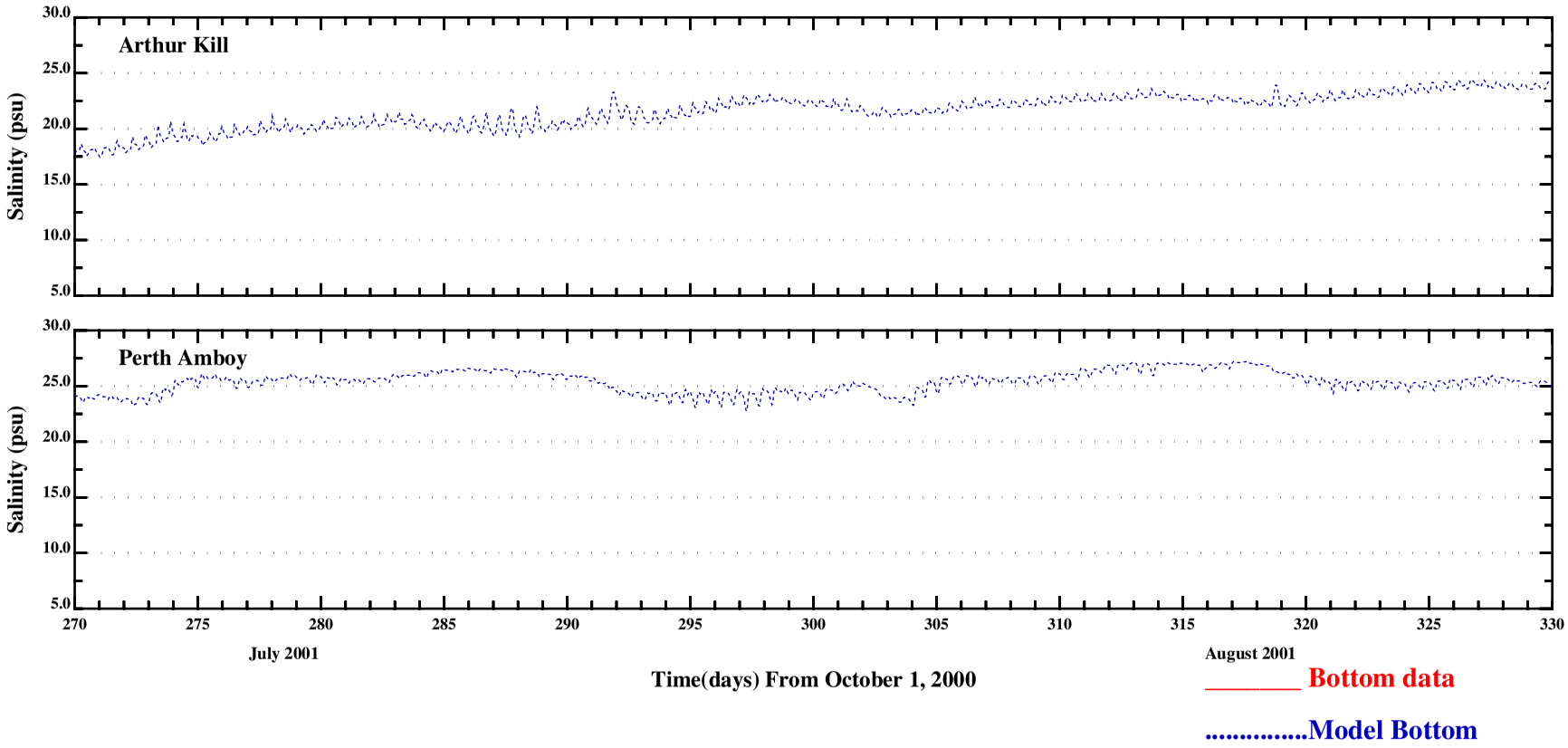

Figure 4-48 Comparison of hourly computed salinity with IMCS mooring data: March-August, 2001 (continued)

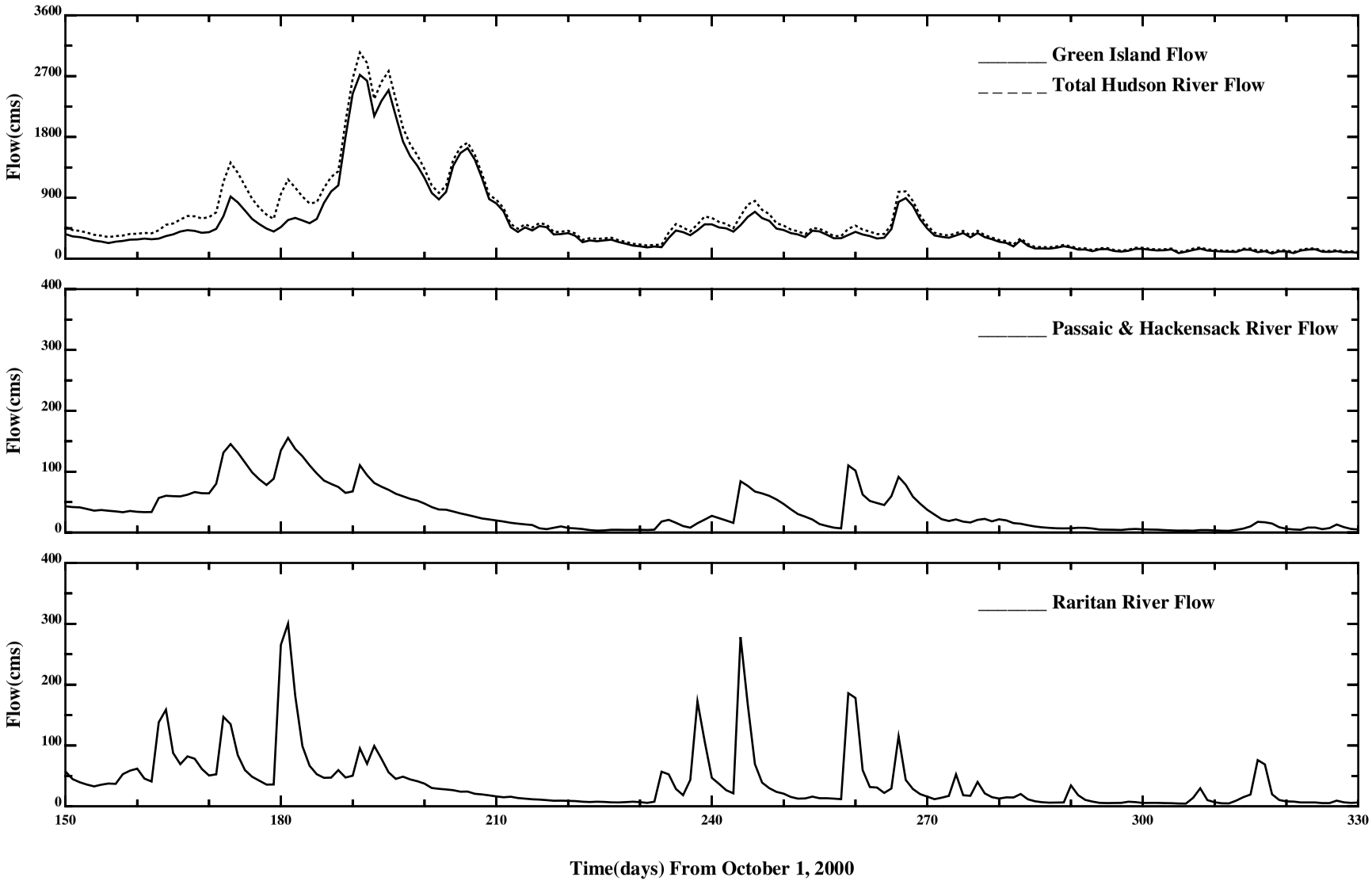

Figure 4-49 Temporal variation of the flow through Hudson, Passaic, Hackensack and Raritan rivers: March-August, 2001

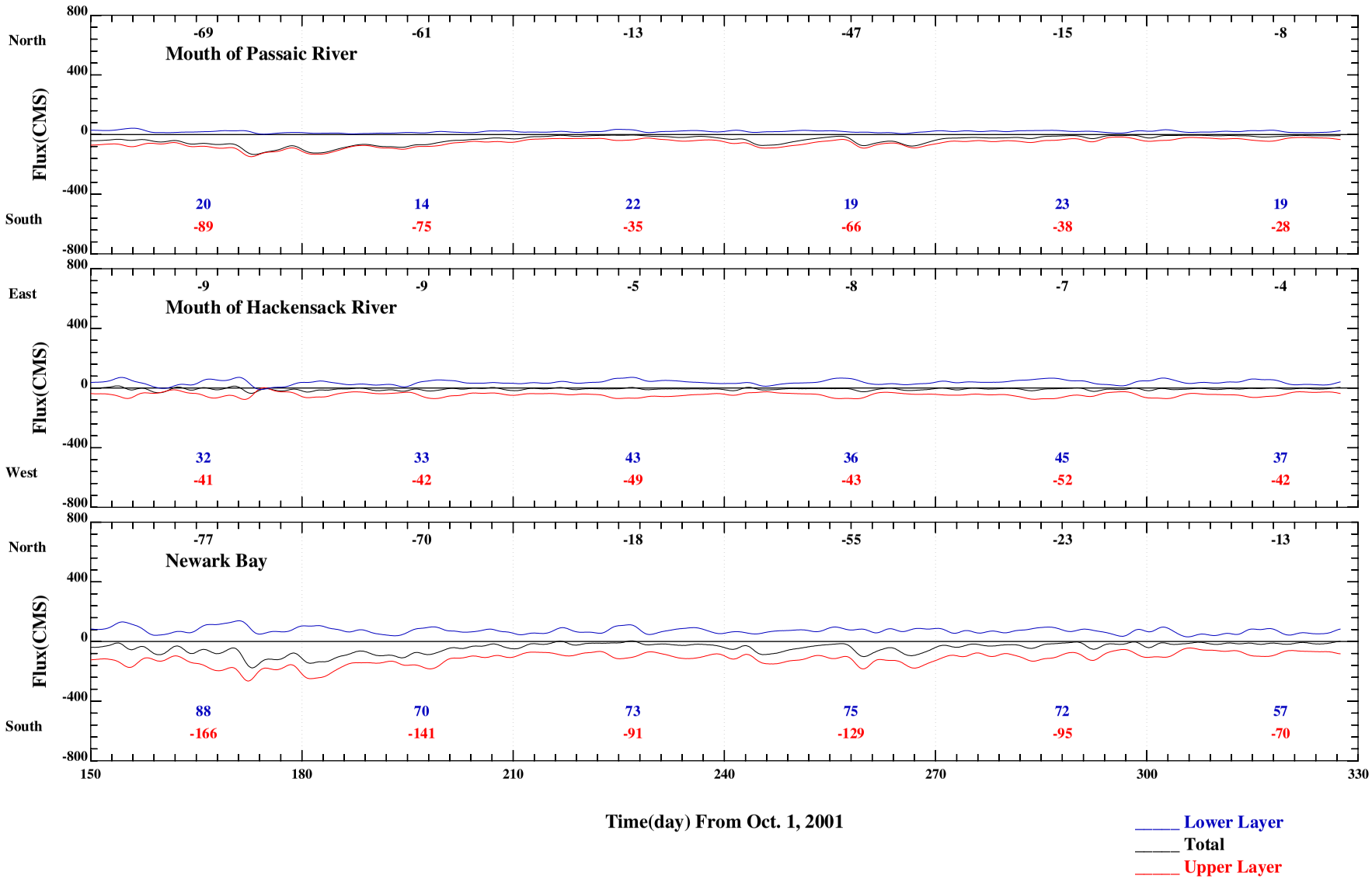

Figure 4-50a Temporal variations of 35 hour low-passed and monthly fluxes through Passaic and Hackensack Rivers, and Newark Bay.

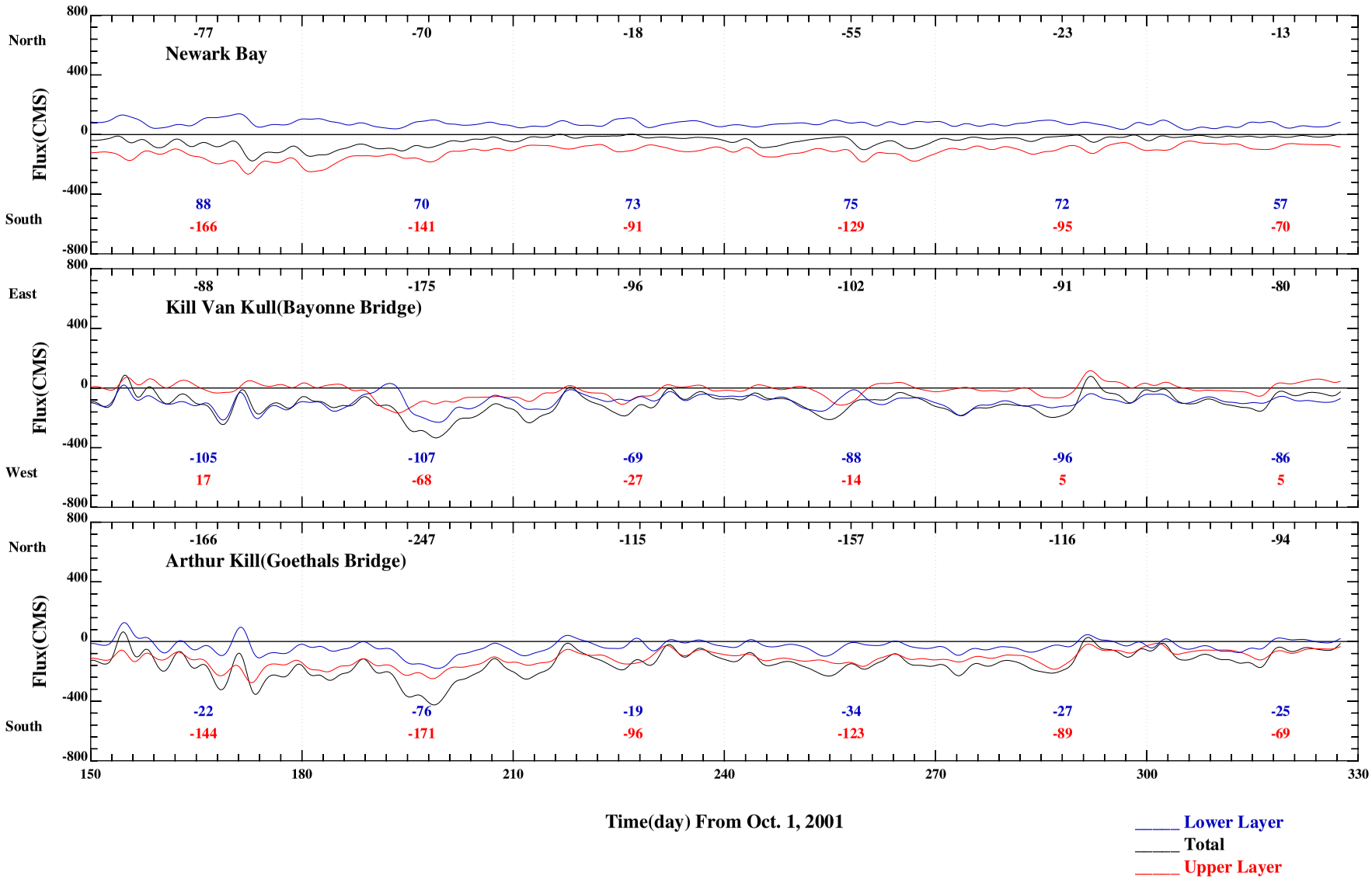

Figure 4-50b Temporal variations of 35 hour low-passed and monthly fluxes through Newark Bay, the Kill van Kull and the Arthur Kill.

SECTION 5

SENSITIVITY

As a part of the calibration process for the LPR hydrodynamic model, several sensitivity runs were conducted to examine the variations of hydrodynamics, i.e. water surface elevations, currents, and temperature and salinity, in response to the selected model parameters. In these sensitivity runs, two important calibration parameters in the model were adjusted: bottom roughness length (Z_0) for bottom stress and the Smagorinsky coefficient (C_S: HORCON) for horizontal mixing. Bottom roughness length, Z_0, controls the bottom friction effect and, hence, the vertical distribution of momentum energy, which, in turn, impacts the level of vertical stratification. The Smagorinsky coefficient (C_S) on the other hand, controls the magnitude of horizontal mixing terms, the horizontal density and momentum gradients, as well as the vertical distribution of density. Commonly, the hydrodynamic model is most responsive to these calibration parameters.

In order to concentrate on the hydrodynamic responses in the LPR, the above-mentioned parameters were only adjusted between RM 0 and 8 during the sensitivity analysis.

5.1 SENSITIVITY TO MODEL PARAMETERS

5.1.1 Bottom Roughness Length

Bottom roughness length (Z_0) represents the characteristics of the bottom sediment, which contributes to the form drag in the bottom boundary layer. The typical value for Z_0 in coastal waters varies from 0.0001 to 0.005 m depending on the type of bottom sediments (Dyer, 1986). This bottom roughness length can affect model-computed fields of water surface elevation and current since in a hydrodynamic model the bottom drag coefficient is directly correlated to sediment grain size. Equation (5-1) shows the formulation used to estimate bottom drag coefficient (C_D) in ECOMSED (Blumberg and Mellor, 1987),

$$C_D = \left[\frac{1}{\kappa} \ln(0.5 * z_b) / z_0 \right]^{-2}, \tag{5-1}$$

where Z_0 is the bottom roughness length, Z_b is the thickness of the grid point nearest the bottom and κ is the von Karman constant. In the above equation, C_D is a function of the local bottom roughness length (Z_0), which is related to sediment grain size (Kamphuis, 1974).

5.1.2 Smagorinsky Coefficient (C_s): HORCON

ECOMSED uses the Smagorinsky formula for calculating horizontal diffusion (A_M) which is expressed as,

$$A_M = C_S \Delta x \Delta y \frac{1}{2} \left| \nabla V + (\nabla V)^T \right|, \tag{5-2}$$

where V is the horizontal velocity vector with components (u, v), ∇ is the horizontal gradient operator, Δx and Δy are the grid spacing, with x increasing eastward and y increasing northward, in a system of orthogonal Cartesian coordinates and

$$\left| \nabla V + (\nabla V)^T \right| \Big/ 2 = \left[(\partial u/\partial x)^2 + (\partial v/\partial x + \partial u/\partial y)^2 / 2 + (\partial v/\partial y)^2 \right]^{1/2}. \tag{5-3}$$

The Smagorinsky coefficient (C_S) is non-dimensional. Values of C_S in the range of 0.10 to 0.20 seem to work well, but, if the grid spacing is small enough (Oey et al., 1985a, b), C_S can be zero. A_M decreases as resolution improves and A_M is small if velocity gradients are small.

5.1.3 Model Sensitivity to Z_0 and C_S

Model sensitivity simulations were conducted using various bottom roughness length and Smagorinsky coefficient values for the period of August through September 2004. The simulations performed with different combinations of the parameters are listed in Table 5-1. 'X' indicates the sensitivity run with the same pair of parameters as those employed for the final model runs. For C_S values larger than 0.1 and smaller than 0.002, the model computation became unstable and crashed. Therefore, the values of C_S for sensitivity runs were selected between 0.005 and 0.075.

Table 5-1. Simulations Performed with Different Combinations of Z_0 and C_S

C_S	Z_0 (m)				
	0.0001	**0.0005**	**0.0010**	**0.0020**	**0.0050**
0.005			X		
0.010	X	X	X	X	X
0.050			X		
0.075			X		

Model sensitivity to the variation in the values of the calibration parameters was examined by comparing the computed water surface elevation, current velocity and temperature/salinity against the observed values at several locations (Figure 4-5). Model/data comparisons were performed at the tidal gauges M1, M3 and M5 for elevation, at ADCP stations M2 and M3 for current velocities and at stations M1, M2, M3, M4, Bridge St. Bridge and M5 for temperature and salinity. The results of the model/data comparisons in terms of the statistical parameters, root mean square error (RMSE), relative RMSE and correlation coefficient for water surface elevations, current velocities and temperature and salinity are presented in the Tables 5-2, 5-3(a-b) and 5-4(a-k), respectively. The numbers of data points used in the statistical analysis are also shown in the tables and the shaded C_S and Z_0 values are the selected parameters for the final model calibration.

Statistically, there are only slight changes in water surface elevation when C_S was held constant (equal to 0.01) and Z_0 was increased from 0.0001 to 0.005 m. This conclusion is evident from the results shown in Table 5-2, with the difference in RMSE values never exceeding 1 cm at all the three tidal gauge stations. When Z_0 was held constant (0.001 m) and C_S was increased from 0.005 to 0.075 m, it was also found that the differences of RMSE values at the three gauges were always less than 1 cm. The results, shown in Table 5-2, clearly indicate that the model computed water surface elevations are not very sensitive to the variation in the values of the calibration parameters.

Tables 5-3(a-b) highlight the outcome of the sensitivity analysis in terms of statistical parameters for current velocity at three depth levels (surface, mid-depth and bottom) at ADCP stations M2 and M3. In contrast to the impact on water surface elevation, increasing mixing in the model reduces the RMSEs and improves the model-data comparisons of current velocity at the two ADCP stations. It shows that the maximum RMSE change can be as large as 2 cm/s. Figure 5-2 shows the sensitivity of model computed current velocities to the variation in the values of C_S and Z_0. The currents at M3 show more significant responses to the changes in model diffusivity than those at M2. As Z_0 or C_S increases, the RMSEs of current velocity decrease by more than 1 cm/s at M3.

Based on the results shown in the Tables 5-3(a-b) and Figure 5-2, it can be concluded that the bottom velocities are more responsive to the variation in the values of the calibration parameters. This observation is supported by the fact that the intensification of horizontal mixing also influences the vertical mixing in estuarine systems. Numerically this occurs through the implementation of the Mellor and Yamada turbulence closure model in the ECOMSED hydrodynamic model which in turn influences the degree of vertical stratification in the water column.

The results of the sensitivity analysis in terms of the statistical parameters for temperature and salinity at the six sampling stations are illustrated in Tables 5-4(a-k). As can

be seen in the table, corresponding to the changes in Z_0 and C_S, the changes of RMSEs are mostly less than 0.1°C except for the changes, related to C_S at the bottom layer of M2, which is about 0.2°C. Due to the larger salinity variability in this portion of the river, the changes of RMSEs between the measured and the computed salinities are relatively large. Most of the changes are one order of magnitude bigger than the changes of the temperature RMSEs. At the bottom layer of M2, the change related to the increase in C_S can be as large as 2.3. Figure 5-3 illustrates the sensitivity of model computed surface and bottom temperature and salinity to the variations in the values of C_S.

Considering that Z_0 and C_S have only been adjusted from RM 0 to RM 8, some downstream stations, M2, M3 and M4, show relatively large RMSE changes and stronger responses to those parameter adjustments as compared to the stations located upstream. Comparing the influence on the temperature and salinity by the Z_0 and C_S adjustments, it is found that the model is more sensitive to the C_S adjustments, especially at the bottom layer. The model output at the upper layer is not quite as sensitive to the variation in the values of the calibration parameters. The temperature and salinity RMSE changes in Tables 5-4(a-k) indicate that large values of C_S produce strong mixing of upstream fresh water and downstream ocean water and are responsible for the largest temperature and salinity changes at the bottom layer of M2 and M3. The above observation can also be understood by comparing the time series of model computed salinities and temperatures for different sensitivity run scenarios. Figures 5-4 and 5-5 illustrate the effect of change of the calibration parameters on the model computed surface and bottom salinities at station M2 over a period of 10 days. Based on the comparison of the time series plots for surface and bottom salinities, it can be concluded that large values of C_S produce the largest salinity changes at the bottom layer of M2. This is also in agreement with the conclusion made earlier based on the statistical analysis of the sensitivity runs.

5.1.4 Summary of Sensitivity to Model Parameters

Based on the statistical parameters in Tables 5-2, 5-3(a-b) and 5-4(a-k), it can be concluded that the model results, in general, are not overly responsive to the changes in the bottom roughness length and Smagorinsky coefficient values. The model computed water surface elevations do not show any significant sensitivity to the variation in the values of the statistical parameters. The current velocities are a little more responsive to the variation in the values of the parameters, with most of the observed response being largely confined to the bottom layer. The changes in horizontal diffusivity do result in significant changes in current and temperature and salinity at the lower layers of the river. Stations M2, M3 and M4 show relatively stronger responses to the bottom roughness length and Smagorinsky coefficient adjustments.

In order to arrive at an optimum combination of the parameter values, a ranking scheme was devised. The ranking scheme involved the averaging of water surface elevation, current and temperature and salinity RMSEs for each combination of Z_0 and C_S in Tables 5-2, 5-3(a-b) and 5-4(a-k). The model performance was then evaluated and ranked for varying Z_0 and C_S, with the lower rank values signifying better performance (i.e., a value of 1 is better than a value of 5). The results obtained from the ranking scheme for water surface elevation, current and temperature and salinity are summarized in Table 5-5 with the last column of the table showing the total rank by adding up the rank's numbers for different variables. The total rank numbers clearly reveal that the selected combination of bottom roughness length and Smagorinsky coefficient for the final model calibration (Z_0 = 0.001 m and C_S = 0.01) is the best (lowest rank) in the group where C_S is held constant and is second best (second lowest) in the group where Z_0 is held constant.

.

Table 5-2. Statistical Comparison of Measured and Computed Elevations (m) where Model Parameters HORCON(C_S) and Z_0 were Varied. The Shaded Values are the Selected Parameters

Location	HORCON (C_S)	Z_0	Number of Observations	RMSE (m)	Correlation Coefficient (R^2)	Relative RMSE (%)
M1	0.01	0.0001	5824	0.15	0.97	5.8
	0.01	0.0005	5824	0.15	0.97	5.8
	0.01	0.001	5824	0.15	0.97	5.8
	0.01	0.002	5824	0.15	0.97	5.8
	0.01	0.005	5824	0.15	0.97	5.8
	0.005	0.001	5824	0.15	0.97	5.8
	0.01	0.001	5824	0.15	0.97	5.8
	0.05	0.001	5824	0.15	0.97	5.8
	0.075	0.001	5824	0.15	0.97	5.8
M3	0.01	0.0001	1417	0.14	0.98	5.7
	0.01	0.0005	1417	0.14	0.98	5.8
	0.01	0.001	1417	0.14	0.98	5.8
	0.01	0.002	1417	0.14	0.98	5.9
	0.01	0.005	1417	0.14	0.98	6.0
	0.005	0.001	1417	0.14	0.98	5.8
	0.01	0.001	1417	0.14	0.98	5.8
	0.05	0.001	1417	0.14	0.98	5.9
	0.075	0.001	1417	0.14	0.98	5.9
M5	0.01	0.0001	6264	0.20	0.92	6.3
	0.01	0.0005	6264	0.19	0.92	6.2
	0.01	0.001	6264	0.19	0.92	6.2
	0.01	0.002	6264	0.19	0.92	6.2
	0.01	0.005	6264	0.19	0.92	6.2
	0.005	0.001	6264	0.19	0.92	6.2
	0.01	0.001	6264	0.19	0.92	6.2
	0.05	0.001	6264	0.19	0.92	6.3
	0.075	0.001	6264	0.19	0.92	6.2

Table 5-3a. Statistical Comparison of Measured ADCP Velocities (m/s) to Computed Results at M2, where Model Parameters HORCON(C_S) and Z_0 were Varied. The Shaded Values are the Selected Parameters

Layer	HORCON (C_S)	Z_0	Number of Observations	RMSE (m/s)	Correlation Coefficient (R^2)	Relative RMSE (%)
Near Surface	0.01	0.0001	2004	0.19	0.89	8.8
	0.01	0.0005	2004	0.19	0.89	9.0
	0.01	0.001	2004	0.19	0.89	9.1
	0.01	0.002	2004	0.19	0.89	9.3
	0.01	0.005	2004	0.20	0.88	9.6
	0.005	0.001	2004	0.19	0.89	9.1
	0.01	0.001	2004	0.19	0.89	9.1
	0.05	0.001	2004	0.19	0.89	9.0
	0.075	0.001	2004	0.19	0.89	9.0
Mid-Depth	0.01	0.0001	3106	0.15	0.86	7.4
	0.01	0.0005	3106	0.15	0.87	7.3
	0.01	0.001	3106	0.14	0.87	7.3
	0.01	0.002	3106	0.15	0.87	7.3
	0.01	0.005	3106	0.15	0.87	7.4
	0.005	0.001	3106	0.15	0.86	7.4
	0.01	0.001	3106	0.14	0.87	7.3
	0.05	0.001	3106	0.14	0.87	7.2
	0.075	0.001	3106	0.14	0.87	7.2
Near Bottom	0.01	0.0001	3074	0.12	0.79	8.6
	0.01	0.0005	3074	0.11	0.80	8.2
	0.01	0.001	3074	0.11	0.80	8.0
	0.01	0.002	3074	0.11	0.80	7.9
	0.01	0.005	3074	0.11	0.80	8.0
	0.005	0.001	3074	0.12	0.77	8.7
	0.01	0.001	3074	0.11	0.80	8.0
	0.05	0.001	3074	0.10	0.84	7.3
	0.075	0.001	3074	0.10	0.84	7.3

Table 5-3b. Statistical Comparison of Measured ADP Velocities (m/s) to Computed Results at M3, where Model Parameters HORCON(C_S) and Z_0 were Varied. The Shaded Values are the Selected Parameters

Layer	HORCON (C_S)	Z_0	Number of Observations	RMSE (m/s)	Correlation Coefficient (R^2)	Relative RMSE (%)
Near Surface	0.01	0.0001	648	0.159	0.853	9.49
	0.01	0.0005	648	0.153	0.859	9.13
	0.01	0.001	648	0.151	0.861	9.00
	0.01	0.002	648	0.150	0.861	8.93
	0.01	0.005	648	0.149	0.858	8.91
	0.005	0.001	648	0.152	0.862	9.08
	0.01	0.001	648	0.151	0.861	9.00
	0.05	0.001	648	0.146	0.857	8.74
	0.075	0.001	648	0.146	0.857	8.71
Mid-Depth	0.01	0.0001	648	0.177	0.787	10.48
	0.01	0.0005	648	0.172	0.796	10.15
	0.01	0.001	648	0.169	0.802	9.96
	0.01	0.002	648	0.167	0.804	9.85
	0.01	0.005	648	0.164	0.807	9.67
	0.005	0.001	648	0.170	0.807	10.04
	0.01	0.001	648	0.169	0.802	9.96
	0.05	0.001	648	0.160	0.802	9.45
	0.075	0.001	648	0.158	0.802	9.36
Near Bottom	0.01	0.0001	648	0.172	0.709	10.51
	0.01	0.0005	648	0.165	0.721	10.09
	0.01	0.001	648	0.163	0.722	9.98
	0.01	0.002	648	0.162	0.721	9.93
	0.01	0.005	648	0.161	0.720	9.83
	0.005	0.001	648	0.177	0.680	10.85
	0.01	0.001	648	0.163	0.722	9.98
	0.05	0.001	648	0.167	0.705	10.18
	0.075	0.001	648	0.167	0.703	10.20

Table 5-4a. Statistical Comparison of Measured and Computed Salinity (psu) at M1, where Model Parameters HORCON (C_S) and Z_0 were Varied. The Shaded Values are the Selected Parameters

Variable	Layer	HORCON (C_S)	Z_0	Number of Observations	RMSE (psu)	Correlation Coefficient (R^2)	Relative RMSE (%)
Salinity	Surface	0.01	0.0001	972	1.7	0.87	9.9
		0.01	0.0005	972	1.7	0.87	9.8
		0.01	0.001	972	1.7	0.88	9.7
		0.01	0.002	972	1.7	0.88	9.7
		0.01	0.005	972	1.7	0.88	9.8
		0.005	0.001	972	1.6	0.88	9.4
		0.01	0.001	972	1.7	0.88	9.7
		0.05	0.001	972	1.8	0.86	10.7
		0.075	0.001	972	1.9	0.85	11.0
	Bottom	0.01	0.0001	709	1.7	0.73	8.9
		0.01	0.0005	709	1.7	0.72	8.8
		0.01	0.001	709	1.7	0.72	8.9
		0.01	0.002	709	1.7	0.71	8.8
		0.01	0.005	709	1.7	0.71	8.8
		0.005	0.001	709	1.7	0.69	8.8
		0.01	0.001	709	1.7	0.72	8.9
		0.05	0.001	709	2.4	0.73	12.4
		0.075	0.001	709	2.6	0.73	13.7

Table 5-4b. Statistical Comparison of Measured and Computed Salinity (psu) at M2, where Model Parameters HORCON (C_S) and Z_0 were Varied. The Shaded Values are the Selected Parameters

Variable	Layer	HORCON (C_S)	Z_0	Number of Observations	RMSE (psu)	Correlation Coefficient (R^2)	Relative RMSE (%)
Salinity	Surface	0.01	0.0001	972	1.8	0.86	10.9
		0.01	0.0005	972	1.8	0.86	10.8
		0.01	0.001	972	1.8	0.86	10.9
		0.01	0.002	972	1.8	0.86	11.0
		0.01	0.005	972	1.8	0.87	11.2
		0.005	0.001	972	1.8	0.85	11.0
		0.01	0.001	972	1.8	0.86	10.9
		0.05	0.001	972	2.0	0.86	12.4
		0.075	0.001	972	2.1	0.86	12.6
	Bottom	0.01	0.0001	1007	3.7	0.51	21.3
		0.01	0.0005	1007	3.8	0.51	22.0
		0.01	0.001	1007	3.9	0.51	22.5
		0.01	0.002	1007	4.0	0.51	23.3
		0.01	0.005	1007	4.3	0.51	24.6
		0.005	0.001	1007	3.4	0.54	19.5
		0.01	0.001	1007	3.9	0.51	22.5
		0.05	0.001	1007	5.5	0.40	31.7
		0.075	0.001	1007	5.6	0.39	32.3

Table 5-4c. Statistical Comparison of Measured and Computed Salinity (psu) at M3, where Model Parameters HORCON (C_S) and Z_0 were Varied. The Shaded Values are the Selected Parameters

Variable	Layer	HORCON (C_S)	Z_0	Number of Observations	RMSE (psu)	Correlation Coefficient (R^2)	Relative RMSE (%)
Salinity	Surface	0.01	0.0001	637	1.5	0.85	12.3
		0.01	0.0005	637	1.5	0.85	12.0
		0.01	0.001	637	1.5	0.85	11.7
		0.01	0.002	637	1.4	0.86	11.4
		0.01	0.005	637	1.4	0.86	11.3
		0.005	0.001	637	1.5	0.85	12.2
		0.01	0.001	637	1.5	0.85	11.7
		0.05	0.001	637	1.7	0.83	13.4
		0.075	0.001	637	1.7	0.82	13.8
	Bottom	0.01	0.0001	369	3.7	0.58	22.9
		0.01	0.0005	369	3.7	0.59	23.4
		0.01	0.001	369	3.8	0.59	23.9
		0.01	0.002	369	3.9	0.59	24.5
		0.01	0.005	369	4.1	0.60	25.8
		0.005	0.001	369	3.3	0.62	20.7
		0.01	0.001	369	3.8	0.59	23.9
		0.05	0.001	369	5.5	0.46	34.2
		0.075	0.001	369	5.6	0.44	35.0

Table 5-4d. Statistical Comparison of Measured and Computed Salinity (psu) at M4, where Model Parameters HORCON (C_S) and Z_0 were Varied. The Shaded Values are the Selected Parameters

Variable	Layer	HORCON (C_S)	Z_0	Number of Observations	RMSE (psu)	Correlation Coefficient (R^2)	Relative RMSE (%)
Salinity	Surface	0.01	0.0001	900	1.1	0.89	9.0
		0.01	0.0005	900	1.1	0.90	8.7
		0.01	0.001	900	1.0	0.90	8.6
		0.01	0.002	900	1.0	0.89	8.7
		0.01	0.005	900	1.1	0.88	9.2
		0.005	0.001	900	1.1	0.89	9.0
		0.01	0.001	900	1.0	0.90	8.6
		0.05	0.001	900	1.3	0.86	11.0
		0.075	0.001	900	1.4	0.86	11.3
	Bottom				No Data		

Table 5-4e. Statistical Comparison of Measured and Computed Salinity (psu) at Bridge St. Bridge, where Model Parameters HORCON (C_S) and Z_0 were Varied. The Shaded Values are the Selected Parameters

Variable	Layer	HORCON (C_S)	Z_0	Number of Observations	RMSE (psu)	Correlation Coefficient (R^2)	Relative RMSE (%)
Salinity	Surface	0.01	0.0001	318	1.1	0.48	17.7
		0.01	0.0005	318	1.1	0.49	17.0
		0.01	0.001	318	1.0	0.50	16.3
		0.01	0.002	318	1.0	0.53	15.6
		0.01	0.005	318	0.9	0.56	14.8
		0.005	0.001	318	1.1	0.52	17.0
		0.01	0.001	318	1.0	0.50	16.3
		0.05	0.001	318	1.1	0.44	17.1
		0.075	0.001	318	1.1	0.44	17.1
	Bottom	0.01	0.0001	98	2.0	0.66	18.6
		0.01	0.0005	98	2.0	0.68	18.0
		0.01	0.001	98	1.9	0.70	17.7
		0.01	0.002	98	1.9	0.71	17.6
		0.01	0.005	98	2.1	0.71	19.1
		0.005	0.001	98	2.0	0.67	18.4
		0.01	0.001	98	1.9	0.70	17.7
		0.05	0.001	98	2.8	0.54	25.1
		0.075	0.001	98	2.8	0.52	25.5

Table 5-4f. Statistical Comparison of Measured and Computed Salinity (psu) at M5, where Model Parameters HORCON (C_S) and Z_0 were Varied. The Shaded Values are the Selected Parameters

Variable	Layer	HORCON (C_S)	Z_0	Number of Observations	RMSE (psu)	Correlation Coefficient (R^2)	Relative RMSE (%)
Salinity	Surface				No Data		
	Bottom	0.01	0.0001	35	1.5	0.11	32.7
		0.01	0.0005	35	1.4	0.11	31.4
		0.01	0.001	35	1.4	0.12	30.3
		0.01	0.002	35	1.4	0.10	30.2
		0.01	0.005	35	1.4	0.12	30.3
		0.005	0.001	35	1.5	0.12	33.8
		0.01	0.001	35	1.4	0.12	30.3
		0.05	0.001	35	1.4	0.13	31.7
		0.075	0.001	35	1.4	0.12	31.4

Table 5-4g. Statistical Comparison of Measured and Computed Temperature (°C) at M1, where Model Parameters HORCON (C_S) and Z_0 were Varied. The Shaded Values are the Selected Parameters

Variable	Layer	HORCON (C_S)	Z_0	Number of Observations	RMSE (°C)	Correlation Coefficient (R^2)	Relative RMSE (%)
Temperature	Surface	0.01	0.0001	1007	1.0	0.77	12.4
		0.01	0.0005	1007	1.0	0.78	12.3
		0.01	0.001	1007	1.0	0.78	12.3
		0.01	0.002	1007	1.0	0.78	12.2
		0.01	0.005	1007	1.0	0.78	12.1
		0.005	0.001	1007	1.0	0.78	12.3
		0.01	0.001	1007	1.0	0.78	12.3
		0.05	0.001	1007	1.0	0.78	12.2
		0.075	0.001	1007	1.0	0.78	12.2
	Bottom	0.01	0.0001	709	0.9	0.85	15.4
		0.01	0.0005	709	0.9	0.85	15.2
		0.01	0.001	709	0.9	0.85	15.3
		0.01	0.002	709	0.9	0.85	15.2
		0.01	0.005	709	0.9	0.85	15.1
		0.005	0.001	709	0.9	0.85	14.9
		0.01	0.001	709	0.9	0.85	15.3
		0.05	0.001	709	1.0	0.82	17.3
		0.075	0.001	709	1.0	0.81	18.1

Table 5-4h. Statistical Comparison of Measured and Computed Temperature (°C) at M2, where Model Parameters HORCON (C_S) and Z_0 were Varied. The Shaded Values are the Selected Parameters

Variable	Layer	HORCON (C_S)	Z_0	Number of Observations	RMSE (°C)	Correlation Coefficient (R^2)	Relative RMSE (%)
Temperature	Surface	0.01	0.0001	1007	1.1	0.73	13.9
		0.01	0.0005	1007	1.1	0.73	13.8
		0.01	0.001	1007	1.1	0.73	13.9
		0.01	0.002	1007	1.1	0.73	13.9
		0.01	0.005	1007	1.1	0.73	14.0
		0.005	0.001	1007	1.1	0.73	13.8
		0.01	0.001	1007	1.1	0.73	13.9
		0.05	0.001	1007	1.1	0.73	14.0
		0.075	0.001	1007	1.1	0.73	14.1
	Bottom	0.01	0.0001	1007	1.1	0.73	14.2
		0.01	0.0005	1007	1.1	0.73	14.3
		0.01	0.001	1007	1.2	0.73	14.5
		0.01	0.002	1007	1.2	0.72	14.6
		0.01	0.005	1007	1.2	0.72	14.9
		0.005	0.001	1007	1.1	0.75	13.7
		0.01	0.001	1007	1.2	0.73	14.5
		0.05	0.001	1007	1.3	0.68	16.2
		0.075	0.001	1007	1.3	0.67	16.4

Table 5-4i. Statistical Comparison of Measured and Computed Temperature (°C) at M4, where Model Parameters HORCON (C_S) and Z_0 were Varied. The Shaded Values are the Selected Parameters

Variable	Layer	HORCON (C_S)	Z_0	Number of Observations	RMSE (°C)	Correlation Coefficient (R^2)	Relative RMSE (%)
Temperature	Surface	0.01	0.0001	935	1.3	0.66	15.5
		0.01	0.0005	935	1.3	0.66	15.5
		0.01	0.001	935	1.3	0.66	15.5
		0.01	0.002	935	1.3	0.66	15.5
		0.01	0.005	935	1.3	0.66	15.5
		0.005	0.001	935	1.3	0.66	15.5
		0.01	0.001	935	1.3	0.66	15.5
		0.05	0.001	935	1.3	0.66	15.5
		0.075	0.001	935	1.3	0.66	15.5
	Bottom				No Data		

Table 5-4j. Statistical Comparison of Measured and Computed Temperature (°C) at Bridge St. Bridge, where Model Parameters HORCON(C_S) and Z_0 were Varied. The Shaded Values are the Selected Parameters

Variable	Layer	HORCON (C_S)	Z_0	Number of Observations	RMSE (°C)	Correlation Coefficient (R^2)	Relative RMSE (%)
Temperature	Surface	0.01	0.0001	335	1.6	0.45	31.2
		0.01	0.0005	335	1.6	0.45	31.1
		0.01	0.001	335	1.6	0.45	31.1
		0.01	0.002	335	1.6	0.44	31.1
		0.01	0.005	335	1.6	0.44	31.1
		0.005	0.001	335	1.6	0.45	31.1
		0.01	0.001	335	1.6	0.45	31.1
		0.05	0.001	335	1.6	0.44	31.1
		0.075	0.001	335	1.6	0.44	31.1
	Bottom	0.01	0.0001	400	1.8	0.53	22.1
		0.01	0.0005	400	1.8	0.52	22.1
		0.01	0.001	400	1.8	0.52	22.1
		0.01	0.002	400	1.8	0.52	22.1
		0.01	0.005	400	1.8	0.52	22.1
		0.005	0.001	400	1.8	0.53	21.9
		0.01	0.001	400	1.8	0.52	22.1
		0.05	0.001	400	1.8	0.52	22.3
		0.075	0.001	400	1.8	0.52	22.3

Table 5-4k. Statistical Comparison of Measured and Computed Temperature (°C) at M5, where Model Parameters HORCON (C_S) and Z_0 were Varied. The Shaded Values are the Selected Parameters

Variable	Layer	HORCON (C_S)	Z_0	Number of Observations	RMSE (°C)	Correlation Coefficient (R^2)	Relative RMSE (%)
Temperature	Surface				No Data		
	Bottom	0.01	0.0001	35	1.3	0.78	42.9
		0.01	0.0005	35	1.3	0.78	42.8
		0.01	0.001	35	1.3	0.78	42.8
		0.01	0.002	35	1.3	0.78	42.8
		0.01	0.005	35	1.3	0.78	42.7
		0.005	0.001	35	1.3	0.78	42.7
		0.01	0.001	35	1.3	0.78	42.8
		0.05	0.001	35	1.3	0.77	43.1
		0.075	0.001	35	1.3	0.78	43.0

Table 5-5. Ranks based on the Water Surface Elevation, Current and Temperature and Salinity RMSEs for each Combination of Z_0 and C_s in Tables 5-2, 5-3, and 5-4

Z_0 (m)	C_S	Elevation	Current	T/S	Total Rank
0.0001	0.010	3	7	4	14
0.0005	0.010	2	6	2	10
0.0010	0.010	4	3	3	10
0.0020	0.010	5	3	5	13
0.0050	0.010	8	5	6	19
0.0010	0.005	1	7	1	9
0.0010	0.050	6	2	7	15
0.0010	0.075	6	1	8	15

5.2 GRID CONVERGENCE TEST

Proper computation grid design and its grid resolution are essential elements of a successful modeling study. Often times, the grid resolution used in a modeling study is determined by the level of accuracy required within the overall modeling objectives. Usually the finer the grid resolution is, the more accurate the results computed by the model will be. However, how much finer a grid resolution one can afford is usually limited by the computational resources available for the study. For example, one may not be able to afford to perform simulations of a one month period if it requires several days to a few weeks of computation time. Therefore a balance must be achieved between the "number" of grid cells (i.e., high resolution) versus the "clock-time" required to complete a simulation. It is often a difficult task to determine 'How much is enough' as far as the grid resolution is concerned. For the current modeling study of the Lower Passaic River, a computational grid was designed with four lateral grid cells covering the downstream section of the LPR. The average grid size is about 40m x 150m between RM 0 to RM 5 (Figure 5-6). With this grid resolution, most of the lateral variation of the bathymetric features including shallow and relatively deep areas, including the historical navigational channel in the downstream five miles are reasonably represented. A grid convergence test was conducted to determine whether this resolution is adequate enough to resolve the complicated hydrodynamic features of the study area.

For the practical operation of this grid-convergence test, a subset of the entire model domain was prepared covering only the Kills and Newark Bay as well as the LPR and Hackensack River sections. The lower eight miles of the LPR section of the grid were doubled in resolution both in lateral and longitudinal directions. A zoomed-in view of the high resolution grid is shown in Figure 5-7. Bathymetry of the high resolution grid was configured with the 2004 USACE bathymetric survey data

Two one-month periods, April 1996 and August 2004, were selected to evaluate the grid-convergence test. In the spring and summer of 1996, TSI conducted a field survey program including transect surveys of vertical velocity profiles as well as temperature and salinity casts. IMCS field data collected in the LPR in the summer of 2004 was used for the comparison of model performances. Open boundary conditions at the Kills and freshwater inflows were extracted from archives of the results of the original model for the same period. Both the original and high resolution grids were configured with the same boundary forcing data.

5.2.1 Model Results

Each model was run for one month and the model results were compared at select locations where field sampling stations were located. Computed surface elevations, current

velocities at depths, and surface and bottom salinity were compared with data as well as between two models. Statistical analyses were also conducted to cross compare the model performances. It is found during the test that there were no meaningful differences in computed water temperature by both grids so discussion on the water temperature is omitted.

5.2.2 Elevations

Table 5-6 lists the statistical analysis of model computed and observed elevations at three pressure sensor stations in the LPR in August 2004. The results of both the original and high resolution grids are shown for comparison in the table. The table indicates that RMSEs for water elevations improve with the high resolution grid but the improvements are less than 1cm at M1 and M2 and a little more than 1 cm at M5. Correlation coefficients (R^2) are identical between the water surface elevations computed by the original and high resolution grids at all stations. Figure 5-8 also indicates that there are no differences in model results as far as the surface water elevations are concerned.

5.2.3 Current Velocity

Figure 5-9 shows the comparison of vertical profiles of current velocities at two transect locations in 1996 (Transect 10 at RM 3 and Transect 15 at RM 4.5), in which the left frame depicts the current velocities computed by the original grid and the right frame shows the result of the high resolution grid. Two periods were shown in Figure 5-9: one during flood and the other during ebb currents. The vertical profiles depict the transects looking upstream. The approximate positions in river miles of each transect are also shown along the figures. Circles in the figures depict the measured current velocities at various points in the lateral section of each transect. Positive values indicate the upstream currents and negative values are downstream currents. The figures indicate that with twice the number of grid cells in the lateral direction, the high resolution grid produced a more detailed distribution of current velocities. However, the original grid also produced relatively the same level lateral structure of current velocities and the magnitudes of the computed current velocities are comparable. Currents velocities at few locations where river bends are shown in Figure 5-10. In rivers, these bends typically exhibit more lateral velocity structures during high flow events as compared to the relatively straight sections. The locations of these cross sections are shown in Figure 5-1. As the Figure 5-10 indicates, there are relatively strong lateral current structures at these locations than those shown in earlier figures at Transect 10 and 15. Although results from the high resolution grid shows more details of the velocity profile as compared to results from the original grid, the basic quantitative and qualitative features of the velocity profile remain the same. The velocity profiles from both the original and double grid shows similar distribution in the vertical direction and the velocity values are

in the same range. These observations indicate that the high resolution and the original grids show quite comparable general behavior of the velocity profiles.

Time series of current velocities at M2 computed by both the original and high resolution grids are shown with observed currents at depths in Figure 5-11. For visual clarity, only the five days of worth of results are presented. The figure indicates that there are only slight differences in computed velocities between the two versions of the model grid and that the differences in computed current velocities at the bottom are greater than at the surface. The differences are minimal in the mid-depth. Table 5-7 lists the statistical analysis of model computed current velocities and observed current velocities at depths at M2. The results indicate that RMSEs are nearly identical for both grids near the bottom at station M2 but that the correlation coefficient improved for the high resolution grid; 0.80 for the original grid versus 0.86 for the high resolution grid. At mid-depth and near surface, the statistics of model-data comparison shows that high resolution grid produced better RMSE by 2 cm/sec but resulted in the same correlation coefficients. The percent RMSE is 1% better for the high resolution grid. Figure 5-12 compares the time series of bottom velocity generated by the original and the high resolution grids at three shallow locations in the Harrison Reach. For the sake of comparison, the velocity generated by the parent cell of the original grid was compared against the average of velocities generated by the two daughter cells that share the same interface (in terms of the location of velocity computation in ECOMSED). The present discussion focuses only on the bottom velocities because the discussion is driven by the need to address the question: What is the sensitivity of bottom shear stress (or bottom velocities) to the grid resolution? The sensitivity of bottom shear stress to grid resolution is of significance here because the bottom shear stresses dictate the erosion and deposition of the contaminated sediments. As can be seen in the Figure 5-12, both the original and the high resolution grid show very similar bottom velocity structures, with the difference in bottom velocities never exceeding 0.05 m/s. The maximum ebb and flood current velocities generated by the two grids are quite similar. It is to be noted that since the water depth of the cells in the original grid and the double grid are not identical, some differences in the prediction of bottom velocities by the two grids are expected. The velocity difference is minimum at location 3 and maximum at location 1. This observation is in good standing with the differences between the original and the double grid depths, with the minimum depth difference occurring at location3 and the maximum at location1.

5.2.4 Salinity

Figure 5-13 shows the comparison of vertical profiles of salinity at two transect locations in 1996 (Transect 10 at RM 3 and Transect 15 at RM 4.5), in which the left frame depicts the salinity computed by the original grid and the right frame shows the result of the high resolution grid. The vertical profiles depict the transects looking upstream. The figures

indicate that with twice the number of grid cells in the lateral direction, the high resolution grid produced a more detailed distribution of salinity, both in lateral and vertical directions. However, the original grid also produced about the same level of lateral structure in the salinity. The spatial distribution of the salinity contours for both grids are comparable. Figure 5-14 shows the hourly computed and observed salinity, where available, at six locations for the surface and the bottom in 2004. The plots indicate that there are no significant differences in computed salinity by the original and high resolution grids at the upstream stations. However, at the downstream locations at M1 and M2, particularly at the bottom, the high resolution grid compared better against the observed salinity. However, at most locations, the differences in computed salinities are less than 1 psu.

Figure 5-15 shows the vertical profile of salinity along the longitudinal section of the LPR from RM 0 through RM 7 in 2004. The upper panel shows the vertical profile of salinity computed by the original grid while the lower panel presents the results from the high resolution grid. In each panel, observed salinity values are also posted. The colors of each circle correspond to the observed value of salinity. Three different hours within a tidal cycle are shown in the figures: maximum ebb, slack before flood, and maximum flood (Figure 5-15). The figures show that both the original and high resolution model performed well reproducing observed salinity in the lower seven miles of the LPR. While there are slight differences in the position of each contour line of salinity both in the horizontal and vertical positions between the two grids, overall, there is no significant disagreement in the positions of the salinity contours between the two grids.

Table 5-8 presents the statistical analysis of model computed and observed salinity at the surface and the bottom at six IMCS field sampling locations. The table provides mixed results for salinity. At M1 and M3, the high resolution grid produced better RMSEs and correlation coefficients compared to those computed by the original grid at both surface and the bottom. However, at M2, the high resolution grid produced larger RMSE and smaller correlation coefficients compared to the results from the original grid. However, the differences between the original and high resolution grids for RMSE are less than 0.5 psu at all stations both at surface and the bottom. The differences in correlation coefficients are less than 0.06.

5.2.5 Bottom Shear Stress

Bottom shear stresses computed by the original and high resolution grids are shown in Figure 5-16. The plots depict hourly averaged bottom shear stresses in dyne-cm^{-2} from the mouth of the LPR to about RM 8 during a maximum flooding condition. The high resolution grid results have been spatially averaged (i.e., each of four high resolution grid cells have been aggregated or spatially-averaged) to provide a direct comparison against the bottom sheer stresses computed by the original LPR grid. The plots indicate that around

RM 4 and 5 (near the upper end of the Harrison Reach) the bottom shear stresses are relatively higher than other locations. The high resolution grid produced relatively detailed variation of bottom shear stresses compared to the ones by the original grid. However, both grids reproduce the similar pattern of spatial distribution of bottom shear stresses for both areas of high bottom shear stress as well as the low bottom stress in the lower section of the LPR.

5.2.6 Tracer Simulations: Estimates of flushing time

For the final test of the grids, a tracer run was conducted for each period to estimate the residence time (flushing time) of the LPR. The entire LPR was initially filled with a conservative tracer with an initial concentration of 1 mg/l. The models were run for 10 days. The change in mass is computed as the ratio of the mass at a given time (M) divided by the initial mass, M_o. The flushing time has been defined according to the e-folding time of the total mass of the tracer in the LPR (e.g. Hagy, Boynton and Sanford, 2000). The results of the tracer simulations in 1996 and 2004 are shown in Figure 5-17. As the figure indicates, there are no significant differences in flushing times between the two models. Both models show similar e-folding times of the total mass of the tracer for both simulation periods: around 1.2 days in 1996 and 2.5 days in 2004. The net differences in the flushing time estimates between the two models are less than a few hours.

5.2.7 Summary of Grid Convergence Test

A grid convergence test for the LPR region was conducted to quantify the model performances between the original grid designed for the LPR study and a high resolution grid (doubled its resolution both in lateral and longitudinal directions). The various model outputs were compared statistically and graphically. The results indicate that the high resolution grid shows improvement of model performance compared to the lower resolution grid. However, the improvements are minor and some times the lower resolution grid performed as well as the high resolution grid despite the fact that the high resolution grid requires roughly eight times longer computational time (factor of four for the increased number of grids cells and another factor of two for the requirement of a smaller computational timestep to maintain stability for the high resolution grid). Therefore, the overall assessment of the results indicates that the original grid designed for the LPR study is adequate to address the hydrodynamics in the system.

Table 5-6. Statistical Comparisons of Original LPR Grid and High Resolution Grid Model Results with Rutgers DOT1 Survey Data for Elevations

		Original LPR Grid			High Resolution Grid		
Station	**No. Data**	**RMSE(m)**	**R^2**	**RMSE (%)**	**RMSE(m)**	**R^2**	**RMSE (%)**
M1	2801	0.14	0.97	5.8	0.13	0.98	5.8
M3	938	0.14	0.97	5.9	0.14	0.97	5.8
M5	2810	0.16	0.95	6.1	0.17	0.95	6.5

Table 5-7. Statistical Comparisons of Original LPR Grid and High Resolution Grid Model Results with Rutgers DOT1 Survey Data for ADCP at M2

Distance From		**Original LPR Grid**			**High Resolution Grid**		
Bottom(m)	**No. Data**	**RMSE(m/s)**	**R^2**	**RMSE (%)**	**RMSE(m/s)**	**R^2**	**RMSE (%)**
3.62	844	0.23	0.89	12.4	0.21	0.89	11.6
2.12	1392	0.15	0.86	9.1	0.14	0.88	8.3
0.37	1389	0.11	0.80	11.7	0.11	0.86	11.2

Table 5-8. Statistical Comparisons of Original LPR Grid and High Resolution Grid Model Results with Rutgers DOT1 Survey Data for Salinity

			Original LPR Grid			High Resolution Grid		
Station	**Layer**	**No. Data**	**RMSE(psu)**	**R^2**	**RMSE (%)**	**RMSE(psu)**	**R^2**	**RMSE (%)**
M1								
	Surface	428	1.60	0.88	10.90	1.43	0.89	9.76
	Bottom	371	1.61	0.64	15.35	1.29	0.69	12.33
M2								
	Surface	428	2.01	0.86	12.32	2.09	0.88	12.79
	Bottom	456	4.44	0.45	25.72	4.73	0.43	27.43
M3								
	Surface	415	1.61	0.83	12.88	1.43	0.87	11.39
	Bottom	153	3.42	0.60	21.75	3.53	0.61	22.45
M4								
	Surface	428	1.30	0.88	10.78	1.21	0.90	10.04
Bridge St.								
	Bottom	64	1.92	0.76	17.48	2.22	0.70	20.18

5.3 SENSITIVITY TO FRESHWATER INFLOWS IN THE HACKENSACK RIVER

Although it was not vigorously pursued as revisions to the final model calibration report were made, initial model calibration efforts included the simulation of water year 1995, comparing the model results with the data collected by Battelle as part of the SWEM study. In earlier runs, model computed salinity in the Hackensack River was higher than observed salinity at all Hackensack River stations. Figure 5-19 shows the model results at three upstream stations. These stations are located about 13 miles from the mouth of the river. The model over-computes salinity by as much as 5 psu. A careful examination of model configuration and input data, such as freshwater inflows, was conducted. There is confidence that the model accounts for all available freshwater sources, such as the flow over the Oradell Dam, wastewater effluent from the three municipal sewage treatment plants including the Bergen County Utility Authority Secaucus and North Bergen plants, as well as CSO/SWO runoff estimates based on RAINMAN rainfall-runoff model. A literature search on the freshwater budget yielded no additional sources of freshwater (Carswell et al., 1976).

However, based on a close examination of freshwater inflows from the Third River discussed in Section 3.5.3, possible groundwater inflow associated with post-rainfall infiltration to the course of the river bed along the length of the river may be unaccounted for in the Hackensack River below the Oradell Dam. This may be a reasonable assumption given the low percent imperviousness of the Hackensack River basin and given elevation gradients within the watershed. A number of sensitivity runs were conducted to estimate the freshwater deficit. It was found that if the model was configured with an additional 100 cfs of freshwater inflow to the Hackensack River (in addition to the flow over the Oradell Dam, three sewage treatment inflows, and CSO/SWO inflows computed by RAINMAN), the model computed salinity would compare favorably to the observed data. Figure 5-19 shows the results of the sensitivity run assuming 100 cfs additional inflow. As a consequence, all model runs presented in this study assume the existence of the additional, as yet undefined, source of freshwater. Further investigation of the freshwater budget in the Hackensack River basin would be required to better quantify and support this model assumption.

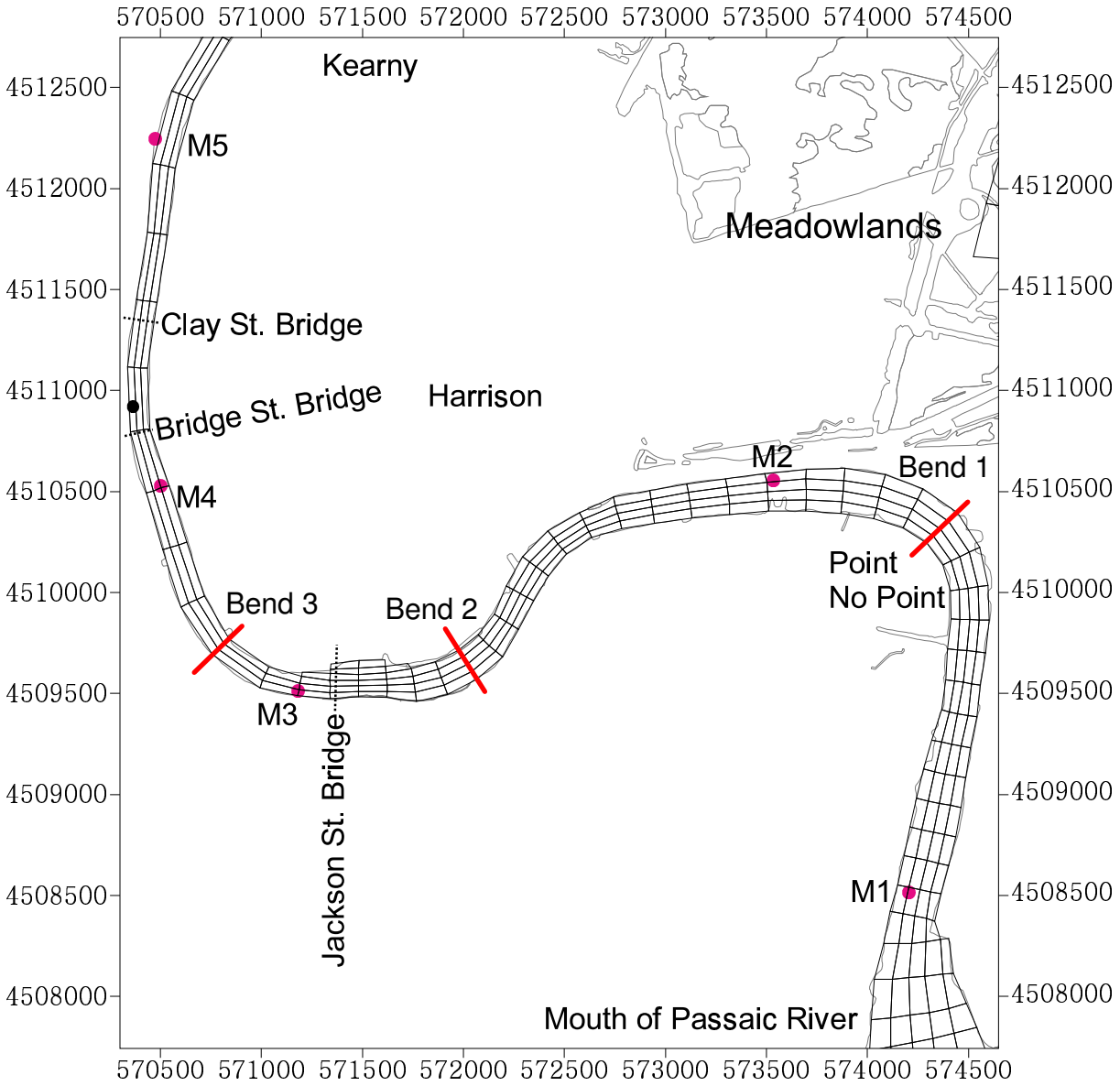

Figure 5-1 Locations of IMCS field sampling stations in the Lower Passaic River (2004)

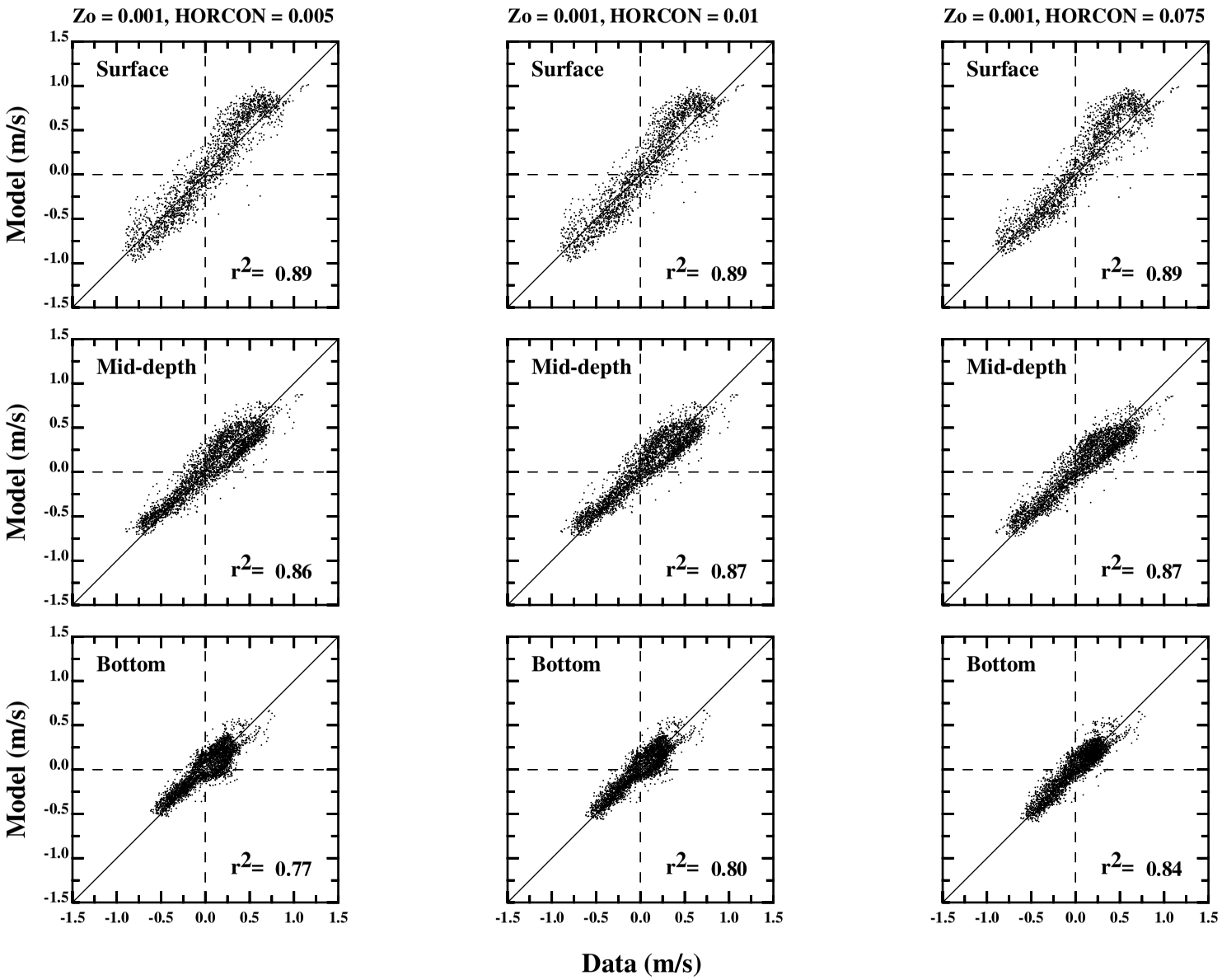

Figure 5-2 Scatter plot of computed current velocities with observed data for sensitivity to Cs and Zo.

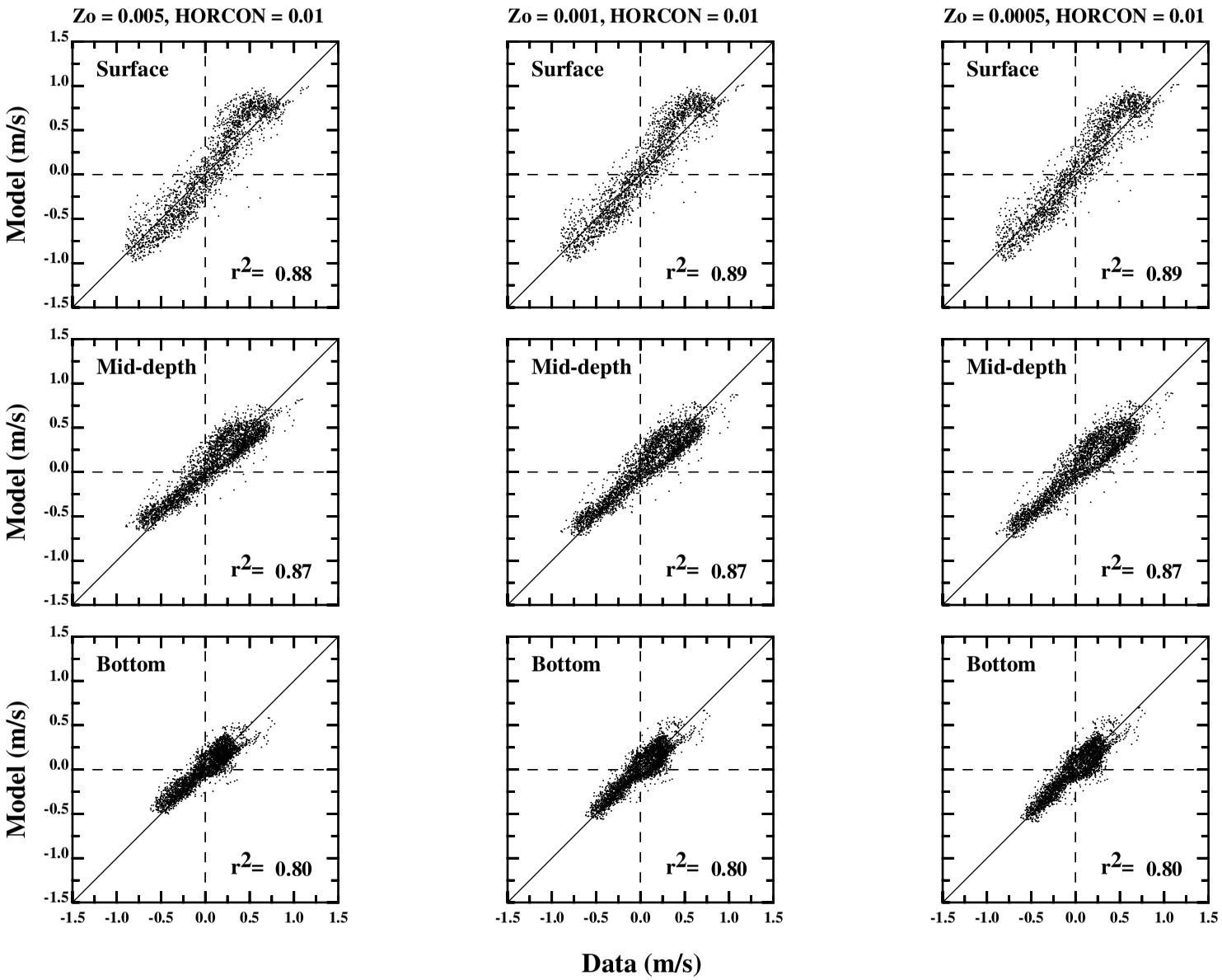

Figure 5-2 Scatter plot of computed current velocities with observed data for sensitivity to Cs and Zo (continued)

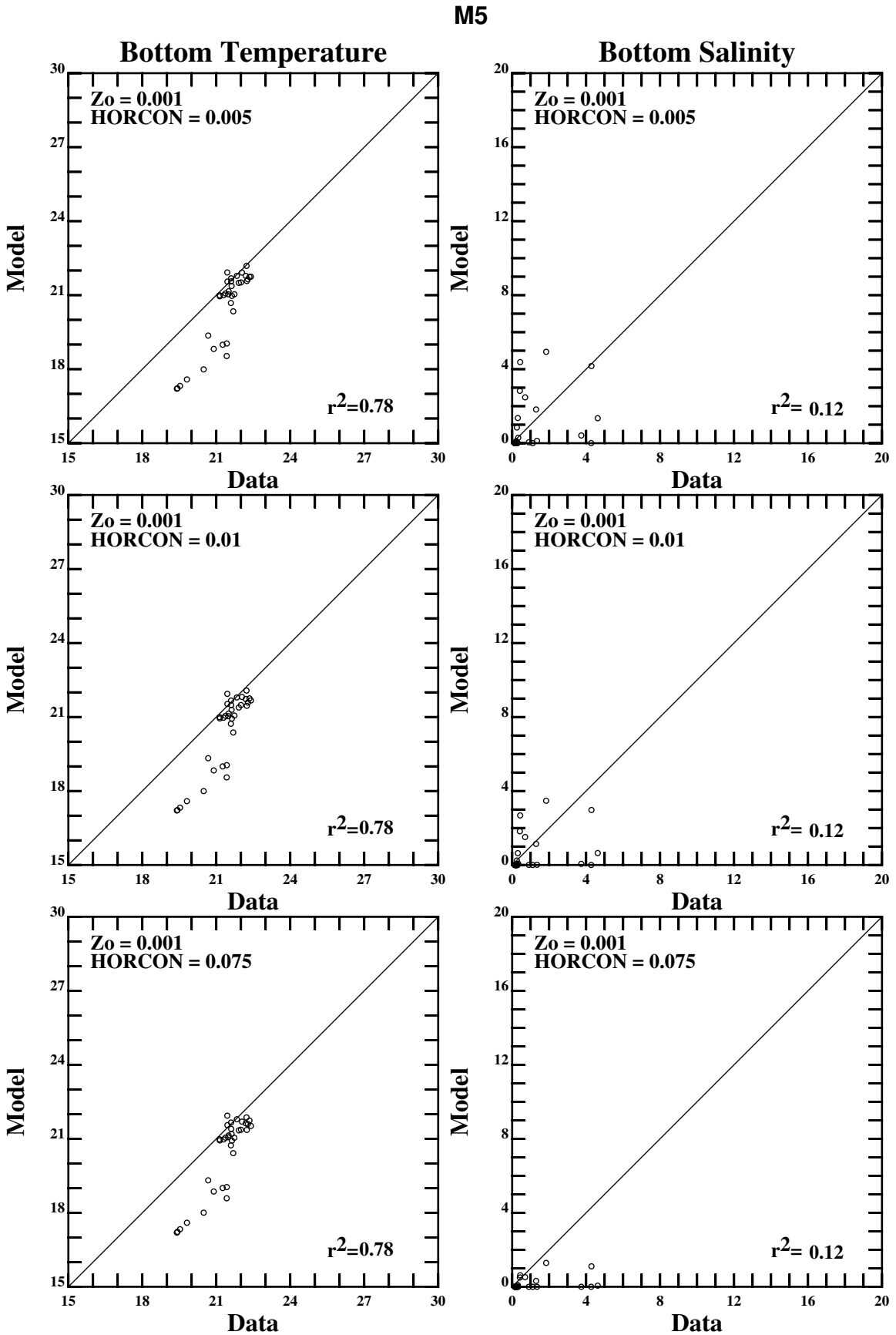

Figure 5-3 Scatter plot of computed surface and bottom temperature and salinity with observed data for sensitivity to Cs

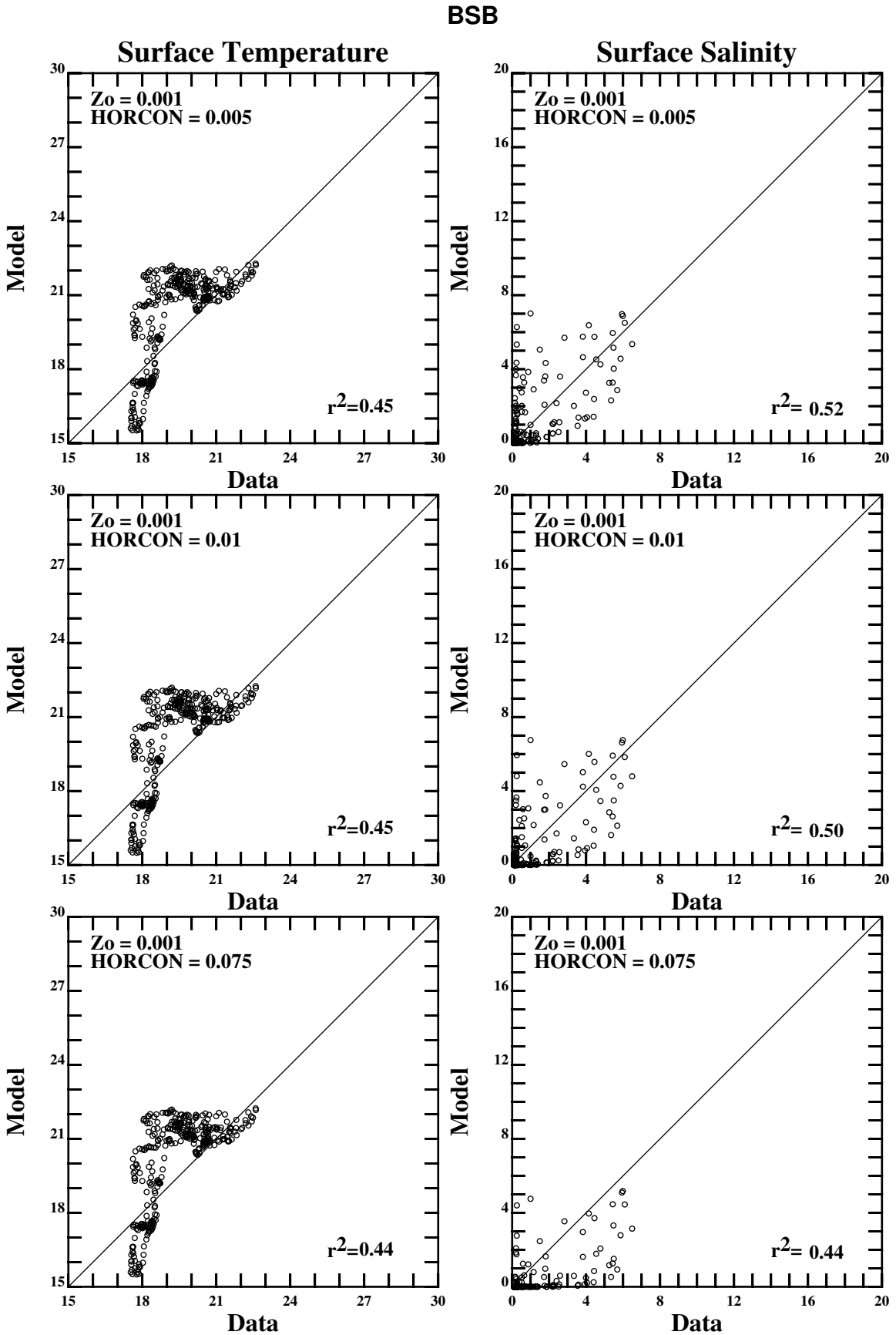

Figure 5-3 Scatter plot of computed surface and bottom temperature and salinity with observed data for sensitivity to Cs (continued)

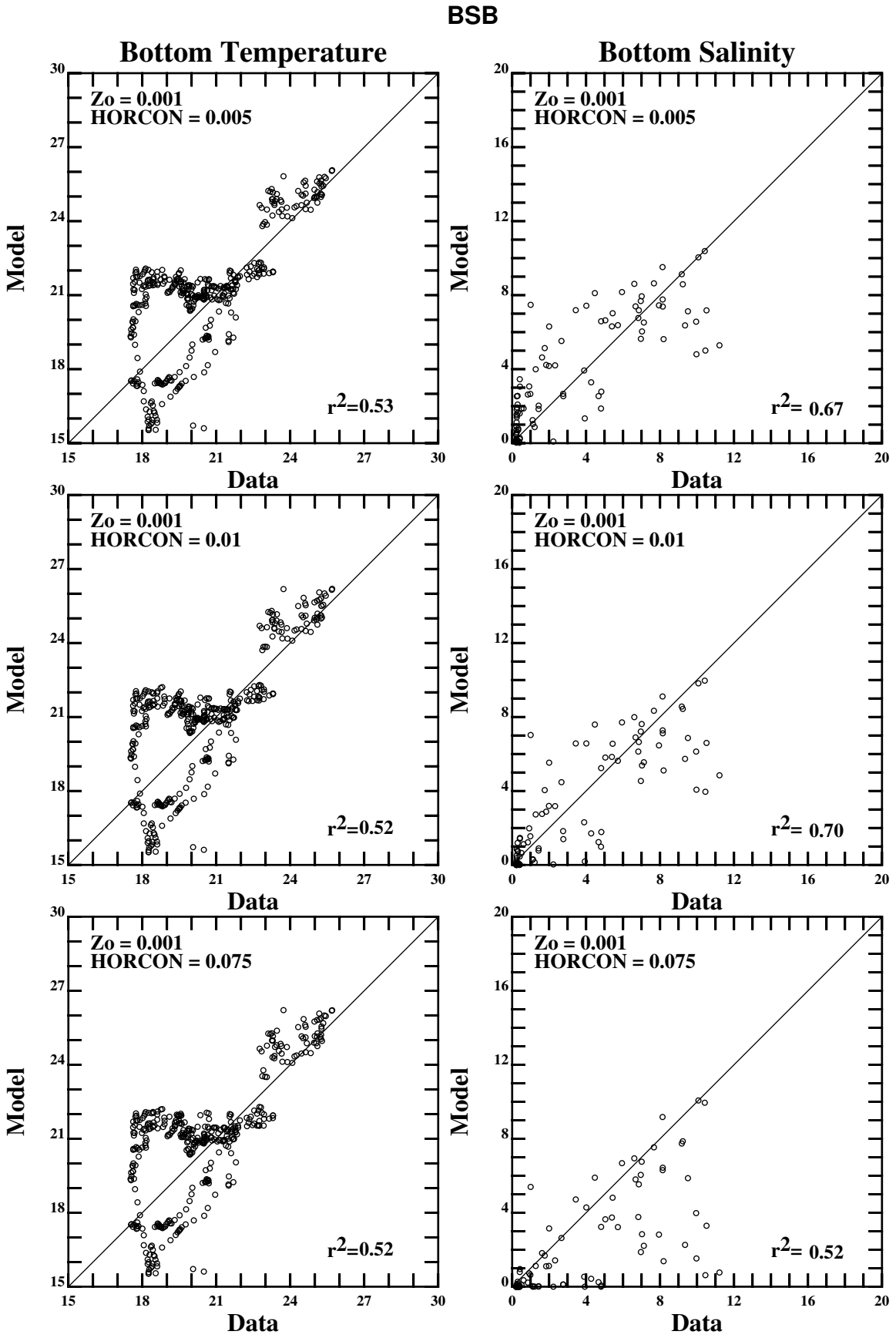

Figure 5-3 Scatter plot of computed surface and bottom temperature and salinity with observed data for sensitivity to Cs (continued)

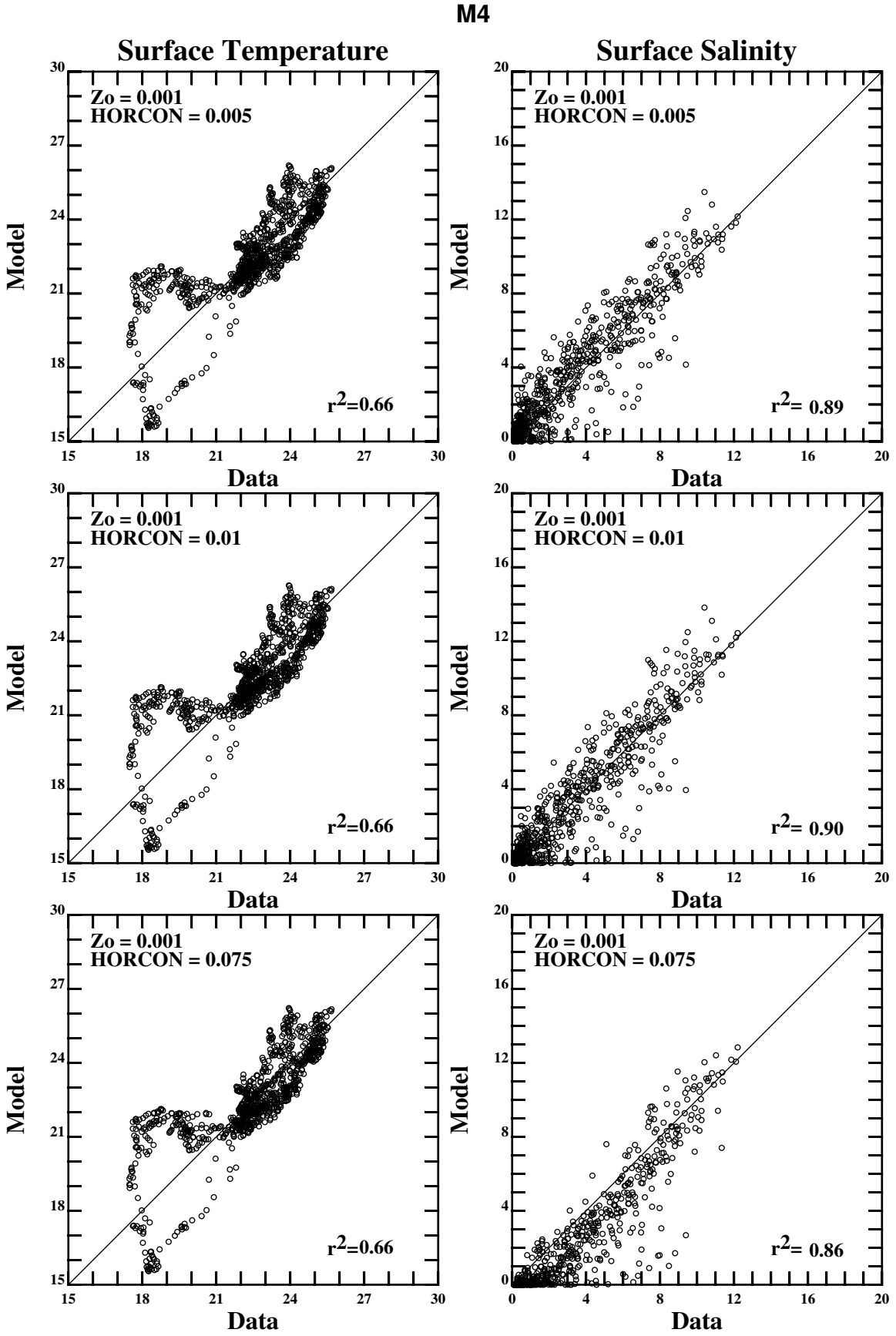

Figure 5-3 Scatter plot of computed surface and bottom temperature and salinity with observed data for sensitivity to Cs (continued)

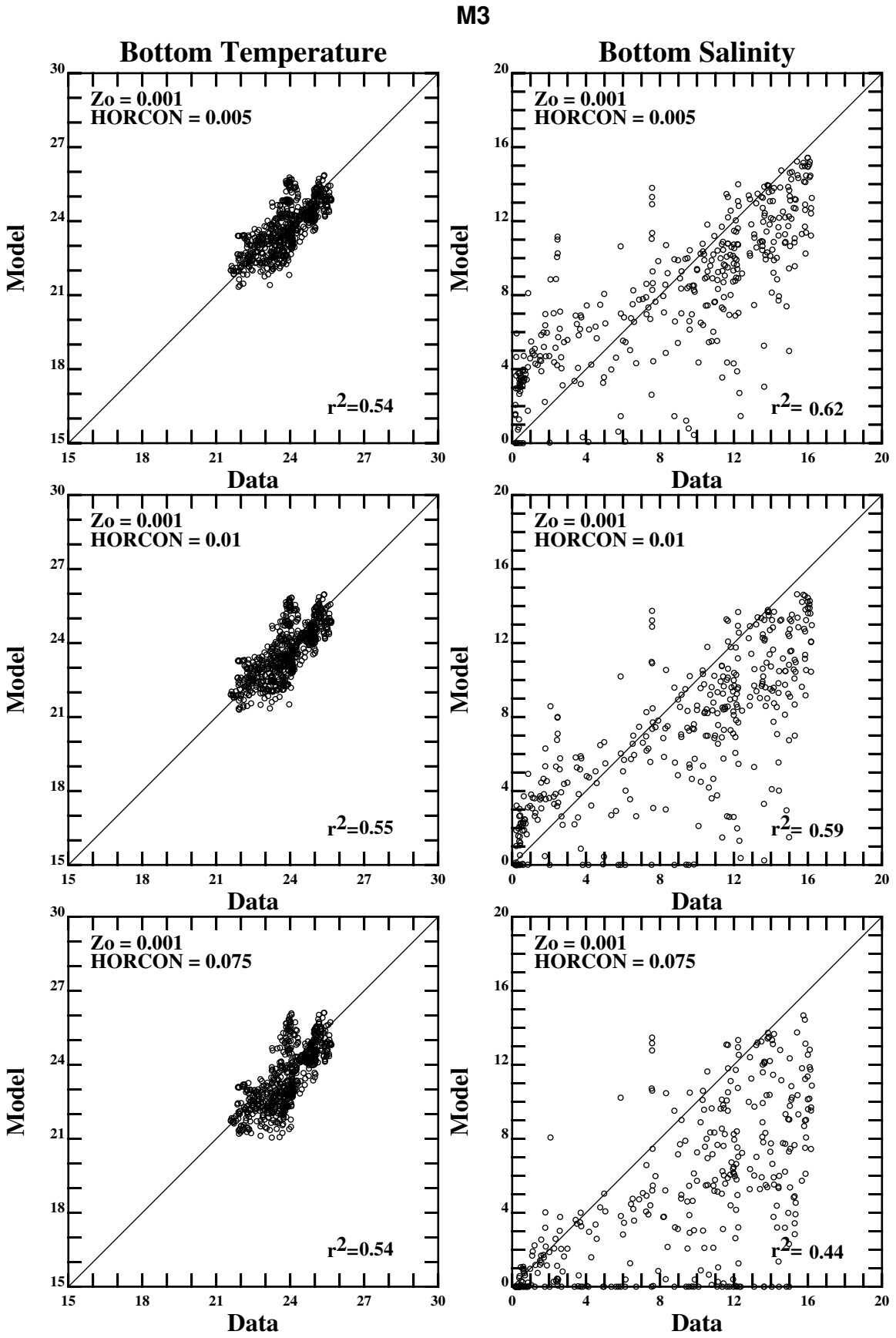

Figure 5-3 Scatter plot of computed surface and bottom temperature and salinity with observed data for sensitivity to Cs (continued)

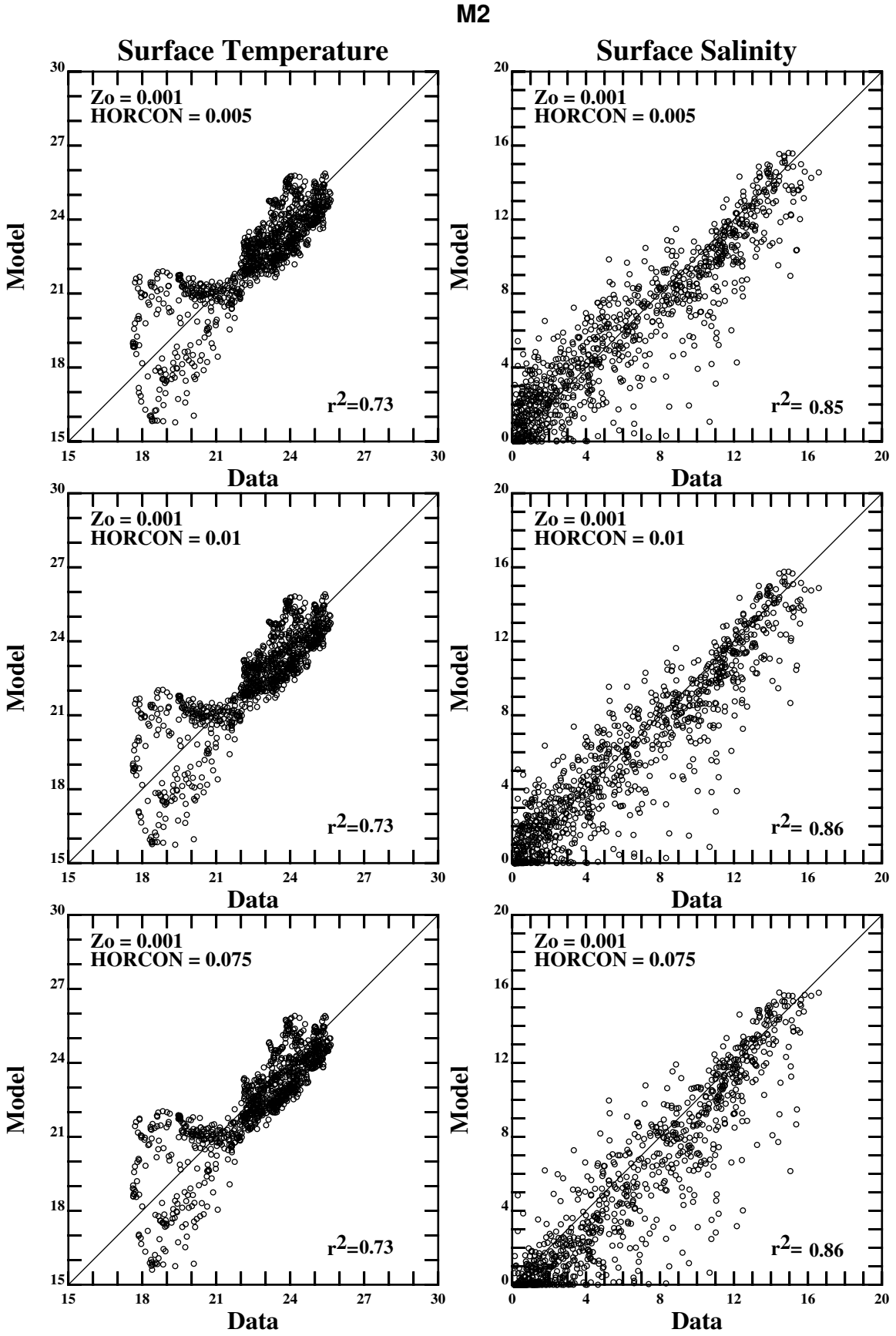

Figure 5-3 Scatter plot of computed surface and bottom temperature and salinity with observed data for sensitivity to Cs (continued)

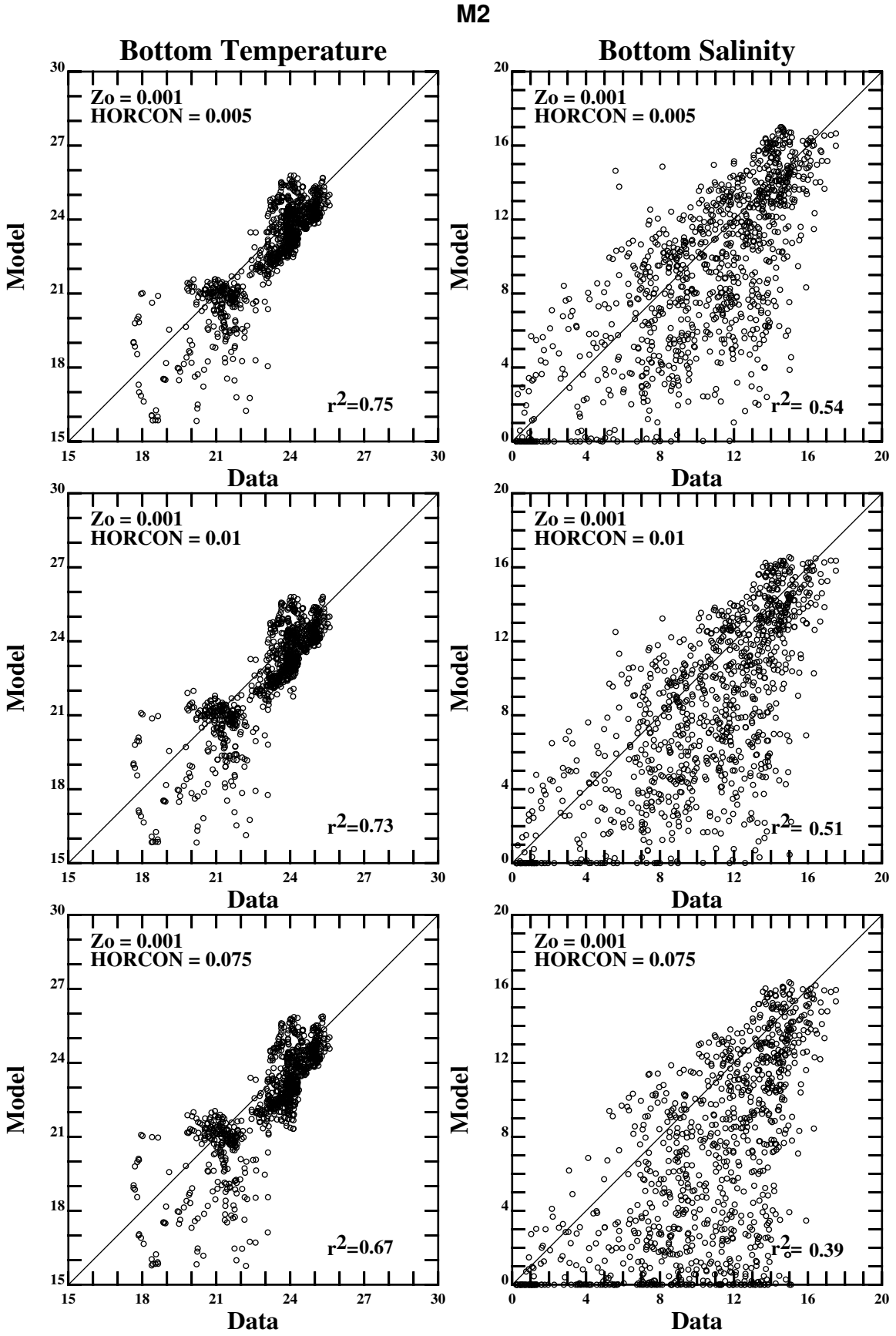

Figure 5-3 Scatter plot of computed surface and bottom temperature and salinity with observed data for sensitivity to Cs (continued)

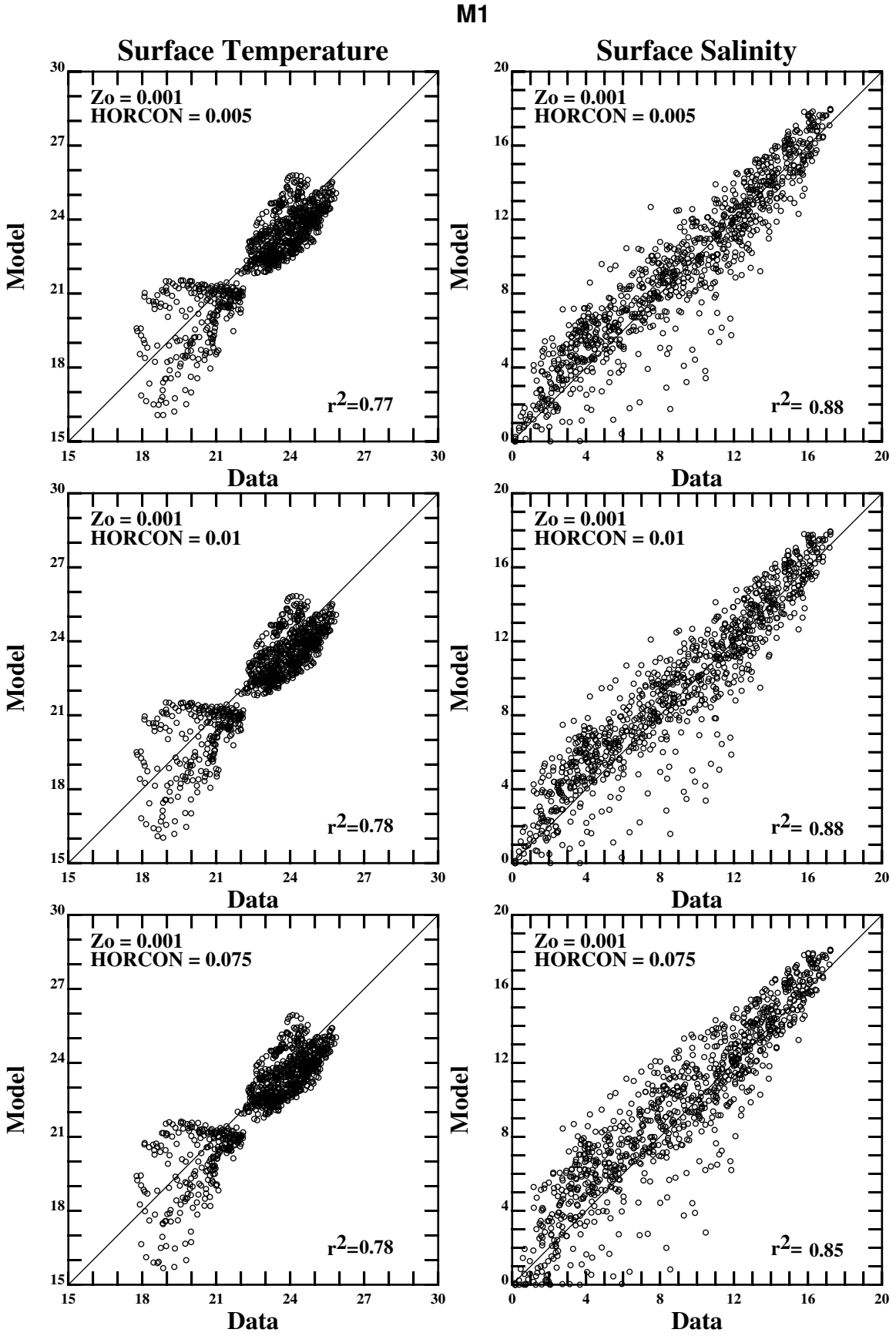

Figure 5-3 Scatter plot of computed surface and bottom temperature and salinity with observed data for sensitivity to Cs (continued)

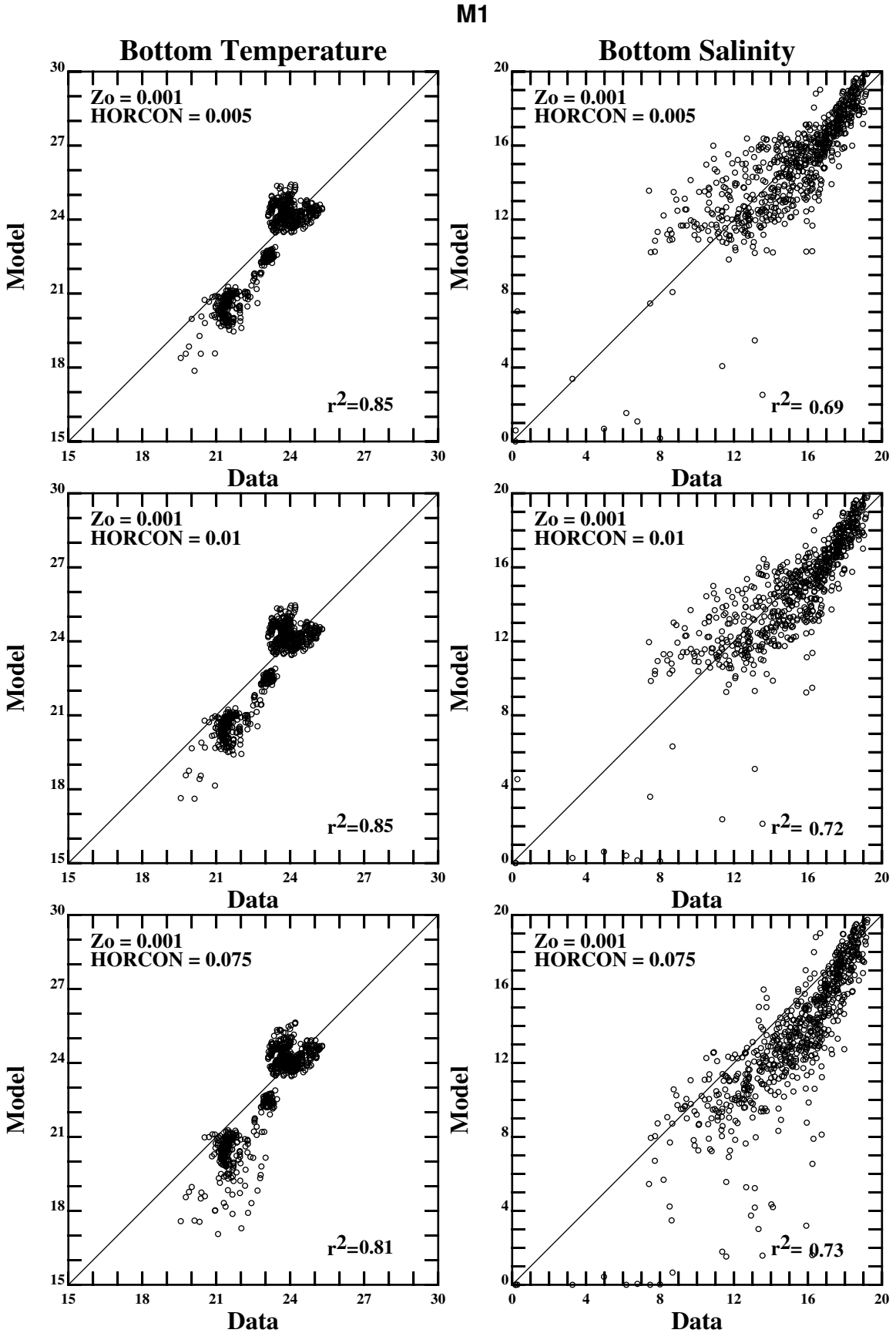

Figure 5-3 Scatter plot of computed surface and bottom temperature and salinity with observed data for sensitivity to Cs (continued)

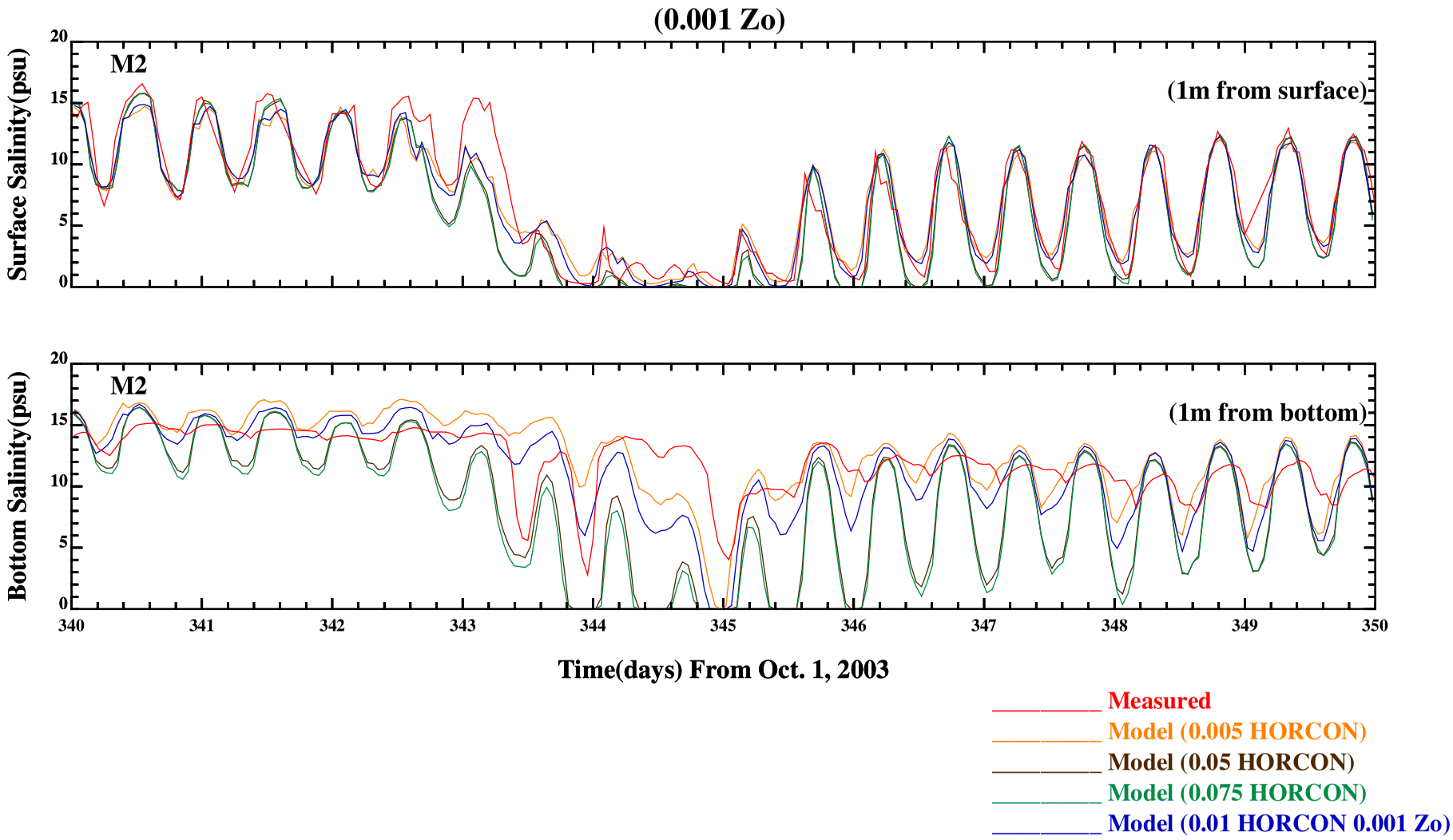

Figure 5-4 Comparison of surface and bottom salinities under different Cs values at M2

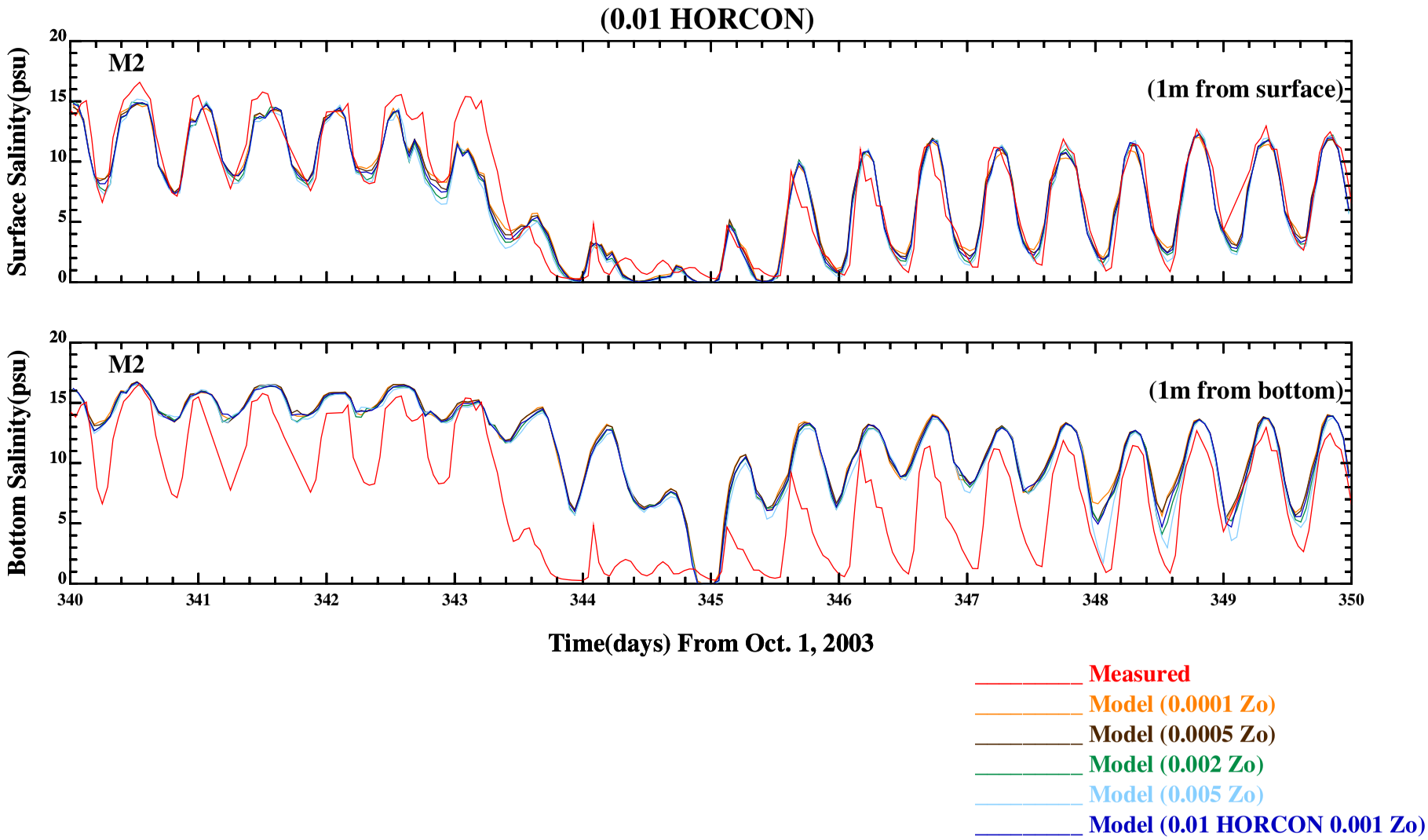

Figure 5-5 Comparison of surface and bottom salinities under different Zo values at M2

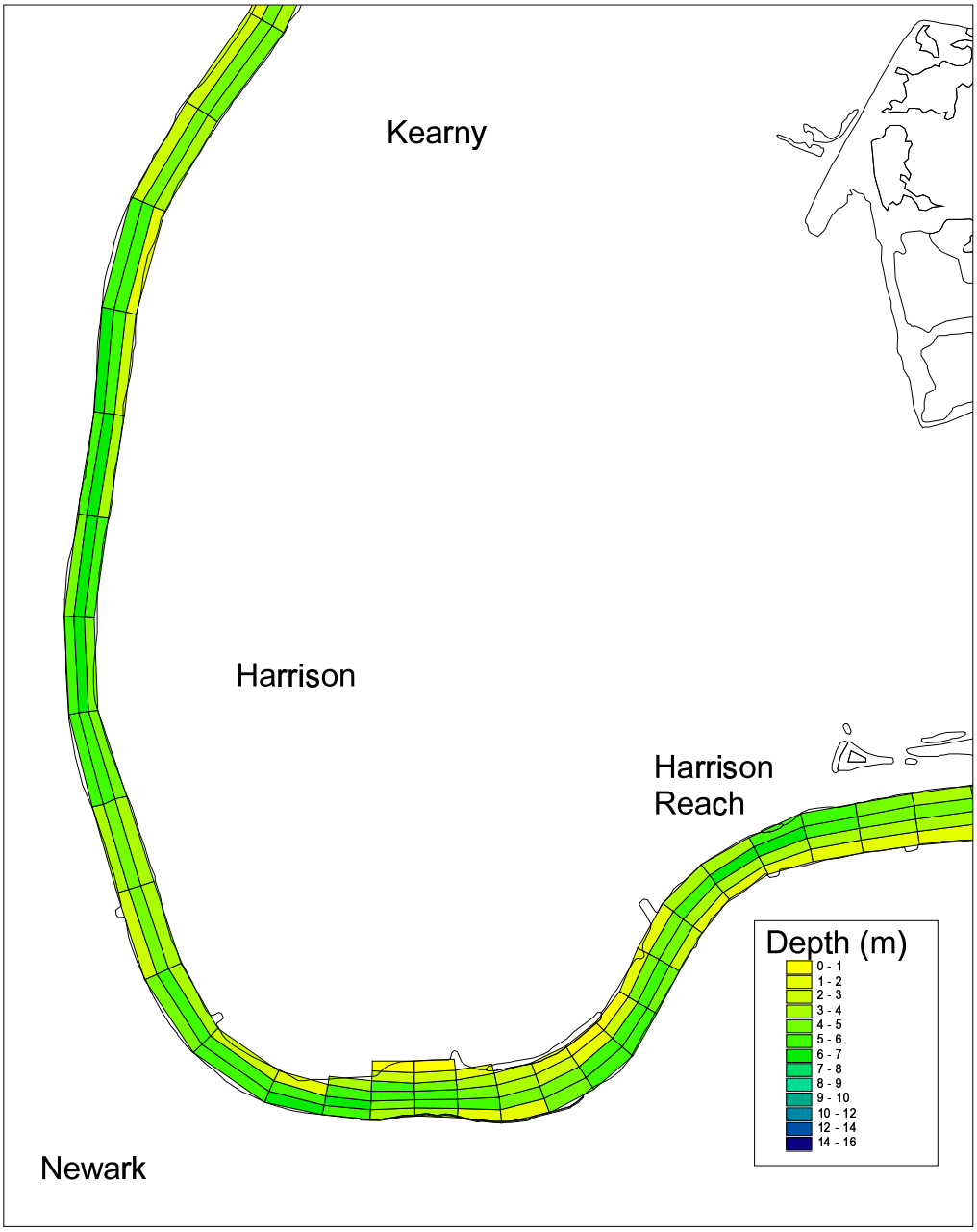

Figure 5-6 Original grid for the Lower Passaic River

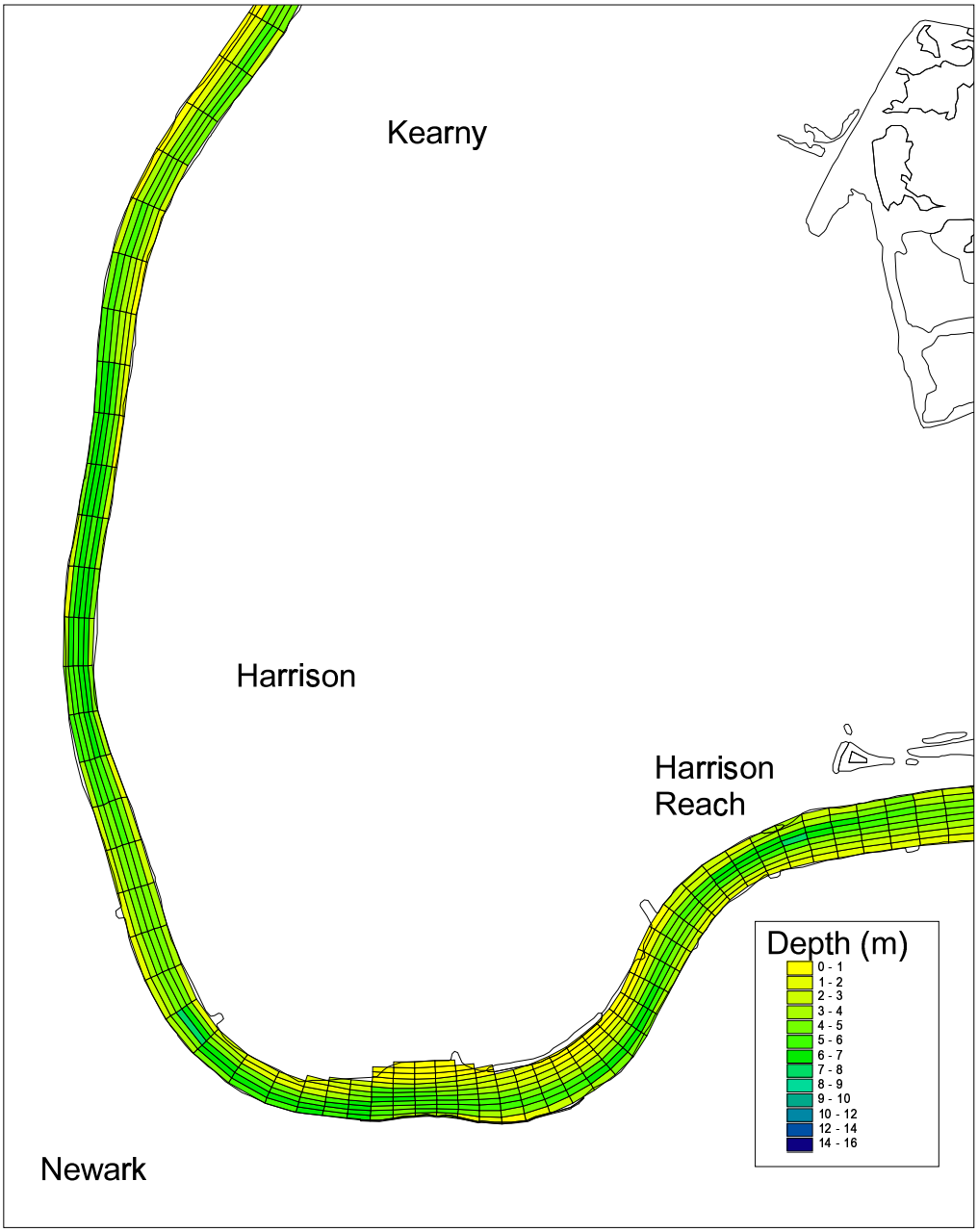

Figure 5-7 High-resolution grid used for the grid convergence test for the Lower Passaic River

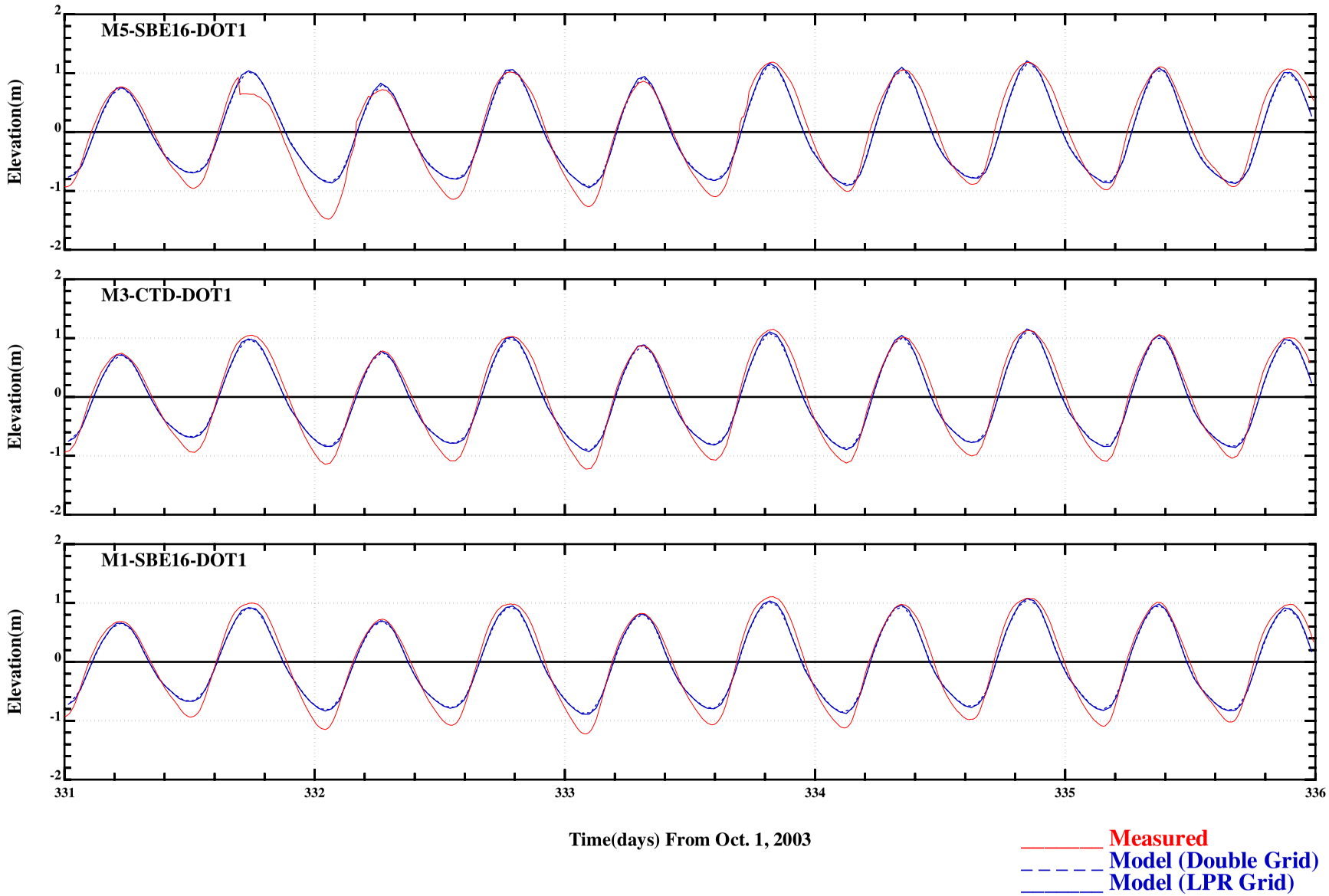

Figure 5-8 Comparison of hourly water surface elevation with data for the original and high-resolution grids

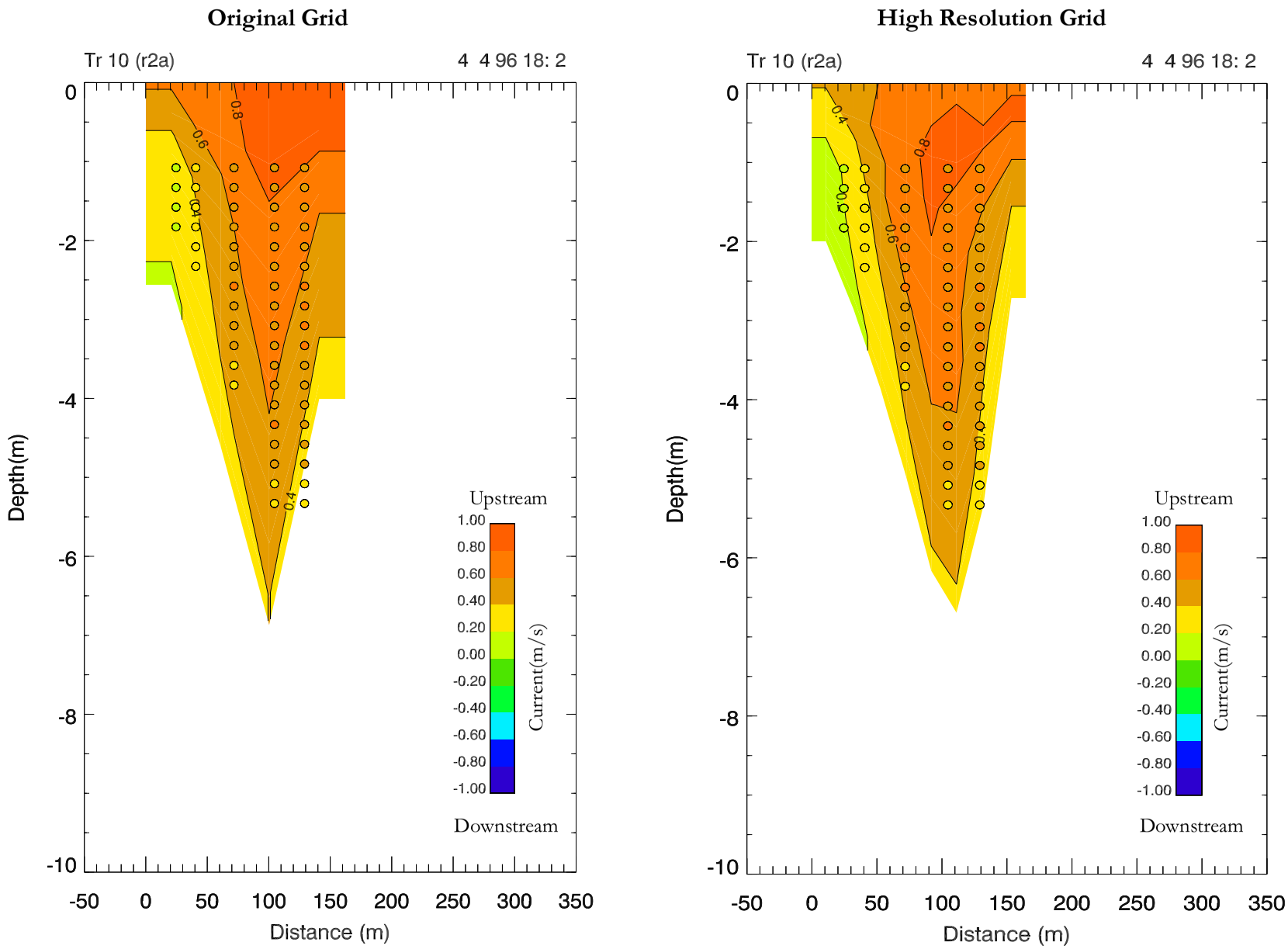

Figure 5-9 Comparison of computed cross-sectional velocities with data (Round 2a & 3) at Transect 10 and 15 for the original and high-resolution grids

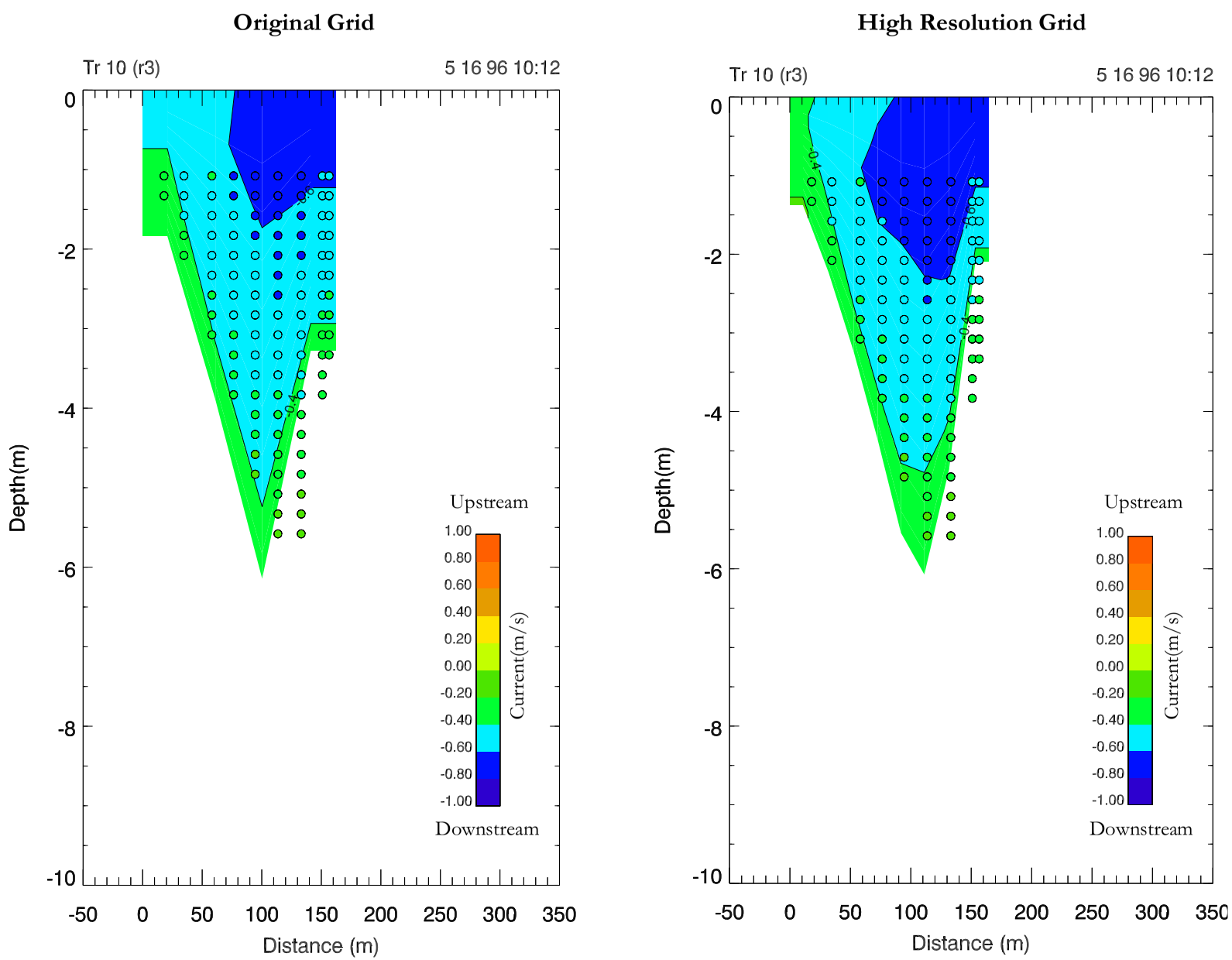

Figure 5-9 Comparison of computed cross-sectional velocities with data (Round 2a & 3) at Transect 10 and 15 for the original and high-resolution grids (continued)

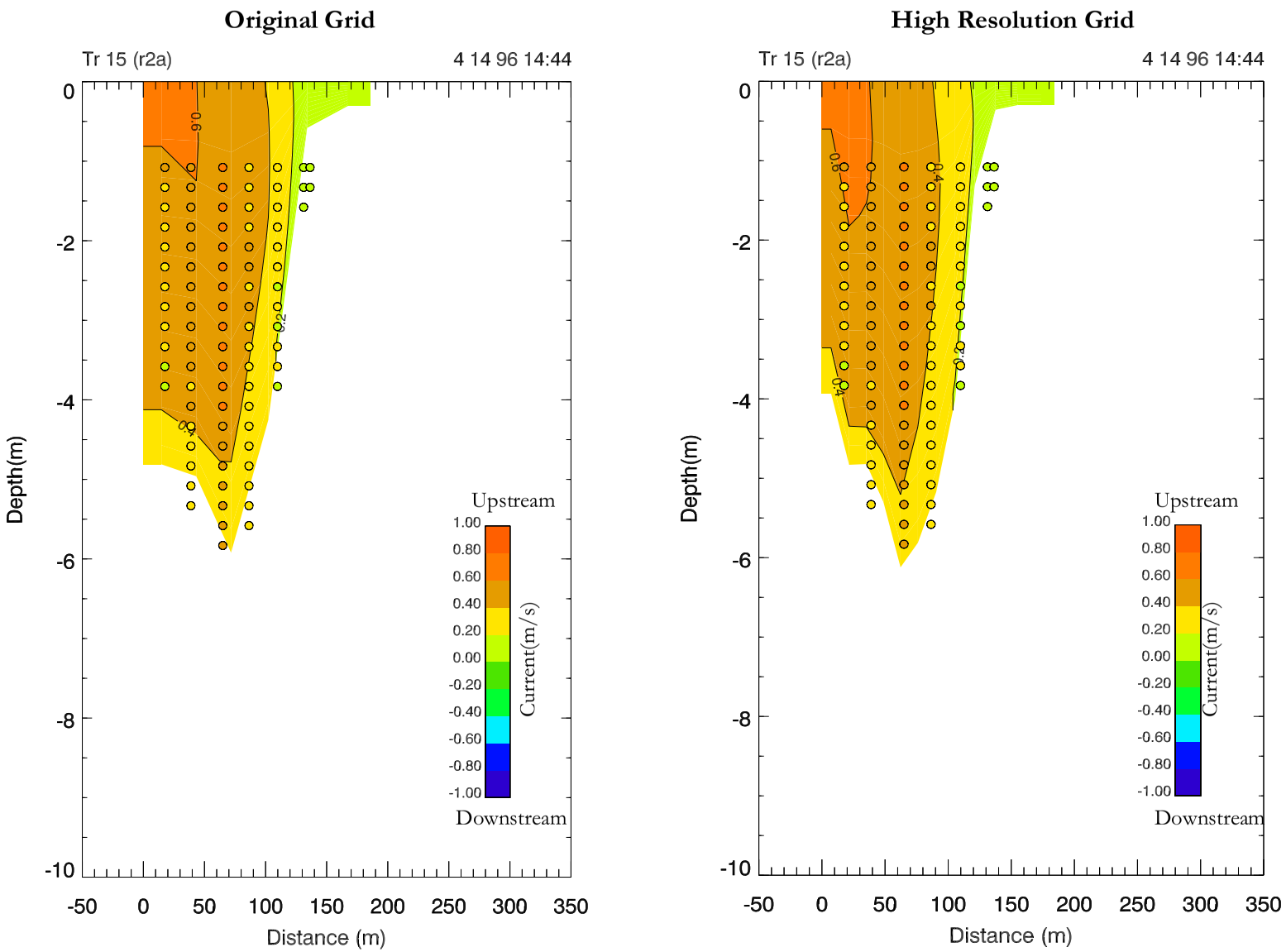

Figure 5-9 Comparison of computed cross-sectional velocities with data (Round 2a & 3) at Transect 10 and 15 for the original and high-resolution grids (continued)

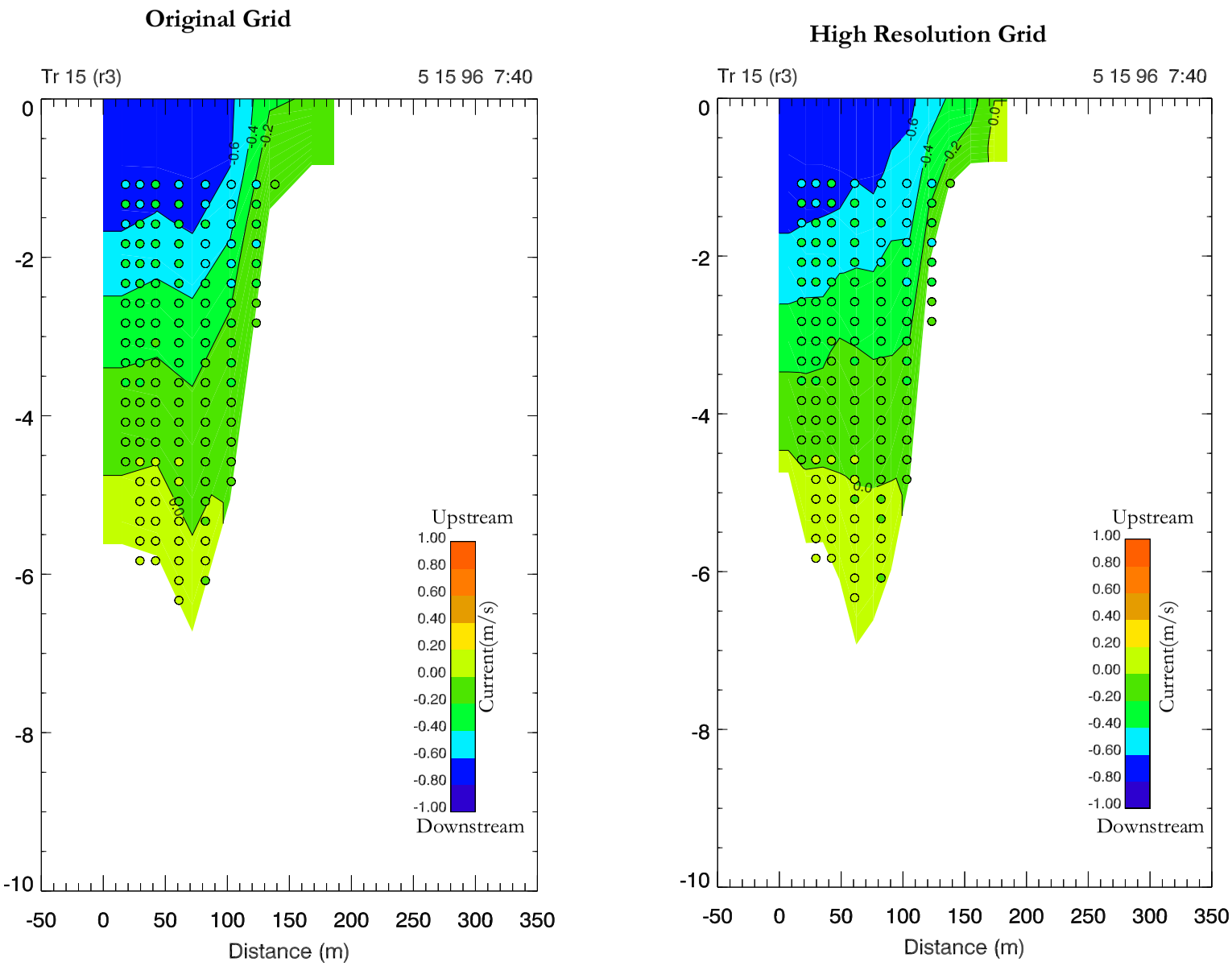

Figure 5-9 Comparison of computed cross-sectional velocities with data (Round 2a & 3) at Transect 10 and 15 for the original and high-resolution grids (continued)

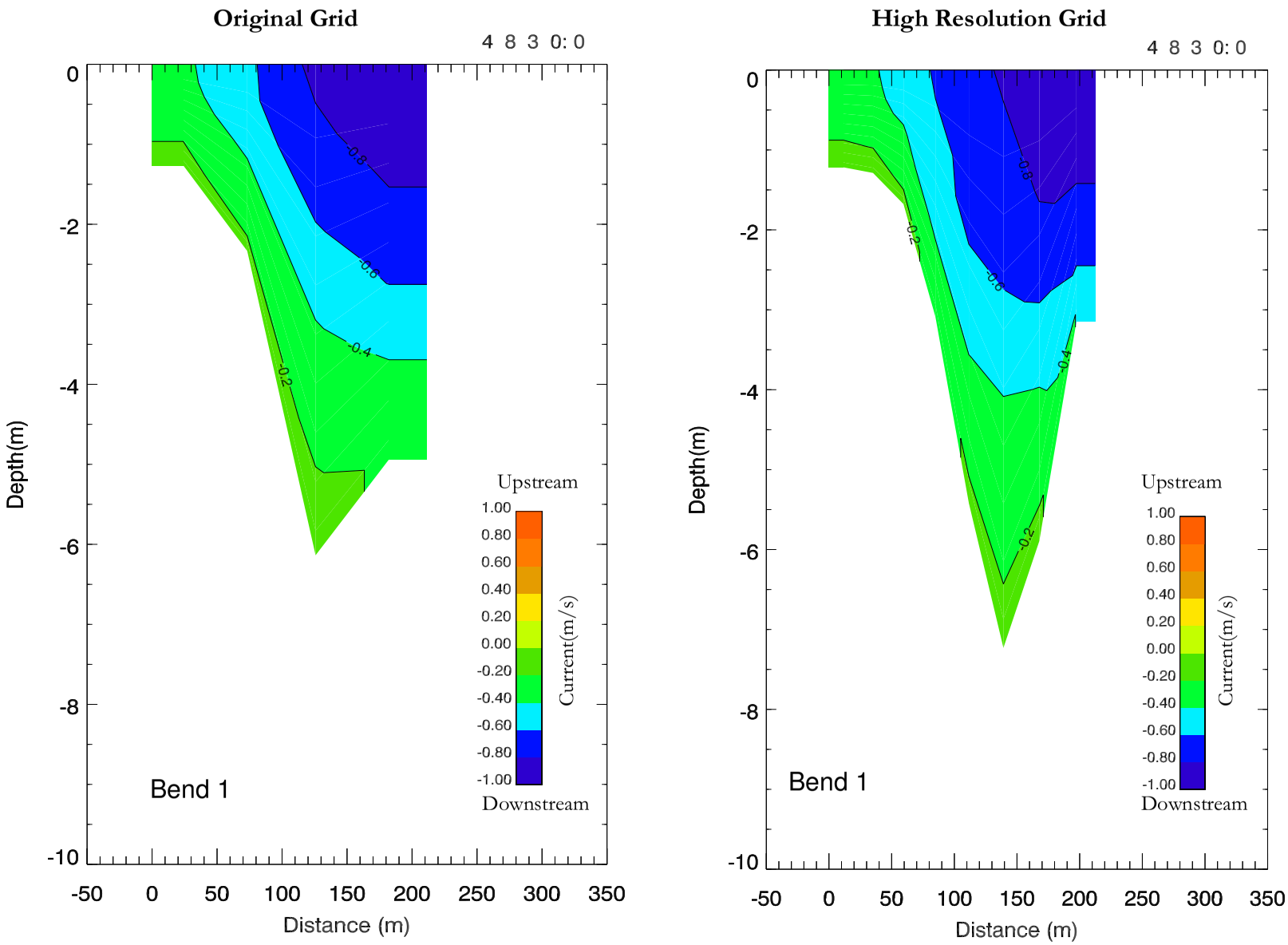

Figure 5-10 Comparison of computed cross-sectional velocities at three transect locations along the river bends for the original and high-resolution grids

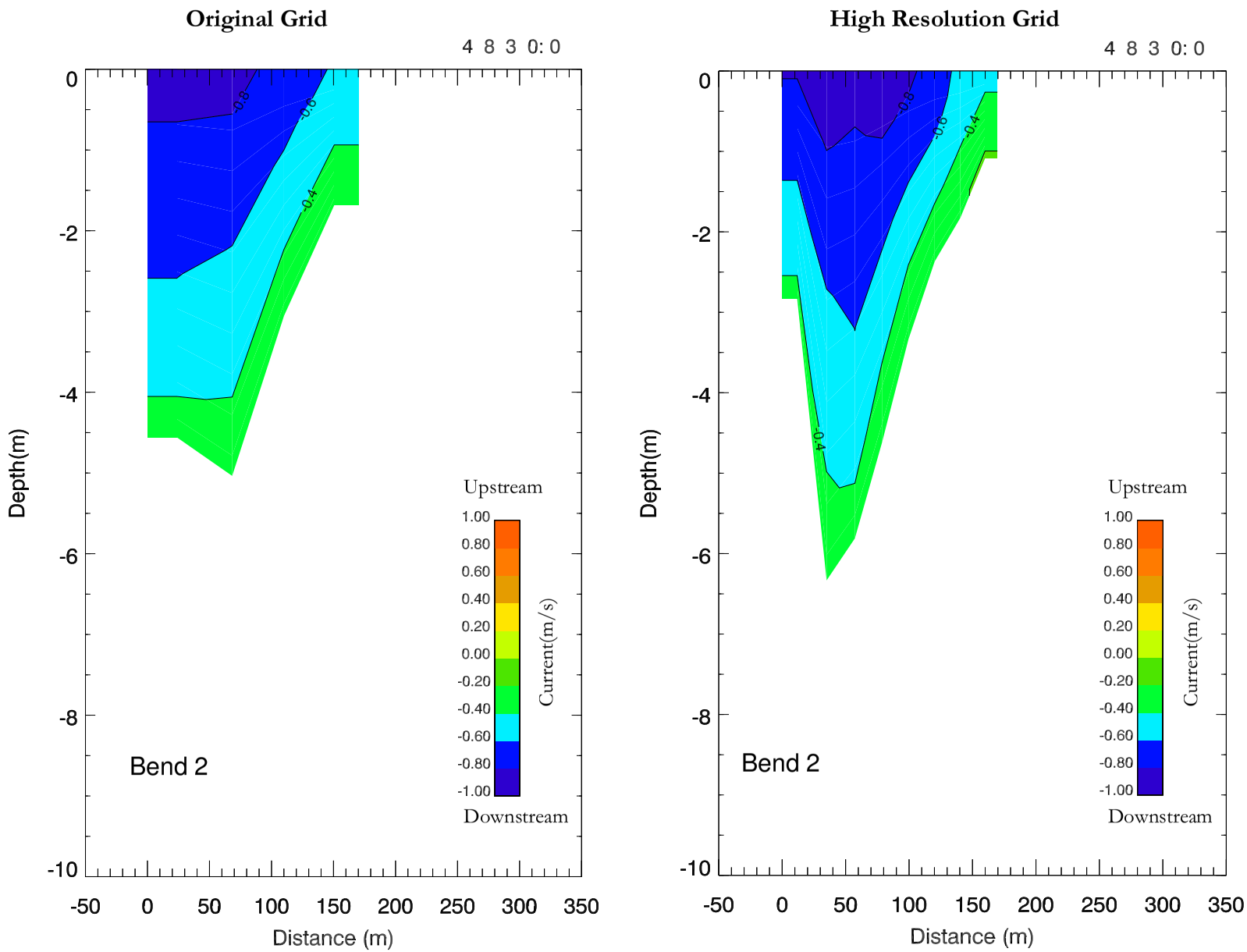

Figure 5-10 Comparison of computed cross-sectional velocities at three transect locations along the river bends for the original and high-resolution grids (continued)

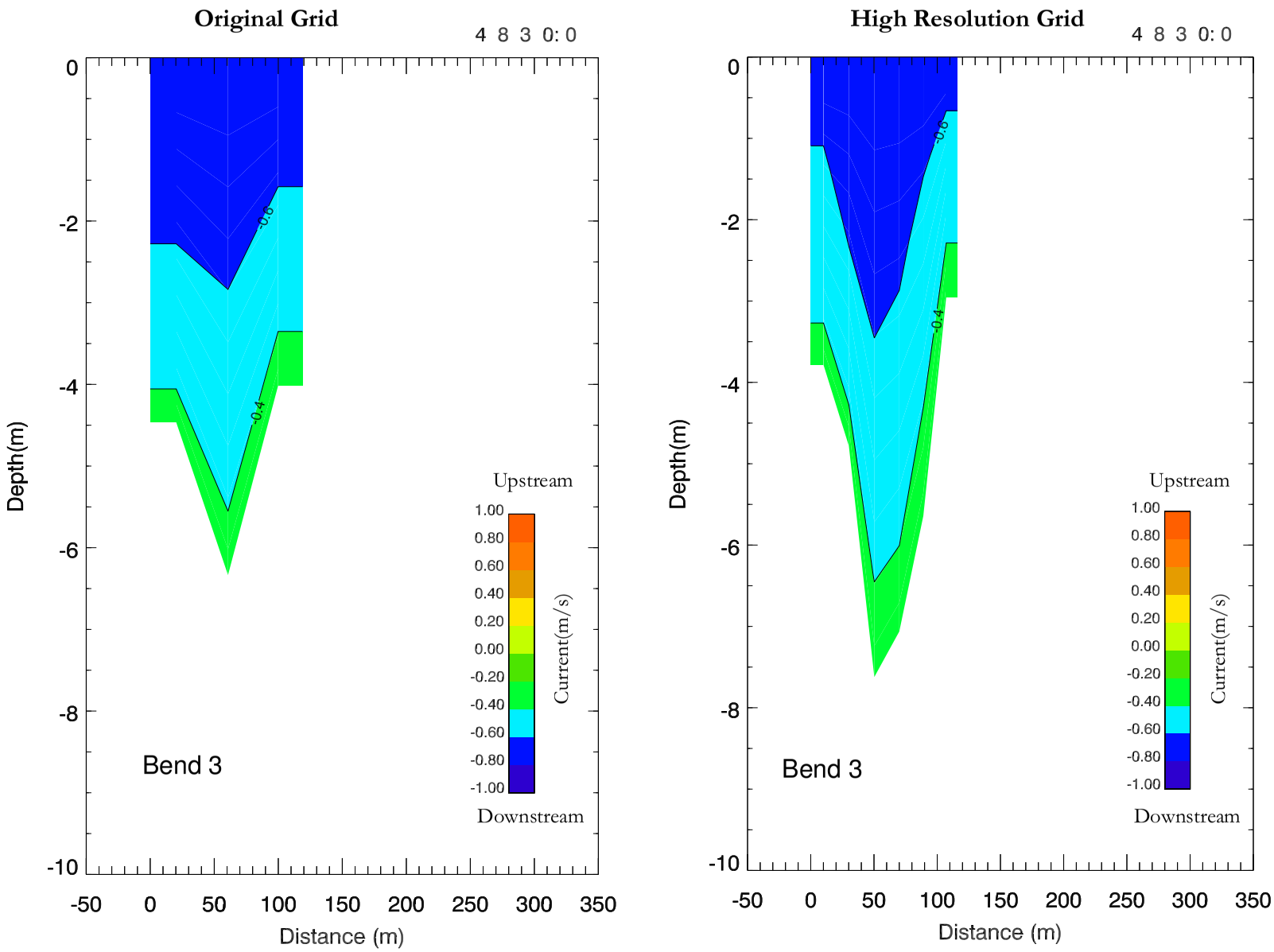

Figure 5-10 Comparison of computed cross-sectional velocities at three transect locations along the river bends for the original and high-resolution grids (continued)

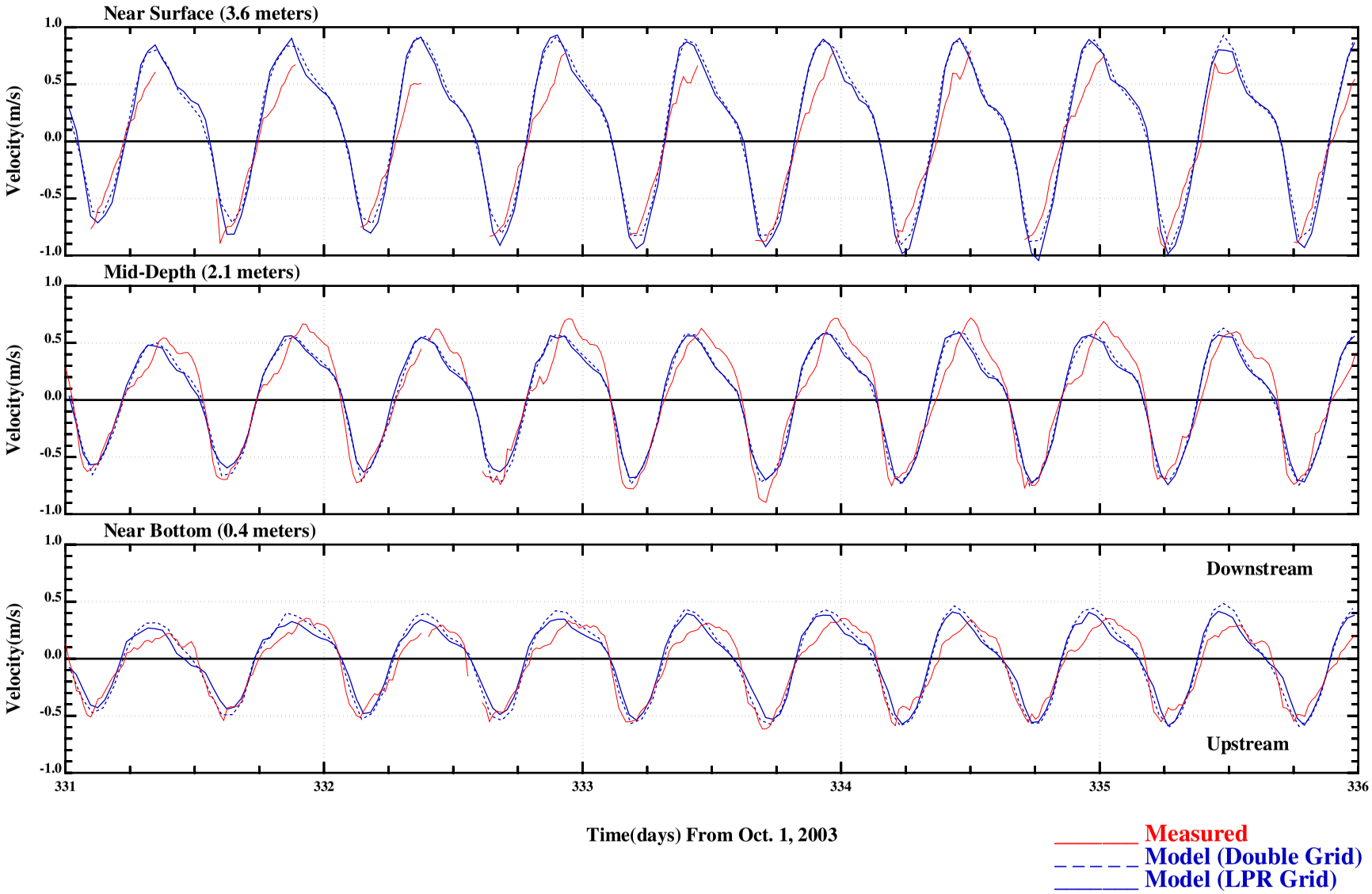

Figure 5-11 Comparison of computed velocities with data at station M2 for the original and high-resolution grids

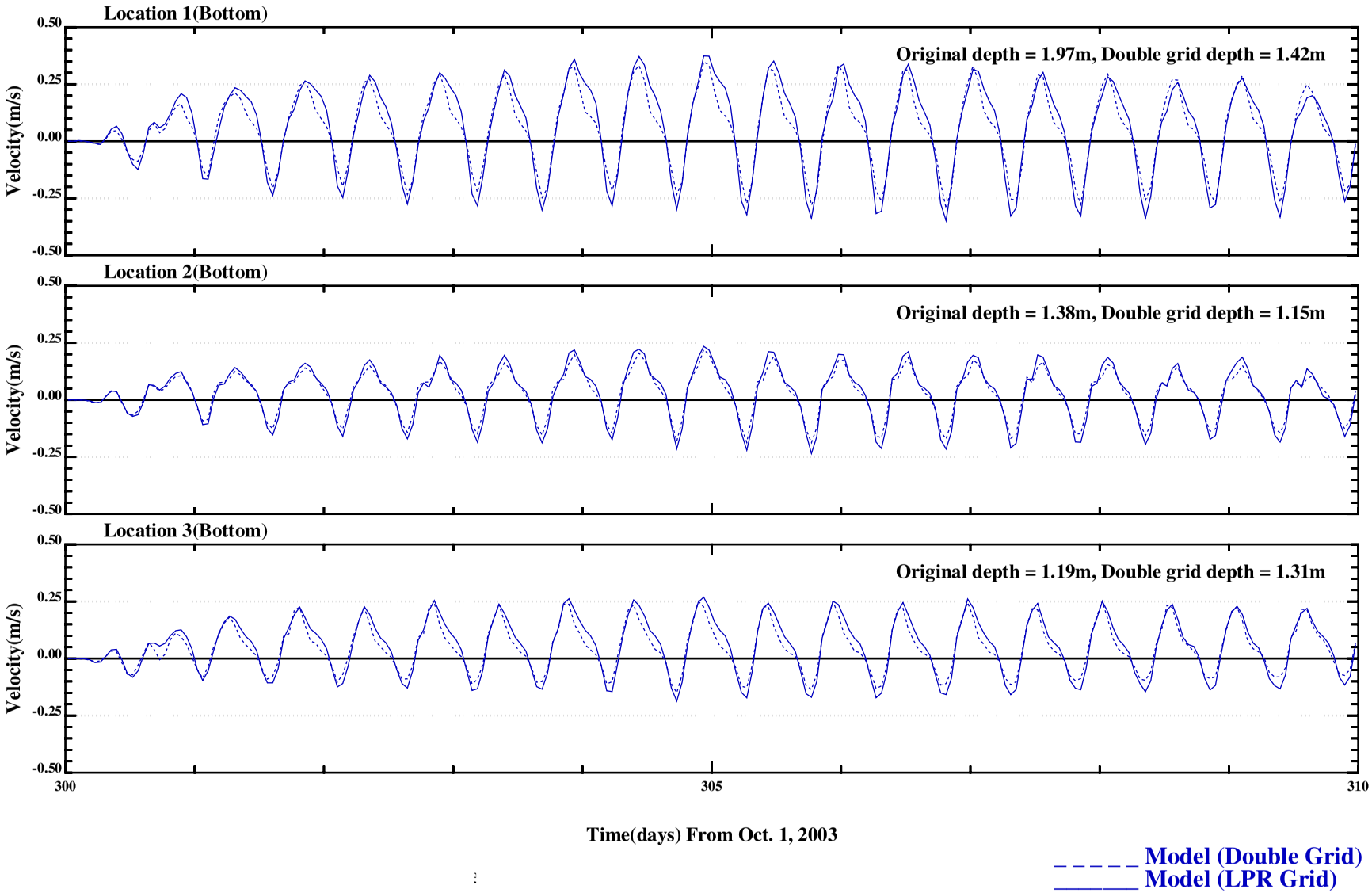

Figure 5-12 Comparison of hourly computed bottom velocities at three shallow locations for the original and high-resolution grids

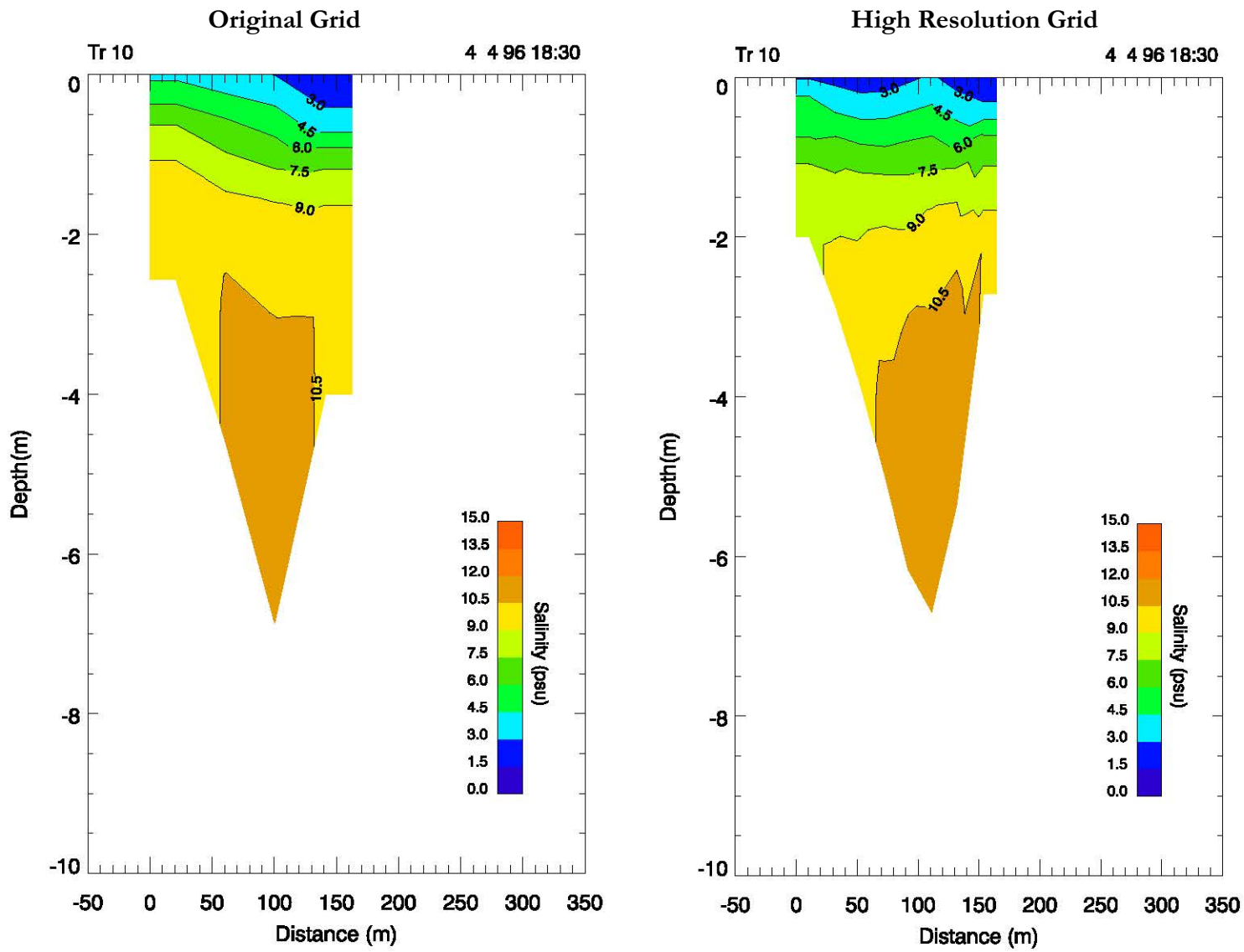

Figure 5-13 Comparison of computed cross-sectional salinities for two different times at Transect 10 and 15 for the original and high-resolution grids

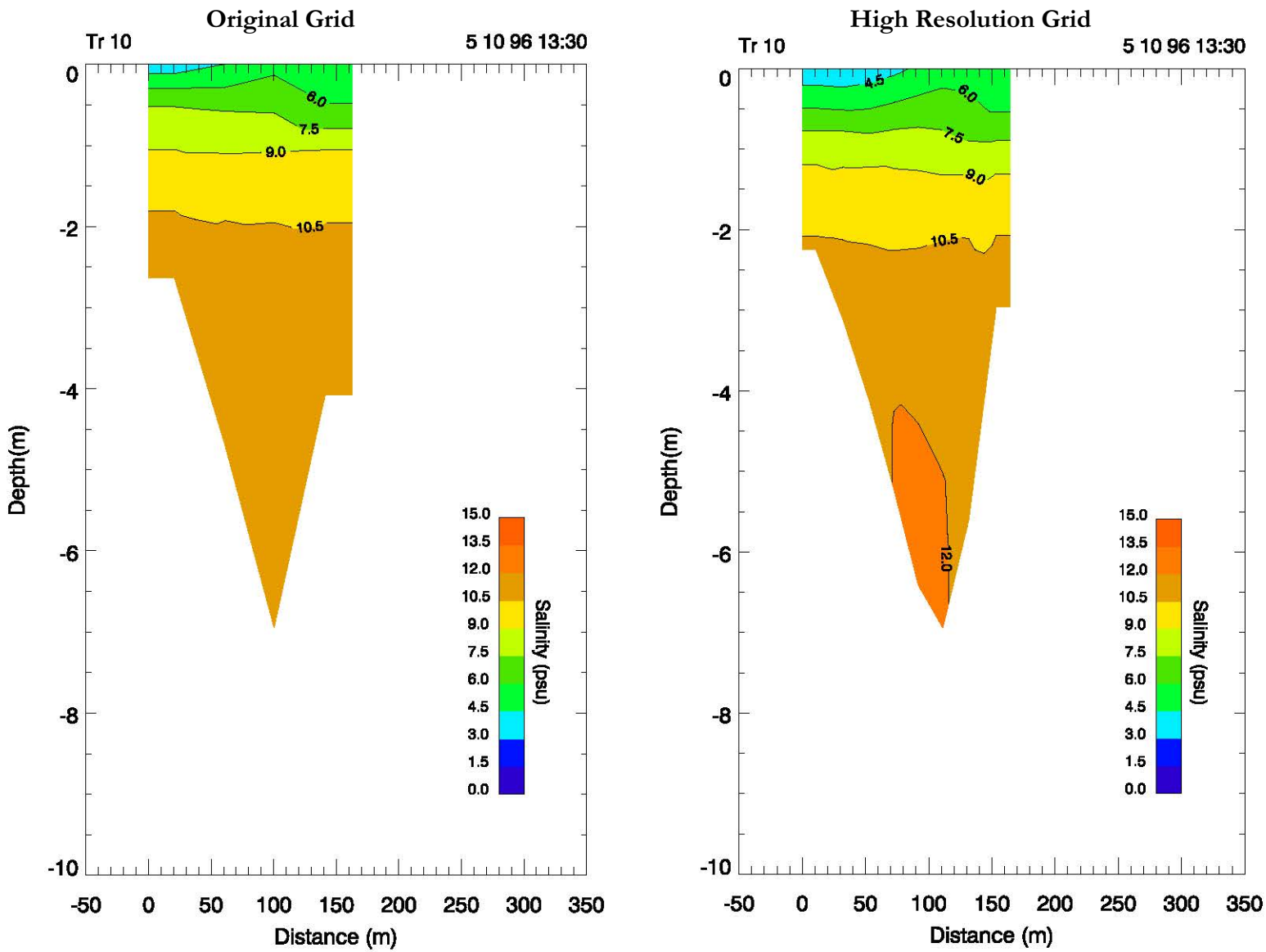

Figure 5-13 Comparison of computed cross-sectional salinities for two different times at Transect 10 and 15 for the original and high-resolution grids (continued)

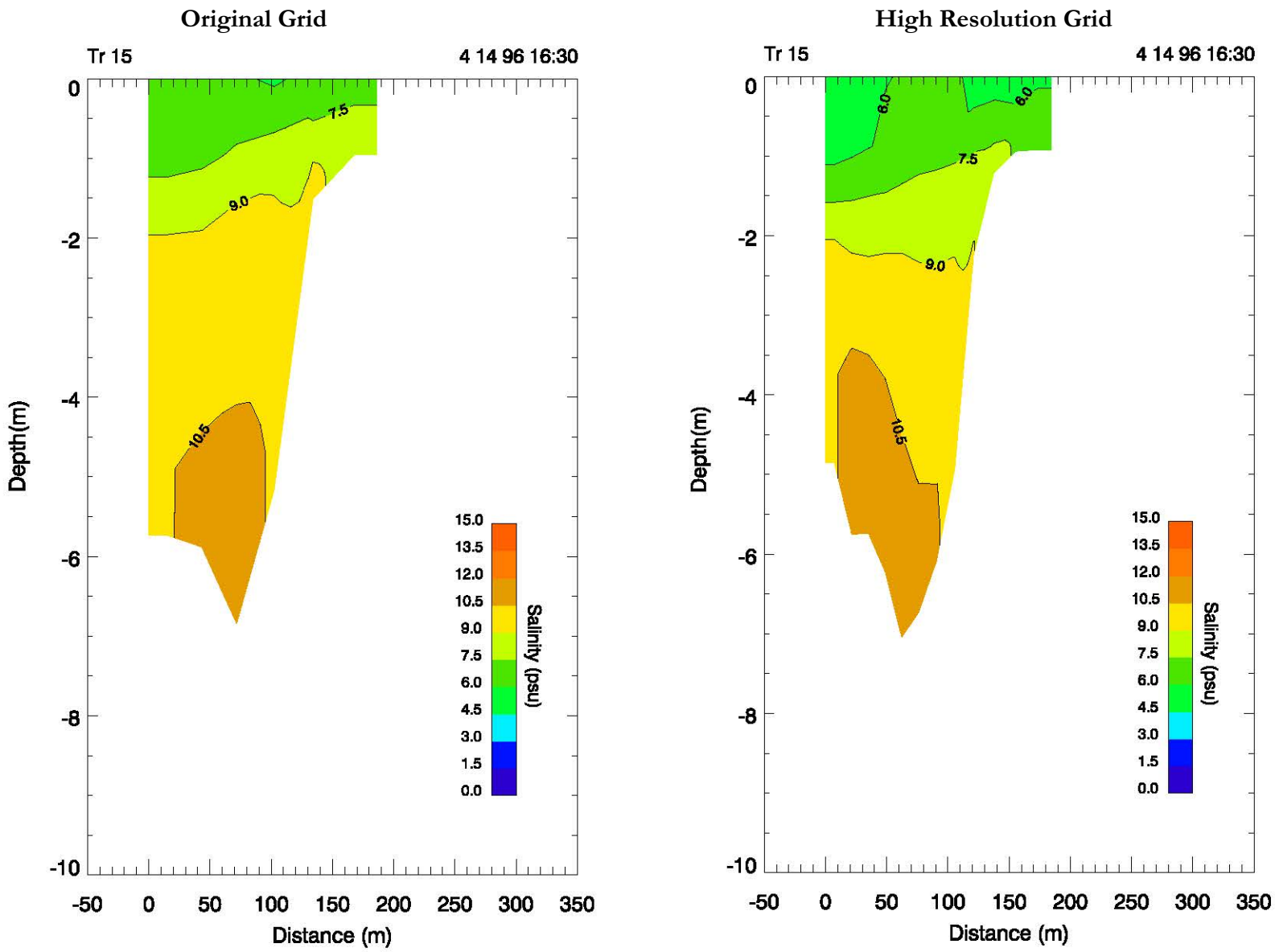

Figure 5-13 Comparison of computed cross-sectional salinities for two different times at Transect 10 and 15 for the original and high-resolution grids (continued)

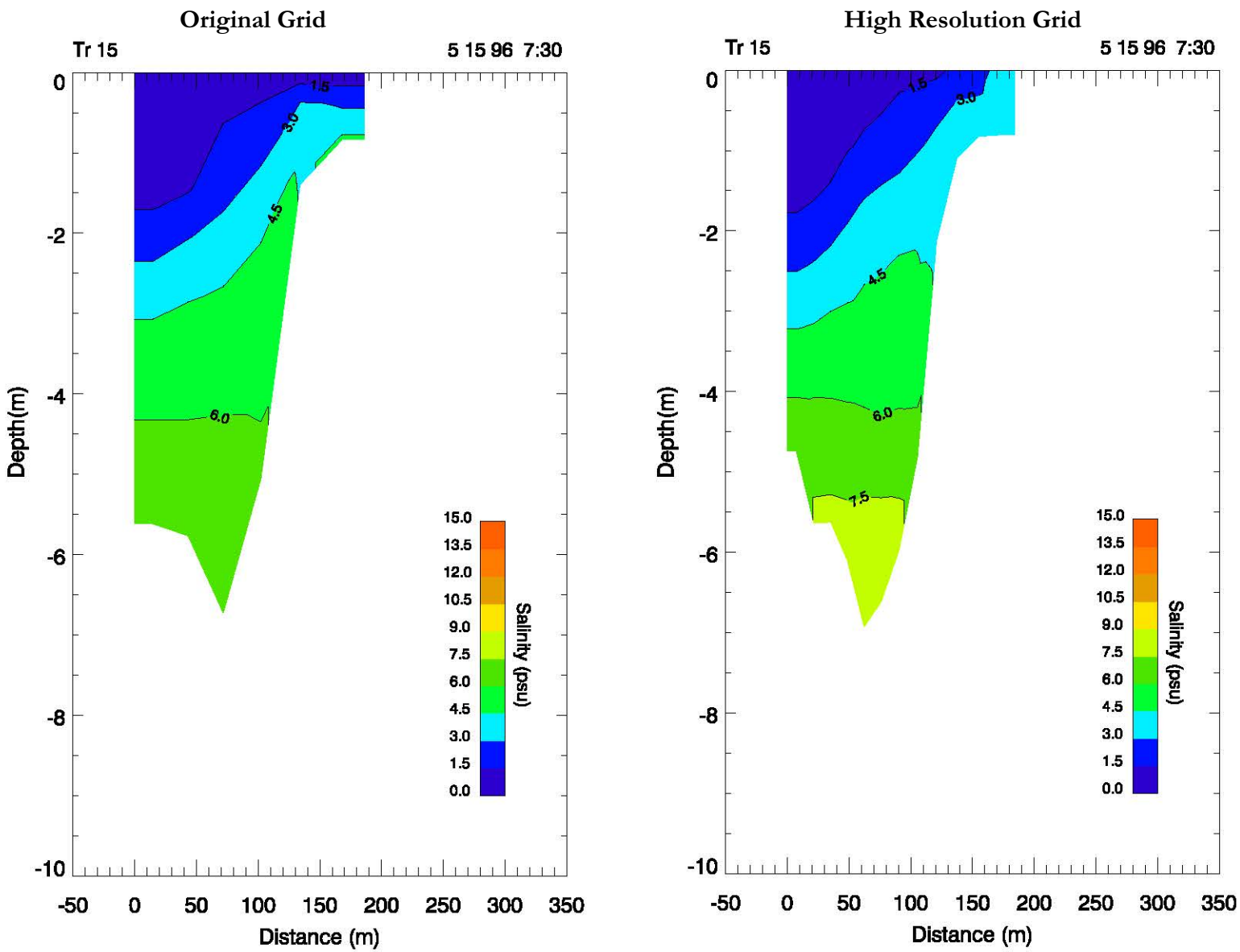

Figure 5-13 Comparison of computed cross-sectional salinities for two different times at Transect 10 and 15 for the original and high-resolution grids (continued)

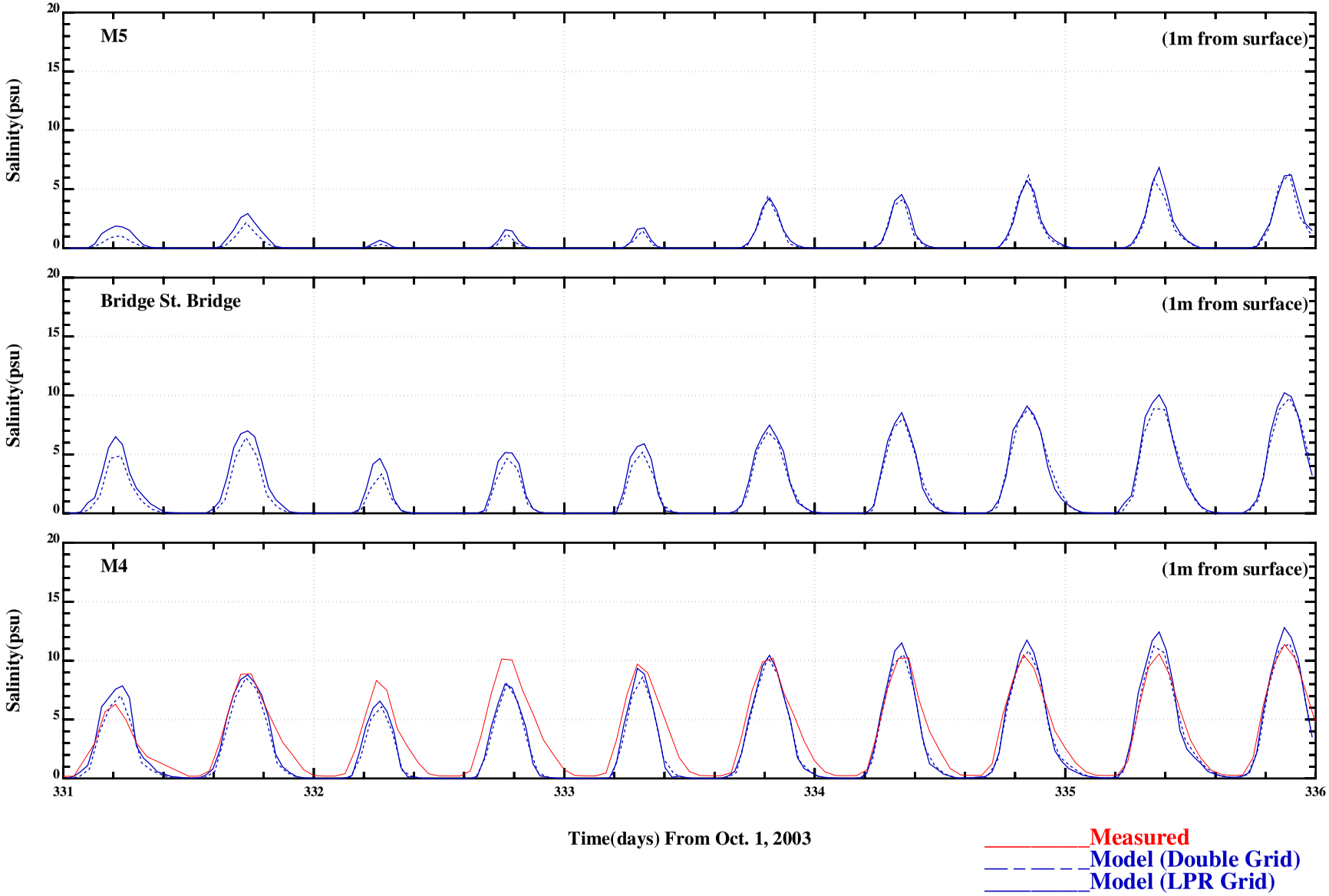

Figure 5-14 Comparison of computed surface and bottom salinities with data for the original and high-resolution grids

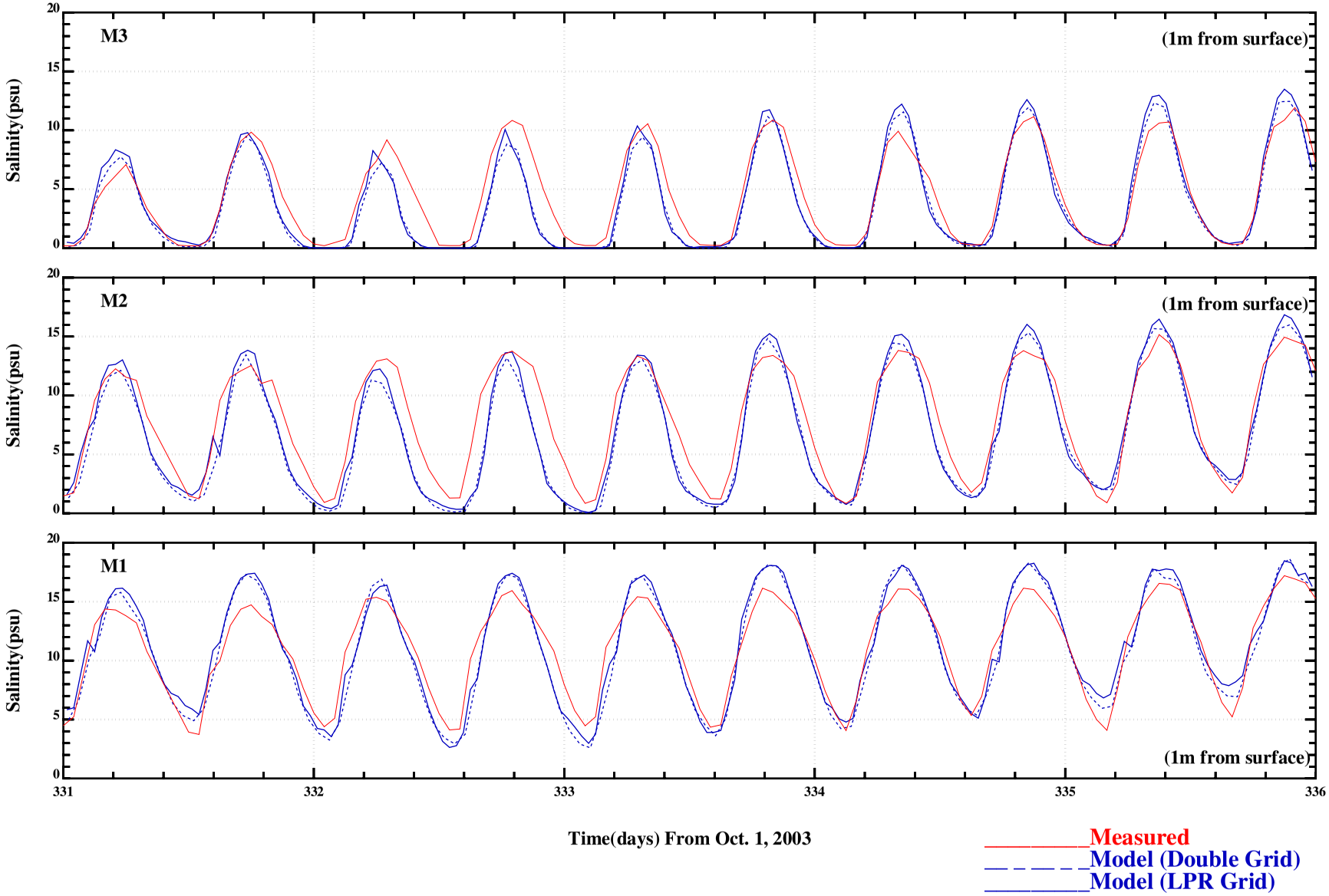

Figure 5-14 Comparison of computed surface and bottom salinities with data for the original and high-resolution grids (continued)

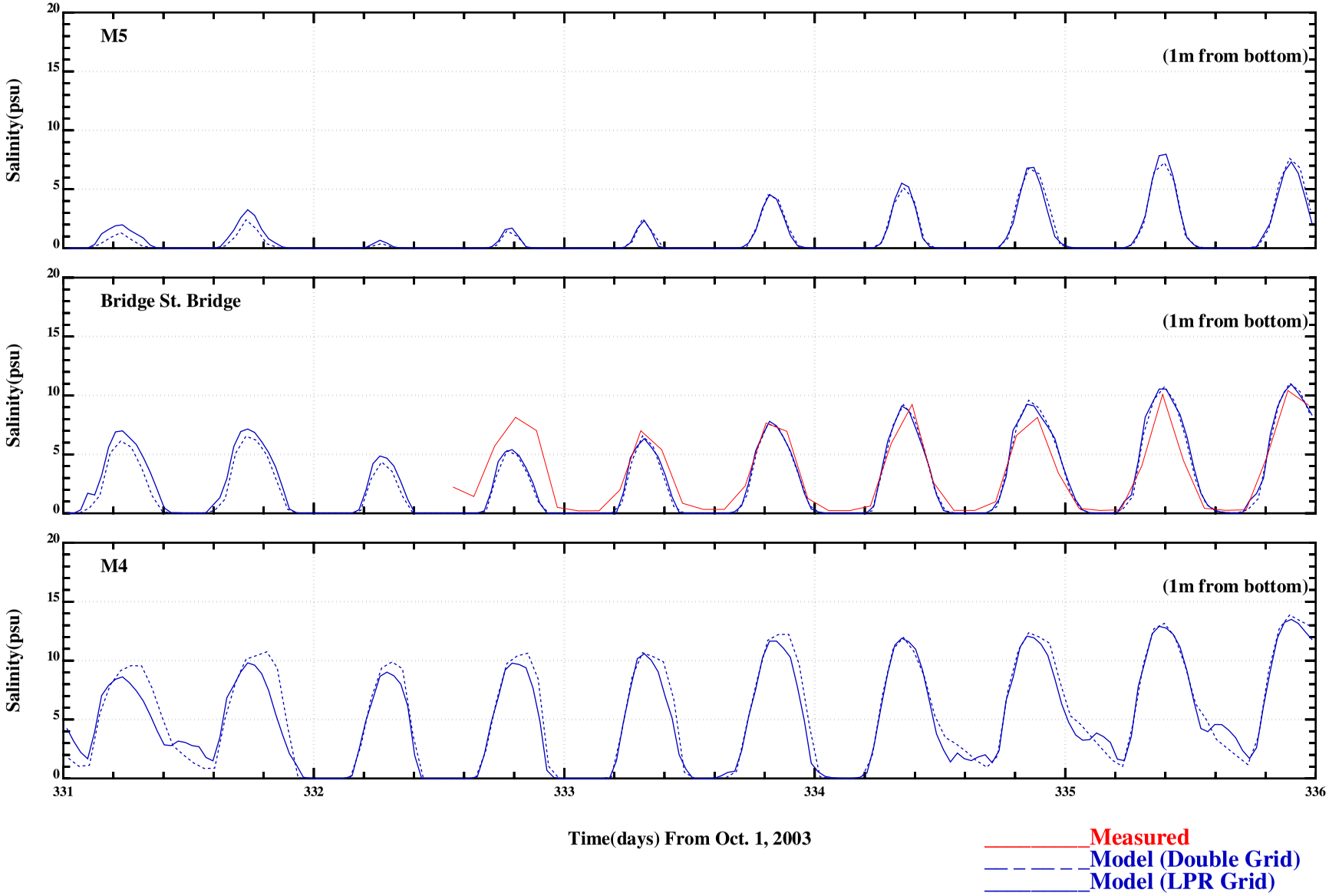

Figure 5-14 Comparison of computed surface and bottom salinities with data for the original and high-resolution grids (continued)

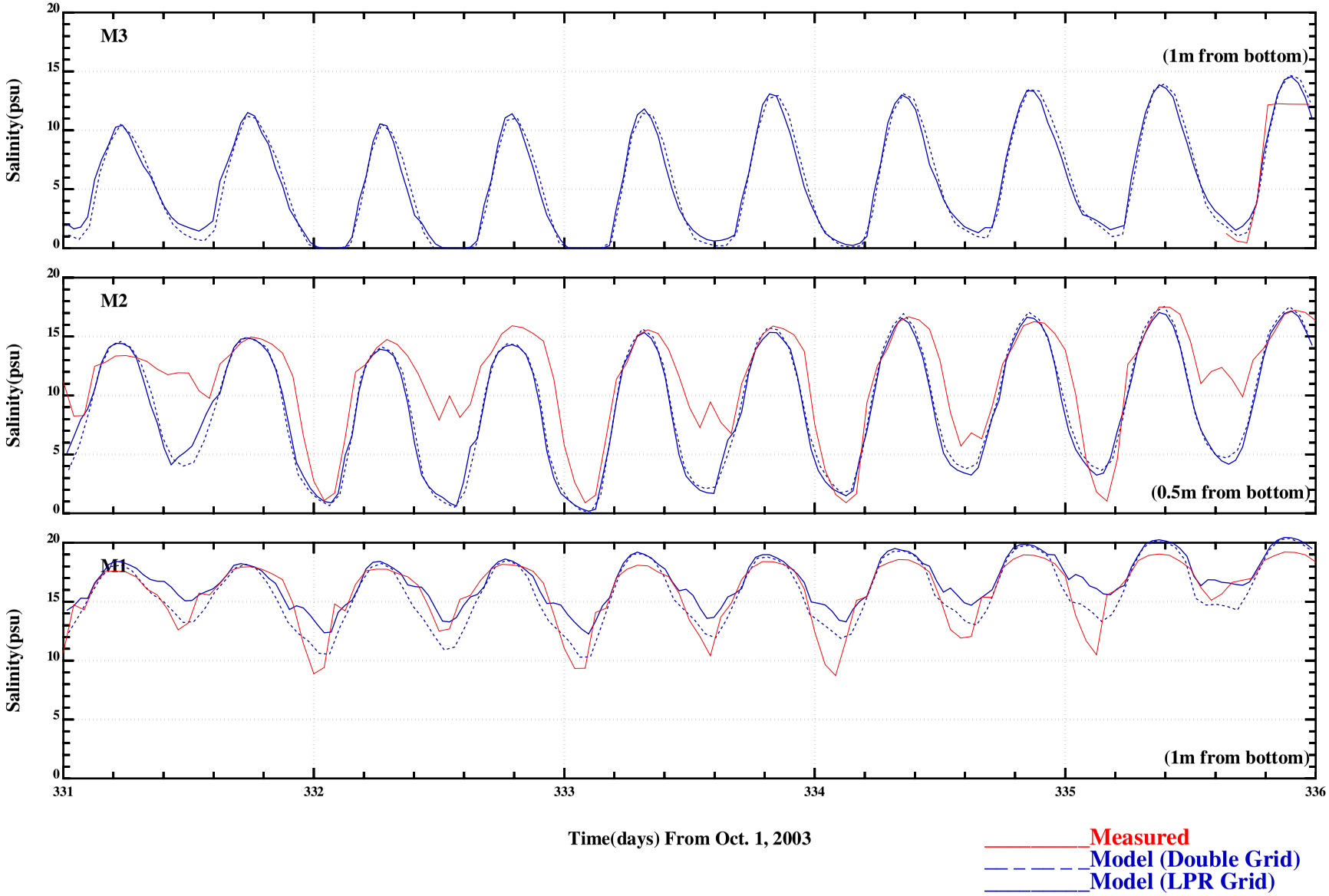

Figure 5-14 Comparison of computed surface and bottom salinities with data for the original and high-resolution grids (continued)

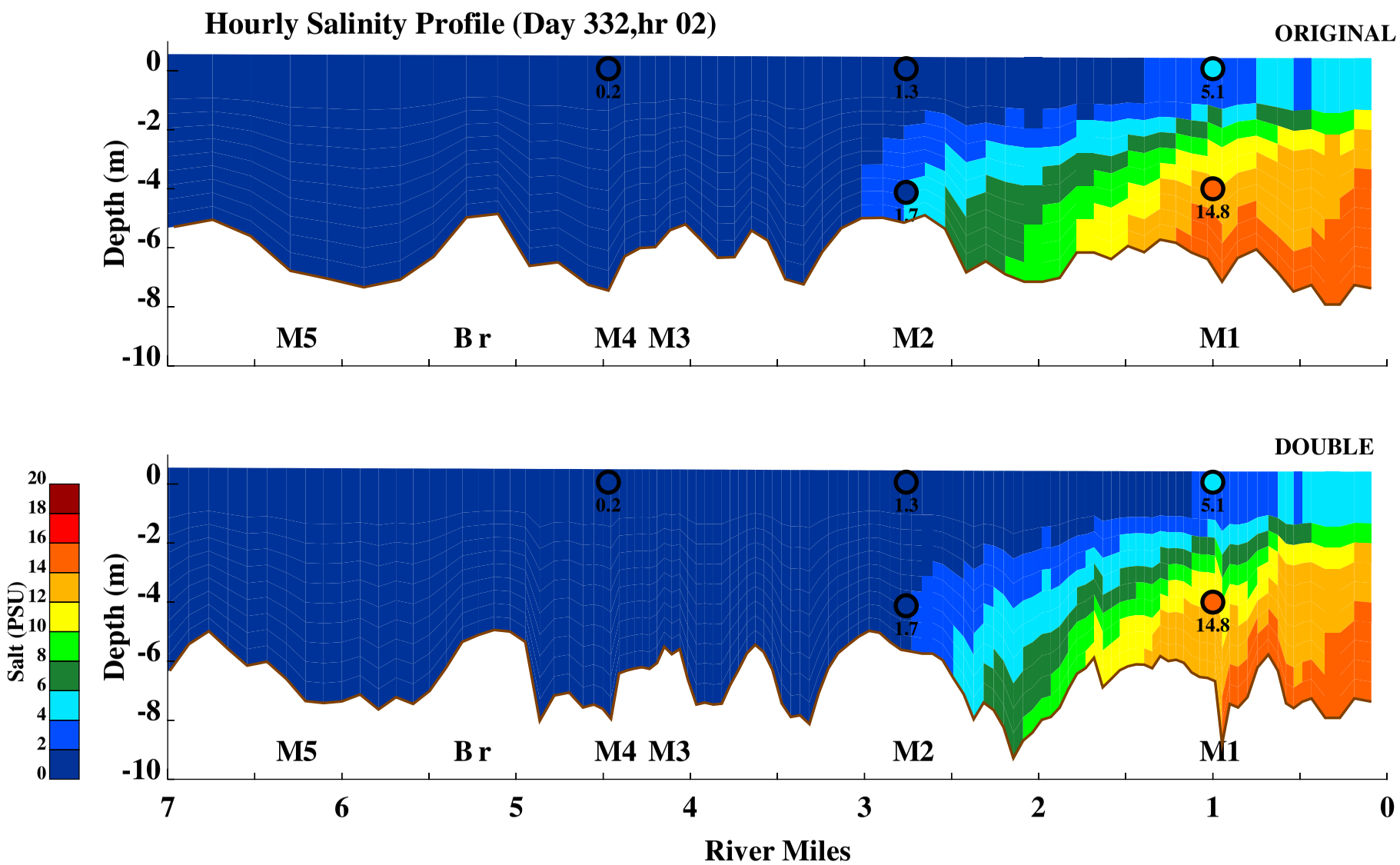

Figure 5-15 Comparison of longitudinal profile of computed salinities with data along Lower Passaic River for the original and high-resolution grids

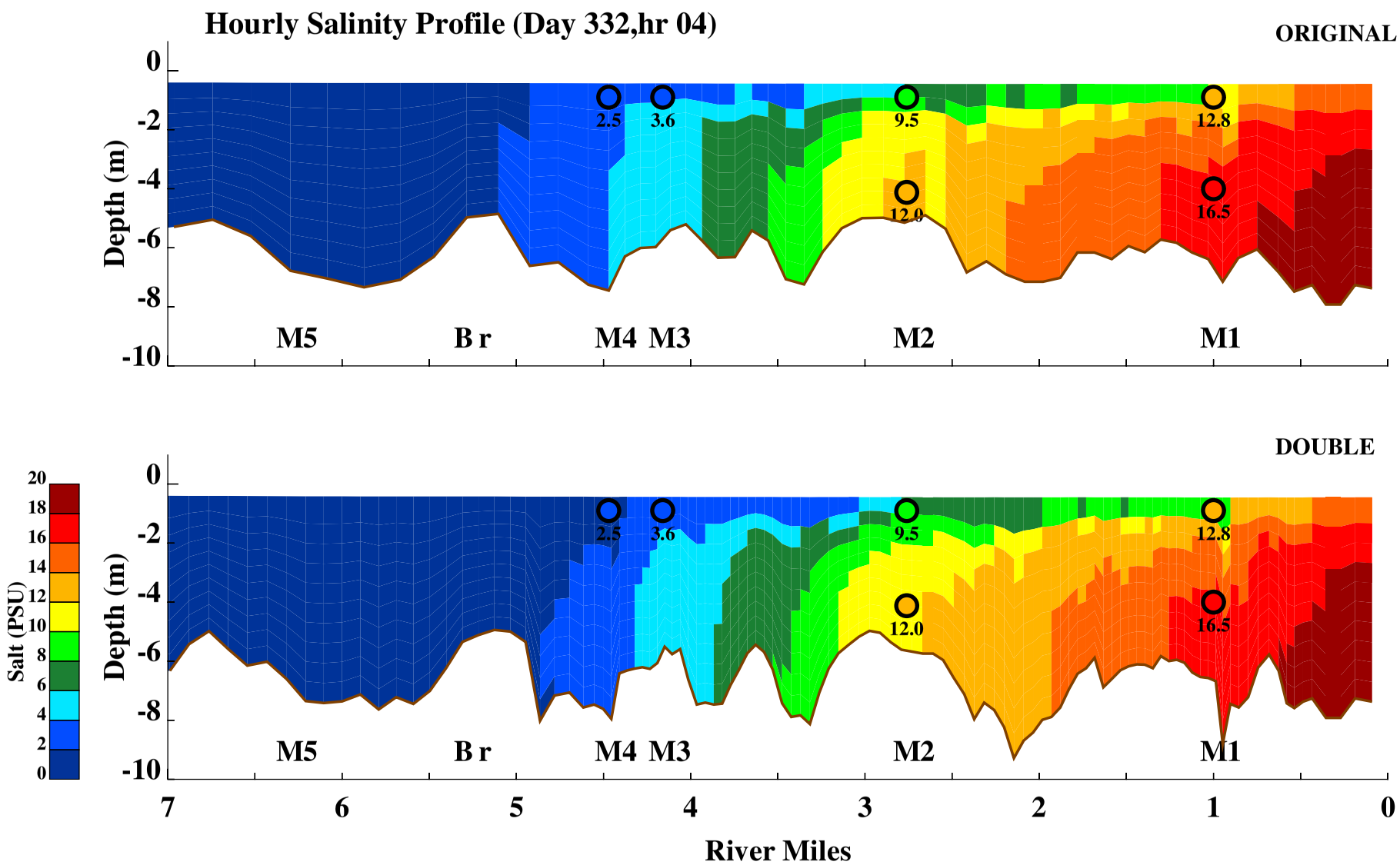

Figure 5-15 Comparison of longitudinal profile of computed salinities with data along Lower Passaic River for the original and high-resolution grids (continued)

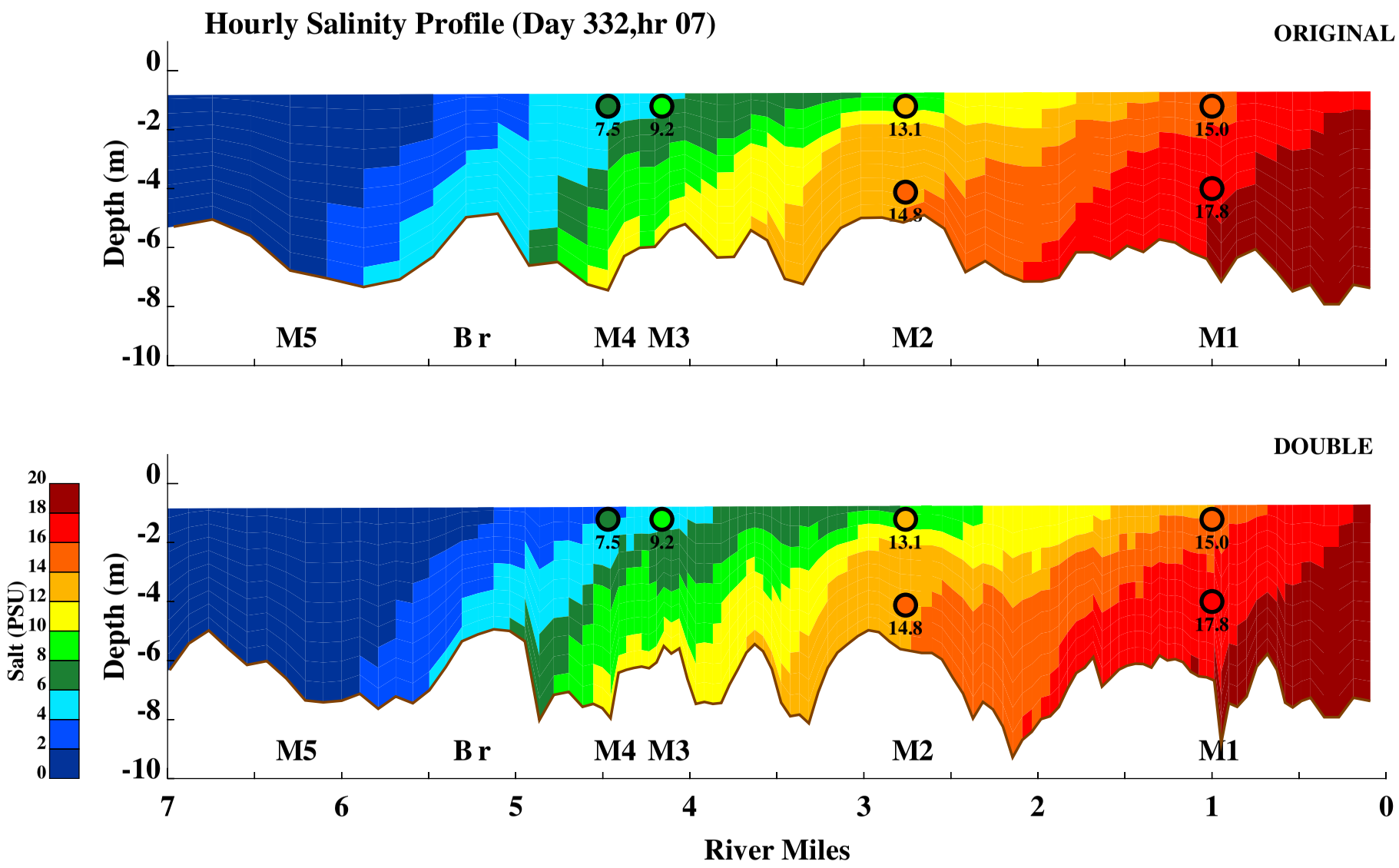

Figure 5-15 Comparison of longitudinal profile of computed salinities with data along Lower Passaic River for the original and high-resolution grids (continued)

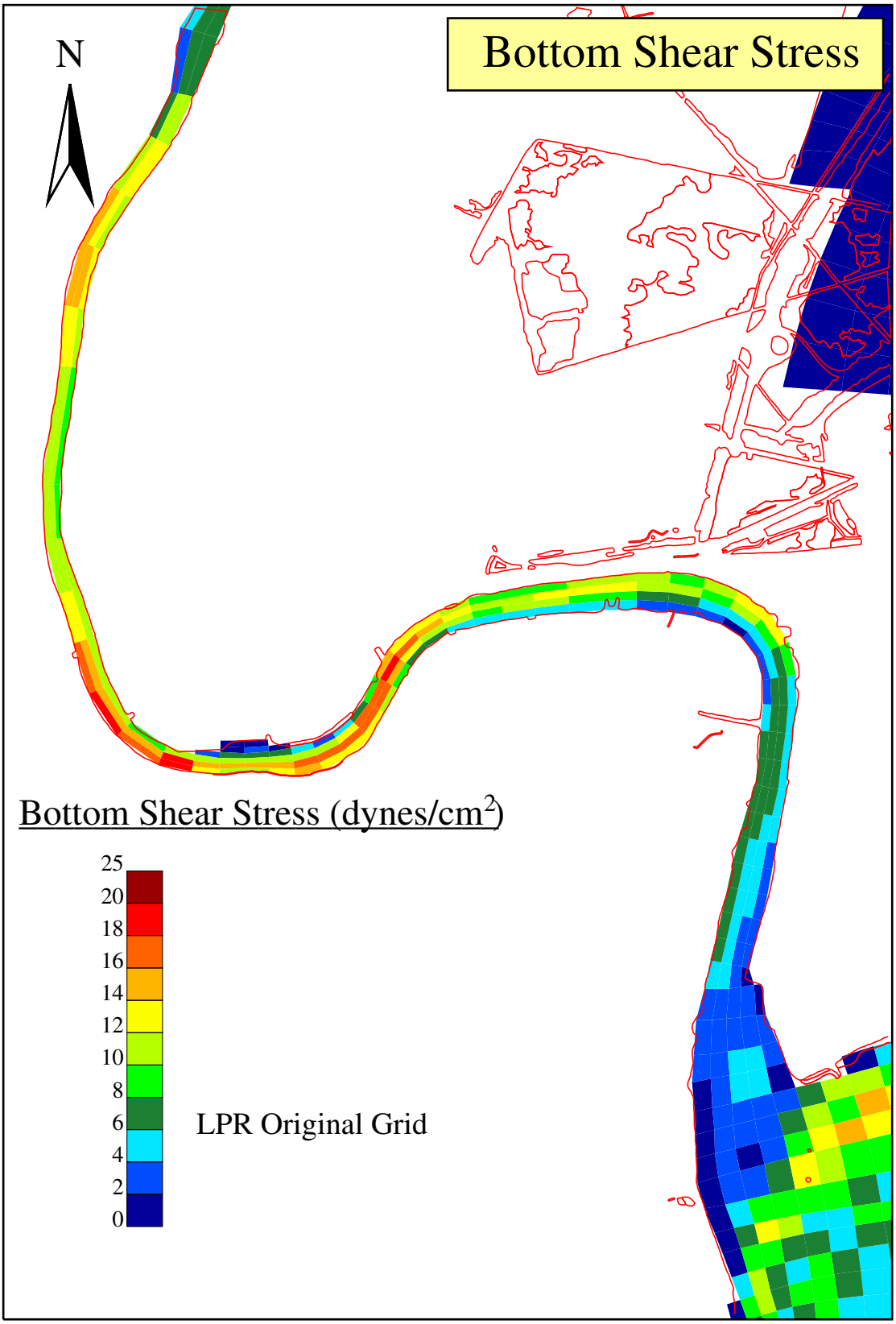

Figure 5-16 Comparison of hourly computed bottom shear stress for the original and high-resolution grids

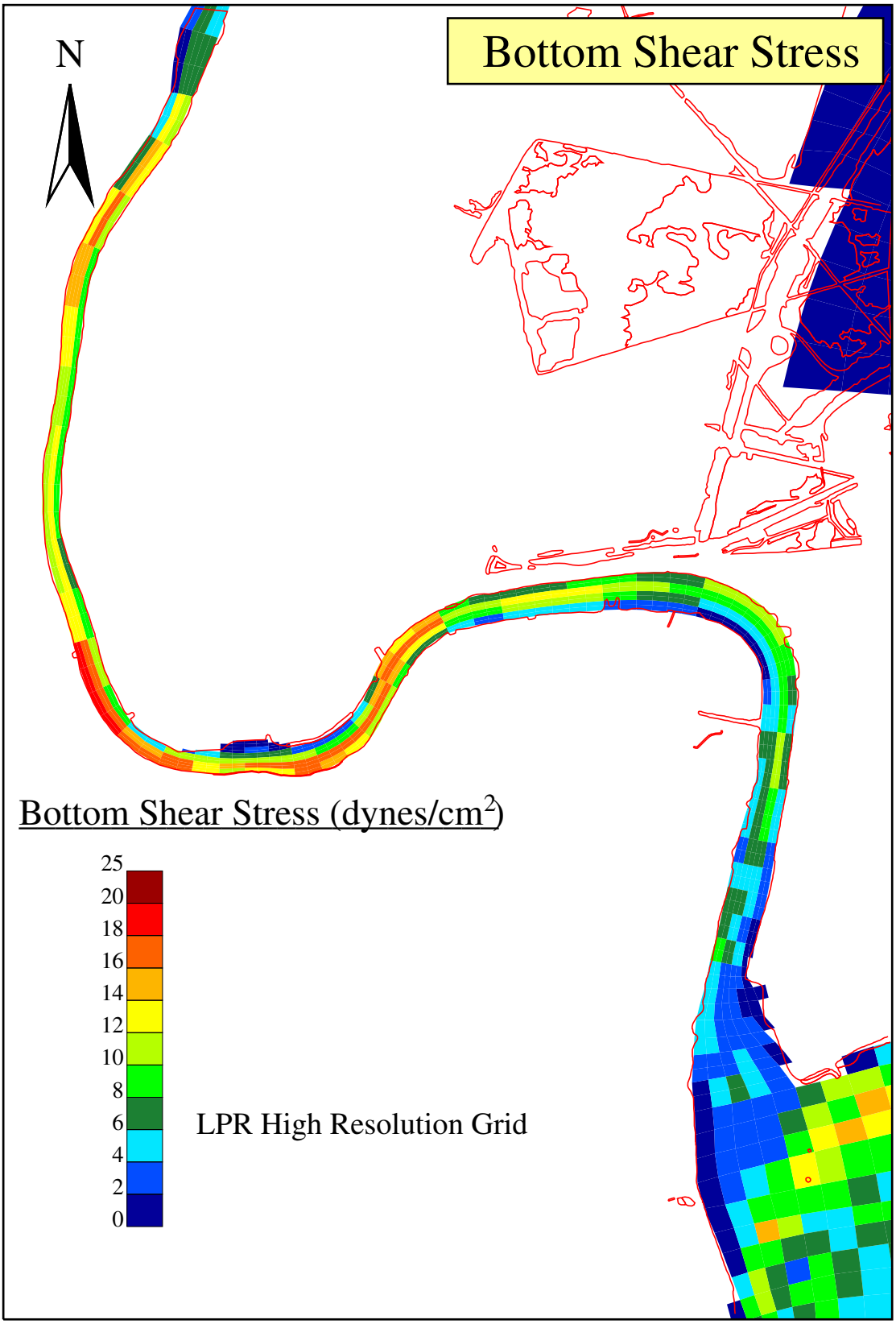

Figure 5-16 Comparison of hourly computed bottom shear stress for the original and high-resolution grids (continued)

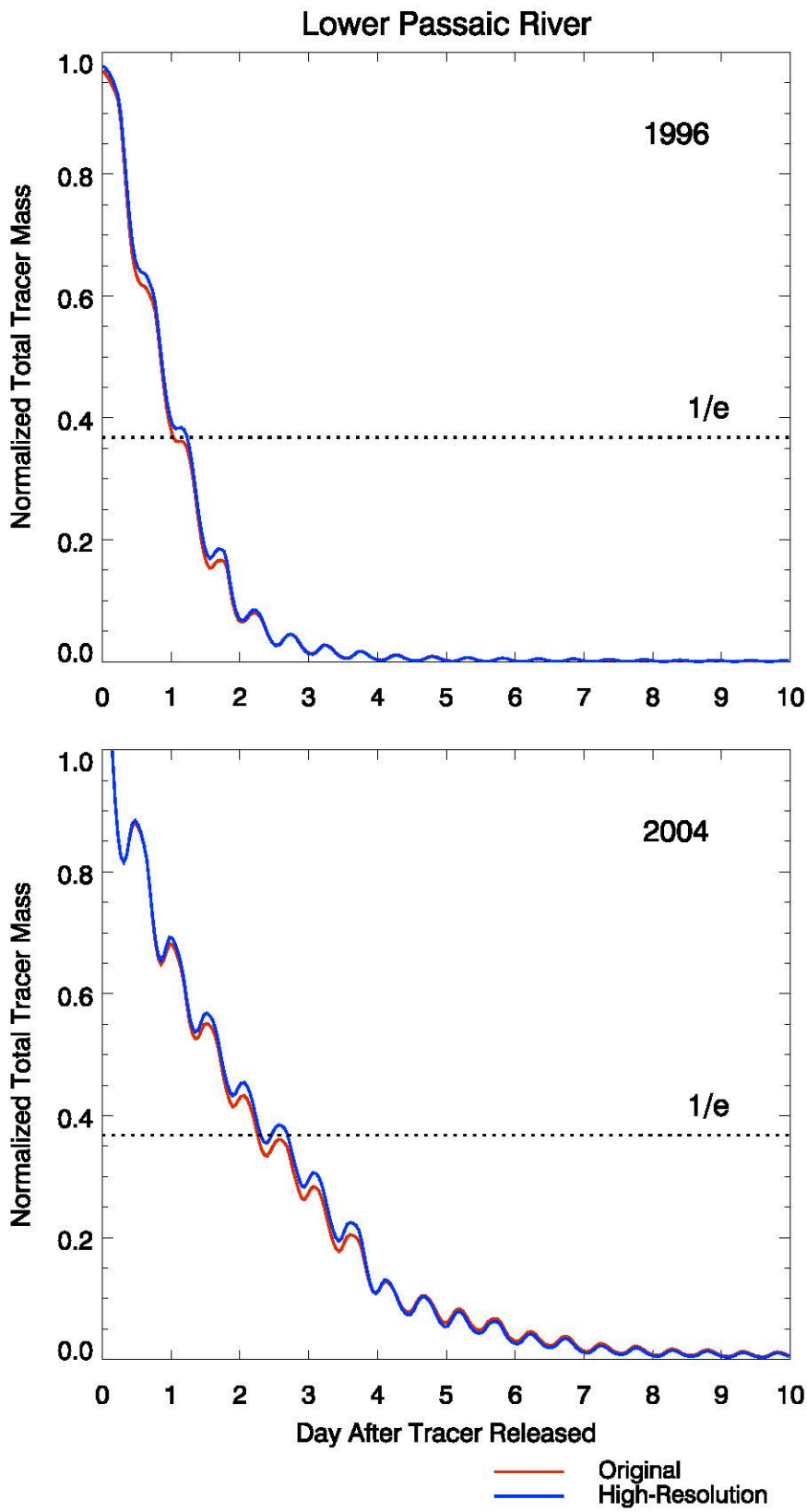

Figure 5-17 Comparison of the flushing time of the Lower Passaic River for the original and high-resolution grids for 1996 (upper frame) and 2004 (lower frame)

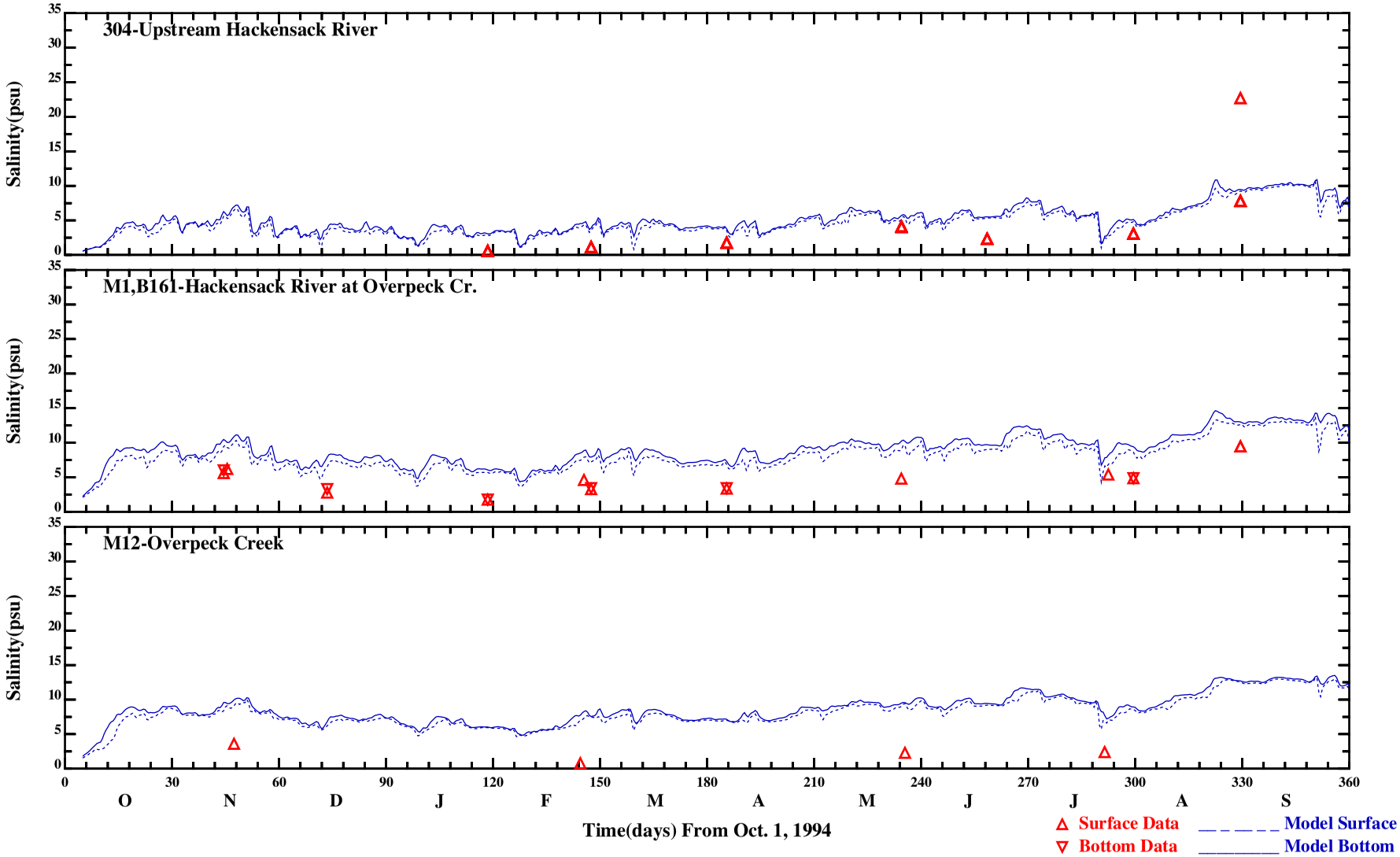

Figure 5-18 Comparison of 35 hour low-passed computed salinity with Battelle and MERI data over a period of one year (1994-1995)

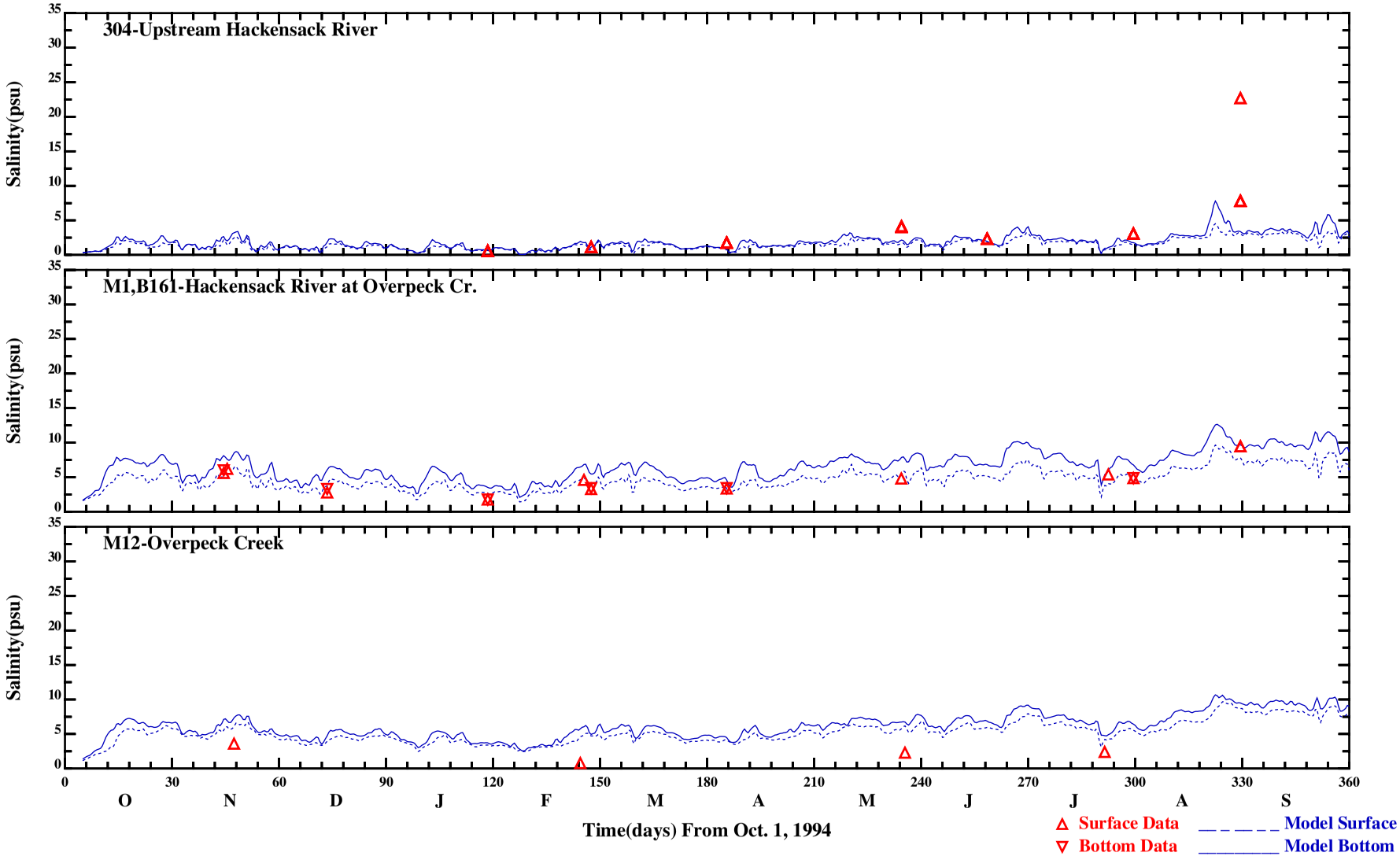

Figure 5-19 Sensitivity run results using additional 100 cfs in the Hackensack River

SECTION 6

SUMMARY OF CALIBRATION/VALIDATION FINDINGS

An extensive database coupled with a three-dimensional, high resolution, physically comprehensive hydrodynamic model has been used to reproduce the major hydrographic features of the Lower Passaic River, the Hackensack River, Newark Bay and the Kills. The computational framework (or computer code) used in this analysis is the Estuarine, Coastal and Ocean Model (ECOMSED). ECOMSED has a long history of successful applications of coastal and estuarine waters. The success of the model was highly dependent on the specification of model boundary forcings. A detailed description of the derived boundary conditions – elevations, salinity, temperature, surface heat flux, freshwater inflows from rivers, wastewater treatment plants and storm runoff – has been presented.

Because the lower section of the Hackensack River consists of about 1,500 acres area of tidal wetlands that are submerged at high tide under average tidal condition, and of a much larger area that can be flooded during extreme flood conditions, the water storage that occurs in the marsh land is expected to have an effect on hydrodynamic transport in the Hackensack River and ultimately the Passaic River. As a result, ECOMSED was reconfigured to explicitly consider the processes of wetting and drying in the hydrodynamic model calculations. In addition, the computational domain included the Meadowlands themselves. The wetting and drying formulations were based on the approaches published by Flather and Heaps (1975) and Kim (1999). Testing of the wetting/drying scheme was conducted under various scenarios and confidence has been established in its suitability for use in the Lower Passaic River domain.

The model grid used in this application is an orthogonal, curvilinear grid system consisting of 74x268 segments in the horizontal plane and 10 equally spaced σ-layers in the vertical plane. The transformed σ-coordinate system in the vertical plane allows the model to have an equal number of vertical segments in all of the computational grid cells. It should be noted that the curvilinear grid allows for finest grid resolution in the areas of interest, such as the Passaic River, Hackensack River and Newark Bay proper. A coarser grid system has been adopted for the rest of the model domain. This technique allows for an efficient and computationally time-effective modeling framework.

Extensive model sensitivity analyses were conducted to ensure that the selection of the model grid and parameters employed in the study was appropriate to address the detailed hydrodynamics of the study area. A series of sensitivity runs, varying key model parameters including bottom roughness lengths, and mixing parameters, were conducted and the best combination of model parameters were obtained, which yielded optimal model calibration

results for water surface elevations, current velocities, and density variations in the LPR. Grid convergence tests were also conducted to verify that the designed grid was fine enough to address the detailed hydrodynamic features of the study area.

Model calibration/validation was driven by high quality sets of observations of tidal elevation, salinity, temperature and velocity collected throughout the domain. Three major data sources were used: (1) the 1995-1996 field data collected by Tierra Solutions Inc. (TSI) 2) the 2000-2002 data set collected by the Institute of Marine & Coastal Sciences (IMCS) of Rutgers University in the Kills and Newark Bay, and 3) 2004 data collected by the IMCS in the lower section of the LPR. Of these data sets, 1995-6 and 2004 data sets were used for the calibration and validation of the LPR area, respectively. 2002 and 2001 data sets were used for the calibration and validation of Newark Bay and the Kills area, respectively. Model simulations were performed for the periods when the field data were available. A model skill assessment has been conducted by visual comparison with observed data and quantified in terms of RMSE and correlation coefficients.

In general, the hydrodynamic model is capable of reproducing the entire range of the observed water elevation, velocity, temperature and salinity data in the Lower Passaic River /Newark Bay domain. A summary of the major findings is given below.

Computed water elevations agreed very well with the observed data. The model is capable of reproducing the spectrum of times scales of the observed quantities, including the semi-diurnal tidal scale, the diurnal scale, the meteorological scale (a few days), spring and neap tidal scale (15 days). There were, however, times, e.g., May 1995, when the model slightly over estimated the amplitudes measured at tidal gauges in the lower section of the LPR, although for these same locations the computed elevations were in full agreement when compared against the 2002 and 2004 measurements. The statistical evaluation of model performance showed that for all stations, the mean correlation coefficient was about 0.95 between measured and computed water elevations, and about 0.83 and 0.79 for the subtidal 35-hr and 5-day low-passed water levels, respectively. The RMSE at all stations were about 6% for most stations, and remained under 10% for the 5-day low-passed water surface elevations, resulting overall in very good agreement between the model and data.

Except for a few discrepancies, the comparison of computed versus measured current velocities showed that at all locations the model was able to reproduce the magnitudes and lateral and vertical structure of velocities during the ebb-, ebb-to-flood transition, and flood tidal periods. The model was also able to reproduce the strong near-surface currents observed in the deep channel. Along some transects in the LPR, the model produced reasonable lateral and vertical variations of current velocities. In general, the resulting RMSE between model and data are about 10%, while the correlation coefficients range between 0.72 and 0.89.

The model was also calibrated by comparing computed near-surface and near-bottom salinity and temperature at a number of stations across the model domain. Although the data density was not uniform across the stations, as some measurements were temporally and spatially sparse, the model was able to reproduce the seasonal cooling and heating cycle of water temperature within the model domain, as well as the range of salinity due to tidal fluctuations. Due to a lack of continuous observations of water temperature at the upstream boundary of the LPR, the computed water temperatures show notable discrepancies during high flow events. There are instances, such as the spring 1996 event, when computed temperatures were persistently lower than the data by 2-3 °C over the tidal cycle. Again, this is due to uncertainties in the boundary forcing water temperatures. The correlation coefficients are lower in the LPR with values ranging from 0.45 in the upstream locations to 0.8 in downstream locations. However, correlation coefficients are above 0.92 for all locations in Newark Bay and the Kills, where the receiving waters are less impacted by uncertainties in boundary river water temperature.

Tidal variations in salinity are larger than those for temperature in the LPR. The model reproduced surface and bottom hourly salinity variations quite well along the length of the river. The computed and observed temporal variations of surface salinity as well as the vertical stratification due to tidal movement of the water were, generally, in good agreement. Both model and data indicate that salinity intrusion into the LPR is about 8 miles during relatively low river flow periods. The tidal excursion of salinity reaches about 10 psu in the downstream stations, indicating the existence of a sharp horizontal gradient between the lower Passaic River and Newark Bay. In Newark Bay and the Kills, computed-bottom salinity followed the general pattern of the observations. However, sudden increases in bottom salinity during neap tides in Newark Bay and the Kills in the spring of 2002 were not reproduced by the model. Based on a sensitivity analysis, it is more likely that the uncertainty is due to problems with salinity computed in NY-NJ Harbor. This in turn is due to uncertainty in the estimates of freshwater inflows in the Lower Hudson Valley that result from rainfall events occurring within that region. Results show relatively little effect on calibration scores and bottom velocities/shear stress.

Finally, the analysis of net volume fluxes in Newark Bay and the Kills confirmed that the depth-averaged volume flux in the Passaic River is always in the downstream direction, reflecting the dominant freshwater inflows from upstream. However, the analysis also indicated a conventional estuarine density-driven circulation with a net landward bottom layer flow and a net seaward surface layer flow in the LPR and Newark Bay system. The analysis also indicates that the fluxes in Newark Bay are consistently balanced by the sum of the Passaic and Hackensack Rivers inflows. It was also found that net fluxes through the

Kills are predominantly towards Raritan Bay, but short-term variations are influenced by wind events.

This calibrated/validated model is expected to be a useful tool for sediment transport and water quality modeling.

SECTION 7

REFERENCES

Adams, E. E., D. R. F. Harleman, G. H. Jirka, K. D. Stolzenbach, 1981."Heat Disposal in the Water Environment", Ralph M. Parsons Laboratory for Water resources and Hydrodynamics, Department of Civil Engineering, MIT, Cambridge, MA 02139.

Ahsan, Q., and A. F. Blumberg, 1998. A Three-Dimensional Hydrothermal Model of Onondaga Lake, New York. Journal of Hydraulic Engineering, Vol. 125, No. 9, September, 1999.

Ashizawa, D. and J.J. Cole, 1994. Long-Term Temperature Trends of the Hudson River: A Study of the Historical Data, Estuaries, 17(1B), 166-71.

Beardsley, R.C., and W.C. Boicourt, 1981. On Estuarine and Continental-Shelf Circulation in the Middle Atlantic Bight. Evolution of Physical Oceanography, Scientific Surveys in Honor of Henry Stommel; B.A. Warren and C. Wunsch, Eds., The MIT Press, 198-233.

Beardsley, R.C. and B. Butman, 1974. Circulation on the New England Continental Shelf: Response to Strong Winter Storms; Geophysical Res. Let. 1(4).

Beardsley, R.C., D.C. Chapman, K.H. Brink, S.R. Ramp and R. Schlitz, 1985. The Nantucket Shoals Flux Experiment (NSFE79). Part I: A Basic Description of the Current and Temperature Variability; J. Phys. Oceanogr. 15:713-748.

Beardsley, R.C. and C.D. Winant, 1979. On The Mean Circulation in the Middle Atlantic Bight; J. Phys. Oceanogr., 9.

Blumberg, A.F., L.A. Khan, and J.P. St. John, 1999. Three dimensional hydrodynamic model of New York Harbor. J. Hyd. Engr., ASCE. 125(8), 799-816.

Blumberg, A.F. and B. Galperin, 1990. On the Summer Circulation in New York Bight and Contiguous Estuarine Waters. In: Coastal and Estuarine Studies, Vol. 38, Residual Currents and Long-Term Transport, D.T. Cheng (Ed.), Springer-Verlag, New York.

Blumberg, A.F. and D.M. Goodrich, 1990. Modeling of Wind-Induced Destratification in Chesapeake Bay, Estuaries, 13(3):236-249, September 1990.

Blumberg, A.F. and H.J. Herring. 1987. Circulation Modeling Using Orthogonal Curvilinear Coordinates. In: Three-Dimensional Models of Marine and Estuarine Dynamics, J.C.J. Nihoul and B.M. Jamart, Eds., Elsevier Pub. Company, 55-88.

Blumberg, A.F. and L.H. Kantha, 1985. Open Boundary Condition for Circulation Models, J. Hydraul. Eng., 111:237-255.

Blumberg, A.F. and L.A. Khan, and J.P. St. John, 1999. Three Dimensional Hydrodynamic Model of New York Harbor Region. J. Hydraulic Engineering, 125, 799-816.

Blumberg, A. F. and B. N. Kim, 2000. Flow Balances in St. Andrew Bay Revealed Through Hydrodynamic Simulations, Estuaries. 23:21-33

Blumberg, A.F. and G.L. Mellor, 1983. Diagnostic and Prognostic Numerical Circulation Studies of the South Atlantic Bight. J. Geophys. Res., 88, 4579 4592.

Blumberg, A.F. and G.L. Mellor, 1987. A Description of a Three-Dimensional Coastal Ocean Circulation Model. In: Three-Dimensional Coastal Ocean Models, Coastal and Estuarine Sciences, 4, N. Heaps, Ed., American Geophysical Union, Washington, D.C., 1-16.

Blumberg, A.F. and G.L. Mellor, 1980. A Coastal Ocean Numerical Model, In: Mathematical Modelling of Estuarine Physics. Proceedings of an International Symposium, Hamburg, August 24-26, 1978. J. Sundermann and K.P. Holz, Eds. Springer-Verlag, Berlin.

Blumberg, A.F. and G.L. Mellor, 1985. A Simulation of the Circulation in the Gulf of Mexico. Israel J. of Earth Sciences, 34, 122 144.

Blumberg, A.F. and L.Y. Oey, 1985, Modeling Circulation and Mixing in Estuaries and Coastal Oceans; Adv. In Geophysics, 28A.

Brown, W.S., N.R. Pettigrew and J.D. Irish, 1985. The Nantucket Shoals Flux Experiment (NSFE79). Part II: The Structure and Variability of Across-Shelf Pressure Gradients, J. Phys. Oceanogr., 15:749-771.

Bumpus, D.F., 1969. Reversal in the Surface Drift in the Middle Atlantic Bight Areas; Deep-Sea res. 16 (suppl.)

Caplow, T., P. Schlosser, D. T. Ho, and N. Santella. 2003. Transport dynamics in a sheltered estuary and connecting tidal straits: SF6 tracer study in New York harbor. *Environ Sci. Technol.,* 37(22): 5116-5126

Carswell, L.D. 1976. Appraisal of Water Resources in the Hackensack River Basin, New Jersey, USGS Water Resources Investigations 76-74

Chant, R.J., 2006. Hydrodynamics of the Newark Bay/Kills System: The New Jersey Toxics Reduction Workplan for New York-New Jersey Harbor – Study I-E, April 2006, 66 pp. prepared for NJ Dept of Env Protection

Chapman, J., A. Barth, R.C. Beardsley and R.G. Fairbanks, 1986. On the Continuity of Mean Flow Between the Scotian Shelf and the Middle Atlantic Bight, J. Phys. Oceangr., 16.

Cole, T. M., and Buchak, E. M., 1995. "CE-QUAL-W2: a two-dimensional, laterally averaged, hydrodynamic and water quality model, version 2.0 user manuaL" Instruction Rep. EL-95-I, U.S. Army Corps of Engineers, Washington, D.C.

Davies, A.M., S.C.M. Kwong and R.A. Flather, 1997. A Three-Dimensional Model of Diurnal and Semi-Diurnal Tides on the European Shelf, J. Geophy. Res., 102(C4), 8625-8656.

Donelan, M.A., 1977. A Simple Numerical Model for Wave and Wind Stress Application, Report, National Water Research Institute, Burlington, Ontario, Canada, 28pp

Edinger, J.E. Brady, D.K., and Greyer, J.C., 1974. Heat exchange and transport in the environment, Rep No 14, Cooling Water Res. Project (RP-49), Electric Power Research Institute, Palo Alto, Calif.

Egbert, G.D., A.F. Bennett and M.G.G. Forman, 1994. TOPE/POSEIDON Tides Estimated Using a Global Inverse Model. J. Geophy. Res., 99 (C12), 24, 821-852.

Flather, R.A. and N.S. Heaps, 1975. Tidal computations for Morecambe Bay, Geophy. J. of Royal Asstro. Society, 42:489-518

Galperin, B., L.H. Kantha, S. Hassid and A. Rosati, 1988. A Quasi-Equilibrium Turbulent Energy Model for Geophysical Flows. J. Almos. Sci., 45, 55-62.

Galperin, B. and G.L. Mellor, 1990a. Time-Dependent, Three-Dimensional Model of the Delaware Bay and River System. Part 1: Description of the Model and Tidal Analysis. Estuarine, Coastal and Shelf Sciences, 31: 231-253.

Galperin, B. and G.L. Mellor, 1990b. Time-Dependent, Three-Dimensional Model of the Delaware Bay and River System, Part 2: Three-Dimensional Flow Fields and Residual Circulation. Estuarine, Coastal and Shelf Sciences, 31: 255-281.

Galperin, B. and G.L. Mellor, 1990c. Salinity Intrusion and Residual Circulation in Delaware Bay During the Drought of 1984. In: Coastal and Estuarine Studies, Vol. 38, Residual Currents and Long-Term Transport, D.T. Cheng (Ed.), Springer-Verlag, New York. 469-480.

Garvine, R.W., K.-C. Wong, G.G. Gawarkiewicz, R.K. McCarthy, R.W. Houghton and F. Aikman III, 1988. The Morphology of Shelf-Break Eddies; J. Geo. Res., 93, 15, December 1988; pp. 593, 607.

Hagy, J.D., L.P. Sanford and W.R. Boynton. 2000. Estimation of net physical transport and hydraulic residence times for a coastal plain estuary using box models. Estuaries 23(3):328-340.

Han, G., D.V. Hansen and J.A. Galt, 1980. Steady-State Diagnostic Model of the New York Bight; J. Phys. Oceanogr., 10.

Hellweger, F. L., A. B. Blumberg, P. Schlosser, D. T. Ho, T. Caplow, U. Lall, and H. Li. 2004. Transport in the Hudson estuary: a model study of estuarine circulation and tidal trapping. *Estuaries*, 27(3): 527-538.

Hopkins, T.S. and D.A. Dieterle, 1983. An Externally Forced Barotropic Circulation Model for the New York Bight; Cont. Shelf Res., 2.

Hopkins, T.S. and D.A. Dieterle, 1987. Analysis of the Baroclinic Circulation of the New York Bight with a 3-D Diagnostic Model, Cont. Shelf Res., 7:237-265.

HydroQual, Inc., 2001. Newtown Creek Water Pollution Control Project, East River Water Quality Plan, Task 10.0 – System-wide Eutrophication Model (SWEM) Sub-Task 10.6, Validate SWEM Hydrodynamics, Report prepared for City of New York Department of Environmental Protection.

HydroQual, Inc., 2002. Calibration Enhancement of the System-Wide Eutrophication Model (SWEM) in the New Jersey Tributaries, Report prepared for New Jersey Department of Environmental Protection under agreement with the Passaic Valley Sewerage Commissioners

Interstate Sanitation Commission, 1989. ISC Report.

Jay, D.A., M.J. Bowman, 1975. The Physical Oceanography and Water Quality of New York Harbor and Western Long Island Sound. Tech. Rpt. 23, Marine Sciences Research Center, State University of New York at Stony Brook.

Johnson, B.H., K.W. Kim, R.E. Heath, B.B. Hsieh, H.L. Butler, 1993, Validation of Three Dimensional Hydrodynamic Model of Chesapeake Bay, J. Hydraulic Eng. 119:2-20

Joyce, T.M. (Editor), 1985. Warm-Core Rings Collection, J. Geophys. Res. (Special Section), 90:8801-8951.

Kim, K.Y., 1999. A Study on the Characteristic Temperature Distribution in the Thermal Discharged Coastal Water – on the Wolsung Nuclear Power Plant, PhD thesis, Seoul National Univ.

Levitus, S., 1982. Climatological Atlas of the Word Ocean, NOAA Professional Paper 13, NOAA, Rockville, MD.

Malcolm Pirnie, Inc. 2005. Lower Passaic River Restoration Project Draft Quality Assurance Project Plan (QAPP)

Malcolm Pirnie, Inc. 2005. Lower Passaic River Restoration Project Draft Work Plan (WP).

Mayer, D.A., G.C. Han and D.V. Hansen, 1982. The Structure of Circulation: MESA Physical Oceanographic Studies in New York Bight, 2, J. Geophys. Res., 87:9579-9588.

Mellor, G.L. and A.F. Blumberg, 1984. Modeling Vertical and Horizontal Viscosity and the Sigma Coordinate System, Mon. Wea. Rev., 113, 1379 1383.

Mellor, G.L. and T. Yamada, 1982. Development of a Turbulence Closure Model for Geophysical Fluid Problems, Rev. Geophys. Space Phys., 20, 851-875.

New Jersey Department of Environmental Protection (NJDEP), 1986. NJDEP Freshwater Wetlands of New Jersey, Office of Information Resources Management (OIRM), Bureau of Geographic Information and Analysis (BGIA)

NOAA, 1990. Tidal Current Tables, Atlantic Coast of North America. National Ocean Survey, U.S. Department of Commerce.

Oey, L.Y., G.L. Mellor and R.I. Hires, 1985a. Tidal Modeling of the Hudson Raritan Estuary. Estuarine Coastal Shelf Science. 20, 511-527.

Oey, L.Y., G.L. Mellor and R.I. Hires, 1985b. A Three Dimensional Simulation of the Hudson-Raritan Estuary. Part I: Description of the Model and Model Simulations, Journal of Physical Oceanography, 15, 1676-1692.

Oey, L.Y., G.L. Mellor and R.I. Hires, 1985c. A Three Dimensional Simulation of the Hudson-Raritan Estuary. Part II: Comparison with Observations, Journal of Physical Oceanography, 15, 1693-1709.

Pecchioli, Joel A., M.S. Bruno, R. Chant, A.M. Pence, A.F. Blumberg, D. Fugate, B.J. Fullerton, S. Glenn, C. Haldeman, E. Hunter, and K.L. Rankin, 2006. The New Jersey Toxics Reduction Workplan for New York – New Jersey Harbor: Study I-E-Hydrodynamic Studies in the Newark Bay Complex, Research Project Summary, Div. of Science, Research and Technology, N.J. Dept of Env. Protection

Pence, Anne Marie, 2004. Dominant Forces in an Estuarine Complex with Multiple Tributaries and Free Connections to the Open Ocean with Application to Sediment Transport, PhD thesis, Stevens Institute of Technology

Scheffner, N.W., S.R. Vermulakonda, D.J. Mark, H.L. Butler and K.W. Kim, 1994. New York Bight Study, Report 1: Hydrodynamic Modeling, Tech-Rept. CERC-94-4, U.S. Army Corps of Engineers, Vicksburg, MS.

Schmalz, Jr., R.A., M.F. Devine and P.H. Richardson, 1994. Long Island Sound Oceanography Project, Summary Report, Volume 2: Residual Circulation and Thermohaline Structure, NOAA Tech. Rpt. NOSOES 003, Silver Spring, Maryland.

Smagorinsky, J., 1963. General Circulation Experiments with the Primitive Equations, I. The Basic Experiment. Monthly Weather Review, 91, 99-164.

Schwab, D.J., J.R. Bennett, P.C. Liu, and M.A. Donelan, 1984. Application of a simple numerical wave prediction model to Lake Erie. Journal of Geophysical Research 89:3586-3592.

Tierra Solutions Inc. 2004. Newark Bay Work Plan - Supplement.

Tierra Solutions Inc. 2003. Executive Summary: Passaic River Study Area: Preliminary Findings.

Tsay, T., G.J. Ruggaber, S.W. Effler, and C.T. Driscoll, 1992. Thermal Stratification Modeling of Lakes with Sediment Heat Flux. J. of Hydraulic Eng. 118, 407-419.